

Antonius Kies

A contribution to the analysis of fuel efficiency measures for heavy-duty vehicles

MONOGRAPHIC SERIES TU GRAZ



Antonius Kies

**A contribution to the analysis of fuel efficiency
measures for heavy-duty vehicles**

Monographic Series TU Graz

Monographic Series TU Graz

Antonius Kies

A contribution to the analysis of fuel efficiency measures for heavy-duty vehicles

This work is based on the dissertation
“A contribution to the analysis of fuel efficiency measures for heavy-duty vehicles”,
presented by Antonius Kies on 27 Sep 2017 at
Technische Universität Graz, Institut für Verbrennungskraftmaschinen und Thermodynamik.

Assessed by
Ao. Univ.Prof. Dr.techn. Dipl.-Ing. Stefan Hausberger, Technische Universität Graz, and
Univ.Prof. Dr.techn. Dipl.-Ing. Bernhard Geringer, Technische Universität Wien.

© 2018 Verlag der Technischen Universität Graz

Cover photo Lunghammer, TU Graz
Layout Christina Fraueneder, TU Graz
 Stefan Schleich, TU Graz

Verlag der Technischen Universität Graz
www.ub.tugraz.at/Verlag

E-Book

ISBN 978-3-85125-578-2

DOI 10.3217/978-3-85125-578-2



<https://creativecommons.org/licenses/by/4.0/>

Acknowledgement

The author wants to thank all the helpful people who assisted him directly or indirectly with this thesis and dedicate it to them:

His dissertation supervisor and first auditor Prof. Hausberger S. for the support and counselling during the creation of this thesis plus the examination and copy editing.

His second auditor Prof. Geringer B. for the additional examination and the valuable proposals.

The whole team at TU Graz, Institut für Verbrennungskraftmaschinen und Thermodynamik, Forschungsbereich Emissionen, for the support and the good cooperation: Blassnegger J., Deutsch M., Dippold M., Lipp S., Luz R., Matzer C., Nöhner G., Quaritsch M., Rexeis M., Röck M., Silberholz G., Stadlhofer W., Stiermair A., Vuckovic T., Weller K.

The IT crowd of the institute, Ilic S. and Neubacher C. for administering our calculating machines, keeping the servers up and restoring many accidentally deleted files.

The library of TU Graz for keeping and obtaining literature with priceless data.

Lutz R. from MAHLE Behr, Stuttgart, for supporting the creation of the fan-model and sharing the necessary measurement data.

Kies D. and Zach B. for proofreading chapter 1 "Introduction and Motivation" for comprehensibility.

The whole ACEA Workgroup-CO2HDV for the support of the VECTO Project with measurement vehicles, decisive data and knowledge.

These ladies and gentlemen for providing driving cycles or help with specific requests: Benita D. (ADEME), Besch M. (WVU), Breemersch T. (TML), Dreger S. (TÜV Nord), Gallo J. (CALSTART), Gao Z. (ORNL), Hahn S. (SSB), Hayes D. (LowCVP), Katsis P. (Emisia), Kotzulla M. (UBA), Kytö M. (VTT), Milojevic S. (Uni Kragujevac), Prohaska R. (NREL), Pütz R. (HAW Landshut), Ragatz A. (NREL), Schumann A. (Deutsche Bahn), Veldhuizen R. (WABCO Optiflow), Verheij J. (Allison), Walkowicz K. (NREL), Wu Y. (Uni Tsinghua), Zhang S. (Uni Michigan).

The scientific workers, publishers and institutions, who make their results available for free.

The publishers who grant the universities access to their archives.

The governmental and private institutions which fund research projects in the public interest.

The operators of the online dictionary leo.org.

The authors of Wikipedia for creating the encyclopaedia and linking to useful resources.

His family and friends for their affection and support, and for their tolerance towards his temporary total retreat into the office.

Skiljan I. for IrfanView, Mitchell M. for Engauge and ASDD for XIXtrFun.

The crews of Linux and Debian and all FOSS communities for producing and maintaining free alternative operating systems and programs.

The operators of privacy-friendly search engines like DuckDuckGo, Ixquick, Qwant or Startpage, which are very helpful to find relevant publications on many topics without feeding the data collectors.

The musicians who produce sophisticated heavy metal music from melodious to brutal and tolerate the distribution via streaming channels, amongst others for the entertainment of simulation engineers.

Table of contents

1	INTRODUCTION AND MOTIVATION	1
1.1	Economics - Save fuel cost	1
1.2	Ecology - Global warming	3
1.3	Decarbonisation and fuel efficiency measures.....	7
1.4	The VECTO project	9
2	SIMULATION OF THE ENERGY CONSUMPTION OF HEAVY-DUTY VEHICLES	12
2.1	Backward and forward simulation.....	12
2.2	Calculation of the energy demand of wheeled motors vehicles	15
2.2.1	Power demand at the hubs of the driven wheels	15
2.2.1.1	The road load curve	17
2.2.1.2	Rolling resistance of tires	17
2.2.1.3	Air drag and cross wind.....	18
2.2.2	Drivetrain losses between wheel hubs and engine	22
2.2.3	Engine auxiliary consumers and the "FC-line"	24
2.2.3.1	Air conditioning system of buses	29
2.2.4	Vehicle control: Acceleration, deceleration and gear shift	33
2.2.5	Engine operation point and fuel consumption.....	35
2.3	Models of engine auxiliary consumers.....	37
2.3.1	Cooling fan	37
2.3.2	Compressor	50
2.3.2.1	Measurement of the pneumatic system of a delivery truck	50
2.3.2.2	Calculating air consumption and compressor power demand.....	55
2.3.2.3	Consumption of pressurised air on bus cycles	61
2.4	Models for energy recovery and start-stop automatic	62
2.4.1	Regenerative braking with engine auxiliaries	62
2.4.2	Start-stop automatic	66
2.4.3	Exhaust heat power generation	68
2.5	Models of electrified powertrains	72
2.5.1	Diesel-electrical parallel hybrid trucks	73
2.5.2	Diesel-electrical parallel hybrid buses	75
2.5.3	Diesel-electrical serial hybrid rigid bus	77
2.5.4	Battery-electrical delivery truck and rigid bus	79
2.5.5	Overload of the models of electrical machines	80
2.6	Basis vehicle models EURO VI, state of technology 2014	83
2.6.1	Creation of basis vehicle models.....	83
2.6.1.1	Tractor-trailer and delivery truck.....	83
2.6.1.2	Rigid city bus 12 m.....	86
2.6.2	Overview of basis vehicle models.....	87
2.6.3	Check for plausibility of basis vehicle models.....	89
2.6.3.1	Models of tractor-trailer and of delivery truck	89
2.6.3.2	Rigid city bus 12 m.....	91
2.6.3.3	Comparison with existing FC limits for trucks and buses	93
2.6.3.4	Additional model of articulated city bus 18 m.....	94
2.6.4	Comparison of the basis HDV models in VECTO 2 and VECTO 3.....	97

3	RESULTS FOR SINGLE AND BUNDLED EFFICIENCY MEASURES	98
3.1	Selected single saving measures and alternative powertrains	99
3.1.1	Tires lowest rolling resistance	99
3.1.2	Aero packages and speed limit 80 km/h.....	100
3.1.3	Lightweighting.....	101
3.1.4	Reduced drivetrain friction	102
3.1.5	Start-stop automatic and efficient engine auxiliaries	103
3.1.6	Exhaust heat power generation	104
3.1.7	Synthetic fuels from regenerative sources	104
3.1.8	Improved engine efficiency	105
3.1.9	EcoRoll and limited braking deceleration	106
3.1.9.1	Tractor-trailer, EcoRoll and Coasting.....	106
3.1.9.2	Urban vehicles, limited deceleration	107
3.1.10	Stoichiometric gas engine	108
3.1.11	Diesel-electrical parallel hybrid vehicles	109
3.1.11.1	Tractor-trailer	110
3.1.11.2	Delivery truck.....	111
3.1.11.3	Rigid bus.....	114
3.1.11.4	Articulated bus.....	115
3.1.12	Diesel-electrical serial hybrid vehicles.....	117
3.1.13	Comparison of parallel and serial hybrid powertrain for rigid buses	119
3.1.14	Battery-electrical powertrain.....	122
3.1.14.1	Delivery Truck.....	122
3.1.14.2	Rigid bus.....	124
3.1.14.3	Battery-electrical vehicle models, payload and energy consumption	125
3.1.15	Overview of results for selected single measures and alternative powertrains	126
3.2	Bundled saving measures, levels "current" and "future"	128
3.2.1	Comparison of models with technology bundles to basis vehicle models	129
3.2.1.1	Partial check for plausibility of bundled saving measures, level "current".....	130
3.2.2	Comparison of alternative powertrains of equal technical levels.....	132
3.2.3	Comparison of results from other studies	134
4	SUMMARY AND OUTLOOK.....	136
5	SUPPORTING DATA	139
5.1	Abbreviations.....	139
5.2	Notations.....	142
5.2.1	Greek and mathematical notations	142
5.2.2	Latin notations	144
5.3	Units.....	150
5.4	Driving cycles.....	153
5.4.1	VECTO target speed driving cycles.....	153
5.4.1.1	Variations of VECTO target speed driving cycles	155
5.4.2	Further driving cycles	156
5.4.3	Characteristic factors of driving cycles.....	163
5.5	Fuel properties.....	165
5.6	Detailed data of basis vehicle models and data sources	166
5.6.1	Basis vehicle models.....	166
5.6.2	Aerodynamic measures	168

5.7	Technical data of vehicle variants and saving measures	169
5.7.1	Single saving measures	169
5.7.2	Alternative powertrain concepts	172
5.7.3	Bundles of current possible saving measures	173
5.7.4	Bundles of future possible saving measures	175
5.7.5	Vehicle models to simulate own measurements.....	176
5.7.6	Additional vehicle models for check of plausibility	178
5.7.7	Driving performance of models with alternative powertrains.....	179
5.8	Engine performance data	180
5.8.1	Performance maps, diesel and gas engines, basis electrical machine	180
5.8.2	Internal combustion engines, check of performance maps	183
5.9	Transmission performance data.....	186
5.10	Average payload of analysed vehicle classes	187
5.11	Cooling capacity of air conditioners of city buses.....	188
5.12	Organic Rankine Cycle performance data	189
5.13	Current consumption standards for heavy-duty vehicles.....	190
5.14	Published values for fuel consumption	192
5.14.1	Tractors 4x2	192
5.14.1.1	Conventional tractors, diesel-fuelled	192
5.14.1.2	Payload-specific GHG emission factors, tractor-trailers, diesel-fuelled.....	194
5.14.1.3	Conventional tractors, CNG-fuelled	195
5.14.2	Delivery trucks 4x2	195
5.14.2.1	Conventional delivery trucks, diesel-fuelled	195
5.14.2.2	Hybrid diesel-electrical delivery trucks	196
5.14.2.3	Battery-electrical delivery trucks.....	198
5.14.3	City buses 12 m 4x2.....	199
5.14.3.1	Conventional city buses 12 m, diesel-fuelled	199
5.14.3.2	Conventional city buses 12 m, CNG-fuelled	202
5.14.3.3	Diesel-electrical parallel hybrid city buses 12 m.....	204
5.14.3.4	Diesel-electrical serial hybrid city buses 12 m	206
5.14.3.5	Battery-electrical city buses 12 m.....	207
5.14.4	City buses 18 m 6x2.....	209
5.14.4.1	Conventional city buses 18 m, diesel-fuelled	209
5.14.4.2	Diesel-electrical parallel hybrid city buses 18 m.....	211
5.15	Fan power demand.....	213
5.16	Miscellaneous	214
5.16.1	Utilised simulation programs	214
6	REFERENCES.....	215
6.1	Institutions and abbreviations	215
6.2	References.....	219

Abstract

In this thesis a selection of efficiency measures to reduce the fuel consumption (FC) of European heavy-duty vehicles (HDV) was analysed by simulation. Efficiency is motivated by saved fuel costs, by lower emissions of greenhouse gases (GHG) and by a reduced dependence on oil imports.

The analysis of the efficiency measures was done by the simulation of longitudinal vehicle dynamics with the program VECTO, which is mandatory from 2019 for the CO₂ certification of new European trucks. The inputs are characteristic parameters to describe the power consumption of every relevant vehicle component, which are explained in the theory chapter. Amongst others the parameters for rolling resistance, air drag, masses and inertias, drivetrain friction, auxiliary power and engine performance are input values to simulate FC and GHG on standardised driving cycles.

New models were created to calculate the power demand of the cooling fan and the saving potential of regenerative braking with auxiliaries. For the compressor of the pneumatic system an existing model was further elaborated. Gas engines were considered by changing the engine performance map. To depict further alternative powertrains like diesel-electrical parallel and serial hybrids plus battery-electrical vehicles, new models were created, and for parallel hybrid buses an existing model was revised.

An extensive effort was spent to collect and sort measurement values for the FC and energy consumption (EC) of many vehicle variations, to check the simulations of single efficiency measures and alternative powertrains for plausibility.

The saving measures were analysed separately, and bundled to packages and simulated for all powertrain concepts. The reduction potentials for the EC and GHG were elaborated for future HDV in the mid-2020ies, the results are shown in Figure 1.

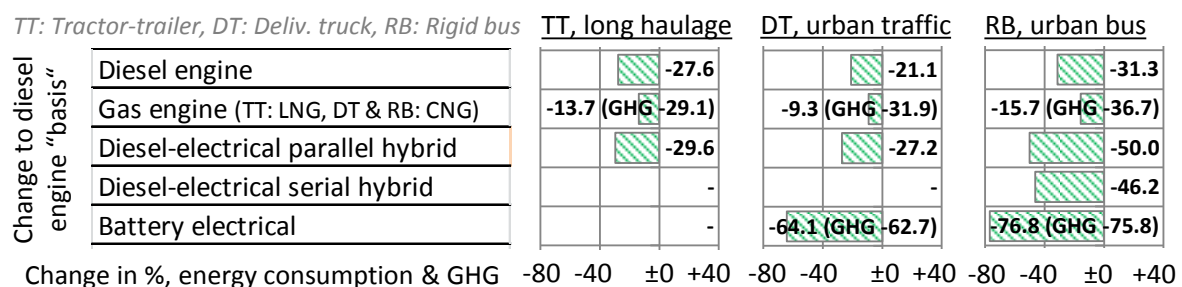


Figure 1. Results for different propulsion systems with bundled saving measures.

FC HDV models "basis", average payload, in L-Diesel/100km: TT 27.8, DT 19.0, RB 41.0

Change in % of EC tank-to-wheel and of GHG well-to-wheel towards the HDV models of technical level basis, year 2014. GHG labelled separately, if not diesel fuel. LNG: Liquefied natural gas.

CNG: Compressed natural gas. Battery-electrical: EC including 10 % charging losses grid to battery.

GHG factor electricity 0.34 kg-CO₂e/kWh_{el}, grid ENTSO-E continental Europe 2014.

Thus with the selected and bundled efficiency measures the energy consumption and GHG emissions from driving can be reduced by ca. 21 to ca. 76 %, depending on application and powertrain. The highest reduction is possible with battery-electrical vehicles.

But also HDV with conventional diesel powertrains still offer significant reduction potentials, and can be combined with GHG-reduced fuels from partly regenerative sources.

Kurzfassung

In dieser Arbeit wurde eine Auswahl von Sparmaßnahmen zur Verringerung des Kraftstoffverbrauchs (KV) von europäischen Nutzfahrzeugen (Nfz) mittels Simulation untersucht. Die Motivation für Sparmaßnahmen ist verringerte Kraftstoffkosten, niedrigere Treibhausgasemission (THG) und eine geringere Abhängigkeit von Ölimporten.

Die Untersuchung der Sparmaßnahmen wurde durch Simulation der Fahrzeug-Längsdynamik mit dem Programm VECTO durchgeführt, welches ab 2019 für die CO₂-Zertifizierung neuer europäischer Lastkraftwagen vorgeschrieben ist. Die Eingabegrößen sind Kennwerte, welche den Leistungsbedarf jeder relevanten Fahrzeugkomponente angeben und im Theorieteil beschrieben werden. Die Eingabedaten bestehen unter anderem aus den Kennwerten für den Rollwiderstand, den Luftwiderstand, die Massen und Massenträgheitsmomente, die Antriebstrangreibung, den Leistungsbedarf der Nebenverbraucher und für die Motorleistung.

Neue Modelle wurden erstellt, um den Leistungsbedarf des Lüfters und das Einsparpotential der Nutzbremmung mit Nebenverbrauchern zu berechnen. Für den Kompressor des Druckluftsystems wurde ein bestehendes Modell weiter ausgearbeitet. Gasmotoren wurden durch den Austausch des Verbrauchskennfeldes simuliert. Um weitere alternative Antriebssysteme wie diesel-elektrische parallele und serielle Hybride sowie batterie-elektrische Fahrzeuge darzustellen, wurden neue Modelle erstellt, oder für parallele Hybridbusse ein bestehendes Modell überarbeitet.

Ein beträchtlicher Aufwand wurde betrieben, um Messwerte für KV und Energieverbrauch (EV) von vielen Fahrzeugvariationen zu sammeln und zu sortieren, um die Simulationen der einzelnen Sparmaßnahmen und alternativen Antriebssysteme zu plausibilisieren.

Die Maßnahmen wurden getrennt analysiert sowie zu Paketen gebündelt und für alle Antriebssysteme simuliert. Die Reduktionspotentiale für EV und THG wurden für zukünftige Nfz für Mitte der 2020er Jahre erarbeitet, die Ergebnisse werden in Figure 2 gezeigt.

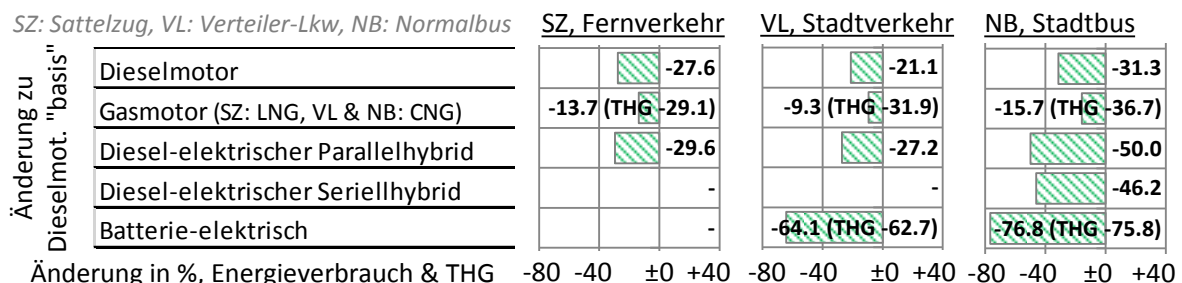


Figure 2 Ergebnisse für verschiedene Antriebssysteme mit gebündelten Sparmaßnahmen.

KV Nfz Modelle "basis", durchschnittliche Zuladung, in L-Diesel/100km: SZ 27.8, VL 19.0, NB 41.0

Änderung in % von EV Tank-zu-Rad und THG Quelle-zu-Rad zu Nfz Modellen auf technischem Niveau "basis", Jahr 2014. THG separat eingetragen, falls kein Dieselmotorkraftstoff. LNG: Liquefied natural gas.

CNG: Compressed natural gas. Batterie-elektrisch: EV inkl. 10 % Ladeverluste Netz zu Batterie.

THG Faktor Strom 0.34 kg-CO₂e/kWh_{el}, Netz ENTSO-E Kontinentaleuropa 2014.

Mit den ausgewählten und gebündelten Sparmaßnahmen können Energieverbrauch und THG-Emissionen für den Fahrbetrieb um ca. 21 bis ca. 76 % reduziert werden, abhängig von Anwendungsfall und Antriebssystem. Die höchste Reduzierung ist mit batterie-elektrischen Fahrzeugen möglich.

Aber auch Nfz mit konventionellen Diesel-Antriebssystemen bieten weiterhin beträchtliche Einsparpotentiale, und können mit THG-reduziertem Kraftstoff aus teilweise regenerativen Quellen kombiniert werden.

Erratum and updates, status 22 Nov. 2017

p. 6, chapter 1.2 "Ecology - Global warming", section on greenhouse gases (GHG) from European heavy-duty vehicles (HDV)

"Concerning the GHG emissions from land transport with HDV, one option are mandatory CO₂ limits, which need to be met to get the type approval for the vehicle"

Since Nov. 2017 there are concrete plans from the European Commission to introduce CO₂ emissions standards for HDV (1), after a monitoring phase (2).

p. 21-22. Section on "effective wind velocity"

The whole logarithmic wind profile in the boundary layer between ground and open sky (p. 22, figure 21, left) needs to be added to the air flow from headwind, not only the averaged effective wind velocity (3).

Then the calculation for the average air drag force (p. 19, equation 5) shall be conducted for all vehicle velocities plus the logarithmic wind profile at all wind angles from 0 ° to 359 °. The result will be an air flow profile (headwind plus wind profile) for every wind angle.

p. 100, chapter 3.1.2 "Aero packages and speed limit 80 km/h"

"To reach a low drag coefficient when moving through fluids, bodies should be streamlined like a submarine: A round bow, a closed and smooth outer layer, and a tapered stern to avoid stall."

Correct is: "To reach a low drag coefficient when moving through fluids, bodies should be streamlined similar to a submarine: A bow with rounded edges, a closed and smooth outer layer, and a tapered stern to avoid stall."

The whole vehicle bow does not need to be round, but needs rounded edges to avoid flow separation. After reaching a certain edge radius there is no further reduction of the drag coefficient. This was found early and reproduced multiple times (4 p. 11) (5 p. 154 ff.) (6 p. 3.13) (7 p. 34 ff.) (8 p. 4) (9 p. 179) (10 p. 11 ff.) (11 pp. 40-41, 199).

p. 220, source no. 55, Commission Regulation (EU) .../... of XXX

The latest version of the draft rule on the certification of CO₂ from HDV can be found at

[http://eur-lex.europa.eu/legal-content/EN/TXT/?uri=PI_COM:Ares\(2017\)1900557](http://eur-lex.europa.eu/legal-content/EN/TXT/?uri=PI_COM:Ares(2017)1900557) .

Its final version, voted in the European Parliament, is expected at latest mid-2018.

p. 222, source no. 88, Regulation (EC) No 1222/2009

The correct CELEX no. is 32009R1222

p. 230, source no. 316, Commission Regulation (EU) 2016/1718

The correct CELEX no. is 32016R1718

References for Erratum and updates:

1. **EuCom-C.** Heavy Duty Vehicles CO₂ emission standards. [Info]. Bruxelles : Europ. Commiss., DG Climate, 20 11 2017. p. 8. [eur-lex.europa.eu/legal-content/EN/TXT/?uri=PI_COM:Ares\(2017\)5654183](http://eur-lex.europa.eu/legal-content/EN/TXT/?uri=PI_COM:Ares(2017)5654183).

2. —. Monitoring and reporting of CO₂ emissions from and fuel consumption of new heavy-duty vehicles. [Proposed rule]. Bruxelles : Europ. Commiss., DG Climate, 31 05 2017. p. 16 + Ann. 23. CELEX no. 52017PC0279.

3. **Brenn, G.** Remark to wind profile and effective wind velocity. *Doctoral examination Kies A.* [Verbal info]. Graz : TU, Inst. f. Strömungslehre u. Wärmeübertragung, 27 09 2017.
4. **Pawlowski, F.** Wind Resistance of Automobiles. *S.A.E. Journal.* 1930, Vol. XXVII, 1, pp. 5-14,86. magazine.sae.org/saej0730/.
5. **Möller, E.** Luftwiderstandsmessungen am VW-Lieferwagen. *ATZ.* 1951, Vol. 53, 6, pp. 153-156. ISSN 0001-2785.
6. **Hoerner, S.** *Fluid-dynamic drag.* 2. Midland Park NJ : Hoerner, 1965. p. 440. OCLC no. 518197.
7. **Schlichting, H.** *Grenzschicht-Theorie.* 5. Karlsruhe : Braun, 1965. p. 736. OCLC no. 703370824.
8. **Saltzman, E.** Drag reduction obtained by rounding vertical corners on a box-shaped ground vehicle. [Rep.]. Edwards CA : NASA, Flight Research Center, 03 1974. p. 19. Rep. no. TM X-56023, hdl.handle.net/2060/19740009590.
9. **Hucho, W.** Aerodynamische Formoptimierung, ein Weg zur Steigerung der Wirtschaftlichkeit von Nutzfahrzeugen. *Fortschr.-Ber. VDI-Z. 12, Verkehrstechnik,* 1978, Vol. 31, pp. 163-185. ISSN 0506-3167.
10. **Muirhead, V.** An investigation of drag reduction for a box-shaped vehicle with various modifications. [Rep.]. Edwards CA : NASA, Flight Research Center, 08 1981. p. 38. Rep. no. NASA CR-163111, hdl.handle.net/2060/19810020559.
11. **Schütz, T. (ed.).** *Hucho - Aerodynamik Des Automobils.* 6. Wiesbaden : Springer Vieweg, 2013. p. 1150. ISBN 9783834819192.

1 Introduction and Motivation

In this thesis the potentials of a selection of technical measures to reduce the fuel consumption and greenhouse gas emissions of heavy-duty vehicles (HDV)¹ are described and assessed by simulation.

Depending on the country in the European Union, HDV contribute from 17 to 100 % to the land transport of goods, in average 71 %, and from 5 to 22 % to the land transport of passengers, in average 9 % (1 pp. 37, 49)² (2 pp. 221, 243) (3 p. 37).

In 2012 the operation of HDV in the EU consumed 15 % of the oil demand, where ca. 9/10 were imported (4 p. 67), and contributed 6 % to the overall greenhouse gas emissions³. The reduction of FC and GHG is necessary due to economic and ecological reasons. In addition the strong dependency on the oil exporters (4 pp. 26, 64) would be reduced.

1.1 Economics - Save fuel cost

The main economic driver is a financial benefit for the first owner due to saved fuel cost. That can only be reached, if the benefit from fuel saving is higher than the additional start investment for a more efficient vehicle when compared to standard products. Additional parts or costlier components, improved for reduced energy consumption, are usually necessary to achieve savings. Therefore, the task is to reach the return on investment (ROI) in an acceptable payback period. For typical customers in Western Europe that ranges for commercially used trucks from 1.5 to 3 years, dependent on the application (5 p. 211).

The saving potential, investment cost and payback period of efficiency measures for typical HDV have been analysed based on German diesel prices mid 2014 (5 pp. 35-52). One result was, that not all measures are cost efficient. In the case of a tractor-trailer the components

aerodynamic fairings at the trailer, gears with reduced friction, improved engine efficiency, tempo limit 80 km/h and tires with low rolling resistance can reach the payback in a 3 year period, but other complex measures probably not (5 p. 45).

For the application of efficiency measures high diesel prices are supporting a short payback period for the first owner. So components which cause a surcharge of the vehicle but reduced fuel cost during the operation will be successful at first in markets with expensive fuel.

¹ Commercial vehicles, trucks and buses, gross vehicle weight rating (GVWR, max. permitted mass) > 3.5 t

² Citations according ISO 690, numerical reference. E. g. (1 pp. 37, 49) means source no. (1), there p. 37 and 49, from list of references in this thesis, here p. 219 ff, section 6.2.

³ HDV, EU-28, 2012: CO₂ emissions of 230.1 Mt tank-to-wheel (526); converted with CO₂-factors to 71.68 Mt fossil diesel fuel, 279.6 Mt CO₂-equivalents well-to-wheel and to an energy consumption of 3.677 EJ well-to-wheel (208 p. 24). EU-28, 2012: Gross inland consumption of oil products ca. 24.05 EJ, (1 p. 119); overall GHG emissions of 4'713Mt CO₂-equivalents (33).

The anticipation of vehicle customers in terms of future fuel cost is an additional factor for the market opportunities of efficiency devices. The diesel price is currently falling from a high level, see Figure 3.

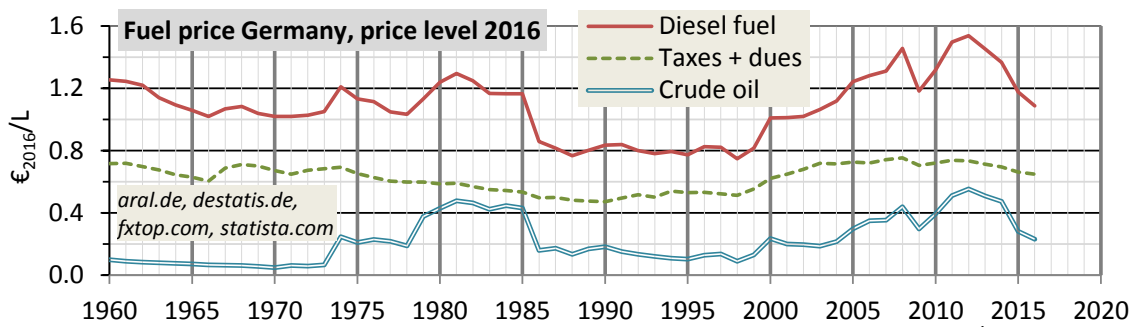


Figure 3. German fuel prices incl. taxes, 1960 to 2016, inflation-adjusted⁴

Since 2012 the fuel prices go down. Hence it is difficult to sell efficiency components for fuel-consuming machinery, because the payback period becomes too long.

When looking at the global reserve-to-production ratios of coal, gas and oil, one can expect that fossil fuels will be available in sufficient quantities in the near future, see Figure 4.

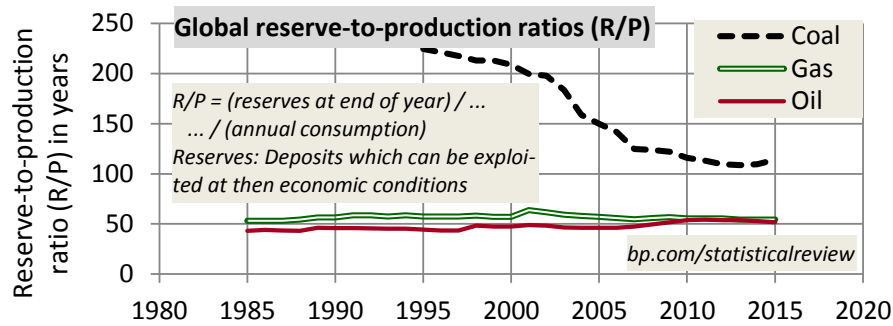


Figure 4. Global reserve-to-production ratio (6 pp. 7,21,31)

The reserves which can be exploited profitably will decrease only slowly, if at all, because with increasing scarcity the fuel prices rise. Thus more expensive equipment can be used to produce from deposits in very remote locations. Concerning liquid fuels for motor vehicles, which offer the highest energy density, it is only a question of the oil price, if gas-to-liquid or coal-to-liquid become profitable.

From the economic perspective it is very likely that liquid or gaseous hydrocarbons will be the main fuel for motor vehicles during the next decades. But they will probably become more expensive after the current period of low prices, due to rising demand and higher production cost. This leads to the assumption that efficiency measures will become more profitable during the next period of rising prices.

⁴ Crude oil prices in US\$_{nom} from statista.com, "Average annual OPEC crude oil price from 1960 to 2016 (in U.S. dollars per barrel)"; fuel prices and tax shares Germany from aral.de, "Kraftstoffpreis-Archiv"; exchange rates DM/\$ for 1960 to 1998 (1 DM = 0.5112 €) and €/€ for 1999 to 2015 from fxtop.com, "Historical rates"; price indices Germany from destatis.de, "Verbraucherpreisindex für Deutschland - Lange Reihen ab 1948"; conversion of oil prices from \$_{nom} with exchange rates to €_{nom}; calculation of oil prices, tax cost and diesel prices from €_{nom} with price indices to €₂₀₁₆

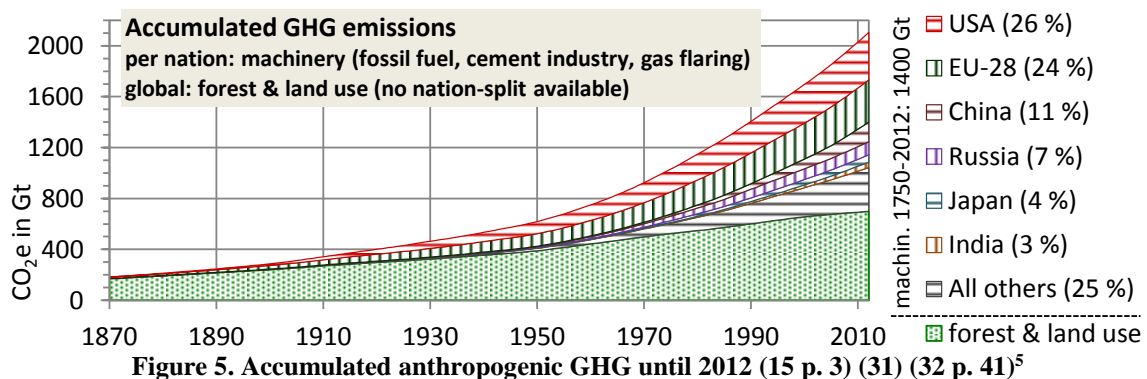
1.2 Ecology - Global warming

Concerning the ongoing global warming, the climate scientists are convinced that more than half of the temperature increase since industrialisation is caused by the anthropogenic greenhouse effect, compare e. g. (7) (8) (9) (10) (11) (12) (13) (14) (15 p. 5) (16) (17) (18) (19) (20) (21) (22) (23).

The greenhouse effect and the resulting global warming mean the following: Short-wave light from the sun is traversing the atmosphere, and a part of it, the terrestrial albedo, is reflected by earth's surface as long-wave infrared radiation (24 pp. 126,181-182). The molecules of the main GHG carbon dioxide (CO₂), methane (CH₄), nitrous oxide ("laughing gas", N₂O), ozone (O₃) and water vapour (H₂O) absorb a part of the albedo and become warmer. The higher the GHG content in the atmosphere, the more radiation is absorbed. One of multiple proofs for the greenhouse effect is, that at wavenumbers which are partly absorbed by CO₂ and CH₄ less radiation energy is emitted than at other wavenumbers, as was shown by satellite measurements (25 p. 356) (26 p. 3/4). In addition there are multiple positive and some negative feedback effects (27). One example is the positive water-vapour climate feedback (28). The storage capacity of air for water vapour increases with the temperature, what is known from thermodynamics (29 p. 518 ff.) (30 p. 289 ff.), and H₂O itself is a GHG (24 pp. 42, 170). Hence the CO₂ emissions act via this positive feedback as a lever and cause higher concentrations of H₂O, what leads to an additional greenhouse effect.

As result of these processes the atmosphere is warming, what is probably a self-accelerating process, and over 90 % of the absorbed energy is transferred as heat to the cooler ocean water at its surface, what is shown later.

From the beginning of industrialisation in 1750 until 2012 GHG with a warming potential of ca. 2100 Gt CO₂e were emitted into the atmosphere, see Figure 5.



40 % of the anthropogenic CO₂e remained in the atmosphere, 30 % were absorbed by the acidifying oceans and 30 % were stored in plants and soil (15 p. 4). Before industrialisation a CO₂-content of ca 300 ppmv was in the atmosphere, and the natural CO₂ cycle of ca. 670 Gt/year by plants, soil and oceans as sources and sinks was nearly closed (24 p. 471).

⁵ Nation-split available since 1870. Assumption: 1750 to 1844 1.28 Gt CO₂e p. a. from forest & land use

This cycle is disturbed by additional GHG, the current emissions are shown in Figure 6.

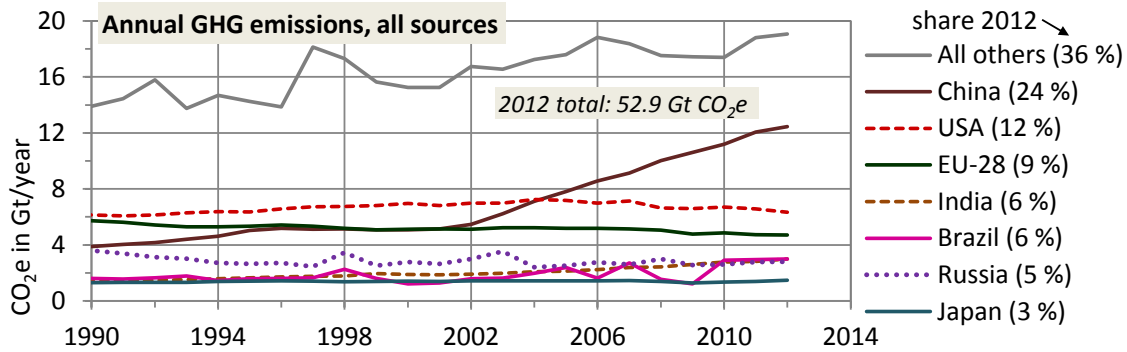


Figure 6. Annual GHG emissions from all sources (33)

The effect of global warming on air temperature and sea level is shown in Figure 7. The sea level is affected amongst others by the melting water from ice sheets and glaciers.

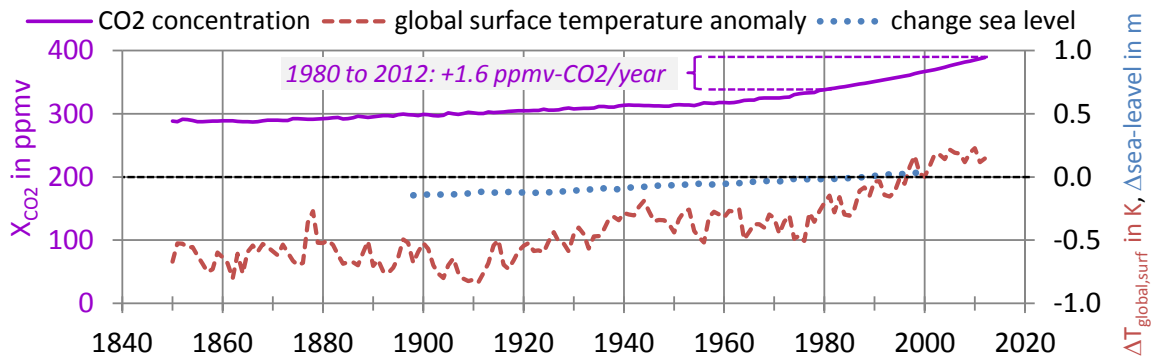


Figure 7. CO₂ concentration, global surface temperature anomaly and sea level (15 p. 3)

When looking at CO₂ concentration, surface temperature anomaly and sea level, it shall be considered that this is a retrospective view over 162 years (temperature) and 100 years (sea level), and that CO₂ is not the only factor for global warming. Effects like other GHG, heat content of the oceans, cloud formation, melting of ice masses and exterior influences like solar radiation or volcanic eruptions are not depicted and difficult to foresee for the future. Therefore it is likely, that temperature and sea level will rise with a different rate in future.

From ca. 2000 to 2010 the global surface temperature did not increase much, but the warming continued in the oceans. From 2000 to 2014 the upper 700 m of ocean water gained ca. 84 ZJ heat (= 84 10²¹ J) (15 p. 42), what can be estimated to +0.08 K increase in average temperature⁶, but with a very unequal distribution (34 p. 65).

⁶ 84 ZJ / (361.8 · 10⁶ km² · 700 m · 1020 kg/m³ · 4.180 kJ/(kg·K)) ≈ 0.078 K, ocean's surface area (527 p. 113)

The whole heat absorption since the 1950ies is shown in Figure 8 left, including the heat in the deeper sea below -700 m and in ice sheets, land mass and atmosphere.

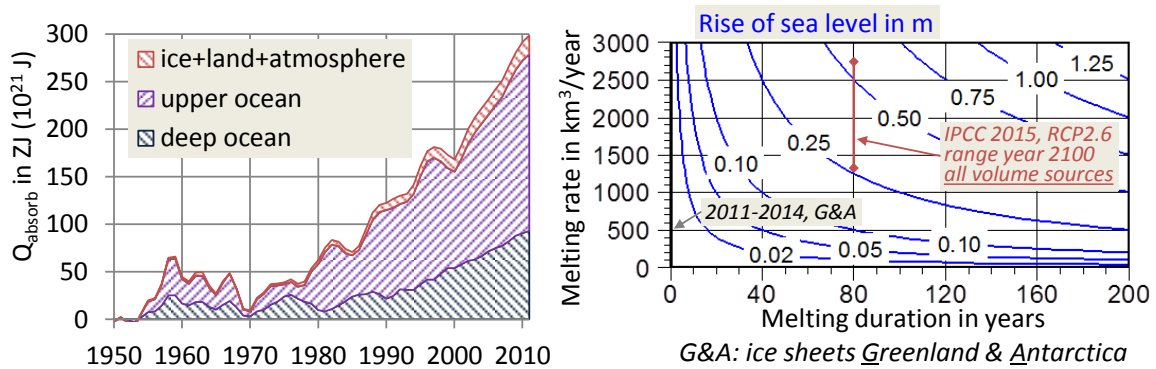


Figure 8. Left: Heat absorbed by oceans and earth surface (ice+land+atmosphere) (15 p. 42) (35 p. 10). Right: Melting of ice masses, duration, rate and rise of sea level (36)⁷

From 1950 to 2011 ca. 300 ZJ heat were absorbed by the climate system, 93 % by the oceans and 7 % by the earth surface, consisting of the ice sheets of Greenland and Antarctica, the land mass and the gaseous atmosphere. Only ca. 1 % of the absorbed heat is stored in the air mass of the atmosphere (15 p. 40) and increase its temperature. The ice sheets are slowly warming and melting (24 p. 347/348), currently at a rate of ca 500 km^3/year (36 p. 1551). The future increased melting rate will lead to a rise of the sea level of a few dm, only from that source, until the end of this century, see Figure 8 right. IPCC predicts for the scenario RCP2.6 ($\Delta T_{\text{global, surf}} \leq 2 \text{ K}$) a range from 2.6 to 5.5 dm, including the melting water from shelf ice, marine ice and glaciers plus the volumetric expansion of the warming sea water (15 p. 12/13).

Concerning the effects and potential damage from global warming, detailed studies on national level are underway. E. g. for industrialised and densely populated countries in central and western Europe these problems can occur (37 p. 52/53):

- Damage caused by rising heat stress on people in agglomerations.
- Adverse effects on water use through increased warming and droughts.
- Damage to buildings and infrastructure through heavy rains and river- or sea floods.

It shall be also considered, that the majority of the world population lives in regions with warm or moderate temperatures, and big cities are near the sea (38 p. 17) (39). In these areas human and material damage by extreme warm-weather events and floods will accumulate.

Thus it can be assumed, that the long-term disadvantages of global warming will outweigh the short-term benefits from the unregulated use of fossil fuel and forest plus land, and that the implementation of countermeasures today will reduce the future cost of damages.

⁷ 2011 to 2014: melting rate both sheets 503 km^3/year (36 p. 1551); density ice ca. 920 kg/m^3 , density ocean water ca. 1020 kg/m^3 , \rightarrow ca. 0.9 $\text{m}^3_{\text{sea-water}}/\text{m}^3_{\text{ice}}$; volume Greenland ice sheet ca. 2.82 10^6 km^3 (528 p. 385), volume Antarctica ice sheet ca. 26.5 10^6 km^3 (529 p. 390)

To get an impression of the lever against global warming, which one gains when concentrating on European HDV, their share at global GHG was determined, see Figure 9.

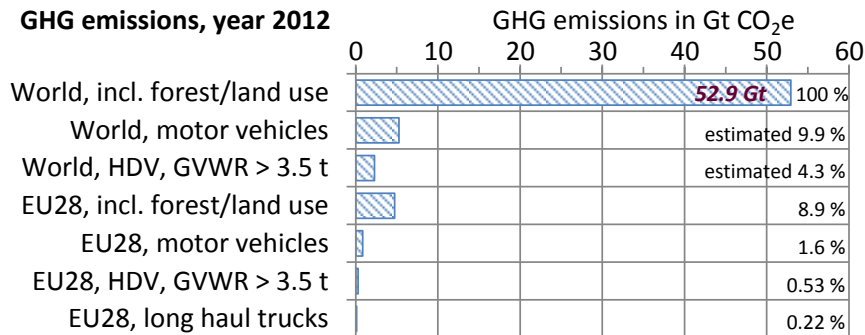


Figure 9. Share of motor vehicles and HDV at GHG emissions.⁸

The lever is short and a change of the European HDV GHG will influence the global warming very little. Thus this could lead to the decision not to act, because that is normally affected with financial disadvantages. Technical measures are more or less expensive and not necessarily cost-effective in terms of an acceptable payback period. Also additional governmental effort would be necessary for administration, control and sanction. When one market participant, an enterprise or country, in an economic region with similar conditions acts alone, he may experience disadvantages. His products or services may become more expensive due to the necessary investment in efficiency measures. And because there is no financial benefit for the investment in most cases, but only the good feeling “to emit less CO₂”, most market actors do not enforce costly CO₂ saving measures.

The economic problem, that individuals who act rationally in the self-interest can counteract the well-being of the group, is well known and was first described by the economist Lloyd W. F.. He used the example of the overexploitation of a conjointly used pasture by multiple herders, where everyone would try to put as many cattle as possible on the meadow (40 pp. 31-32). Later the ecologist Hardin G. transferred this deduction to the problem of population control and created the term “*tragedy of the commons*”. He found that this case is also valid for environmental pollution:

“The rational man finds that his share of the cost of the wastes he discharges into the commons is less than the cost of purifying his wastes before releasing them. Since this is true for everyone, we are locked into a system of ‘fouling our own nest,’ so long as we behave only as independent, rational, free-enterprisers.” (41 p. 1245)

This problem can only be solved with regulations from a superior entity like a government or by international treaties, because in this case the free market fails totally. The task is to create regulations which distribute the financial disadvantages, here the investment for efficiency measures, equally among all market participants. Hence the desired effect will be reached and there is an equal basis for all actors. Without such regulations no automotive OEM would ever have applied exhaust aftertreatment devices to reduce the pollutant emissions, due to the high cost. After 22 years of stepwise tightening these emissions reached in 2014 the low level of EURO VI. Concerning the GHG emissions from land transport with HDV, one option are mandatory CO₂ limits, which need to be met to get the type approval for the vehicle.

⁸ Global GHG in 2012: 52.854 Gt CO₂e (33) || Change of global GHG from fossil fuel, cement, flaring (530): 2009 to 2012 +9.3 %, 2010 to 2012 +4.0 % || Assumption: Global GHG motor vehicles changed at same rate like global GHG fossil fuel, cement, flaring || Global GHG motor vehicles in 2010: 5.044 Gt CO₂e (531 p. 606), → 5.246 Gt CO₂e in 2012 (+4.0 %) || Global final energy consumption (TTW) HDV in 2009: 23 EJ_{th} (531 p. 609), assumed to be diesel fuel [43.1 MJ_{th}/kg TTW, 3.90 kgCO₂e/kg WTW (208 p. 24)] → 0.534 Gt diesel fuel in 2009, → 2.083 Gt CO₂e in 2009, → 2.276 Gt CO₂e in 2012 (+9.3 %) || EU-28 GHG in 2012: 4.713 Gt CO₂e (33) || EU-28 GHG motor vehicles in 2012: 0.843 Gt CO₂e (532 p. 130) || EU-28 GHG HDV GVWR > 3.5 t and long haul trucks in 2012: 0.280 and 0.114 Gt CO₂e (526)

1.3 Decarbonisation and fuel efficiency measures

The transition from the energy supply mainly by fossil fuels to low-carbon or zero-carbon power sources like geothermal, nuclear, solar, water or wind power stations is called decarbonisation. Fuel efficiency measures for all technical devices are a key-factor to reduce the demand of electrical, gaseous or liquid fuel from low-carbon sources and facilitate this transition. There are obvious signs that the decarbonisation will gain momentum in near future and concern also the HDV sector.

Since the UN Climate Change Conference 2015 in Paris there is a political consensus to start implementing measures against GHG and global warming. The conference participants noted that a global limit of 40 GtCO_{2e}/year in 2030 is necessary to keep the global warming likely below +2 K, compared to the pre-industrial level (42 p. 3 § 17). That is scenario RPC2.6 (15 p. 11), and from ca. 2080 on the anthropogenic GHG emissions shall be zero (15 p. 9).

GHG are not harmful at present, but will provoke damage to material and people in future, where the loss expenses can only be estimated. Cost for preventive measures like structures to protect against floods and storms or for the resettlement of people from coastal lowlands can be well calculated. But not for the damage caused by unanticipated disasters like dam failures or strong cyclones. The sum of these investments are the future social cost of carbon dioxide (SCC), expressed in \$/tCO_{2e}. To allocate these future cost to the present originators, carbon prices are already partly applied. In 2015 thirty-six national, regional or urban administrations put prices on GHG, ranging from 1 to 130 \$/tCO_{2e} (43 pp. 10-14).

A selection of GHG prices is given in Table 1.

Table 1. Selection of GHG prices (1 \$₂₀₁₅ ≈ 0.90 €₂₀₁₅ (OnVista))

GHG price, \$/tCO _{2e}	Source	Description
7.1	(43 pp. 10,13)	Weighted average GHG price 2015
8.4	(44)	European Emission Allowance (EUA)
10 to 25	multiple ⁹	GHG prices from literature

The effect of additional GHG prices on fuel- and electricity cost is shown in Figure 10.

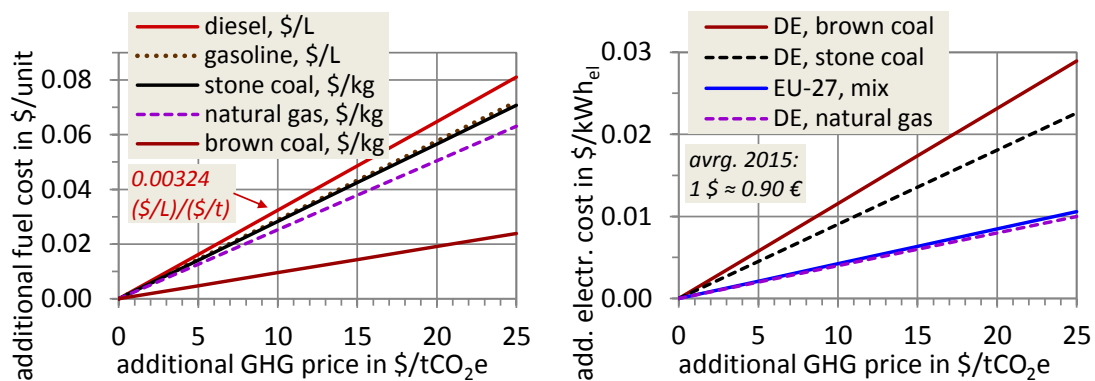


Figure 10. Effect of additional GHG prices on fuel- and electricity cost¹⁰

E. g. a GHG price of 10 \$/tCO_{2e} would cause surcharges on vehicle fuels from 0.029 to 0.032 \$/L, additional 0.001 to 0.028 \$/kg on industrial fuels like coal or gas and 0.004 to 0.012 \$/kWh_{el} on electricity from different sources.

⁹ (533 p. 10) (534 p. 25) (535) (536 p. 308) (537 p. 26), converted to \$₂₀₁₅, US price index from (538 p. 70/71)

¹⁰ CO_{2e} factors WTW, fossil vehicle fuels: Diesel 3.24 kg/L, gasoline 2.88 kg/L || CO_{2e} factors WTW industry fuels: stone coal (DE, bituminous coal & semi-anthracite) 2.83 kg/kg, natural gas 2.52 kg/kg, brown coal (DE, lignite & sub-bituminous coal) 0.96 kg/kg || CO_{2e} WTW factors electricity (mainly DE): from brown coal 1.158 kg/kWh_{el}, from stone coal 0.904 kg/kWh_{el}, EU-27 mix 0.424 kg/kWh_{el}, from natural gas 0.399 kg/kWh_{el} || (208 p. 24) (539 pp. 9, 21) (540 p. 78) , exchange rate €/ \$ from onvista.de

The EU-28 economy would be charged with ca. $38.7 \cdot 10^9 \text{ €}_{2015}$ p. a. in addition, what is below 0.3 % of the nominal gross domestic product and results in ca $76 \text{ €}_{2015}/\text{a}$ per capita¹¹. This additional cost would be distributed among the consumers dependent on the GHG-intensity of their lifestyle. People with small income or high GHG awareness, who buy typically less energy, meat products and material goods will be affected less than those with a more GHG-intense consumerism. That would be a desired guidance to a low-GHG economy.

For long haul trucks a GHG price of 10 $\text{\$/tCO}_2\text{e}$ means $0.008 \text{ €}_{2015}/\text{km}$ in addition, what is ca. 2.4 % of the current fuel cost¹². In case of long haulage the fuel cost contribute 26 % to the overall transport cost¹³, so these would increase by 0.6 %. Thus the shipping rates would be marginally higher and/or the ROI for investments in transport companies slightly smaller.

If GHG pricing is applied for HDV transportation, the market introduction of efficiency components would be supported, see Figure 11.

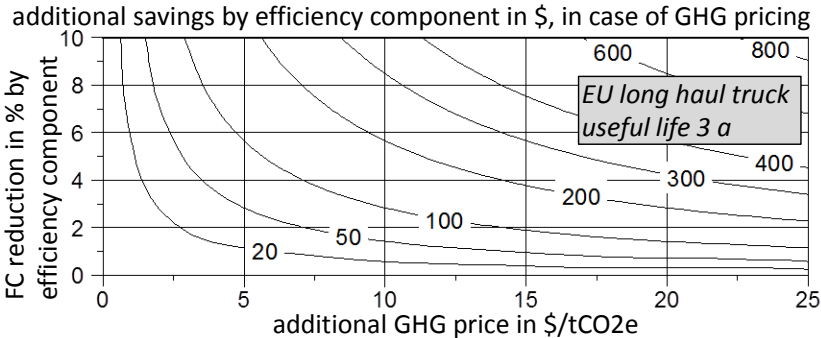


Figure 11. Effect of GHG price on financial attractiveness of efficiency components for long haul trucks

To read the diagram: A EU long haul truck causes during 3 years GHG of ca. 354 tCO₂e from FC¹⁴, which would result in additional GHG cost of 3'540 \$ in case of 10 $\text{\$/tCO}_2\text{e}$. Hence a component, which reduces FC by 4 % would save 142 \$ more during 3 years than in the case without GHG pricing. Thus devices for fuel saving may be more expensive for the first vehicle operator in case of GHG fees, what increases the incentive of the whole HDV business (suppliers, OEM, dealers, operators, drivers) to produce, buy and use them.

¹¹ Estimations EU-28 for 2015: GHG 4.30 Gt CO₂e (33) (530) → $38.7 \cdot 10^9 \text{ €}$ GHG cost for 10 $\text{\$/CO}_2\text{e}$, GDP $14'640 \cdot 10^9 \text{ €}$ (imf.org), population $0.5082 \cdot 10^9$ people (ec.europa.eu/eurostat)
¹² Avg. diesel price DE 2015 1.19 €/L-diesel (aral.de), FC 28 L/100km, → 0.333 €/km
¹³ Regional delivery 22 %, urban delivery 13 %, data for DE 2013 (541)
¹⁴ 28 L/100km · 130'000 km/year · 3.24 kgCO₂e/L · 3 year ≈ 354 tCO₂e

1.4 The VECTO project

The European Commission is working on the reduction of GHG from all sources. In the transport sector the specific CO₂ emissions from new registrations of passenger cars and light commercial vehicles are monitored and limited.

For HDV such a regulation is yet not in force in the EU. The analysis of the last decades showed that there was not much progress in the fuel efficiency and thus the GHG emissions from the vehicle generation EURO I (1992 to 1996) to early EURO VI (since 2013) (45 p. 150 ff.) (46 p. 31) (47 p. 11) (48 p. 30) (49 p. 28)¹⁵. During these 20 years the manufacturers had to fulfil continuously more stringent exhaust gas limits for pollutant emissions. Thus the OEMs introduced complex emission control systems. The engines became substantially cleaner but the overall vehicle did not become significantly more efficient, since several emission control technologies contradicted fuel efficiency improvements.

Because all consumers of fossil fuels, also HDV, must contribute to the reduction of GHG, the Commission started in 2010 the project “Reduction and testing of Greenhouse Gas Emissions from Heavy duty vehicles”, where one part (LOT2) dealt with “Development and Testing of a certification procedure for CO₂ emissions and fuel consumption of HDV” (50). This part resulted in an EU regulation for the certification of all new registered trucks. The method is based on the measurement and certification of the efficiency-relevant components and the simulation of the FC of the entire vehicle with the component test data as input. The simulation software is called “Vehicle Energy Consumption calculation Tool” (VECTO). The first objective of the regulation is to provide a methodology for the comparison of HDV in terms of FC and CO₂ emissions. A label shall support customers at the purchase decision (51 p. 7/8) and be the basis for possible regulations. The project is described in multiple reports (50) (52) (53) (54), and the procedure defined in a draft rule from the Commission (55).

The main ideas behind VECTO are:

- Identify, which components of HDV contribute significantly to the consumption of mechanical power and fuel.
- Measure the consumption characteristics of these components in standardised test procedures. The measurement results are characteristic numbers, curves or maps for every component. These results become certified and are the basis for the following simulation procedure.
- Use standard table values for bodies, trailers, payload and other parts, which are usually not influenced by the manufacturers of the motor vehicles.¹⁶
- Feed the certified measurement results together with the complementary, standard table values into the standardised VECTO simulation tool¹⁷.
- Simulate the FC and CO₂ emissions for every single HDV model on typical, standardised driving cycles. The simulated numbers for FC and CO₂ become the certified values for the type approval.
- Publish the results to support customers in their buying decision.

¹⁵ E. g. the avrg. FC of French tractor-trailers GCWR 40 t from 2000 to 2012 changed by -5 %. The main reason for the visible decrease from 2013 on was likely the anticipation of the additional "contribution climat énergie" on diesel fuel (gazole), which started in 2014-04 (542 p. 68) (543).

¹⁶ If other vehicle parts than the motor vehicle, e. g. lightweight bodies or trailers with improved aerodynamics, shall be considered in a later stage of VECTO, is part of an ongoing discussion.

¹⁷ The latest version of the simulation tool can be downloaded from the Commission: <https://webgate.ec.europa.eu/CITnet/confluence/display/VECTO> ; link as of 2017-07 ; user account necessary.

An overview on the simulation procedure and the data sources is given in Figure 12.

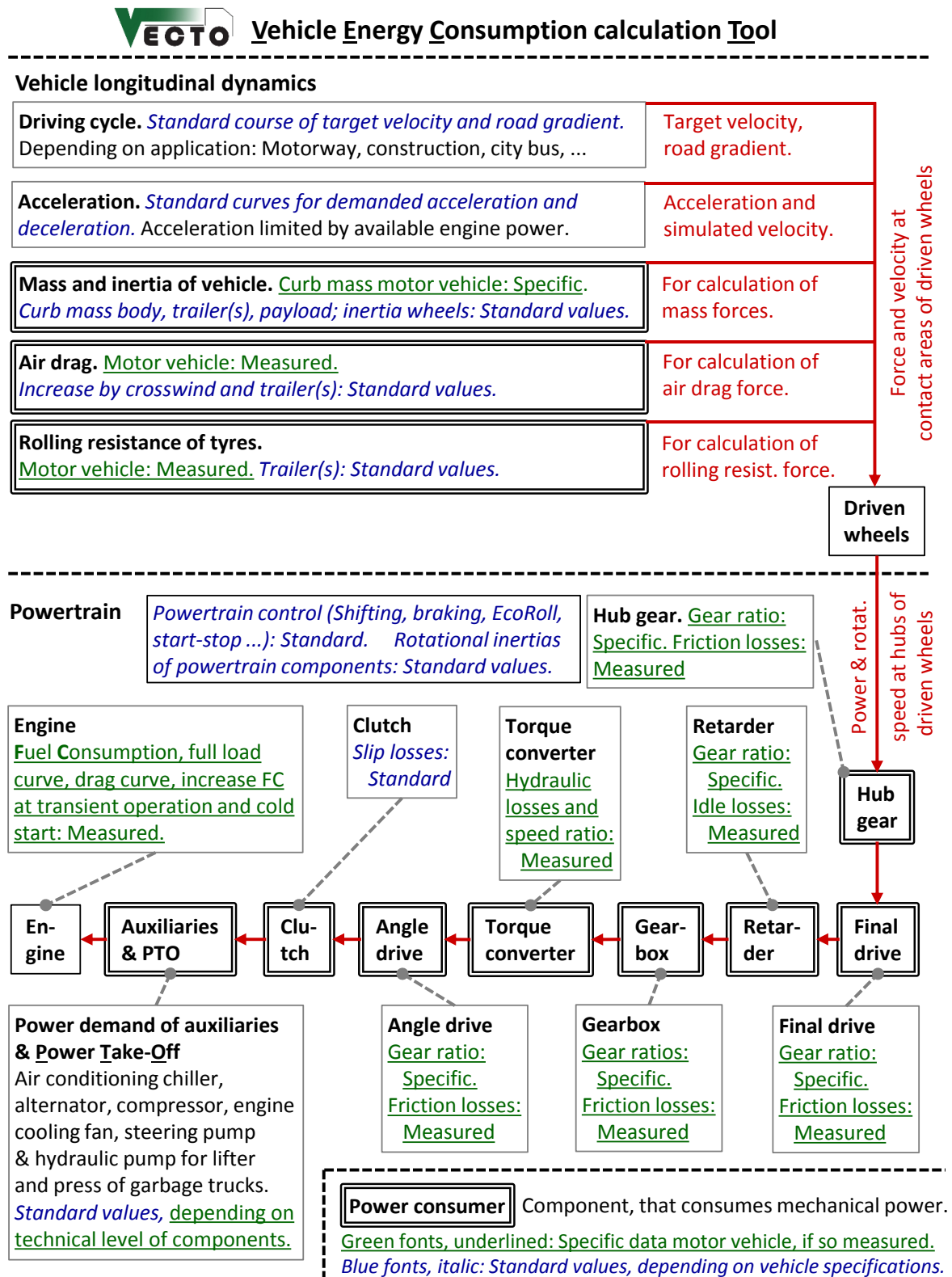


Figure 12. Calculation principle of VECTO, indication of data sources¹⁸

¹⁸ In this sketch most components of the powertrain are shown, which can be depicted in VECTO v3.2.0/925. In addition portal axles can be input. The effectively utilized components depend on the application of the HDV. E. g. a common powertrain of long haul trucks in western Europe consists of a final drive, a retarder, a gearbox, a clutch, auxiliaries and an engine.

If the HDV is equipped with multiple driven (portal) axles and/or hub gears, the gear ratios and loss maps of the transfer gearbox(es), the final drive(s), the portal gear(s) and the hub gears are combined to one virtual final gear as input for VECTO.

In case of garbage trucks the PTO can be connected to the engine or to the gearbox.

From the vehicle longitudinal dynamics on the driving cycle the course of velocity and force at the contact area of the driven wheels is calculated for every timestep. By taking into account the radius and rotational inertia of the driven wheels, the course of mechanical power and rotational speed at the hubs is determined. Subsequently the power losses from the hub gears to the clutch are added, and the rotational speed at every stage is calculated with the gear ratios. The power demand of engine auxiliaries and power take-off is added to the power at the clutch, and the result is the course of power and speed at the engine crankshaft. These values are used together with the rotational inertia of the engine to calculate the course of power and rotational speed for the interpolation of the FC from the engine map.

VECTO utilises the approach of an extended backward simulation. This calculation principle was first applied in the 1950ies by US-American engineers. An overview on the simulation of vehicle's FC and the main formulas for the model are given in sections 2.1 and 2.2 on p. 12 ff.

With this certification approach, the single power consumers of motor vehicles can be combined in a modular way to cheaply create models of complete trucks and buses and simulate the resulting FC and CO₂. These vehicles are ordered and produced in the same modular way, what makes this certification process most economic if all possible variants in one model range of HDV shall be depicted. There the components engine, gearbox, final drive, cabin, type of suspension, tires, additional tanks, air conditioning, speed control etc. are chosen individually. E. g. a delivery truck is offered with >> 1'000 variations relevant in terms of FC (5 p. 70).

Simulation-based regulations similar to VECTO, already with mandatory limits for FC and/or CO₂, are active in Canada, China, Japan and USA (56) (57) (58) (59) (60). In Brazil, India, Mexico and South Korea rules for the GHG from HDV are under consideration (61) (62).

2 Simulation of the energy consumption of heavy-duty vehicles

In this chapter an overview of the simulation method is given, which was used to calculate the energy demand of the basis vehicle models and the possible reduction by saving measures on vehicle level. The approach uses the equations of longitudinal dynamics and thus is valid for all wheeled land vehicles, differing in powertrain¹⁹ structure and energy sources: Trains, on- and off-road motor-vehicles of all sizes, motorcycles and bicycles. Here it is applied to calculate the engine power demand and energy consumption of heavy-duty road vehicles, i. e. trucks and buses of gross vehicle weight rating (GVWR) > 3.5 t, with an internal combustion engine or electrical machine.

The analysed models are a tractor-trailer (TT), gross combined weight rating (GCWR) 40 t, a delivery truck (DT), GVWR 12 t, and an urban rigid bus (RB) 18 t, compare p. 83 section 2.6.1 for an overview and p. 166 section 5.6.1 for details. Typical target-speed driving cycles are available, from long haul and coach operation to municipal utility and city bus traffic, see p. 153 ff. section 5.4.1.

2.1 Backward and forward simulation

For the simulation of longitudinal vehicle dynamics one can make the main difference between backward and forward models, quasistatic and dynamic.

For the backward simulation the courses of velocity and altitude or road gradient are given and the power at the wheels is calculated, the procedure is explained on p. 15 ff. chapter 2.2. The calculation flow from wheel to engines is shown in Figure 13.

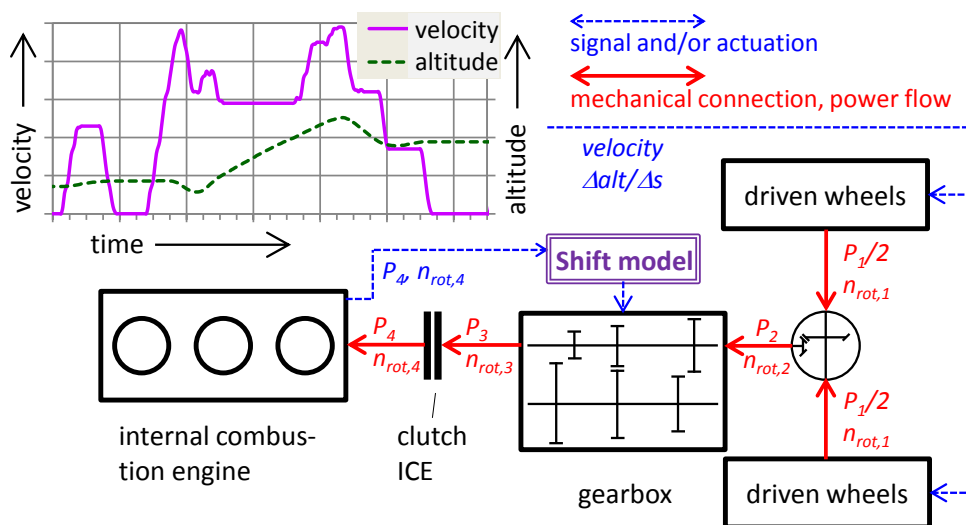


Figure 13. Calculation flow of a backward simulation

The first researchers started with backward simulation, as soon as computers were commercially available. If so the models were modified to depict performance limits due to the maximum available engine power. Lukey calculated the full throttle acceleration of a Buick passenger car in the mid-1950ies on an IBM 650 mainframe (63). With these results as basis, a Buick Third Member was simulated on a complete driving cycle (64). At the same time the

¹⁹ Definitions used in this work:

Powertrain. All components from the energy storages and power machines to the hubs of the driven wheels, hence fuel tanks, batteries, heat engines, electrical machines, auxiliary consumers, clutches, gear pairs and shafts.

Drivetrain. All components between the power machines and the hubs of the driven wheels, hence clutches, gear pairs, shafts. Thus the drivetrain depicts those parts of the powertrain, which transmitt the mechanical power from the machine(s) to the wheels, and back in case of regenerative braking. Following this definition, a vehicle with wheel hub motors does not contain a drivetrain.

engineers at Detroit Arsenal investigated the acceleration performance of the light truck XM521, GVWR 2.27 t (65). In the early 1960ies the results of the simulation of a tractor-trailer on a typical motorway cycle were published by the GMC Truck and Coach Division (66). Also the computational analysis of regenerative braking of hybrid passenger cars started (67). More details on the current state of backward simulation is given the literature, e. g. the sections "quasistatic modelling" for every powertrain component in (68).

In contrast to the backward model, the calculation flow of the forward simulation is from engine to wheel. The input values for the driver model, which is represented by a virtual controller, are the target velocity (v_{targ}), the current simulated velocity (v_{sim}) and the desired values for acceleration and deceleration. The driver model generates the signals for accelerator and brake pedal, which are the input for the virtual vehicle controller and the model of the brake system. Current HDV are equipped with a sensor pedal, the signal is forwarded to the real vehicle controller, which actuates the engine(s) and the whole powertrain.

From a mechanical point of view this is the calculation of a multibody system with all reaction forces among each other. The system consists in case of a vehicle of the moving parts of the powertrain²⁰ and the driving resistance forces, acting at the wheels. The calculation scheme with the main feedback loops is shown in Figure 14.

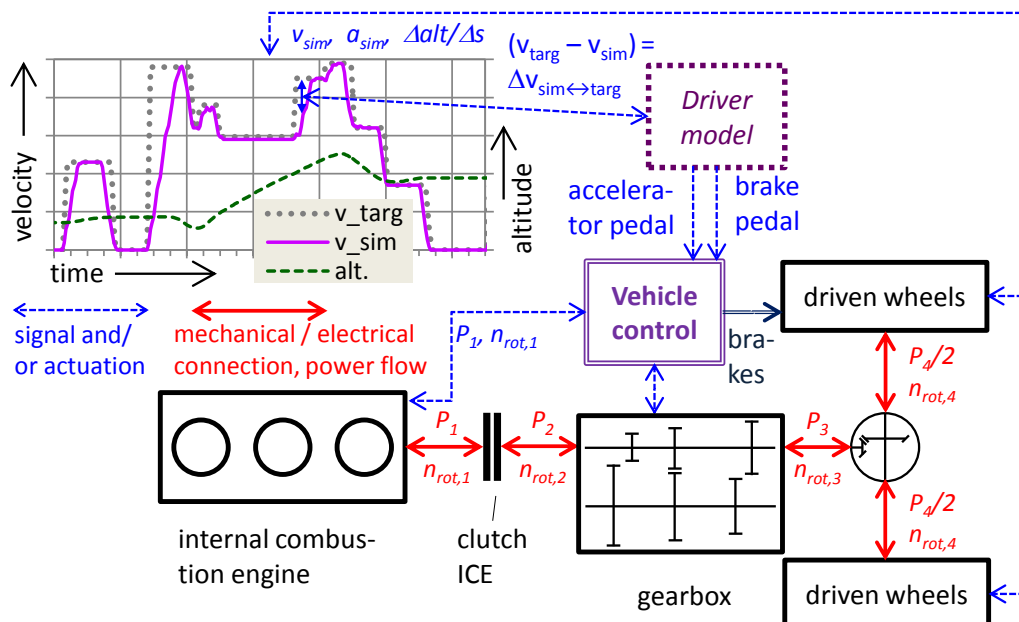


Figure 14. Calculation flow of the forward simulation.

²⁰ For the task to simulate the FC, the parts of the powertrain can be modelled as rigid bodies, connected by stiff couplings. This assumption is only valid, when oscillations, e. g. due to the elasticity of gears and shafts, are not relevant. That is the case, if only the power demand at the driving machine(s) shall be simulated.

The equations of motion for every powertrain part²¹ need to be solved numerically. This offers the possibility to simulate the custom vehicle controllers with the original datasets, if the reactions of the coupled models of the components to the actuation are calculated. Hence the influence of manufacturer-specific control strategies can be assessed.

The basis for the computerised analysis of motion in all three directions, stability and power demand of wheeled vehicles via forward simulation was elaborated in the 1950ies, where the calculation methods for the motion of airplanes were applied on models of automobiles (69) (70). The work on driver models started during the same time (71) (72) (73) (74), and one of the first forward simulating vehicle models with a virtual driver was published in 1967 (75). The data from pilots, trained in jet simulators, was used to calibrate the driver model in terms of reaction time delay, acceleration sensing capability etc. (76). An early German work on a forward vehicle simulation with a driver model is (77) from 1972.

The actual state of the simulation of vehicle dynamics in terms of general motion in all directions, stability, vibrations, suspension and power demand is described in detail in the literature, see e. g. (78), (79) or (80).

²¹ The driven wheels, in a simplified model reduced to one rigid disk, are actuated with a certain torque ($T_{q_{wh,act}}$) in the hub. Then the reaction force is calculated from ($F_{roll} + F_{grade} + F_{air} + F_{inert,transl} + F_{inert,wh,non-dr}$), acting at the centre of tire contact, plus the force to overcome the rotational inertia of the driven wheels ($d^2\varphi_{wh}/dt^2 \cdot J_{wh,dr}$).

The resulting equation of motion for a rigid disk (544 p. 80), here the driven wheel, is shown below. The formulas are explained on p. 15 ff. section 2.2.1 and the notations on p. 142 ff. section 5.2.

$$d^2\varphi_{wh}/dt^2 \cdot J_{wh,dr} = T_{q_{wh,act}} - (F_{roll} + F_{grade} + F_{air} + F_{inert,transl} + F_{inert,wh,non-dr}) \cdot r_{dyn} ;$$

$$\text{where } d^2\varphi_{wh}/dt^2 = a_{veh} / r_{dyn}$$

$$\Leftrightarrow a_{veh} = \{ T_{q_{wh,act}} \cdot r_{dyn} - v_{veh}^2 \cdot (C_d \cdot A_{cr} \cdot \rho_{air} / 2 \cdot r_{dyn}^2) - [(RRC + \Delta alt / \Delta s) \cdot (m_{curb} + m_{payl}) \cdot g \cdot r_{dyn}^2] \} / \dots$$

$$\dots / [(J_{wh,dr} + J_{wh,non-dr}) + (m_{curb} + m_{payl}) \cdot r_{dyn}^2]$$

$$\Leftrightarrow a_{veh} = T_{q_{wh,act}} \cdot A + v_{veh}^2 \cdot B + C ; \text{ where } A, B, C, \text{ are constant parameters}$$

This non-linear differential equation can be solved with appropriate numerical methods, but this approach is not further treated in this thesis.

2.2 Calculation of the energy demand of wheeled motors vehicles

In this chapter the basics of the backward simulation of the longitudinal dynamics and of the power demand for wheeled vehicles are described. Below in Table 2 the single fractions of the power demand at the engine are listed, from wheel to engine.

Table 2. Composition of the power demand at the engine

1)	Rolling resistance of tires	5)	Drivetrain losses and its rotational inertia
2)	Gradient force of vehicle mass	6)	Power demand of engine auxiliaries
3)	Air drag of vehicle body	7)	Rotational inertia of engine
4)	Inertia of translationally moved vehicle masses		

In the next sections the single power consumers and the simulation approaches are explained.

2.2.1 Power demand at the hubs of the driven wheels

For the simulation of longitudinal dynamics the vehicle is assumed to be a conglomerate of rigid bodies, without elasticity or deformation. Because one only wants to know the power at the hubs of the driven wheels, this simplification is acceptable. When one applies Newton's 2nd law²², the equilibrium of forces can be set up, see Figure 15 and Equation 1.

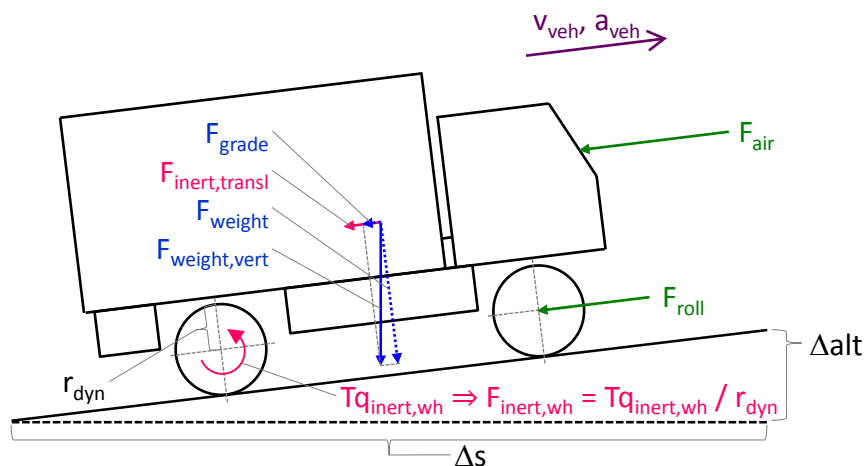


Figure 15. Longitudinal forces at driving vehicle

where:	Δalt	Altitude difference of road section
	Δs	Horizontal distance of road section
	a_{veh}	Acceleration in driving direction
	F_{air}	Air drag force between vehicle body and surrounding air
	F_{grade}	Gradient force, component of weight force parallel to road surface
	$F_{inert,transl}$	Inertia force of translationally accelerated vehicle masses
	$F_{inert,wh}$	Equivalent inertia force of all rotating accelerated wheels
	F_{roll}	Rolling resistance force of tires
	F_{weight}	Weight force of laden vehicle
	$F_{weight,vert}$	Weight force, component vertical to road surface

²² (545 p. 12 ff.). Newton I. founded the basis for classical mechanics, an explanation of his laws can be found e. g. in (546 pp. 3-7). The method of equilibrium of forces and the resulting (differential) equations are standard in engineering since the first half of the 19th century, see e. g (544 pp. 27-35, 74-85).

r_{dyn}	Dynamic rolling radius of driven wheels
$Tq_{inert,wh}$	Inertia torque of all accelerated rotating wheels
v_{veh}	Vehicle velocity

Equation 1: Force to drive or brake a wheeled vehicle

$$\begin{aligned}
F_{wh} &= F_{roll} + F_{grade} + F_{air} + (F_{inert,transl} + F_{inert,wh}) = \dots \\
&= \sum_{i=1}^{no_{ax}} (RRC_i \cdot sh_i) \cdot \cos\left(\arctan\frac{\Delta alt}{\Delta s}\right) \cdot (m_{curb} + m_{payl}) \cdot g + \dots \\
&\dots + \sin\left(\arctan\frac{\Delta alt}{\Delta s}\right) \cdot (m_{curb} + m_{payl}) \cdot g + \dots \\
&\dots + C_{d,\beta} \cdot A_{cr} \cdot \frac{\rho_{air}}{2} \cdot v_{air}^2 + \left(m_{curb} + m_{payl} + \frac{\sum_{i=1}^{no_{ax}} (J_{wh,i})}{r_{dyn}^2} \right) \cdot a_{veh}
\end{aligned}$$

where: β	Yaw angle of the air flow around the moving vehicle
ρ_{air}	Air density (= 1.188 kg/m ³ at standard ambient conditions)
A_{cr}	Cross sectional area of vehicle
$C_{d,\beta}$	Air drag coefficient, dependent on yaw angle of air flow
F_{wh}	Driving force: Tractive or brake force, parallel to longitudinal vehicle axis. Including the inertia forces of the rotating wheels.
g	Acceleration due to gravity (= 9.81 m/s ²)
$J_{wh,i}$	Rotational inertia of wheels, axle "i"
m_{curb}	Curb mass of vehicle
m_{payl}	Mass of payload
no_{ax}	Number of axles
RRC_i	Rolling resistance coefficient of tires at axle "i"
sh_i	Share of axle load "i" at vehicle's total weight force
v_{air}	Air flow velocity around moving vehicle, dependent on vehicle velocity, wind velocity and relative wind angle

For the simplified variant see Equation 2: RRC is $\Sigma (RRC_i \cdot sh_i)$, for small values $\Delta alt/\Delta s$ the expression $\sin(\arctan(\Delta alt/\Delta s))$ becomes $\approx \Delta alt/\Delta s$ and $\cos(\arctan(\Delta alt/\Delta s))$ gets ≈ 1 . Without crosswind C_d is constant, v_{air} equals v_{veh} , and finally $\Sigma (J_{wh,i}) / r_{dyn}^2$ is $m_{rot,eq,wh}$.

Equation 2: Force to drive or brake a wheeled vehicle, simplified formula

$$F_{wh} = \left(\frac{\Delta alt}{\Delta s} + RRC \right) \cdot (m_{curb} + m_{payl}) \cdot g + C_d \cdot A_{cr} \cdot \frac{\rho_{air}}{2} \cdot v_{veh}^2 + (m_{curb} + m_{payl} + m_{rot,eq,wh}) \cdot a_{veh}$$

where: C_d	Air drag coefficient for straight air flow, without cross wind
$m_{rot,eq,wh}$	Equivalent mass of rotating wheels
RRC	Average rolling resistance, weighted by share of axle load

The driving or braking power at the propelled hubs is calculated with Equation 3. The simplification is made, that all propelled wheels, for HDV usually two twin wheels at one axle, are combined to one virtual wheel, which propels or brakes the vehicle. For the calculation of power and speed this simplification is feasible.

Equation 3: Power to drive or brake a wheeled vehicle

$$P_{wh} = (F_{wh} \cdot r_{dyn}) \cdot (v_{veh}/r_{dyn}) = F_{wh} \cdot v_{veh} = T_{qwh} \cdot \omega_{wh}$$

where: ω_{wh} Angular speed of propelled wheel, here in rad/s
 P_{wh} Power at wheel hubs to drive or brake the vehicle
 T_{qwh} Sum torque at hubs of driven wheels

2.2.1.1 The road load curve

The sum of rolling resistance force and air drag force is called "road load" and is split into a constant and a variable part (F_0 , F_2), what was found in the 19th century by railway engineers. An early measurement of "friction and resistance" of carriages on a rail-way was done in 1818, where already an influence of velocity and wind was found (81 p. 169 ff.). Later the engineer Pambour F.-M. used the knowledge, that the friction force between a rigid body and the surrounding fluid depends on the square of the relative velocity (82) (83), in case of turbulent flows (84 pp. 131-144). Taking this into account, he set up for the first known time the road load curve in the 1830ies (85 pp. 114 ff., 131, 161), compare also (86 pp. 162-178).

The comparison of the measured road load of a delivery truck 12 t and a fitted polynomial of 2nd order is shown in Figure 16.

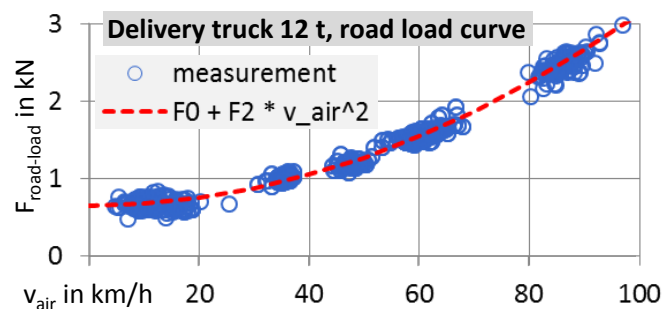


Figure 16. Road load curve of delivery truck 12 t²³, own measurement 2011

The reduction of the road load can be reached by tires with reduced rolling resistance (→ smaller F_0 or RRC) and aerodynamic improvements of the vehicle (→ smaller F_2 or C_d).

2.2.1.2 Rolling resistance of tires

The rolling resistance of the tires is caused by the friction between the material layers and in the rubber itself due to the continuous deformation when running through the tire contact area. It generates a horizontal driving resistance force (F_{roll}) and is calculated by the product of the rolling resistance coefficient (RRC) and the vertical wheel load, see Equation 1. The RRC is a product-specific value, in Europe measured by the manufacturers according to (87 p. 64) and will be approved following (55), Annex X. It is subdivided into classes following (88 p. 51) and printed on the product label which is mandatory since 2012-11. For HDV tires, segment C3, the classes range from "A" ($RRC \leq 4$ N/kN) and "B" (4.1 to 5 N/kN) up to "F" (≥ 8.1 N/kN). I. e. a tire of efficiency class "B" causes during rolling a horizontal resistance force in the range from 4.1 to 5 N per kN vertical wheel load. The RRC is measured at standardised conditions on a steel drum with a diameter of at least 1.7 m.

²³ Constant speed measurement, track Klettwitz 2011-06-28 to 2011-07-01, description of procedure in (50 p. 166).
 With: $F_0 = RRC \cdot (m_{curb} + m_{payl}) \cdot g$; $F_2 = C_d \cdot A_{cr} \cdot \rho_{air}/2 \cdot v_{veh}^2$

For real-world operation it is changed amongst others by the influences shown in Table 3.

Table 3. Influences on the tire rolling resistance (89 p. 49) (90 p. 9) (91) (92 p. 68)

Tire profile depth	Tire slip angle	Curvature of road surface
Tire inflation pressure	Vehicle velocity	Roughness of road surface
Tire material temperature	Ambient temperature	Stiffness of road surface
Vertical wheel load		

It is not feasible to generate an "overall correction factor" to convert the RRC from drum conditions to average European conditions of usage on the roads. Thus it was decided for the VECTO project to take the exact RRC-value from the manufacturer's test bench and do a correction for the virtual vertical wheel load according (93 p. 84) (94 p. 6).

The result from road measurements is, that the RRC from the drum comes at least close to the real-world value on rough pavements (90 p. 49) (92 p. 69) (95 p. 244) (96 pp. 6/7, 14-18) (97 pp. 21-29). For the sake of convenience an inevitable deviation is accepted, but the main objective is still reached: The distinction between more and less energy-efficient components.

The rotational wheel slip, dependent on the tractive force between tire and pavement, is also neglected in Equation 3. There it would cause a deviation in the range $\pm 2\%$ from the circumferential velocity of the driven wheels from the vehicle velocity. That was the outcome from the analysis of own measurements on the chassis dyno and on the road.

For the simulations described later in this work no exact RRCs were available, hence upper values from the tire efficiency classes were chosen. In addition a correction of -12% compared to a new tire's RRC for half wear was conducted, to depict the decrease of the rolling resistance with mileage. The RRC is highest for the full profile depth of 16 mm and decreases by 20 to 40 % when the remaining profile is at 2 mm, because less rubber mass causes internal friction (94 p. 11) (95 p. 241). For this work the effective RRC for the tires at one axle was calculated by Equation 4, where also its change due to the varying vertical load is depicted.

Equation 4. Effective rolling resistance coefficient (derivate from (93 p. 84) and manual VECTO v2.2)

$$RRC_i = RRC_{cl,upper} \cdot fact_{wear} \cdot \left(\frac{(m_{veh} \cdot g \cdot sh_i) / no_{wh,i}}{F_{z,lab}} \right)^{-0.1}$$

where: $fact_{wear}$ Factor to depict half worn tires, here $fact_{wear} = 0.88$
 $F_{z,lab}$ Vertical load on tire during official RRC-measurement in laboratory
 m_{veh} Sum of vehicle curb weight and payload
 $no_{wh,i}$ Number of wheels at axle "i", two or four
 $RRC_{cl,upper}$ Upper RRC from tire efficiency class, e. g. B: 4.9 N/kN, C: 5.9 N/kN, ...

Since 2016 tires of the lowest RRC class A are available for all axles of tractor-trailers (98) (99) and will become subsequently available also for other HDV classes.

2.2.1.3 Air drag and cross wind

For VECTO the air drag coefficient (C_d) of HDV will be measured according to a new standard, see (52), (100) or (55) Annex VIII. For the basis truck models of this work C_d was determined by the evaluation of constant speed measurements for trucks while for urban buses a default value was chosen.

In addition the crosswind was considered in this work as defined for VECTO version 2.2 (101 pp. 107-111). The air flows around the driving vehicle with a yaw angle (β), which

depends on the relative wind angle (φ_{wind}), the effective wind velocity²⁴ ($v_{\text{wind,eff}}$) and the vehicle velocity (v_{veh}), see Figure 17 left. When the lateral air flow enters gaps between cabin/body/trailer or in the fissured underbody, it causes swirls and increases the air drag force (F_{air}).

One example for the resulting change in $C_{d,\beta}$ (C_d depending on the yaw angle) is shown in Figure 17 right. The factor $\text{fact}_{C_d,\text{yaw}}(\beta)$ is the ratio of the air drag coefficient with cross wind to the coefficient for longitudinal airflow, i. e. the ratio $C_{d,\beta} / C_{d,\beta=0}$. Data from a tractor-trailer was available for the yaw angle between 0 and ca. 30 ° (101 p. 111), for bigger angles the curve was estimated from literature values (84 p. 484) (102 p. 18). As shown later, the factor $\text{fact}_{C_d,\text{yaw}}(\beta)$ needs only to be known for the yaw angle from 0 to 10.4 °.

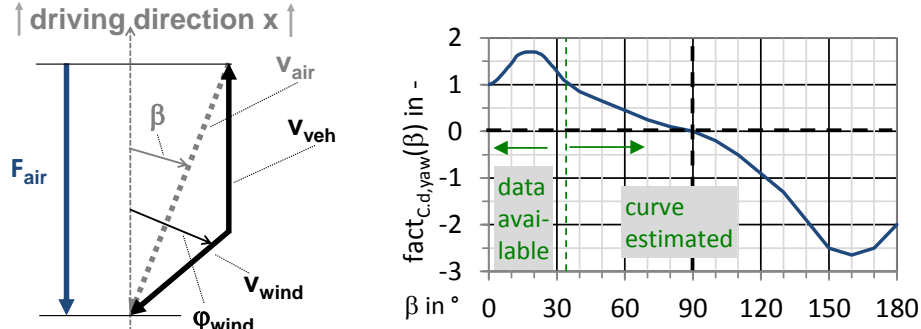


Figure 17. Left: Air flow around vehicle. Right: Yaw angle & change of air drag coefficient

To include the effect of the crosswind, an approach proposed from industry was applied and shall be explained for the case tractor-trailer (101 pp. 107-111) (103 p. 57).

For VECTO v2.2 and the models of this thesis it is assumed, that the average effective wind velocity is 3 m/s (101 p. 109) and that during driving the wind comes from all sides, i. e. the relative wind angle φ_{wind} varies from 0 to 359 °. For every combination of wind angle and vehicle velocity the air flow velocity, the yaw angle and the change of C_d ($\text{fact}_{C_d,\text{yaw}}$) were calculated. The C_d -values and the air flow velocities were used to calculate the air drag forces, 360 times per velocity node. Finally the average air drag force per velocity node ($F_{\text{air,avrg}}$, for φ_{wind} from 0 to 359 ° in steps of 1 °) is divided by the theoretical air drag force without cross wind, and the result is the correction factor for that node ($\text{fact}_{C_d,\text{vel}}$).

The calculation is shown in Equation 5.

Equation 5. Correction of air drag coefficient due to cross wind, dependent on vehicle velocity

Calculation of the air drag force due to the velocities of vehicle and wind, plus the wind angle :

$$v_{\text{air}} = \sqrt{(v_{\text{veh}} + v_{\text{wind,eff}} \cdot \cos \varphi_{\text{wind}})^2 + (v_{\text{wind,eff}} \cdot \sin \varphi_{\text{wind}})^2} ;$$

$$\beta = \arctan \frac{v_{\text{wind,eff}} \cdot \sin \varphi_{\text{wind}}}{v_{\text{veh}} + v_{\text{wind,eff}} \cdot \cos \varphi_{\text{wind}}} ; \quad F_{\text{air}} = \text{fact}_{C_d,\text{yaw}}(\beta) \cdot C_d \cdot A_{\text{cr}} \cdot \rho_{\text{air}} / 2 \cdot v_{\text{air}}^2$$

Calculation of the average air drag force from all wind angles per velocity node :

$$F_{\text{air,avrg}}(v_{\text{veh}}) = \sum_{\varphi=0^{\circ}}^{\varphi=359^{\circ}} F_{\text{air}} / 360$$

Calculation of the correction due to crosswind, for the air drag coefficient of straight air flow :

$$\text{fact}_{C_d,\text{vel}}(v_{\text{veh}}) = F_{\text{air,avrg}}(v_{\text{veh}}) / (C_d \cdot A_{\text{cr}} \cdot \rho_{\text{air}} / 2 \cdot v_{\text{veh}}^2)$$

where: φ_{wind} Relative angle between driving and wind direction, see Figure 17.
 C_d Air drag coefficient of straight air flow, without crosswind correction.

²⁴ The effective wind velocity is calculated from the so-called "logarithmic wind profile" in the boundary layer between ground and the reference height of the wind measurement, see the description on p. 21 ff.

- fact_{C_d,vel} Correction due to cross wind, for the air drag coefficient of straight air flow (C_d), at one node of vehicle velocity, see Figure 19 left.
- fact_{C_d,yaw} Change of air drag coefficient with yaw angle, see Figure 17 right.
- F_{air,avrg} Average air drag force at one velocity node, for φ_{wind} from 0 to 359 °, see Figure 17 right.
- V_{wind,eff} Effective wind velocity. Equals the air flow velocity, which causes the same air drag like the logarithmic wind profile from ground to vehicle height. Here set to 3 m/s, see also the description on p. 21 ff..

HDV are assumed to be symmetrical to the vertical longitudinal section, hence only the range 0 to 180° for the wind angle is relevant to calculate the cross wind correction for C_d. The results for some node velocities are shown in Figure 18.

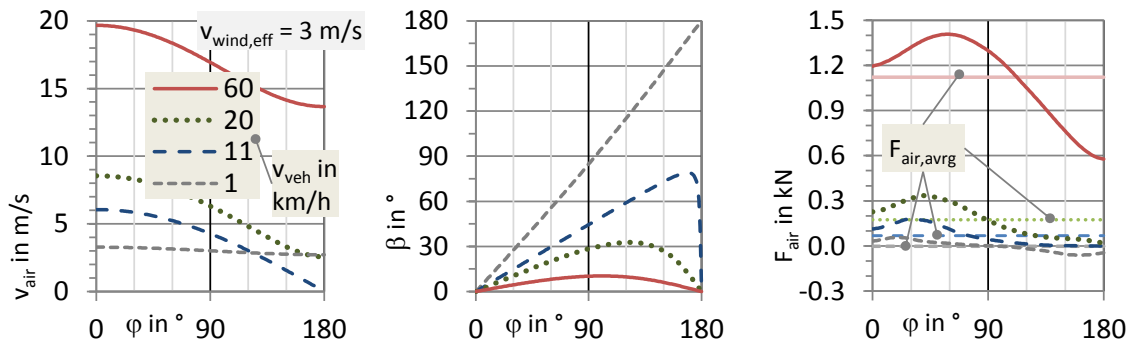


Figure 18. Air flow velocity, yaw angle and average air drag force for the tractor-trailer model

Only for very low vehicle velocities < 10.8 km/h (= 3 m/s) the air is flowing from the rear and causing a negative air drag force, what equals a driving force.

The resulting correction factor of C_d (fact_{C_d,vel}) according Equation 5 is shown in Figure 19 left. The case "full" means a correction for cross wind in the full velocity range, the case "60" a correction for velocities ≥ 60 km/h and the constant factor from that node for velocities below.

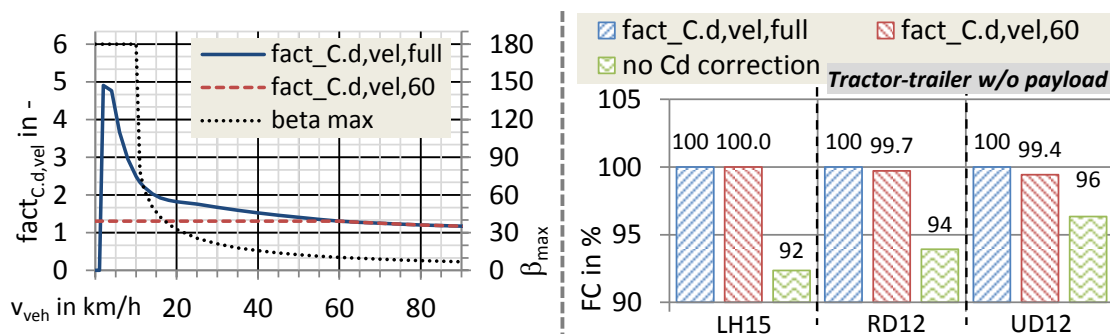


Figure 19. Left: Correction of air drag coefficient of tractor-trailer. Right: Simulation results for three variations of correction for cross wind. All data for effective wind velocity (v_{wind,eff}) 3 m/s (= 10.8 km/h).

For low vehicle velocities below 10 km/h the correction factor fact_{C_d,vel,full} gets high, because the additional average air drag force (F_{air,avrg}) by the wind is up to 5 times higher than the air drag force generated by the headwind of the slow vehicle.

The current proposal from the industry is to consider only the changing yaw angle at vehicle velocities equal or above 60 km/h and keep the correction constant for velocities below that limit, see fact_{C_d,vel,60} in Figure 19 left. That is reasonable, because the influence on the simulated FC is low at max. -0.6 %, see Figure 19 right. The max. yaw angle at 60 km/h vehicle velocity and 3 m/s effective wind velocity is 10.4 °.

For the HDV classes tractor-trailer, rigid truck, rigid truck with trailer and bus default curves for the absolute increase of C_d · A_{cr} in m² are available, see (103 p. 57). For tractor-trailers with side panels, which reduce the susceptibility to crosswind due to less air flow entering the trailer chassis, measurement values were researched (104) (105 pp. 4, fig. 5b) (106).

The results for the tractor-trailer and the final curves as input for VECTO ($\text{fact}_{C_d, \text{vel}, 60}$) for the three analysed vehicle models are shown in Figure 20.

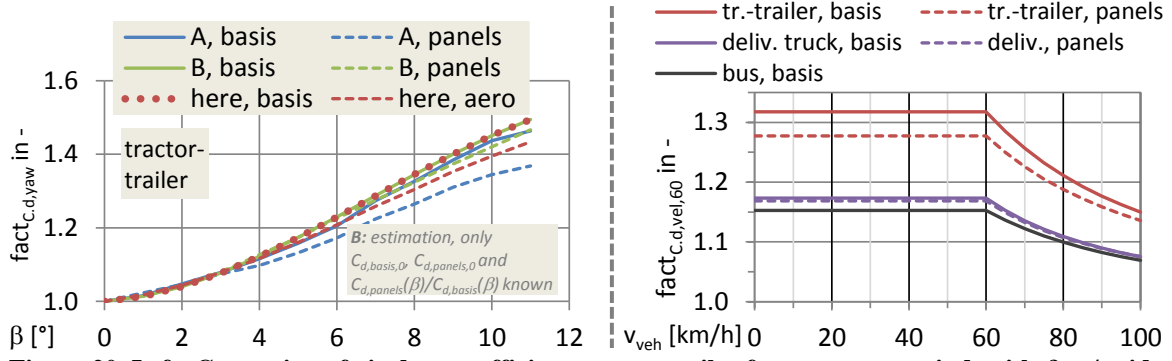


Figure 20. Left: Correction of air drag coefficient tractor-trailer for avrg. cross wind, with & w/o side panels, sources A and B. Right: Input data for VECTO for the three basis vehicle models.

All data for effective wind velocity ($v_{\text{wind,eff}}$) 3 m/s (= 10.8 km/h).

By adding side-panels the air drag is reduced due to a lower C_d -value, compare p. 168 Table 31, and in addition due to a lower C_d -increase by side wind. The latter effect is depicted by appropriate curves for the influence of the cross wind for the vehicle models without and with panels. For the delivery truck as solo vehicle the sensitivity towards cross wind is small, because the vehicle itself is short and contains no bigger gaps in the chassis.

Concerning the effective wind velocity ($v_{\text{wind,eff}}$) it shall be mentioned, that this value is not constant for all European regions or terrains beside the roads. E. g. motorways are usually surrounded by fields or woods, and urban streets by higher buildings. In addition vehicles drive in the boundary layer of the wind between the road surface and the open sky, which can be described by the so-called logarithmic wind profile. The effective wind velocity can be calculated from the wind profile and the resulting aerodynamic force, see Equation 6.

Equation 6. Effective wind velocity ($v_{\text{wind,eff}}$) for case direct headwind²⁵. See also p. 22 Figure 21 left.

$$\begin{aligned} v_{\text{wind,eff}} &= \sqrt{F_{\text{air,wind}} / (C_d \cdot A_{\text{cr}} \cdot \rho_{\text{air}} / 2)} \\ &= \sqrt{(\int_0^{h_{\text{veh}}} C_d \cdot w_{\text{veh}} \cdot \rho_{\text{air}} / 2 \cdot v_{\text{wind}}^2 dz) / (C_d \cdot w_{\text{veh}} \cdot h_{\text{veh}} \cdot \rho_{\text{air}} / 2)} \\ &= \sqrt{(\int_0^{h_{\text{veh}}} v_{\text{wind}}^2 dz) / h_{\text{veh}}} \\ \text{with } v_{\text{wind}} &= v_{\text{wind,ref}} \cdot \frac{\ln(\max(z, z_0) / z_0)}{\ln(z_{\text{ref}} / z_0)} \end{aligned}$$

- where:
- $F_{\text{air,wind}}$ Force by wind, acting on vehicle body against driving direction
 - h_{veh} Height of vehicle
 - v_{wind} Wind velocity in boundary layer, dependent on altitude above road surface
 - $v_{\text{wind,eff}}$ Effective wind velocity.
 - $v_{\text{wind,ref}}$ Reference wind velocity at reference altitude z_{ref} , from wind atlas
 - w_{veh} Width of vehicle
 - z Coordinate for altitude above ground, here the road surface
 - z_0 Aerodynamic roughness length. Altitude above ground, where the wind velocity becomes zero.
 - z_{ref} Reference height, altitude above ground where the wind velocity is known

The aerodynamic roughness length (z_0) is the altitude above ground, where the wind velocity becomes zero due to the surrounding terrain, e. g. grass, crops, wood or buildings. It is

²⁵ Formula wind velocity (v_{wind}) from (547 p. 131). C_d const. for all vehicle sections from ground to max. height.

segmented in classes, and beside roads its values can range from 0.03 m, class 3 "open flat terrain", to 2 m, class 8 "city centre" (107 pp. I.5-13).

The effective wind velocity generates an aerodynamic force equal to that of the wind profile between the road surface and the height of vehicle.

From wind atlases some examples for the annual average wind velocity were taken, which can be used as $v_{wind,ref}$. For western Europe in the 1980ies at the reference altitude (z_{ref}) 50 m the range 3.5 m/s to 8.5 m/s was found (108 p. 37). High values occurred only over flat terrain, and for the majority of interior regions the wind velocity was between 4 m/s and 6 m/s. More current and detailed data was found for Germany. The annual average wind velocity 10 m above ground reaches from 1 m/s to 7 m/s (109) (110) (111 pp. 7, 10). High values occur at the northern coast, for the most interior areas the velocity ranges from 1 m/s to 4 m/s.

An example for the wind profile and for the effective wind velocity is given in Figure 21 left, here calculated with an aerodynamic roughness length of 0.25 m, class 5 "high crops".

Due to the significance of the air drag for HDV on motorways, the basis model of the tractor-trailer was simulated for different effective wind velocities on the cycle Long Haul 2015. The correction curves for the air drag coefficient due to cross wind ($fact_{C,d,vel,60}$) were calculated like described above. For the technical data of the vehicle model data see p. 87 Table 17. The results are shown in Figure 21 right.

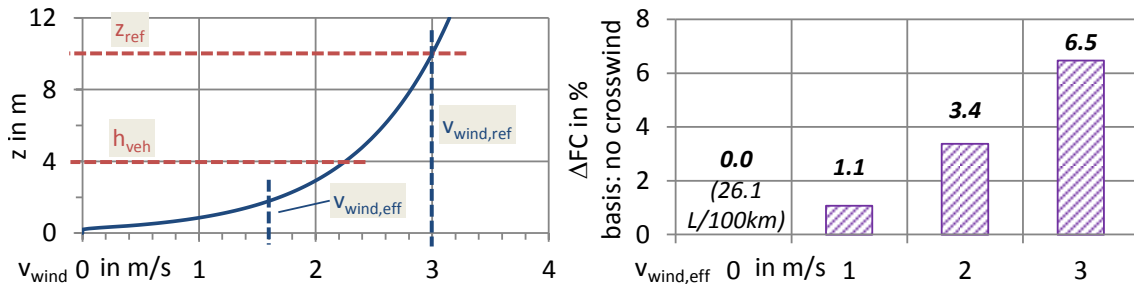


Figure 21. Model tractor-trailer (TT). Left: Wind profile & effective wind velocity. Right: Increase of simulated FC with wind velocity; model TT, payload 14.5 t, cycle LH15.

The default effective wind velocity of 3 m/s, state 2017-01, caused for the basis model of a tractor-trailer on the Long Haul cycle 2015 an increase in FC of ca. 1.6 L/100km, what are +6.5 %. It is shown later, that this leads to somewhat high absolute simulated FC values, when compared to measurements in regions with lower average wind velocities²⁶.

2.2.2 Drivetrain losses between wheel hubs and engine

The drivetrain includes all components between wheel hubs and clutch, see also p. 10 Figure 12. According to this definition the engine, the auxiliaries, the PTO and the wheels are not part of the drivetrain. During the power transmission from the engine to the wheel hubs, and vice versa in case of coasting or regenerative braking, losses occur in the shift gearbox and in the final drive. They are caused by mechanical friction between the gears and in the bearings and if so by the power demand of an integrated oil pump.

There are additional losses due to the friction in the bearings of wheels and shafts, also sliding brake pads can cause friction. But these losses are small compared to the other drivetrain parts, hence they are neglected.

Trucks, coaches and intercity buses are usually equipped with manually or automatically actuated gearboxes in spur-gear design in combination with a friction clutch: MT - Manual Transmission, AMT - Automated Manual Transmission. In city buses and some garbage trucks

²⁶ In VECTO v3.2.0 from 2017-07, the boundary layer is considered for the internal calculation of the cross wind correction.

a planetary gearbox with a hydraulic clutch or hydraulic torque converter is used: AT - Automated Transmission.

The standard to measure the drivetrain losses is underway, see (55), Annexes VI and VII.

The overall losses from gearbox inlet to outlet are depicted by maps, where the current power loss is interpolated from the operating point in terms of input speed and input power²⁷. An example and the full load curve of a HDV engine 185 kW are shown in Figure 22.

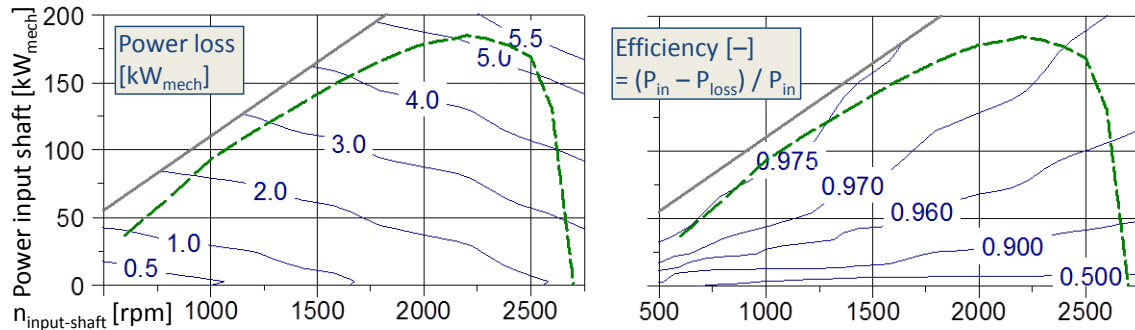


Figure 22. Example for map of transmission power loss, calculated from default torque-based map²⁸

In case of city buses or of some garbage trucks a hydraulic clutch or torque converter is the connection between crankshaft and gearbox input shaft. Due to the permanent driveaways from bus stops or trash cans such a wearless clutch offers benefits in terms of working cost, because no disks of a friction clutch need to be replaced frequently.

The power loss in a hydraulic torque converter depends on the ratio of output to input speed (ν , latinised Nu), the ratio of output to input torque (μ , latinised Mu) and the torque at reference input speed ($T_{q_{ref}}$). That leads to three characteristic curves which describe the torque converter, compare (55), Annex VI section 4 and (112), and the VECTO manual.

For this work the provisional submodel of a 4-stage AT in VECTO v2.2 was utilised, where the first gear has a power split between hydraulic and mechanical transfer, compare (113 pp. 174 ff., 185). An example for the loss in the hydro-mechanical first gear is given in Figure 23 left.

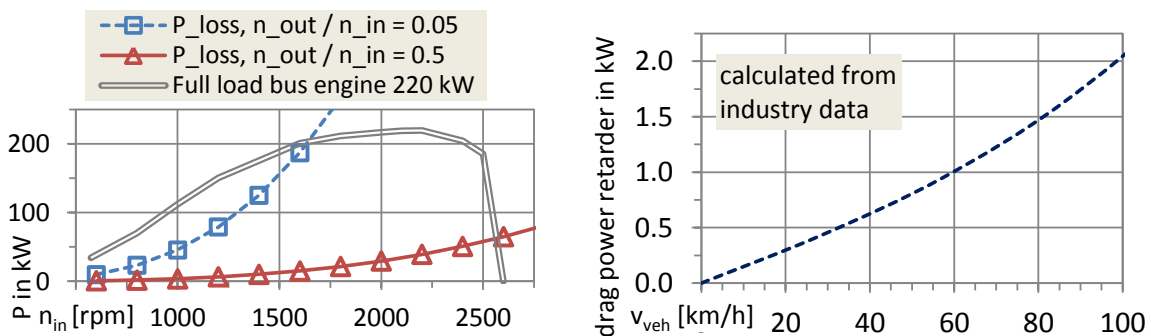


Figure 23. Left: Power loss in hydro-mechanical first gear of 4-stage automated transmission. Right: Power loss in idle from a retarder²⁹, connected to the cardan shaft

If the vehicle is equipped with a hydraulic retarder, a permanent brake running on oil or water, its idle losses are considered by a characteristic curve of the power loss. The standard data for VECTO is shown in Figure 23 right.

²⁷ The original format for VECTO are maps {input speed [rpm], input torque [Nm], torque loss referred to input shaft [Nm]}, these can be used to calculate the power.

²⁸ Standard data of VECTO for the stepped-up indirect gear of a delivery truck 12 t.

²⁹ Both diagrams were elaborated from industry data. In case of the idling retarder the dependence of the torque loss on the rotational speed is given (103 p. 135). For a typical long haul tractor the power loss of a secondary retarder at the cardan shaft was calculated: Tires 315/70R22.5, r_{dyn} 0.492 m, ratio final drive 2.65.

In addition the rotational inertia of the drivetrain parts from engine to wheel axles are regarded, see Equation 7.

Equation 7. Power demand of rotating drivetrain parts³⁰ (114 p. 61)

$$P_{\text{inert,dt}} = F_{\text{inert,dt}} \cdot v_{\text{veh}} = (m_{\text{rot,eq,dt}} \cdot a_{\text{veh}}) \cdot v_{\text{veh}} = \left(\frac{\sum_k (J_{\text{dt,k}} \cdot i_{\text{dt,k-wh}}^2)}{r_{\text{dyn}}^2} \cdot a_{\text{veh}} \right) \cdot v_{\text{veh}}$$

- where: $F_{\text{inert,dt}}$ Equivalent inertia force of rotating drivetrain parts at wheel axles
 $i_{\text{dt,k-wh}}$ Ratio of component k's speed to driven hub's speed.
 $J_{\text{dt,k}}$ Rotational inertia of component "k" (clutches, gears, shafts)
 $m_{\text{rot,eq,dt}}$ Equivalent mass of rotating drivetrain parts
 $P_{\text{inert,dt}}$ Mechanical power to accelerate all rotating drivetrain parts

The sum of the power consumers described until here is the power demand at the clutch.

2.2.3 Engine auxiliary consumers and the "FC-line"

To the power at the clutch the additional demand of the auxiliary consumers

air conditioning chiller, alternator, compressor, cooling fan, steering pump is added. For all auxiliaries default values for the average power or calculation schemes to elaborate these values are available in the VECTO draft certification method (55), Annex IX, (103 pp. 166-234) and (115). Here in section 2.2.3 the application of the average power values is analysed and on p. 37 ff., chapters 2.3 and 2.4, new or revised models for fan, compressor and regenerative braking with auxiliaries are presented.

For alternator, compressor, cooling fan and steering pump of a delivery truck 12 t with a 6-cylinder engine, 175 kW EURO V (50 p. 156) the characteristic curves for the power demand were available, see Figure 24 left. From chassis dynamometer measurements with an identical truck, see p. 195 Table 59 first entry, where engine speed, fan speed and air pressure at the compressor outlet were recorded in addition, the operation of the auxiliaries could be determined, see Figure 24 right.

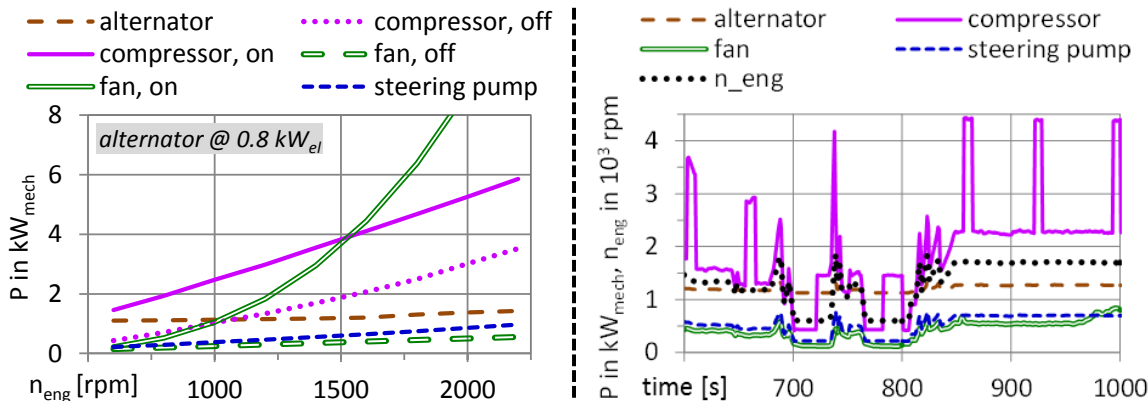


Figure 24. Delivery truck 12 t. Left: Power curves auxiliaries. Right: Auxiliary power, part of cycle RD12.

³⁰ $(J_{\text{dt,k}} \cdot i_{\text{dt,k-wh}}^2)$ is the rotational inertia of drivetrain component k, referred to the wheel hub. The rotational energy remains constant : $E_{\text{rot}} = 1/2 \cdot J_{\text{dt,k}} \cdot \omega_{\text{dt,k}}^2 = 1/2 \cdot J_{\text{dt,k}} \cdot (\omega_{\text{wh}} \cdot i_{\text{dt,k-wh}})^2 = 1/2 \cdot (J_{\text{dt,k}} \cdot i_{\text{dt,k-wh}}^2) \cdot \omega_{\text{wh}}^2$

The power curve for the alternator was interpolated from its performance map, see Figure 25 left. In case of a constant electrical power demand this interpolated mechanical power becomes a characteristic curve, compare Figure 25 right.

The input data for VECTO was the alternator performance map and a constant electrical power demand. The characteristic curves in Figure 25 right were used for the model of regenerative braking, described later on p. 62 ff. chapter 2.4.1.

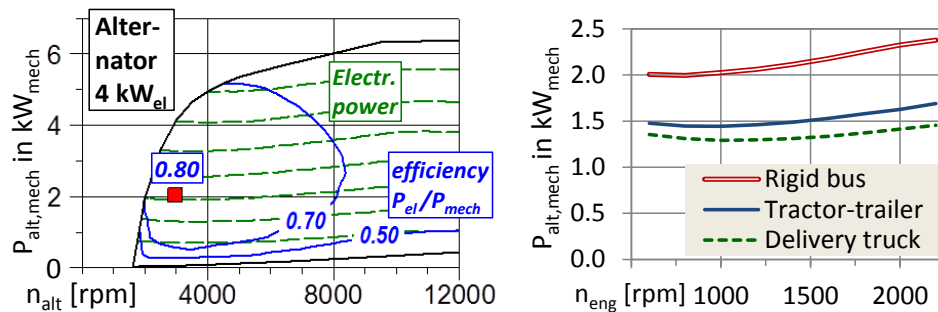


Figure 25. Left: Alternator performance map (Bosch). Right: Power curves for basis HDV models

For every vehicle model generic data for the average electrical power demand is available, see p. 167 Table 30. The characteristic curves for the mechanical power demand from the alternator are calculated with the electrical power, the alternator map, its gear ratio to the engine crankshaft and the efficiency of the transmission from crankshaft to alternator, here 0.98.

Compressor, fan and steering pump are intermittent consumers, switching regularly from low to high power and back, where the steering pump is not used on chassis dynamometers. During the driving cycle shown in Figure 24 right the fan is not engaged appreciably, a better picture from the measurement of another vehicle is shown on p. 213 Figure 206.

To simulate the exact engine operation points in terms of load, detailed models for the variable power demand of the intermittent consumers are necessary, what increases the grade of detail and the burden of data collection plus model calibration significantly. An impression of the effort for a more in-depth model of the fan is given on p. 37 ff. section 2.3.1. It is not manageable to reach this grade of detail for type approval and implementation in VECTO.

Thus the approach is to take average power values, varying by HDV class, driving cycle and technology stage of the device. E. g. a compressor with clutch to avoid idle losses gets a lower mean power than without clutch, hence the more efficient technology is privileged.

This simplification of using constant power values over a cycle does not lead to a bigger deviation of the calculated FC. There is an almost linear relation between engine power and FC, with exception of very low engine load.

Here this relation is called the "Fuel Consumption Line" (FC-line), and it was elaborated by other workers from the concept of the "Willans Line" (116 p. 23) (117) (118 p. 248 ff.) (119 pp. 9-11, 34-37) (120 p. 18 ff.) (121 pp. 19 ff., 67 ff.) (122 p. 785).

Examples for the Willans Lines and the FC-Line are shown in Figure 26.

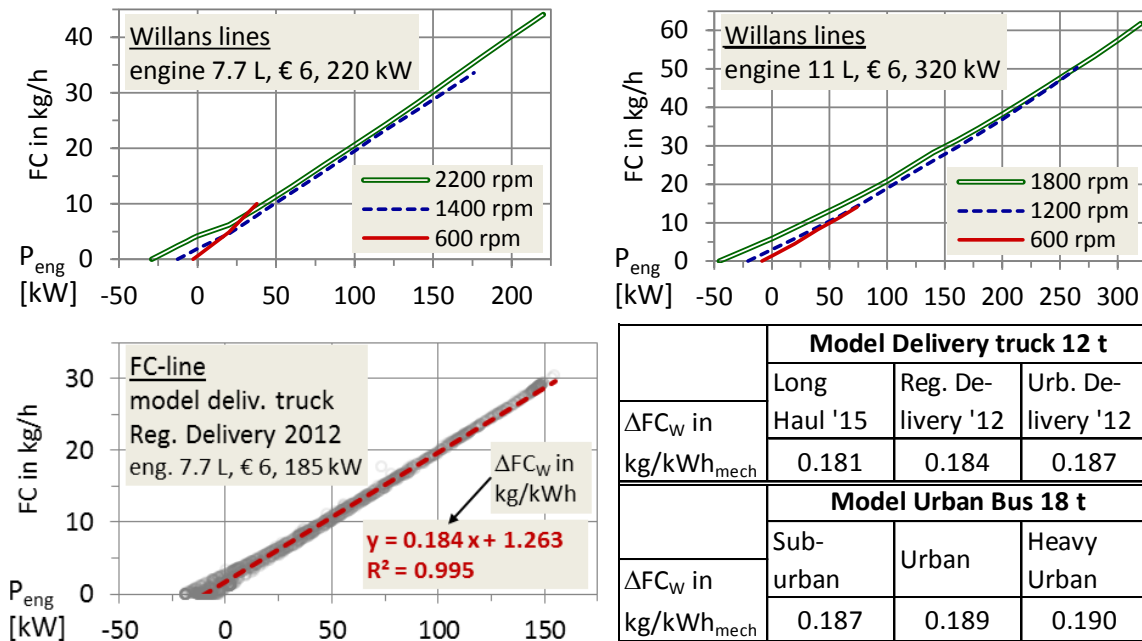


Figure 26. Examples for Willans lines, for the FC-line and for Willans factors (ΔFC_w)

The Willans Lines are the nearly linear correlations between FC and engine power at each engine speed, and are individual for a certain engine type. Because the Willans Lines for all speeds are close to each other, the engine operation points from typical duty cycles are also located with good approximation on a straight line, the so-called FC-Line. It is individual for every measured or simulated combination of engine, vehicle and driving cycle.

There is a nearly constant relation, the Willans factor (ΔFC_w) in (kg/h)/kW_{mech} or kg/(kW·h)_{mech}, between the change of FC and the change of engine cycle work.

This approximation is not valid at low engine loads. Especially at low engine power and increased speed, at high idle, the Willans Lines are no more linear, compare Figure 26 the upper diagrams.

The FC-Line means for the auxiliaries, that the temporal distribution of their mechanical work, i. e. their power course, is not very relevant, only the accumulated work shall be the same for the intermittent and the constant simulation. The calculated additional FC for an intermittent consumer, switching between high and low power, is very similar for the real variable power course or its average constant equivalent.

This was checked by simulation for different power courses of fictive variable additional consumers, shown in Table 4.

Table 4. Intermittent behaviour of fictive variable consumers

a) Shifting between 200 and 0 % load	d) 15 kW _{mech} for total 60 s at stand, min. duration intervals 10 s
b) Shifting between 175 and 25 % load	e) 15 kW _{mech} for total 60 s during driving
c) Shifting between 150, 100 and 50 % load	f) Constant 2 kW _{mech} during all stand phases
a) to c): Variable power, shifting interval $t_{interval}$ 6 s, in average 100 % load	g) Constant 2 kW _{mech} during driving phases.

These fictive auxiliaries were simulated with intermittent and constant average power demand, the accumulated work during the whole driving cycle was the same for both cases.

The influence of the change in engine efficiency (η_{eng}) at idle speed 600 rpm, from 0.00 at no load to 0.31 at full load, was assessed for the consumers a) to c), see Figure 27.

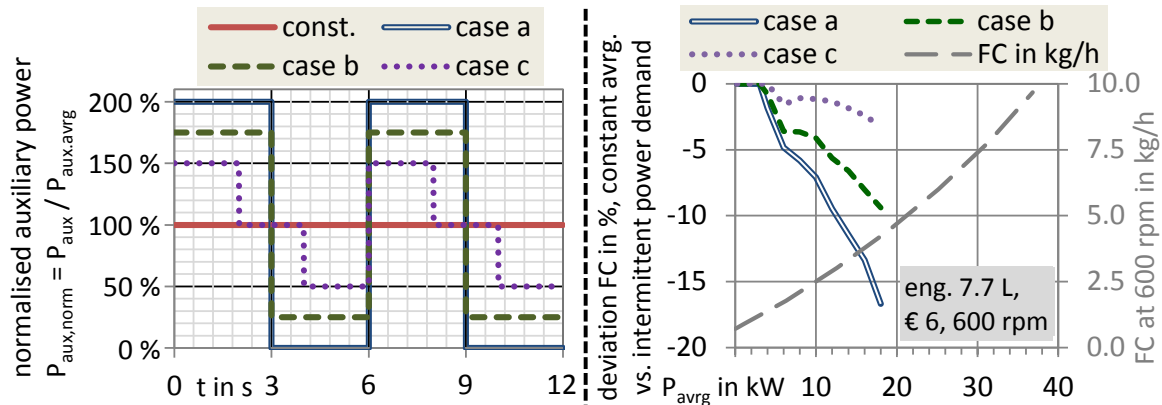


Figure 27. Left: Power course of fictional shifting consumers a) to c). Right: Shifting and constant power consumers of same average power at engine idle speed.

To read the right diagram: A consumer which shifts from 0 to 200 % load and back (“case a”) with an average power of $6 \text{ kW}_{\text{mech}}$ (\rightarrow steps 0 and $12 \text{ kW}_{\text{mech}}$) causes a deviation of -5 % for its simulated FC at idle speed, when depicted as constant consumer of $6 \text{ kW}_{\text{mech}}$. That extreme case can be neglected in this thesis, because there are no big consumers which switch between zero and high load, there is always some basis load from alternator and idling pumps.

For the depiction of power take-offs in VECTO, which show a behaviour similar to “case a”, standardised courses for power and speed are available. For other less variable consumers the deviation in the simulated FC at idle from constant to intermittent power is smaller.

An example for the fictive consumers d) to g) is shown in Figure 28.

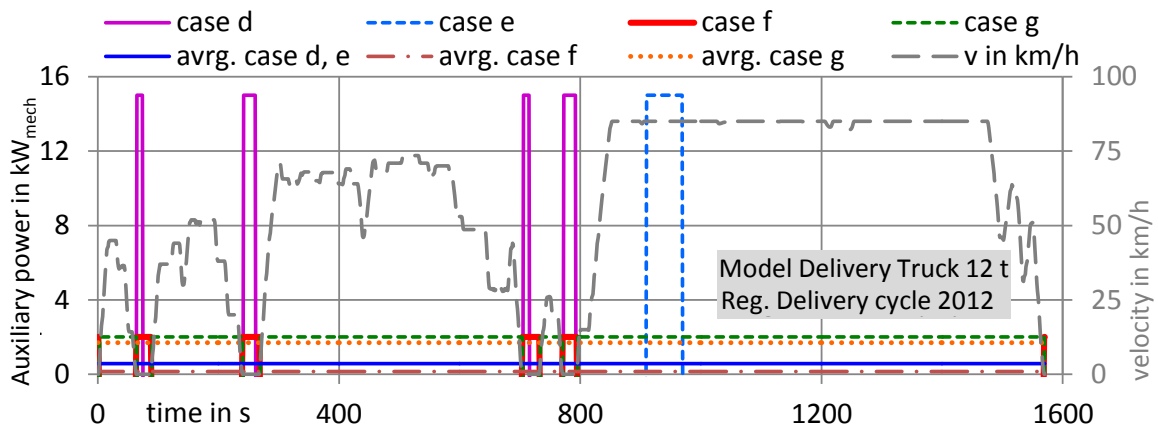


Figure 28. Example for fictive, highly intermittent consumers for test cases

As next step the cases a) to g) of additional shifting consumers were simulated for the models delivery truck and rigid bus on multiple cycles, with the intermittent power course and the constant average equivalent. The average auxiliaries' power for the cases a) to c) ranged from 3.1 to 3.6 kW for the truck and from 8.1 to 8.2 kW for the bus. The deviation of the additional FC of the consumers from constant to intermittent simulation is shown in Figure 29.

	Model Delivery Truck 12 t									Model Rigid City Bus								
	Long Haul 2015			Regional Delivery 2012			Urban Delivery 2012			Heavy Urban			Urban			Suburban		
case a	99.9	99.9	99.9	99.7	99.7	99.7	99.6	99.6	99.6	97.1	97.1	97.1	97.8	97.8	97.8	99.0	99.0	99.0
case b	99.8	99.8	99.8	99.5	99.5	99.5	100.5	100.5	100.5	98.1	98.1	98.1	98.5	98.5	98.5	99.5	99.5	99.5
case c	99.7	99.7	99.7	98.4	98.4	98.4	101.1	101.1	101.1	99.5	99.5	99.5	99.6	99.6	99.6	100.1	100.1	100.1
case d	100.4	100.4	100.4	89.2	89.2	89.2	97.3	97.3	97.3	91.9	91.9	91.9	91.9	91.9	91.9	95.0	95.0	95.0
case e	98.5	98.5	98.5	93.0	93.0	93.0	106.2	106.2	106.2	92.0	92.0	92.0	92.0	92.0	92.0	99.4	99.4	99.4
case f	111.4	111.4	111.4	95.4	95.4	95.4	106.5	106.5	106.5	105.5	105.5	105.5	105.5	105.5	105.5	107.0	107.0	107.0
case g	99.9	99.9	99.9	100.2	100.2	100.2	96.1	96.1	96.1	96.9	96.9	96.9	96.9	96.9	96.9	98.5	98.5	98.5
	85 100 115	85 100 115	85 100 115	85 100 115	85 100 115	85 100 115	85 100 115	85 100 115	85 100 115	85 100 115	85 100 115	85 100 115	85 100 115	85 100 115	85 100 115	85 100 115	85 100 115	85 100 115

Figure 29. FC of additional consumers in %, constant average vs. intermittent additional power

The deviation in the additional FC ranges from -11 % (case d, Regional Delivery '12), to +11 % (case f, Long Haul). In 30 of 42 cases it is in a range of ± 5 %, and bigger differences occur only for cases d), e) and f). Cases d) and f) are not relevant for the practical use of VECTO, because there are no engine auxiliaries, which are only active during vehicle stop, and power take-offs are treated separately. Case e) is similar to a cooling fan with clutch, which causes no idle losses and is turned on only once at steep uphill driving with hot engine, see e. g. p. 213 Figure 207. For this special case a deviation for the *additional* FC of the auxiliary in the range ± 10 % instead of ± 5 % can occur, if simulated with the constant average power value.

The change of the overall FC from the HDV models, constant vs. intermittent auxiliaries, ranged for all cases from -1.1 to +0.3 %, what was elaborated also from the simulation results. Bigger deviations from -1.1 to -0.6 % occurred only for the model of the rigid bus on the cycles Heavy Urban and Urban for cases a) and b), due to the high share of engine idling at stops. There the averaging of the intermittent auxiliary power can cause bigger deviations in FC, compare also p. 27 Figure 27. Without these four outliers (rigid bus, cycles Heavy Urban and Urban, cases a) and b)) the overall FC deviated in the smaller range of -0.4 to +0.3 %.

The deviations between the simulations with constant and intermittent auxiliary power are probably caused by the non-linear correlation between engine power and FC at low loads, especially at high idle, see Figure 26 upper diagrams. Hence at these operating points the FC-Line is not valid. If a correction can be introduced, shall be the subject of future work.

The delivery truck 12 t, where the auxiliary operation was known, compare p. 24 Figure 24, was measured on the chassis dynamometer on the cycles Regional Delivery 2012 (RD12) and Urban Delivery 2012 flat³¹ (UD12-flat), and also a short road cycle at TU Graz Inffeldgasse was recorded (IG), see p. 159 Figure 172. The latter consisted only of driveaway and braking events to check the air consumption of the brakes, but also the auxiliaries' signals were recorded. During the road test the FC was not measured, hence only a simulation result is available with an estimated max. deviation from the unknown FC of ± 10 %. A model of the truck was set up, see p. 176, Table 37 "Delivery truck € 5", and all three cycles were simulated with intermittent and constant auxiliaries. The result is shown in Figure 30.

³¹ Only in this case the Urban Delivery cycle 2012 was measured w/o road gradient, due to technical reasons.

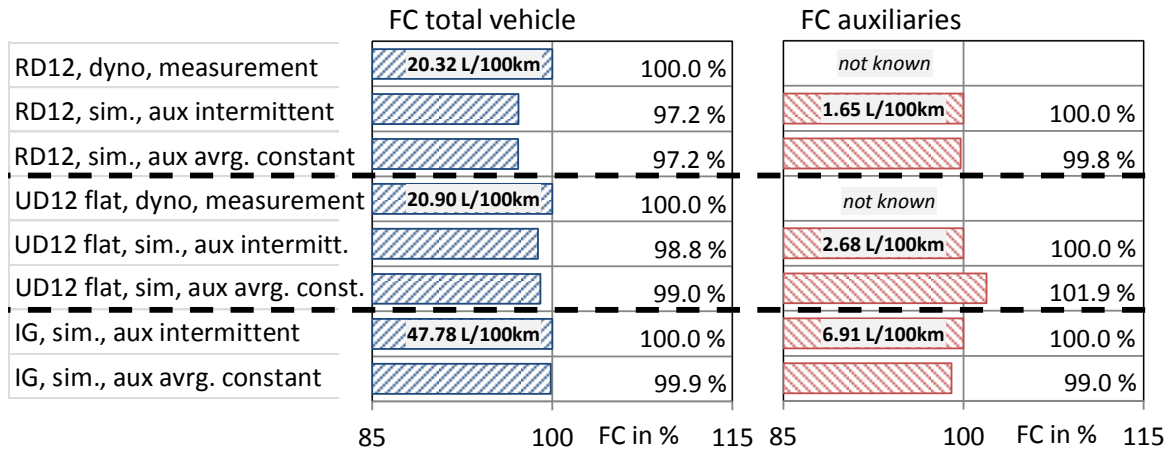


Figure 30. Delivery truck. Fuel consumption simulated for auxiliary power with intermittent and constant average course.

For the RD12 and UD12-flat cycle the deviation of the additional auxiliaries' FC is low at -0.2 and +1.9 %, and for the highly transient Inffeldgasse cycle at -1.0 %. The influence on the simulated total FC is lower at ±0.0, +0.2 and -0.1 %.

⇒ The conclusion from all simulations is, that the depiction of the engine auxiliaries as constant power consumers is a reasonable simplification since a simulation of on/off phases of intermittently operating auxiliaries would also include uncertainties. For a good accuracy of the additional FC from the auxiliaries the accumulated work demand of their constant average power shall be equal or near the work that would be consumed during the real intermittent operation. The deviation of the *additional* FC for the auxiliaries will be in most cases below 5 % from the result of intermittent operation, and the deviation of the *overall* FC below 1 %.

2.2.3.1 Air conditioning system of buses

The chiller of the air conditioning's (A/C) refrigerator of buses is one big power consumer, for the basis model of a city bus it causes just under 8 % of the total FC, compare p. 89 Figure 89. Here the determination of its power demand shall be described in more detail.

For city buses the requirement for the cooling capacity is to reach a cabin temperature of +32 °C at an ambient temperature of +35 °C, for a load factor of 75 % (123 p. 6), what are 60 passengers in a 12 m rigid bus or ca. 100 passengers in an 18 m articulated bus. For this thesis the A/C of the rigid bus models has got a max. cooling capacity³² of 40 kW_{th} and the A/C of the articulated bus model has got 60 kW_{th}. Both values are at the upper end of typical A/C sizes, some numbers were researched from real vehicles, see p. 188 section 5.11.

For this work the simulation tool "Heating, Ventilation and Air Conditioning Carbon Dioxide Simulator" (HVACCO2SIM) for buses was used, which was developed for VECTO by Fraunhofer-Institut für Verkehrs- und Infrastruktursysteme (IVI), Dresden (124) (125). The necessary heat transmission from the bus cabin to the ambient is calculated by a simplified heat balance. The heat sources are solar radiation, the passengers and in summer thermal transmission through the cabin walls. In winter the thermal transmission becomes a heat sink.

³² The maximum heat flow which can be transferred by the A/C from the bus cabin to the ambient air. Expressed in thermic kilowatt (kW_{th}).

Input values are amongst others:

- Chiller propulsion. Mechanical from the engine crankshaft via a transmission, or electrical from the on-board power supply.
- Control of the chiller. For the mechanically driven machine 2-point (0 %, 100 %), 3-point (0 %, 50 %, 100 %), 4-point (0 %, 25 %, 50 %, 100 %) or continuous. The control of the electrically powered chiller is continuous by default.
- Maximum cooling capacity of the A/C system ($\dot{Q}_{A/C,cool,max}$)
- Bus type. Surface and volume of cabin, surface of floor, surface of windows.
- Number of passengers.
- Application of efficiency measures for the A/C: Insulation, more efficient blower motors, heat pump for the winter, low temperature storage etc..

The thermal system of the bus cabin is simulated for southern, central and northern Europe during a whole year in the resolution of 5 minutes, with varying values for the angle of incidence of the sun and the ambient temperature. If the air temperature in the cabin becomes too high, the A/C is virtually turned on for cooling, if it becomes too low, the heating starts.

The output values are annual average numbers, separate for the three European temperature zones, and one overall result for

- Mechanical power demand of the chiller (= 0 in case of electrical drive).
- Electrical power demand of the A/C, at least from the blower motors, if so plus the power of the electrically driven chiller.
- Fuel consumption of the separate heater³³.

For the basis technical level 2014 the chiller is equipped with a 2-point control and regulated mechanically for a refrigerant temperature in the evaporator from 0 °C to +5 °C. Chillers with 2-point control operate at full cooling power or are turned off³⁴. This causes for low cooling demands in spring or autumn the need for reheating the chilled air downstream the evaporator with engine waste heat, when the air temperature became uncomfortable low.

For chillers with a multistage or continuous control the power demand is smaller, because less or no work is wasted to overcool air which is reheated afterwards.

The demand not to overcool the air can cause a trade-off with the need to dry it during phases of high humidity. Then the air is overcooled in the evaporator to that extend, where enough water vapour condenses to reach the maximum relative humidity for thermal comfort. This value ranges from 50 to 70 %, depending on the cabin temperature (123 p. 9).

During phases of low cooling demand and high humidity, the chilled and dried air needs to be reheated in any case to avoid uncomfortable low temperatures. With the available tools and data it was not possible to analyse separately the increase of FC due to this effect.

³³ This additional FC was not considered in this thesis. The HVACCO2SIM tool allows to choose the amount of engine waste heat for heating, where the additional FC depends on. The avrg. positive engine power over the UB cycle is 31 kW_{mech} and its avrg. efficiency 0.371. Hence the waste heat to the coolant can be estimated to $(31 \text{ kW}_{\text{mech}} / 0.371 - 31 \text{ kW}_{\text{mech}}) / 2 \approx 26 \text{ kW}_{\text{th}}$. HVACCO2SIM's default value is 3 kW_{th}, (124 p. 38), what leads to a heating fuel flow of 0.19 L/h at 16 passengers, and the demand gets 0 L/h for waste heats above 19 kW_{th}. Currently it is not known, what fraction of the waste heat from the coolant can be used for cabin heating.

³⁴ For this standard control strategy see (548 p. 1457) (549 p. 20) (550 p. 81) (551 p. 7) (552 p. 1258) (553 p. 270) (554 p. 215) (555 p. 7460) (556 p. 1202).

The ratio of the cooling capacity to the chiller power demand is the energy efficiency ratio (EER). For HVACCO2SIM an average value of 3.5 is assumed (124 p. 39), there called coefficient of performance for cooling (COP_{cool}). Currently no default values or mandatory standards for the measurement of the chillers of vehicle's A/C are known, but the number 3.5 is close to manufacturer's data³⁵. For building technology much literature is available, and the average EER matches the default value for room air conditioning systems with capacities above 12 kW_{th}, compare (126 p. 126) Table I.11 or (127 p. 7/52) Table 25³⁶.

For this thesis the bus model was simulated for different levels of technology to depict current and future possible saving potentials. Details on the technical levels and components are given on p. 128 chapter 3.2 and p. 169 chapter 5.7.1 ff.. In addition to the 12 m rigid bus an 18 m articulated bus 28 t was simulated for comparison reasons.

For the A/C systems of the buses these properties were chosen for the technology levels, where the chillers are powered mechanically for every level:

- A/C Basis: Chiller with 2-point control; no insulation measures.
- A/C Current: Chiller with 3-point control (full, half, off); insulated glazing, walls, doors.
- A/C Future: Chiller with continuous control; insulated glazing, walls, doors.

The results from the simulation tool HVACCO2SIM for the annual average A/C power are shown in Figure 31, in addition the power demand of a fully electrical A/C.

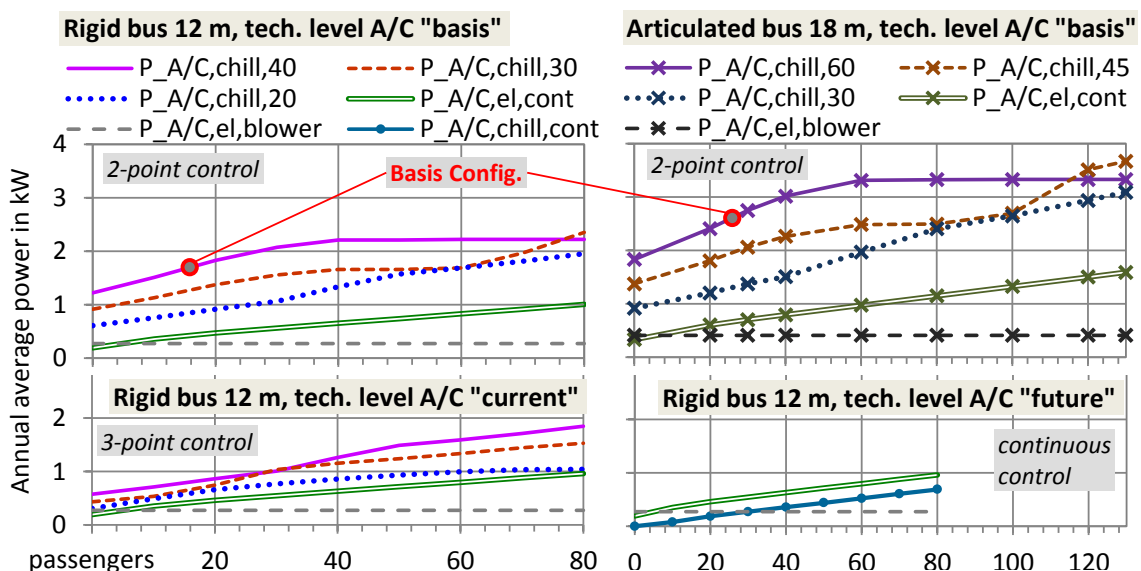


Figure 31. Annual average A/C power from HVACCO2SIM; southern, central and northern Europe; variation of passenger number, maximum cooling capacity and technology level³⁷

where: $P_{A/C,chill,20...60}$ Mechanical power demand of chiller for max. cooling capacities 20, 30 and 40 kW_{th} for rigid bus; 30, 45 and 60 kW_{th} for articulated bus.

$P_{A/C,chill,cont}$ Mechanical power demand of chiller with continuous control, only for the rigid bus A/C model, level "future".

³⁵ Examples for rated EER, refrigerant R134a, evaporator temperature +5 °C, condenser temperature +50 °C: Bitzer F400Y, EER = 3.46 (557 p. 3); Bock FKX30/275 to FKX50/980, EER in range 3.38 to 3.43 (558 p. 16/17). The EER is highly dependent on the temperature levels and can vary for one machine from ca. 1.00 (low evaporator temperature, high condenser temperature) to ca. 11.00 (vice versa). The temperatures for the examples are assumed to be close to the settings in vehicle's A/C, compare (559 p. 49 ff.).

³⁶ In case of A/C for buildings it needs to be regarded, that EER is the ratio of the rated cooling capacity to the rated electrical power demand from chiller plus blowers, these systems are purely electrically driven.

³⁷ HVACCO2SIM, rigid bus: MB Citaro 12 m low floor. Articulated bus: MB Citaro G 18 m low floor.

$P_{A/C,el,blower}$	Electrical power demand of the air conditioning blower motors
$P_{A/C,el,cont}$	Electrical power demand of a fully electrical A/C with continuously controlled chiller. Power demand of motors for chiller <u>and</u> blower.

For the A/C with mechanically driven chillers with 2-point or 3-point control, levels "basis" and "current", the influence of the maximum cooling capacity is obvious. Over the year the chillers run for the same duration, when cool air is demanded, and the big machines consume more power for the delivery of colder air. Because during the transitional season the chilled air becomes too cold, it needs to be reheated downstream the evaporator with engine waste heat, and the chiller power was partial for nothing or just for drying the air stream. For a multi-point control with additional stages this loss becomes smaller than for the 2-point control.

Because the basis A/C models for this thesis had high cooling capacities, and the simulation included the share of the power demand for the southern European countries, the A/C power became too high for central Europe. The mean chiller power for the three temperature zones and its overall average value are shown in Figure 33.

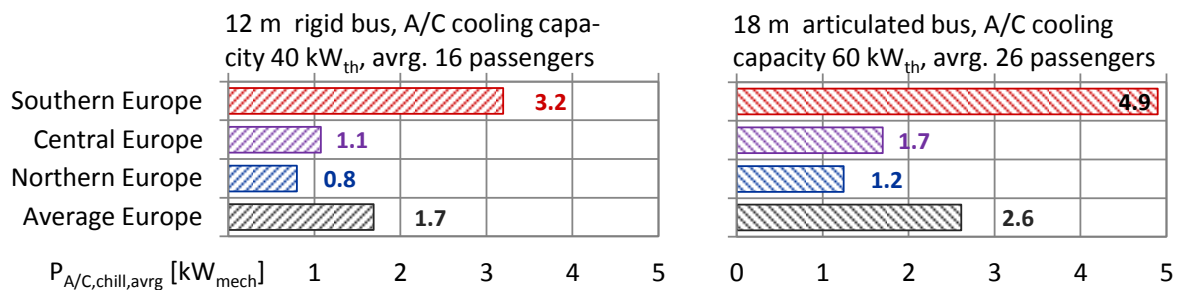


Figure 32. Average annual power demand of A/C chiller, 2-point control, different temperature zones

The share of the calculated chiller power in southern Europe at high ambient temperatures increased the overall average value for whole Europe significantly. Together with the high cooling capacities of the basis A/C this resulted in somewhat high FCs for the basis bus models when compared with results from fleet tests, see p. 92 Figure 94 for rigid buses and p. 96 Figure 98 for articulated vehicles. The tests were mainly conducted in middle Europe and the buses were probably equipped with smaller A/Cs, for an overview see p. 188 Table 46. To check the bus models with a medium A/C, the average power demand of an A/C with 30 kW_{th} maximum cooling capacity for the rigid bus model and 45 kW_{th} for the articulated bus model, only for central Europe, was extracted from the simulation tool, see Figure 33.

To make a fair comparison between conventional diesel buses with mechanically driven chillers and (hybrid) electrical buses with fully electrical A/C, the systems for the latter vehicles had the same control like those for the diesel buses. That means for level "basis" the mechanical power demand of the chiller with 2-point control was divided by the assumed efficiency 0.90 of an electrical motor to depict the electrically powered chiller with the same control. The electrical power demand of the blower motors was added and the result was the total electrical power for an A/C with a 2-point controlled chiller. If the electrical vehicles were equipped with the simulated electrical A/C from HVACCO2SIM, with a continuously controlled chiller, they would have an advantage for energy consumption. The curves for the total electrical power of the basis A/C with 2-point control are also shown in Figure 33.

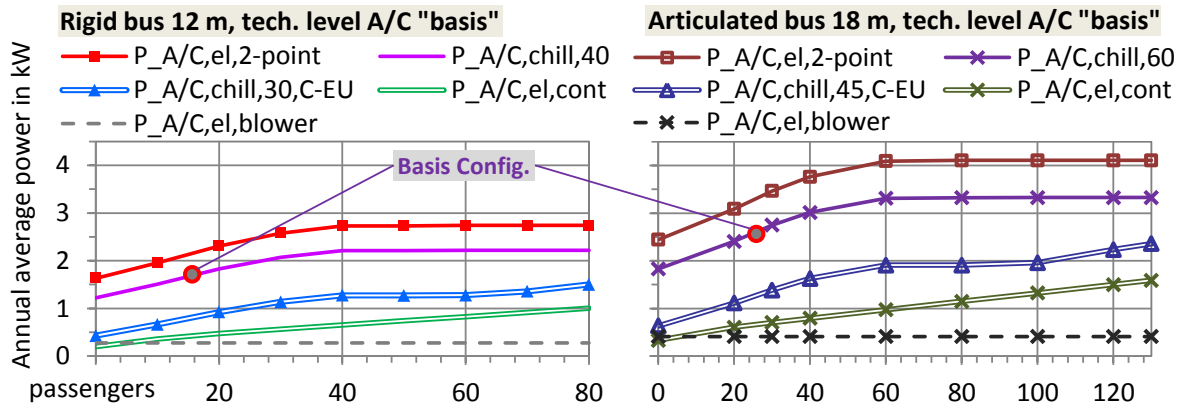


Figure 33. Variations of the A/C systems for the simulation.

- where: $P_{A/C,chill,30,C-EU}$ Mechanical power demand of the chiller 30 kW_{th} with 2-point control, 12 m rigid bus, only for the zone central Europe. *The other curves in the diagram w/o the index "C-EU" depict the overall mean values for southern, central and northern countries.*
- $P_{A/C,chill,45,C-EU}$ Mechanical power demand of the chiller 45 kW_{th} with 2-point control, 18 m articulated bus, only for the zone central Europe.
- $P_{A/C,el,2-point}$ Electrical power demand of a fully electrical A/C with 2-point controlled chiller. Power demand of motors for chiller and blower.

For the rigid bus with average 16 passengers the difference between the chiller power for an A/C of 40 kW_{th} including the southern countries and the power for a system of 30 kW_{th} only in central Europe is 0.9 kW_{mech}.

In case of the electrical A/C the differences between the big systems of 40 or 60 kW_{th} with 2-point control for the rigid bus, 16 passengers, or for the articulated bus, 26 passengers, and the continuously controlled A/C are 1.7 kW_{el} or 2.6 kW_{el}.

Those are additional advantages in consumption for (hybrid) electrical vehicles with electrical, continuously controlled A/C, when they are compared to diesel vehicles with a mechanical, 2-point controlled A/C. The reason is the control strategy, continuous versus 2-point, which eliminates the loss of A/C due to running always at full power when turned on. This effect is described on p. 30

This advantage is significant, as will be shown on p. 114 ff., sections 3.1.11.3 to 3.1.12 about the models of hybrid buses.

2.2.4 Vehicle control: Acceleration, deceleration and gear shift

The main control functions of the basis models are the curves for desired acceleration and deceleration and for the gear shift behaviour. By defined calculation steps the target speed driving cycles, demanded velocity as function of cycle distance, are converted in VECTO v2.2 to time-based velocity courses, like described in (53 pp. 101-17)³⁸. The curves for max. acceleration and min. deceleration are used to shape the velocity course, compare Figure 34.

³⁸ The main simulation program for this thesis was VECTO v2.2, where the pre-processing from distance- to time-based cycles was conducted internally. The current VECTO v3 calculates only distance-based.

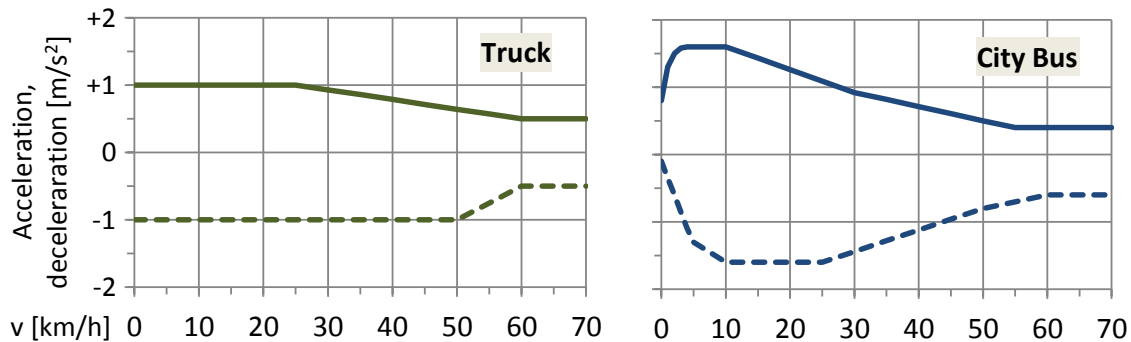


Figure 34. Input curves for demanded max. acceleration and min. deceleration, truck and city bus³⁹

The standard gear shift control for trucks with (A)MT is simple, see Figure 35 left. When the current gear is below the highest gear and the demanded engine operation point on or right of the "shift up" curve, the next higher gear is selected. In case of a current gear above the 1st and an engine operation point on or left of the "shift down" curve, the next lower gear is chosen.

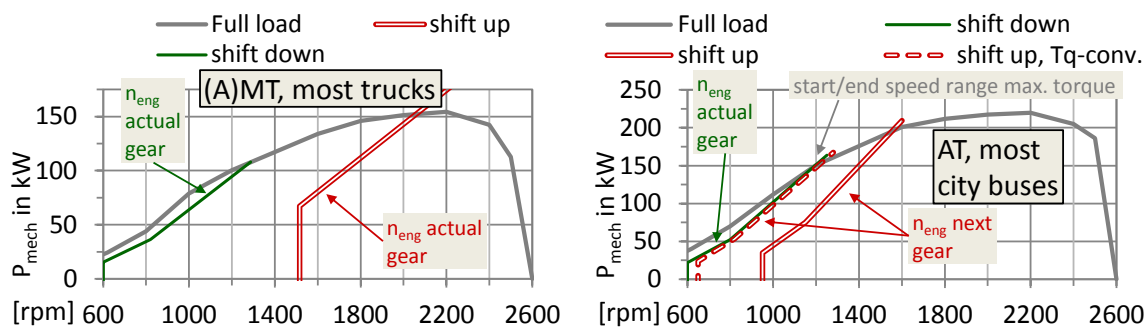


Figure 35. Curves for gear shift control in VECTO v2.2⁴⁰

In case of AT with hydraulic torque converters the curve "shift up" refers to the engine speed in the *next higher* gear, see Figure 35 right. For the 1st gear, where the hydraulic torque converter is unlocked, it is shifted up as soon as possible, when the engine speed in the 2nd gear reached the range of maximum torque. The average losses in the hydro-mechanical 1st gear are high at ca. 25 %, thus the residence time in this gear is limited to the minimum.

It shall be mentioned, that the shifting model for AT in VECTO is work in progress at the time of writing, hence it is provisional. As will be shown later on p. 94 ff. section 2.6.3.4, the utilised model of a 4-speed AT in VECTO v2.2 seems to produce an overestimation of the total FC especially for buses of higher mass in heavy urban traffic.

The described features are the main functions of the shifting model of VECTO v2.2. In addition some extra-rules are regarded (54 p. 55), like an early upshift for the AMT when the engine speed is still below the "shift up" curve, but enough torque is available in the next gear.

³⁹ Acceleration curves for truck from (149 p. 139/140), acceleration curves for city bus elaborated from measurement of bus line 31 Graz in 2012-04 (243 p. 136/137) (161 p. 35), rigid bus 12 m, 3.8 t payload, halt at every bus stop, usual driving style "aggressive".

⁴⁰ Gear shift curves truck calculated according (101 pp. 168-170). City bus shifting curves adopted to meet average engine speed: $n_{eng,rel,avrg} = (n_{eng,curr,avrg} - n_{eng,idle}) / (n_{eng,rated} - n_{eng,idle})$. Measured engine speed ($n_{eng,curr}$) from city bus with 4-speed AT, see p. 199 Table 62, first case.

The shifting model for the early versions of VECTO v3 is similar to VECTO v2.2. The model will be completely reworked and will be probably available in the 2018 versions of VECTO v3.

2.2.5 Engine operation point and fuel consumption

The gross engine torque and the subsequent power in VECTO and for this thesis consist of

- 1) Rolling resistance of tires. $P_{roll} = RRC \cdot (m_{curb} + m_{payl}) \cdot g \cdot v_{veh}$.
- 2) Gradient force of vehicle mass. $P_{grad} = \Delta alt / \Delta s \cdot (m_{curb} + m_{payl}) \cdot g \cdot v_{veh}$.
- 3) Air drag of vehicle body. $P_{air} = C_d \cdot \text{fact}_{C,d,vel,60} \cdot A_{cr} \cdot \rho_{air} / 2 \cdot v_{veh}^3$.
- 4) Inertia of vehicle. Vehicle mass plus rotational inertia of wheels and drivetrain parts
 $P_{inert,veh} = (m_{curb} + m_{payl} + m_{rot,eq,wh} + m_{rot,eq,dt}) \cdot a_{veh} \cdot v_{veh}$.
- 5) Drivetrain friction. Friction between gears and in bearings, power consumption of lubricant pumps, idle losses of retarder, if so hydraulic losses of torque converter.
 $P_{dt,loss}$ (calculated from maps or characteristic curves).
- 6) Power demand of engine auxiliaries. Air conditioning chiller, alternator, compressor, cooling fan, steering pump and PTO. P_{aux} (average constant table values in most cases).
- 7) Inertia of engine. Equivalent inertia of moving engine parts, referred to crankshaft.

$$P_{inert,eng} = J_{eng} \cdot \dot{\omega}_{eng} \cdot \omega_{eng}$$

where: J_{eng} Rotational inertia of moving engine parts, referred to crankshaft
 ω_{eng} Rotational engine speed, here in rad/s

It is calculated according to Equation 8.

Equation 8: Calculation of the gross engine power

$$P_{eng,gross} = P_{roll} + P_{grad} + P_{air} + P_{inert,veh} + P_{dt,loss} + P_{aux} + P_{inert,engine}$$

where: $P_{eng,gross}$ Gross engine power

The engine speed is determined via Equation 9.

Equation 9: Relation between engine speed and vehicle velocity, clutch fully closed

$$n_{eng} = \omega_{wh} \cdot i_{fd} \cdot i_{gb} \cdot 30 / \pi$$

where: i_{fd} Gear ratio of final drive (ratio of input to output speed)
 i_{gb} Gear ratio of gear box (ratio of input to output speed)
 n_{eng} Rotational engine speed, here in rpm

With the values for gross engine power and engine speed the current FC is interpolated from a map ("FC-map"), measured under stationary conditions (55), Annex V. The maps of the engines for the HDV models tractor-trailer and rigid bus of this thesis are shown in Figure 36.

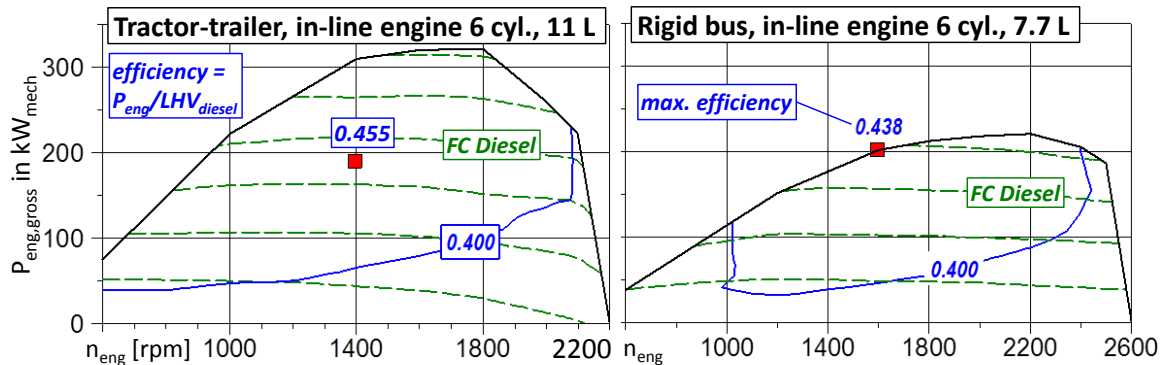


Figure 36. Maps of diesel engines, fuel flow and efficiency, tractor engine 320 kW and bus engine 220 kW

The engine efficiency from 0.43 to 0.45 is of the magnitude of EURO VI diesel engines, compare (128 pp. 8-16). The applicate of the performance maps can be the consumption of any

liquid or gaseous fuel in [unit/time], and in case of electrical machines the consumption or generation of electrical power. The maps for all combustion engines and the electrical machine plus a comparison with measured results are given on p. 180 ff. chapter 5.8.

The single consumed (or generated) units of mass, volume or energy are summarised over the cycle and the result is the overall fuel consumption (FC) or energy consumption (EC).

To depict transient effects for internal combustion engines, here diesel- or gas-fuelled, the summarised FC from the engine map is multiplied with a transient correction factor (TCF) (53 pp. 19-22). For driving cycles with frequent load changes the real FC is slightly higher than the summarised FC from a stationary engine map, the factor ranges from 1.00 for motorway operation up to ca. 1.04 for urban bus cycles.

The main reason is, that during the many load steps of transient urban operation the rotational inertia of the turbocharger needs to be overcome, what delays its acceleration and thus delays also the buildup of boost pressure, what is called “turbo lag”. During this dynamic process of increasing the load and speeding up the engine plus the turbocharger, the air-fuel-ratio (AFR) is lower than during the stationary measurement of the FC-map. A lower AFR leads to a lower engine efficiency, what is known from engine analysis (129 pp. 138, Abb. 3.13a). Thus the engine efficiency during load steps is below the value from the stationary FC-map.

Another reason is, that during transient urban cycles the temperature of the engine block is lower than during the stationary measurement of the FC-map. In urban driving the engine operates with a low average load and with many phases of drag or idle, what reduces the average waste heat to the engine block significantly, in comparison to the stationary measurement. This causes lower temperatures of oil and coolant in the engine block.

Oil of lower temperature has got a higher viscosity, what increases its internal friction. The lower temperature of the coolant leads to lower temperatures of the cylinder walls, what increases the wall heat losses of the burning gas mass in the cylinder. A higher share of the heat is lost to the engine block and cannot be used for the expansion of the gas mass in the cylinder.

E. g. it is known from measurement, that the FC of HDV diesel engines during the World Harmonised Transient test Cycle (WHTC, (130 pp. 29 ff., 87 ff.)) with cold start is a few % higher than the FC during the same cycle with warm start.

This increase of FC in the same operating points from warm to cool engine affects the interpolated values from the FC-map especially for transient operation. Like described above, the engine temperature during the measurement of the FC-map is higher than the temperature of the virtual engine, simulated on transient cycles with partly high shares of drag plus idle.

The attribution of the transient correction factors (TCF) to the driving cycles is given on p. 163 ff. Table 28, where some characteristic factors for the analysed cycles are shown.

In VECTO additional correction factors for cold start and the regeneration of the particle filter are applied. Due to the low temperature of the cylinder walls, lube oil, etc. during cold start the engine efficiency is lower than in the stationary FC-map, which is measured under hot engine conditions, as described in the paragraph above. For the active regeneration of the particle filter additional fuel needs to be injected to increase the exhaust temperature. For typical engine cycles these effects cause an increase of the overall FC below 0.4 %, what was elaborated from measurement data, and were neglected here.

All of these correction factors (transient, cold start and DPF regeneration) are calculated from the test results in the WHTC as described in (55), Annex V.

The VECTO results for FC or EC can be combined with the factors for greenhouse gases well-to-wheel, compare p. 165 Table 29, to get the impact on global warming.

2.3 Models of engine auxiliary consumers

A new model was developed to calculate the power demand of the cooling fan, and an existing model for the compressor of the pneumatic system was revised to allow a more detailed simulation than just using constant power values as foreseen for VECTO today.

The models can be used to determine the additional load on the engine by these consumers, or to generate values for their average constant power consumption.

2.3.1 Cooling fan

In this section a model for the simulation of the intermittent power demand of the fan is described. This consumer contributes ca. 0.5 % to the FC of a tractor-trailer on the Long Haul cycle 2015. The current approach in VECTO is to choose a constant table value for the average power demand. There the distinction is made between different power transmission technologies from engine crankshaft to fan shaft, e. g. on-off clutch or viscous clutch.

An alternative approach is to determine the input values for a more detailed model of the fan and to calculate its power demand timestep by timestep. Multiple publications on HDV cooling systems and fans were found, but no complete model which was simple enough to be implemented without additional software or much programming effort (131) (132) (133) (134) (135) (136) (137) (138) (139) (140). Hence a new model of the cooling system was created to calculate the fan power demand.

The manufacturer of HDV cooling systems MAHLE Behr GmbH, Stuttgart, kindly shared the measurement data of an EURO VI tractor engine 326 kW with cooling circuit, so the model could be validated. All measurement values shown in this chapter were provided by MAHLE. The engine operation when powering a typical tractor-trailer with 19.3 t payload on the old Long Haul cycle 2012 was simulated in VECTO. Subsequently the resulting engine cycle was measured on a test bench where the engine was equipped with its original cooling system, and the headwind was generated by a blower.

All model parameters have been fitted based on these measurement data.

The approach of the elaborated model is:

- Determine the fan state, on or off, and its rotational speed, depending on the coolant temperature.
- Model the air flow through grille, radiator, (idling) fan and engine compartment to the undersurface as pipe flow with flow resistances.
- Calculate the air flow velocity with Bernoulli's principle.
- Assume the ram pressure by headwind and the increase of static pressure by the activated fan as energy sources, and grille, radiator, idling fan plus engine compartment as flow resistances.
- Depict the fan as additional flow resistance in idle state, or calculate its operating point in terms of flow velocity and pressure increase when actuated.
- Determine the fan power consumption from a measured characteristic curve.
- Model the heat flow from coolant to air in the radiator as characteristic curve, dependent on the air flow velocity.
- Determine for each timestep the heat input to coolant and engine, calculated by the heat balance from the fuel energy flow and the waste heat flow to the radiator.
- Calculate with a heat balance the temperature of coolant and engine for the next time step, assuming one effective thermal mass.

The general structure of an engine cooling system and the curve of the actuation grade for the fan are shown in Figure 37.

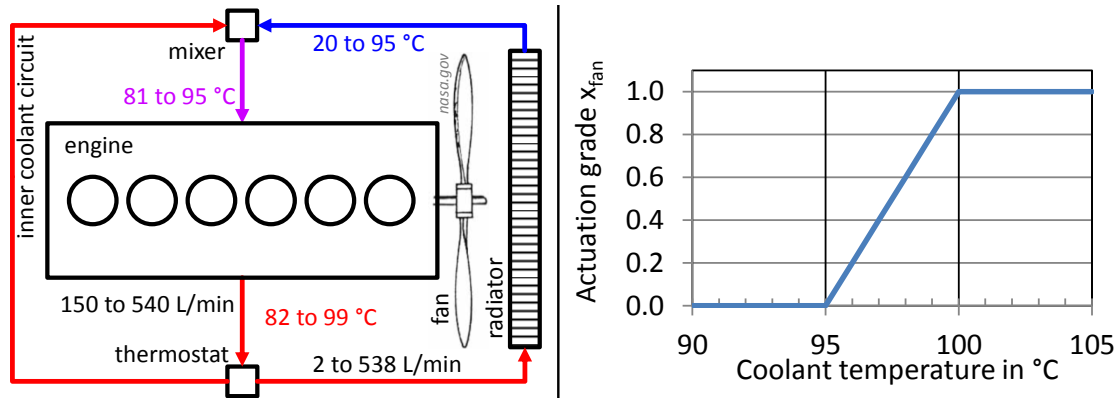


Figure 37. Left: Structure of analysed engine cooling system. Right: Fan actuation grade x_{fan}

The cooling system consists of an inner and an outer circuit, where the radiator is located in the outer circuit. The coolant flow from the engine can be split by the thermostat, and a fraction from 0 to 100 % can be lead through the radiator. Engine's waste heat is transmitted to the coolant in the inner circuit and afterwards to the air flow in the radiator. Between engine and radiator the fan is mounted and boosts additional air, when the headwind is not sufficient to gain enough heat transfer.

The thermostat is controlled by the coolant temperature at engine outlet (T_{cool}) and opens the outer circuit partly in case of higher cooling demand. If the thermostat is closed, the radiator can be cooled down almost to ambient temperature by the headwind and be used as low temperature storage for the next phase with high waste heat.

In the model, which is described below, the thermostat is neglected and the lower limit for the coolant temperature is set to 82 °C by definition.

One of the main simplifications of the model is the depiction of engine and coolant circuits as one effective thermal mass. In reality the lower limit for the temperature of the inner coolant circuit is 82 °C, hence this number was also chosen as lowest temperature of the effective thermal mass. If the temperature, calculated from the heat balance, compare p. 46 Equation 20, would become lower than 82 °C, this is neglected and it is held constant until the next phase of heat excess.

In case of the measured cooling system the fan speed (n_{fan}) was set by the actuation grade x_{fan} , which is dependent on the coolant temperature, see Figure 37 right. The fan speed is calculated by Equation 10.

Equation 10. Calculation of rotational fan speed

$$n_{fan} = x_{fan} \cdot (n_{eng} \cdot i_{cl,fan} - n_{fan,idle}) + n_{fan,idle}$$

- where:
- n_{fan} Rotational fan speed, at output of viscous clutch, see Figure 38 left
 - x_{fan} Fan actuation grade, interpolated each time step from curve Figure 37 right
 - n_{eng} Rotational engine speed
 - $i_{cl,fan}$ Ratio of rotational speed of fan clutch to engine speed
 - $n_{fan,idle}$ Rotational speed of idling fan

This relation is only valid for the analysed viscous clutch, which is electronically controlled. For other power transmission types like viscous clutches with bimetallic temperature control or on-off clutches other relations have to be chosen.

The speed ratio of fan to clutch input shaft $n_{fan} / n_{fan,cl}$ is adjusted by changing the oil volume in the viscous clutch. A higher oil volume leads to a higher speed ratio due to more fluid friction between in- and output plate, a drawing is shown left in Figure 38.

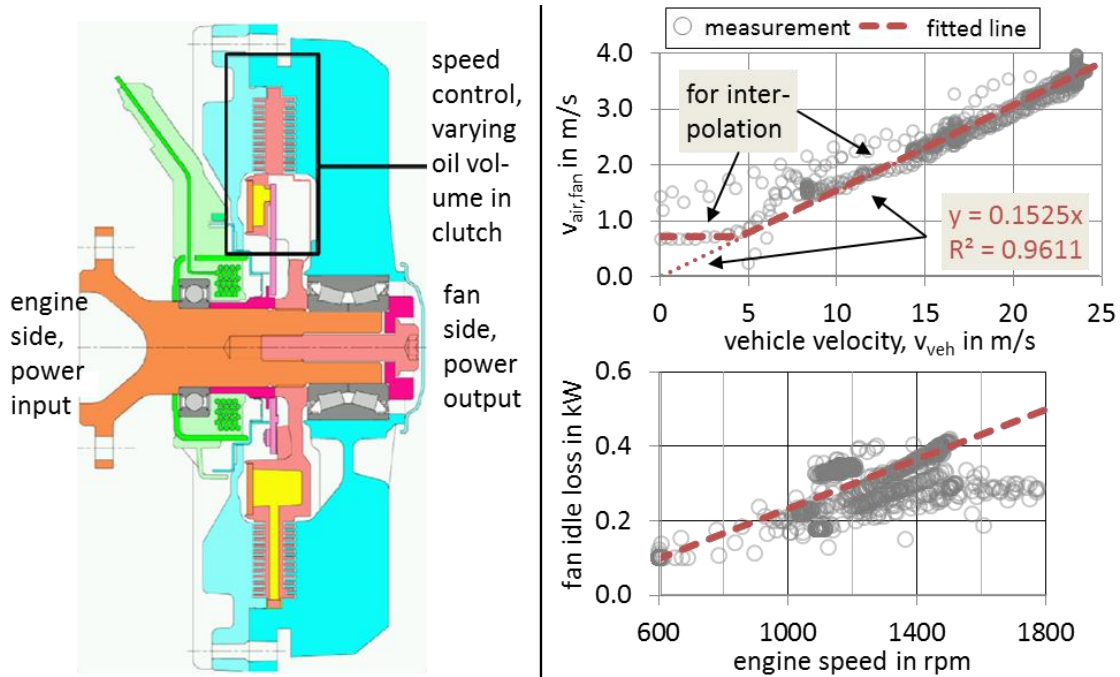


Figure 38. Left: Viscous fan clutch (141 p. 4). Right: Air flow velocity ($V_{air,fan}$), idling fan ($0 \text{ m/s} < v_{veh} < 4 \text{ m/s}$) & idling fan plus headwind ($v_{veh} > 4 \text{ m/s}$). Power loss in idle state, from fan & clutch.

When the fan is turned off, the air flow velocity can be interpolated from the curve Figure 38 right above, the idling losses of fan and clutch from the curve right below.

For the air flow in the fan cross sectional area a constant value for the average air density was assumed. This simplification is reasonable, since the variability of the density is low. As example the normalised density, calculated with the radiator's heat balance of coolant and air mass flow and the resulting air temperature, limited to ($T_{cool} - 5 \text{ K}$), is shown in Figure 39.

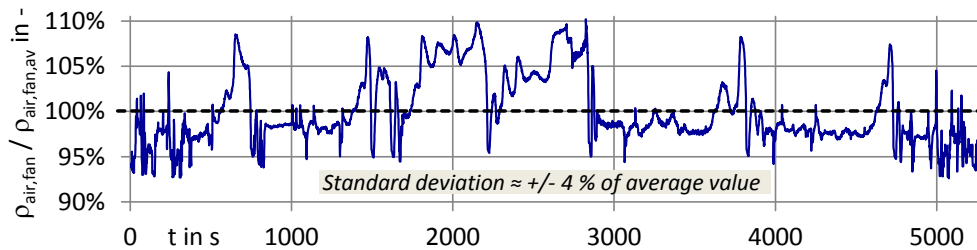


Figure 39. Normalised air density behind radiator in fan cross sectional area.
Calculated from the measured air temperature, and normalised to the average air density.

In the simplified model the average density of the air behind the radiator ($\rho_{air,fan,av}$) was chosen for the calculation of the air flow velocity in the fan cross sectional area ($V_{air,fan}$), see Equation 12 and Equation 13.

For the vehicle the air flow through radiator and fan starts at the vehicle front, where the headwind generates ram pressure ($p_{ram,fr}$), and ends at the vehicle undersurface, where also a usually negative ram pressure ($p_{ram,u}$) occurs. Between front and undersurface the obstacles grille, radiator, idling fan and engine compartment cause drops of the static pressure, which can be summarised to one overall drop (Δp_{drop}). One needs to distinguish the cases fan-off and fan-on, where the idling fan causes an additional pressure drop ($\Delta p_{fan-off}$), or generates a pressure increase (Δp_{fan-on}). The air flow channel is shown in Figure 40.

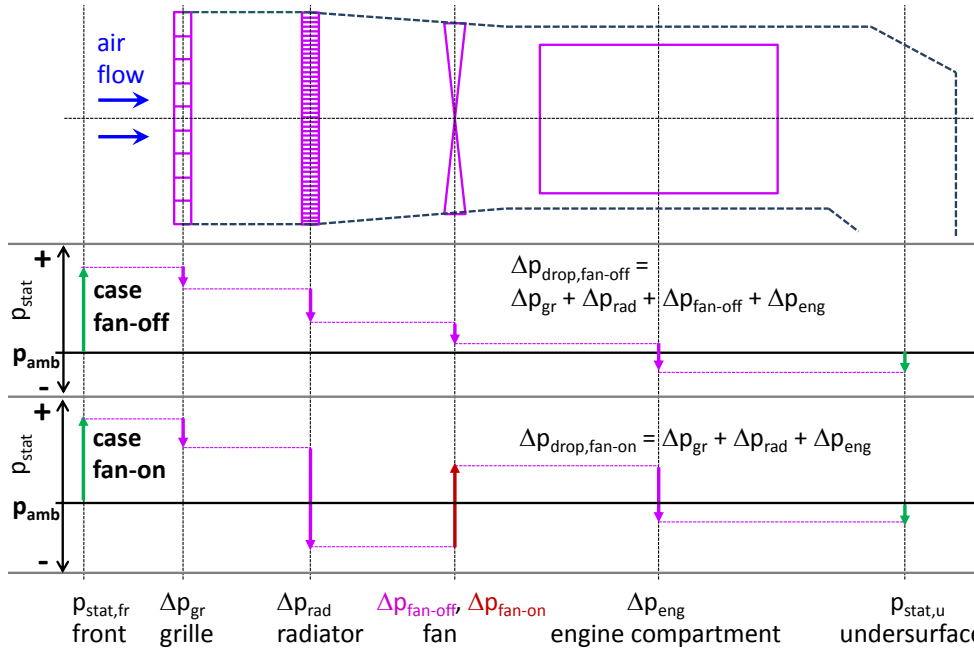


Figure 40. Air flow channel, vehicle front to undersurface, pressure sources and drops (142 p. 40)

- where: $\Delta p_{\text{drop,fan-off/on}}$ Summarised overall pressure drop for cases fan-off (idling fan acts as flow resistance) or fan-on (powered fan acts as pressure source)
- Δp_i Pressure drop of flow resistance "i" (grille, radiator, engine compartment)
- $\Delta p_{\text{fan-off}}$ Pressure drop by idling fan
- $\Delta p_{\text{fan-on}}$ Pressure increase by activated fan
- p_{amb} Ambient pressure
- p_{stat} Static pressure
- $p_{\text{stat,fr}}$ Static pressure at vehicle front, ambient pressure plus ram pressure by headwind ($p_{\text{ram,fr}}$)
- $p_{\text{stat,u}}$ Static pressure at vehicle undersurface, ambient pressure plus ram (under-) pressure by headwind ($p_{\text{ram,u}}$)

The air flow channel was modelled as a horizontal pipe with the constant diameter of the fan cross sectional area, and the pressure drop was assumed to occur in this pipe, see Figure 41.

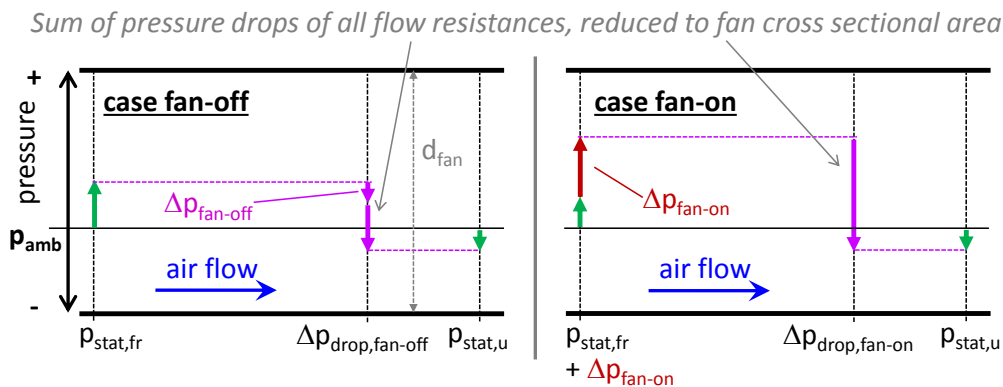


Figure 41. Depiction of the air flow channel as pipe flow with constant fluid density and fix diameter

The air mass flow is calculated by Equation 11.

Equation 11. Air mass flow through fan cross sectional area

$$\dot{m}_{\text{air,fan}} = v_{\text{air,fan}} \cdot \rho_{\text{air,fan,av}} \cdot d_{\text{fan}}^2 \cdot \pi/4 = v_{\text{air,fan}} \cdot \rho_{\text{air,fan,av}} \cdot A_{\text{cr,fan}}$$

where: $\rho_{\text{air,fan,av}}$	Average air density in fan cross sectional area, assumed to be constant during simulated driving cycle
$A_{\text{cr,fan}}$	Fan cross sectional area
d_{fan}	Diameter of fan cross sectional area
$\dot{m}_{\text{air,fan}}$	Air mass flow through fan cross sectional area
$V_{\text{air,fan}}$	Air flow velocity in fan cross sectional area

The pressure drop (Δp_{drop}) is calculated via Equation 12.

Equation 12. Pressure drop, formula of Voisins (143 p. 113), also known as Darcy-Weisbach equation

$$\Delta p_{\text{drop,fan-off/on}} = k_{\text{fan-off/on}} \cdot \frac{\rho_{\text{air,fan,av}}}{2} v_{\text{air,fan}}^2$$

where: $k_{\text{fan-off/on}}$ Combined flow resistance coefficient of obstacles, for cases fan-off or fan-on, with and without idling fan as additional obstacle

To calculate the air flow, Bernoulli's principle of the conservation of energy was applied on the flow of an incompressible fluid in a horizontal pipe, see Equation 13.

Equation 13. Bernoulli's principle (144 p. 30) (84 p. 151) (145 pp. 14-18)

$$E_{\text{kin,air}} + E_{\text{pot,air}} + E_{\text{v,air}} = \text{const.} = m_{\text{air}} \cdot \frac{1}{2} \cdot v_{\text{air,fan}}^2 + m_{\text{air}} \cdot g \cdot \text{alt} + p_{\text{stat}} \cdot V_{\text{air}}$$

• with: $p_{\text{stat,fr}} + \Delta p_{\text{fan-on}} - \Delta p_{\text{drop,fan-off/on}} = p_{\text{stat,u}}$; $\Delta p_{\text{fan-on}} = 0$ for case fan - off,
"fr" or "u" means front or undersurface

$$\begin{aligned} \Rightarrow m_{\text{air}} \cdot \frac{1}{2} \cdot v_{\text{air,fan}}^2 + m_{\text{air}} \cdot g \cdot \text{alt}_{\text{fr}} + (p_{\text{stat,fr}} + \Delta p_{\text{fan-on}} - \Delta p_{\text{drop,fan-off/on}}) \cdot V_{\text{air,fr}} &= \dots \\ \dots = m_{\text{air}} \cdot \frac{1}{2} \cdot v_{\text{air,fan}}^2 + m_{\text{air}} \cdot g \cdot \text{alt}_{\text{u}} + p_{\text{stat,u}} \cdot V_{\text{air,u}} \end{aligned}$$

• with: $\text{alt}_{\text{fr}} = \text{alt}_{\text{u}}$; $p_{\text{stat,fr}} = p_{\text{amb}} + p_{\text{ram,fr}}$; $p_{\text{stat,u}} = p_{\text{amb}} + p_{\text{ram,u}}$; $V_{\text{air}} = m_{\text{air}} / \rho_{\text{air,fan,av}} = \text{const.}$

$$\Rightarrow p_{\text{amb}} + p_{\text{ram,fr}} + \Delta p_{\text{fan-on}} - \Delta p_{\text{drop,fan-off/on}} = p_{\text{amb}} + p_{\text{ram,u}}$$

• with: $\Delta p_{\text{drop,fan-off/on}} = k_{\text{fan-off/on}} \cdot \frac{\rho_{\text{air,fan,av}}}{2} v_{\text{air,fan}}^2$; formula of Voisins

$$\Rightarrow p_{\text{ram,fr}} + \Delta p_{\text{fan-on}} - k_{\text{fan-off/on}} \cdot \frac{\rho_{\text{air,fan,av}}}{2} \cdot v_{\text{air,fan}}^2 = p_{\text{ram,u}}$$

• with $p_{\text{ram,j}} = c_{p,j} \cdot \frac{\rho_{\text{air,amb}}}{2} \cdot v_{\text{veh}}^2$; $\Delta p_{\text{ramfr-u}} = p_{\text{ramfr}} - p_{\text{ramu}}$; $\Delta c_{p,fr-u} = c_{p,fr} - c_{p,u}$

$$\Rightarrow \Delta p_{\text{ramfr-u}} + \Delta p_{\text{fan-on}} - k_{\text{fan-off/on}} \cdot \frac{\rho_{\text{air,fan,av}}}{2} v_{\text{air,fan}}^2 = 0$$

$$\Leftrightarrow \Delta c_{p,fr-u} \cdot \frac{\rho_{\text{air,amb}}}{2} \cdot v_{\text{veh}}^2 + \Delta p_{\text{fan-on}} - k_{\text{fan-off/on}} \cdot \frac{\rho_{\text{air,fan,av}}}{2} v_{\text{air,fan}}^2 = 0$$

where: $\Delta c_{p,fr-u}$ Difference in ram pressure coefficients, *here set to $\Delta c_{p,fr-u} = 0.8$*
 $\Delta p_{\text{ram,fr-u}}$ Difference in ram pressure from vehicle front to undersurface
 $\rho_{\text{air,amb}}$ Air density at ambient conditions, 1.188 kg/m³
alt Altitude of air, here equal at vehicle front and undersurface
 $c_{p,fr}$ Ram pressure coefficient at vehicle front, usually $c_{p,fr} > 0$
 $c_{p,u}$ Ram pressure coefficient at vehicle undersurface, usually $c_{p,u} < 0$

$E_{kin,air}$	Kinetic energy of air mass
$E_{pot,air}$	Potential energy of air mass
$E_{v,air}$	Pressure energy of air volume, equals the mechanical work to move one volume unit: $p_{stat} \cdot V_{air} = p_{stat} \cdot A_{cr,fan} \cdot \Delta S_{air} = F_{fan} \cdot \Delta S_{air} = W_{mech,air}$, where ΔS_{air} is the distance to move the volume unit
j	Index, placeholder for front (fr) or undersurface (u)
m_{air}	Air mass
$p_{ram,fr}$	Ram pressure by headwind, at vehicle front
$p_{ram,u}$	Ram pressure by headwind, at vehicle undersurface
V_{air}	Volume of air

Hence for the case fan-off ($\Delta p_{fan-on} = 0$) it can be written in Equation 14

Equation 14. Calculation of air flow velocity by headwind at idling fan

$$v_{air,fan} = \sqrt{\frac{\Delta c_{p,fr-u}}{k_{fan,off}} \cdot \frac{\rho_{air,amb}}{\rho_{air,fan,av}}} \cdot v_{veh}$$

where: $k_{fan-off}$ Overall flow resistance coefficient of grille, radiator, idling fan and engine compartment, case "fan-off", converted to fan cross sectional area. Calculated to 39.0. Setting $\Delta c_{p,fr-u} = 0.8$. $v_{air,fan} / v_{veh} = 0.1525$, measured, see p. 39 Figure 38 right above.

This simplification is only valid for this one analysed measurement of the examined cooling system.

$\rho_{air,amb} / \rho_{air,fan,av}$ Constant ratio of ambient air density and average air density in fan cross sectional area

When the fan is turned on, its operating point needs to be calculated for every timestep. In this case it acts not as flow resistance, but as pressure source, in addition to the ram pressure. The operating behaviour of fans is depicted by characteristic curves: Static pressure increase (Δp_{fan-on}) as function of a flow quantity. There is one curve for every speed of the rotating fan. The flow quantity can be the fluid velocity in a defined cross section, the volume flow or the mass flow. Here the air flow velocity ($v_{air,fan}$) is chosen. The curve for the pressure increase is measured for the relevant velocity range, and also the curve for the mechanical power demand at the fan hub ($P_{fan,hub}$) is determined. These curves can be normalised.

The fluid flow velocity correlates directly with the rotational speed at equal backpressure:

$$v_{air,fan,1} / n_{fan,1} = v_{air,fan,2} / n_{fan,2} \cdot$$

At equal ratios $v_{air,fan} / n_{fan}$, hence $v_{fan,1} / n_{fan,1} = v_{fan,2} / n_{fan,2}$, the static pressure increase depends on the squared fan speed, and the power demand on n_{fan}^3 (146 p. 123). That is

$$\Delta p_{fan-on,1} / n_{fan,1}^2 = \Delta p_{fan-on,2} / n_{fan,2}^2 \quad \text{and}$$

$$P_{fan,hub,1} / n_{fan,1}^3 = P_{fan,hub,2} / n_{fan,2}^3 \cdot$$

The units for the values, normalised to the fan speed, become:

Air flow velocity:	$v_{air,fan} / n_{fan}$	$= v'_{air,fan}$,	$[v'_{air,fan}] = (m/s)/Hz$
Static pressure increase	$\Delta p_{fan-on} / n_{fan}^2$	$= \Delta p'_{fan-on}$,	$[\Delta p'_{fan-on}] = Pa/Hz^2$
Power demand at fan hub	$P_{fan,hub} / n_{fan}^3$	$= P'_{fan,hub}$,	$[P'_{fan,hub}] = W_{mech}/Hz^3$

The normalised curves for pressure increase and power demand of the investigated fan are shown in Figure 42.

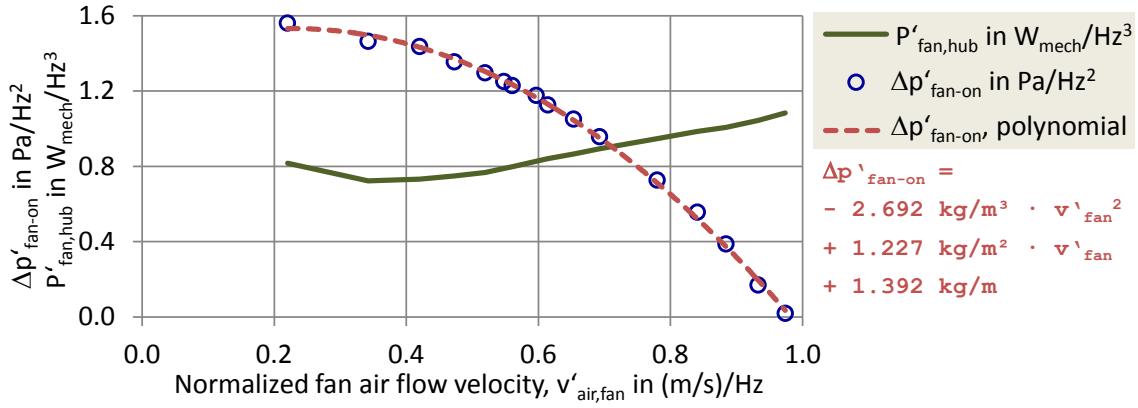


Figure 42. Fan operation: Curves for static pressure increase and power at hub as function of fan air flow velocity, all parameters normalised to fan speed.

It is obvious, that the curve for the normalised pressure increase can be depicted as a 2nd order polynomial. Its 0th order coefficient depends on n_{fan}^2 , its 1st order coefficient on n_{fan}^1 and the 2nd order coefficient is constant, hence it can be written in Equation 15 for the denormalised fan pressure increase:

Equation 15. Polynomial for static pressure increase of fan.

$$\Delta p_{fan-on} = a_2 \cdot v_{air,fan}^2 + a_1 \cdot n_{fan} \cdot v_{fan} + a_0 \cdot n_{fan}^2$$

where: a_0 0th order coefficient of pressure polynomial, here +1.392 kg/m
 a_1 1st order coefficient of pressure polynomial, here +1.227 kg/m²
 a_2 2nd order coefficient of pressure polynomial, here -2.692 kg/m³

The power demand of the fan at its hub can be interpolated from the green curve Figure 42, and is calculated according to Equation 16.

Equation 16. Calculation of fan power demand at hub.

$$P_{fan,hub} = P'_{fan,hub} \cdot n_{fan}^3$$

where: $P_{fan,hub}$ Mechanical power at fan hub
 $P'_{fan,hub}$ Normalised mechanical power at fan hub, normalised to n_{fan}^3 , determined from curve with given value $v_{air,fan}/n_{fan}$ see, Figure 42

With Equation 15 the polynomial for the fan pressure increase and with Equation 16 the characteristic curve for its power demand are calculated for every value of the fan speed, thus only the dependence on the air flow velocity remains.

When the fan is turned on, the pressure balance as outcome of Equation 13 results in an equilibrium between fan pressure increase (Δp_{fan-on}) and ram pressure difference ($\Delta p_{ram,fr-u}$) as pressure sources and the pressure drop for the case fan-on ($\Delta p_{drop,fan-on}$) as pressure sink, see Figure 41 right. For every timestep that air flow velocity ($v_{air,fan}$) is calculated, where this condition is fulfilled, i. e. $\Delta p_{fan-on} + \Delta p_{ram,fr-u} = \Delta p_{drop,fan-on}$.

The expression becomes a binomial equation and can be solved to $v_{air,fan}$, see Equation 17.

Equation 17. Fan air flow velocity for activated fan

$$\Delta p_{fan-on} + \Delta p_{ram,fr-u} = \Delta p_{drop,fan-on}$$

$$\Leftrightarrow a_2 \cdot v_{air,fan}^2 + a_1 \cdot n_{fan} \cdot v_{air,fan} + a_0 \cdot n_{fan}^2 + \Delta p_{ram,fr-u} = k_{fan-on} \cdot \frac{\rho_{air,fan,av}}{2} \cdot v_{air,fan}^2$$

$$\Leftrightarrow v_{air,fan}^2 + 2 \cdot v_{air,fan} \cdot \frac{a_1 \cdot n_{fan}}{2a_2 - k_{fan-on} \cdot \rho_{air,fan,av}} = - \frac{2 \cdot (a_0 \cdot n_{fan}^2 + \Delta p_{ram,fr-u})}{2a_2 - k_{fan-on} \cdot \rho_{air,fan,av}}$$

$$\Leftrightarrow v_{air,fan} = \sqrt{\left(\frac{a_1 \cdot n_{fan}}{2a_2 - k_{fan-on} \cdot \rho_{air,fan,av}} \right)^2 - \frac{2 \cdot (a_0 \cdot n_{fan}^2 + \Delta p_{ram,fr-u})}{2a_2 - k_{fan-on} \cdot \rho_{air,fan,av}}} - \frac{a_1 \cdot n_{fan}}{2a_2 - k_{fan-on} \cdot \rho_{air,fan,av}}$$

where: $\Delta p_{drop,fan-on}$ Combined pressure drop of grille, radiator and engine compartment, converted to fan cross sectional area, case fan-on

k_{fan-on} Combined flow resistance coefficient of grille, radiator and engine compartment, converted to fan cross sectional area, with $\Delta c_{p,fr-u} = 0.8$ calculated to 25.0, see Figure 43.

With the known values from the measurement of the Long Haul cycle 2012, the flow resistance coefficient was determined by solving Equation 17 to k_{fan-on} , see Figure 43 left.

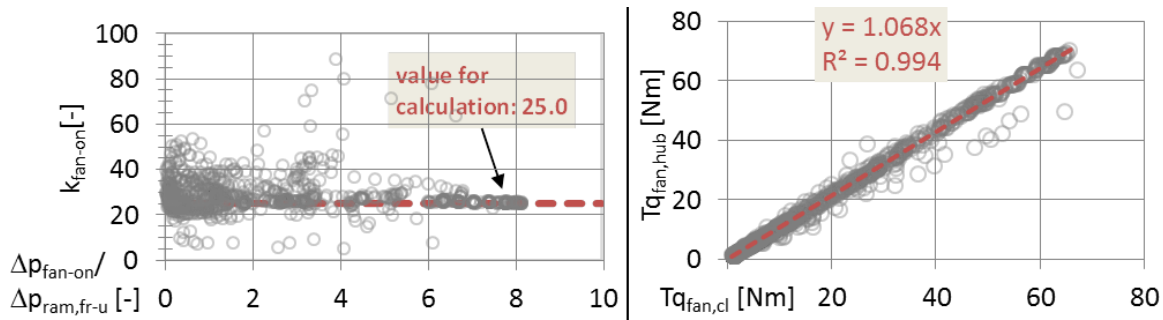


Figure 43. Left: Determination of flow resistance coefficient at activated fan (k_{fan-on}). Right: Torque characteristic of viscous clutch.

k_{fan-on} is smaller than $k_{fan-off}$, because the fan is activated and acts no longer as flow resistance in idling state. When $v_{air,fan}$ was calculated for fan-on, the fan static pressure increase, ranging from 0 to 10 mbar (simulation of Long Haul cycle 2015), and the fan power at the hub are calculated following Equation 15 and Equation 16.

The model for the air flow velocity was checked for accuracy. With the known measurement values vehicle velocity and fan speed the air flow velocity was calculated according Equation 14 and Equation 17, and the resulting air mass flow ($mf_{air,sim} = v_{air,fan} \cdot \rho_{air,fan,av} \cdot A_{cr,fan}$) was compared with the measured value, see Figure 44.

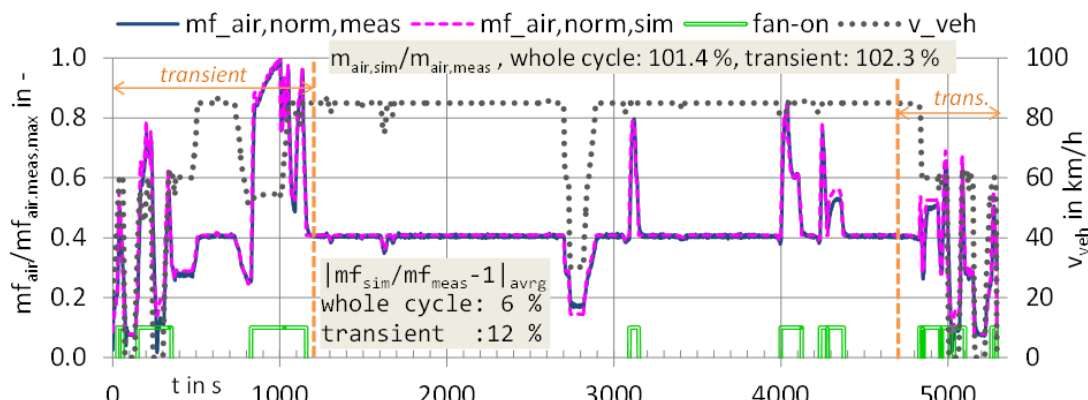


Figure 44. Comparison of simulated with measured air mass flow (mf_{air}), normalised to $mf_{air,meas,max}$

For stationary operation at constant vehicle velocity and/or fan speed the model matches the measured air mass flow very well for this one available dataset, the deviation is small at $\pm 2\%$. For the whole Long Haul cycle 2012 the total measured air mass (≈ 8.36 t) is matched with a deviation of $+1.4\%$, and the average absolute value of the mass flow deviation ($|mf_{sim} / mf_{meas} - 1|_{avrg}$) is 6% .

When looking only at the transient third of the cycle where the vehicle velocity and fan speed change more often, the deviation increases. The total air mass is simulated to $+2.3\%$ and the average absolute mass flow deviation becomes 12% . This value should be similar for the more transient cycles Regional Delivery 2012 and Urban Delivery 2012.

For friction, viscous or rigid clutches the input torque equals the output torque, here $Tq_{fan,cl} = Tq_{fan,hub}$, what is also an outcome of the measurement data, see Figure 43 right. Hence the power demand at the input shaft of the clutch is determined from Equation 18.

Equation 18. Calculation of power demand at fan clutch input shaft

$$P_{fan,cl} = \omega_{fan,cl} \cdot Tq_{fan,cl} = \omega_{fan,cl} \cdot Tq_{fan,hub} = \omega_{fan,cl} \cdot P_{fan,hub} / \omega_{fan} = P_{fan,hub} \cdot n_{fan,cl} / n_{fan}$$

- where:
- ω_{fan} Angular speed of fan
 - $\omega_{fan,cl}$ Angular speed of fan clutch input shaft
 - $n_{fan,cl}$ Rotational speed at fan clutch input shaft, see p. 39 Figure 38 left, $n_{fan,cl} > n_{fan}$ due to slip
 - $P_{fan,cl}$ Power demand at fan clutch input shaft
 - $Tq_{fan,cl}$ Torque at fan clutch input shaft
 - $Tq_{fan,hub}$ Torque at fan hub, at clutch output shaft

The coolant temperature (T_{cool}) was calculated via the balance of engine's waste heat as heat source, coolant and engine as heat storage and the heat transfer to the air in the radiator as heat sink. The main influence on the waste heat is the lower heating value (LHV) of the burned fuel, here diesel. For the engine a stationary map of speed, torque and waste heat to coolant was available. The analysis of the operating points from the driving cycle showed a clear correlation between waste heat and the flow of fuel energy in terms of LHV, here diesel fuel with $9.94 \text{ kWh}_{th}/L$, see Figure 45 left.

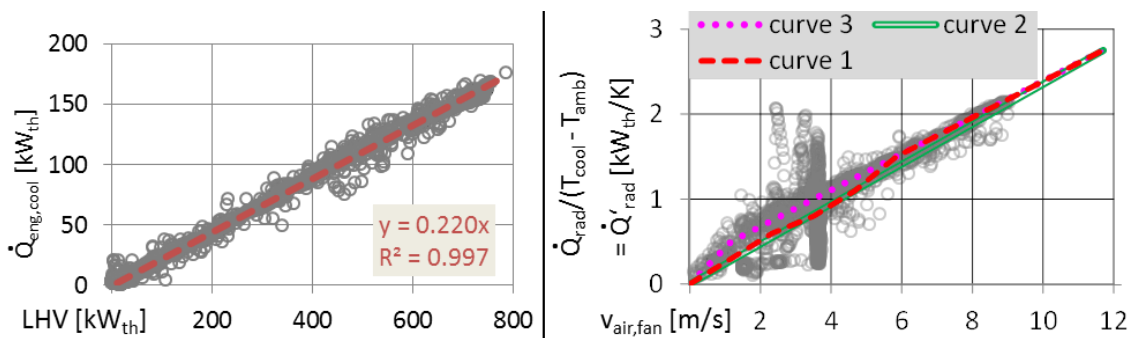


Figure 45. Left: Waste heat engine to coolant ($\dot{Q}_{eng,cool}$). Right: Heat flow coefficient of radiator (\dot{Q}'_{rad}), calculated from heat flow coolant to air (\dot{Q}_{rad}) and temperature difference coolant to ambient

Thus it can be assumed, that ca. 22% of the fuel energy are transmitted as waste heat to the coolant: The inclination of the fitted straight “(Waste heat engine to coolant) as function of (Lower heating value fed to engine)”, see Figure 45 left, is 0.22 . An exception is the idle state at very low load, where only ca. 6% of the fuel energy become waste heat to coolant. The radiators for the cooling of exhaust gas recirculation and charge air were of gas-to-air type and not connected to the coolant circuit in case of this engine.

This correlation between fuel energy and waste heat is only valid for the analysed combination of engine and duty cycle, it will be different for other measurements.

In the simplified model the cooling system transfers heat only into the radiator, a process which can be depicted by a characteristic curve, see Figure 45 right, "curve 1", which was determined from measurement data. Curve 2 and 3 are later used for a parameter variation. From the measured coolant mass flow through the radiator and its calculated heat balance the absolute heat flow to the air was determined (\dot{Q}_{rad}), and divided by the temperature difference from coolant to ambient. Curve 1 reflects the average behaviour of the radiator as heat flow coefficient (\dot{Q}'_{rad}), depending on the air flow velocity. \dot{Q}'_{rad} is the product of the heat transfer coefficient (h_{rad} in $\text{W} / (\text{m}^2 \cdot \text{K})$) and the surface of the radiator (A_{rad}), where both values are unknown. Hence the radiator's heat transfer is determined by Equation 19.

Equation 19. Calculation of the heat transfer in the radiator from coolant to air

$$\dot{Q}_{\text{rad}} = h_{\text{rad}} \cdot A_{\text{rad}} \cdot (T_{\text{cool}} - T_{\text{amb}}) = \dot{Q}'_{\text{rad}} \cdot (T_{\text{cool}} - T_{\text{amb}})$$

where: A_{rad} Surface of the radiator
 h_{rad} Heat transfer coefficient of radiator, dependent on air flow velocity
 \dot{Q}_{rad} Heat flow in radiator from coolant to air
 \dot{Q}'_{rad} Heat flow coefficient, dependent on air flow velocity, determined from measurement data, see p. 45 Figure 45 right, "curve 1".
 T_{amb} Ambient temperature

The chosen "curve 1", see p. 45 Figure 45 right, was manually adjusted to the scatter plot and shows a lower heat flow coefficient around 3.6 m/s, what is the air flow velocity in the fan cross sectional area by headwind at highway speed. This shape is necessary to depict the function of the thermostat to partially close the outer cooling circuit with the radiator at low cooling demand. In that case, when the radiator can be cooled down to ambient temperature, the heat flow coefficient is smaller due to a lower temperature difference from coolant to ambient air.

An additional input value is the cumulative effective heat capacity of coolant, engine oil and engine block (C_{eng}). These components were assumed to be a homogenous mixture with one average specific heat capacity and the mean temperature of the coolant (T_{cool}). This is a very rough simplification, but works for the first approach of a simplified fan model. C_{eng} is a typical calibration factor and was determined from the first simulation results by minimizing the deviation between calculated and measured coolant temperature. The value became

$$C_{\text{eng}} = 700 \text{ kJ/K.}$$

The change of the coolant temperature by the heat balance of engine waste heat to the coolant ($\dot{Q}_{\text{eng,cool}}$), change of heat content in coolant and engine ($C_{\text{eng}} \cdot \Delta T_{\text{cool}}$) and heat transfer in the radiator (\dot{Q}_{rad}) is described by Equation 20.

Equation 20. Change of coolant temperature

$$\Delta T_{\text{cool}} = \frac{(\dot{Q}_{\text{eng,cool}} - \dot{Q}_{\text{rad}})}{C_{\text{eng}}}$$

where: ΔT_{cool} Change of coolant temperature
 C_{eng} Effective average heat capacity of coolant, engine oil and engine
 $\dot{Q}_{\text{eng,cool}}$ Waste heat engine to coolant

To summarise, the simplifications for this model are:

- Negligence of the air density variation behind the radiator, use of one average value.
- Reduction of the obstacles in the air flow channel to one overall flow resistance coefficient
- Calculation of the air flow as horizontal pipe flow of an incompressible fluid.
- Waste heat flow from engine to coolant is linearly dependent on the fuel energy flow.
- Depiction of radiator behaviour by one characteristic curve for the heat flow coefficient, depending on the air flow velocity.
- Negligence of thermostat and outer cooling circuit. Indirect and rough depiction of overcooling of radiator at closed thermostat and higher vehicle velocities by adjusted curve for the heat flow coefficient.
- Depiction of coolant, engine oil and engine block as one effective thermal mass with one average heat capacity and the average temperature of the coolant.

With the above described relations the calculation scheme for time step i is

1. Coolant temperature $T_{cool,i}$ known from heat balance of time step $i - 1$
2. Fan actuation determined from curve x_{fan} , see p. 38 Figure 37 right.
If fan turned off
- 3off. Interpolation of air flow velocity $v_{air,fan}$ from curve, see p. 39 Figure 38 right above
- 4off. Interpolation of fan idle power from curve, see p. 39 Figure 38 right below.
If fan turned on
- 3on. Calculation of air flow velocity $v_{air,fan}$, see p. 44 Equation 17.
- 4on. Calculation of fan power at its clutch input shaft, see p. 43 Equation 16 and p. 45 Equation 18.
5. Calculation of heat transfer to ambient in radiator, see p. 46 Equation 19.
7. Calculation of change of coolant temperature $\Delta T_{cool,i}$ via p. 46 Equation 20.
8. Calculation of coolant temperature for next time step, lower limit 82 °C:
$$T_{cool,i+1} = T_{cool,i} + \Delta T_{cool,i}$$

The simulation results for the coolant temperature and for the fan power at the clutch input shaft in comparison with the measurement values are shown in Figure 46 and Figure 47.

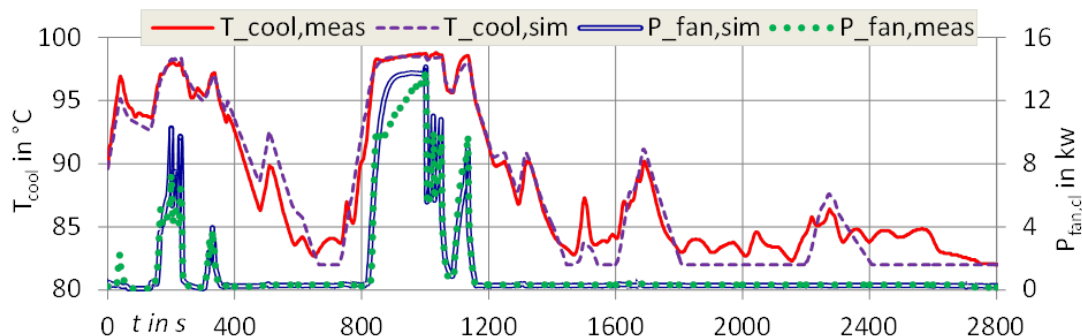


Figure 46. Comparison of simulation and measurement results, coolant temperature engine outlet (T_{cool}) and fan power at its clutch input shaft ($P_{fan,cl}$). VECTO Long Haul cycle 2012, part 1

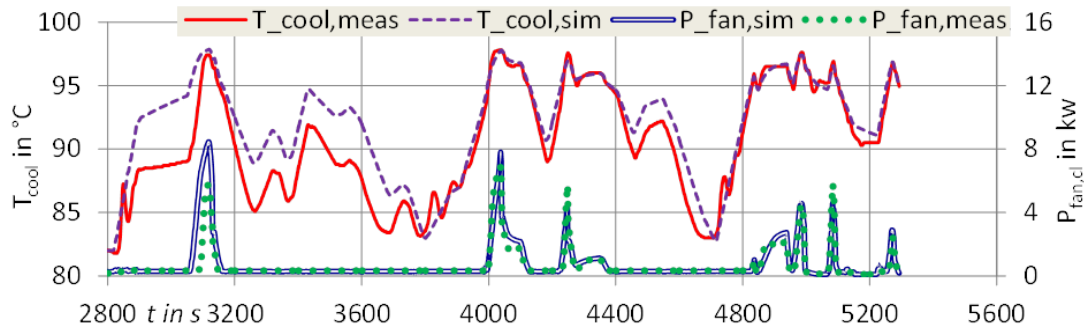


Figure 47. Fan, simulation and measurement results, VECTO Long Haul cycle 2012, part 2

The distinction between the states fan-off and fan-on and the magnitude of the fan power demand are calculated reliably, with a few exceptions, e. g. at second 40. The simple model for the coolant temperature matches the measurement values sometimes well and other times poorly. E. g. at 760 s and 2'850 s the negligence of the outer coolant circuit, where the radiator was cooled down to low temperatures before, leads to a deviation. If the cooling demand increases in that case due to higher waste heat, at first the thermostat is opened and the radiator heats up, hence the coolant temperature remains lower than for an already hot radiator. This behaviour is shown in Figure 48.

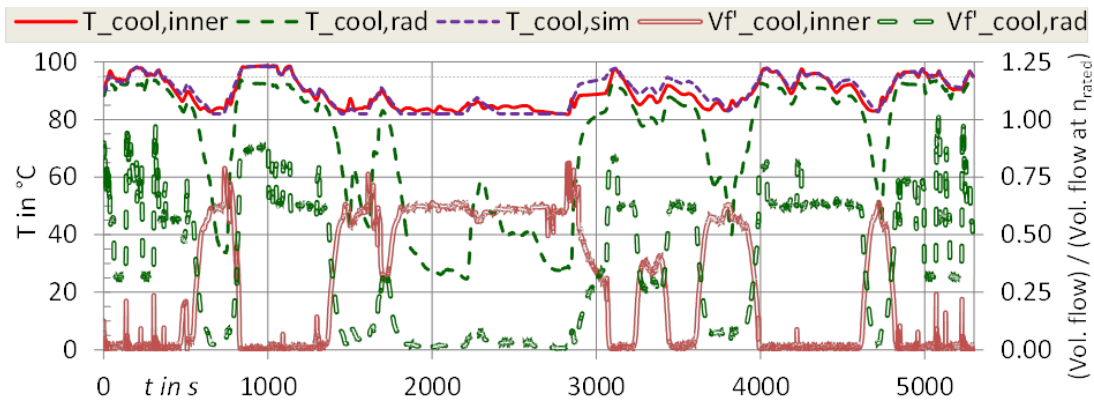


Figure 48. Measurement values for coolant temperature and volume flow of inner engine and outer radiator circuit, simulated coolant temperature of effective thermal mass.

The simplification of one effective thermal mass causes in the two activation phases at 760 s and 2'850 s a longer fan operation at higher power. The simulated fan work is 0.13 kWh_{mech} higher than measured, what increases the overall mean fan power by 0.1 kW_{mech}, hence 9 % of the average value.

A summary of the mean results from measurement, from the simulation with the reference calibration factors and from a simulation with a parameter variation for the calibration factors effective heat capacity C_{eng} and radiator curves 2 and 3, p. 45 Figure 45, is given in Table 5.

Table 5. Mean values; measurement; simulation with reference calibration factors (line "Simulation"); parameter variation for effective heat capacity (C_{eng}) and heat flow coefficient curves of the radiator

	T_{cool}	$ T_{cool,meas} - T_{cool,sim} $	$ \Delta T_{cool}/\Delta t $	$n_{fan,on}$	$W_{fan,on}$	$t_{fan,on}$	$P_{fan,off\&on}$	\dot{m}_{air}	\dot{Q}_{rad}
	°C	°C	K/s	rpm	kWh _{mech}	%t _{cycle}	kW _{mech}	kg/s	kW _{th}
Measurement	89.3		0.059	707	1.19	21.9	1.05	1.579	64.2
Simulation	89.9	1.42	0.049	717	1.35	14%	22.8	1.606	62.6
<i>Parameter variation</i>									
$C_{eng} = 650 \text{ kJ/K}$	89.8	1.39	0.052	731	1.42	19%	23.0	1.61	63.0
$C_{eng} = 750 \text{ kJ/K}$	89.9	1.48	0.047	703	1.29	9%	22.7	1.60	62.3
Q_{rad} : curve 2	89.7	1.39	0.049	746	1.46	23%	22.9	1.62	63.0
Q_{rad} : curve 3	88.2	1.36	0.047	712	0.97	-18%	15.5	1.52	69.2

With the simple model, calibrated to the one available measurement run, the mean value for the fan's power demand is matched acceptably.

It can be assumed that the grade of detail and accuracy are not good enough to depict a cooling system's behaviour without a preceding calibration of heat capacity and radiator curve. These input values influence the simulation results decisively, like shown in Table 5. Hence without further analysis and refinement this model is not suitable for a standardised simulation approach like in VECTO.

Also it shall be stated, that the adjustment of the model to only one set of measurement data is insufficient to judge its quality. More comparisons are necessary to determine, if such a simple model works for other layouts of the cooling system or other driving cycles. These restrictions need to be taken into account when interpreting the further results from the model.

The further analysis showed, that a detailed fan model is currently not necessary for the VECTO approach. The distinction between the fan as intermittent power consumer or one average constant power demand changes the overall FC very little, compare also p. 24 ff. chapter 2.2.3 on the FC-line. The calibrated fan model for a tractor trailer, 330 kW rated engine power and 19.3 t payload, was used to simulate the intermittent fan power for the VECTO truck cycles without Municipal utility⁴¹. The differences between the fan as intermittent or constant power consumer were analysed, also the saving potential of a viscous clutch, which can be decoupled in idling state. With such a device the idling losses from 0.1 to 0.5 kW could be avoided. The mean results are shown in Table 6, and for some time courses see p. 213 section 5.15.

Table 6. Average values of simulation results for the fan's share at the overall FC at different payloads

	FC_{tot} in L/100km	T_{cool} in °C	n_{fan,on} in rpm	W_{fan,on} in kWh	t_{fan,on} in %t_{cycle}	P_{fan,off&on} in kW	P_{fan,off&on} ACEA in kW	FC_{fan} in %FC_{tot}	%FC, P_{fan} = const.	%FC, de- coupl.
Long Haul 2012, 19.3 t	35.6	89.3	707	1.19	22	1.05	0.62	0.9	-0.08	-0.2
Long Haul 2015, 19.3 t	31.5	87.6	662	0.38	9	0.56	0.62	0.5	-0.02	-0.2
0 t	22.2	82.8	off	0.00	0	0.28	0.62	0.3	0.00	-0.3
25.6 t	34.6	89.2	593	0.59	17	0.70	0.62	0.6	-0.03	-0.2
Reg. Delivery '12, 19.3 t	39.5	91.1	395	0.07	14	0.36	0.67	0.3	-0.01	-0.1
0 t	23.7	82.5	off	0.00	0	0.22	0.67	0.3	0.00	-0.3
25.6 t	44.8	92.9	463	0.20	28	0.61	0.67	0.5	-0.02	-0.1
Urb. Delivery, '12 19.3 t	50.3	92.2	397	0.13	15	0.29	0.52	0.4	-0.02	-0.1
Construction, 19.3 t	57.5	91.0	489	0.28	25	0.55	1.05	0.7	-0.05	0.0

Note: FC_{tot} - Total FC of vehicle; T_{cool} - Coolant temp.; n_{fan,on} - Rotational speed of fan, case "fan-on"; W_{fan,on} - Work demand of fan, case "fan-on"; t_{fan,on} - Duration of phases "fan-on"; P_{fan,off&on} - Overall power of fan, cases "fan-off" and "fan-on"; P_{fan,off&on} ACEA - ACEA table values; FC_{fan} - Overall FC of fan, cases "fan-off" and "fan-on"; %FC, P_{fan} = const. - Change of FC_{tot}, when the intermittent fan power is replaced by its average constant value; %FC, decoupl. - Change of FC_{tot}, when the idling fan is decoupled from the engine

It is obvious, that the intermittent change of the fan's power demand can be neglected for the total FC, if a realistic value for the constant average power demand is chosen. The change in total FC is below 0.1 %.

The variation of the payload from empty to full influences the engine power demand, the waste heat and the fan power. For the Long Haul cycle 2015 the average fan power varies from 0.3 to 0.7 kW_{mech} for empty and full vehicle, for the Regional Delivery cycle 2012 from 0.2 to 0.6 kW_{mech}.

⁴¹ The Municipal Utility cycle was not analysed for the fan power, because it aims at garbage trucks and consists of 53 % standstill. There the hydraulic pumps for lifting device and waste press consume up to 30 kW_{mech} from the power take-off at engine or gearbox (525), what is not foreseen for long haul trucks.

Another result is, that a viscous clutch, decoupled when idling, offers a small saving potential from 0.0 to 0.3 %. If such a decoupler will reach the payback in e. g. 3 years, depends on its price, the annual mileage and the development of the fuel price.

An outcome of the time course from MAHLE's measurement and the own simulation is, that for this vehicle model the fan is turned on only during long engine full load, see p. 213 section 5.15, what means long uphill driving or acceleration. Thus on cycles with less road gradient or mainly short acceleration phases the fan power demand is low.

The model for the fan was used to analyse its typical behaviour in HDV cycles and to check the default values for the average fan power provided by industry and used in the standard VECTO mode for CO₂ certification.

For the HDV models of this thesis also the default table values for the average fan power were applied to be in line with the future CO₂ legislation (55), Annex XI p. 265.

2.3.2 Compressor

The compressor is a 2-stroke piston machine, delivering air into pressure vessels to feed the consumers pneumatic brakes, air suspension and pneumatic actuators at engine, clutch, gearbox and drivetrain, seldom also the AdBlue doser. An example is shown in Figure 49.

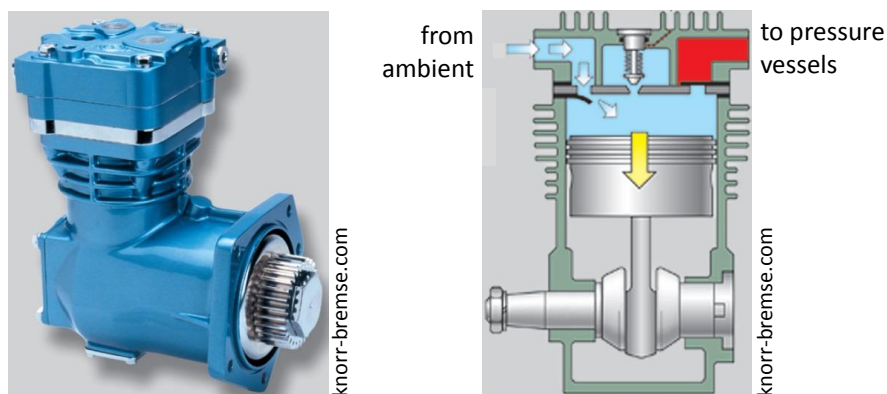


Figure 49. Left: One-cylinder compressor, one-stage, water-cooled. Right: Working principle.

In this section the measurement of the air consumption is described and an existing model (115 p. 79) for the compressor power analysed and elaborated.

2.3.2.1 Measurement of the pneumatic system of a delivery truck

For a delivery truck GVWR 12 t, diesel engine inline-6, 175 kW @ 2200 rpm, compare p. 195 Table 59 first entry, the pneumatic system was measured in 2015-02 for air pressure and air temperature.

The measurement setup is shown in Figure 50.

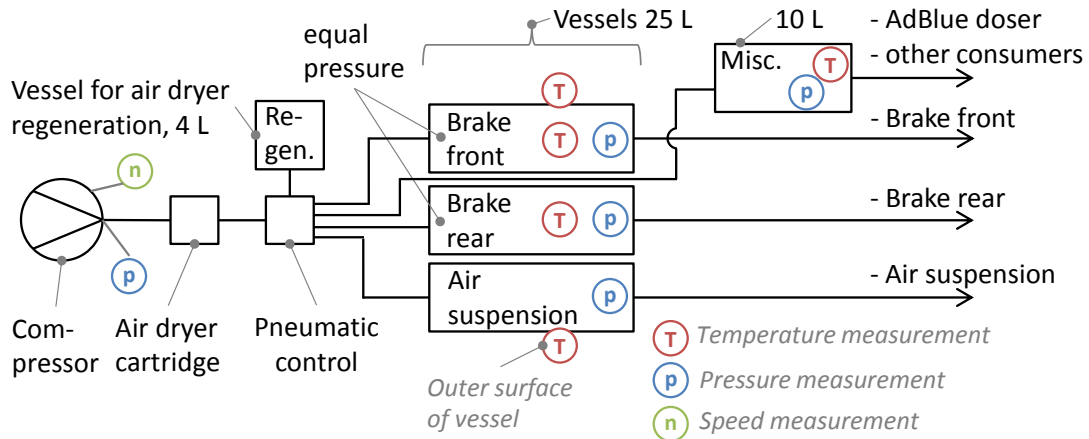


Figure 50. Measurement setup for the pneumatic system of a delivery truck 12 t.⁴²

At first the time course of the air mass in the vessels was elaborated, what will be the basis for the determination of the compressor performance in a later stage. The air mass was calculated by the ideal gas law, where air temperature, air pressure and the vessel volumes were input values. An example for the measured temperature and pressure is shown in Figure 51.

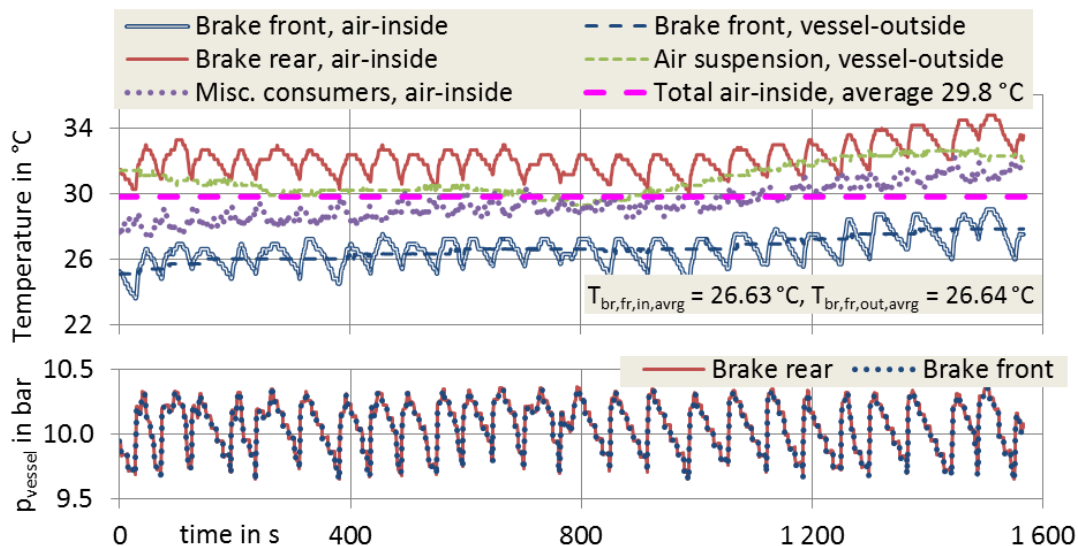


Figure 51. Chassis dyno, Reg. Delivery cycle 2012, air temperature all vessels, air pressure brake vessels

where: p_{vessel} Air pressure in vessel
 $T_{\text{br,fr,in}}$ Air temperature in vessel front brake
 $T_{\text{br,fr,out}}$ Material temperature of outer surface of vessel front brake

The average values of the temperatures of the air inside the vessel “brake-front” and outside on the wall of this vessel were very close to each other. It was assumed, that the same is valid for the vessel air suspension, where the air temperature could not be measured directly due to technical reasons. Hence this temperature should be close the outside wall temperature, the green dotted line in the diagram above.

Another result was, that the air temperatures in the four vessels “brake-front”, “brake-rear”, “air suspension” and “miscellaneous consumers” can be replaced by the total average air temperature. The variation of the temperatures in the vessels are mainly caused by mass changes due to air loss to consumers and air gain by delivery from the compressor.

⁴² The vessel for air dryer regeneration was not measured and neglected in the analysis, what is acceptable due to its small share of 4.5 % at the overall vessel volume.

The absolute air temperatures in K vary from -2.0 % to +1.7 % around the overall average air temperature of 303 K (= +29.8 °C, see e. g. Figure 51 upper diagram), hence it is acceptable to work with the mean value.

The air mass in the four vessels was calculated in steps of 1 s with the ideal gas law for dry air. The volume of the vessels brake front/rear and suspension is equal at 25 L, the volume of the vessel for miscellaneous consumers is 10 L, and the pressure in the two brake vessels is equal, hence it can be written in Equation 21

Equation 21. Ideal gas law (147 p. 164) and calculation of total air mass in vessels

$$p_{\text{vessel}} \cdot V_{\text{vessel}} = m_{\text{air,vessel}} \cdot R_{\text{s,air}} \cdot T_{\text{air,vs,avrg}}$$

$$\text{with: } p_{\text{br-front}} = p_{\text{br-rear}} = p_{\text{br}}, V_{\text{br-front}} = V_{\text{br-rear}} = V_{\text{susp}} = 0.025 \text{ m}^3$$

$$\Rightarrow m_{\text{air,tot}} = \frac{(p_{\text{br}} + p_{\text{br}} + p_{\text{susp}}) \cdot 0.025 \text{ m}^3 + p_{\text{misc}} \cdot 0.010 \text{ m}^3}{R_{\text{s,air}} \cdot T_{\text{air,vs,avrg}}}$$

$$\Rightarrow V_{\text{air,tot,std}} = \frac{m_{\text{air,tot}}}{\rho_{\text{air,std}}}$$

where: $\rho_{\text{air,std}}$ Density of dry air at standard conditions (20 °C, 1.013 bar): 1.204 kg/m³

$m_{\text{air,vessel}}$ Air mass in one vessel

$m_{\text{air,tot}}$ Total air mass, vessels brake front, brake rear, air suspension, miscellaneous

p_{br} Air pressure in brake vessels, equal for both vessels

p_{misc} Air pressure in vessel for miscellaneous consumers

p_{susp} Air pressure in vessel for air suspension

$R_{\text{s,air}}$ Specific gas constant for dry air, 287.1 J/(kg·K)

$T_{\text{air,vs,avrg}}$ Average air temperature in vessels, here 303 K (= +29.8 °C)

$V_{\text{air,tot,std}}$ Total air content, mass unit of standard litres air [sl], = 0.001204 kg

V_{vessel} Volume of air vessel

The pressure in the vessels was measured plus analysed and the temporal course of the total air content in all four vessels was calculated based on the single pressures and the average air temperature, shown in Figure 52.

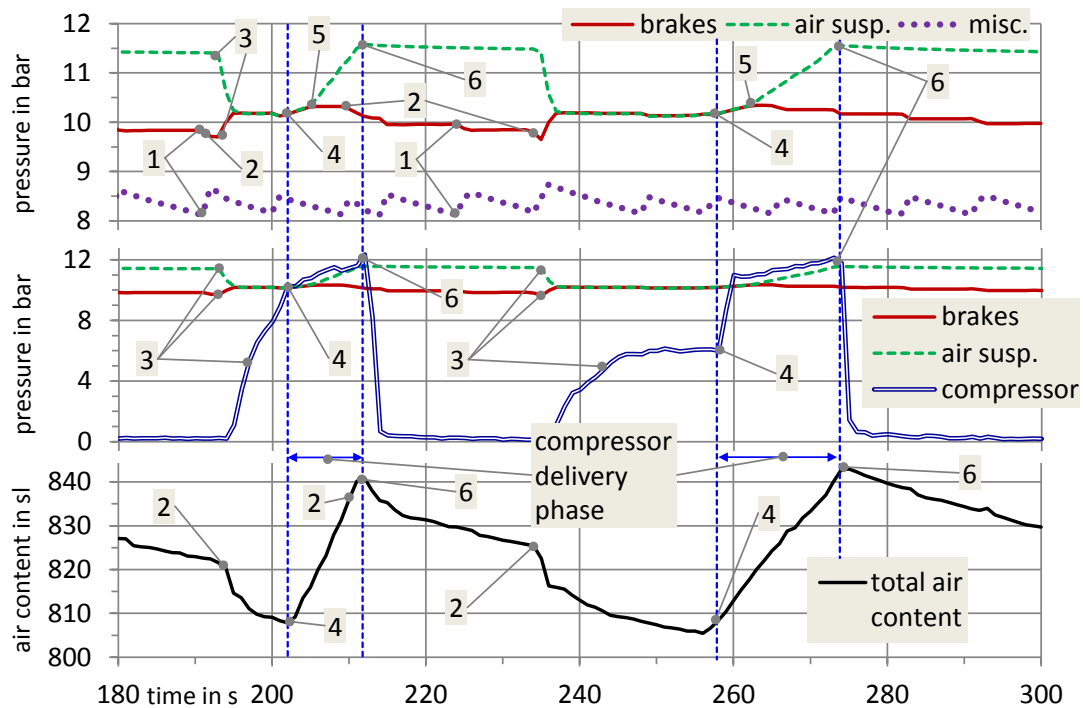


Figure 52. Pressure course in air vessels and total air content, section of Reg. Delivery cycle 2012⁴³
sl – standard litre of dry air. Mass of 1 L dry air at 1.013 bar and +20 °C, equals 0.001204 kg/L

- where:
1. The vessel for miscellaneous consumers is refilled from the brake vessels (trigger: $p_{\text{misc},\text{min}} \approx 8.2$ bar).
 2. Braking: The average pressure drop per brake actuation in the coupled brake vessels is ca. 0.12 bar on the chassis dyno (RD12 and UD-12 flat) and ca. 0.17 bar on the road (cycle "Inffeldgasse").
 3. The brake and suspension vessels are coupled at the start of the filling phase (trigger: $p_{\text{br},\text{min}} \approx 9.7$ bar). Probably due to pressure equalisation between compressor outlet and the vessels and/or regeneration of the air dryer cartridge the overall air content in the four probed vessels decreases. The behaviour of the complete pneumatic system during this phase could not be determined exactly.
 4. The compressor starts, when its outlet pressure equals the vessel pressure.
 5. The brake and suspension vessels are decoupled (trigger: $p_{\text{br},\text{max}} \approx 10.4$ bar) and the compressor continues to deliver into the suspension vessel.
 6. The compressor stops (trigger: $p_{\text{susp},\text{max}} \approx 11.6$ bar).

⁴³ The given courses for measured air pressure and the calculated overall air mass refer only to the four analysed vessels brakes, air suspension and miscellaneous consumers and the pressure at the compressor outlet. Events like pressure equalisation and the behaviour of the small vessel for regeneration could not be measured directly.

With the ideal gas law the consumption per actuation was calculated for the brakes and for the continuous consumption of air suspension and miscellaneous consumers, see Table 7. The calculation of the air delivery rate by the compressor is described below in Equation 22.

Table 7. Air consumption of pneumatics and delivery rate of compressor

	T _{air} in °C		Air consumption								Air delivery	
	Ves- sels	Am- bient	Brakes		Air sus- pension		AdBlue doser		Pneumatic actuators		Compressor	
			bar/ act.	sl/ act.	bar/ min.	sl/ min.	bar/ min.	sl/ min.	bar/ min.	sl/ min.	L _{amb} / stroke	sl/ stroke
Dyno	30	24	0.12	5.8	0.19	4.5	2.1	20.1	0.8	8.5	0.169	0.167
Road	12	6	0.17	8.7	0.36	9.1	2.1	21.3	0.8	8.5	0.169	0.178
VECTO standard	26	20	0.17	8.3	0.36	8.7	2.1	20.3	0.8	8.5	0.169	0.169

Note: Overall average values, air volumes corrected for varying (ambient) temperatures. Cycles RD12 and UD12-flat on chassis dyno, cycle "Inffeldgasse" on road. Air demand AdBlue doser from (103 p. 212). **bar/act.** - Pressure drop [bar] per actuation; **sl/act.** - Air consumption [sl] per actuation; **bar/min.** - Pressure drop [bar] per minute; **sl/min.** - Air consumption [sl] per minute; **L_{amb}/stroke** - Delivered air volume [L] at ambient conditions per stroke; **sl/stroke** - Delivered air mass [sl] per stroke

The air consumption per brake actuation, calculated from the measurement, is close to values delivered by the industry, when corrected to the standard ambient temperature of 20 °C (line "VECTO standard") and referred to the vehicle mass. The result for the truck of test mass 12 t was 0.692 sl/t per braking (= consumption of air [sl], per vehicle mass [t] and per brake-actuation), the default value from industry was 0.600 sl/t (103 p. 212).

Concerning the possible leakage of the pneumatic system of the truck, a vehicle used only for measurements with an age of 3.83 years and a mileage of 13'000 km, it was found that the air loss can be neglected. During 6 h of deactivated vehicle a very low leakage of 0.55 sl/h was determined, what is below 0.1 % of the lowest air demand during the truck cycles.

With the known consumption values the air balance was set up for the compressor delivery phases, given in Equation 22. The simplification is, that the air volume delivered per compressor stroke is constant, independent on rotational speed and backpressure.

Equation 22. Air balance for delivery phases and delivered air volume

$$\Delta m_{\text{air,compr}} = \Delta m_{\text{air,vessels}} + \sum_{\Delta t.\text{compr}} (\Delta m_{\text{br}}) + \left(\frac{\Delta m_{\text{misc}}}{\Delta t} + \frac{\Delta m_{\text{susp}}}{\Delta t} \right) \cdot \Delta t_{\text{compr}}$$

$$\Rightarrow V_{\text{air,amb,deliv}}(i) = \frac{n_{\text{compr}}(i)}{\sum_{\Delta t.\text{compr}} (n_{\text{compr}})} \cdot \frac{\Delta m_{\text{air,compr}}}{\rho_{\text{air,amb}}}$$

- where:
- $\sum_{\Delta t.\text{compr}} (\Delta m_{\text{br}})$ Summarised air consumption of brakes during delivery phase
 - $\sum_{\Delta t.\text{compr}} (n_{\text{compr}})$ Sum of all compressor rotations during delivery phase
 - $\Delta m_{\text{air,compr}}$ Air mass to be delivered by compressor
 - $\Delta m_{\text{air,vessels}}$ Difference of air content in vessels, end to start of deliv. phase
 - $\Delta m_{\text{misc}}/\Delta t$ Average air consumption rate of miscellaneous consumers
 - $\Delta m_{\text{susp}}/\Delta t$ Average air consumption rate of suspension
 - Δt_{compr} Duration of compressor delivery phase
 - $\rho_{\text{air,amb}}$ Ambient air density
 - $n_{\text{compr}}(i)$ Rotational compressor speed at second "i" of delivery phase
 - $V_{\text{air,amb,deliv}}(i)$ Air volume delivered at second "i" of deliv. phase, ambient density

The result for the delivered air volume per minute for all measured delivery phases is shown in Figure 53 left.

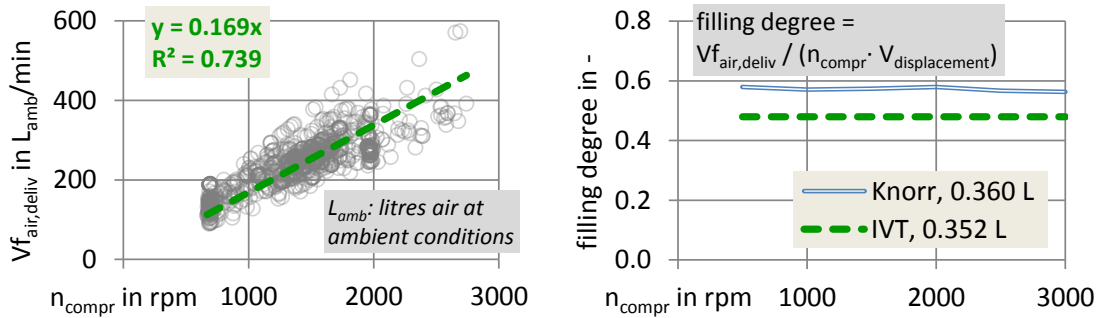


Figure 53. Left: Air volume per compressor stroke. Right: Comparison of filling degree (148 p. 2)⁴⁴

IVT: Compressor analysed at the “*Institut für Verbrennungskraftmaschinen und Thermodynamik*” of TU Graz.
Knorr: Compressor, where data is available, similar to “*IVT*”.

There is a clear correlation between delivery air flow and compressor speed, hence the assumption of a constant delivered volume per stroke was justified, here 0.169 L at ambient conditions. The resulting average filling degree of the analysed compressor with a displacement of 0.352 L is at 0.48 similar to the published value 0.56 of a compressor 0.360 L of the same design, see Figure 53 right. The analysed compressor was measured with the flow resistances air dryer cartridge and pneumatic control downstream its outlet valve, compare p. 51 Figure 50, hence a lower filling degree is plausible.

In addition the measured compressor data was compared to other models, see Figure 54.

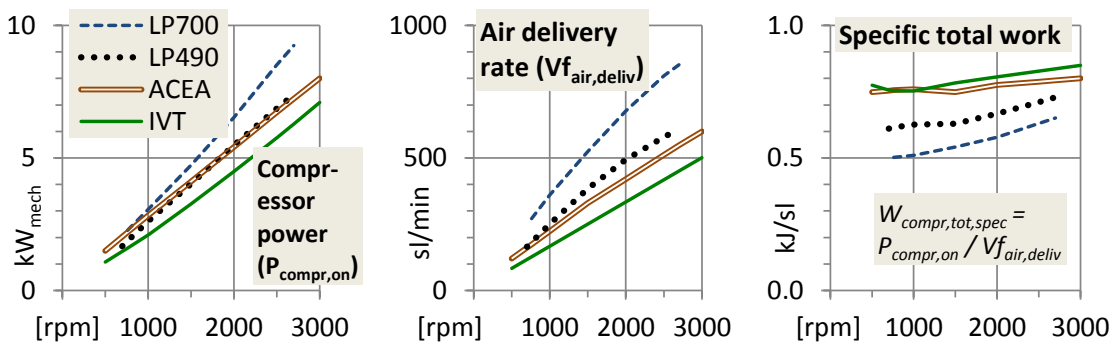


Figure 54. Comparison of compressors. (149 p. 211), (150)

where: $P_{\text{compr,on}}$ Total compressor power at delivery (power curves “*IVT*” available)

$\dot{V}_{\text{air,deliv}}$ Air delivery rate

$W_{\text{compr,tot,spec}}$ Specific total delivery work, $W_{\text{compr,tot,spec}} = P_{\text{compr,on}} / \dot{V}_{\text{air,deliv}}$

In addition to the filling degree also further values like delivery power, delivery rate and specific total work are in-line with other compressor models.

2.3.2.2 Calculating air consumption and compressor power demand

An existing compressor model was analysed and elaborated to calculate the average power demand. It is based on an approach described by Ricardo (115 p. 79), its calculation scheme is shown in the data section, p. 214 Figure 211. A detailed simulation of the pneumatic system with accurate allocation of single consumption events, pressurisation between vessels and delivery phases is complex and out of scope of this work and the VECTO approach.

⁴⁴ Examined compressor (“*IVT*”): Wabco 412 154 004 0, one cylinder, displacement 352 cm³, bore 8.5 cm, stroke 7.2 cm, water cooled, rotational speed up to 3000 rpm. Compressor from literature: Knorr VF00200_370, one cylinder, displacement 360 cm³, bore 9.2 cm, stroke 7.1 cm, water cooled, rotational speed up to 3000 rpm.

For the model the average air consumption, i. e. the total air consumption divided by the cycle duration ($\dot{V}_{\text{air,consumpt}} / \Delta t_{\text{cycle}}$), was assumed to be also the average delivery rate of the compressor ($\dot{V}_{\text{air,deliv,tot}} / \Delta t_{\text{cycle}}$). From the calculated consumption values, compare p. 54 Table 7, the delivery rate was determined for the measured driving cycles, see Table 8.

Table 8. Average air delivery rates as examples for the input data for the compressor model

Driving cycle	Dyno, RD12	Dyno, UD12-flat	Road, "Inffeldgasse"
$\dot{V}_{\text{air,deliv,tot}} / \Delta t_{\text{cycle}}$, calculated from Table 7	39.3 sl/min	40.5 sl/min	62.5 sl/min

To depict the compressor power, first the additional delivery power ($\Delta P_{\text{compr,deliv}}$), i. e. the difference between idle and total delivery power, is defined. This was done for the measured compressor "IVT", which is also treated in the rest of this chapter. Its curves for idle and delivery power were known, for the resulting additional delivery power see Figure 55.

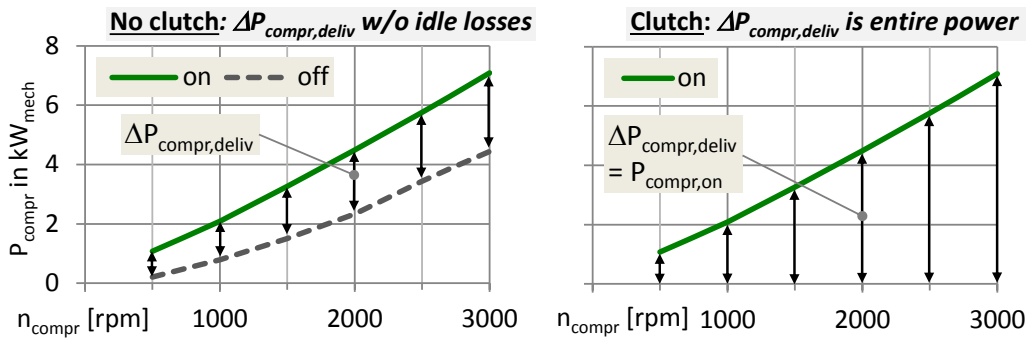


Figure 55. Left: Additional delivery power ($\Delta P_{\text{compr,deliv}}$), compressor "IVT". Right: $\Delta P_{\text{compr,deliv}}$ "IVT with clutch", calculated by omitting the idle losses.

where: $\Delta P_{\text{compr,deliv}}$ Additional compressor delivery power

$$\Delta P_{\text{compr,deliv}} = P_{\text{compr,on}} - P_{\text{compr,off}}$$

$P_{\text{compr,off}}$ Compressor power at idle (= 0 in case of clutch)

The ratio of the additional delivery power to the air delivery rate is the additional specific delivery work ($W_{\text{compr,deliv,spec}}$), which is shown in Figure 56.

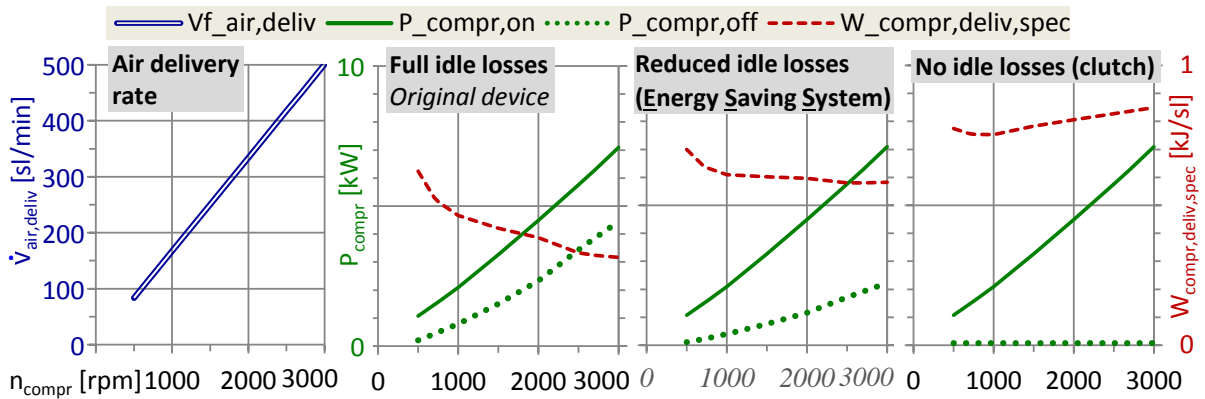


Figure 56. Compressor "IVT", additional specific compressor delivery work ($W_{\text{compr,deliv,spec}}$)

where: $W_{\text{compr,deliv,spec}}$ Additional specific compressor delivery work

$$W_{\text{compr,deliv,spec}} = (P_{\text{compr,on}} - P_{\text{compr,off}}) / \dot{V}_{\text{air,deliv}} = \Delta P_{\text{compr,deliv}} / \dot{V}_{\text{air,deliv}}$$

In case of a high power demand at idle like for the measured compressor "IVT" (Figure 56 "Full idle losses") the specific delivery work becomes small, for no idle power due to a clutch it equals the specific total delivery work, compare Figure 56 right and Figure 54 right.

For the compressor model the following assumptions were made:

- The additional FC of the compressor is independent of the temporal distribution of its accumulated work, compare p. 24 ff. section 2.2.3 on the "FC-line".
- The delivery phases can be of arbitrary duration and distribution, only the total delivered air volume ($V_{\text{air,deliv,tot}}$) needs to match the overall air consumption ($V_{\text{air,consumpt}}$):

$$V_{\text{air,deliv,tot}} = V_{\text{air,consumpt}}$$
- The compressor speed (n_{compr}), its power consumption at idle ($P_{\text{compr,off}}$) and delivery ($P_{\text{compr,on}}$) and its additional specific delivery work ($W_{\text{compr,deliv,spec}}$) are constant during one time step Δt , here 1 s.

With these assumptions the following theoretical conception is made:

- One volume fraction of compressed air ($V_{\text{air,deliv,fract}}$) is delivered per single time step Δt .

$$\rightarrow V_{\text{air,deliv,fract}} / \Delta t = V_{\text{air,deliv,tot}} / \Delta t_{\text{cycle}}; \text{ for } V_{\text{air,deliv,tot}} / \Delta t_{\text{cycle}} \text{ see p. 56 Table 8.}$$
- The compressor turns on and off *within one time step* to deliver the volume fraction $V_{\text{air,deliv,fract}}$: Assumption of a smaller time step $\Delta\tau$ within the calculation time step Δt . This is not feasible in practice, but necessary for the theoretical model.
- The volume fraction $V_{\text{air,deliv,fract}}$ is delivered at the current specific delivery work $W_{\text{compr,deliv,spec}}$, which depends on the current compressor speed, see p. 56 Figure 56.
- The product of the current specific delivery work and the volume fraction is the *additional compressor delivery work* during one time step Δt :

$$\Delta W_{\text{compr,deliv}} = W_{\text{compr,deliv,spec}} \cdot V_{\text{air,deliv,fract}}$$
- Because the additional compressor delivery work ($\Delta W_{\text{compr,deliv}}$) during one time step is calculated, it can be used to calculate the average additional compressor delivery power ($\Delta P_{\text{compr,deliv,\Delta t}}$) in that time step Δt (here 1 s): $\Delta P_{\text{compr,deliv,\Delta t}} = \Delta W_{\text{compr,deliv}} / \Delta t$. Compare Figure 57.

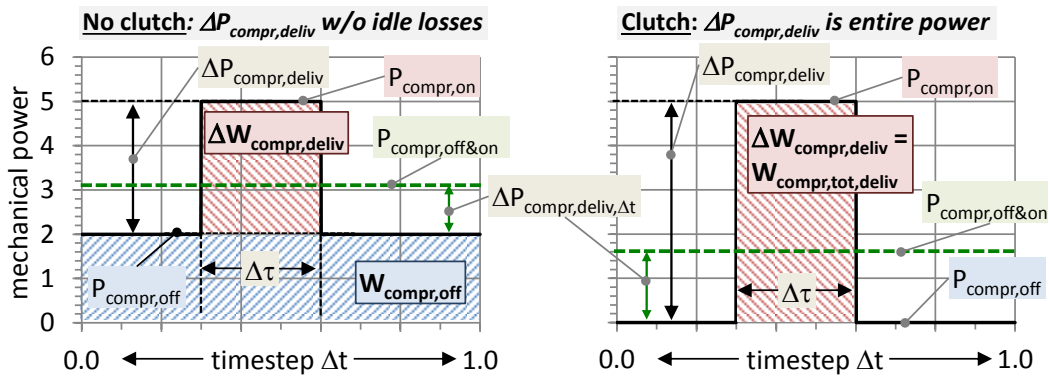


Figure 57. Average additional compressor delivery power in time step Δt .

where: $\Delta\tau$ Smaller time step in which the air volume $V_{\text{air,deliv,fract}}$ is delivered within the calculation time step Δt . Dependent on the current compressor speed: $\Delta\tau = V_{\text{air,deliv,fract}} / \dot{V}_{\text{air,deliv}}(n_{\text{compr}})$

In seldom cases, at very high air demand ($V_{\text{air,deliv,fract}} \uparrow$) and/or very low air delivery from the compressor at low speeds ($\dot{V}_{\text{air,deliv}}(n_{\text{compr}}) \downarrow$) the time step $\Delta\tau$ can get bigger than Δt . In this case the approach would cause an error of the compressor power for these phases. This was not the case for the treated vehicle models.

$\Delta P_{\text{compr,deliv}}$ Additional compressor delivery power, see also p. 56 Figure 55

$\Delta P_{\text{compr,deliv},\Delta t}$	Average additional compressor delivery power in time step Δt $\Delta P_{\text{compr,deliv},\Delta t} = P_{\text{compr,off\&on}} - P_{\text{compr,off}} = \Delta W_{\text{compr,deliv}} / \Delta t$ <i>Because the additional FC of the compressor is independent of the temporal distribution of its accumulated work demand, the expression ($\Delta P_{\text{compr,deliv},\Delta t} = \Delta W_{\text{compr,deliv}} / \Delta t$) is permissible.</i>
Δt	Time step for calculation, here 1 s.
$\Delta W_{\text{compr,deliv}}$	Additional compressor delivery work for air volume fraction. $\Delta W_{\text{compr,deliv}} = W_{\text{compr,deliv,spec}} \cdot V_{\text{air,deliv,fract}} = \Delta P_{\text{compr,deliv}} \cdot \Delta \tau$
$P_{\text{compr,off\&on}}$	Average compressor power for idle and delivery phases, time step Δt $P_{\text{compr,off\&on}} = (W_{\text{compr,off}} + \Delta W_{\text{compr,deliv}}) / \Delta t$
$W_{\text{compr,off}}$	Compressor work at idle, $W_{\text{compr,off}} = P_{\text{compr,off}} \cdot \Delta t. = 0$ for clutch.
$W_{\text{compr,tot,deliv}}$	Total compressor work during air delivery, including all idle losses

➔ *With exception of Δt all values are dependent on the current compressor speed.*

The average compressor power per time step ($P_{\text{compr,off\&on}}$), including idle and delivery, is defined in Equation 23.

Equation 23. Average compressor power in one simulation time step

$$\begin{aligned}
P_{\text{compr,off\&on}} &= W_{\text{compr}} / \Delta t \\
&= (W_{\text{compr,off}} + \Delta W_{\text{compr,deliv}}) / \Delta t \\
&= (P_{\text{compr,off}} \cdot \Delta t + W_{\text{compr,deliv,spec}} \cdot V_{\text{air,deliv,fract}}) / \Delta t \\
&\text{with } V_{\text{air,deliv,fract}} / \Delta t = V_{\text{air,deliv,tot}} / \Delta t_{\text{cycle}} \\
&= P_{\text{compr,off}} + W_{\text{compr,deliv,spec}} \cdot V_{\text{air,deliv,tot}} / \Delta t_{\text{cycle}}
\end{aligned}$$

Note: $P_{\text{compr,off}}$ and $W_{\text{compr,deliv,spec}}$ are dependent on the current compressor speed.

where: Δt_{cycle}	Cycle duration, dependent on vehicle model and cycle characteristics
$V_{\text{air,deliv,tot}}$	Total delivered air volume over driving cycle, equals total air consumption, calculated from air consumption of vehicle model and cycle characteristics
$V_{\text{air,deliv,fract}}$	Air volume fraction, delivered in time step Δt
W_{compr}	Overall compressor work, idle and delivery phases

As result from this model the overall compressor work during the driving cycle equals the sum of the total work from the idle losses plus the product of total delivered air volume and the average additional delivery work, like shown in Equation 24.

Equation 24. Overall compressor work during driving cycle

$$\begin{aligned}
W_{\text{compr}} &= \int_0^{t.\text{end}} (P_{\text{compr,off\&on}}) dt \\
&= \int_0^{t.\text{end}} (P_{\text{compr,off}} + \Delta P_{\text{compr,deliv},\Delta t}) dt \\
&= \int_0^{t.\text{end}} (P_{\text{compr,off}}) dt + \int_0^{t.\text{end}} (W_{\text{compr,deliv,spec}} \cdot V_{\text{air,deliv,tot}} / \Delta t_{\text{cycle}}) dt \\
&= \int_0^{t.\text{end}} (P_{\text{compr,off}}) dt + V_{\text{air,deliv,tot}} \cdot \int_0^{t.\text{end}} (W_{\text{compr,deliv,spec}}) dt / \Delta t_{\text{cycle}} \\
&= \int_0^{t.\text{end}} (P_{\text{compr,off}}) dt + V_{\text{air,deliv,tot}} \cdot W_{\text{compr,deliv,spec,avrg}}
\end{aligned}$$

where: $\int_0^{t.end}$ Integral from start to end of driving cycle

$W_{compr,deliv,spec,avrg}$ Average of additional specific delivery work (p. 56 Figure 56, red dashed curves), average value over all compressor speed values during simulated driving cycle.

The advantage of this model is, that the influence of the compressor speed on the average additional specific delivery work is depicted accurately. The course of the compressor speed is not known at simulation start. In Equation 24 in the 2nd line the summand $\Delta P_{compr,deliv,\Delta t}$ (average additional compressor delivery power per time step Δt) reflects the influence of the current compressor speed. $\Delta P_{compr,deliv,\Delta t}$ depends on the additional specific delivery work ($W_{compr,deliv,spec}$, see p. 56 Figure 56, red dashed curves) and therefore on the speed.

$\Delta P_{compr,deliv,\Delta t}$ can be expressed as a characteristic curve for the simulated combination of air demand and compressor type. The work flow is enlisted below.

1. The input values are the curves for compressor power at delivery ("on", $P_{compr,on}$), compressor power at idle ("off", $P_{compr,off}$, equals 0 in case of clutch) and compressor air delivery rate ($\dot{V}_{air,deliv}$), shown in Figure 58. Necessary are also the values for the total delivered air volume ($V_{air,deliv,tot}$), which equals the overall air consumption from the HDV model, and the cycle duration (Δt_{cycle}), compare p. 56 Table 8.

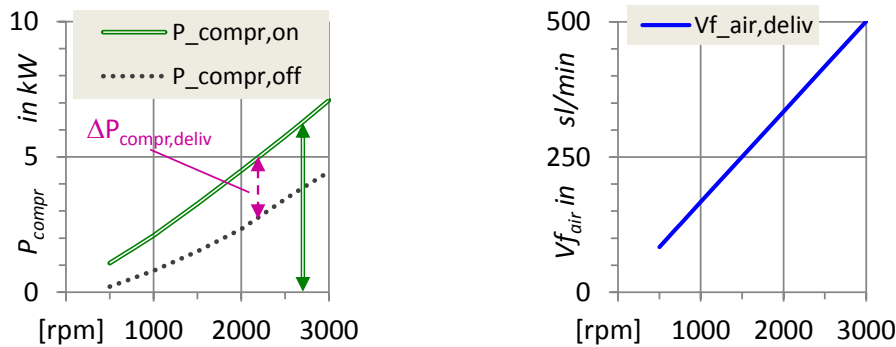


Figure 58. Compressor "IVT". Curves for power at delivery, power at idle and air delivery rate.

2. Divide the difference between delivery and idle power by the delivery rate, the result is the specific additional delivery work: $W_{compr,deliv,spec} = (P_{compr,on} - P_{compr,off}) / \dot{V}_{air,deliv}$, compare Figure 59 left.

3. Multiply the specific additional delivery work with the quotient of total delivered air volume and cycle duration, and add the result to the compressor idle power. The result is the average compressor power for the states idle and delivery, dependent on its speed: $P_{compr,off\&on} = P_{compr,off} + W_{compr,deliv,spec} \cdot V_{air,deliv,tot} / \Delta t_{cycle}$, see Figure 59 right.

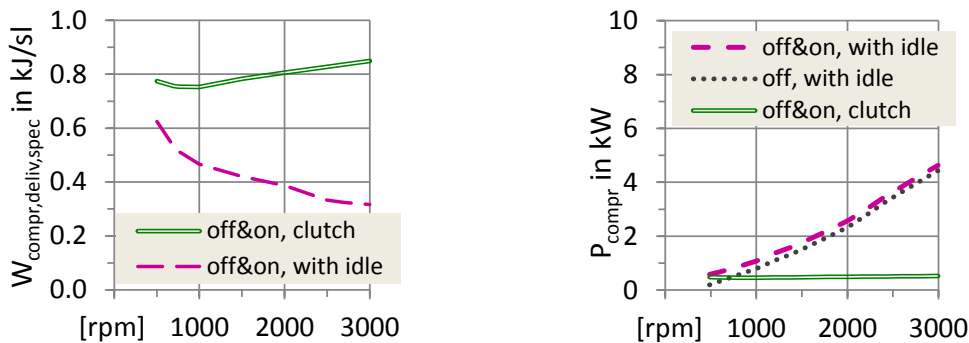


Figure 59. Compressor "IVT". Curves spec. additional delivery work & average power for states off&on

The curves $P_{\text{compr,off\&on}}$ from Figure 59, right diagram, serve as input data for the simulation program. In the time-power diagram the model can be explained by looking at areas, which represent the mechanical work, see Figure 60.

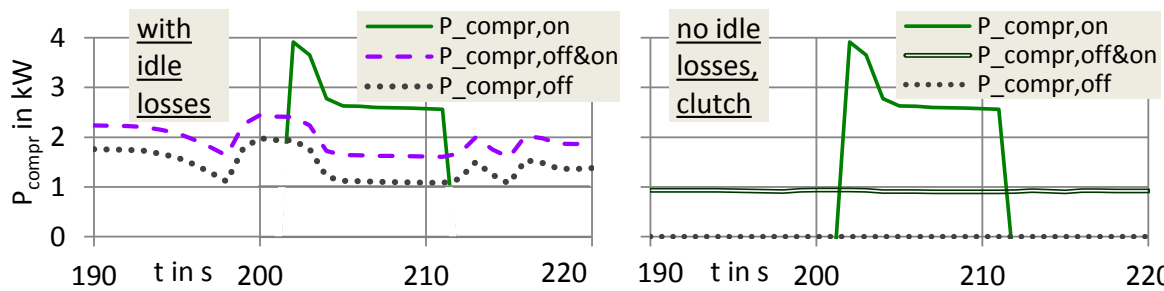


Figure 60. Temporal course of compressor power, cases with and without idle losses (no clutch, w. clutch)

Both diagrams are parts of the compressor operation during the Regional Delivery cycle 2012, measured on the chassis dyno.

In the left diagram, case with idle losses, the area between $P_{\text{compr,off}}$ and the abscissa equals the compressor work at idle ($W_{\text{compr,off}}$). The area between $P_{\text{compr,on}}$ and $P_{\text{compr,off}}$, for the delivering compressor in the interval 202 to 211 s, is the additional compressor work during delivery ($\Delta W_{\text{compr,deliv}}$). Its size equals that of the area between $P_{\text{compr,off\&on}}$ and $P_{\text{compr,off}}$ during the whole part 190 to 220 s. Thus the area between $P_{\text{compr,off\&on}}$ and the abscissa equals the sum of $W_{\text{compr,off}}$ and $\Delta W_{\text{compr,deliv}}$, i. e. the overall compressor work during idle and delivery.

In the right diagram the relations are the same, but it is assumed that the compressor is equipped with a clutch. Thus the idle losses and the work at idle are zero. In this case the area between $P_{\text{compr,on}}$ and the abscissa in the delivery interval 202 to 211 s equals the area between $P_{\text{compr,off\&on}}$ and the abscissa in the whole part from 190 to 220 s.

The theory, that the calculation with the replacement "Average compressor power for idle and delivery phases ($P_{\text{compr,off\&on}}$)" leads to the same accumulated compressor work like its real intermittent power course was checked for the cycles RD12 and UD12-flat. The integrals of the power courses were calculated for the cases with idle losses and with clutch, where the compressor operation was determined from measurement values, compare p. 53 Figure 52. The results show, that the calculated mechanical work is very similar, see Table 9.

Table 9. Comparison of accumulated compressor work from measurement and model

<i>Compressor work in kWh_{mech}/km</i>	$W_{\text{compr,RD12,idle}}$	$W_{\text{compr,RD12,clutch}}$	$W_{\text{compr,UD12-fl,idle}}$	$W_{\text{compr,UD12-fl,clutch}}$
Measurement, intermitt. power	0.034	0.0081	0.050	0.016
Model, $P_{\text{compr,off\&on}}$	0.034	0.0081	0.050	0.016
Deviation	+0.04 %	-0.05 %	-0.02 %	-0.02 %

The deviation of the accumulated compressor work from the model to the real intermittent power course is below 0.1 % in case of four analysed cases.

Using the FC-line in VECTO, compare p. 24 ff. section 2.2.3, it is assumed that the additional FC of an engine auxiliary is nearly independent on the temporal distribution of its accumulated work demand. It was checked if this is also valid for the compressor model. Its additional FC was calculated two times: With its intermittent power course, determined from measurement⁴⁵, and with the model plus the calculated air volume from p. 54 Table 7. For the model of the truck see p. 176 Table 37, and the results are shown in Figure 61.

⁴⁵ This means that the power course of the compressor, determined from measurement, was used as input for the simulation of the delivery truck in VECTO.

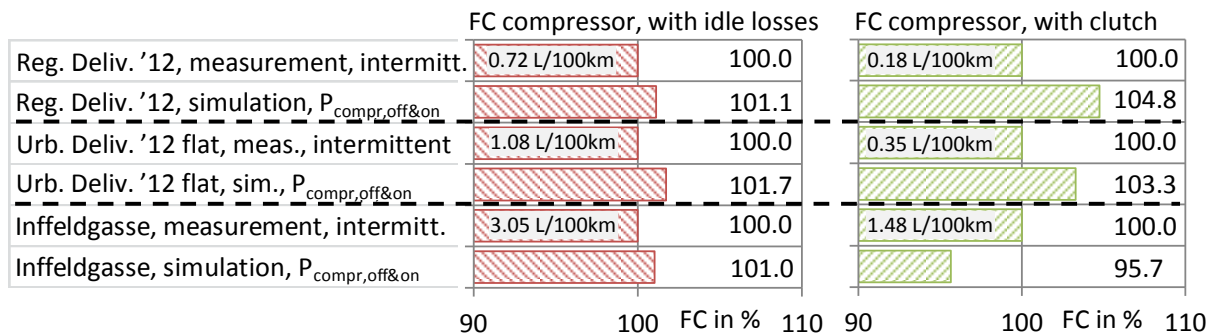


Figure 61. Additional fuel consumption of compressor, determined from measurement and model.

All values for the additional FC of the compressor model are in a range of $\pm 5\%$ from the FC simulated with the intermittent power course, determined from measurement. Hence the model can be used for the purpose to distinct between more and less efficient compressors.

The saving potential for the additional FC of a disengageable compressor in comparison to a device with full idle losses was calculated to 76 % and 68 % reduction for the cycles RD12 and UD12-flat, see p. 60 Table 9. Similar values were found for a tractor-trailer by other workers, when analysing the power in unloaded state: 77 % for "overland" and 59 % for "city" (151 p. 31).

2.3.2.3 Consumption of pressurised air on bus cycles

For the VECTO bus cycles, see p. 153 ff. section 5.4.1 "VECTO target speed driving cycles", the number of events, where pressurised air is consumed, is standardised, see Table 10.

Table 10. Number of events with consumption of pressurised air, bus driving cycles (103 p. 212)

Driving cycle	s in km	Brake-events	Bus-stop brake + doors	Kneeling mechanism
Coach Bus	275.2	27 (0.1/km)	6 (0.0/km)	0 (0.0/km)
Heavy Urban Bus	30.5	191 (6.3/km)	82 (2.7/km)	27 (0.9/km)
Interurban Bus	123.6	190 (1.5/km)	9 (0.1/km)	0 (0.0/km)
Suburban Bus	23.5	49 (2.1/km)	25 (1.1/km)	6 (0.3/km)
Urban bus	39.5	153 (3.9/km)	75 (1.9/km)	25 (0.6/km)

The generic values for the number of events and the amount of air consumption (103 pp. 212-214) were used as input for the compressor model for the city buses.

2.4 Models for energy recovery and start-stop automatic

In this chapter new models for the partial recovery of kinetic energy during braking by recuperation with engine auxiliary consumers and for the recovery of exhaust heat by a small steam power process are described. Because for the model of the start-stop automatic a similar approach was used like for the recuperating auxiliaries, it is also treated here.

Regenerative braking with auxiliaries and the start-stop automatic were simulated by postprocessing the VECTO output. Here the regeneration with the auxiliaries alternator and compressor is described, which deliver electricity and pressurised air during braking into the reservoirs battery and air vessels.

Regeneration is also possible with the steering pump, which can operate at max. power during braking and deliver pressurised oil into a hydraulic bladder accumulator, examples for these components are shown in (152). But at present not enough data is available for a model.

The official approach of the VECTO project for regenerative braking with auxiliaries is described in (115) for the electrical and pneumatic systems of buses, also the air conditioning is respected. These models are included in the current VECTO releases and are still tested at the time of writing.

Hence own models were elaborated to depict recuperation with auxiliaries and the approach can serve as alternative. The necessary input data is shown in Table 11.

Table 11. Input data for models of regenerative braking and start-stop automatic

Input data from vehicle model	Results from simulation run in VECTO
Alternator performance map, p. 25 Figure 25	Cycle duration (Δt_{cycle})
Average electrical power ($P_{\text{el,avrg}}$)	Engine speed (n_{eng})
Average mechanical chiller power ($P_{\text{chill,avrg}}$)	FC-line, e. g. page 26 Figure 26
Average mechanical fan power ($P_{\text{fan,avrg}}$)	Gear
Average mech. idle power steering pump ($P_{\text{steer,idle}}$)	Mechanical brake power at wheel hubs (P_{br})
Average mechanical steering power ($P_{\text{steer,steer}}$)	Mechanical gross engine power ($P_{\text{eng,gross}}$)
Compressor curves power & air flow, p. 59 Figure 58	Mechanical power at wheel hubs (P_{wh})
Dynamic tire radius (r_{dyn})	Vehicle velocity (v_{veh})
FC map diesel engine, e. g. page 35 Figure 36	
Final drive gear ratio (i_{fd})	Storage efficiency of battery (η_{batt})
Shift gearbox gear ratios (i_{gb})	Total air demand pneumatics ($V_{\text{air,consumpt}} = V_{\text{air,deliv,tot}}$)

2.4.1 Regenerative braking with engine auxiliaries

Here the workflow of the model for regenerative braking with alternator and compressor is described. The results are presented for future auxiliaries, where the compressor is assumed to be equipped with a clutch and the steering pump with an electrical drive, see p. 171 Table 33 case m) "Efficient engine auxiliaries, future". In the bus two alternators are installed to feed the higher demand of the electrical engine cooling fan and the also electrical steering pump.

For the future scenario, partly electrified auxiliaries with low or no idle losses were chosen for the analysis. The mechanical auxiliaries fan and steering pump cannot be powered by the regenerated energy, but in case of electrification a part of the energy can be gained by regeneration with the alternator(s).

1) Determine the power curves of the auxiliaries during normal operation

With the alternator performance map and the average electrical power the curve $P_{alt,mech, norm}$ for the mechanical alternator power demand is calculated for normal operation, see p. 25 Figure 25 right. The same is done with the compressor power curves and the total air demand to get the curve $P_{compr, off\&on, norm}$ for the average compressor power, see p. 59 Figure 59 right.

The electrical energy demand ($E_{el, total}$) is calculated from electrical power and cycle duration.

2) Identify the phases, where regenerative braking can be applied

In the simulation it was assumed that for regenerative braking the brake power at the wheels shall be unequal zero for at least three consecutive seconds and that the charging of the energy storages can start in second two, examples are shown on p. 65 in Figure 64. Coasting phases with also negative wheel power but no braking, where the rolling vehicle powers the idling engine and the auxiliaries, are not considered. During these phases the forces between engine and wheels are balanced and no excess power for a higher auxiliary load is available.

The result of this step are time intervals with possible regenerative braking and the total regeneration duration ($\Delta t_{regen, total}$).

3) Calculate the auxiliary work during standing, driving and coasting for normal operation

With the engine speed course and the power curves for alternator and compressor in normal operation without regenerative braking, $P_{alt,mech, norm}$ and $P_{compr, off\&on, norm}$, the accumulated work consumption for the phases standing, driving and coasting is calculated⁴⁶. In these cases the engine is fuelled or the forces in the powertrain of the coasting vehicle are balanced for engine friction, auxiliary propulsion and forces at wheels. A change of the auxiliary power during these phases affects the FC. The result is the work consumption of the auxiliaries during phases which are relevant for FC at normal operation without regenerative braking: $W_{alt, FC, norm}$ and $W_{compr, FC, norm}$.

4) Calculate the engine speed course during regenerative braking

To simplify the simulation it is assumed for non-powershift gearboxes, i. e. for the AMTs of trucks, that the shifted gear is kept constant from the beginning to the end of the regenerative braking phase⁴⁷. Thus shifting at reversed power flow is avoided. For powershift-capable gearboxes like the ATs of city buses the gears are assumed to be shifted from high to low during regenerative braking to reach higher delivery rates of the auxiliaries at high rotational speeds.

The calculation of the gears and the resulting engine speeds is done with vehicle velocity, dynamic tire radius and the gear ratios of final drive and shift gearbox, see p. 35 Equation 9.

The lower limit for the engine speed during regeneration is idle speed minus 50 rpm. When this limit is reached, the regeneration stops and the engine returns to normal idle operation.

An example for regenerative braking from the HDV models rigid bus on the Urban Bus cycle and the delivery truck on the Urban Delivery cycle 2012 is shown on p. 65 Figure 64.

⁴⁶ Powertrain behaviour during standing and driving: $P_{eng, gross} > 0$.

During coasting: ($P_{eng, gross} < 0$ AND $P_{wh} < 0$ AND $P_{br} = 0$).

⁴⁷ Powertrain behaviour during braking: ($P_{eng, gross} < 0$ AND $P_{brake} \neq 0$). It is assumed that the auxiliaries are propelled by the braking vehicle and a change of their power during these phases demand doesn't affect the FC.

5) Subdivide the calculated engine speed points during regenerative braking into classes

The resulting engine speed points during regenerative braking are subdivided into classes, e. g. of width 100 rpm, and the residence time in these classes is calculated, Figure 62 left.

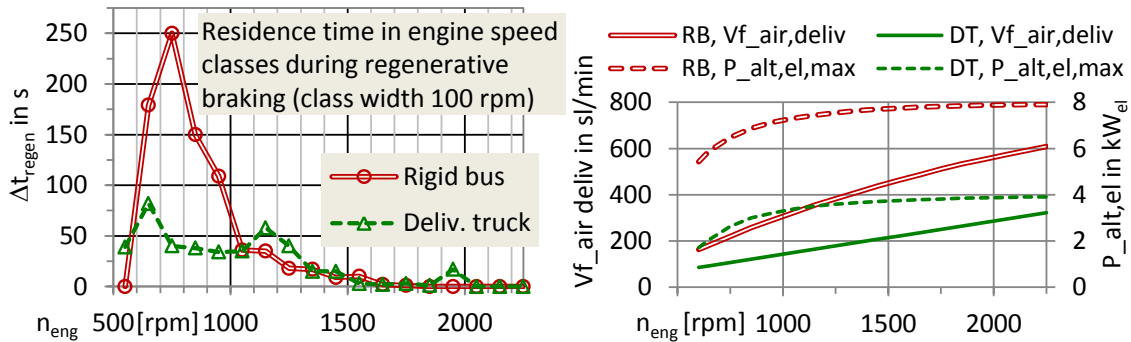


Figure 62. Left: Residence time of engine in speed classes during regen. braking. Right: Max. compressor air delivery ($V_{f_{air,deliv}}$) and max. alternator output ($P_{alt,el,max}$), rigid bus (RB) and deliv. truck (DT)

Driving cycles: Rigid bus - Urban Bus (UB), Delivery truck - Urban delivery 2012 (UD12)

Note: The delivery truck is equipped with one alternator, the rigid city bus with two alternators

6) Calculate the energy gain by regenerative braking

It is estimated, that 90 % of the regenerative braking phases can be used to fill the energy storages, here battery and air vessels, with operating the auxiliaries at full power. Due to a lack of measurement data this estimation was not checked, and serves only as working hypothesis. During urban traffic with manifold, but short retardations this seems to be realistic, because the storages are big enough to absorb the short filling cycles. The %-share of usable braking phases can be adopted for e. g. small storages, longer braking or a very low braking power.

E. g. for the rigid bus it is calculated, that alternator and compressor operate with max. power at engine speed 750 rpm for $(0.9 \cdot 250 \text{ s} = 225 \text{ s})$, see Figure 62 left, at 850 rpm for $(0.9 \cdot 150 \text{ s} = 135 \text{ s})$ and so on. In case of the delivery truck both auxiliaries operate with max. power at engine speed 1150 rpm for $(0.9 \cdot 58 \text{ s} = 52 \text{ s})$, at 1250 rpm for $(0.9 \cdot 40 \text{ s} = 36 \text{ s})$ etc..

The maximum output of alternator and compressor in terms of electrical power and pressurised air is shown in Figure 62 right. This recuperated output is fed to battery and air vessels, which are used as buffer storage. In case of the bus 26 % of the total demand of electrical energy and 45 % of the total pressurised air can be gained by regenerative braking, for the delivery truck the shares are 34 % for both kinds of energy, see Figure 63 left.

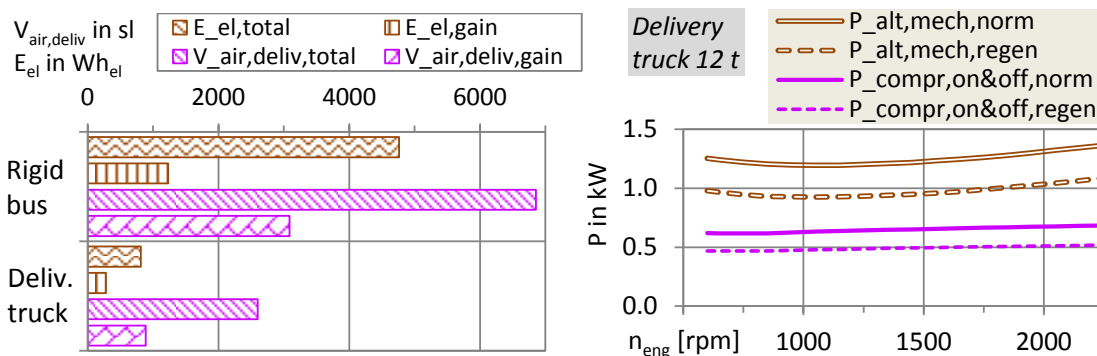


Figure 63. Left: Total demand of electrical energy and pressurised air plus gain by regen. braking Right: Delivery truck, alternator and average compressor power, normal operation and regen. braking

where $E_{el,total}$ Total demand of electrical energy
 $E_{el,gain}$ Gain of electrical energy during regenerative braking
 $V_{air,deliv}$ Total delivered air volume
 $V_{air,deliv,gain}$ Gain of delivered air during regenerative braking

The usable amount of regenerated electrical energy is reduced by double battery losses of $(100\% - (95\%)^2 \approx 10\%)$ during charging and discharging.

7) New power curves of the auxiliaries for the whole cycle with regenerative braking

The differences between the total demands of electrical energy or pressurised air and the gain by regenerative braking, see Figure 63 left, still have to be delivered by the auxiliaries during standing, driving and coasting. This means for the bus, that 74 % of the total electrical energy and 55 % of the total pressurised air need to be generated during these phases. In case of the delivery truck 66 % of both types of energy need to be delivered then.

The new value for the average electrical power demand is calculated via Equation 25.

Equation 25. Avrg. electrical power during standing, driving & coasting, with regenerative braking

$$P_{el,avrg,regen} = \frac{E_{el,total} - E_{el,gain}}{\Delta t_{cycle} - \Delta t_{regen,total}}$$

where $P_{el,avrg,regen}$ Reduced electrical power demand during standing, driving & coasting due to regenerative braking

$\Delta t_{regen,total}$ Total regeneration duration

With the reduced average electrical power demand a new curve for the mechanical power of the alternator is determined ($P_{alt,mech,regen}$).

The new curve for the reduced compressor power is calculated with Equation 26.

Equation 26. Compressor power curve during standing, driving & coasting, with regenerative braking

$$P_{compr,off\&on,regen} = P_{compr,off} + W_{compr,deliv,spec} \cdot \frac{V_{air,deliv} - V_{air,deliv,gain}}{\Delta t_{cycle} - \Delta t_{regen,total}}$$

where $P_{compr,off\&on,regen}$ Reduced compressor power during standing, driving & coasting due to regenerative braking

The workflow to get the compressor curve is shown on p. 59.

Examples for the normal and reduced power of alternator and compressor, without and with recuperation, are shown for the delivery truck on p. 64 Figure 63 right.

Results for phases of regeneration during parts of the driving cycles and the auxiliary power curves for normal operation and regeneration are given in Figure 64.

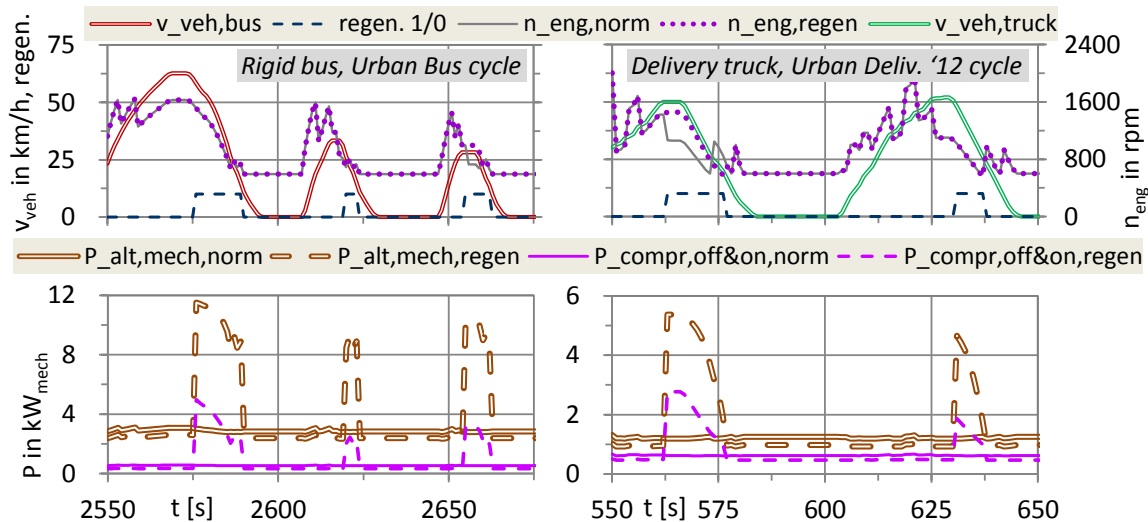


Figure 64. Above: Regenerative braking, vehicle velocity and engine speed.

Below: Alternator and compressor power for normal operation and regenerative braking

Note: (Regenerative) braking occurs not only during deceleration, but also at constant driving downhill

During standing, driving and coasting, where the curve "regen. 1/0" equals zero, the areas between $P_{alt,mech,norm}$ and $P_{alt,mech,regen}$ as well as the area between $P_{compr,off\&on,norm}$ and $P_{compr,off\&on,regen}$ represent the decrease in the auxiliaries work demand.

8) Calculate the auxiliary work during standing, driving and coasting for regen. braking

Like in step 3) with the engine speed course and the new, lower power curves for alternator and compressor, $P_{alt,mech,regen}$ and $P_{compr,off\&on,regen}$, the work consumption is calculated for the phases standing, driving and coasting. The result is the reduced consumption of mechanical work due to regenerative braking: $W_{alt,FC,regen}$ and $W_{compr,FC,regen}$.

9) Calculate the reduced fuel consumption due to regenerative braking

Finally the decrease in FC can be calculated with the reduced auxiliary work during standing, driving plus coasting and the linear factor ΔFC_w from the FC-line, see Equation 27.

Equation 27. Decrease in fuel consumption due to regenerative braking with engine auxiliary consumers.

$$\Delta FC_{regen} = \Delta FC_w \cdot \left(\sum W_{i,FC,regen} - \sum W_{i,FC,norm} \right)$$

where ΔFC_{regen} Decrease in fuel consumption due to regenerative braking, incl. transient correction factor (TCF)

$\sum W_{i,FC,norm}$ Sum of normal work of engine auxiliaries "i" during standing, driving, coasting w/o regen. braking, here ($W_{alt,FC,norm} + W_{compr,FC,norm}$)

$\sum W_{i,FC,regen}$ Sum of reduced work of engine auxiliaries "i" during standing, driving, coasting, w. regen. braking, here ($W_{alt,FC,regen} + W_{compr,FC,regen}$)

ΔFC_w Change of consumed fuel mass per change of positive mechanical engine work, compare p. 26 Figure 26

The relative decrease in FC due to regenerative braking for the rigid bus and the delivery truck with future auxiliaries is shown in Table 12.

Table 12. Change in FC due to regenerative braking, HDV with future auxiliaries

The 2nd alternator for the rigid bus allows to regain more energy, therefore the saving potential is higher.

	Alternator	Compressor
Rigid bus (two alternators)	-1.4 %	-0.9 %
Delivery truck (one alternator)	-0.8 %	-0.5 %

For the check of plausibility no measurement data was available, hence the model could not be validated. From industry the experience value of ca. 1 % FC decrease is known for city buses and regenerative braking with alternators (153 p. 3).

2.4.2 Start-stop automatic

The model for the start-stop automatic is here also done as postprocessing of the VECTO output. The model uses the FC-line and will be described in the following paragraphs. In principle the model allocates auxiliaries' work which cannot be provided during engine stop phases - such as electric energy from the alternator - to the phases where the engine is running. Without such a reallocation the benefit of start/stop systems would be overestimated due to an artificial reduction of the auxiliary work demand over the cycle.

1) Identify the phases of engine stop during vehicle stand

A single stop phase is defined here for the simulation as an interval with a minimum length of 4 s, where the vehicle velocity equals zero, and the engine is assumed to be turned off at the 3rd second. Hence the minimum downtime of the engine is 2 s and shorter stop phases are avoided. E. g. the intervals at zero velocity shown on p. 65 Figure 64 would be suited for a start-stop automatic. Because the starts and durations of the stand phases are already known from the driving cycle, the maximum saving potential by a start-stop automatic is determined.

2) Calculate the work of auxiliaries at engine stop to be shifted to driving phases

The default values for the average power of A/C chiller, fan and *steering pump at steering without idle*, and the power from the curves for alternator and compressor at idle speed, compare p. 25 Figure 25 and p. 59 Figure 59 right, are integrated for engine stop intervals. In case of a preceding calculation of regenerative braking with auxiliaries, the alternator and compressor power are determined from the reduced power curves $P_{alt,mech,regen}$ and $P_{compr,off\&on,regen}$, see the previous section, p. 65 step 7). It is assumed, that this work from idling phases is necessary for the vehicle operation and needs to be shifted to the driving phases ($W_{aux,stop,shift}$). The power of the *steering pump at idle* during vehicle stop is not necessary for the vehicle operation.

3) Shift the auxiliaries work from engine stop to driving phases

The duration of engine downtime (Δt_{stop}) and of the phases driving plus coasting ($\Delta t_{drive+coast}$)⁴⁸ are calculated. It is assumed that the work of auxiliaries during engine stop, determined in the preceding step 2) ($W_{aux,stop,shift}$), is performed at driving vehicle and therefore shifted.

That part of the shifted auxiliaries' work, which is conducted during driving or coasting, is relevant for the FC. That part performed during braking phases is for free due to the excess power from the decelerating vehicle.

4) Calculate the reduction of fuel consumption due to start-stop automatic

With the Willans Factor (ΔFC_W), see p. 26 Figure 26, the additional FC to perform the part of shifted auxiliary work during driving plus coasting is calculated ($\Delta FC_{aux,shift,add}$).

With the default values for the average power of A/C chiller, fan and *steering pump at steering plus idle*, and the power from the curves for alternator and compressor at engine idle speed, the FC at vehicle stand is interpolated from its consumption map and accumulated. The accumulated FC is the total FC during engine stop phases ($\Delta FC_{stop,save}$), it is decreased by the additional FC from shifted auxiliaries' work. See Equation 28 to compute the FC savings.

Equation 28. Decrease in fuel consumption due to start-stop automatic

$$\begin{aligned} \Delta FC_{start-stop} &= \Delta FC_{stop,save} + \Delta FC_{aux,shift,add} \\ &= \Delta FC_{stop,save} + \Delta FC_W \cdot W_{aux,stop,shift} \cdot \frac{\Delta t_{drive+coast}}{\Delta t_{cycle} - \Delta t_{stop}} \end{aligned}$$

where	$\Delta FC_{start-stop}$	Decrease in FC due to start-stop automatic (value < 0)
	$\Delta FC_{stop,save}$	Saved FC (value < 0) during engine stop phases
	$\Delta FC_{aux,shift,add}$	Additional FC (value > 0) during driving + coasting to perform the auxiliary work which was shifted from engine stop
	$\Delta t_{drive+coast}$	Duration of driving and coasting phases

⁴⁸After the calculation of engine downtime: Powertrain behaviour during driving: $P_{eng,gross} > 0$. During coasting: ($P_{eng,gross} < 0$ AND $P_{wh} < 0$ AND $P_{br} = 0$)

Δt_{stop}	Duration of engine stop phases
$W_{\text{aux,stop,shift}}$	Work of engine auxiliaries, shifted from engine stop to driving, without steering pump idle losses

The relative reduction of FC by a start-stop automatic can be combined with that from regenerative braking, see the previous section 2.4.1. The results are shown in Table 13.

Table 13. Change in FC due to start-stop automatic and regen. braking, HDV with future auxiliaries

	Start-stop automatic	Start-stop automatic & regen. braking
Rigid bus (two alternators)	-4.9 %	-6.9 %
Delivery truck (one alternator)	-2.2 %	-3.4 %

2.4.3 Exhaust heat power generation

To estimate the fuel saving potential from exhaust heat power generation, a simplified model for an Organic Rankine cycle (ORC) was set up. The scheme of such a steam power process is shown in Figure 65.

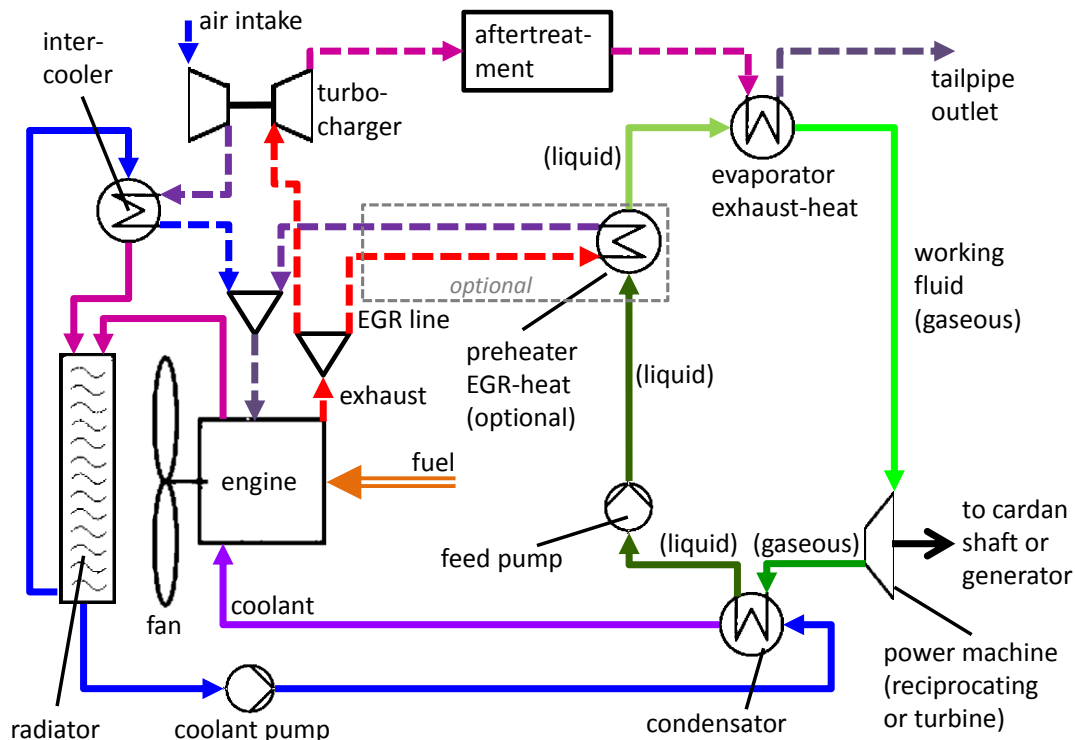


Figure 65. Flow scheme of an ORC process, coupled to an internal combustion engine (142 p. 26)

Brighter colours within a circuit mean a higher temperature level

For these processes organic working fluids are used, hence the name is Organic Rankine Cycle. In comparison with water, the common working fluid of stationary thermic power stations, the specific evaporation enthalpy of these fluids is smaller, thus for small heat sources the mass flow in the circuit becomes higher than for water. This leads to the desired effect, that the proportionate gap losses of the fluid in the power machines are smaller than for fluids of high evaporation enthalpy and low mass flow. Small gaps between piston or turbine and the housing of the power machine cannot be avoided, hence a certain leakage of the working fluid at the pressurised side occurs. The higher the mass flow is, the lower the proportionate leakage and the equivalent power loss become.

The impression of an ORC prototype is given in Figure 66.



Figure 66. ORC prototype (154)

For the model of this thesis the process is driven only by the exhaust downstream the aftertreatment, without the optional EGR-preheater, and the power machine was coupled by a 1-speed reduction gear and a belt-drive to the cardan shaft as described in (155 p. 35). The power of the feed pump is included in the overall efficiency, see p. 70 Figure 68.

The simulated ORC process generated an average mechanical power of $2.9 \text{ kW}_{\text{mech}}$ and at maximum $12.5 \text{ kW}_{\text{mech}}$ for the basis tractor-trailer model with 14.5 t payload on the Long Haul cycle 2015, as will be shown later in the results. Hence the electrical output of a generator connected to the power machine of the Rankine process would be much higher than the average demand by the a tractor, which was modelled to be approx. $1.1 \text{ kW}_{\text{el}}$. Thus only the usage of the mechanical power was investigated.

For an engine EURO V 330 kW of ca. 11 L displacement, the mass flow, composition and temperature of the exhaust downstream the turbocharger were known. This data was used to calculate the exhaust loss, the difference of its enthalpy between turbocharger outlet and ambient, according Equation 29.

Equation 29. Exhaust loss, calculated from exhaust flow and difference of specific enthalpy

$$\dot{H}_{\text{exh,TC}} = \dot{n}_{\text{mol,exh}} \cdot \left(\sum_i X_i \cdot h_i(1 \text{ bar}, T_{\text{exh,TC}}) - \sum_i X_i \cdot h_i(1 \text{ bar}, T_{\text{exh,amb}}) \right)$$

where: $\dot{H}_{\text{exh,TC}}$ Exhaust loss from turbocharger outlet to ambient

h_i Specific enthalpy for main species in exhaust (CO_2 , H_2O , N_2 , O_2), depending on the pressure and temperature of the gas

$\dot{n}_{\text{mol,exh}}$ Molar exhaust flow, [mol/s]

T_{amb} Ambient temperature, here $20 \text{ }^\circ\text{C}$

$T_{\text{exh,TC}}$ Exhaust temperature downstream turbocharger

X_i Mole fraction in [-], for species in exhaust (CO_2 , H_2O , N_2 , O_2)

The fractions of the species in the exhaust were calculated for the ideal combustion of diesel fuel⁴⁹, the table values for the specific enthalpies at 1 bar, depending on the gas temperature, were taken from (156).

⁴⁹ $1 \text{ C}_{13.66}\text{H}_{26.05} + \lambda \cdot 20.18 \cdot (\text{O}_2 + 3.762 \text{ N}_2) = 13.66 \text{ CO}_2 + (\lambda - 1) \cdot 20.18 \text{ O}_2 + 13.03 \text{ H}_2\text{O} + \lambda \cdot 75.92 \text{ N}_2$, with $\lambda = \text{AFR} / \text{AFR}_{\text{stoich}}$, where: AFR - air-fuel-ratio, ratio of air mass to fuel mass; stoich - stoichiometric

The exhaust temperature of the known engine and its exhaust loss are shown in Figure 67. Also the operating points for the ESC are given, which are used later.

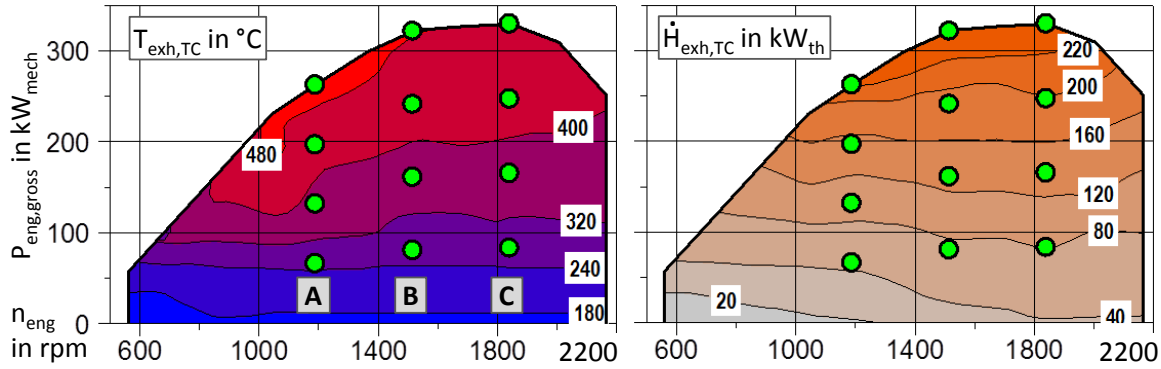


Figure 67. Engine map € 5; exhaust temperature downstream turbocharger ($T_{exh,TC}$); exhaust loss turbocharger outlet to ambient ($\dot{H}_{exh,TC}$); operation points ESC at A, B and C-speed from (157 pp. 10, 55)

From literature the mechanical power output of the expansion machines of ORC processes ($P_{ORC,mech}$) at multiple operation points of diesel engines in the ESC could be determined, the data found is shown on p. 189 section 5.12. The engines EURO V were similar to the known one, hence the published results were combined with the known values for exhaust temperature and exhaust loss, see above Figure 67. For the stationary measurements (“stat”) the heat loss between the turbocharger and the outlet of the aftertreatment was assumed to be small and neglected. Thus the exhaust temperature at the outlet of the aftertreatment ($T_{exh,out,stat}$) was close to that downstream the turbocharger ($T_{exh,TC,stat}$).

This led to the assumption $\dot{H}_{exh,TC,stat} \approx \dot{H}_{exh,out,stat}$, where $\dot{H}_{exh,out}$ is the exhaust loss referred to the outlet of the aftertreatment.

The effective efficiency of the ORC was calculated according Equation 30.

Equation 30. Effective efficiency of ORC process

$$\eta_{ORC} = P_{ORC,mech} / \dot{H}_{exh,out}$$

where: η_{ORC} Efficiency of ORC process.

$\dot{H}_{exh,out}$ Exhaust loss at the outlet of the aftertreatment. Enthalpy difference of exhaust flow between temperature at outlet of aftertreatment and ambient temperature.

$P_{ORC,mech}$ Output of mechanical power at shaft of expander of ORC process

The result was a characteristic curve for the efficiency of ORC processes as function of the exhaust temperature, which is shown in Figure 68.

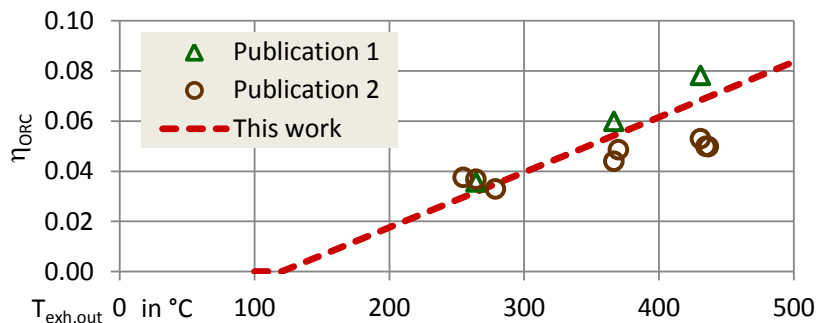


Figure 68. Characteristic curve, effective ORC efficiency as function of exhaust temperature
The data from the two publications and the calculated efficiencies are given on p. 189 section 5.12

Subsequently the model of the basis tractor-trailer was implemented in the program PHEM (158 pp. 12-21), which offers also the possibility to simulate the exhaust gas temperatures.

For the 6-cylinder tractor engine EURO V, which was described above, a calibrated model was available to calculate the exhaust gas mass flow with the temperature downstream the aftertreatment for transient operation ($T_{\text{exh,out}}$) (159 pp. 72-95). The differences between EURO V and EURO VI add a small uncertainty to the result.

From the PHEM results the transient course of the exhaust enthalpy was calculated like described above ($\dot{H}_{\text{exh,out}}$), and with the exhaust temperature ($T_{\text{exh,out}}$) the efficiency of the ORC process was determined from the curve Figure 68. With these data the mechanical power at the expander shaft was calculated. For the transmission from expander to cardan shaft 10 % losses were estimated, and to determine the power gained at the engine crankshaft, the gearbox losses were added. The results are the engine operation points with ORC at lower engine power demand compared to the vehicle model without ORC. The new power course was used to interpolate the reduced FC from the engine performance map. The interdependency (lower engine power) \rightarrow (lower exhaust loss) \rightarrow (lower ORC power) was neglected. In case of negative engine power during coasting or braking nothing was changed.

The results for the simulated exhaust flow and the ORC power are shown in Figure 69.

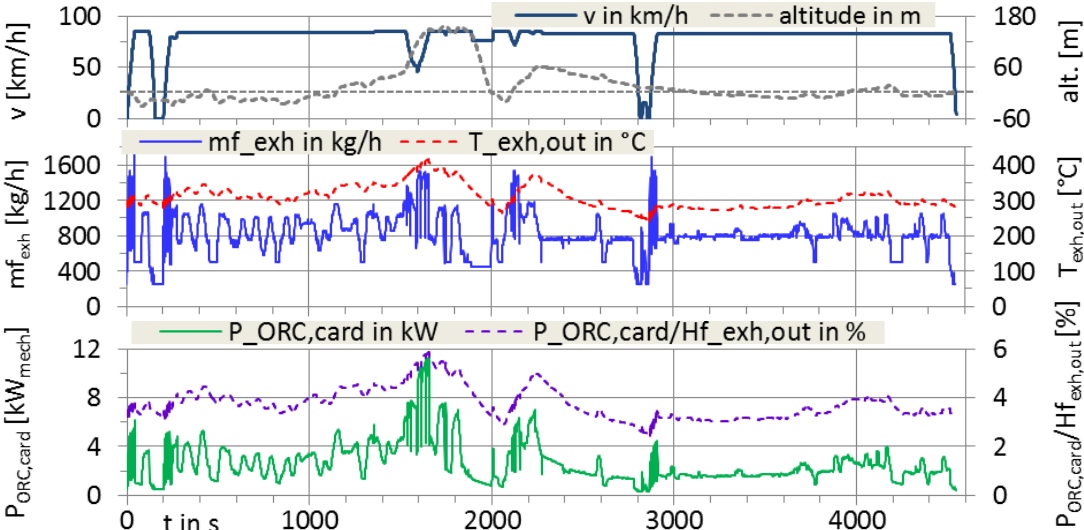


Figure 69. Results for exhaust flow and ORC process, model tractor-trailer, Long Haul cycle 2015

$H_{\text{exh,out}}$ - Exhaust loss, outlet of aftertreatment to ambient, mf_{exh} - Exhaust mass flow, $P_{\text{ORC,mech,card}}$ Mechanical power of ORC expander at cardan shaft, $T_{\text{exh,out}}$ - Exhaust temperature at outlet of aftertreatment

The simplified model of the ORC calculated a stationary behaviour of the components, and a change in mass flow or temperature generated an instantaneous change of efficiency and power output. In reality the thermal inertias of the heat exchangers and of the whole system slow down the change, but were not be depicted by the simple model. Thus it fits best to non-transient cycles like long haul with rather slow changes of the engine operation point.

With the simplified model of an ORC process the saving potential for a tractor-trailer on the Long Haul cycle 2015 was calculated to 2.2 %. That is at the lower end of published values, where the references and further checks are given on p. 104 in section 3.1.6.

2.5 Models of electrified powertrains

In this chapter the simulation approach and the control strategy for the models of hybrid-electrical and battery-electrical vehicles (HEV, BEV) are described. For the technical data of the vehicles see p. 172, Table 34 entries B) to E), p. 178 Table 38 and for the basis performance map of the electrical machines (EM) p. 181 Figure 201. The hybrid types electrical parallel and electrical serial are shown in Figure 70.

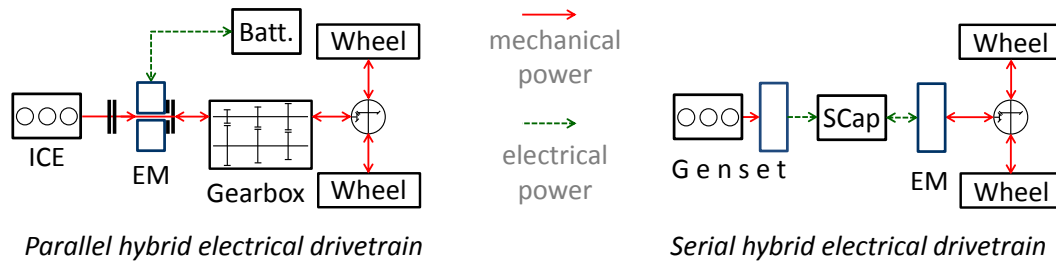


Figure 70. Structure of electrical parallel and electrical serial powertrains⁵⁰

Batt. - Battery; **EM** - Electrical machine; **Genset** - Generator set, combination of heat engine and electrical machine, which works only as generator; **ICE** - Internal combustion engine; **SCap** - Supercapacitor.

The main distinction between parallel and serial hybrid is, that in case of the parallel layout the ICE and the EM can propel the vehicle simultaneously or independent on each other, where the serial hybrid is already an electrical vehicle with a genset as power source.

The map of the permanent magnet synchronous machine (PMSM) was measured at the institute. It was scaled for the maximum torque of the different EM models, and the resulting power curves are shown on p. 182 ff. Figure 204 and Figure 205.

For the electrical one-way efficiencies of the components inverter, battery and supercapacitor, i. e. the ratio of output power to input power for the transfer in one direction, the value 0.95 was assumed⁵¹. The EMs are connected by an inverter to the electrical storages, which converts the alternating current to/from the EM towards direct current from/to the battery or supercapacitor.

Hence the round-trip efficiency between EM and storage cells for regenerative braking

EM output - inverter - storage input - storage output - inverter - EM input
becomes $(0.95)^4 = 0.815$, where inverter and storage contribute each two times 0.95.

The efficiencies of the power conversions mechanical to electrical (EM as braking generator) and vice versa (EM as propelling motor) need to be considered in addition.

EM can be operated for a certain time at overload, up to multiple continuous power. The limit for the duration is the temperature of the copper windings. When it becomes too high, the electrical insulation would melt and/or other damage occurs. The temperature course of the EM depends amongst others on its cooling system (air or liquid), the cooling capacity and the installation situation. During overload the waste heat from the EM, 5 % to 20 % of the electrical power, is higher than the removal by the cooling system, hence the machine heats up. How power and overload for real electrical vehicles are controlled is not known.

E. g. for a parallel hybrid bus Volvo 7700 LH with an EM of $70 \text{ kW}_{\text{mech}}$ continuous and $120 \text{ kW}_{\text{mech}}$ peak power, the limit for motor operation on the road was $+75 \text{ kW}_{\text{mech}}$, for generator operation $-90 \text{ kW}_{\text{mech}}$ (160 p. 9).

⁵⁰ These powertrain structures and components are treated in this thesis and are only one of manifold possibilities to combine energy conversion machines, energy storages and gearboxes. For more examples see the literature.

⁵¹ Published values for the electrical one-way efficiencies of inverters, Li-Ion batteries and supercapacitors, mainly in the range 0.90 to 0.98, are given e. g. in (560 p. 35.41) (561 p. 925) (562 p. 5) (563 p. 56) (564 p. 25) (565 p. 28) (566 p. 320) (567 p. 4) (568 p. 7544) (569 p. 519) (570 p. 443) (571 p. 117) (572 p. 16) (573 p. 1999) (574 p. 39) (575 p. 116) (576 p. 324).

For most hybrid- and battery-electrical vehicle models the EM were assumed to operate in overload during powering and braking. For the parallel hybrid city bus models, rigid and articulated, the motor power of the EM was limited to avoid overheating.

In case of the serial hybrid rigid city bus the electrical motor power was reduced due to the limited rated power of the diesel engine, which propels the genset. The output from the engine is decreased by the electrical conversion losses in the generator, the inverter and the traction machine plus the electrical power demand of the auxiliaries.

To check these operation strategies, some characteristic values to assess the extent of the overload phases were calculated, see p. 80 ff. section 2.5.5. The results from the models of the (hybrid) electrical vehicles are the input for the calculation, hence it is explained afterwards.

2.5.1 Diesel-electrical parallel hybrid trucks

For the tractor-trailer and the delivery truck a parallel hybrid powertrain was analysed by postprocessing the VECTO output of the frequency 1 Hz, which served as input for the hybrid models. Until now there are no models for hybrid powertrains in VECTO, what created the need for a postprocessing. The basis HDV models were simulated on the driving cycles with an extra mass for the hybrid components EM, inverter and battery: 0.80 t for the tractor-trailer and 0.30 t for the delivery truck. For the main data of the truck models with parallel hybrid powertrains see p. 172, Table 34, "B) Diesel-electrical parallel hybrid vehicles", and p. 178 Table 38, "Diesel-electrical parallel hybrid delivery tractor-trailer". Via postprocessing the fuel saving potential due to regenerative braking and a start-stop function was calculated.

The model and the assumptions are described below, where the results of VECTO from the pre-processed cycles were the basis:

- The state of charge (SOC) of the battery model at cycle start shall equal the SOC at end, what was reached by adjusting the SOC at simulation start.
- The model offers the hybrid functions regenerative braking and operation of the EM as auxiliary motor to relieve the diesel engine, plus a start-stop function.
- Regenerative braking with the EM is applied, when the brake power is unequal zero for minimum 3 seconds.
- The gear from the timestep before the braking started is kept constant to avoid shifting. The AMT of trucks are not capable of powershifting, i. e. gear change with load, hence shifting during regenerative braking was assumed to be avoided.
- With the gear ratios the rotational speed of the gearbox input shaft is calculated, where the EM is placed.
- The negative mechanical power consumed by the EM as generator during regenerative braking is limited by one of the three values below, whichever is bigger:
 - The brake power at the wheels plus the deceleration power from the EM's rotational inertia, minus: The drivetrain losses and in case of coupled engine the auxiliary power plus the engine friction power from its drag curve.
 - The minimum power from the EM's generator full load curve.
 - The product of the possible generator power and the factor for charging, which depends on the SOC of the battery, see Figure 71. The product of this factor and the possible electrical generator power is the effectively produced power, to avoid overcharging of the battery.

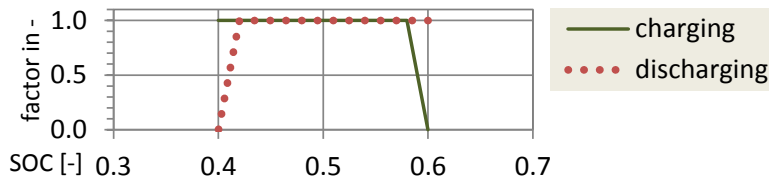


Figure 71. Limiting factors for charging and discharging of the battery, depending on SOC

- During regenerative braking the battery is charged and two times 5 % losses are subtracted from the EM electrical power output, for inverter losses and internal battery losses. The upper SOC limit for charging is 0.60.
- In case of demand for driving power at the gearbox input shaft the EM works as motor. Its positive power is limited by one of the three values below, whichever is smaller:
 - The power demand at the gearbox input shaft.
 - The maximum motor power from the EM's full load curve less the acceleration power from its rotational inertia
 - The product of the possible motor power and the factor for discharging, which depends on the SOC of the battery, see Figure 71. The product of this factor and the possible electrical motor power is the effectively consumed power to avoid exhaustive discharge of the battery.
- During motor operation of the EM the battery is discharged and two times 5 % losses are added to the demanded electrical motor power, for inverter losses and internal battery losses. The lower SOC limit for discharging is 0.40.
- The EM is connected with a clutch to the gearbox input shaft, which is opened during idle when the EM does not work as motor or generator. Thus the idle losses from the EM are avoided.
- For the start-stop function the work of the engine auxiliary consumers during vehicle stand needs to be depicted. Its sum, without idle work of the steering pump, is shifted as average additional power to the phases of rolling vehicle, compare also p. 66 ff. chapter 2.4.2.
- The power demand at the diesel engine is the difference of gearbox input power minus EM motor power, plus the auxiliaries power demand, the shifted auxiliaries' power from stand phases and the acceleration power of the engine inertia.
- With the reduced power demand at the diesel engine ($P_{eng,gross,hybrid}$) and its speed the FC is interpolated from the engine performance map.
- The implemented control strategy was simple: During braking phases ($P_{brake} \neq 0$ for at least 3 s) the EM works as generator and recovers as much energy as possible. During phases of driving ($P_{gearbox-in} > 0$) the virtual EM is operated as motor with its maximum possible power, where the limits are explained above. If the power from the EM is not sufficient to drive the vehicle model, the diesel engine delivers the rest of the demanded power. Thus the diesel engine is still the prime mover for the vehicle and the EM relieves it when possible.

This model was implemented in MS Excel, for its output see Figure 72 and Figure 73.

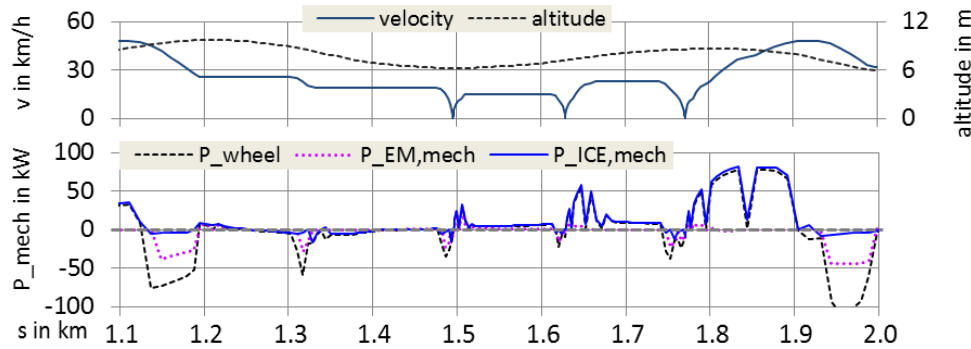


Figure 72. Model diesel-electrical parallel hybrid deliv. truck, section of Urban Delivery cycle 2012, part 1

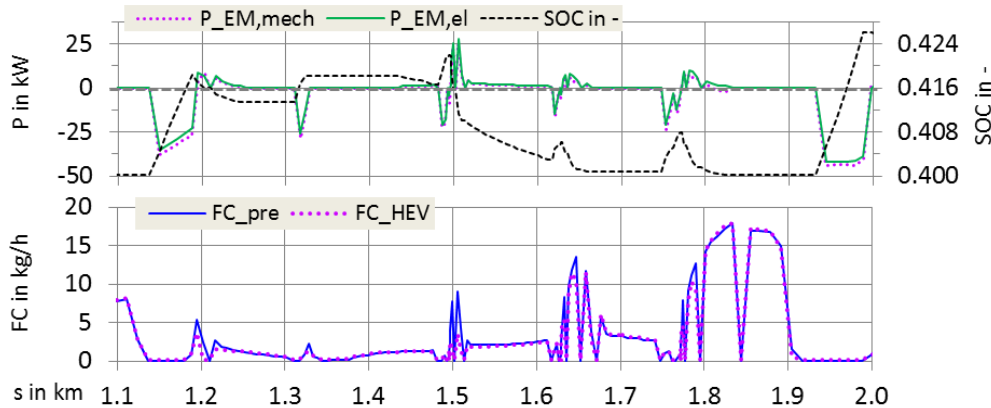


Figure 73. Model diesel-electrical parallel hybrid deliv. truck, section of Urban Delivery cycle 2012, part 2
 FC_{HEV} - FC of hybrid electrical vehicle; FC_{pre} - FC from pre-processed vehicle model, without hybrid functions;
 $P_{EM,el}$ - Electrical power of EM; $P_{EM,mech}$ - Mechanical power of EM; $P_{ICE,mech}$ - Mech. power output from ICE;
 P_{wheel} - Mech. power at wheels; SOC - State of charge of electrical energy storage

As described above, the model of the EM balances a part of the transient power at the gearbox input shaft by working as generator and motor, and relieves the diesel engine.

2.5.2 Diesel-electrical parallel hybrid buses

For the simulation of parallel hybrid buses a separate version of the in-house program PHEM was created during a preceding project, compare (161 p. 24 ff.), and for this thesis combined with a postprocessing in MS Excel.

The model of the hybrid bus in PHEM offered the possibility of adding the power of the EM to the power of the diesel engine, and simulating with a higher power than from the diesel engine alone (“boosting”). This was necessary, because the models of the parallel hybrid buses were equipped with smaller diesel engines than the conventional buses, and needed the additional power of the EM to reach a similar driving performance. Boosting was not possible with the simple hybrid model in MS Excel, which was used for the trucks and where the EM operated only as auxiliary motor to relieve the diesel engine.

The main data of the bus models with parallel hybrid powertrain is given on p. 172, Table 34, "B) Diesel-electrical parallel hybrid vehicles", and p. 178 Table 38, "Diesel-electrical parallel hybrid articulated bus".

The model and the assumptions are described below:

- The applied PHEM version does not accept distance-based target speed driving cycles, but the time-based course of the demanded speed in steps of 1 s. Hence the target speed cycles are simulated in VECTO with a bus model of equal road load and total mass, to get the velocity course in 1 Hz as output.
- From the first VECTO run the consumed mechanical work to overcome rolling resistance and air drag is known. In PHEM the coefficients for rolling resistance and air drag are adapted to meet the work for each driving resistance from VECTO. Thus for driving resistances the PHEM model behaves like a VECTO model of equal mass.
- The state of charge (SOC) of the battery model at cycle start equals the SOC at end, what was reached by adjusting the SOC at simulation start.
- The model offers the hybrid functions regenerative braking, boosting of the propulsion power with the EM and load point shift, in addition a start-stop function was simulated.
- The PHEM routine for gear-shifting is used.
- From the vehicle speed, the power at the wheels, the drivetrain losses and the gear ratios the values rotational speed, torque and mechanical power at the gearbox input shaft are calculated.
- The torque demand at the EM is interpolated from a control map, in the next step its maximum mechanical power is limited, depending on the SOC. The maps and curves were deduced from the measurement of a parallel hybrid city bus, compare (161 p. 25), and are shown in Figure 74 and Figure 75.

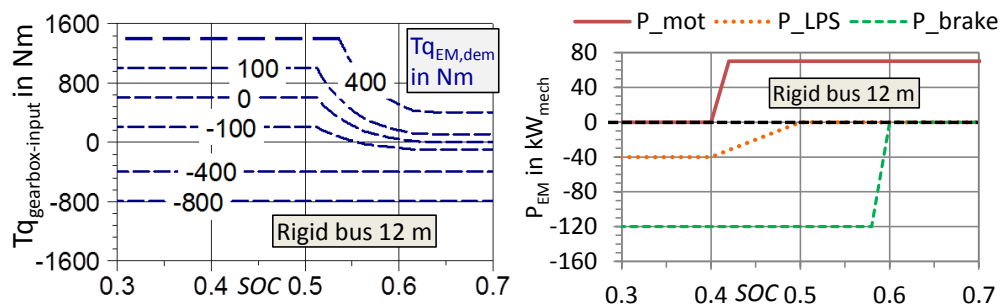


Figure 74. Parallel hybrid-electrical rigid bus. Left: Control map for torque of EM. Right: Curve for power-limit of EM for the states motor operation, Load Point Shift and regenerative braking.
Negative values for torque or power mean generator operation.

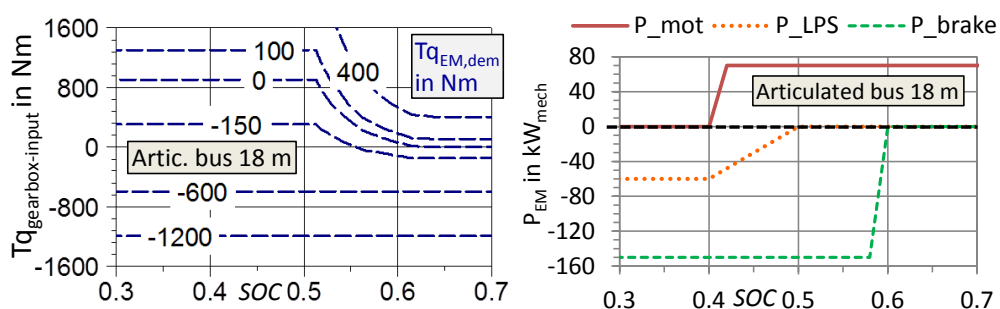


Figure 75. Parallel hybrid-electrical articulated bus. Map and curves for control of electrical machine.

With the values for the calculated torque demand at the gearbox input shaft ($T_{q_{gearbox-input}}$) and the SOC of the battery, the torque demand at the EM ($T_{q_{EM,dem}}$) is interpolated from the left maps. Afterwards with $T_{q_{EM,dem}}$ and the rotational speed of the gearbox input shaft the demanded mechanical power of the EM is determined and limited by one of the curves from the right diagrams. The limits for maximum or minimum power depend on the state of operation (motor, load point shift or regenerative braking) and SOC.

The map for the demanded torque from the EM and the curves for the power limits are the control strategy for this model of a parallel hybrid powertrain.

- A start-stop function is implemented. At every stop the diesel engine is turned off and the electrical consumers are fed from the battery.
- For a SOC below 44 % the diesel engine remains running at stops or is turned on again, powers the EM as generator and feeds the electrical consumers to spare the battery.
- For velocities above 15 km/h the diesel engine is turned always on and becomes the prime motor.
- The power of the diesel engine is the difference between the power at the gearbox input shaft and the power of the EM. In case of EM operation as motor the diesel engine is relieved, and for load point shift its excess power is used to load the battery.
- With the engine speed and its power the FC is interpolated from the performance map.

An example for the model output is shown in Figure 76 and Figure 77.

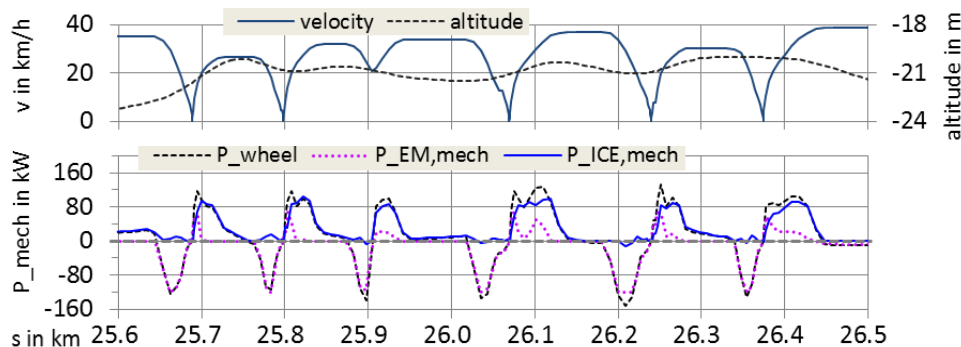


Figure 76. Model of diesel-electrical parallel hybrid rigid bus, section of Urban Bus cycle, part 1

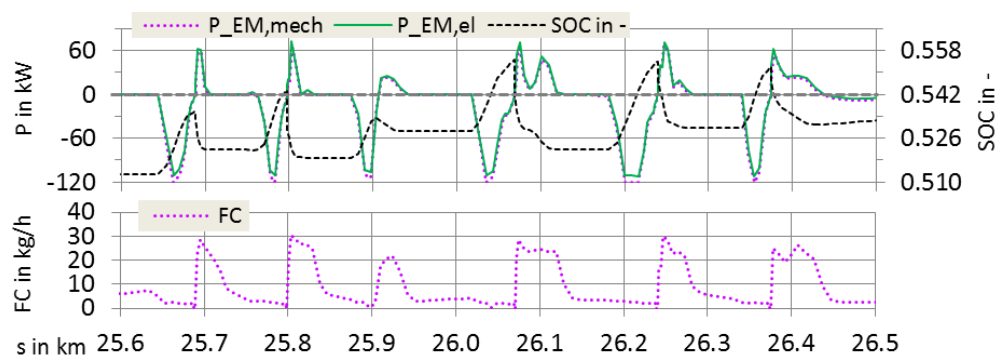


Figure 77. Model of diesel-electrical parallel hybrid rigid bus, section of Urban Bus cycle, part 2

The phases where the EM works as motor, as generator during load point shift and as generator during regenerative braking, are clearly visible.

2.5.3 Diesel-electrical serial hybrid rigid bus

For the HDV class rigid bus also the model of a serial hybrid powertrain was created. The main data of the bus model is given on p. 172, Table 34, "C) Diesel-electrical serial hybrid vehicle". The models of the (serial hybrid) electrical buses were simulated with VECTO v1.4 for technical reasons, and the output was the course of engine operation points for the EM. Below the further calculation is described, what was developed as a postprocessing in Excel.

- The state of charge (SOC) of the supercapacitor at cycle start equals the SOC at end, what was reached by adjusting the SOC at simulation start.
- The model offers the hybrid functions regenerative braking and electrical driving. A start-stop function was implemented indirectly. The auxiliary consumers were powered electrically, and the diesel engine starts only to propel the genset, when the supercapacitor reaches the lower SOC limit.
- From the course of EM operation points from the VECTO output the course of electrical power at the EM clamps was interpolated from its performance map.

- During regenerative braking, where the EM operates as generator, the supercapacitor is charged, and at the beginning of electrical driving it is discharged.
- For both directions of the power flow two times 5 % losses are considered, for the inverter and the internal losses in the capacitor.
- When the capacitor is full during phases of longer downhill braking, the EM does not work longer as generator, and a higher actuation of the mechanical friction brakes at the wheels is assumed.
- For SOC values ≤ 0.30 of the capacitor the genset is turned on. The minimum SOC is 0.20 to ensure a minimum voltage at the capacitor output.
- When the capacitor is discharged at SOC = 0.20 during standing or driveaway, the total demand of electrical power is fulfilled by the genset.
- The FC-map of the diesel engine was combined with the scaled generator map of the EM, and the result is the map of electrical efficiency of the genset: $\eta_{el,genset} = P_{el,genset} / LHV_{diesel}$. $\eta_{el,genset}$ is the ratio of (generated electrical power) to (lower heating value of the consumed diesel fuel). The genset worked mainly on the curve of highest efficiency per electrical power, see Figure 78.

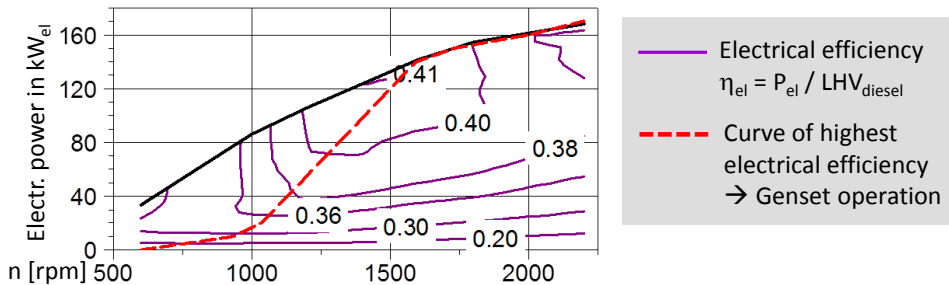


Figure 78. Map for electrical efficiency of diesel genset, curve of best efficiency per power.

- The effective power of the diesel engine is calculated from the mechanical power demand for the generator and the acceleration power demand to overcome the inertias of engine and generator. With the speed of the genset and the power demand at the diesel engine the FC is interpolated from the performance map.
- A simple control strategy was assumed: During driving the EM works as motor and is fed at first from the supercapacitor. When the SOC gets below 0.30, the genset starts, and when the SOC reaches the lower limit 0.20, the demanded electrical power is provided only by the genset. During braking the EM works as generator and charges the capacitor until the upper SOC of 1.00 is reached. The brake power below the generator power of the EM is provided by the friction brakes at the wheels.

The output for a section of the Urban Bus cycle is shown in Figure 79 and Figure 80.

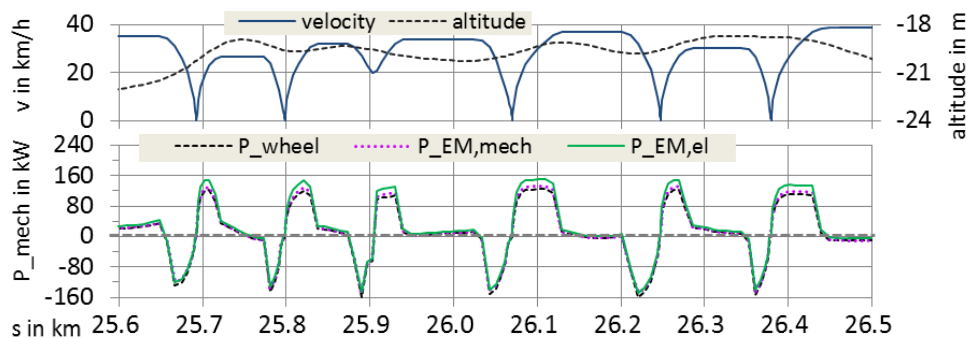


Figure 79. Model of diesel-electrical serial hybrid rigid bus, section of Urban Bus cycle, part 1

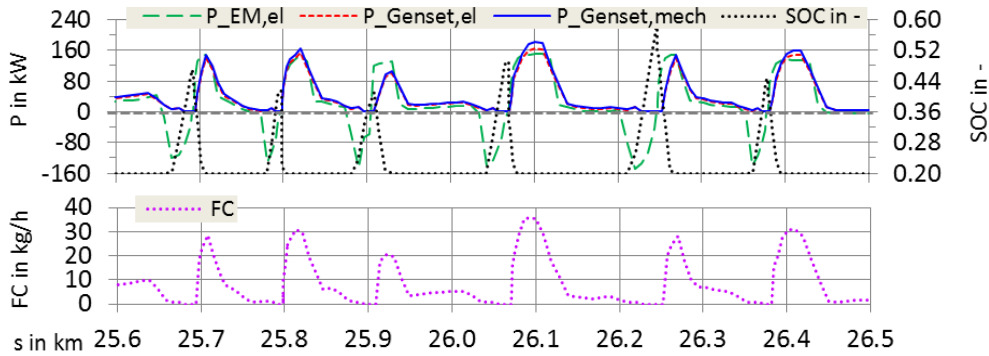


Figure 80. Model of diesel-electrical serial hybrid rigid bus, section of Urban Bus cycle, part 2

2.5.4 Battery-electrical delivery truck and rigid bus

The models for battery-electrical HDV were the combination of a VECTO simulation and a postprocessing in MS Excel. The main data of the vehicle models is given on p. 173, Table 34, "D) Battery-electrical vehicle" and p. 178 Table 38 " Battery-electrical delivery truck 'Smith'". For the powertrain structure of the bus models see p 72. Figure 70 right "Serial hybrid", where supercondensator and diesel genset are replaced by a Li-Ion battery. In case of the model for an electrical delivery truck the EM is connected with a 3-speed AT to the cardan shaft, and for the BEV truck "Smith" with a 1-speed reduction gear.

The vehicle models were simulated with VECTO v1.4 due to technical reasons and the output were the operation points for the EM. Below the subsequent postprocessing is described.

- From the course of EM operation points from the VECTO output the course of electrical power at the EM clamps was interpolated from its performance map.
- During driving and standing the battery is discharged by the EM, working as motor, and/or the electrical auxiliary consumers. During regenerative braking, where the EM operates as generator, the battery is charged.
- For both directions of the electrical power flow 2 times 5 % losses are considered, for the inverter and the internal losses in the battery.

The output for a section of the Urban Bus cycle is shown in and Figure 82.

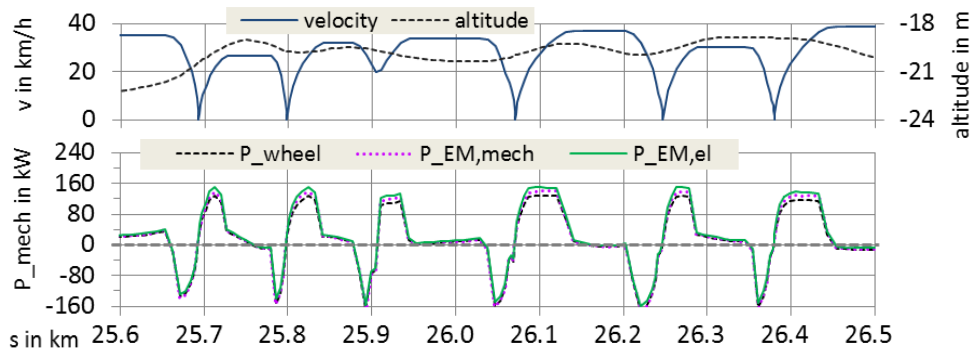


Figure 81. Model of battery-electrical rigid bus, section of Urban Bus cycle, part 1

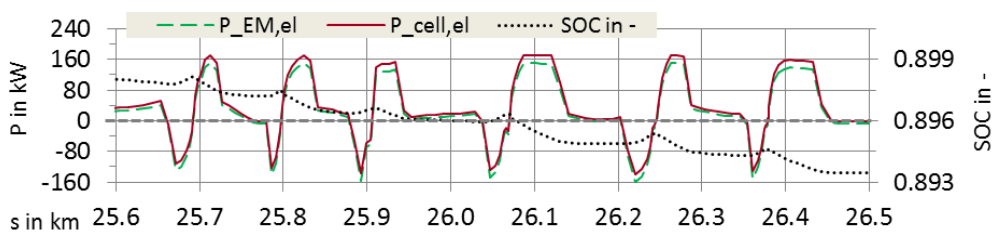


Figure 82. Model of battery-electrical rigid bus, section of Urban Bus cycle, part 2

For the battery-electrical vehicle models 10 % charging losses from grid to battery are added to the energy consumption from the battery (162 p. 10) (163 p. 1).

2.5.5 Overload of the models of electrical machines

Like written above on p. 72 in the introduction to chapter 2.5, electrical machines (EM), here permanent magnet synchronous machines (PMSM), can be operated for a certain duration at multiple overload. The limit is the temperature of the copper windings of the stator, which are usually the hottest parts in the machine⁵². When it gets too high, the electrical insulation material becomes damaged, which is available for temperature classes from 90 °C to 250 °C (164 p. 7) (165 p. 16 ff.). The thermal stability of the insulation of the copper windings of the stator is the effective limit for the duration of the overload.

For the detailed analysis of the temperature distribution in the EM finite-elements programs are used to simulate the thermal masses in the machine as a network, where heat flows are exchanged⁵³. This way the temperature course of the EM can be simulated during transient load cycles, also for the traction machines of motor vehicles⁵⁴.

Such a thermal model and the necessary input data was not available for the PMSM, which served as basis for the machines in this thesis. Hence the overload was assessed by characteristic values, which were calculated from the simulation results of the (hybrid) electrical HDV models. Thus it was at least possible to estimate where thermal problems may occur and where likely not. The characteristic values are:

$(P/P_{\text{cont}})_{\text{avrg}}$	Energised electrical machine ($P_{\text{EM,el}} \neq 0$): Average ratio of (mechanical power) to (continuous mechanical power).
share overload	Energised electrical machine ($P_{\text{EM,el}} \neq 0$): Ratio of (duration of overload) to (overall duration of operation).
$(P_{\text{overload}}/P_{\text{cont}})_{\text{avrg}}$	During overload: Average ratio of (mechanical overload power) to (mechanical continuous power).
overload _{1min,avrg}	Subdivision of simulation results into intervals of one minute: Average ratio of (overload duration) to (interval duration), only for those intervals, where overload occurs. In literature a ratio of 0.17 at triple overload is assumed to be possible in intervals of one minute, when the overall average power equals the continuous power (166 p. 2624). For double overload the ratio was estimated to 0.25 for this thesis.
overload _{1min,max}	Subdivision of results into intervals of one minute: Maximum ratio of (overload duration) to (interval duration), only for those intervals, where overload occurs.

⁵² See e. g. (577 pp. 91, 192) (578 pp. 18, 62 ff.) (579 pp. 412, 417) (580 pp. 24, 111 ff.)

⁵³ For the thermal models of EM see e. g. (581) (582 pp. 31-46) (583 pp. 13-39) (584 pp. 42-87).

⁵⁴ Transient thermal simulations of EM are shown e. g. in (585) (586) (587) (588) (589) (590).

The results for the vehicle models with full payload are shown in Figure 83.

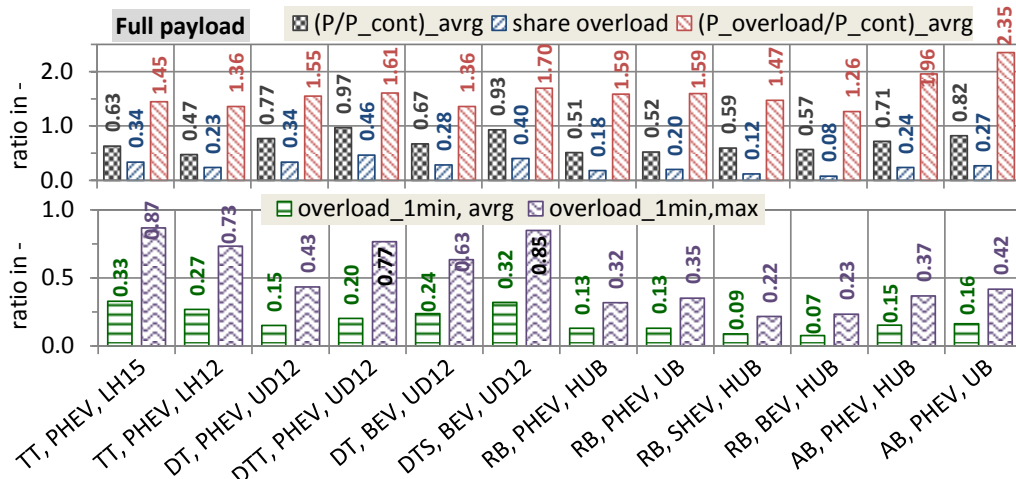


Figure 83. Models of (hybrid) electrical vehicles, full payload⁵⁵. Characteristic values for overload.

For the vehicle models at full payload the average ratio of the power of the EM to its continuous power ranges from 0.47 to 0.97, where the model of the parallel hybrid delivery tractor-trailer on the Urban Delivery Cycle 2012 produces the highest value. The share of overload at the total EM operation is 0.08 to 0.46. When looking only at the overload phases, the average ratio of the power to the continuous power ranges from 1.26 to 2.35, the highest value is found for the parallel hybrid articulated bus on the Urban Bus cycle. For this vehicle the permitted overload is the highest at 300 % of the continuous load.

The analysis of the temporal distribution showed, that in those intervals of one minute length where overload occurred, the average share of the operation with increased power at the interval length ranges from 0.07 to 0.33, with peak values from 0.22 to 0.87. The maximum value resulted from the model of the parallel hybrid long haul tractor-trailer on the Long Haul cycle 2015, which includes one long braking phase of 1¹/₄ minute during downhill driving. The same model on the Long Haul cycle 2012, the parallel hybrid delivery tractor-trailer, the battery-electrical delivery truck "Smith" and the battery-electrical rigid bus reached also high overload shares above 0.50 in single minutes. In case of the urban vehicles phases of driving and braking at overload followed each other subsequently at some occasions.

With these results it can be estimated for the simulations with full payload, that for the models parallel hybrid tractor-trailers long haul and delivery, battery-electrical delivery truck "Smith", battery-electrical rigid bus and parallel hybrid articulated bus temperature problems may occur during some phases. In reality the motor- or generator power of the electrical machines would be reduced to avoid damage. Thus for full payload the applied curves for maximum and minimum power of the machines seem to be too high for some models.

For a better assessment of the thermal stress a detailed simulation of the heat exchange plus the measurement of a machine on a typical duty cycle for the adjustment of the model can be conducted in future research.

⁵⁵ AB - Articulated bus, BEV - Battery electrical vehicle, DT - Delivery truck, DTS - Battery-electrical delivery truck "Smith", DTT - Delivery tractor-trailer, HUB - Cycle Heavy Urban Bus, LH12 - Cycle Long Haul 2012, PHEV - Parallel hybrid electrical vehicle, RB - Rigid bus, SHEV - Serial hybrid electrical vehicle, TT - Tractor-trailer, UB - Cycle Urban Bus, UD12 - Cycle Urban Delivery 2012.

Full payload: TT 25.8 t; DTs 5.1 t to 5.9 t; DTT 14.7 t; RB 80 Pass., ~ 5.4 t; AB 130 Pass., ~ 8.8 t

In addition the models were simulated with average payload, see Figure 84.

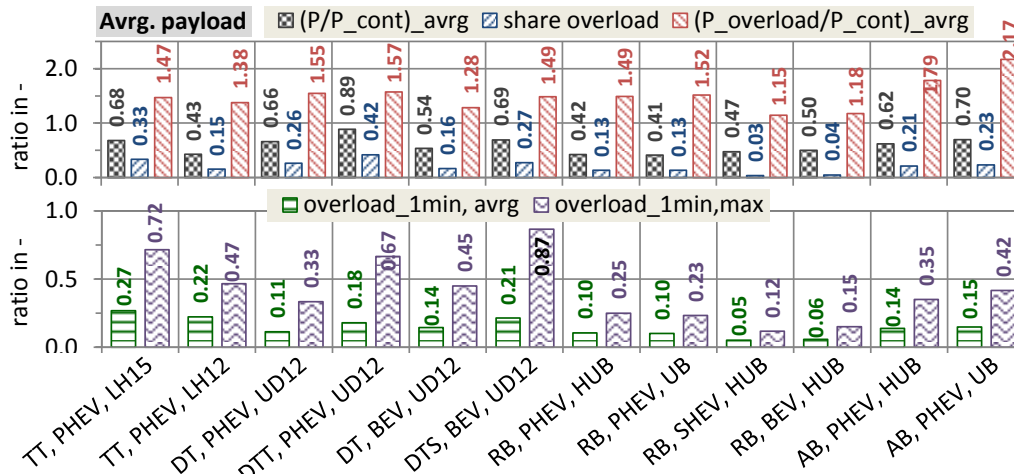


Figure 84. Models of (hybrid) electrical vehicles, average payload⁵⁶. Characteristic values for overload

For the simulations with average payload the stress of the virtual electrical machines is lower than for full payload. E. g. the average ratio of the power to the continuous power ranges from 0.41 to 0.89 instead 0.47 to 0.97, also the share of overload operation gets lower to 0.03 to 0.42 instead of 0.08 to 0.46. In case of the parallel hybrid articulated bus the average ratio of overload to continuous power is still high at 1.79 and 2.17, but lower than for full payload. The temporal distribution of the overload phases showed for the parallel hybrid tractor-trailers long haul and delivery or for the battery-electrical delivery truck "Smith" one minute or two minutes at different parts of the cycle, where the share of overload was above 0.50. In case of the hybrid long haul tractor-trailer the longest continuous overload phase was 1¹/₄ minute during downhill driving, like for the simulation with full payload. The average of the share of overload in the intervals of 1 minute from all models was 0.05 to 0.27, thus lower than with full payload, where it was 0.07 to 0.33.

It is estimated, that the curves for maximum and minimum power of the electrical machines work for the simulations with average payload and real machines would likely not overheat.

⁵⁶ Average payload: TT 14.5 t; DT 1.8 t; DTT 9.14 t; DTS 1.8 t; RB 16 Pass., 1.1 t; AB 26 Pass., 1.8 t.

2.6 Basis vehicle models EURO VI, state of technology 2014

The VECTO program was applied to generic, representative models of three selected EURO VI HDV: Tractor-trailer GCWR 40 t, delivery truck GVWR 12 t and rigid city bus 18 t. For a preceding project the technical level of the basis HDV models, MY 2014, was discussed with the industry (5 pp. 55, 98, 211). The models were simulated on the corresponding driving cycles: Long haul 2015, Urban Delivery 2012 and Urban Bus. Examples for the HDV classes are shown in Figure 85.



Figure 85. Examples for simulated HDV classes. F.l.t.r.: Tractor-trailer, delivery truck, rigid city bus

2.6.1 Creation of basis vehicle models

The basis vehicle models of this thesis exist only virtually and could not be compared with test results. Hence it was evaluated, if the single steps when deriving them from models close to test vehicles EURO V are plausible. The models of the EURO V HDV were compared directly with test results, and afterwards single components were changed to get to the basis EURO VI models. For every step the relative change in the simulated FC was analysed.

2.6.1.1 Tractor-trailer and delivery truck

The basis models for tractor-trailer and delivery truck were derived from separate models, which could be compared directly with measured vehicles. The FC was measured in both cases with a mobile fuel flowmeter of 0.1 %-of-reading accuracy (AVL KMA Mobile Typ 150, year 2010).

The tested tractor-trailer was a vehicle EURO V 350 kW with a curtainsider trailer, see (50 pp. 146, HDV4) and here p. 192, Table 56, first entry. The driving cycle was a trip on the motorway near Graz, starting at junction "Wundschuh", see p. 162 Figure 189.

The measured delivery truck 12 t was a chassis of wheelbase 4.8 m, with a small cabin, a 6-cylinder engine EURO V 175 kW, a rigid body and a tail-lift 1.5 t·m⁵⁷, see p. 195, Table 59 first entry. A very similar truck of wheelbase 4.2 m was investigated during a preceding project (50 pp. 146, HDV6). The measurement cycles were "Regional Delivery 2012" and "Urban Delivery 2012 flat", on the HDV chassis dyno of IVT, TU Graz.

⁵⁷ Lifting capacity of tail-lift. Horizontal distance of mass on tail-lift to rear loading sill. 1 t·m \approx 9.81 kNm

For the models similar to the specimen the input data is given on p. 176, Table 37, first two entries. The simulated FC was compared directly with the recorded FC, see Figure 86.

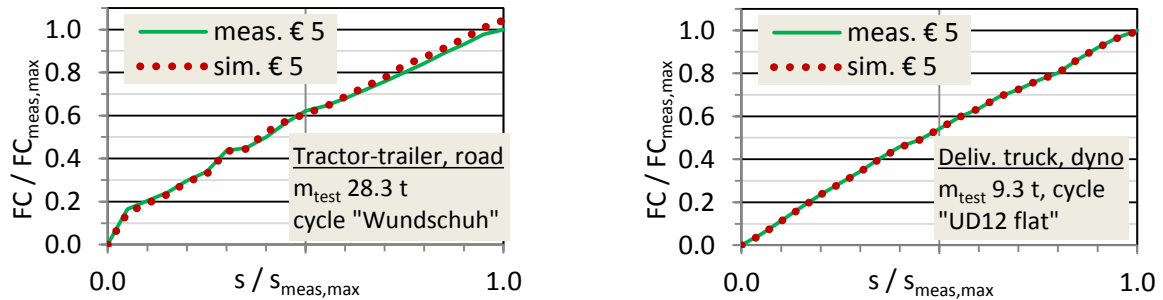


Figure 86. Validation, models of measured trucks EURO V (€ 5)

After the comparison with the measurement results, the models of the EURO V trucks were changed stepwise to the basis truck models EURO VI for this thesis. The steps for the tractor model are shown in Table 14.

Table 14. Derivation of basis tractor-trailer model EURO VI from measured EURO V vehicle

	Variant	$v_{roll,avg}$ km/h	$W_{tract,wh}$ kWh _{mech} /km	$\eta_{ICE,avg}$ ⁵⁸ -	FC L/100km	Dev. %
0)	Measurement motorway, cycle "Wundschuh", <u>Original vehicle</u>	80.25	<i>not known</i>		25.35	<i>basis</i>
1)	Simulation → Model of measured tractor EURO V ⁵⁹ For the model data see p. 176 Table 37	80.23	0.954	0.407	26.39	+4.1
1a)	Variation: Model 1) w/o crosswind correction	80.29	0.880	0.402	24.87	-1.9
2)	1) + final drive ratio 2.65, instead of 3.07	80.29	0.956	0.413	25.78	+1.7
3)	2) + tires 315/70R22.5 instead of 385/55R22.5; r_{dyn} 0.492 m, instead of 0.522 m	80.22	0.956	0.411	25.97	+2.5
4)	3) + engine 6 cyl. 12 L € 6 350 kW; map 12 L € 6 350 kW with FL curve 12 L € 5/6 350 kW; instead of map 12 L € 5 350 kW with full load curve 12 L € 5/6 350 kW	80.22	0.956	0.417	25.61	+1.0
5)	4) + engine 6 cyl. 11 L € 6 330 kW; map 11 L € 6 320 kW with full load curve 11 L € 6 316 kW, instead of map 12 L € 6 350 kW with full load curve 12 L € 5/6 350 kW	80.08	0.957	0.420	25.48	+0.5
6)	5) + tractor 7.2 t, instead of 8.5 t → Basis model tractor EURO VI for this thesis, compare p. 87 Table 17	80.09	0.934	0.420	24.89	-1.8

⁵⁸ $\eta_{eng,avg} = \int (P_{eng,gross,pos}) dt / \int (FC(P_{eng,gross,pos}) \cdot LHV_{diesel}) dt = W_{eng,gross,pos} / \int (FC(P_{eng,gross,pos}) \cdot LHV_{diesel}) dt$; thus the ratio of (positive gross engine cycle work) to [(fuel consumed during positive gross engine power) times (lower heating value of diesel fuel, 11.94 kWh_{th}/kg)]. Transient correction factor (TCF) considered, compare p. 36.

⁵⁹ Simulation with the VECTO shifting model, the real gears were not recorded. But the deviation should be small, on the motorway the direct 12th gear was engaged most times.

For the model 1) of the measured tractor-trailer EURO V the deviation of the simulated FC of + 4.1 % is higher than expected for a dataset, where the powertrain data is known well. For comparison reasons variation 1a) without the default crosswind correction was simulated, and the calculated FC decreases by 5.8 %, compared to variant 1). As described on p. 21 ff. at the end of section 2.2.1.3, the default effective wind velocity of 3 m/s seems to be too high for some interior regions, when the vehicle in the boundary layer near to the ground is investigated. But because the measurement was conducted during a light breeze⁶⁰, no wind would be too low.

→ Taking into account that also the rolling resistance of the utilised tires is not known, it can only be stated, that the model of the tractor-trailer EURO V produces results, which are likely less than 5 % away from the measurements.

The change of FC for every single changed component is credible, and the resulting basis model of a tractor EURO VI for this thesis produces plausible results, as will be shown later.

The steps to get from the model of the tested EURO V delivery truck to the basis model EURO VI for this thesis is shown in Table 15.

Table 15. Derivation of basis delivery truck model EURO VI from measured EURO V vehicle

	Variation	$v_{roll,avrg}$ km/h	$W_{tract,wh}$ kWh _{mech} /km	$\eta_{ICE,avrg}$ -	FC L/100km	Dev. %
Regional Delivery Cycle 2012						
0)	Measurement chassis dyno <u>Original vehicle</u>	63.62	0.640	<i>not known</i>	20.32	<i>basis</i>
1)	Simulation → Model of measured truck EURO V For the model data see p. 176 Table 37	63.34	0.651	0.395	19.74	-2.8
2)	1) + VECTO shifting model <i>instead of measured gears</i>	63.29	0.651	0.395	19.86	-2.3
Urban Delivery Cycle 2012, flat						
0)	Measurement chassis dyno <u>Original vehicle</u>	38.19	0.572	<i>not known</i>	20.90	<i>basis</i>
1)	Simulation → Model of measured truck EURO V For the model data see p. 176 Table 37	37.54	0.566	0.366	20.65	-1.2
2)	1) + VECTO shifting model <i>instead of measured gears</i>	37.31	0.565	0.373	20.79	-0.5
3)	2) + 6-cyl. engine 6.4 L € 6 175 kW; map 6.4 L € 6 228 kW with full load curve 6.4 L € 5/6 175 kW; <i>instead of map 6.4 L € 5 228 kW w. full load curve 6.4 L € 5/6 175 kW</i>	37.31	0.565	0.388	19.96	-4.5
4)	3) + Standard average auxiliary power of EURO VI delivery truck, incl. alternator, 2.9 kW _{mech} <i>instead of 3.5 kW_{mech}</i> (avrg. power of intermittent auxiliaries of tested truck)	37.39	0.566	0.387	19.58	-6.3
5)	4) + wheel base 4.4 m (-0.15 t) <i>instead of 4.8 m</i> ; rigid body 6.1 m 15 pallets (-0.4 t) <i>instead of 7.2 m 17 pallets</i> ; rear axle leaf suspension (-0.05 t) <i>instead of air suspension</i> curb mass 6.3 t <i>instead of 6.9 t</i>	37.36	0.538	0.386	18.74	-10.3

⁶⁰ The meteorological station of the airport Graz Thalerhof recorded during the measurement, 2010-10-10 from 15⁰⁰ to 15³⁰ CEST (UTC +2), wind in the range from 2.0 to 2.6 m/s from southeast by south, against the driving direction. The distance from the station to the motorway section was 6 km to 31 km, hence at the vehicle other wind velocities have occurred.

	Variation	$v_{roll,avrg}$ km/h	$W_{tract,wh}$ kWh _{mech} /km	$\eta_{ICE,avrg}$ -	FC L/100km	Dev. %
6)	5) + 4-cyl. engine 5.1 L € 6 154 kW; map 5.1 L € 6 177 kW with full load curve 5.1 L € 6 154 kW; <i>instead of</i> map 6.4 L € 6 228 kW with full load curve 6.4 L € 5/6 175 kW curb mass 6.1 t <i>instead of</i> 6.3 t	37.28	0.537	0.394	18.26	-12.6
7)	6) + final drive ratio 4.63, <i>instead of</i> 4.30 → Basis model delivery truck EURO VI for this thesis, compare p. 87 Table 17.	37.39	0.538	0.395	18.22	-12.8

Also for the delivery truck EURO VI the change of FC during the stepwise conversion from the model EURO V of the measured truck to the basis model of this thesis is credible.

2.6.1.2 Rigid city bus 12 m

The basis model for the 12 m rigid bus was also derived from a vehicle model, which could be compared directly with a measured vehicle. Here the FC was calculated via the carbon balance from the CO₂ emissions⁶¹, recorded at the HDV dyno of IVT, TU Graz.

The measured EURO V bus was from public transportation Brussels (STIB), p. 199, Table 62, first entry, and the measurement cycles were "Braunschweig" and "Graz", see p. 156 Figure 157 and p. 158 Figure 166.

For the model similar to the specimen the input data are given on p. 176, Table 37, "Rigid Bus € 5". The simulated FC from was compared with the recorded FC, Figure 87.

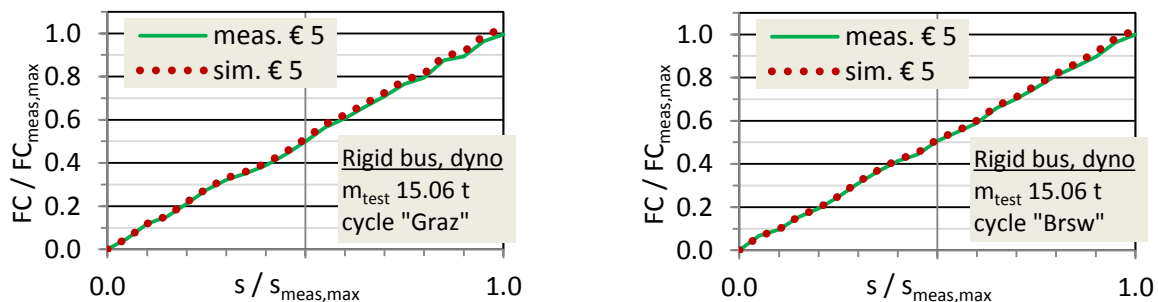


Figure 87. Validation, model of measured bus EURO V

Subsequently the basis bus model EURO VI for this thesis was derived step-by-step from the model of the test vehicle, compare Table 16.

Table 16. Derivation of EURO VI rigid bus model from measured EURO V vehicle

	Variation	$v_{roll,avrg}$ km/h	$W_{tract,wh}$ kWh _{mech} /km	$n_{eng,rel,avrg}$ ⁶² -	FC, L/ 100km	Dev. %
Graz cycle						
0)	Measurement chassis dyno <u>Original vehicle</u>	19.57	1.218	0.156	48.03	<i>basis</i>
1)	Simulation → Model of measured bus EURO V For the model data see p. 176 Table 37	19.67	1.202	0.160	49.15	+2.3

⁶¹ mass shares carbon: $Y_{C,Diesel} \approx 0.860$; CO_2 : $Y_{C,CO_2} \approx 0.272$; \Rightarrow ca. 3.16 kgCO₂ from 1 kg-Diesel

⁶² Average relative engine speed: $n_{eng,rel} = (n_{eng,curr} - n_{eng,idle}) / (n_{eng,rated} - n_{eng,idle})$

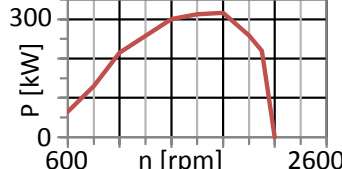
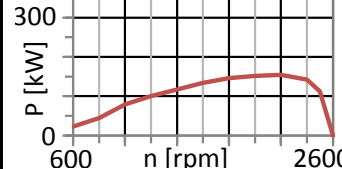
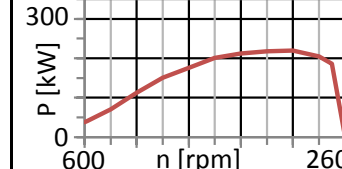
	Variation	$V_{roll,avg}$ km/h	$W_{tract,wh}$ kWh _{mech} /km	$n_{eng,rel,avg}$ ⁶² -	FC, L/ 100km	Dev. %
Braunschweig cycle						
0)	Measurement chassis dyno <u>Original vehicle</u>	28.57	1.178	0.198	42.79	<i>basis</i>
1)	Simulation ➔ Model of measured bus EURO V For the model data see p. 176 Table 37	28.97	1.179	0.205	43.46	+1.4
2)	1) + 6 cyl. engine 7.7 L € 6 220 kW <i>instead of</i> 6 cyl. engine 11.0 L € 5 235 kW; map 7.7 L € 6 260 kW with full load curve 7.7 L € 6 220 kW; <i>instead of</i> map 11.0 L € 5 320 kW with full load curve 11 L € 5 235 kW Average engine efficiency ($\eta_{ICE,avg}$) 0.389 (7.7 L, € 6) <i>instead of</i> 0.372 (11.0 L, € 5)	29.06	1.177	0.171	41.17	-3.9
3)	2) + curb mass 11.00 t <i>instead of</i> 12.44 t	28.95	1.078	0.162	38.47	-10.2
4)	3) + final drive ratio 5.77 <i>instead of</i> 5.47 ➔ Basis model rigid bus EURO VI for this thesis, compare p. 87 Table 17.	28.96	1.078	0.171	38.32	-10.6

With the model of the measured bus EURO V the FC is matched with +1.4 % and +2.3 % accuracy. The changes in FC when converting the model of the measured bus virtually to the model of a lighter EURO VI vehicle with a smaller engine and an final drive with a higher gear ratio are credible, when assessed severally.

2.6.2 Overview of basis vehicle models

The main technical data as input for the vehicle models is shown here in Table 17, more details and the sources for the data are given in the data section, p. 166 ff. Table 30.

Table 17. Technical data, simulated FC and GHG emissions of basis vehicle models EURO VI, MY 2014

	Tractor-trailer, GCWR 40 t	Delivery truck, GVWR 12 t	Rigid city bus, GVWR 18 t
Technical data of vehicle models			
Vehicle	Tractor 4x2, wheelbase 3.5 m Long-haul cabin 3-axle trailer, curtainsider, 13.62 m, 34 pallets	Chassis 4x2, wheelbase 4.4 m Small cabin Rigid body 6.1 m, 15 pallets, tail-lift 1.5 t·m (14.72 kNm)	Bus 4x2, wheelbase 5.9 m Rigid cabin 12 m 35 seats, 45 stances
Cycle	Long Haul 2015 (LH15) p. 154 Figure 146	Urban Delivery 2012 (UD12) p. 155 Figure 152	Urban Bus (UB) p. 155 Figure 151
For the cycle statistics like average velocities, stand ratio, stops per km etc. see p. 163 ff. section 5.4.3			
En- gine	In-line 6, 11 L $P_{rat} = 316 \text{ kW @ } 1800 \text{ rpm}$ $\eta_{ICE,avg} \mathbf{0.424}$, $\eta_{ICE,max} 0.455$	In-line 4, 5.1 L $P_{rat} = 154 \text{ kW @ } 2200 \text{ rpm}$ $\eta_{ICE,avg} \mathbf{0.387}$, $\eta_{ICE,max} 0.438$	In-line 6, 7.7 L, $P_{rat} = 220 \text{ kW @ } 2200 \text{ rpm}$ $\eta_{ICE,avg} \mathbf{0.371}$, $\eta_{ICE,max} 0.438$
Full load curve			

	Tractor-trailer, GCWR 40 t	Delivery truck, GVWR 12 t	Rigid city bus, GVWR 18 t
Gearbox, average efficiency	12-speed AMT, 14.90 to 1.00 i_{fd} 2.65 $\eta_{mech,gear,indir} = 0.973$ $\eta_{mech,gear,dir} = 0.981$ $\eta_{mech,ret-idle} = 0.985$ $\eta_{mech,FD} = 0.959$ $\eta_{mech,drivetr} = 0.925$	6-speed AMT, 6.75 to 0.78 i_{fd} 4.63 $\eta_{mech,gear,indir} = 0.965$ $\eta_{mech,gear,dir} = 0.981$ $\eta_{mech,FD} = 0.957$ $\eta_{mech,drivetr} = 0.926$	4-speed AT, 1.36 to 0.74 Power split 1 st gear, activated hydraulic torque converter i_{fd} 5.77 $\eta_{mech,gear,1,Tq-conv} = 0.728$ $\eta_{mech,gear,2} = 0.952$ $\eta_{mech,gear,3} = 0.925^{63}$ $\eta_{mech,gear,4} = 0.891$ $\eta_{mech,FD} = 0.953$ $\eta_{mech,drivetr} = 0.840$
RRC classes	Steer 315/70R22.5, RRC B Drive 315/70R22.5, RRC B Trailer 385/65R22.5, RRC B $RRC_{total} = 4.5$ N/kN	Steer 265/70R19.5, RRC D Drive 265/70R19.5, RRC D $RRC_{total} = 6.7$ N/kN	Steer 275/70R22.5, RRC D Drive 275/70R22.5, RRC D $RRC_{total} = 6.4$ N/kN
Aerodynamics	$C_d = 0.51$, $A_{cr} = 10.00$ m ² <u>Tractor</u> : Fairings cabin to trailer, closable grille, side panels, partial lining underbody <u>Trailer</u> : No measures <u>Side wind</u> : Standard curve	$C_d = 0.57$, $A_{cr} = 9.10$ m ² Fairing cabin-roof to body <u>Side wind</u> : Standard curve	$C_d = 0.64$, $A_{cr} = 8.00$ m ² Cuboid shape, rounded edges <u>Side wind</u> : Standard curve
Engine auxiliaries: Constant average values from (103 p. 166 ff.)			
	$P_{aux,avrg} = 4.8$ kW	$P_{aux,avrg} = 3.1$ kW	$P_{aux,avrg} = 7.4$ kW
Mass	<u>Tractor</u> : 7.20 t, tank 800 L, half full <u>Trailer</u> : 6.2 t <u>Payload</u> 14.5 t (max. 26.6 t)	<u>Chassis</u> : 4.5 t; <u>Body</u> : 1.1 t <u>Tail-lift</u> : 0.5 t <u>Payload</u> 1.8 t (max. 5.9 t)	<u>Curb weight</u> : 11.0 t avrg. 16 passengers \approx 1.10 t max. 80 passengers \approx 5.44 t
<i>For the average payload of the HDV classes see p. 187 section 5.10</i>			
Simulation results for FC tank-to-wheel and for GHG emissions well-to-wheel⁶⁴			
FC, GHG	27.8 L/100km 62 gCO _{2e} /tkm	19.0 L/100km 343 gCO _{2e} /tkm	41.0 L/100km 83 gCO _{2e} /pkm

The models were also simulated for variations of payload from empty to full, see Figure 88.

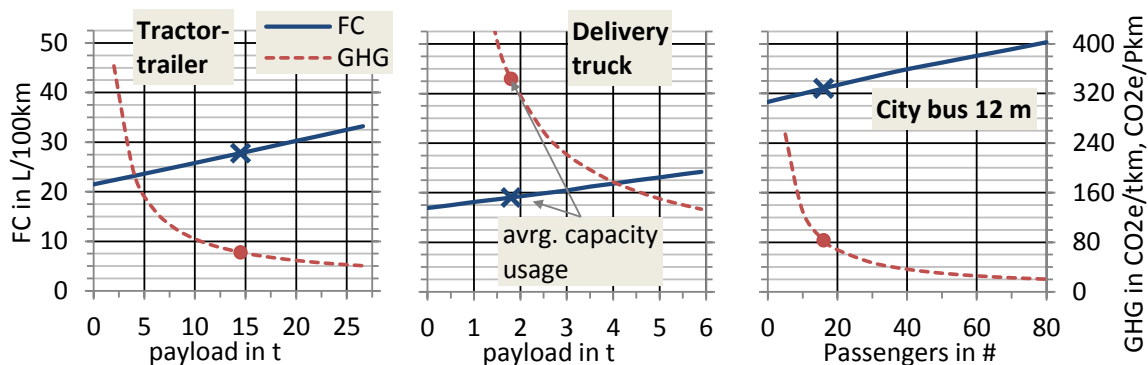


Figure 88. Capacity usage, fuel consumption and payload-specific greenhouse gases

⁶³ In this case the lower power loss of the direct 3rd gear is outweighed by a small average input power, what leads to a lower average efficiency, compare the example map for a truck on p. 23 Figure 22. Usually the average efficiency of direct gears is higher than of stepped-up indirect gears, see the results for the trucks.

⁶⁴ GHG emissions well-to-wheel (WTW) in CO_{2e} for 100 % fossil diesel: Emissions from combustion (tank-to-wheel, TTW) plus production of fuel (well-to-tank, WTT) in CO₂-equivalents. I. e. the sum of GHG, converted to an overall equivalent of CO₂ with the same warming potential. GHG factors see p. 165 Table 29

For tractor-trailer, delivery truck and rigid bus the empty vehicle models output 21.5, 16.9 and 38.3 L/100km. At full payload the results are 33.2, 24.2 and 50.3 L/100km, where the FC is with good approximation linearly dependent on the payload.

The payload-specific GHG emissions decrease for a higher capacity usage. For the average loaded basis HDV models tractor-trailer, delivery truck and rigid bus the ratios of payload to total vehicle mass are 52, 23 and 9 %. In addition to the much more transient urban driving cycles this leads to significantly higher specific GHG emissions: 343 and 1221 gCO_{2e}/tkm for the delivery truck and for the rigid bus respectively, vs. 62 gCO_{2e}/tkm for the tractor-trailer. On every driving cycle it is prodigal to move 75 to 90 % vehicle mass for 25 to 10 % payload.

To get an impression of possible savings, the split of engine work output is useful, Figure 89.

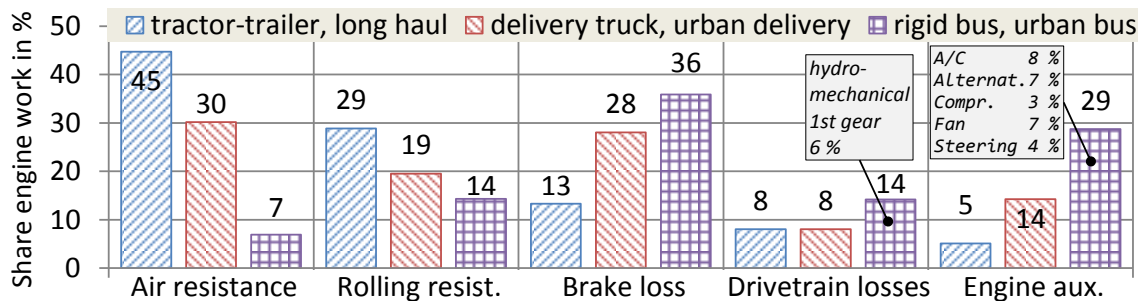


Figure 89. Split of engine work output, basis heavy-duty vehicle models with average payload

For the tractor-trailer model 45 % of the work are consumed by the air drag, 29 % by the rolling resistance of the tires, 13 % by the friction brakes at the wheels, 8 % by the drivetrain friction incl. idling retarder and 5 % by the engine auxiliary consumers. Thus for this vehicle class saving measures for air drag and rolling resistance are particularly effective.

In case of the delivery truck model, where the Urban Delivery cycle 2012 is much slower than the Long Haul cycle 2015 (v_{avg} 30.8 vs. 79.6 km/h) and more transient, the split is another: 30, 19, 28, 8 and 14 %. The share of air drag and rolling resistance is lower and the brake loss significantly higher. Also the engine auxiliaries consume a higher share.

On the slow and transient Urban Bus cycle with the bus model (v_{avg} 17.7 km/h) the air drag is not very significant at 7 %, hence aerodynamic measures for city buses are not efficient. On the other hand the brake loss is high at 36 %, the drivetrain friction contributes 14 %, incl. 6 % losses in the first hydro-mechanical gear during drive off, and the engine auxiliaries consume 29 % of the work. Thus for this vehicle class regenerative braking should be useful, also efficient auxiliaries with reduced idle losses.

2.6.3 Check for plausibility of basis vehicle models

In this chapter the basis models of the HDV are checked for plausibility. FC values from own measurements and publications were collected, and the model results were compared.

The engine performance maps of all HDV models were compared with measurement results and showed conformity, and also the average efficiencies of the truck transmissions are in line with guidance- and default values, compare p. 180 ff. sections 5.8 and 5.9.

2.6.3.1 Models of tractor-trailer and of delivery truck

In the following paragraphs the basis model for a tractor-trailer, p. 87 Table 17, is compared with published measurement and simulation data. The collected FC numbers are shown on p. 192 ff. Table 56, and the calculated payload-specific GHG values on p. 194 ff. Table 57.

The model was simulated on the cycles Flat-80km/h, Long Haul 2012 and Long Haul 2015, from empty to full payload in steps of 2 t. The measurands are from tractor-trailers with known payload, EURO III, MY ca. 2000, to early EURO VI, MY 2014. For that decade no significant

change in average FC is reported (45 p. 150 ff.) (46 p. 31) (47 p. 11) (48 p. 30) (49 p. 28)⁶⁵, hence the values are comparable. The results are shown in Figure 90 and Figure 91.

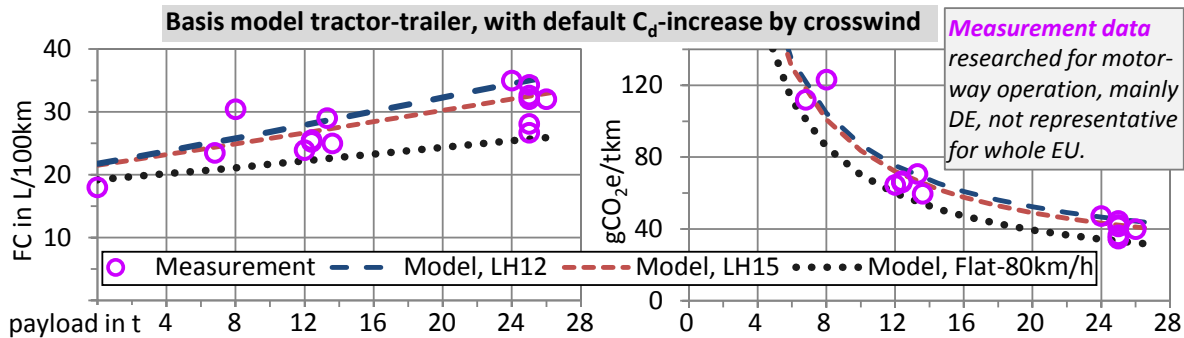


Figure 90. Basis model tractor-trailer, comparison with measurement, w. default correction for crosswind.

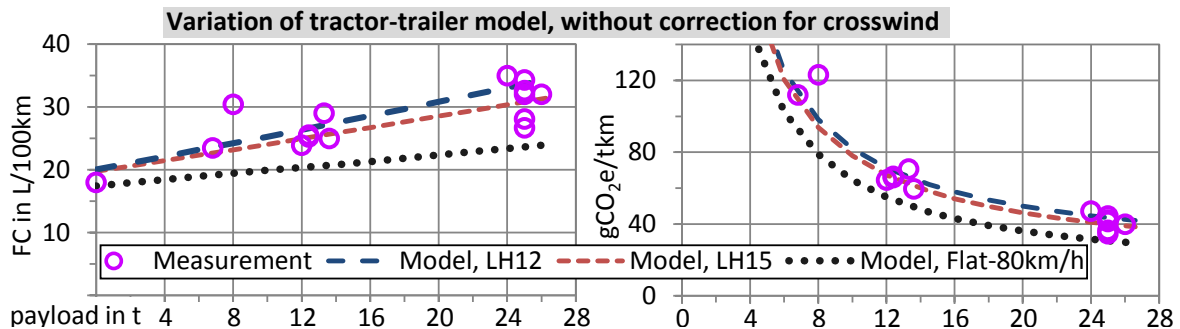


Figure 91. Basis model tractor-trailer, comparison with measurement, w/o correction for crosswind.

With the default correction for crosswind the model outputs FC values which are at the upper end of the scatter plot of measurement results from tractor-trailers on motorways. As described on p. 21 ff. at the end of section 2.2.1.3, an average effective wind velocity of 3 m/s seems to be too high for mid- and south-Germany, where most of the measurements took place in the corridors of the motorways. Thus the model was simulated without crosswind and then the results are in the range of measurements, or in case of the cycle Flat-80km/h below.

It shall be mentioned that the unknown RRC of the tires of the measured vehicles and also uncharted properties of other components like the real air drag coefficients or the auxiliary consumers add additional uncertainty to the comparison.

Thus it can only be stated that the model produces FC numbers which are in the range of measurement values, and the default effective wind velocity can be too high for some regions. A detailed validation of the model of an EURO VI tractor-trailer, which existed only virtually, was not possible.

The basis model tractor-trailer was also compared to a reference model in VECTO from the manufacturers. In 2013 TML collected data from the European OEM to forecast FC reduction potentials (167). The scenario for tractor-trailers was the old Long Haul cycle 2012 with a test mass of 34.4 t (167 p. 9). The corresponding basis model EURO VI of this thesis with the same test mass outputs 32.9 L/100km. That is 1 % above the VECTO simulation result from the manufacturers of 32.5 L/100km for the same HDV class (167 pp. 7, 10).

Also the basis model of the delivery truck EURO VI was compared with published FC values, as is described in the paragraphs below. For the numbers see p. 195 Table 59.

The simulated FC from the basis model EURO VI with average payload, 19.0 L/100km, is in the range of 16.1 to 21.5 L/100km from 12 t trucks EURO V in urban delivery traffic in multiple European cities. For these measured trucks the average values for payload or test mass are not known.

⁶⁵ The visible decrease of the avrg. FC of French tractor-trailers from 2013 on was likely caused by the introduction of an additional energy tax on diesel fuel, compare also the corresponding footnote on p. 9.

The simulation for a test mass of 11.7 t outputs 23.8 L/100km, what is also in the range of 20.5 to 25.2 L/100km from two measured trucks EURO V with similar mass in urban traffic. The engines of the test trucks were of different rated power, 118 to 185 kW, hence it can only be stated that the simulation results are in a plausible range, not more.

2.6.3.2 Rigid city bus 12 m

To compare the model of the rigid city bus with other 12 m buses, published FC values for this HDV class were researched, compare p. 199, Table 62.

The measured FC numbers result from tests of buses with 4-speed AT and with 7-speed AT. The available transmissions for city buses and other urban vehicles from the manufacturers Allison (7-speed), Voith (4-speed) and ZF (7-speed) differ in the design. In the first gear of the 4-speed AT the transmitted power is split between the hydraulic torque converter and the first mechanical gear of the planetary gearbox. In case of the 7-speed ATs the torque converter is mounted in front of the planetary gearbox, and in the first gear the whole engine power is transmitted through the converter and subsequently through the mechanical section.

For the bus model of this thesis a 4-speed AT was implemented, but the results could be compared also to measurements of buses with 7-speed AT. Published numbers (168 p. 18) and data from buses which were measured for the VECTO project in 2016 showed, that the difference in FC between the two AT designs is small. For equal rigid and articulated buses, which differ only in a 4-speed AT or a 7-speed AT, the changes in FC on the SORT cycles and for road tests range from $\pm 1\%$ to $\pm 4\%$. On some cycles the FC of the bus with a 4-speed AT was lower, in other cases the vehicle with the 7-speed AT consumed less fuel.

The simulation results for the SORT cycles with 3.2 t payload according UITP conditions⁶⁶ in comparison with collected measurement values are shown in Figure 92. For the measurement vehicles the curb weight was not known, hence the test mass was estimated.

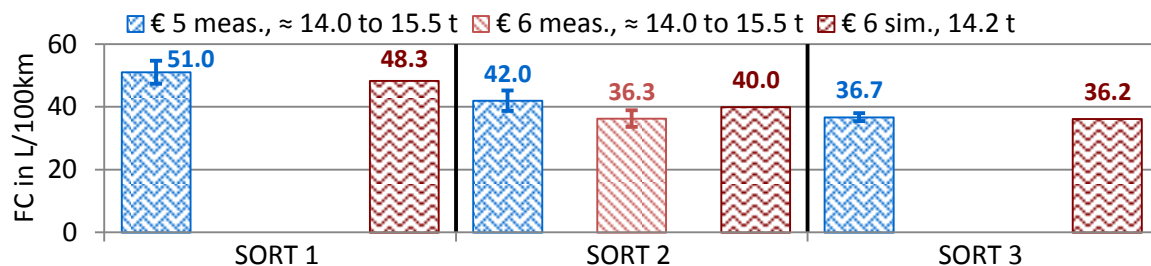


Figure 92. Fuel consumption on SORT cycles, rigid bus 12 m, measurement and simulation
Measurand is avrg. from max. and min. found FC, where the range is also shown. Case multiple buses only.

The simulated FC values from the EURO VI bus model are at the lower end of the range for EURO V vehicles and at the upper end of the EURO VI range.

⁶⁶ SORT, test track, settings: No A/C; steering pump idle + banking; 1 x door opening; no kneeling; payload 3.2 t

Measurement and simulation results are also available for Stuttgart Line 42⁶⁷, see Figure 93.

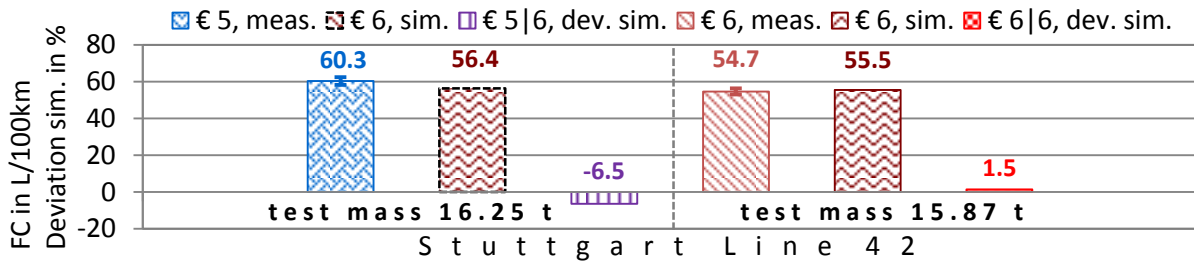


Figure 93. Fuel consumption on Stuttgart Line 42, rigid bus 12 m

Measurand is avrg. from each two published FC numbers, where the range is also shown.

In this case the simulated FC is lower when compared with two EURO V buses and slightly above the average result from two EURO VI vehicles. The small deviation to the EURO VI buses happened by chance, because the measurements took place in normal urban traffic, and even on one bus line with the same driver differences in the velocity courses are usual. Hence the cycle for the simulation, elaborated from own GPS measurements, differs a bit from the measured cycles. The deduction is, that the bus model produces results in the right magnitude.

The published FC numbers, which were found for fleet tests and line operation, were segmented into heavy urban, urban and suburban bus lines according to the average velocity, compare p. 200 Table 62 “Fleet tests and line operation”. With VECTO the appropriate urban bus cycles were simulated⁶⁸, see Figure 94.

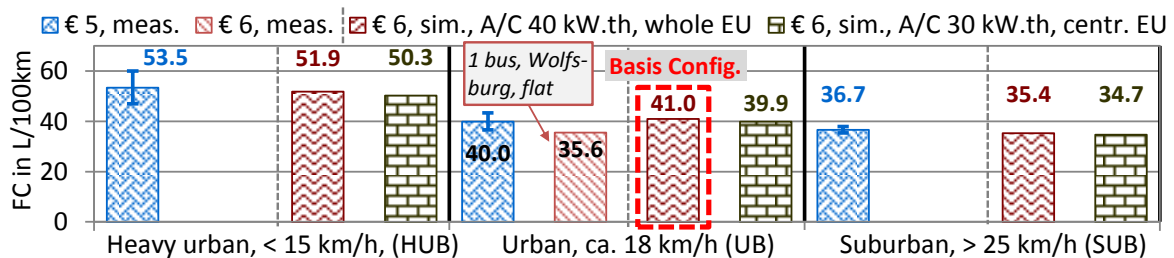


Figure 94. Fuel consumption for urban bus operation, rigid bus 12 m, measurement and simulation

Measurand is avrg. from max. and min. found FC, where the range is also shown. Case multiple buses only.

Concerning the A/C, the basis bus model is equipped with a system of a max. cooling capacity of 40 kW_{th}, and the average chiller’s power demand was determined for the zones southern, central and northern Europe, compare p. 29 ff. section 2.2.3.1 on bus A/C. As described there, this leads to a higher FC of the A/C than for the measured buses, which were probably equipped with smaller A/C and operated mainly in central Europe. An overview of typical A/C for (inter-) city buses is given on p. 188 Table 46. Thus the bus model was simulated also with a medium A/C of 30 kW_{th} only for central Europe. In this case the calculated average power demand of the chiller is 0.9 kW_{mech} below the demand from the chiller of the A/C 40 kW_{th} in all three temperature zones: 0.8 kW_{mech} vs. 1.7 kW_{mech}. The simulation of the smaller A/C showed a decrease in FC from 0.7 to 1.6 L/100km.

Because for current EURO VI buses only little data was found, it can only be stated, that the results from the EURO VI bus model on the standard urban bus cycles are in or somewhat below the FC-range for EURO V vehicles.

The idle FC at stand without A/C is 2.17 L/h, what is 20 % above the average measurement value of 1.81 L/h (1.1 to 2.4 L/h) from five EURO VI city buses 12 m (169 p. 19). Because a share of the auxiliary work at driving from fan and steering pump is included in the average constant power demand, a higher idle FC than measured is plausible.

⁶⁷ Stuttgart Line 42, road, settings: No A/C; stand at all 52 bus stops; no door opening or kneeling

⁶⁸ Line operation, settings: A/C turned on; default auxiliary power demand; default values for no. of braking and bus-stops; actuation of doors and kneeling; average capacity usage 20 % → 16 passengers ≈ 1.10 t

2.6.3.3 Comparison with existing FC limits for trucks and buses

Currently in Canada, China, Japan and the USA the FC and/or the CO₂ emissions of HDV are limited. The vehicles are measured on a chassis dynamometer or models are simulated with standardised programs. The Canadian procedure is aligned to the US-American one, e. g. the same CO₂ limits are applied, see (58 pp. 482-484) and (170 pp. 133-134). As driving cycles EPA GHG (CA & US), C-WTVC (CN), and JE05 plus IDM (JP) are used, compare p. 156 ff.. The consumption from the single parts of the cycles is weighted, dependent on the HDV class, and the sum is the resulting FC, which shall be lower than the limit.

In China the vehicle is tested at maximum permitted GVW and in the USA a fix payload per HDV class is prescribed. The road load coefficients are determined from a coastdown measurement in both cases.

In Japan the input data for the HDV models are mostly table values, only the full load curve of the engine, its performance map, the gear ratios and the dynamic tire radius are specific vehicle data. Thus only those vehicle parameters are covered, which affect the engine speed, and the rest is set to default. In addition the model is simulated without engine auxiliaries. This procedure is in fact an engine test with default vehicle models for each HDV class.

More details for the procedures and model settings are given on p. 190 ff., chapter 5.13.

The simulation results from the basis HDV models of this thesis with the prescribed payloads on the standard cycles of each national regulation are shown in Table 18.

Table 18. Results from basis HDV models on current certification driving cycles
Details on the test settings and the single FC limits are given on p. 190 ff. in section 5.13

Country	Test mass in t	Changes of input data	FC limit L/100km	FC sim. L/100km	% FC _{sim} to FC _{limit}
<u>Tractor-trailer, basis model of this thesis</u>					
China	40.00	No crosswind, steering pump only idle power, no A/C	40.0	30.7	-23
Japan	39.08	Default vehicle model see p. 191, Table 55	49.8	48.9	-2
USA & Canada	30.64	No crosswind, steering pump only idle power, no A/C	32.6	28.3	-13
<u>Delivery truck, basis model of this thesis</u>					
China	12.00	No crosswind, steering pump only idle power, no A/C	25.0	20.0	-20
Japan	7.85	Default vehicle model see p. 191, Table 55	16.7	15.2	-9
USA & Canada	11.18	No crosswind, steering pump only idle power, no A/C	30.3	23.4	-23
<u>Rigid bus, basis model of this thesis</u>					
China	18.00	No crosswind, steering pump only idle power, no A/C	37.5	36.0	-4
Japan	11.96	Default vehicle model see p. 191, Table 55	23.6	20.7	-12
USA & Canada		<i>Buses not covered in phase 1 until 2017</i>			

In all cases the simulated FC and therefore the CO₂ emissions from the basis HDV models EURO VI, MY 2014, fall short of the limits, by 2 to 23 %. Hence the models would become type approved in terms of CO₂ emissions.

2.6.3.4 Additional model of articulated city bus 18 m

The vehicle models of a conventional and of a hybrid articulated bus 6x2 of GVWR 28 t, stage EURO VI 2014, were created to assess the powertrain model of the parallel hybrid bus by comparing the simulated FC values with published numbers for this HDV class.

An overview of the technical data of conventional articulated buses is given on p. 209, Table 71, where also the researched FC values are enlisted. The data of the basis simulation model can be found on p. 178, Table 38, "Articulated bus".

Because the basis model for this bus class was improvisationally created from generic data which were available when simulations started, in addition a reference model was elaborated with original data from the manufacturer which were attained later in 2016. The basis model was converted to the reference model by changing only those components, where original input was available⁶⁹, the rest remained the same. The reference model was simulated on the SORT cycles⁷⁰, where measurands were available from the manufacturer. The comparison with the measured FC is shown in Figure 95.

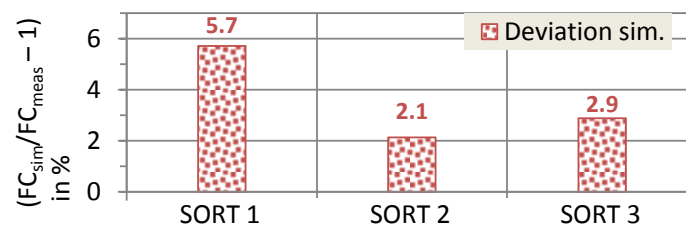


Figure 95. Reference model artic. bus, simulation with measured velocity and VECTO v2.2 shifting model

With one reference model of one articulated bus, of a test mass in the range 21 to 23 t, the utilised VECTO v2.2 with a preliminary AT model overestimates the FC for the SORT cycles on a flat test track by 2 to 6 %, when the measured velocity is used as input. The deviation is highest for SORT 1, which represents heavy urban traffic.

One reference model and one set of measurement data from the same source are generally too little to assess a simulation, and further checks are necessary, when more data from separate sources become available. But it is assumed that this one model produces plausible results for urban and suburban bus cycles with medium and higher average velocities.

In the following paragraphs the basis model of the articulated bus is compared with published FC values, and for the VECTO cycles also with the outcome from the reference model.

The found measured FC and the simulation results for SORT are shown in Figure 96.

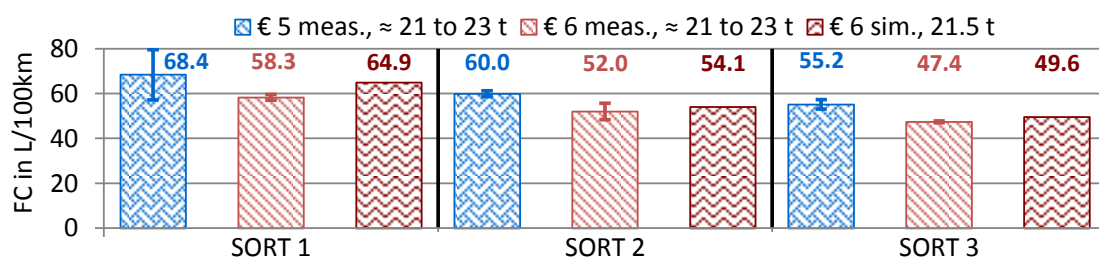


Figure 96. Fuel consumption on SORT cycles, measurement and basis model articulated bus 18 m
Measurand is avrg. from max. and min. found FC, where the range is also shown. Case multiple buses only.

The simulated FC is at the lower range of or below the found FC from EURO V buses and in the range or above the numbers for EURO VI vehicles.

⁶⁹ **Original data from bus manufacturer for reference model:** Curb weight; effective air drag area ($C_d \cdot A_{cr}$); rolling resistance coefficient of tires (RRC), for wheels of same size like basis model; full load curve, FC-map, rotational inertia and idle speed of engine (260 to 280 kW); gear ratio final drive; efficiency values and loss maps for final drive and gearbox; 4-speed AT, shifting curves & torque-converter data

⁷⁰ SORT, test track, settings: No A/C; steering pump idle + banking; 1 x door opening; no kneeling; payload 5.0 t

The basis model of the articulated bus was also checked for FC on the cycles Stuttgart Line 42⁷¹ and Wien Line 26A⁷², compare Figure 97.

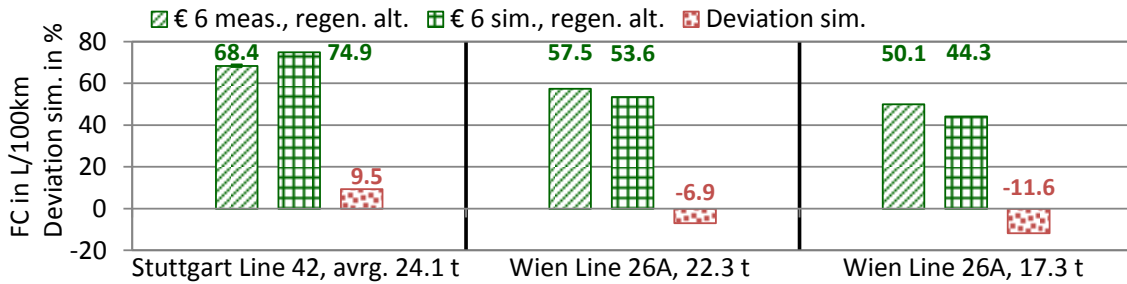


Figure 97. Fuel consumption on bus lines Stuttgart 42 and Wien 26A, basis model articulated bus 18 m
Measured and simulated vehicles utilised three alternators for regenerative braking.

Measurand is avrg. from max. and min. found FC, where the range is also shown. Case multiple buses only.

For the comparison of simulation and measurement for Stuttgart and Wien it shall be mentioned, that the measured buses were equipped with a bigger engine with higher torque. That could not be implemented in this work, because the simulated 4-speed AT allowed only medium input torques up to 1600 Nm. In addition the measured Stuttgart bus had a 7-speed AT, the gearbox for the Wien bus is not known, but probably the same. Hence the simulated bus model could not follow the measured velocity during high acceleration phases due to the weaker engine. Thus with this comparison only the magnitude of the simulated FC can be assessed, not its exact value, which is too high for Stuttgart and too low for Wien.

For an articulated bus EURO III with a 4-speed AT on the Düsseldorf cycle⁷³ the results for FC, average relative engine speed and positive engine cycle work at the clutch ($W_{eng,pos,cl}$) are available, for the comparison see Table 19.

Table 19. Results on the Düsseldorf cycle for a conventional 18 m articulated bus, basis model

Cycle	Measurement, € 3				Simulation, € 6			
	m_{test} [t]	FC [L/ 100km]	$n_{rel,avrg}$ [-]	$W_{eng,pos,cl}$ kWh/km	m_{test} [t]	FC [L/ 100km]	$n_{eng,rel,avrg}$ [-]	$W_{eng,pos,cl}$ kWh/km
Düsseldorf	21.4	38.9	0.282	1.48	21.4	39.7	0.294	1.50
% sim. to meas.			-			+2.0	+4.1	+1.4

That an early EURO VI engine consumes equal fuel than an older EURO III machine is not surprising, compare the researched FC values for engines on p. 185 Table 41. The shifting control and the sum of drivetrain losses and driving resistances are met due to the matching relative engine speed and cycle work. One part of the deviation +4.1 % of the relative engine speed can be explained with the 7.6 % higher gear ratio of the final drive of the simulation model, 6.21 versus 5.77 for the measured bus.

For the urban bus cycles⁷⁴ the model results were also assessed. The published FC numbers from articulated buses were segmented into heavy urban and urban bus lines according to the average velocity, compare p. 210 Table 71 “Fleet tests and line operation”.

Like the model of a rigid bus, the model of the articulated vehicle is equipped with a big A/C, here with a max cooling capacity of 60 kW_{th}, and the average chiller’s power demand is the overall mean value for the temperature zones southern, central and northern Europe. As described on p. 29 ff., section 2.2.3.1 on bus A/C, this leads to a higher FC of the simulated A/C than for the measured vehicles, which were operated mainly in central Europe and where

⁷¹ Stuttgart Line 42, road, settings: No A/C; stand at all 52 bus stops; no door opening or kneeling

⁷² Wien Line 26A, road, settings: No A/C; stand at all 46 bus stops; no door opening or kneeling

⁷³ Engine cycle derivated from road measurement with articulated bus: i_{FD} 5.77, no auxiliary consumers

⁷⁴ Line operation, settings: A/C turned on; default auxiliary power demand; default values for no. of braking and bus-stops; actuation of doors and kneeling; average capacity usage 20 % → 26 passengers ≈ 1.8 t

the A/Cs were probably smaller. Thus the bus was simulated also with a medium A/C of 45 kW_{th}, only for the zone central Europe. Then the calculated chiller power is 1.4 kW_{mech} below the demand from the chiller of the A/C 60 kW_{th} in whole Europe, 1.2 vs. 2.6 kW_{mech}.

The simulated results from all the variations are shown in Figure 98.

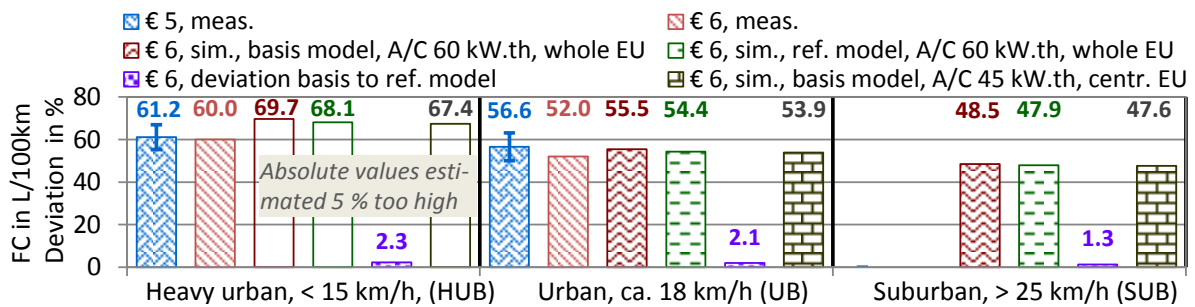


Figure 98. Fuel consumption urban bus lines, basis & reference model 18 m artic. bus, test mass 18.3 t. Measurand is avrg. from max. and min. found FC, where the range is also shown. Case multiple buses only.

As for the 12 m rigid bus, the basis model of the articulated bus 18 m EURO VI outputs FC values somewhere between measurement results from EURO V and EURO VI buses.

The comparison of the basis model with the reference model shows conformity with a deviation from +1 to +2 %. On the slow Heavy Urban Bus cycle only the relative change from the basis to the reference model can be assessed. As explained below Figure 95, the provisional AT-model of VECTO v2.2 probably leads to an overestimation of the FC in slow heavy urban traffic of 5 to 6 %.

Concerning the size of the A/C the basis model outputs 2.3 to 0.9 L/100km less FC, when simulated with a smaller system only for the temperature zone central Europe.

The check for plausibility of the basis model of an articulated bus is less clear than for the other vehicle models. The simulated SORT results are at the upper range of or above the measured values from EURO VI buses and below EURO V results. In comparison with road measurements the results are 12 % below, 6 % below and 9.6 % above the FC of the measured EURO VI buses with other powertrain specifications. The comparison of the net engine cycle work showed a good approximation to a measured value, and the check with published FC numbers from line operation produced, that the model results are in or somewhat above the FC ranges of EURO V and EURO VI buses.

The check of the basis model with a more credible reference model showed an acceptable deviation of FC from the basis model of max. +2.3 % for the urban bus cycles, see Figure 98.

In addition it was found, that VECTO v2.2 seems to overestimate the simulated FC for articulated buses of higher mass with a 4-speed AT in heavy urban traffic by ca. 5 %. This is the result from the comparison with one single measurement, and more data is necessary for a better justified assessment. One reason are shortcomings in the provisional submodel of the automatic transmission with a hydraulic torque converter in VECTO v2.2.

2.6.4 Comparison of the basis HDV models in VECTO 2 and VECTO 3

The main simulation program for this thesis was VECTO v2.2 of 2015-09-10. Afterwards the program was rewritten from scratch and labelled version 3, where the modelling approach remained similar to version 2. The basis HDV models of this thesis were implemented in VECTO v3.2.0/925 of 2017-07-14 to investigate the differences in FC between the old and the new program for identical input data. The results shown in Figure 99 and Figure 100.

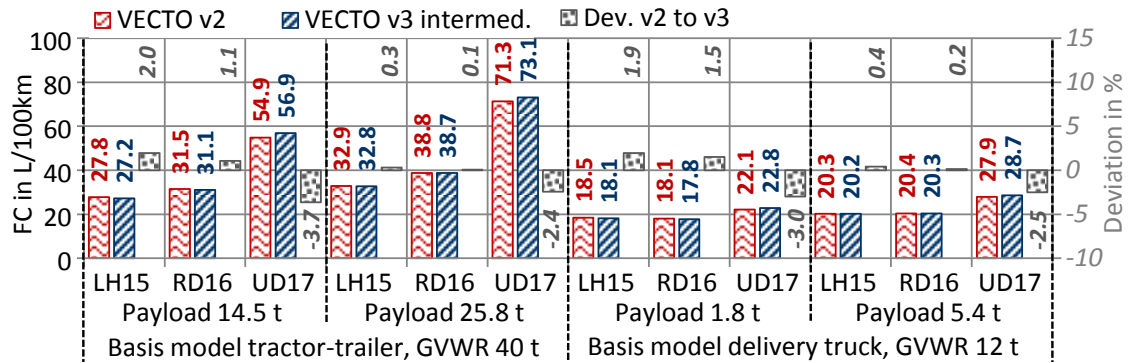


Figure 99. Basis truck models, comparison of FC, simulation with VECTO v2.2 and v3.2.0/925

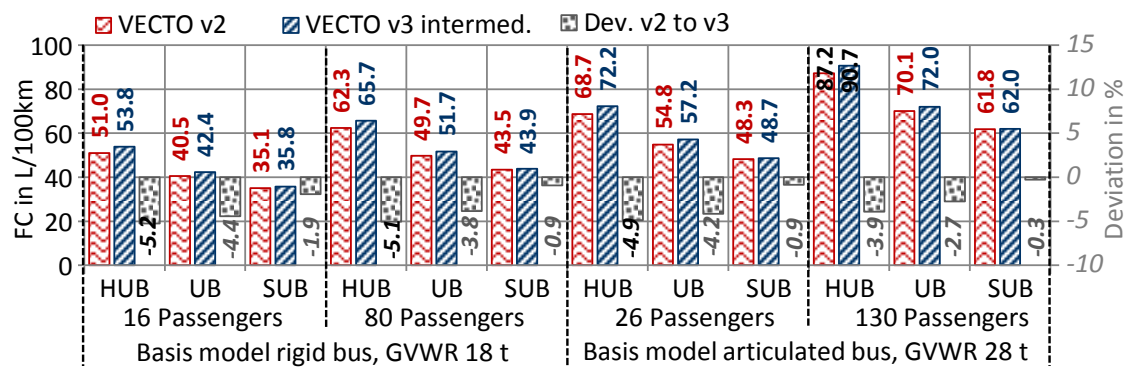


Figure 100. Basis bus models, comparison of FC, simulation with VECTO v2.2 and v3.2.0/925⁷⁵

When interpreting the results of v3.2.0/925 and the resulting deviations v2 to v3, it shall be considered, that v3 is still an intermediate version and will be further refined until the final release for the official certification in 2019.

For the truck cycles Long Haul 2015 and Regional Delivery 2016 the deviation is small, but becomes higher for the more transient Urban Delivery 2017 cycle. The biggest deviation was found at -5.2 % for the rigid bus with 16 passengers on the Heavy Urban Bus cycle.

For the time being it can be stated, that the older VECTO 2 outputs FC numbers with deviations of max. ca. ± 5 % when compared to an intermediate version of the new VECTO 3. For the truck models the max. deviation is ca. -4 %, and for the average loaded rigid bus it is biggest at ca. -5 %. The main reason for the simulated changes of the FC from the bus models is the reworked and improved submodel for the automatic transmissions in v3.2.0/925.

⁷⁵ The input data for the bus models needed to be modified slightly to work with VECTO 3, e. g. in case of the acceleration curves for the bus models. This is the explanations for the small deviations for the FC numbers VECTO 2 to the other results from this work.

3 Results for single and bundled efficiency measures

In this chapter the simulation results for the selected single and bundled efficiency measures are given and checked for plausibility, if data for a comparison was found.

An overview, how the measures and powertrain concepts were simulated, is given in Table 20.

Table 20. Simulation procedures for investigated saving measures and powertrain concepts

If not mentioned otherwise, VECTO v2.2 was the simulation program

Measure	Simulation procedure
Lower tire rolling resistance	Change of number for RRC in input data. See p. 17 ff. section 2.2.1.2 on the rolling resistance.
Lower air drag	Change of number for $C_d \cdot A_{cr}$ in input data, change of curve for increase of C_d with crosswind in case of truck models with side panels. See p. 18 ff. section 2.2.1.3 on the air drag.
Lightweighting	Change of masses of vehicle, body and accessories in input data.
Reduced drivetrain friction	Change of maps for torque loss of final drive and gearbox in input data. See p. 22 ff. section 2.2.2 on the drivetrain losses.
Start-stop automatic	Postprocessing of VECTO output in MS Excel, application of model for start-stop automatic. See p. 66 ff. for the corresponding section 2.4.2.
Efficient engine auxiliaries	Change of numbers for average constant power demand of auxiliaries in input data. See p. 24 ff. section 2.2.3 on engine auxiliary consumers. For city buses: Application of compressor model, see p. 55 ff. section 2.3.2.2.
Regenerative braking, auxiliaries	Postprocessing of VECTO output in MS Excel, application of model for regen. braking with engine auxiliaries. See p. 62 ff section 2.4.1. Application of model for compressor power, see p. 55 ff. section 2.3.2.2.
Exhaust heat power generation	Postprocessing of PHEM v11.4 output for exhaust and VECTO output for basis model tractor-trailer in MS Excel. Application of model for exhaust heat power generation, see. p. 68 section 2.4.3 for the description.
EcoRoll and Look Ahead Coasting	Activation of the functions in the VECTO
Limited braking deceleration	Change of curve for demanded deceleration, see p. 33 section 2.2.4 on the simulated vehicle control.
Gas engine	Change of the engine performance map, its full load curve and the rotational inertia in the input data.
Diesel-electrical parallel hybrid trucks	Postprocessing of VECTO output in MS Excel, application of model for parallel hybrid electrical powertrain for trucks, see p. 73 section 2.5.1.
Diesel-electrical parallel hybrid city buses	Simulation of the complete vehicle model in PHEM v7.2, postprocessing in MS Excel. See p. 75 section 2.5.2 for the description.
Diesel-electrical serial hybrid city bus	Simulation of the vehicle model in VECTO v1.4, postprocessing of the output in MS Excel. Application of the model for serial hybrid-electrical powertrains, see p. 77 section 2.5.3.
Battery-electrical vehicles	Simulation of the vehicle model in VECTO v1.4, postprocessing of the output in MS Excel. Application of the model for battery-electrical powertrains, see p. 79 section 2.5.4.

3.1 Selected single saving measures and alternative powertrains

Here the outcome for the selected single saving measures like improved aerodynamics or reduced drivetrain friction is described, and the findings from the models with alternative powertrains are presented. An overview of all results is given on p. 126 section 3.1.15.

The technical data of the vehicle models for each variant is enlisted in the data section on p. 169, chapter 5.7.1 and on p. 172, chapter 5.7.2. The properties of the fuels for the alternative powertrains are shown on p. 165 Table 29.

Some measures were grouped into the technical levels “current” and “future”. The current measures could be applied immediately, the components are already available, and the future measures are expected to enter the market until the mid-2020ies.

3.1.1 Tires lowest rolling resistance

For the simulation of the possible reduction of FC by tires with a lower rolling resistance coefficient (RRC) it was assumed, that the basis vehicle models are equipped with tires of typical RRC state 2014 (5 pp. 61 ff., 211). For the basis tractor-trailer model class B was chosen, and for the basis models delivery truck and rigid bus class D.

For the configuration "current" tires of RRC-class B for tractors⁷⁶, A for semitrailers, C for the steering axles of the urban vehicles and D for their drive axles were chosen and offer FC savings from 0.6 to 2.7 %. The current saving potential for the urban vehicles is small, because the share of the RRC at the overall FC is with 19 % (delivery truck) and 14 % (rigid bus) lower than for tractor-trailers with 29 %, see also p. 89 Figure 89.

For the future the potential for all tires of class A was simulated. Here the possible reduction for the urban vehicles is high at 6.0 % (delivery truck) and 4.4 % (rigid bus), because the step from class D/D to A/A is big.

In Figure 101 the relation between the change of FC and RRC is shown.

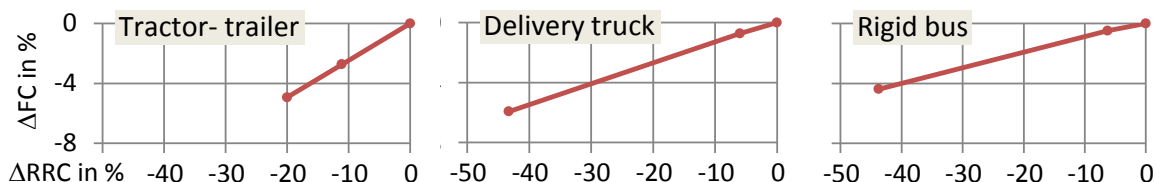


Figure 101. Change of fuel consumption vs. change of rolling resistance coefficient

For the tractor-trailer the FC is reduced by 0.25 % per 1 %-reduction of RRC or by 5.5 % per N/kN-reduction of RRC. For the urban vehicles delivery truck or rigid bus the potential of RRC is lower at 0.14 or 0.10 %/% (2.0 or 1.6 %/(N/kN)).

Such linear relations between FC and change of rolling resistances were found also by other workers, compare e. g. (171 pp. 46-49).

⁷⁶ State 2015-10, Continental, Goodyear, Michelin, CP Reifen Trading GmbH (reifenleader.de).

The announcement of tractor tires class A, here Michelin X Line Energy, models F and D2, for MY 2016 was published after the research on RRC for this work (98) (99).

3.1.2 Aero packages and speed limit 80 km/h

To reach a low drag coefficient when moving through fluids, bodies should be streamlined like a submarine: A round bow, a closed and smooth outer layer, and a tapered stern to avoid stall. Such a stern is also called boat tail. One of the first measurements of these modifications for HDV was done in the 1950ies at the Wind Tunnel Operations Dept. of the Uni Maryland with the model of a tractor-trailer (172) (173 p. 14). Since these early experiments the aerodynamics of HDV were continuously improved. E. g. from 1980 to 2014 the performance of European tractor-trailers in terms of the effective air drag area ($C_d \cdot A_{cr}$) decreased by ca. 16 %⁷⁷.

Pictures of current aerodynamic trucks are shown in Figure 102 and Figure 103, and details for the aerodynamic devices are described on p. 168, Table 31.



Figure 102. Tractor-trailer with aerodynamic improvements (renault-trucks.com)



Figure 103. Delivery truck with aerodynamic improvements (174)

In case of the city bus aerodynamic measures were not investigated, because the share of the air drag at the overall FC is small at 7 %, compare also p. 89 Figure 89.

For the current aero package such add-ons were chosen, which are possible with the present permitted dimensions (175 p. 53/54) and vehicle technology. At a trailer side panels and a boat tail up to 0.5 m can be mounted, for the delivery truck in addition an underbody cover and fairings from cabin to body were assumed.

In the next years longer boat tails plus small rear-view cameras instead of mirrors will become permitted (176) (177 pp. 1,5) (178), hence these were added to the future aero packages.

The current and future aero packages and the reduction of the air drag are shown in Table 21.

Table 21. Aero packages 1 and 2 for tractor-trailer and delivery truck, for sources see p. 168 Table 31

	Basis		a) Rear view cameras	b) Fairing cabin to trailer/body	c) Side panels	d) Underbody cover	e) Boat tail 50 cm	f) Boat tail 100 cm	Aero package actual	Aero package future	
	C_d in -	A_{cr} in m^2									
Tractor-trailer	0.51	10	- 3 %	basis	- 8 %	- 2 %	- 8 %	- 10 %	c) e), +200kg ΔC_d : - 16 %; $C_d = 0.428$	a) c) d) f), +250kg ΔC_d : - 23 %; $C_d = 0.393$	
Deliv. Truck	0.57	9.1	estimated overall change of C_d						-	b) c) d) e), +130kg ΔC_d : - 10 %; $C_d = 0.513$	a) b) c) d) e), +130kg ΔC_d : - 13 %; $C_d = 0.496$

⁷⁷ End 1970ies: $C_d \cdot A_{cr} = C_d \cdot h_{veh} \cdot w_{veh} = 0.70 \cdot 3.7 \text{ m} \cdot 2.4 \text{ m} = 6.22 \text{ m}^2$ (591 p. 192) (592 p. 202) (593 p. 278)
Beginning 2010s: $C_d \cdot A_{cr} = 0.52 \cdot 4.0 \text{ m} \cdot 2.5 \text{ m} = 5.20 \text{ m}^2$. (335 pp. 660, 702), p. 166 Table 30, C_d tractor-trailer

For the simulated relation between air drag and FC for the truck models see Figure 104.

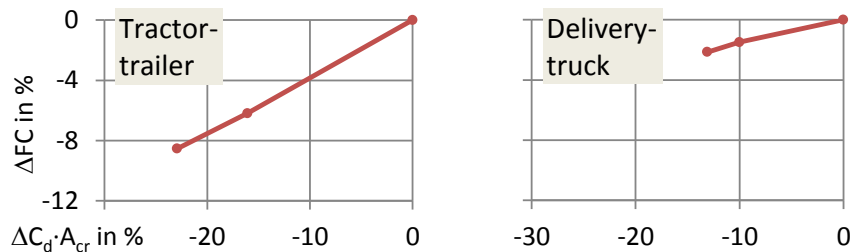


Figure 104. Change of fuel consumption vs. change of effective air drag area, truck models avrg. payload

Per 1 %-reduction of the effective air drag area ($C_d \cdot A_{cr}$) the tractor-trailer model outputs a fuel saving of 0.37 % and the model of the delivery truck a potential of 0.16 %. The current aero packages allow a FC reduction of 6.2 % for the tractor-trailer and 1.5 % for the delivery truck, in future 8.5 % and 2.1 % will be possible, compared to the basis models. Due to the lower velocity the impact of aerodynamics in cities is smaller than on motorways.

At full payload of 26.6 t the simulated reduction of FC with the current aero package for the tractor-trailer model is lower at 5.2 % (30.7 vs. 32.4 L/100km), due to the smaller share of the air drag at the FC for a higher vehicle mass. This calculated number is similar to a manufacturer's measurement result, where a change in FC of -4.5 % was measured for a tractor-trailer of test mass 40 t, with side panels and a short boat tail in long haul traffic (179). A similar change in FC of -4.8 %, 29.8 vs. 31.3 L/100km, was measured with a tractor-trailer of test mass 40 t on the flat/wavy route "Verkehrsrundschau full" (171 p. 54/55). There the optimised trailer was also equipped with side panels and a short boat tail, the route is described in the footnote on p. 192. For a tractor-trailer where the test mass is not known another manufacturer reports fuel savings of ca. 7 % for aerodynamic improvements similar to aero package "current", with an additional underbody cover (180 p. 36).

In addition a speed limit of 80 km/h was researched, instead of the max. 85 km/h for the standard cycles. The max. velocity is reduced by ca. 6 %, but due to its quadratic nature the air drag is reduced by ca. 11 %: $(80 \text{ km/h})^2 / (85 \text{ km/h})^2 \approx 0.89$. For the tractor-trailer on the LH15 cycle this offers an additional saving potential of 1.0 L/100km or 3.4 %. For the delivery truck on the UD12 cycle the effect is lower at 0.1 L/100km or 0.8 %.

The time loss is small with +3.0 min/100km for long haulage and +0.7 min/100km for mainly urban traffic.

The comparison with measurements showed, that for long haul cycles the saving potential by a speed limit was slightly underestimated. For two tractor-trailers of ca. 320 kW with 12.4 t payload a reduction of FC of 6 %, 26.6 vs. 28.3 L/100km, was measured for a reduction of the max. velocity from 88 to 82 km/h. The comparison was conducted during multiple days on German motorways of mixed altitude profile (181). In case of a reduction of the max. velocity from 89 to 82 km/h a FC change of -5.7 % was measured with a tractor-trailer 331 kW EURO V of test mass 39.6 t on a mixed motorway trip, 38.3 vs. 40.6 L/100km (182 p. 12).

3.1.3 Lightweighting

In case of the tractor-trailer model a standard 3-axle semitrailer with reduced curb weight was chosen, with 5.5 t instead of 6.2 t. Such trailers are available, e. g. Berger Ecotrail LTCn (5.33 t), Krone ProfiLiner Ultra (5.66 t), Schmitz S.CS Universal X-Light (5.41 t) or Schwarzmüller 3-axle ultralight (5.20 t).

The curb weight of the delivery truck model was reduced by 0.2 t with a smaller tail-lift, mass 0.3 t vs. 0.5 t. At the same time the max. lifting capacity decreased from 1.5 t·m ($\approx 14.7 \text{ kNm}$) to 0.6 t·m ($\approx 5.9 \text{ kNm}$). That is still enough to handle a heavy good in urban delivery traffic, a palette of full beverage bottles with ca. 0.85 t.

For the lightweight 12 m rigid bus a curb weight of 10.5 t instead of 11 t was assumed. These or similar vehicles are already available, e.g. MB Citaro, GVWR 19 t, 2-doors, with 10.5 t or VDL Citea LLE-120, GVWR 14.9 t, with 9.0 t (183 pp. 19, 26) (184). The lower GVWR of the VDL bus is not a problem, its max. capacity is still 85 passengers⁷⁸. Due to the practical limit of ca. 4 passengers per m² in the standing areas, the effective capacity is around 80 passengers, independent on the GVWR. The references for the max. capacity usage of rigid buses are given on p. 187 ff in section 5.10 on the average payload. Hence with the lightweight Citaro GVWR 19 t the calculated theoretical capacity of 123 passengers cannot be reached.

For the future measures a moderate weight reduction for the tractor, the delivery truck chassis and the already light rigid bus of further 0.2 t was assumed.

The simulated reduction of FC with the current lightweight measures is 1.1 % for the models of tractor-trailer and delivery truck and 2.4 % for the rigid bus. With the future measures savings of 1.4, 2.6 and 3.3 % were calculated.

The dependence of the fuel saving on the reduction of weight is shown in Figure 105.

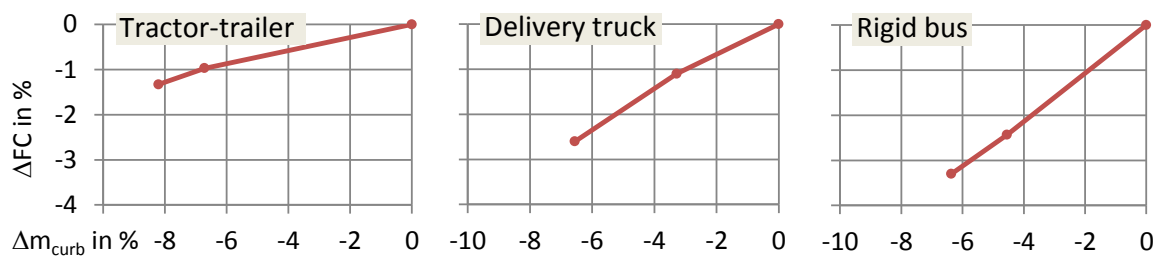


Figure 105. Change of fuel consumption vs. change of curb weight

Per 1 % of reduced curb weight 0.16 % fuel saving were calculated with the tractor-trailer model, 0.4 % with the delivery truck model and 0.5 % with the rigid bus model. The saving potential is higher for the urban HDV, where the typical driving cycles are transient with frequent acceleration and braking events. When the urban HDV are lighter, less energy is necessary during acceleration and later wasted in the friction brakes.

Also a 2-axle semitrailer was simulated for the tractor-trailer, where the omission of the 3rd axle saves around 0.65 t (185 p. 92), but limits the GCWR of the whole vehicle to 38 t. The net loss of 1.35 t payload is a disadvantage, but it should be asked, how often the tractor-trailer really carries the full payload. The current average payload usage is around 55 % ≈ 14.5 t, compare p. 187 section 5.10. The abandonment of the max. transport capacity, here a net loss of 1.35 t max. payload, offers via the reduced curb weight a fuel saving potential of 1.4 %.

3.1.4 Reduced drivetrain friction

For all HDV models around 8 % of the engine work output are consumed by the mechanical friction in the drivetrain from gearbox input to the wheel hub, where gears and bearings contribute to these losses. In case of the bus model additionally ca. 6 % are lost in the power split hydro-mechanical 1st gear during the frequent driveaway events.

In literature multiple efficiency measures for gearboxes are described, see Table 22.

Table 22. Efficiency measures for gearboxes and final drives

Superfinished or coated gear surfaces to reduce the friction	Lubricants with decreased internal friction
Bearings with lower friction losses	Dry sump lubrication with reduced oil fill
<i>Sources:</i> (186 p. 37) (187 p. 923) (188 p. 56) (189 pp. 123-126) (190 p. 486) (191 p. 55) (192 p. 61) (193 p. 302) (194 p. 313) (195 p. 320) (196 p. 83) (197 p. 322)	

⁷⁸ (GVWR 14.9 t - curb weight 9 t - driver weight 0.075 t) / (0.068 t/passenger) ≈ 85 passengers

E. g. for truck gearboxes a reduction of the losses in a range from 17 to 66 % was measured, reached by different techniques (189 pp. 123-126).

For this thesis lump sum 25 % decrease of the mechanical friction in the gearbox and final drive were assumed without focusing on single measures. This was depicted by changing the maps of the torque losses. The model of the power split 1st gear of the AT was not altered.

The tractor-trailer model was also analysed for a retarder with clutch. During idling this device causes losses up to 1.6 kW_{mech}, compare p. 23 Figure 23 right, and a consumption of 1.5 % of the input work. E. g. Scania offers retarders with clutches (198 p. 14).

The simulation results for reduced drivetrain friction are saving potentials of 1.4 %, 1.2 % and 1.7 % for the HDV models tractor-trailer, delivery truck and rigid bus, plus additional 1.3 % for the tractor-trailer with disengageable retarder.

For tractor-trailers retarder idle losses of max. 1.5 kW are known (199 p. 84). But the effect of its omission could not be determined due to the measurement uncertainty of ca. 1.6 %, what was the width of the 95 % confidence interval (199 p. 92).

3.1.5 Start-stop automatic and efficient engine auxiliaries

For the urban vehicles the effect of a start-stop automatic was investigated, where the engine is turned off during longer stand phases. Because the Long Haul cycle 2015 contains only 1.5 % stand phases, start-stop was not analysed for the tractor-trailer model.

For the auxiliary technology level "current" these devices were chosen: A compressor with clutch, a variable steering pump and LED lighting with reduced electrical power demand. The rigid bus was equipped in addition with a variable hydraulic fan, insulation of glazing and side walls plus an A/C with 3-point control with reduced energy demand.

At level "future" for the truck models also the viscous fan drive becomes disengageable and the steering pump gets an electrical drive to avoid its idle losses. In the future bus model fan and steering pump become electrified, what adds the need for a 2nd alternator. The future bus A/C was simulated with a continuous power control, see also p. 29 ff. section 2.2.3.1.

In addition regenerative braking with alternator and compressor was simulated in the level "future" for the urban vehicles. This level was chosen, because the electrification allows the gain of propulsion energy for the auxiliaries during braking with the alternator(s).

The models and assumptions for regenerative braking with auxiliaries and start-stop are described on p. 62 ff. chapter 2.4.1 and chapter 2.4.2.

The simulation of the start-stop function for the basis auxiliaries resulted in a decrease of FC of 2.3 % for the delivery truck and 5.7 % for the rigid bus.

The auxiliaries "current" offer saving potentials of 1.0 %, 1.2 % and 6.3 % for the models tractor-trailer, delivery truck and rigid bus. At stage "future" the potentials increase to 1.5 %, 2.4 % and 11.7 %.

If the models for regenerative braking with alternator(s) and compressor are applied to the future auxiliaries, a possible FC reduction of 3.7 % and 13.6 % was calculated for delivery truck and rigid bus, compared to the basis models.

3.1.6 Exhaust heat power generation

With the model of the tractor-trailer it was calculated that about 30 % of the fuel energy in terms of lower heating value are lost as hot exhaust downstream the aftertreatment devices. The average exhaust loss is 66 kW_{th} (10 to 193 kW_{th}) and its average temperature 310 °C (244 to 417 °C), what is enough to be used as heat source for a small steam power process.

A simplified model of an ORC process was set up to estimate the fuel saving potential for the model of the tractor-trailer on the Long Haul cycle 2015, see p. 68 ff. section 2.4.3 "Exhaust heat power generation". The calculated possible reduction of 2.2 % is at the lower end of published values from manufacturers, ranging from 2 to 5 % (154) (200 p. 44) (201 p. 5).

The model was also compared in the ETC cycle with measurement results from a HDV engine 13 L, equipped with an ORC system (202 p. 35), see Figure 106.

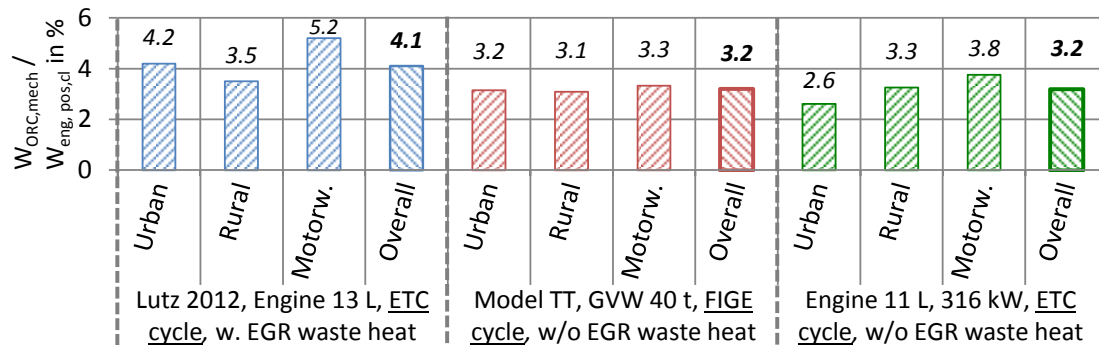


Figure 106. Comparison of results from ORC model with measurement (202 p. 35), ETC from (157 p. 79)

The model of the diesel engine with ORC was simulated with the tractor-trailer model at full payload on the FIGE cycle and in the "engine only" mode in the ETC. The vehicle cycle FIGE was the basis for the engine cycle ETC in the early 1990ies, but here the calculated positive engine work at the clutch ($W_{eng,pos,cl}$) was lower than from the ETC, 43.5 vs. 53.2 kWh. Nevertheless in both cases the overall ratio of the work output from the ORC expander ($W_{ORC,mech}$) to the positive engine work is 3.2 %, lower than for the measured system. The measured ORC was fed also with the waste heat from the EGR cooler and the simplified model not, hence a lower saving is credible.

3.1.7 Synthetic fuels from regenerative sources

Synthetic liquid or gaseous hydrocarbons from vegetable or animal feedstocks, what is called "biofuel" in general, contribute to the reduction of GHG from transport. Another possibility is to produce hydrocarbons with CO₂ from the atmosphere and water as feedstocks, plus electricity from regenerative sources to power the process, what is named "E-Fuel".

The main idea for both cases is, that a share, from a few % to 100 %, of the fossil fuel is replaced by a substance with very similar properties in terms of injection and combustion, and with a lower GHG-factor. Thus the GHG-factor of the blend gets lower, but not necessarily the fuel efficiency of the engine or of the overall vehicle.

Regenerative fuel for the compression ignition engine was used by the inventor Mr. Diesel himself as early as 1900. At the World's Fair in Paris he demonstrated his engine to the audience, fuelled with earth-nut oil (203 p. 7) (204 p. 115) (205 p. 1104). He wrote in 1912:

"The use of vegetable oils may seem insignificant to-day, but such oils may become in course of time as equally important as some natural mineral oils and the tar products are at the present time. (...) In any case, they make it certain that motor power can still be produced from the heat of the sun, which is always available for agricultural purposes, even when all our natural stores of solid and liquid fuels are exhausted." (203 p. 7)

Such a statement before the general motorisation and the steep increase of the oil demand is remarkable. Since these beginnings, regenerative fuels have been investigated consistently (206 p. 4 ff.), but did not become competitive in comparison to the cheap fossil fuels.

As example biodiesel shall be treated, which is standardised and available in larger quantities. In 2014 its share at the diesel consumption of transport in EU-28 was 6 %⁷⁹, and for 2016 the mandatory admixture was increased to 7 % (207 p. 31) Biodiesel's GHG factor is 1.92 kgCO_{2e}/L (208 p. 24), a reduction of 41 % versus fossil diesel (3.24 kgCO_{2e}/L).

Because the LHV of biodiesel is 9 % lower than of fossil diesel, the GHG factor was corrected for the increase in FC, assuming a constant engine efficiency. Thus the effective reduction of GHG assuming pure biodiesel becomes 35 %. The weighted GHG factors for blends of fossil and biogenous diesel were calculated and are shown in Figure 107.

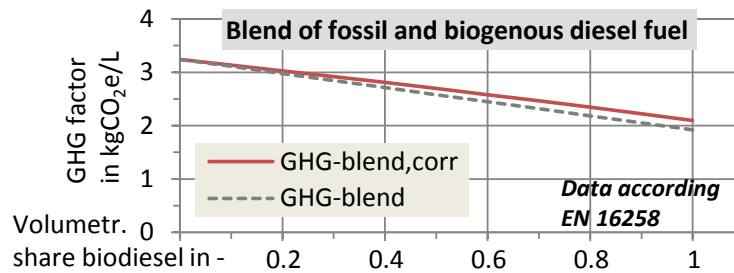


Figure 107. Greenhouse gas factors for blends of fossil and biogenous diesel fuels
GHG-blend,corr: Corrected for change of LHV: Biodiesel 9.11 kW_{it}/L, fossil diesel 9.97 kW_{it}/L

Depending on the share of biodiesel the reduced GHG emissions can easily be determined. For the current mandatory blend of 93 vol-% fossil diesel and 7 vol-% biodiesel the GHG factor is 3.16 kgCO_{2e}/L, corrected for LHV. That is 2.4 % less GHG than pure fossil diesel.

The GHG factors for blends of other fossil and carbon-reduced fuels can be calculated the same way with the specific parameters. For more information about liquid and gaseous fuels from regenerative sources in terms of feedstocks, production, refinement and the use in engines see the literature, e. g. (206) (209) (210) (211) (212) (213) (214) (215).

3.1.8 Improved engine efficiency

Around 60 % of the fuel energy in terms of heat from combustion are lost in the engine, compare the calculated average efficiencies of ca. 40 % on p. 87 Table 17. To reduce the losses in diesel engines, multiple measures were analysed by other researchers, see the selection in Table 23.

Table 23. Selection of efficiency measures for diesel engines

Honed and coated cylinder liners for reduced friction	Reduced backpressure downstream turbocharger
Sealings with reduced friction	Miller Valve Timing
Lubricants w. lower viscosity, reduced internal frict.	Cylinder deactivation
Increased compression ratio	DeNO _x of exhaust with reduced EGR or SCR-only
Reduced losses in the injection system	Variable pumps for oil and coolant
Higher coolant temperature for reduced heat losses	
<i>Sources:</i> (216) (217 p. 34) (218 p. 32) (219 p. 28) (220 p. 12) (221 p. 39) (222 p. 316) (223 p. 630) (224 p. 56/57) (225 p. 1456/1457) (226 p. 204) (227 p. 216) (228 p. 1631) (229 p. 42) (230 p. 5) (231 p. 164) (232 p. 6) (196 p. 82) (233) (234 p. 2383/2385) (235 p. 6/11) (236 p. 2)	

⁷⁹ EU-28, 2014, transport. Production & consumption biodiesel: 11'342 ktOE → 472.8 PJ → 14.41 GL. Consumption fossil diesel: 195'107 ktOE → 8'133 PJ → 226.5 GL. || → Overall consumption 240.9 GL diesel for transport. Volumetric share biodiesel 6.0 %. || (4 p. 112) (208 p. 24) (594 p. 56).

E. g. EGR decreases the engine efficiency slightly because the combustion is slowed and its centre of gravity moves to late (237 p. 499), hence Iveco and Scania offer already SCR-only engines, which reach the low NO_x level of EURO VI without EGR. Tractors with these engines showed very low FC values during testing (238) (239). Thus it can be assumed, that in future the market share of EGR engines may get smaller as long if no more stringent NO_x emission limits are introduced.

For this thesis a lump sum increase of the absolute average engine efficiency ($\eta_{\text{eng,avg}}$) of 0.01 was assumed, e. g. $0.41 + 0.01 = 0.42$, without further detailing.

The improved average engine efficiencies from the models of tractor-trailer, delivery truck and rigid bus are 0.434, 0.397 and 0.381, the resulting savings are 2.2 %, 2.5 % and 2.6 %.

3.1.9 EcoRoll and limited braking deceleration

3.1.9.1 Tractor-trailer, EcoRoll and Coasting

Manual or automatic powertrain control measures offer additional fuel saving possibilities. The electronic control units of the powertrain were coupled with GPS systems plus digital topographic maps of the motorways and take over the work of trained drivers. The vehicle computer itself can apply a forward-looking behaviour for the actuation of accelerator pedal or (permanent) brake. In the utilised simulation program VECTO v2.2 the functions EcoRoll (ER) and Look-Ahead Coasting (LAC) were implemented.

The main idea of EcoRoll is to save fuel on hilly motorways by allowing negative and positive deviations from the target velocity. During uphill driving the fuel supply is stopped at a certain distance before the crest, the vehicle slows down and rolls with a defined minimum velocity over the hill. At downhill driving it speeds up to the maximum permitted velocity and consumes the excess of kinetic energy on the next section, when powering becomes necessary. With this measure the duration of fuel supply at the end and start of uphill sections in wavy terrain is shorter than for normal driving. In VECTO EcoRoll was activated above 50 km/h and deviations from the target velocity of ± 5 km/h were allowed.

For Look-Ahead Coasting the target deceleration, compare p. 34 Figure 34, was set to VECTO's default value for this measure, -0.5 m/s^2 , to simulate the driver's behaviour of cutting the fuel supply before the desired stop point and let the vehicle roll.

Both functions were analysed separately to check the fuel saving potential. For MY 2014 the GPS-supported EcoRoll function was not standard for all European long haul tractors (240 p. 3). Today EcoRoll and Look-Ahead Coasting are quite usual for new vehicles. An impression of these functions is given in Figure 108.

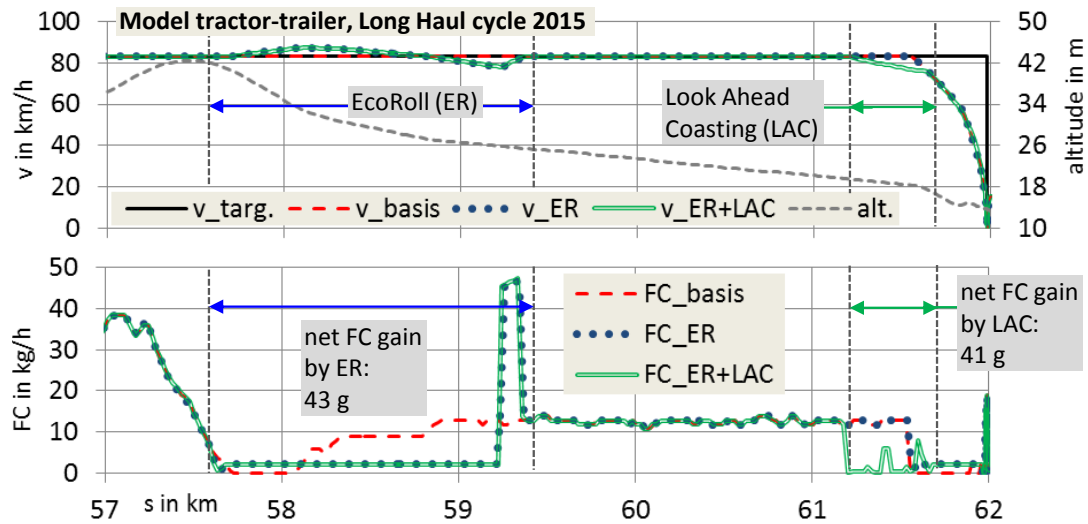


Figure 108. EcoRoll (ER) and Look-Ahead Coasting (LAC), tractor trailer model, section of LH15 cycle

On the downhill section starting at 57.5 km the model with EcoRoll accelerates up to 87.2 km/h, driven by the positive gradient force. Hence on the following part with less road gradient, where powering becomes necessary, the fuelling starts later when the surplus of kinetic energy is consumed and the velocity gets near 59.0 km close to its target value. For the subsequent braking event the model with Look-Ahead Coasting starts earlier at 61.2 km to decelerate and thus the fuelling duration becomes shorter.

In VECTO v2.2 a preliminary version of EcoRoll was implemented, therefore the deceleration before the crest at 57.5 km and the subsequent coasting until and not below the target velocity at 59.0 km did not work. Nevertheless a fuel saving was calculated for every EcoRoll phase.

For the tractor-trailer a fuel saving by EcoRoll of 1.4 % and with EcoRoll plus Look-Ahead Coasting of 1.7 % was calculated for the cycle LH15.

At full payload 26.6 t and only with EcoRoll the saving potential is 2.3 % on the LH15 cycle and 4.0 % on the more hilly LH12 cycle.

The result with full payload and EcoRoll on the hilly motorway cycle LH12 meets the measurement from three tractors, also with full payload in wavy terrain. A reduction from 0.4 % to 5.9 % was determined, dependent on the OEM (241 p. 18). Savings of 3 % to 5 % were already simulated in the early 2000s by an OEM for a US tractor-trailer (242 p. 7).

3.1.9.2 Urban vehicles, limited deceleration

For the urban vehicles with frequent braking EcoRoll is not effective, hence only the deceleration was limited to -0.8 m/s^2 . This limit was found during a preceding project with a parallel hybrid city bus (243 p. 136) (244 p. 6). It is especially useful for hybrid vehicles with limited generator power of the electrical machine. The less braking power is lost due to strong deceleration, the more kinetic energy can be recuperated and the fuel saving potential becomes higher. The effect is shown in Figure 109.

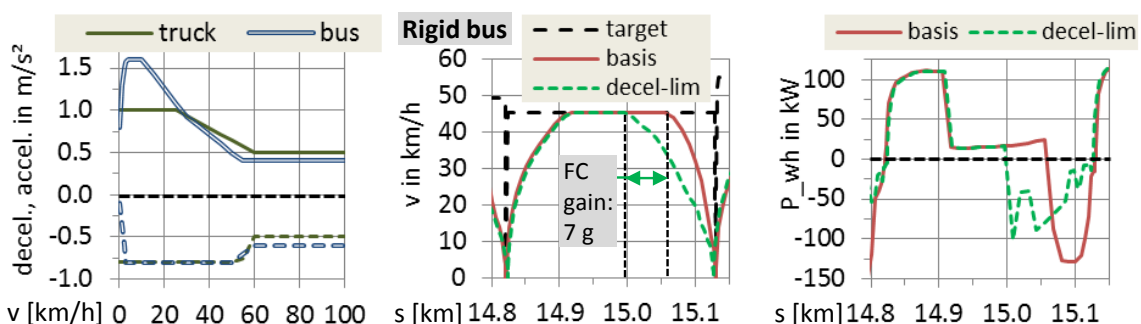


Figure 109. Limited deceleration, vehicle velocity and power at wheels (changing road gradient not shown)

Every braking event becomes longer and therefore the duration of fuel supply shorter.

In addition hybrid vehicles with a low ratio of electrical power to vehicle mass can recuperate more kinetic energy during regenerative braking. In case of harsh deceleration the braking power usually exceeds the max. generator power of a small electrical machine, hence more kinetic energy is lost in the friction brakes at the wheels. During soft deceleration the average braking power becomes lower, thus for the same HDV also with a smaller machine a significant part of the kinetic energy can be recuperated. This was one of the outcomes from a preceding research project with a diesel-electrical parallel hybrid city bus (161 pp. 15 ff., 57 ff.).

With the basis model of the delivery truck a reduction of FC of 0.7 % was simulated on the urban delivery cycle (0.9 stops/km), and for the rigid bus on the urban bus cycle (3.0 stops/km) the saving potential was 2.2 %.

On the other hand the driving time got longer, 1.9 min/100km for the delivery truck and 14.8 min/100km for the bus. For one round of 40 km on the Urban Bus cycle this results in +6 min. A compromise between fuel saving and timeliness needs to be found by the drivers.

3.1.10 Stoichiometric gas engine

The application of gas engines with LNG or CNG as fuel was simulated for every vehicle class. One engine map for a gas-fuelled HDV engine of stoichiometric type was available, the specific rated power was 26 kW_{mech} per litre displacement, at 1900 rpm. The displacement was adapted to meet the rated power of the equivalent diesel engines, and the full load curves for the gas engines are shown on p. 181 ff. Figure 200 and Figure 201. To reach the rated power at the same velocity like the diesel vehicles, the gear ratio of the final drive was adapted due to the different rated engine speeds: Gas 1900 rpm compared to diesel with 1800 or 2200 rpm, depending on the basic diesel engine simulated for the single vehicle types.

The results for the acceleration performance of the HDV models with gas engines are shown on p. 179 ff. in section 5.7.7 and showed no worsening towards the diesel HDV models.

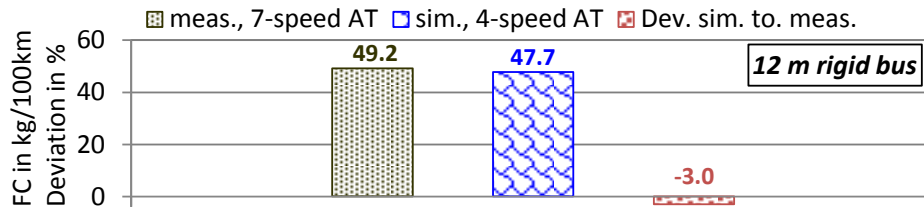
The performance map of the gas engine was compared to published measurement data and showed good agreement, compare p. 185 ff. Table 42 and Table 43. A minimum brake specific fuel consumption (bsfc) of ca. 195 to 200 g/kWh is currently usual for stoichiometric gas engines as treated in this thesis.

In case of gas engines with direct injection and a lean burning concept, which are available for HDV or under development, the best bsfc is lower at ca. 180 to 183 g/kWh (245 p. 19) (246 p. 128) (247 p. 12).

For the tractor-trailer model a LNG tank with liquefied natural gas was assumed, for the urban vehicles CNG tanks with gaseous, pressurised gas.

For the rigid city bus with a gas engine one test was found which could be compared directly. The data of the specimen is given on p. 203 Table 64 "Road measurement", first entry, the results for the FC from measurement and simulation⁸⁰ are shown in Figure 110.

⁸⁰ Stuttgart Line 42, road, settings: No A/C; stand at all 52 bus stops; no door opening or kneeling



Stuttgart Line 42, test mass 15.6 t, three regenerating alternators

Figure 110. CNG-fuelled rigid bus, stoichiometr. gas engines, comparison of measurement and simulation.

The regenerating alternators were calculated like described on p. 62 ff. in section 2.4.1, and on p. 91 it is explained, that the difference in FC is small between buses with 4- or 7-speed AT. As mentioned for the previous checks of models on Stuttgart Line 42, the small deviations between the unknown real driving cycle and the own GPS tracks as basis for the VECTO input add a few % uncertainty to the comparison.

The FC for the gas vehicles tractor-trailer, delivery truck and rigid bus was simulated to 25.9, 17.4 and 39.3 kg/100km. The resulting energy consumption (EC) in terms of lower heating value (LHV) and GHG in comparison with the basis diesel models is shown in Figure 111.

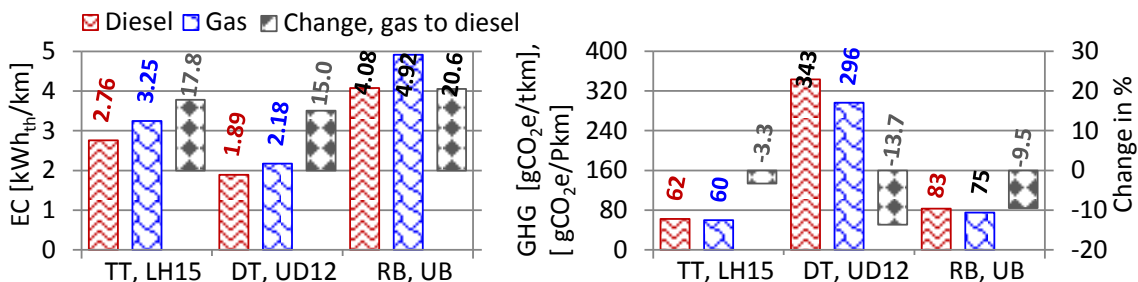


Figure 111. Simulated energy consumption and GHG emissions for diesel and gas models, stoichiometric gas engines, average payload

DT - Delivery truck, LH15 - Long Haul cycle 2015, RB - 12 m Rigid bus, TT - Tractor-trailer, UB - Urban Bus cycle, UD12 - Urban Delivery cycle 2012

Because of the engine process, the efficiency of the analysed stoichiometric gas engines is lower than for the diesel engines of the same rated power, what is the reason for the increase of EC. But due to the lower LHV-specific GHG of the gaseous fuels, LNG 0.268 and CNG 0.245 versus diesel 0.325 kgCO_{2e}/kW_{th}, nevertheless a reduction of GHG is possible.

The simulated excess consumption of fuel energy in comparison with diesel-fuelled vehicles is at the lower end of measured values. Published values for tractor-trailers and rigid city buses are given on p. 195 Table 58 and p. 202 Table 64. For a CNG-fuelled tractor-trailer 28 % more energy consumption were measured and for city buses the range was +18 to +38 %. The simulated values from the two HDV models are +17.8 % and +20.6 %.

3.1.11 Diesel-electrical parallel hybrid vehicles

All HDV models were simulated with a diesel-electrical parallel hybrid powertrain, for the structure see p. 72 Figure 70 left. The main benefit of hybrids is the possibility to recover a part of the kinetic energy during braking, by running the electrical machine in generator mode to charge the battery. In addition the hybrid models were equipped with a start-stop function. The simulation approaches are described on p. 73, chapter 2.5.1 "Diesel-electrical parallel hybrid trucks" and p. 75, chapter 2.5.2 "Diesel-electrical parallel hybrid buses". For the data of the vehicle models see p. 172 Table 34, "B) Diesel-electrical parallel hybrid vehicles".

To check the driving performance of the models with (hybrid) electrical powertrains, these were simulated with max. payload for full load acceleration and on demanding hilly and/or transient driving cycles. No significant slowdown in comparison with the basis models of conventional HDV were found, for the detailed results see p. 179 ff. section 5.7.7.

3.1.11.1 Tractor-trailer

For European tractor-trailers with a parallel hybrid powertrain no measurement or simulation results from independent institutions were found for comparison purposes. Hence the simulation of a US vehicle on the motorway cycle FDHDT-A (248) (249) (250) (251) was used to check the EU-model of this thesis, see Figure 127.

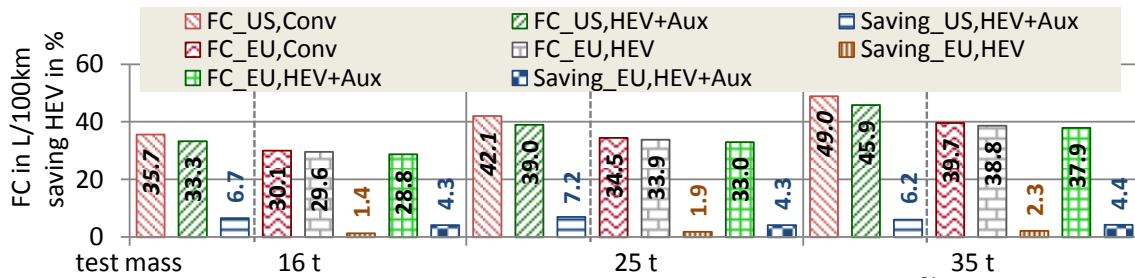


Figure 112. Cycle FDHDT-A, comparison of simulation results⁸¹, conventional and hybrid tractor-trailers, results for US-model from (249 p. 102)

The FC of the EU-model from this thesis is lower than calculated for the US-model, but the resulting saving of the parallel hybrid *with* advanced auxiliaries ("HEV+Aux") is in a similar range, albeit somewhat lower.

For the case HEV-only, *without* advanced auxiliaries, the simulation engineer who worked with the US-model confirmed a saving potential in the range 1 % to 3% (251), what is also the outcome from the model of this thesis.

In general the comparison with only one external value, in this case from a simulation, is too little to assess the own results, but here no more data was found. At least it can be stated that the model does not seem to produce evident errors.

The hybrid tractor-trailer was also compared on multiple driving cycles, with and without the default correction for crosswind. The results are shown in Figure 113 and Figure 114.

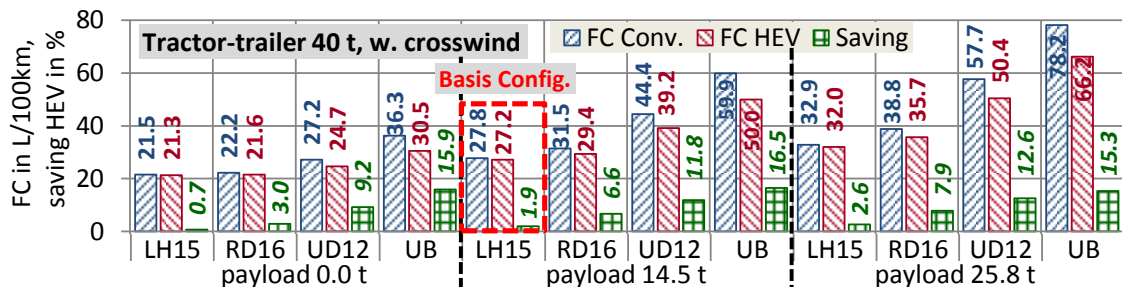


Figure 113. Models of conventional and hybrid tractor-trailers, with default correction for crosswind.

⁸¹ "HEV": Hybrid Electric Vehicle, "Aux": Advanced auxiliaries, lower average power.

US-model: Simulation program ANL Autonomie; Conventional: Tractor 6x4, 2-axle trailer, GCWR 36 t; curb weight 12.5 t; engine Cummins ISX15, 6 cyl. 15 L EPA '10, 2400 Nm @ 1300 rpm, 391 kW @ 1700 rpm, bsfc_{min} 186 g/kWh; 10-speed MT, 14.78 to 1.00; i_{FD} 2.64; r_{dyn} 0.53 m; $C_d \cdot A_{cr}$ 6.02 m², RRC 7 N/kN; $P_{aux,avrg}$ 8.2 kW_{mech}; Electrical parallel hybrid, differences to conventional: Curb weight 12.9 t; EM on gearbox input shaft, 100 (220) kW_{mech}; Li-Ion battery 35 kWh_{el}; $P_{aux,avrg}$ 4.2 kW_{el}

EU-model: Conventional & hybrid tractor-trailer from this thesis. Models with basis auxiliaries: $P_{aux,avrg}$ 8.2 kW_{mech}, like US-model. Hybrid with advanced auxiliaries: $P_{aux,avrg}$ 4.7 kW_{mech} (4.2 kW_{el} from US-model, divided by assumed 90 % efficiency of electrical generator).

The different battery sizes, EU 12 kWh_{el} & US 35 kWh_{el}, did not influence the results from the EU-model. E. g. for the cases test mass 25 or 35 t, "HEV+Aux", the simulated FC with a battery 35 kWh_{el} was 0.02 L/100km higher than with the standard battery 12 kWh_{el}: 33.06 or 37.96 L/100km vs. 33.04 or 37.94 L/100km.

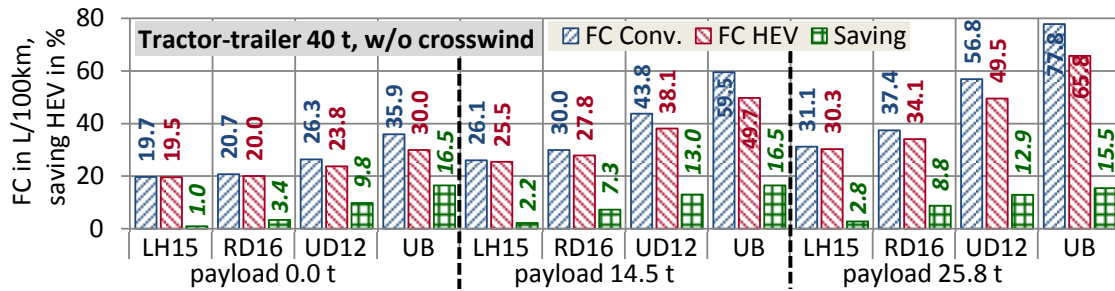


Figure 114. Models of conventional and hybrid tractor-trailers, w/o correction for crosswind.

The output from the tractor-trailer model with a parallel hybrid powertrain for the basis configuration, cycle LH15, 14.5 t payload and crosswind, is a fuel saving potential of 1.9 %.

The simulated changes of the saving potential from the hybrid vehicle model on different driving cycles are clearly visible. On the motorway cycle LH15 without payload the potential is lowest at ca. 1 %. On the transient bus cycle UB, which is not typical for tractor-trailers and was simulated only as example, the potential becomes highest around 15 %.

The default crosswind correction increases the weighted average FC from all variants on the truck cycles LH15, RD16 and UD12 by 5.4 % or 1.5 L/100km, and decreases slightly the saving potential from the hybrid models. The reason is, that the increase of the air drag consumes kinetic energy during braking, what would be available otherwise for recuperation. E. g. with 14.5 t payload on the cycle LH15 the average brake losses with crosswind are 0.164 kWh_{mech}/km and without wind 0.172 kWh_{mech}/km, hence more kinetic energy can be recovered with the EM in the latter case. The absolute saving in L/100km remains the same for most variants with or without crosswind, but due to the lower FC in the second case the relative saving becomes higher.

3.1.11.2 Delivery truck

The model of the parallel hybrid powertrain for delivery trucks could be examined for several HDV, compare (252) (253) (254 p. 28 ff.) and (255). The main data is given on p. 196 Table 60. The test vehicles "Delivery trucks, pair 1", "Delivery trucks, pair 2" and "Delivery tractor-trailer" are marked in Table 60 and consistently in the following diagrams.

For every pair of vehicles appropriate models⁸² were created to depict the measured ones. Nevertheless the simulated absolute FC cannot be compared to the measurement, because too little data is available for the specimen. Thus the comparison shall focus on the matching of the relative changes from hybrid to conventional.

⁸² All models: $\eta_{\text{mech,FD}} 0.96$, $\eta_{\text{mech,gear,indir}} 0.96$, $\eta_{\text{mech,gear,dir}} 0.98$;

Delivery trucks, differences to basis models *Conventional* and *Hybrid* of this thesis,

Pair 1, Conventional: Engine map 6.4 L € 6, full load curve 155 kW; test mass 14.3 t; no crosswind

Hybrid: Engine map 6.4 L € 6, full load curve 220 kW; test mass 14.8 t; no crosswind

Pair 2, Conventional: Engine map 6.4 L € 6, full load curve 220 kW; $i_{\text{FD}} 4.30$, wheels 11R22.5, $r_{\text{dyn}} 0.51$ m; test mass 12.5 t;

Hybrid: Engine map 6.4 L € 6, full load curve 185 kW; $i_{\text{FD}} 5.57$, wheels 11R22.5, $r_{\text{dyn}} 0.51$ m; test mass 12.2 t

Delivery tractor-trailer: Entire new models, technical data see p. 178 Table 38 "DTT - Delivery tractor-trailer"

The comparison of measurement and simulation for rigid delivery trucks on multiple driving cycles with conventional and parallel hybrid electrical powertrains, is shown in Figure 115.

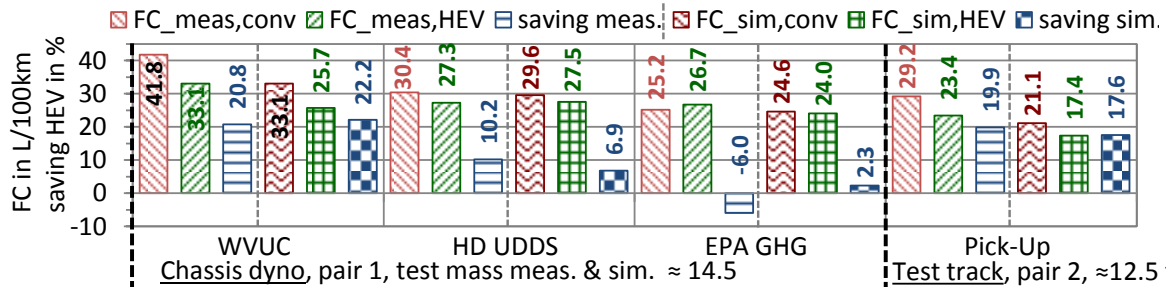


Figure 115. Measured and simulated fuel savings for conventional and hybrid electrical delivery trucks

For the case "Chassis dyno" the simulated change in FC from hybrid to conventional conforms well for the transient urban cycle WVUC, medium for the faster HD UDDS and not for the certification cycle EPA GHG. In the latter case the measured hybrid truck consumed 6 % more fuel than the conventional one, and in the simulation the FC is 2 % below. Because the dyno settings are not known, a more detailed analysis was not possible.

In the second case "Test track" the simulated relative change of FC fits well to the measured difference between hybrid and conventional.

For the conventional and hybrid delivery tractor-trailers results were available for measurements on the chassis dyno and for 1 year of real world urban delivery traffic in Miami, FL. By chance the average characteristic values of the real world traffic were similar to the VECTO cycle UD12-flat⁸³, hence this cycle was also analysed. For the vehicles the road load coefficients were known. The results are shown in Figure 116.

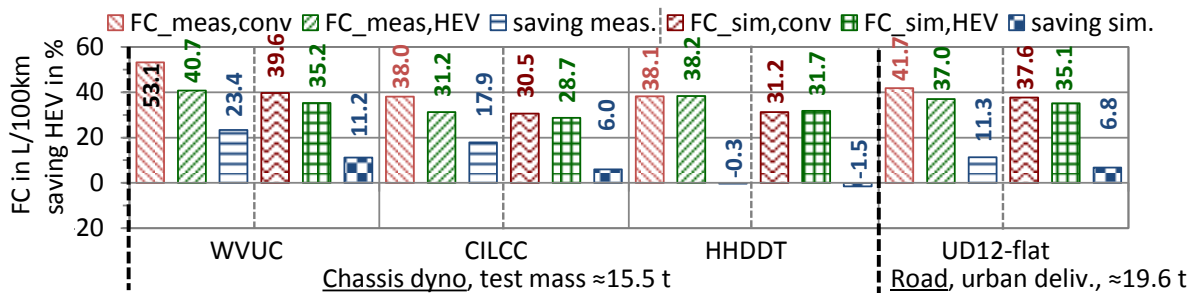


Figure 116. Measured and sim. fuel savings for conventional and hybrid electrical delivery tractor-trailers

Here the relative changes in FC from the dyno are not met in two of three cases. For the urban cycles WVUC and CILCC the measured saving is significantly higher than simulated. Only for the HHDDT cycle with a high share of motorway driving the relative change from hybrid to conventional, a small saving, is met. For real world urban delivery the deviation from the simulated to the measured change of FC is also obvious, but at least smaller than for the dyno.

Further road measurements and long-term fleet tests, published by other researchers, resulted in changes of FC from hybrid to conventional trucks in a range from -24 % to +0.5 %, where the majority of recorded changes was around -10 %. The collected numbers are shown on p. 197 ff. Table 60, "Road measurement" and "Fleet operation".

⁸³ (253 p. 7), Real world: weighted averages: $v_{roll,avg}$ 36.5 km/h, 1.0 stops/km, k_i 0.468 1/km; UD12-flat: $v_{roll,avg}$ 38.2 km/h, 0.9 stops/km, k_i 0.479 1/km. Characteristic values for UD12-flat simulated with model of conventional delivery tractor-trailer, test mass 19.5 t

The models of the conventional and hybrid delivery truck were also varied for driving cycles, payload and the correction for crosswind, the results are shown in Figure 117 and Figure 118.

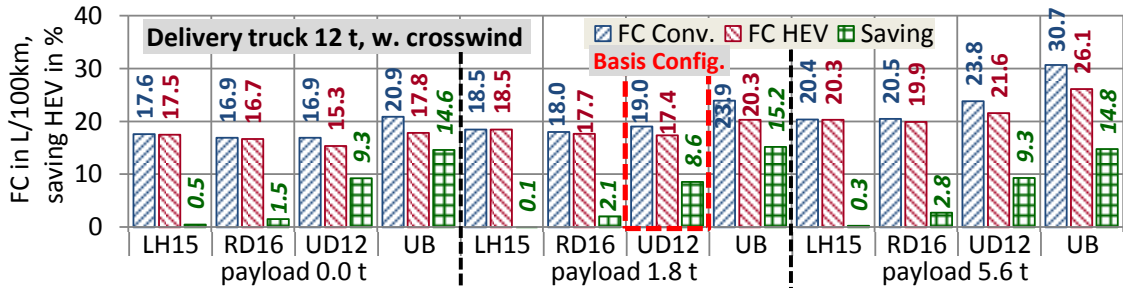


Figure 117. Models of conventional and hybrid delivery truck, with default correction for crosswind.

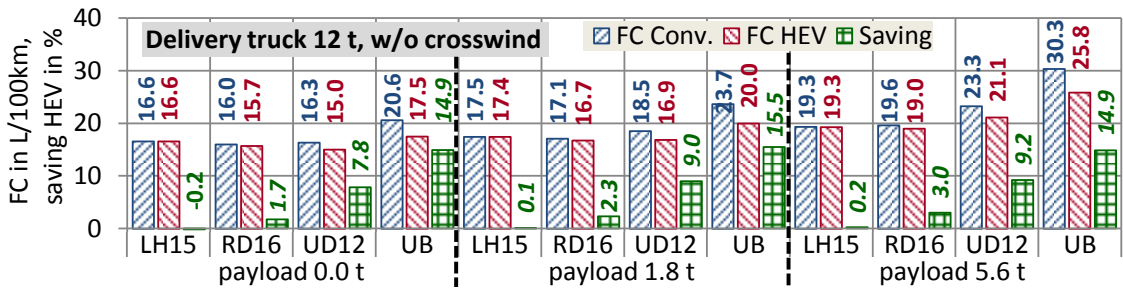


Figure 118. Models of conventional and hybrid delivery truck, w/o correction for crosswind.

The output from the delivery truck model with a parallel hybrid powertrain for the basis configuration, cycle UD12, 1.8 t payload and crosswind, is a fuel saving potential of 8.6 %. In comparison with the fleet tests this is plausible, but at the lower end of possible fuel savings.

Similar to the model of the hybrid tractor-trailer, the simulated potential of the hybrid is higher for urban cycles, where the bus cycle UB was also calculated only as example.

On the fast cycles LH15 and RD16 the potential is small or zero for this model, because the air drag consumes a higher share of the kinetic energy during braking than for the tractor-trailer. The effective air drag area $C_d \cdot A_{cr}$ of the tractor-trailer is 5.1 m² at vehicle masses from 13.4 t to 40.0 t. For the delivery truck $C_d \cdot A_{cr}$ is 5.2 m² for masses from 6.1 t to 12 t. Thus during braking there is significantly less kinetic energy available for recuperation from the lighter delivery truck, and the air drag consumes a bigger share.

For this model the crosswind correction increases the weighted average FC of all variants on the truck cycles LH15, RD16 and UD12 by 5.1 % or 0.90 L/100km. In addition the saving potential is slightly changed and for the basis configuration increased by 0.4 %-points.

3.1.11.3 Rigid bus

For parallel hybrid rigid buses some FC values are published from vehicles with powertrains similar to the modelled one, see p. 204 Table 65.

From a chassis dyno measurement the relative changes of FC from a parallel hybrid bus to a conventional bus are known and were compared with the results from the models for the bus cycles, see Figure 119.

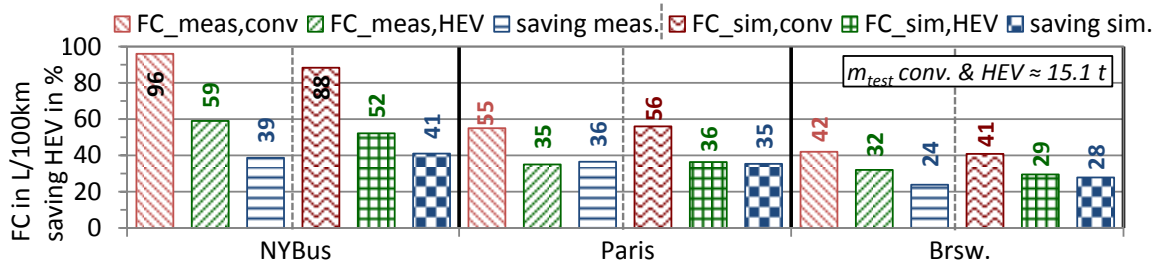


Figure 119. Parallel hybrid rigid bus, measurement chassis dyno (256 pp. 176, 179 ff.), own simulation⁸⁴

The deviation from the simulated to the measured savings hybrid vs. conventional ranges from -1 to +2 %-points, e. g. for the NYBus cycle 39 % saving measured and 41 % simulated. Because no details for the road load parameters of the dyno or for the vehicles are known, compare (256 pp. 81-85, 107), this good approximation happened by chance due to several unknown parameters from the measurement. It can only be reasoned, that the parallel hybrid model produces results of a realistic magnitude, when compared with the basis bus model.

From multiple publications the FC of parallel hybrid rigid buses EURO V and VI during fleet tests was collected and the change towards the FC of conventional buses. The range for the FC was 28.8 to 36.5 L/100km, and the difference to diesel buses varied from -20 to -30 %.

The parallel hybrid rigid bus was simulated for the conditions urban traffic on multiple urban bus cycles and for two variants of the average A/C power, for the results see Figure 120.

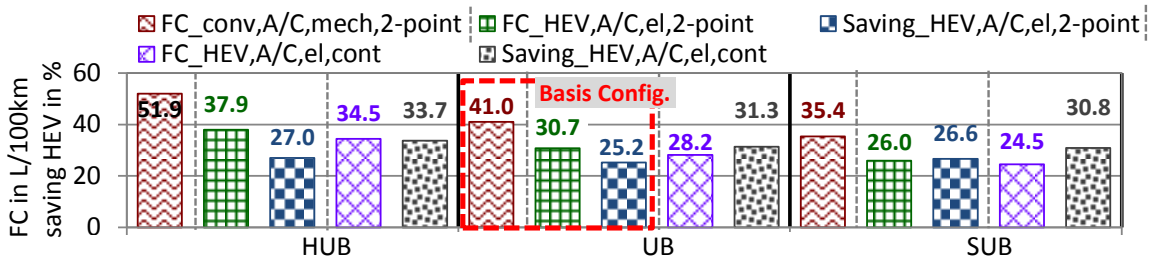


Figure 120. Models of conventional and parallel hybrid rigid bus, variation of A/C for hybrid⁸⁵

A/C,mech,2-point - mechanically driven A/C, 2-point control on/off; *A/C,el,2-point* - electrically driven A/C, 2-point control on/off; *A/C,el,cont* - electrically driven A/C, continuous control

The output from the rigid bus model with a parallel hybrid powertrain for the basis configuration, cycle UB, 16 passengers and 2-point A/C control, is a fuel saving potential of 25.2 %. In comparison with the fleet tests this is in the middle.

As shown on p. 188 Table 46 the hybrid buses are usually equipped with fully electrical A/C systems, which can be operated also at stops and during electrical driving, when the combustion engine is turned off. In addition the A/C of the hybrids are of lower cooling capacity in some cases and assumed to be equipped with a continuous control. As described on p. 29 ff. section 2.2.3.1 this leads to a lower average power demand of the A/C in comparison to the conventional bus with a simple 2-point control, see also p. 33 Figure 33.

⁸⁴ Chassis dyno, settings: No A/C, steering pump idle, no door-opening or kneeling

⁸⁵ Line operation, settings: A/C turned on; default auxiliary power demand; default values for no. of braking and bus-stops; actuation of doors and kneeling; average capacity usage 20 % → 16 passengers ≈ 1.1 t

Thus the hybrid bus was also simulated with the lower average power demand of an electrical A/C with continuous control, what increased the saving potential to 31.3 % on the UB cycle. If the assumption of a continuously controlled electrical A/C is right for all measured hybrid buses, could not be determined by remote diagnosis. But the additional saving effect of a more efficient A/C for city buses is clear and can be depicted with the model.

Depending on the state of technology of the A/C, the parallel hybrid bus model produces saving potentials which are in the range or slightly above of measured changes of FC.

3.1.11.4 Articulated bus

To assess the model of the parallel hybrid powertrain for buses complementarily, the vehicle model for an articulated hybrid bus was created, see p. 178 Table 38, "AB-PHEV, Diesel-electrical parallel hybrid articulated bus".

For articulated hybrid buses three numbers for the absolute FC and/or the change towards conventional vehicles were found, compare p. 211 Table 72.

The FC on the SORT 2 cycle is available for a parallel hybrid articulated bus. Here the main technical data of the measured vehicle is known, hence a similar model could be set up. The results of the comparison are given in Figure 121.

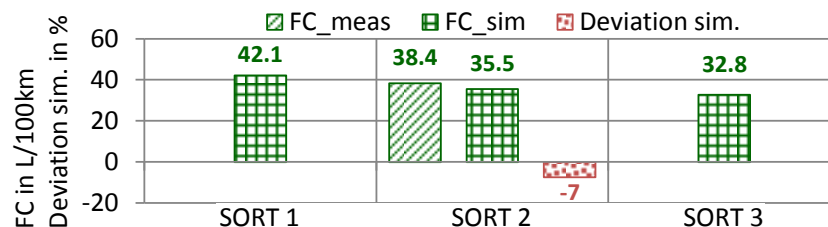


Figure 121. Parallel hybrid artic. bus, test mass 21.4 t, measurement result (257 p. 9), own simulation⁸⁶

Missing parameters for the model are the tire rolling resistance, details on the auxiliaries, the performance maps of diesel engine and electrical machine and the whole hybrid control. Facing these uncertainties, an approximation of -7 % to the measured FC is acceptable.

In comparison with the simulated SORT results for the articulated diesel bus, see p. 94 Figure 96, the model of the articulated parallel hybrid bus outputs savings from 34 % to 35 %. That is somewhat above the savings on the SORT cycles, which were calculated for the rigid parallel hybrid bus, as will be shown later on p. 119 in Figure 127.

For Luzern data is published (258 p. 16/17) from a 1 year comparison between an unspecified articulated bus EURO VI and a parallel hybrid articulated bus Volvo 7900LAH, where the technical data is available. The exact velocity patterns are not known, only the average velocities from 13 to 26 km/h of 7 bus lines, which point to heavy urban to suburban routes. In addition for Aarau the FC of a Volvo 7900LAH in mixed urban bus traffic with average values similar to SORT 2 is available for 2015/2016 (259 p. 15).

⁸⁶ SORT, test track, settings: No A/C; steering pump idle + banking; 1 x door opening; no kneeling; payload 5.0 t

The models of conventional and parallel hybrid articulated buses were compared on the appropriate VECTO cycles, also for a variation of the A/C power, see Figure 122

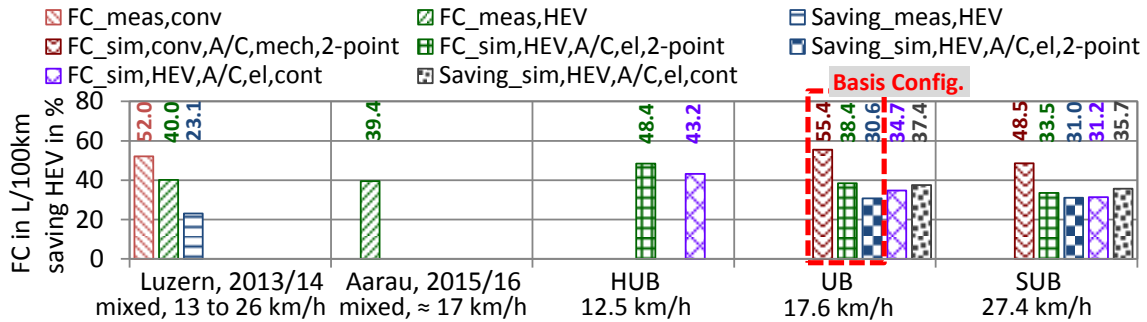


Figure 122. Measurement and sim., conventional and hybrid artic. buses € 6, variation A/C for hybrid⁸⁷
Measurement data (258 p. 16/17) (259 p. 15). A/C,mch,2-point - mech. driven A/C, 2-point control on/off; A/C,el,2-point - electr. driven A/C, 2-point control on/off; A/C,el,cont - electr. driven A/C, continuous control

The comparison for the HUB cycle is not shown, because the basis model of the articulated bus overestimates the FC on this cycle likely for > 5% and fits better for the other urban cycles, see p. 96 Figure 98.

The output from the articulated bus model with a parallel hybrid powertrain for the basis configuration, cycle UB, 26 passengers and A/C control 2-point, is a saving potential of 30.6 %, what is above the one known saving from one fleet test.

It shall be reminded, that the simulated FC from the conventional articulated bus model seems to be slightly too high, as described on p. 94 section 2.6.3.4.

Like described in the preceding section 3.1.11.3 on the hybrid rigid bus, the simulation of an electrically powered A/C with continuous control is more realistic for a hybrid electrical vehicle than an A/C with 2-point control. In this case the fuel saving from the hybrid model is significantly overestimated when compared to the one known fleet test.

From the complementary simulation of the articulated parallel hybrid bus it can only be deduced, that the calculated FC is of the right magnitude, but too low. It is estimated, that the model outputs FC values, which are 5 % to 10 % too low, when compared with few measurement values from SORT cycles and fleet tests. Hence blatant errors in the model of the diesel-electrical parallel hybrid powertrain for buses are at least unlikely. Because this bus model was set up only to check the powertrain model for parallel hybrid buses, the reasons for the deviation were not further investigated.

⁸⁷ Line operation, settings: A/C turned on; default auxiliary power demand; default values for no. of braking and bus-stops; actuation of doors and kneeling; average capacity usage 20 % → 26 passengers ≈ 1.8 t

3.1.12 Diesel-electrical serial hybrid vehicles

The model of the rigid city bus was also simulated with a serial hybrid powertrain. The structure is shown on p. 72 Figure 70 right, and the model is described on p. 77 chapter 2.5.3.

Like the parallel hybrid HDV, also this model was checked with max. payload for driving performance and could follow the basis bus, for details compare p. 179 ff. section 5.7.7.

For a bus with powertrain specifications similar to the model published FC values are given on p. 206 Table 67. The simulated FC for SORT and the comparison are shown in Figure 123.

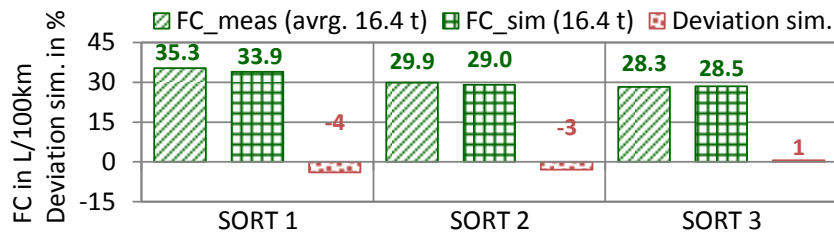


Figure 123. Serial hybrid rigid bus, avg. measurement (260 p. 30) (261 p. 13) (262 p. 81), own simulation⁸⁸

In this case the model EURO VI meets the measured FC of a serial hybrid bus EURO V with a few percent deviation. Because technical details for the measurement vehicle like rolling resistance, air drag and hybrid control are unknown, this is acceptable.

Also the simulated FC of the serial hybrid bus and the reduction versus a conventional vehicle on the Altoona cycle were investigated and compared with measurement data, see Figure 124.

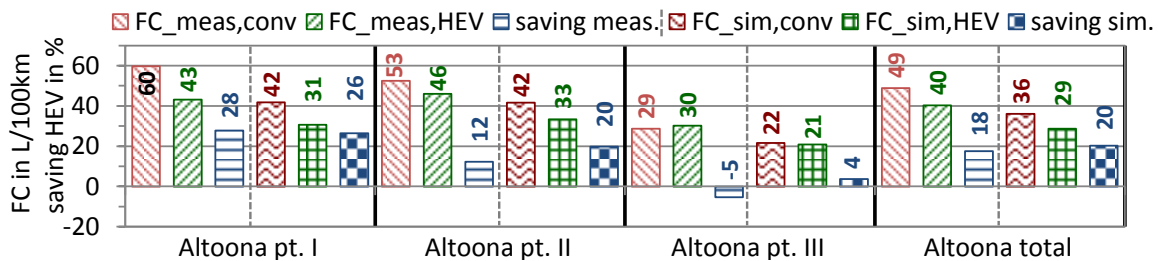


Figure 124. Serial hybrid rigid bus, measurement results from (263 p. 41) (264 p. 40), own simulation⁸⁹

On the Altoona cycle the absolute consumption is not met, but the relative change from hybrid to conventional vehicle is depicted acceptably. The simulated very small saving and the measured surcharge of FC during the third cycle part, constant driving at 64 km/h, are interesting. Because of the double power conversion in generator and electrical machine, the drivetrain losses from engine to wheel shafts are higher than for a conventional bus. That effect can lead to a higher FC of the serial hybrid bus, since no brake energy can be recovered on constant speed cycles to compensate these losses.

⁸⁸ SORT, test track, settings: No A/C; steering pump idle + banking; 1 x door opening; no kneeling; payload 3.2 t

⁸⁹ Altoona, test track : No A/C., steering pump idle + banking, door opening every stop, no kneeling. Test masses measurement and simulation: Conventional 15.1 t, serial hybrid 15.4 t.

For the road measurement on Stuttgart Line 42 the reduction of FC from a serial hybrid bus in comparison with conventional buses is known, all vehicles of stage EURO V. This driving cycle was also simulated with the bus models EURO VI, see Figure 125.

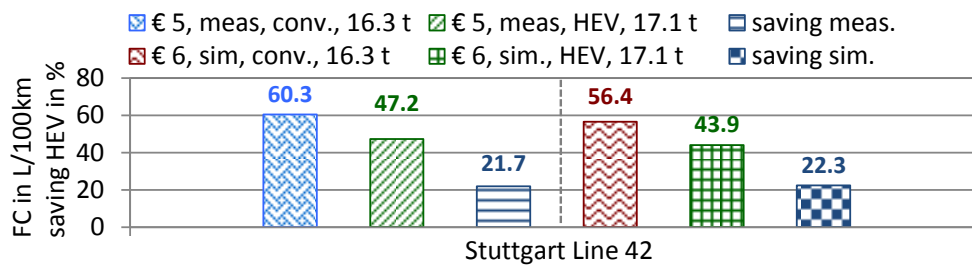


Figure 125. Serial hybrid rigid bus, avrg. measurement (265 p. 50) (266 p. 48) (267 p. 74), own simulation⁹⁰

Here the absolute simulated FC values are lower than measured and the calculated fuel saving by the hybrid is somewhat higher. As described above, the unknown measured driving cycles deviate slightly among each other and to the measured GPS track, which was the basis of the VECTO input. Hence only the magnitude of the results can be compared, which matches.

From fleet tests of European serial hybrid buses a range of savings 15 to 28 % versus conventional diesel buses is known, compare p. 206 Table 67. The FC of the hybrid buses ranged from 29.1 to 33.3 L/100km.

The model of the serial hybrid rigid bus was simulated on the VECTO urban bus cycles, like the others hybrids also for a variation of the A/C power. For the results see Figure 126.

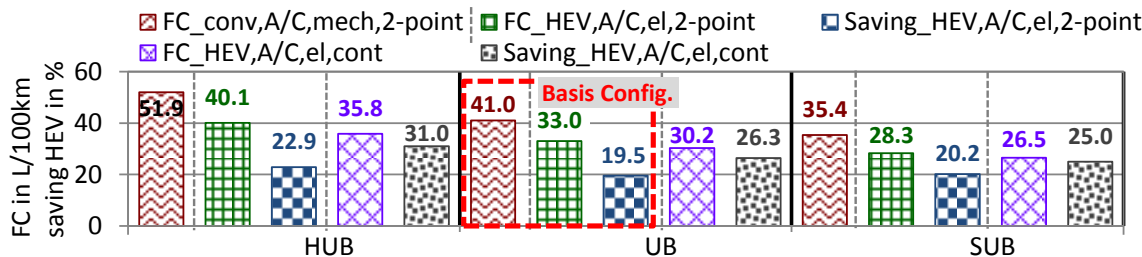


Figure 126. Models of conventional and serial hybrid rigid bus, variation of A/C for hybrid⁹¹
A/C,mech,2-point - mechanically driven A/C, 2-point control on/off; *A/C,el,2-point* - electrically driven A/C, 2-point control on/off; *A/C,el,cont* - electrically driven A/C, continuous control

The output from the rigid bus model with a serial hybrid powertrain for the basis configuration, cycle UB, average 16 passengers and an A/C with 2-point control, is a fuel saving potential of 19.5 %. That is in the range of published savings from fleet tests, but at the lower end.

The model of the serial hybrid rigid bus was also simulated with the average power demand of an electrically driven A/C with continuous control, instead a system with 2-point control. Then the saving potential on the three urban bus cycles gets higher to 25 to 31 % and is at the upper end or above of the published savings. Like described on p. 29 ff. section 2.2.3.1 on bus A/C systems and on p. 114 at the end of part 3.1.11.3 on the parallel hybrid rigid bus, also the measured serial hybrid buses were likely equipped with electrically driven A/C with advanced control functions. These devices reduce the FC in addition to the hybrid powertrain.

⁹⁰ Stuttgart Line 42, road, settings: No A/C; stand at all 52 bus stops; no door opening or kneeling.

⁹¹ Line operation, settings: A/C turned on; default auxiliary power demand; default values for no. of braking and bus-stops; actuation of doors and kneeling; average capacity usage 20 % → 16 passengers ≈ 1.1 t

3.1.13 Comparison of parallel and serial hybrid powertrain for rigid buses

To check, if the models of the parallel and serial hybrid bus are plausible when compared with each other, the results from the cycles SORT 1-2-3, (Heavy) Urban Bus, Suburban & Interurban Bus plus Long Haul 2015 were compared, where the latter two cycles were limited to 80 km/h due to model restrictions. For the SORT results see Figure 127 and Figure 128.

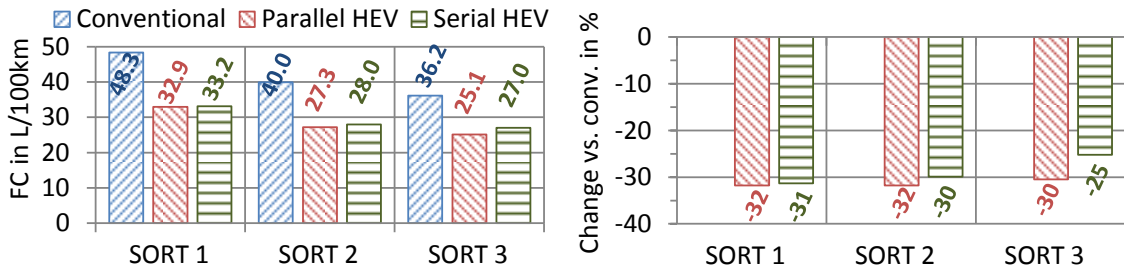


Figure 127. Simulation results SORT cycles, conventional, parallel- and serial hybrid bus models

On the cycles SORT 1 and 2 the saving potential from the parallel and serial hybrid bus model is nearly the same, on the SORT 3 the parallel bus consumed less fuel.

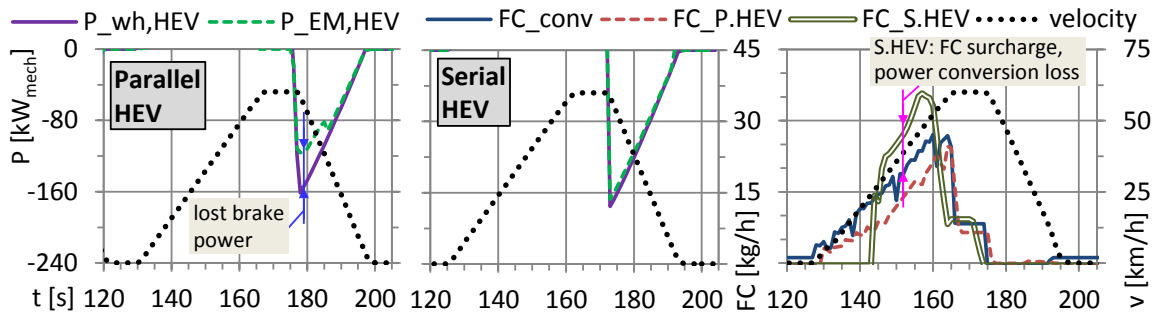


Figure 128. SORT 3 cycle, 3rd trapezoid. Parallel and serial hybrid electrical bus (P.HEV, S.HEV), mech. power at wheels and at electrical machine. Fuel consumption for conventional and hybrid buses.

During regenerative braking the serial hybrid has got an advantage by the high generator power of its motor-generator, $-240 \text{ kW}_{\text{mech}}$ vs. $-120 \text{ kW}_{\text{mech}}$ for the parallel hybrid. Hence more braking power can be recovered by the serial hybrid, as is shown in Figure 128 middle.

While driving with the diesel engine the parallel hybrid takes advantage of its good powertrain efficiency due to the mechanical power transmission. The serial hybrid powertrain comprises three power conversions, mechanical to electrical in the generator, electrical to electrical in the inverter and electrical to mechanical in the motor-generator, what causes significantly higher losses and a FC surcharge, see Figure 128 right. This effect causes the FC penalty on the SORT 3 cycle in comparison to the parallel hybrid bus model. The SORT 3 is the fastest of the SORT cycles, where the diesel engine is utilised most.

The hybrid architecture, parallel, serial or power-split, does not determine the generator power of the electrical machine(s) (EM). It would be also possible to construct a parallel hybrid with a big and a serial hybrid with a small EM. But there are practical requirements to be considered. In a parallel hybrid the EM is only the second propulsion machine to relieve the diesel engine. Also the total mass of the powertrain needs to be limited, which consists of diesel engine, mechanical gearbox, EM and battery. A serial hybrid is in fact an electrical vehicle with a genset as power source and needs an EM of a minimum size. Torque and power at the wheels shall be sufficient to reach similar acceleration values like conventional vehicles. Hence the EM of a serial hybrid is in most cases bigger than of parallel hybrid.

The results with average and full payload on the VECTO target speed cycles HUB, UB, SUB, IUB (80 km/h) and LH15 (80 km/h) are shown in Figure 129.

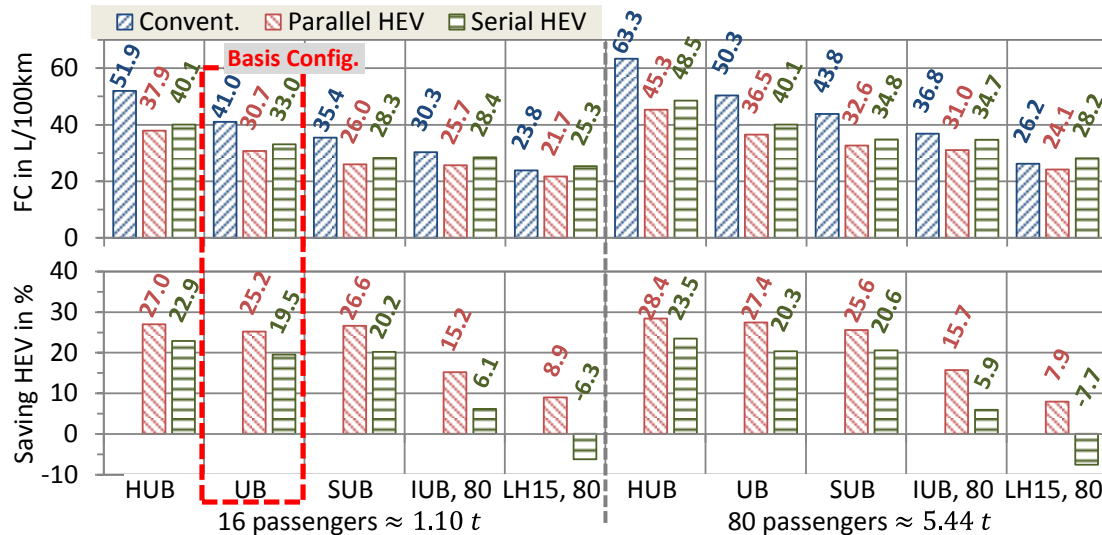


Figure 129. Fuel consumption and relative change of FC for conventional and hybrid rigid buses.
Convent. or hybrid bus models w. mech. or electr. A/C 2-point control, compare p. 29 ff. section 2.2.3.1

With an average payload of 16 passengers on the urban bus cycles the hybrid buses offer saving potentials from ca. 20 to 27 %, where the potential of the parallel hybrid is higher. On the IUB cycle (80 km/h) the saving for the serial hybrid model decreases significantly due to the higher drivetrain losses. In case of average payload on the LH15 cycle (80 km/h) it outputs a FC surcharge of ca. 6 %, caused by the conversion losses in the drivetrain. The parallel hybrid still offers a saving of ca. 9 %.

For full payload the relation between the savings from the parallel and the serial hybrid bus model are similar to the case of average payload. Here the FC penalty for the serial hybrid on the motorway cycle LH15 (80 km/h) increases slightly to 7.7 %.

For a better understanding of the differences between the parallel and the serial hybrid bus model a closer look at the results from the bus cycles was taken. Especially the reason for the higher FC of the serial hybrid instead of its bigger potential for regenerative braking needed to be found. The overall average values for the rolling velocity ($v_{veh} > 0$ km/h, $v_{roll,avg}$), the positive tractive work at the wheels ($W_{tract,wh}$) and the mechanical drivetrain efficiency for the tractive power from the combustion engine ($\eta_{mech,drivetr,ice}$)⁹² were compared, see Figure 130.

⁹² Positive power at wheel hubs and at engine shaft: Traction, driving mainly with engine power.

Ratio of (tractive work at wheel hubs) to (work output at engine shaft). If so corrected for share of tractive power from electrical machine of hybrid powertrain, and for auxiliary power.

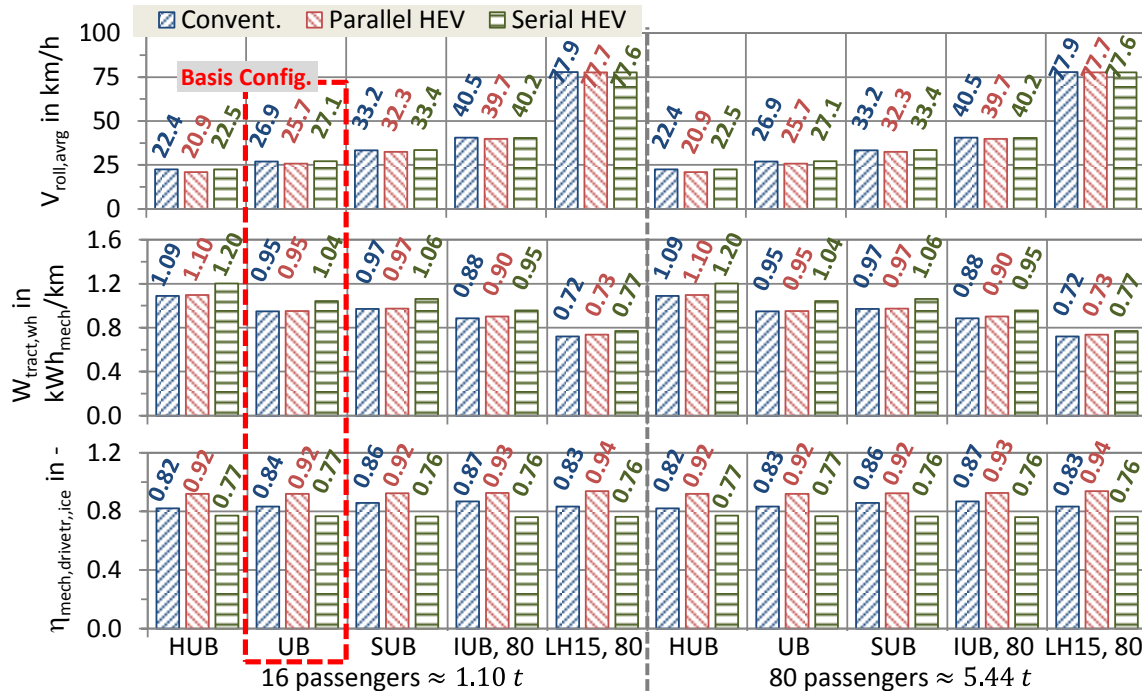


Figure 130. Average values for rolling velocity, tractive work and drivetrain efficiency for ICE power

Due to the powertrain characteristic the parallel hybrid bus model accelerates slightly less than the conventional and serial hybrid models, what was also found during a preceding project in collaboration with bus drivers (161 p. 51). This leads to less tractive work at the wheels in comparison to the serial hybrid, in addition to the lower curb weight of 11.7 vs. 12.3 t. The differences in the acceleration behaviour reflect the real behaviour of drivers to use a higher available engine torque for a better driving performance, also for HDV.

Another reason for the higher FC from the serial hybrid bus model is its lower drivetrain efficiency when driving with the diesel engine, caused by the triple power conversion in generator, inverter and EM.

From the comparison above it can be reasoned, that the single models for hybrid rigid buses seem to be plausible. E. g. the influences of drivetrain efficiency and acceleration behaviour are depicted accurately.

The result, that the model of the parallel hybrid rigid bus outputs less FC than the serial hybrid, is in contrast to the outcome from a preceding project (5 p. 92). The reasons are amongst others completely revised and improved models and an error in the simulation program PHEM, which was applied to the parallel hybrid bus. The error was found after the end of the preceding project and was fixed manually for this work in the postprocessing.

The question, if a parallel or serial hybrid bus is more efficient, could not be answered finally. Multiple different simulation programs (VECTO v1.4 & v2.2, PHEM) were utilised in combination with custom postprocessing routines in MS Excel. The vehicle models were aligned as well as possible for road load, driving dynamics and drivetrain losses, but the remaining uncertainty is higher than in case of one universal simulation tool.

For the future theoretical analysis of different hybrid concepts the application of one standardised simulation program for all vehicle models is highly recommended.

3.1.14 Battery-electrical powertrain

The HDV delivery truck and rigid bus were simulated as battery-electrical vehicles (BEV), compare p. 173 Table 34 "D) Battery-electrical vehicle". The modelling approach is explained on p. 79, chapter 2.5.4 "Battery-electrical delivery truck and rigid bus". With the electrical HDV models the energy consumption was determined on battery level (EC_{batt}), and for the consumption from the grid (EC_{grid}) 10 % charging losses were added (162 p. 10) (163 p. 1).

For the comparison of the consumed energy storage-to-wheel it shall be considered, that electricity from the battery is compared with lower heating value of diesel fuel from the tank. The energy conversion machine of the electrical vehicle, the motor-generator, has a much higher efficiency than the diesel engine, ca. 95 % vs. ca. 40 %, due to its working principle. Also it offers regenerative braking, what cannot be done with a diesel engine.

The power conversion electrical \rightarrow mechanical or vice versa in a motor-generator by electromagnetic induction causes significantly lower losses than the conversion chemical \rightarrow mechanical in a diesel engine. The working principle of heat engines is combustion with a resulting temperature increase of a gas mass, where the following volume expansion is used to conduct mechanical work.

During the generation of electrical energy in thermal power stations, e. g. fired with gas, coal, solar or nuclear decay heat, losses of the similar type like in combustion engines occur, but not in wind or water power stations. Dependent on the share of fossil plants in the grid the GHG-factor is calculated. For the ENTSO-E-Mix in continental Europe it was in 2014

$$0.34 \text{ kg-CO}_2\text{e/kWh}_{el} \quad (268 \text{ p. } 37).$$

It is multiplied with the energy consumption from the grid (EC_{grid}), to get the GHG emissions.

The amount of radioactive waste from the electricity grid continental Europe was in 2014

$$7.11 \cdot 10^{-7} \text{ kg-radioact./kWh}_{el} \quad (268 \text{ p. } 37),$$

what can be taken into account for the analysis of the overall environmental damage.

The results of the simulation of driving performance for the BEV models are shown on p. 179 ff. in section 5.7.7, where no worsening in comparison to the basis HDV was found.

3.1.14.1 Delivery Truck

For the modelled 12 t BEV delivery truck no values for the EC are available for a direct comparison, but for a slightly other US truck, see p. 198 Table 61 first entry. During 19 months in 2013/2014 the EC of 200 BEV delivery trucks, make Smith, model "Newton", was recorded in the urban traffic of 40 US cities (163). From GPS velocity patterns the representative driving cycle Smith Newton (SN) was elaborated (269 p. 7), see p. 161 Figure 181. A model similar to the measurement vehicle was created, compare p. 178 Table 38 "DTS: Battery-electrical delivery truck 'Smith'", and it was tried to match the energy consumption only during driving ($EC_{batt,drv}$, without stops). The model of the BEV delivery truck for this thesis was derived step by step from the model of the measured vehicle. The results of the comparison and the stepwise conversion towards the model for this thesis are shown on Table 24.

Table 24. Derivation of battery-electrical delivery truck (BEV DT) from delivery truck "Smith" (DTS)⁹³

	Variation	$W_{\text{tract,wh}}$ kWh _{mech} / km	$\eta_{\text{mech, drivetr,tot}}$ in -	$\eta_{\text{EM,tot}}$ in -	$EC_{\text{batt,drv}}$ kWh _{el} / km	Dev. %	EC_{batt} kWh _{el} / km
0)	Measurement urban traffic Fleet of original vehicles, "Smith Newton"	-	-	-	0.786	<i>basis</i>	-
1)	Simulation, cycle "Smith Newton"(SN) ➔ Model similar to measured trucks Compare p. 178 Table 38	0.647	0.922	0.900	0.783	-0.4	0.814
2)	1) + curb mass 5.30 t <i>instead of</i> 4.52 t	0.690	0.908	0.902	0.833	+6.0	0.864
3)	2) + tires 265/70R19.5 <i>instead of</i> 245/ 70R19.5; $J_{\text{wh,tot}}$ 39 vs. 36 kg·m ² , r_{dyn} 0.421 vs. 0.403 m, RRC 6.1 vs. 9 N/kN	0.642	0.905	0.900	0.763	-2.9	0.794
4)	3) + bigger cabin and body $C_d \cdot A_{\text{cr}}$ 5.19 m ² and crosswind curve "Delivery truck" <i>instead of</i> $C_d \cdot A_{\text{cr}}$ 4.68 m ² and crosswind curve "DTS"	0.658	0.906	0.901	0.785	-0.1	0.817
5)	4) + EM & powertr. BEV DT EM 1100 Nm & 160 kW <i>instead of</i> EM 600 Nm & 120 kW 3-speed AT, w/o torque-converter (1.85, 1.36, 1.00) <i>instead of</i> 1-speed gear 4.00 Loss maps AT <i>instead of</i> efficiency 0.97	0.661	0.874	0.905	0.794	+1.0	0.825
6)	5) + final drive 3.70 <i>instead of</i> 3.42, loss map final drive <i>instead of</i> efficiency 0.96 ➔ Model battery electrical delivery truck for this thesis, compare p. 173 Table 34	0.662	0.873	0.904	0.800	+1.8	0.832

From step 2) to 3) the EC decreases due to the lower rolling resistance. In the US this value is in general higher for smaller truck tires than in the EU (270 p. 3) (271 pp. C-3). When changing the powertrain, step 4) to 5), EC increases by 5 % mainly due to the higher friction losses in the automated transmission (AT) in comparison with the single speed reduction gear. A multi-stage gearbox was necessary to couple the bigger EM 160 kW with the cardan shaft, because its max. speed is 2100 rpm instead of 8100 rpm for the smaller 120 kW machine. An AT is useful due to its powershift capability, i. e. shifting during power transmission, because for regenerative braking a continuous power flow without traction interruption is desired.

For the model of the battery-electrical delivery truck with average 1.8 t payload the energy consumption EC_{grid} on the Urban Delivery 2012 cycle was simulated to 0.86 kWh_{el}/km, including 10 % charging losses from grid to battery. That is 54.5 % less final energy, when compared with the FC of the basis diesel truck, 19.0 L/100km or 1.89 kWh_{th}/km. The resulting GHG emissions based on the ENTSO-E-Mix 2014 are 52.6 % lower than from the diesel vehicle.

⁹³ $\eta_{\text{mech, drivetr,tot}}$ - Total mechanical drivetrain efficiency, driving and regenerative braking;

$\eta_{\text{EM,tot}}$ - Total efficiency electrical machine, motor and generator operation.

3.1.14.2 Rigid bus

For the BEV rigid bus more EC_{batt} values are available to check the model, compare p. 207 Table 69 for BEV buses with motor-generators of similar power like the model and p. 208 Table 70 for vehicles with weaker machines.

The comparison of the simulation with several measurements is shown in Figure 131.

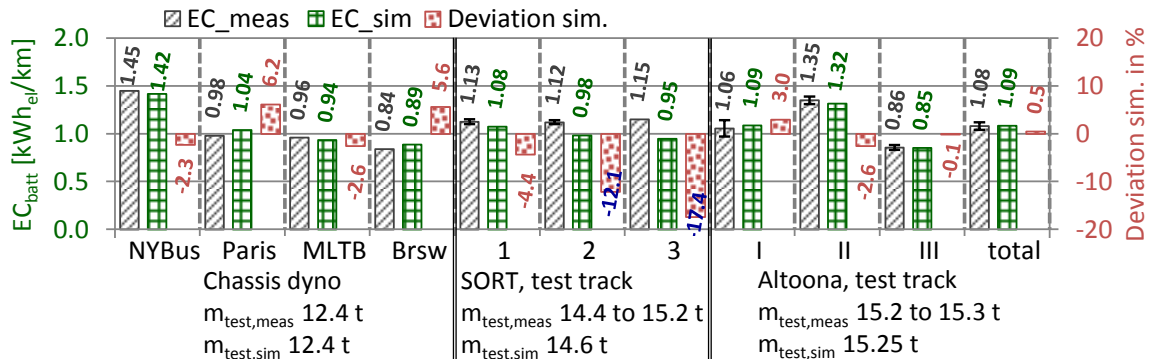


Figure 131. 12 m battery-electrical rigid bus, measured and simulated energy consumption⁹⁴

Measurand is avrg. from max. and min. found EC_{batt} , where the range is also shown. Case multiple buses only.

The deviation from simulation to measurement ranges from -17 to +6 %, with an average absolute value of ca. 5 %. Concerning the bigger deviations for the SORT cycles it is less plausible, that the measured EC remains nearly constant for cycles of different characteristics. Thus the test results in the SORT cycles may not be fully representative. When looking at the other two comparisons, the simulated EC is closer to the measurands.

The simulation on the VECTO urban bus cycles and a comparison with published EC_{batt} values for line operation (see p. 207 ff. Table 69 & Table 70) is shown in Figure 132.

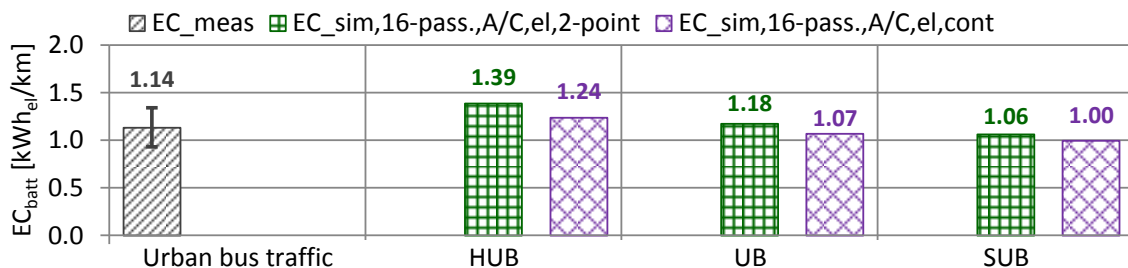


Figure 132. 12 m battery-electrical rigid bus, energy consumption for line operation⁹⁵

A/C, el, 2-point - electr. driven A/C, 2-point control on/off; *A/C, el, cont* - electr. driven A/C, continuous control
Measurand is avrg. from max. and min. found EC_{batt} , where the range is also shown.

The result for the Heavy Urban Bus cycle is at the upper end of the measured EC_{batt} range, the results for Urban and Suburban Bus cycle are in the middle.

The bus model was also simulated with an A/C with continuous control. As described on p. 29 ff. in section 2.2.3.1 that decreases the average power demand of the chiller substantially, when compared to a standard device with 2-point control. For the BEV urban bus the overall energy consumption decreases by 0.06 to 0.15 kWh_{el}/km or by ca. 6 to 11 %.

After 4 rounds on the Urban Bus cycle the basis BEV bus model with a battery of a capacity 300 kWh_{el} needs to be recharged for min. 0.75 h with a power of 300 kW_{el}. 4 rounds equal 160 km in 8.8 h and that is a half or third day of operation, dependent on the shift system.

⁹⁴ Chassis dyno: No A/C, no door opening or kneeling. SORT test track: No A/C, steering pump only banking, 1 x door opening, no kneeling. Altoona test track: No A/C., steering pump only banking, door opening every stop, no kneeling.

⁹⁵ Line operation, settings: A/C turned on; default auxiliary power demand; default values for no. of braking and bus-stops; actuation of doors and kneeling; average capacity usage 20 % → 16 passengers ≈ 1.1 t

The alternative is a BEV bus with a smaller battery 80 kWh_{el}, what is enough capacity for 1 round with 80 passengers. At the final bus stop, where the drivers usually take a short rest, the battery is recharged for 0.25 h with 200 kW_{el}, what is sufficient for the next round. The curb weight of the bus becomes lower than for the variant with a big battery, 11.5 vs. 13.5 t, and the EC decreases. The simulated EC_{batt} on the Urban Bus cycle with 16 passengers is 1.08 kWh_{el}/km from the battery, 8 % less than for the bus with the bigger battery.

3.1.14.3 Battery-electrical vehicle models, payload and energy consumption

The models of the battery-electrical delivery truck and 12 m rigid bus, w/o intermediate charging, were simulated for a variation of the payload. The results are shown in Figure 133.

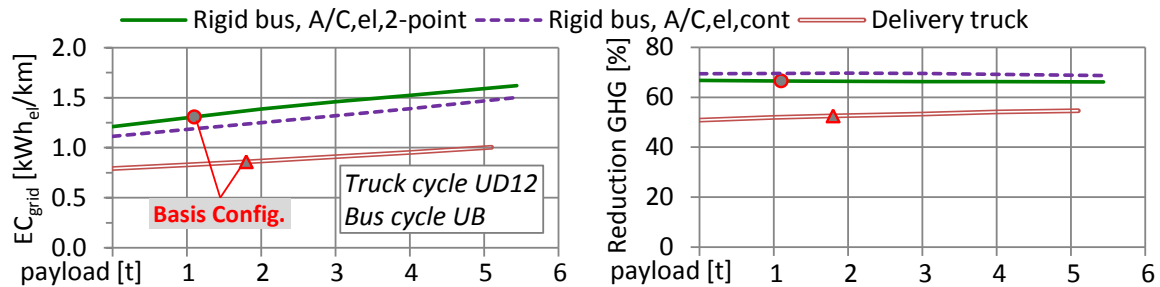


Figure 133. Payload of battery-electrical vehicles, energy consumption from grid and reduction of GHG vs. conventional diesel-fuelled HDV models (GHG factor ENTSO-E-Mix 2014, 0.34 kg-CO_{2e}/kWh_{el})

The model of the battery-electrical delivery truck outputs reduction potentials for GHG from 51 % to 55 % in comparison with the conventional diesel truck.

For all payloads the reduction of GHG from the bus model with a standard A/C, 2-point control, is around 66 %, with a slight decrease for higher capacity usages. An A/C with continuous control magnifies the reduction to ca. 69 %.

The model of the battery-electrical delivery truck has got in average a higher power-to-mass ratio than the battery-electrical rigid bus, when comparing the available generator power of the EM to the vehicle mass⁹⁶. This is the reason for the slight increase of the reduction of GHG at higher payloads. Especially at low payloads the virtual EM in the truck can recuperate a higher share of the brake power in comparison to the EM in the bus.

⁹⁶ The ratio of (rated generator power) to (vehicle test mass) for the delivery truck decreases from 0 to 5.1 t payload from 23.2 to 13.3 kW_{mech, rated}/t. For the rigid bus the ratio is smaller and changes from 0 to 5.44 t payload (≈ 80 Pass.) from 18.0 to 12.8 kW_{mech, rated}/t. From empty to full payload this ratio, thus the max. potential for regenerative braking, changes for the truck by -9.9 kW_{mech, rated}/t and for the bus by -5.2 kW_{mech, rated}/t. That decreases for the bus model the dependence of the change of GHG vs. the diesel vehicle on the payload.

During regen. braking the EM operates most times below its rated generator power on the line of max. generator torque, but the above mentioned ratio can be used as first estimation for the max. potential for recuperation.

3.1.15 Overview of results for selected single measures and alternative powertrains

In Figure 134 and Figure 135 the results for the selected single measures are summarised, in terms of the change of fuel consumption (FC, tank-to-wheel, diesel) and greenhouse gases (GHG, well-to-wheel).

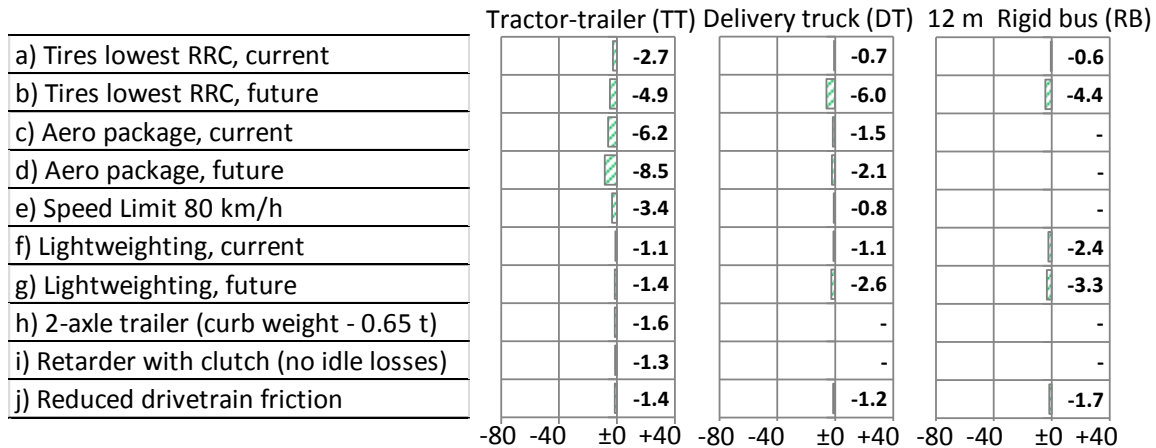


Figure 134. Results for single efficiency measures, change in % of FC (TTW, base unit [L]) and of GHG (WTW, base unit [gCO_{2e}]), towards the HDV models of technical level “basis”, MY 2014. Part 1

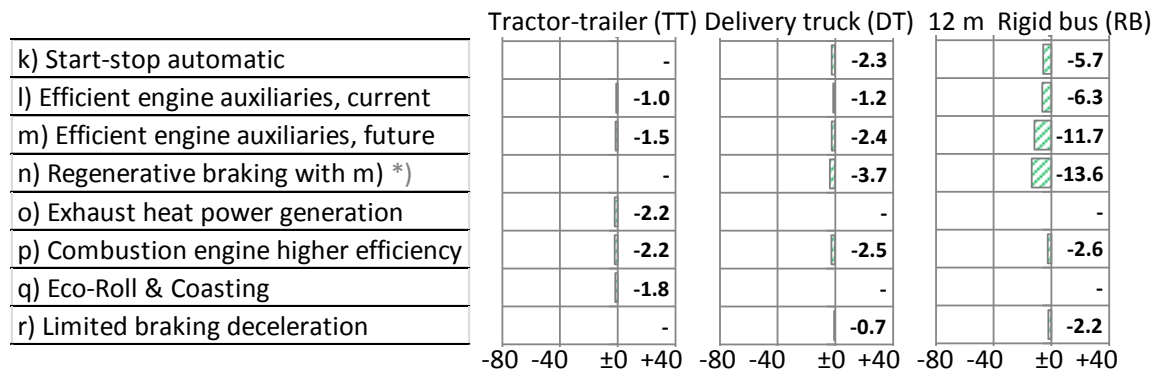
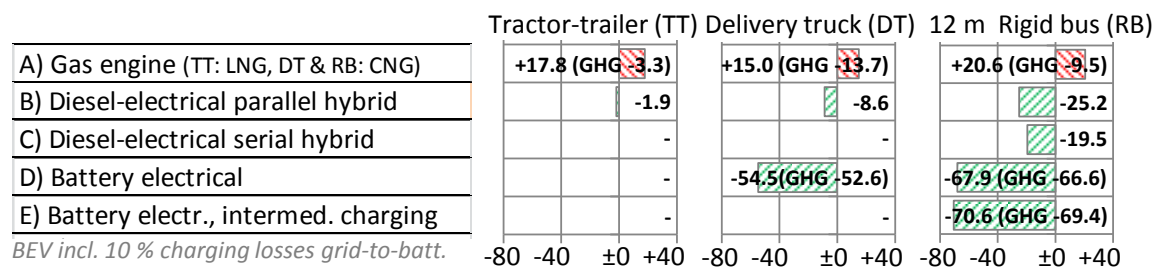


Figure 135. Results for single efficiency measures, change in % of FC (TTW, base unit [L]) and of GHG (WTW, base unit [gCO_{2e}]), towards the HDV models of technical level “basis”, MY 2014. Part 2

*) Alternator and compressor at max power during braking

With the measures a) to r) the simulated changes of fuel consumption range from -0.6 % to -13.6 %. For the model of the tractor-trailer the future aero package, measure d), offers the highest saving of 8.5 %. For the delivery truck the highest reduction of ca. 6.0 % can be reached with future tires of rolling resistance class A, measure b), instead of the current tires class C & D. In case of the rigid bus the most efficient single measure with a potential of 13.6 % is the bundle of future auxiliary consumers with regenerative braking, measure n).

A summary of the results for the alternative powertrains is shown in Figure 136. There the change of energy consumption (EC, diesel, natural gas, electricity) and GHG is enlisted. For other fuel than diesel the change of GHG is labelled separately due to the other GHG factors.



BEV incl. 10 % charging losses grid-to-batt.

Figure 136. Results for alternative powertrains, change in % of EC (TTW, base unit [kWh]) and of GHG (WTW, base unit [gCO_{2e}]), towards the HDV models of technical level “basis”, MY 2014. GHG labelled separately if not diesel fuel.

Looking at alternative powertrains instead of diesel-only, the gas engines, measure A), offer potentials for GHG reduction from 3 % to 14 %. The energy consumption increases by 15 % to 21 % due to the lower efficiency of the analysed stoichiometric gas engines in comparison to the basis diesel engines. The low GHG factors of liquefied and compressed natural gas allow nevertheless a reduction of GHG emissions.

With the diesel-electrical parallel and serial hybrid powertrains, measures B) and C), the fuel consumption is reduced by 2 % to 25 %, dependent on driving cycle and vehicle type.

In case of the battery-electrical vehicles, measures D) and E), the electricity demand from the grid was simulated to be 55 to 71 % lower than the consumption of lower heating value from the diesel tanks of the conventional vehicles. The resulting GHG emissions well-to-wheel, calculated with the GHG factor for the ENTSO-E-Mix 2014 (0.34 kg-CO₂e/kWh_{el}, (268 p. 37)), were 53 % to 69 % lower than for the diesel vehicles.

3.2 Bundled saving measures, levels "current" and "future"

The selected single saving measures, see p. 126 ff. Figure 134 and Figure 135, a) to r), were combined to bundles and simulated for each of the standard diesel engine and alternative powertrain concepts. As technology levels "current" and "future" were chosen. "Current" means measures, where the components or control settings are already available on the market and could be applied in a short time frame to HDV. The level "future" includes the measures from the first stage "current" plus advanced components, which are currently not on the market, but where the main part can be expected until the mid of the 2020ies.

The allocation of single saving measures to bundles and HDV classes is shown in Table 25. Most "future" components, such as electrified engine auxiliaries or systems for exhaust heat power recuperation are already available as prototypes or small series, but for trucks not in big series or as option. Some city buses, e.g. the MB Citaro and Solaris Urbino are already offered with three regenerating alternators and a supercap as energy storage. For the tires RRC in the "future" bundle class A was assumed for all axles (see chapter 3.1.1).

Table 25. Bundles of efficiency measures, current and future, simulated for all powertrain concepts.

	Tractor-trailer	Delivery truck	Rigid bus 12 m
current possible saving measures	a) Tires lowest RRC, current c) Aero package, current e) Speed limit 80 km/h f) Lightweight trailer h) Trailer 2-axles i) Retarder with clutch l) Efficient auxiliaries, curr. q) EcoRoll & Coasting	a) Tires lowest RRC, current c) Aero package, current e) Speed limit 80 km/h f) Lightweight tail-lift k) Start-stop automatic l) Efficient auxiliaries, curr. r) Limited braking deceleration	a) Tires lowest RRC, current f) Lightweight chassis, curr. k) Start-stop automatic l) Efficient auxiliaries, curr. r) Limited braking deceleration
future possible saving measures	b) Tires lowest RRC, future d) Aero package, future e) Speed limit 80 km/h g) Lightweight trailer and tractor h) Trailer 2-axles i) Retarder with clutch j) Reduced gearbox losses m) Efficient auxiliaries, future o) Exh. heat power generation p) ICE higher efficiency q) EcoRoll & Coasting	b) Tires lowest RRC, future d) Aero package, future e) Speed limit 80 km/h g) Lightw. tail-lift & chassis j) Reduced gearbox losses k) Start-stop automatic m) Efficient auxiliaries, future n) Regen. braking with m) p) ICE higher efficiency r) Limited braking deceleration	b) Tires lowest RRC, future g) Lightweight chassis, future j) Reduced gearbox losses k) Start-stop automatic m) Efficient auxiliaries, future n) Regen. braking with m) p) ICE higher efficiency r) Limited braking deceleration

Not every measure was simulated for every HDV class, because some are not useful for certain applications. The tractor-trailer model on the Long Haul cycle 2015 with a stand ratio of 1.5 % does not profit by a start-stop automatic, on the other hand for a slow city bus aerodynamic measures are useless. In addition there are some limitations by the simplified simulation models. Because no models were created for the charging level of the 24 V battery of conventional HDV and of the air vessels, regenerative braking could not be simulated for the Long Haul cycle 2015. This cycle contains multiple downhill phases with longer braking, where the storages would be full sometimes and the regeneration stops. For the urban cycles with many short braking phases it was assumed, that in the driving phases enough electrical energy and pressurised air are consumed to allow recharging during the next braking phase.

The modifications of the HDV with bundled saving measures towards the basis models are enlisted on p. 173, chapter 5.7.3 "Bundles of current possible saving measures" and p. 175 chapter 5.7.4 "Bundles of future possible saving measures".

3.2.1 Comparison of models with technology bundles to basis vehicle models

The simulation results for the combinations of saving measures and powertrain concepts are shown in Figure 137. The numbers are the changes of the energy consumption tank-to-wheel and GHG emissions well-to-wheel towards the vehicle models with conventional powertrain at basis level 2014, as given on p. 87 Table 17.

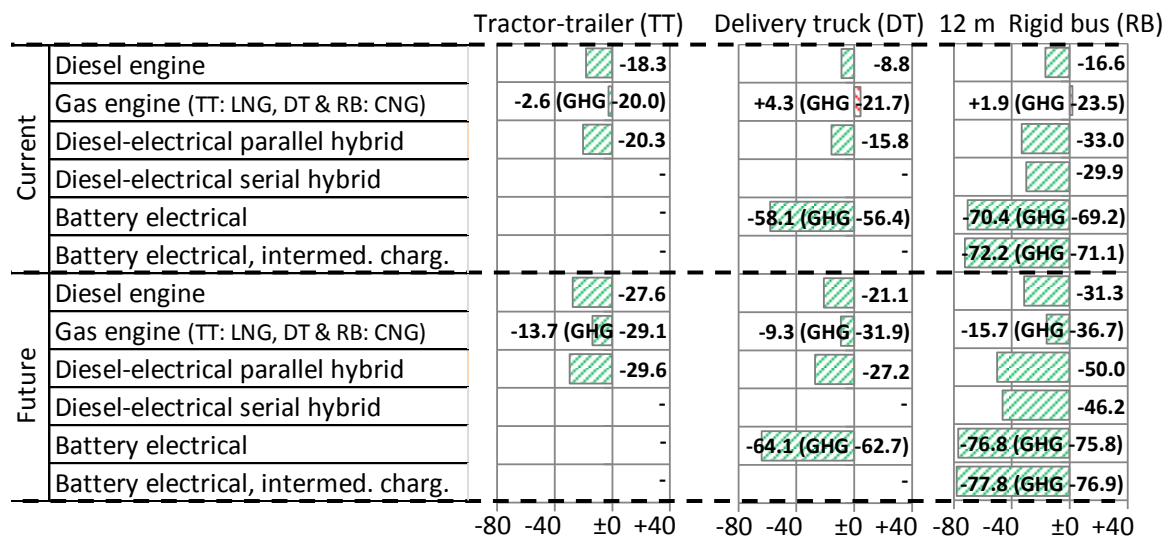


Figure 137. Results for different propulsion systems with bundled saving measures. Change in % of EC (TTW, base unit [kWh]) and of GHG (WTW, base unit [gCO₂e]) towards the HDV models of technical level “basis”, MY 2014.

GHG labelled separately if not diesel fuel. BEVs: Including 10 % charging losses grid-to-battery.

The VECTO simulation results shown in Figure 137 are compared below with results gained by a simple multiplicative accumulation of technology effects. There the FC from the basis models was subsequently multiplied with the consumption factors of the single saving measures (CF_i). The CF_i are the sums of 1 and the single relative changes of FC, which are enlisted on p. 126 ff. Figure 134 and Figure 135. E. g. for the model of the rigid bus with current tires of lowest RRC, measure a), it is CF = 1 + (-0.006) = 0.994. The comparison of the VECTO results and the overall changes of FC from the products of the single CF_i for the powertrain "diesel engine"⁹⁷ are shown in Table 26.

Table 26. Change of FC relative to basis models, tech. bundles “current” and “future” for conventional powertrain diesel engine, comparison of VECTO results with a simple multiplicative accumulation.

	Tractor-trailer, change of FC		Delivery truck, change of FC		Rigid bus, change of FC	
	VECTO	∏ _i (CF _i) - 1	VECTO	∏ _i (CF _i) - 1	VECTO	∏ _i (CF _i) - 1
Current	-0.183	-0.177	-0.088	-0.080	-0.166	-0.162
Future	-0.276	-0.269	-0.211	-0.219	-0.313	-0.315

There are no bigger deviations between the results from the VECTO simulation and the simple multiplicative accumulation. The simple accumulation of technology effects can overestimate the reduction compared to VECTO, which can be explained by overlapping effects of single technologies: E. g. less exhaust heat is available for power generation at a higher engine efficiency, or a lower road load increases the potential of hybrid vehicles for regenerative braking.

⁹⁷ For the rigid bus, bundle "current" of measures a) f) k) l) r), the product of the consumption factors is ∏_i (CF_i) = [1 + (-0.006)] · [1 + (-0.024)] · [1 + (-0.057)] · [1 + (-0.063)] · [1 + (-0.022)] = 0.838, thus the overall relative change of FC is ∏_i (CF_i) - 1 = -0.162.

Looking again at the VECTO results from Figure 137 one sees, that for the technology bundle of the level “current” a possible reduction of fuel and GHG of 18.3 % was calculated for the tractor-trailer model with a conventional diesel powertrain. For the bundle with a gas engine the change of fuel energy became -2.6 % and the GHG emissions were reduced by 20.0 % due to the lower GHG-factor of gas. The technology bundle including the diesel-electrical parallel hybrid offered a saving potential of 20.3 %.

In case of the delivery truck, bundle “current”, the energy demand for the powertrains diesel engine, gas engine and parallel hybrid changed by -8.8, +4.3 (GHG -21.7) and -15.8 %. For the gas engine in the delivery truck the ratio of the change of fuel energy to GHG emissions is another than for the tractor-trailer. For the truck CNG with a GHG-factor well-to-wheel of 3.07 kgCO_{2e}/kg was used instead of LNG for the tractor-trailer. There the GHG factor was 3.36 kgCO_{2e}/kg due to the energy demand of liquefaction. In addition a battery-electrical powertrain was simulated for the delivery truck, where the reduction of the energy consumption became 58.1 % (GHG 56.4 %). For BEV only the GHG emissions from the electricity mix ENTSO-E (0.34 kgCO_{2e}/kWh_{el}, (268 p. 37)) can be compared directly, because in this case the fuel is electricity and no hydrocarbons.

The highest number of variations of the powertrain was simulated for the model of the rigid bus. The energy demand with the bundle “current” for diesel engine, gas engine and parallel hybrid changed by -16.6, +1.9 (GHG -23.5) and -33.0 %, compared to the basis vehicle model. The serial hybrid powertrain at the same level offered a fuel saving potential of 29.9 %. When the diesel genset and the supercap of the electrical vehicle "serial hybrid" were virtually replaced by a battery, the energy demand decreased by 70.4 % (GHG 69.2 %). For the electrical bus with a smaller and lighter battery plus intermediate charging the current saving potential was biggest at 72.2 % final energy and 71.1 % GHG.

Certainly higher reductions of energy and GHG could be possible in the future, when more efficiency technologies become available in series than analysed here.

With the model of the future conventional tractor-trailer a fuel saving of 27.6 % was simulated. With a LNG-fuelled gas engine the reduction of fuel energy and GHG became 13.7 and 29.1 % and with a diesel-electrical parallel hybrid 29.6 %.

For the future conventional delivery truck the saving of energy was simulated to 21.1 %, for the CNG-fuelled variant to 9.3 % (GHG 31.9 %). With a parallel hybrid vehicle of stage "future" the fuel consumption can be reduced by 27.2 %, and with a battery-electrical vehicle the energy consumption and GHG emissions decrease by 64.1 and 62.7 %.

In case of the rigid bus the future diesel vehicle model output -31.3 % FC compared to the base model MY 2014, and the model with a CNG-fuelled gas engine resulted in -15.7 % fuel energy and -36.7 % GHG. With the models of diesel-electrical parallel and serial hybrids -50.0 and -46.2 % FC were simulated. Like before the highest savings were enabled with the models of battery-electrical vehicles without and with intermediate charging: -76.8 % energy consumption (-75.8 % GHG) and -77.8 % energy (-76.9 % GHG).

3.2.1.1 Partial check for plausibility of bundled saving measures, level "current"

Most of the technology bundles could not be compared to existing vehicle test results due to a lack of measurement data, but this is a typical situation when models are used to predict technology effects.

For current European optimised tractor-trailers data from a comparison with standard vehicles is available (272). The optimised vehicles comprised these measures:

- a) Tires lowest rolling resistance, current; here tires of classes B-B-AAA
- c) Aero package current; hence a trailer with side panels and a short boat tail
- f) Lightweight current

The average fuel saving at two hauliers during one week of normal long haulage was 12.9 %, 27.0 L/100km from the optimised vehicles compared to 31.1 L/100 from the basis trucks.

The simulated fuel saving for the tractor-trailer with measures a), c) and f) became 9.7 %⁹⁸, i. e. 25.1 vs. 27.8 L/100km, lower than measured. The simulated absolute saving, 2.7 L/100km, is also lower than the average measurand 4.1 L/100km.

The tested optimised tractors were equipped with aerodynamically improved "StreamSpace" cabins in comparison with the "standard" reference tractors. In the simulation only the air drag reduction from the add-ons for the trailer was considered, hence this can be one part of the missing potential. In addition the average payload, the driving cycle, its altitude profile and the tires of the basis trucks are not known, what makes a direct comparison difficult. Thus only the magnitude of the relative change of FC can be compared, which is at least similar.

For an optimised rigid bus measurement data is available (183) (273) (274), the vehicle parameters are summarised on p. 202 in Table 63, first entry. The bus is already equipped with efficient engine auxiliaries, and regenerative braking with three alternators is applied. The VECTO model similar to the specimen consists of the basis bus model EURO VI plus:

- a) Tires lowest RRC, current
- l) Efficient auxiliaries, current
- n) Regenerative braking with auxiliaries. Here three alternators, w/o the compressor.
- r) Limited braking deceleration (distance-based target cycles only). The equivalent of Eco-Driving for urban buses.

The bus was measured on Stuttgart Line 42 and Wiesbaden Line 17. For Line 42 the whole cycle is available, and for Line 17 the average velocity and the cumulated absolute value of the change of altitude ($|\Delta alt / \Delta s|_{norm}$)⁹⁹ are given (183 p. 17).

The average velocity of the VECTO Urban Bus cycle UB matched the value from the measurement on Wiesbaden Line 17, and the road gradient of the UB cycle was scaled with the factor 1.554 to get the same cumulated absolute value of the change of altitude. This variant of the UB cycle was named UB-hilly, compare also p. 155 Figure 154. The original UB cycle was elaborated from a real bus line in Offenbach. It is assumed, that the other characteristic values of UB-hilly like average rolling velocity and stops/km etc. are not that far away from the corresponding unknown values of Line 17, which is of the same overall average velocity.

⁹⁸ Compare p. 126 Figure 134: $\prod_i (CF_i) - 1 = [1 + (-0.027)] \cdot [1 + (-0.062)] \cdot [1 + (-0.011)] - 1 = -0.097$

⁹⁹ $|\Delta alt / \Delta s|_{norm} = \sum_{q=1}^{q=q_{max}} |\Delta alt_q / \Delta s_q| / s_{max}$

The model of the optimised bus was simulated on Stuttgart Line 42 and UB-hilly, and the outcome compared with the measured FC values, see Figure 138.

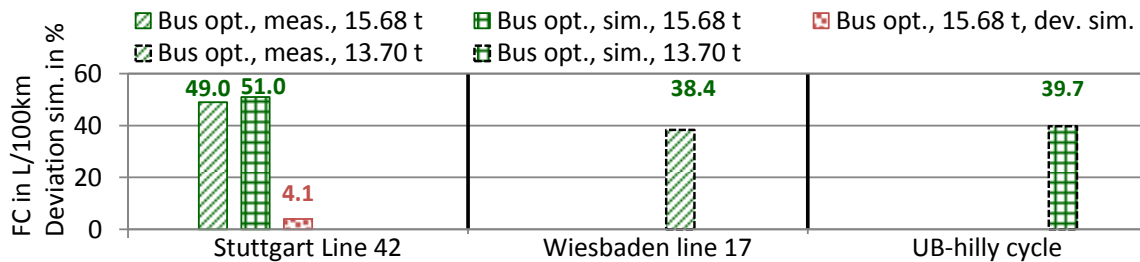


Figure 138. Optimised rigid bus, comparison of measured and simulated fuel consumption¹⁰⁰
Current tires low RRC, current efficient engine auxiliaries, regenerative braking with three alternators

On the known cycle Stuttgart Line 42 the model deviates by ca. +4 % from the measured FC. The unknown driving style during the measurement adds a few percent uncertainty to the comparison.

The simulated FC on the UB-hilly cycle is also slightly above the measurand from Wiesbaden Line 17, where the higher uncertainty due to the unknown real driving cycle needs to be considered. UB-hilly matches Line 17 only for the average velocity and the cumulated absolute value of the change of altitude. Big deviations for other unknown characteristics are assumed to be unlikely, but possible.

Taking into account these results and uncertainties, this model of an optimised bus seems to produce FC numbers of a plausible magnitude which are probably a few percent above real measured consumption values.

3.2.2 Comparison of alternative powertrains of equal technical levels

In the preceding chapter 3.2.1 the HDV models with all powertrain variants, each simulated with the technology bundles "current" and "future", were compared with the basis HDV models state 2014. Thus the maximum potential for the reduction of energy consumption and GHG emissions by efficiency measures and alternative powertrains was determined. E. g. for the basis model of the rigid bus with a diesel engine the simulated FC was 41.0 L/100, and for the diesel-electrical parallel hybrid with the bundle "future" the outcome was 20.5 L/100km, hence the saving potential became 50.0 %. The data of all HDV models plus the results for FC and GHG are given on p. 169 ff. in the sections 5.7 to 5.7.4.

In this section the saving potential only by alternative powertrains for all technical levels shall be analysed. Looking again at the urban bus, the result from the model with a diesel powertrain and the bundle "future" was 28.2 L/100km. Thus the saving potential of the parallel hybrid bus "future", with a FC of 20.5 L/100km, versus the diesel bus with equal efficiency measures became 27.2 %. This differentiation is important to assess the impact of the bundled efficiency measures on the relative and absolute saving potentials by alternative powertrains.

For potential HDV buyers, hauliers or public transport companies, the benchmarks in terms of cost effectiveness will always be conventional diesel vehicles, optimised for a low FC. Blends of fossil and carbon-reduced diesel from regenerative sources further increase the reduction of GHG from conventional HDV. Alternative powertrain concepts like gas engines, hybrid-electrical or battery-electrical, for vehicles of the same technical level, need to beat the

¹⁰⁰ Stuttgart Line 42: Measured & simulated cycle very similar. No A/C, stand at all 52 bus stops, no door opening or kneeling.

Wiesbaden Line 17: Only measured FC, exact cycle unknown. No A/C, 1.35 bus-stops/km with opening of 1 door and kneeling. Cycle characteristics: 18.6 km, $|\Delta alt/\Delta s|_{norm} = 2.26\%$, Eco-Driving, $v_{avrg} = 16.6$ km/h.

UB-hilly: Only simulated FC, cycle assumed to be similar to Wiesbaden Line 17. No A/C, 1.35 bus-stops/km with opening of 1 door and kneeling. Cycle characteristics: 39.6 km, $|\Delta alt/\Delta s|_{norm} = 2.25\%$, limited deceleration, $v_{avrg} = 16.9$ km/h.

diesel powertrain for the total cost of ownership to become attractive. Otherwise it is not possible to get into the market without political measures, e. g. subsidies, GHG-limits or bans on driving for fossil-fuelled vehicles.

The comparison of energy consumption and GHG emissions for the HDV models of equal technical levels and with different powertrain concepts is shown in Figure 139.

		Tractor-trailer (TT)	Delivery truck (DT)	12 m Rigid bus (RB)
Diesel engine	model "basis"	per km: 2.76 kWh, 901 gCO _{2e}	per km: 1.89 kWh, 617 gCO _{2e}	per km: 4.08 kWh, 1331 gCO _{2e}
	bundle "current"	per km: 2.25 kWh, 736 gCO _{2e}	per km: 1.73 kWh, 563 gCO _{2e}	per km: 3.40 kWh, 1110 gCO _{2e}
	bundle "future"	per km: 2.00 kWh, 653 gCO _{2e}	per km: 1.49 kWh, 487 gCO _{2e}	per km: 2.80 kWh, 0914 gCO _{2e}
Gas engine (TT: LNG, DT & RB: CNG)	model "basis"	+17.8 (GHG -3.3)	+15.0 (GHG -13.7)	+20.6 (GHG -9.5)
	bundle "current"	+19.6 (GHG -2.1)	+13.9 (GHG -14.2)	+22.4 (GHG -8.4)
	bundle "future"	+19.0 (GHG -2.1)	+15.4 (GHG -13.7)	+22.9 (GHG -7.9)
Diesel-electr. parallel hybrid	model "basis"	-1.9	-8.6	-25.2
	bundle "current"	-2.3	-8.0	-19.6
	bundle "future"	-2.9	-7.6	-27.2
Diesel-electr. serial hybrid	model "basis"	-	-	-19.5
	bundle "current"	-	-	-15.9
	bundle "future"	-	-	-21.9
Battery-electr.	model "basis"	-	-54.5 (GHG -52.6)	-67.9 (GHG -66.6)
	bundle "current"	-	-54.2 (GHG -52.2)	-64.5 (GHG -63.0)
	bundle "future"	-	-54.5 (GHG -52.7)	-66.1 (GHG -64.7)
Battery-electr., inter-med. charg.	model "basis"	-	-	-70.6 (GHG -69.4)
	bundle "current"	-	-	-66.7 (GHG -65.3)
	bundle "future"	-	-	-67.7 (GHG -66.3)

Figure 139. Results for different propulsion systems with bundled saving measures.
 Change in % of EC (TTW, base unit [kWh]) and of GHG (WTW, base unit [gCO_{2e}])
 towards the HDV models with a diesel-only powertrain (1st line "Diesel only") of the equal technical level.
 GHG labelled separately if not diesel fuel. BEVs: Including 10 % charging losses grid-to-battery.

The changes in energy consumption and GHG emissions from the models with alternative powertrains of level "basis", red fonts, were already described on p. 108 ff., chapters 3.1.10 to 3.1.14, and shown on p. 126 Figure 136.

Here also the models of level "current", blue fonts, and "future", green fronts, were compared with the standard diesel powertrain at equal technical level. It is interesting, that the change of energy consumption and GHG emissions towards the diesel powertrain is less dependent on the technical level. E. g. for the tractor-trailer with gas engine the surcharge in fuel energy is 17.8, 19.6 and 19.0 % for the stages "basis", "current" and "future". For the battery-electrical rigid bus of these levels the decrease in energy consumption, i. e. electrical energy vs. lower heating value, remains similar at 67.9, 64.5 and 66.1 %.

The reason is, that the saving measures except the powertrain concepts, compare p. 128 Table 25, were the same for all vehicle models. One exception are the hybrids, where the start-stop automatic was already implemented at level "basis". Therefore the FC advantage of the hybrids gets lower for the advanced stages, e. g. 19.6 instead of 25.2 % for the parallel hybrid rigid bus "current", because the diesel bus "current" also saves fuel during vehicle stop. In case of the hybrids also the dependence of the brake loss on the rolling resistance shall be regarded. For the diesel-electrical serial hybrid bus "current" the negative work at the wheels during deceleration is 0.654 kWh_{mech}/km, what can be used for regenerative braking. When in future the road load is lowered by tires with lowest rolling resistance, the brake loss increases to 0.679 kWh_{mech}/km, because at equal deceleration less driving resistances are braking "for free". This effect contributes to the increased saving potential, 21.9 % for the "future" vehicle compared to 15.9 % for the "current" model.

It was also found, that for future HDV with alternative powertrains the absolute reduction of the energy consumption in comparison with the diesel-only model of the equal technical level will decrease. E. g. for the level "basis" the parallel and serial hybrid bus models output an absolute saving of 10.3 and 8.0 L/100km in comparison to the diesel bus, i.e. 30.7 and 33.0 versus 41.0 L/100km. For the models "future" of the parallel and serial hybrid bus the absolute savings got lower to 7.7 and 6.1 L/100km; 20.5 and 22.1 versus 28.2 L/100km.

These lower future absolute fuel savings increase the difficulty for alternative powertrains to become attractive in financial terms for the first buyer. For lower absolute fuel savings in comparison with an optimised diesel-only vehicle also the absolute monetary savings get lower. A future higher diesel price caused by the underlying oil price or by additional taxes could outweigh this disadvantage for alternative powertrains partially. If the diesel price stays similar or becomes lower, it will remain difficult for alternative powertrains to get into the market only due to savings of fuel cost.

3.2.3 Comparison of results from other studies

A current simulation study on fuel saving measures for tractor-trailers was published by TU München, Lehrstuhl für Fahrzeugtechnik (171 p. 50). There the savings for 1 t less curb weight and for a semitrailer with side panels plus a short boat tail for improved aerodynamics were calculated to 1.9 and 4.4 %, with a payload of 12 t on motorways.

The results from this work for the equivalent measures are potentials of 1.4 % (lightweighting 0.9 t) and 6.2 % (trailer with sidepanels and short boat tail), simulated with the tractor-trailer model, payload 14.5 t, on the Long Haul cycle 2015. Details for the model data can be found on p. 170 Table 33, "g) Lightweight future" and "c) Aero package current".

In this work for the aerodynamics also the sensitivity towards cross wind was lowered. Hence the saving potential by aerodynamics is higher than in the mentioned study, where crosswind was not considered (171 p. 55).

Another source of simulation results for the FC reduction potential of European tractor-trailers in long haulage is from TM Leuven (TML) (167) (275), where these measures were investigated:

- reduced rolling resistance
- reduced drivetrain friction
- driver assistance systems.
- improved aerodynamics
- economical auxiliaries
- lightweighting
- improved engine efficiency

The research consisted of a literature review about the potentials of several measures, the consultation of engineers from HDV manufacturers and the collection and consolidation of calculation results from the industry. There the technicians simulated models of current tractor-trailers on the Long Haul cycle 2012, and delivered the numbers to TML (167 pp. 5-6). A comparison with the results from this work is shown in Table 27. The consumption factors (CF) are the ratios of the FC with saving measure to the basis FC.

Table 27. Consumption factors for tractor-trailers (167 p. 15)

	tires lower	RRC, actual	aero package, actual	lightweighting	less gearbox friction	less axle gear friction	efficient auxiliaries	better engine efficiency	multiplied
This work. Basis model tractor-trailer, LH12 cycle	0.959	0.950	0.987	0.986		0.991	0.977	0.86	
TM Leuven, Consumption factor	0.960	0.960	0.995	0.995	0.995	0.985	0.950	0.89	

With exception of the potentials for lightweighting and the improved diesel engine, the consumption factors are similar. Multiplied to an overall value, the measures which were analysed by both labs resulted in a possible fuel saving of 11 to 14 %. That the method of multiplication of single CF is admissible, was shown above, compare p. 129 Table 26.

An additional overview of efficiency measures for European trucks, based amongst others on an extensive literature review and interviews with industry experts, is given in (276 pp. 37-39). Because only the saving potentials and no details on the vehicle models are given, the results were not compared in detail with this thesis.

4 Summary and outlook

In this thesis a selection of efficiency measures to reduce the fuel consumption (FC) of European heavy-duty vehicles (HDV) was analysed, and the reduction potentials were simulated. Efficiency is motivated by saved fuel costs, by lower emissions of greenhouse gases (GHG) and by a reduced dependence on oil imports. In addition the probable future decarbonisation of all economy sectors will create the need for HDV with low CO₂ emissions. In any case an acceptable payback period and/or regulative inducements for saving measures are the pre-condition for the commercial success.

The analysis of efficiency measures was done with the simulation of longitudinal vehicle dynamics with the program VECTO which will be mandatory from 2019 for the CO₂-labelling of new European trucks. The buses will follow later. Because HDV are produced on-demand from a modular system and a high number of possible variants is reached per model, such a simulation-based approach is the most cost-efficient way to cover all possible vehicle variants. In Canada, China, Japan and the US similar procedures with own simulation programs are already mandatory to proof the compliance with CO₂-limits.

The inputs for VECTO are characteristic parameters to determine the power consumption of every relevant vehicle component, which are explained in the theory chapter. Amongst others the parameters for rolling resistance, air drag, masses and inertias, gearbox friction, auxiliary power and engine performance are input values to simulate FC and GHG on standardised driving cycles.

New models were created to calculate the power demand of the cooling fan and the saving potential of regenerative braking with auxiliaries. For the compressor of the pneumatic system an existing model was further elaborated. To determine the compressor power, its operation and the air consumption of a truck during tests on a chassis dynamometer and on the road were measured.

Gas engines were considered by changing the engine performance map. To depict further alternative powertrains like diesel-electrical parallel and serial hybrids plus battery-electrical vehicles, new models were created, and for parallel hybrid buses an existing model was revised. For the HDV-classes long haul tractor-trailer (TT), max. permitted mass 40 t, urban delivery truck (DT) 12 t, and urban rigid bus (RB) 18 t the fuel saving potential for multiple measures to reduce the power demand was simulated on appropriate driving cycles. Amongst others the effects of reduced rolling resistance, air drag, curb weight, gearbox friction and auxiliary power were investigated. The focus was set on realistic measures, where the components are already available or will probably be introduced into the market in the next ten years.

An extensive effort was spent to collect and sort measurement values for the FC and energy consumption (EC) of multiple vehicle variations to check the simulations for plausibility.

The analysis of the single saving measures resulted in potentials for the reduction of FC in a range from 1 % for current bus tires up to 9 % for future aerodynamics of tractor-trailers, or 14 % for future bus auxiliaries with regenerative braking. For biodiesel as partial replacement for fossil diesel a maximum reduction of GHG of 35 % was calculated.

Looking at alternative powertrains, a surcharge in fuel energy from 15 to 21 % was found for stoichiometric gas engines, where the GHG emissions decreased by 14 to 3 % due to the lower GHG-factor of natural gas. For the hybrid powertrains a saving potential from 2 to 25 % was simulated depending on the use case, such as long haulage or dense urban traffic. It was also found that higher savings from hybrid buses in fleet tests resulted likely from smaller and/or more efficient air conditioning systems, which further increased the potential of the hybrid systems. The highest saving is possible with battery-electrical vehicles, where the EC was reduced by 55 to 71 % and GHG emissions by 53 to 69 %.

As second step the single saving measures were bundled to packages and simulated for all powertrain concepts. The level "current" can be already implemented, the equipment is there, and the level "future" can be applied when the components become subsequently available in the near future. The resulting saving potentials for the HDV models with the technology bundles "current" and "future" are shown in Figure 140.

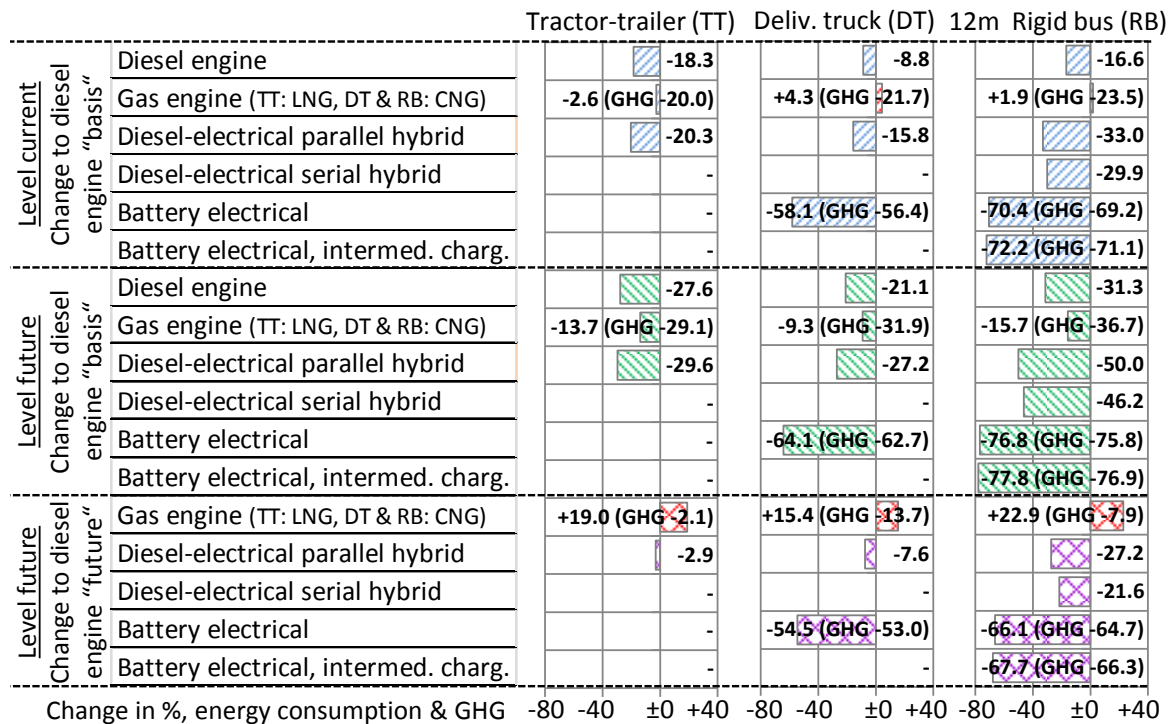


Figure 140. Simulated potentials for reduction of energy consumption and GHG emissions of HDV¹⁰¹

For the assessment of alternative powertrains also the change towards the diesel vehicle of the equal technical level is important, not only the comparison with the diesel model "basis". E. g. the parallel hybrid bus "future" offers a saving of 50.0 % versus the diesel bus "basis". But when compared with the diesel bus "future" the saving becomes 27.2 %, what is only slightly better than the parallel hybrid bus "basis" versus the diesel bus "basis". Thus for a fair comparison HDV with alternative powertrains shall always be compared to diesel vehicles which are equipped with the same efficiency components.

Also HDV with conventional diesel powertrains offer significant saving potentials for energy consumption and GHG emissions. Blends of fossil diesel and synthetic diesel from regenerative sources could contribute further to the necessary decrease of GHG. Hence it can be assumed that the diesel engine in combination with a mechanical gearbox will remain a strong competitor for alternative propulsion systems in terms of total cost of ownership and GHG emissions.

From a technical point of view considerable lower values for energy consumption and GHG emissions from HDV are feasible or will be enabled by new components. The possible reduction is highest for battery-electrical vehicles. The political task is to generate financial and regulative incentives to make more efficient vehicles attractive for potential customers.

¹⁰¹ "Basis", standard tech. 2014, FC fossil diesel [L/100km]: Tractor-trailer 27.8, delivery truck 19.0, bus 41.0. Energy consumption tank-to-wheel, GHG well-to-wheel. Basis model tractor-trailer with 3-axle trailer and max. mass 40 t, optimised model with 2-axle trailer and max. mass 38 t. For other fuel than diesel the GHG reduction is labelled separately (Gas engines: Stoichiometric types). For the comparison of the parallel and serial hybrid buses see p. 119 section 3.1.13 and the remarks on p. 121. In case of battery-electrical vehicles 10 % charging losses grid-to-battery are added. GHG-factor electricity for the ENTSO-E-Mix 2014, grid continental Europe: 0.34 kgCO_{2e}/kWh_{el}. Radioactive waste of ca. 7.1 10⁻⁷ kg-radioact./kWh_{el} needs to be considered in addition.

For future theoretical work on fuel efficiency measures for HDV all vehicle models should be simulated with the same program, e. g. prospective versions of VECTO with hybrid- and battery-electrical powertrains, or if so with other tools. That was not possible for this thesis, because the whole VECTO project was work in progress, where the focus was set at the beginning on conventional diesel powertrains.

Also more HDV types can be analysed, here a tractor-trailer 40 t, a delivery truck 12 t and a rigid bus 18 t were chosen as examples.

Only a selection of fuel efficiency measures was analysed, which covered some of the most relevant technologies, but was not complete. More efficiency measures are available, and new ones are continuously developed, which need to be assessed.

Examples are wire-electrical long haul trucks, which are fed by a pantograph directly from the grid; regenerative braking with the steering pump; final drives with lower gear ratios to reduce speed and friction of the engines of long haul trucks; platooning to reduce the air drag of the rear trucks; and overlong trucks with two semitrailers, which are already permitted in Sweden and multiple countries outside of Europe.

A standardised simulation procedure for the energy consumption of HDV is a very cost efficient way to rate fuel saving components for effectiveness, and to compare them at equal conditions. In any case the simulation results need to be checked for plausibility by comparing them to measurement results from multiple independent sources.

Thus the simulation will only be one tool for the future vehicle development, and the validation of the models with measurement results remains indispensable.

5 Supporting data

5.1 Abbreviations

€ 3, € 4, € 5, € 6	EU emission standard EURO III (2001-10), IV (2006-10), V (2009-10), VI (2014-01)
A/C	Air conditioning
AB	Articulated bus
act.	Actuation
AFR	Air-fuel-ratio, ratio of (air mass) to (fuel mass)
AFR _{stoich}	Air-fuel-ratio, ratio of (air mass) to (fuel mass), stoichiometric case, for diesel fuel = 14.5 (237 p. 109)
AMT	Automated manual transmission, spur-gear design
assoc.	Association
AT	Automated transmission, hydraulic element & planetary gearbox
avrg	Average
B25, B50, B75 ...	Measurement points at B-speed in engine map, ESC test
BEV	Battery-electrical vehicle
BJBC	Beijing Bus Cycle
Brsw	Braunschweig bus cycle
CB	VECTO Coach Bus cycle
CBD	Central Business District bus cycle
CEST	Central European Summer Time
ch.	Fully charged battery, models of parallel hybrid electrical vehicles
CH ₄	Methane
CILCC	Combined International Local and Commuter Cycle
CNG	Compressed natural gas, 200 bar, +20 °C
CO	Carbon monoxide
CO ₂	Carbon dioxide
CO _{2e}	CO ₂ equivalents, warming potential of greenhouse gases, normed to CO ₂
COE	Cab over engine, type of truck
conv.	Conventional vehicle, standard diesel powertrain
CS	VECTO Construction cycle
C-WTVC	Chinese World Transient Vehicle Cycle
cyl.	Cylinders of internal combustion engine
DeNO _x	Denitrification process for exhaust
Dev.	Deviation
disch.	Discharged battery, models of parallel hybrid electrical vehicles
DT	Delivery truck
dyno	Dynamometer
EC	Energy consumption, lower heating value (diesel or gas from the tank) or electrical energy (from the battery or from the grid)
EC _{batt}	Energy consumption, electrical energy battery, without charging losses
EC _{batt,drv}	Energy consumption from battery during driving, without stand phases
EC _{grid}	Energy consumption, electrical energy from grid, = EC _{batt} · 1.10, incl. 10 % charging losses
ECU	Electronic control unit
EER	Energy Efficiency Ratio, air conditioners, ratio of (cooling capacity) to (power demand)
EEV	Enhanced environmentally friendly vehicle

EGR	Exhaust gas recirculation
EM	Electrical machine
ENTSO-E	European Network of Transmission System Operators for Electricity
EPA-GHG	EPA GreenHouse Gas cycle
ER	EcoRoll, powertrain control function
ESC	European Steady state Cycle, duty cycle for heavy-duty diesel engines
ESS	Energy Saving System, air compressor with reduced idle losses
ETC	European Transient Cycle, duty cycle for heavy-duty diesel engines
ETF	Empty trip factor, share of trips without payload at overall mileage
FC	Fuel consumption, usually ratio of (consumed fuel) to (driven distance)
FC-line	Fuel consumption line, linear relation between fuel consumption and engine power
FDHDT	Freeway-Dominant Heavy-Duty Truck cycle
FE	Fuel efficiency, usually ratio of (driven distance) per (consumed fuel)
FL	Full load, max. power of internal combustion engine
FTP	Federal Test Procedure, US duty cycle for heavy-duty diesel engines
GCWR	Gross Combined Weight Rating, max. permitted weight of truck and trailer
GDP	Gross domestic product
GEM	Greenhouse Gas Emissions Model, c/o USEPA
gen.	Generator operation
genset	Generating set, electrical generator powered by heat engine
GES	Gaz à Effet de Serre (French for greenhouse gas)
GHG	Greenhouse gas
GVW	Gross vehicle weight, current value, curb weight plus payload.
GVWR	Gross vehicle weight rating, max. permitted vehicle weight
HC	Hydrocarbons
HD UDDS	Heavy Duty Urban Dynamometer Driving Schedule cycle
HDV	Heavy-duty vehicle, maximum permitted vehicle mass > 3.5 t
HEV	Hybrid electrical vehicle
HHDDT	Heavy Heavy-Duty Diesel Truck cycle
HUB	VECTO Heavy Urban Bus cycle
HVAC	Heating, Ventilation and Air Conditioning
HVACCO2SIM	Heating, Ventilation and Air Conditioning Carbon Dioxide Simulator, Fraunhofer IVI
ICE	Internal combustion engine
IDM	Interurban Driving Mode cycle
IG	Inffeldgasse cycle
IUB	VECTO Interurban Bus
JE05	JE05 cycle
KCM	King County Metro bus cycle
LAC	Look-ahead coasting, powertrain control function
LF	Load factor, usage of maximum payload during laden trips
LH12	VECTO Long Haul cycle 2012
LH15	VECTO Long Haul cycle 2015
LHV	Lower heating value
Li-Ion	Lithium-ion battery type
LNG	Liquefied natural gas, 6 bar, -140°C
LPS	Load point shift, electrical machine works as generator during driving and is propelled by excess power from internal combustion engine
LUB	LowCVP UK Bus cycle
meas.	Measured

misc.	miscellaneous
MLTB	Millbrooks London Transport Bus cycle
mot.	Motor operation
MS Excel	Microsoft Excel, spreadsheet and calculation program
MT	Manual transmission, spur-gear design
MU	VECTO Municipal Utility cycle (garbage truck)
MY	Model year
N ₂ O	Nitrous oxide, “laughing gas”
no.	Number
NO _x	Nitrogen oxides, sum of nitrogen monoxide (NO) and nitrogen dioxide (NO ₂)
NYBus	New York Bus cycle
OCBC	Orange County Bus Cycle
OEM	Original Equipment Manufacturer
ORC	Organic Rankine cycle, steam power process
P.HEV	Parallel hybrid electrical vehicle
PHEM	Passenger car and Heavy duty vehicle Emission Model
PM	Particulate matter
PMSM	Permanent magnet synchronous machine
pt.	Part
R/P	Reserve to production ratio, resources
RB	Rigid bus
RCP	Representative Concentration Pathways
RD12	VECTO Regional Delivery cycle 2012
RD16	VECTO Regional Delivery cycle 2016
regen.	Regenerative braking, recoument of part of kinetic energy by charging of buffer storages
ROI	Return on investment
rot.	Rotational
S.HEV	Serial hybrid electrical vehicle
SCap	Supercapacitor
SCC	Social costs of carbon dioxide
SCR	Selective catalytic reduction, process for denitrification of exhaust
SET	Supplemental Emission Test, US stationary engine cycle, equals ETC
share overload	Energised EM ($P_{EM,el} \neq 0$): Ratio (duration of overload) to (overall duration of operation)
SI	Système international d’unités
sim.	Simulated
SN	Smith Newton truck cycle
SOC	State of charge, energy storage, battery or supercapacitor
SORT 1, 2, 3	Standardised OnRoad Test 1, 2, 3 bus cycle
spec.	Specific
Sped.	Spedition (German for haulier)
SUB	VECTO Suburban Bus cycle
susp.	suspension
TCF	Transient Correction Factor. Depiction of increase of fuel consumption for transient operation, when interpolated from a stationary performance map.
TT	Tractor-trailer
TTW	Tank-to-wheel, referred only to the operation of the vehicle
UB	VECTO Urban Bus cycle
UB-hilly	VECTO Urban Bus cycle, hilly variant, original road gradient scaled with factor 1.554
UCTE	Union for the Co-ordination of Transmission of Electricity

UD12	VECTO Urban Delivery cycle 2012
UD12–flat	VECTO Urban Delivery cycle 2012, flat variant without road gradient
UD17	VECTO Urban Delivery cycle 2017
UTC	Universal Time Coordinated
VECTO	Vehicle Energy Consumption calculation TOol
w.	with
w/o	without
WHR	Waste heat recovery
WHTC	World Harmonised Transient test Cycle
WHTC-factor	Transient correction for simulated fuel consumption on WHTC engine cycle. Ratio of (FC measured at engine dynamometer) to (FC interpolated from stationary engine map).
WHVC	World Harmonized Vehicle Cycle
WTW	Well-to-wheel, referred to the vehicle operation <u>and</u> the production process of the fuel
WVUC	West Virginia University City cycle

5.2 Notations

5.2.1 Greek and mathematical notations

$ x $	Absolute value of x
$ \Delta alt/\Delta s _{norm}$	Cumulated absolute value of the change of altitude, normalised to cycle length
Δalt	Altitude difference of road section
$\Delta alt/\Delta s$	Longitudinal road gradient, ratio of (change of altitude) to (change of distance)
$\Delta C_{p,fr-u}$	Difference in ram pressure coefficients, front to undersurface of vehicle
$\Delta FC_{aux,shift,add}$	Additional FC (> 0) during driving + coasting to perform the auxiliary work, which was shifted from engine stop, without steering pump idle losses
ΔFC_{regen}	Decrease in FC (< 0) due to regenerative braking with engine auxiliary consumers
$\Delta FC_{start-stop}$	Decrease in FC (< 0) due to start-stop automatic
$\Delta FC_{stop,save}$	Saved FC (< 0) during engine stop phases, with steering pump idle losses
ΔFC_W	Willans factor, change of (fuel mass) per (change of positive mechanical engine work)
$\Delta m_{air,compr}$	Air mass to be delivered by compressor
$\Delta m_{air,vessels}$	Difference of air content in vessels, end to start of delivery phase
$\Delta m_{misc}/\Delta t$	Average air consumption rate of miscellaneous consumers
$\Delta m_{susp}/\Delta t$	Average air consumption rate of air suspension
$\Delta p'_{fan-on}$	Static pressure increase by activated fan, normalised to squared rotational fan speed
$\Delta p_{br,avrg}$	Average pressure loss in brake vessels during braking
$\Delta P_{compr,deliv}$	Additional compressor delivery power
$\Delta P_{compr,deliv,\Delta t}$	Average additional compressor delivery power in simulation time step Δt
$\Delta p_{drop,fan-off/on}$	Overall static pressure drop for cases fan-off or fan-on
$\Delta p_{drop,fan-on}$	Combined pressure drop of grille, radiator and engine compartment, converted to fan cross sectional area
$\Delta p_{drop,i}$	Static pressure drop of flow resistance "i"
$\Delta p_{fan-off}$	Static pressure drop by idling fan
Δp_{fan-on}	Static pressure increase by activated fan
$\Delta p_{ram,fr-u}$	Difference in ram pressure from vehicle front to undersurface
Δs	Horizontal distance of road section in current time step
Δt	Time step for calculation
Δt_{compr}	Duration of compressor delivery phase

ΔT_{cool}	Change of coolant temperature
Δt_{cycle}	Cycle duration
$\Delta t_{drive+coast}$	Duration of driving and coasting phases
$\Delta T_{global,surf}$	Global surface temperature anomaly
Δt_{regen}	Residence time in engine speed class during regenerative braking
$\Delta t_{regen,total}$	Total duration of regeneration, for regenerative braking with auxiliaries
Δt_{stop}	Duration of engine stop phases
$\Delta V_{sim \leftrightarrow targ}$	Difference between simulated and target velocity
$\Delta W_{compr,deliv}$	Additional compressor delivery work for air volume fraction
$\Delta \tau$	Smaller time step for delivery of air volume fraction $V_{air,deliv,frac}$ in sim. time step Δt
$\Sigma W_{i,FC,norm}$	Sum of work of engine auxiliaries "i" during standing, driving, coasting, normal operation w/o regenerative braking
$\Sigma W_{i,FC,regen}$	Sum of work of engine auxiliaries "i" during standing, driving, coasting, with regenerative braking
$\Sigma \Delta t_{compr}(n_{compr})$	Sum of all compressor rotations during delivery phase
$\Sigma \Delta t_{compr}(\Delta m_{br})$	Summarised air consumption of brakes during delivery phase
β	Yaw angle of air flow around moving vehicle
$\eta_{el,batt}$	Electrical efficiency battery, one-way, energy output to energy input, equal value for both directions of power flow (clamps to cells or cells to clamps)
$\eta_{el,genset}$	Electrical efficiency of generating set, powered by a heat machine, ratio of (electrical power) to (lower heating value of fuel)
$\eta_{el,inv}$	Electrical efficiency power inverter, one-way, energy output to energy input, equal value for both directions of power flow
η_{EM}	Efficiency of electrical machine, one-way, ratio of (mech. power output) to (electr. power input), case motor; or (electr. power output) to (mech. power input), case generator
$\eta_{EM,tot}$	Total efficiency of electrical machine, ratio of (mech. work output motor + electr. energy output generator) to (electr. energy input motor + mech. work input generator)
η_{ICE}	Efficiency of internal combustion engine, ratio of (mechanical power output) to (lower heating value input of fuel); only for positive power output
$\eta_{ICE,avrg}$	Average efficiency of internal combustion engine, ratio of (positive work output) to (lower heating value input during positive power output)
$\eta_{mech,drivetr}$	Mechanical efficiency of drivetrain, one-way, ratio of (work-output at wheel hubs, driving) to (work-input at clutch, driving).
$\eta_{mech,drivetr,ice}$	Positive power at wheel hub and at engine shaft: Traction, driving with engine power. Ratio of (tractive work at wheels) to (work output at engine shaft). If so corrected for share of tractive power from EM of hybrid powertrain, and for auxiliary power.
$\eta_{mech,drivetr,tot}$	Total mechanical efficiency of drivetrain for (hybrid) electrical vehicles, ratio of (work-output at wheel hubs, driving + work-output at gearbox, regen. braking) / (work-input at gearbox, driving + work-input at wheel hubs, regen. braking)
$\eta_{mech,FD}$	Mechanical efficiency of final drive gear, ratio of (traction work-output) to (traction work-input)
$\eta_{mech,gear,1,Tq-conv}$	Automated transmission, power split in 1 st gear with hydraulic and mechanical transfer, ratio of (traction work-output) to (traction work-input) of whole gearbox
$\eta_{mech,gear,dir}$	Mechanical efficiency of direct gear (gear ratio = 1.00), ratio of (traction work-output) to (traction work-input)
$\eta_{mech,gear,indir}$	Mechanical efficiency of indirect, stepped-up gears (gear ratios \neq 1.00), ratio of (traction work-output) to (traction work-input)
$\eta_{mech,ret-idle}$	Mechanical efficiency of idling retarder, ratio of (traction work-output) to (traction work-input)
η_{ORC}	Effective efficiency of ORC steam power process, ratio of (power output from ORC expander) to (Enthalpy difference of exhaust flow between temperature at outlet of aftertreatment and ambient temperature)
$\eta_{tm,mesh}$	Mechanical mesh efficiency of a transmission, gear pair, only friction between gears, without bearing loss, churning loss etc.
$\eta_{tm,ova}$	Mechanical overall efficiency of a transmission, ratio (work output) to (work input)
ϕ_{wh}	Angular position of driven wheels

ϕ_{wind}	Relative angle between driving and wind direction
λ	Ratio of (air-fuel-ratio) to (stoichiometric air-fuel-ratio)
μ	Ratio of (output torque) to (input torque), hydraulic torque converter
ν	Ratio of (output speed) to (input speed) of a hydraulic torque converter
ρ	Density
ρ_{air}	Air density
$\rho_{\text{air,amb}}$	Air density at ambient conditions, 1.188 kg/m ³
$\rho_{\text{air,fan}}$	Air density in fan cross sectional area
$\rho_{\text{air,fan,av}}$	Average air density in fan cross sectional area
$\rho_{\text{air,std}}$	Density of 1 m ³ dry air at standard conditions (20 °C, 1.013 bar): 1.204 kg/m ³
ω_{eng}	Rotational engine speed, angular velocity
ω_{fan}	Angular speed of fan
$\omega_{\text{fan,cl}}$	Angular speed of fan clutch input shaft
ω_{wh}	Angular speed of driven wheels

5.2.2 Latin notations

$\dot{H}_{\text{exh,TC}}$ or $Hf_{\text{exh,TC}}$	Exhaust loss from outlet of turbocharger to ambient (20 °C)
$\dot{H}_{\text{exh,TC,stat}}$	Exhaust loss from outlet of turbocharger to ambient (20 °C), stationary case
$\dot{H}_{\text{exh,out}}$ or $Hf_{\text{exh,out}}$	Exhaust loss from outlet of aftertreatment to ambient (20 °C)
$\dot{H}_{\text{exh,out,stat}}$	Exhaust loss from outlet of aftertreatment to ambient (20 °C), stationary case
$\dot{m}_{\text{air,fan}}$	Air mass flow through fan cross sectional area
\dot{Q}'_{rad}	Heat flow coefficient of radiator, calculated from measurement. Dependence of [ratio of (heat flow in radiator from coolant to air) to (temperature difference coolant to ambient)] on (air flow velocity in fan cross sectional area).
$\dot{Q}_{A/C,\text{cool,max}}$	Maximum cooling capacity of air conditioning unit
$\dot{Q}_{\text{eng,cool}}$	Waste heat engine to coolant
\dot{Q}_{rad}	Heat flow in radiator from coolant to air
$\dot{n}_{\text{mol,exh}}$	Molar exhaust flow
$\dot{V}_{\text{air,deliv}}$ or $Vf_{\text{air,deliv}}$	Air delivery rate of compressor
$(P/P_{\text{cont}})_{\text{avrg}}$	Energised electrical machine ($P_{\text{EM,el}} \neq 0$): Average ratio of (mechanical power) to (continuous mechanical power)
$(P_{\text{overload}}/P_{\text{cont}})_{\text{avrg}}$	During overload of electrical machine: Average ratio of (mechanical power) to (continuous mechanical power)
2015	Subscript, correction for inflation, here conversion to price level 2015
\tilde{a}	Characteristic acceleration, according (277 p. 4 ff.)
a_0, a_1, a_2	0 th , 1 st , 2 nd order coefficient of pressure polynomial for fan operation
A_{cr}	Cross sectional area of vehicle
$A_{\text{cr,fan}}$	Cross sectional area of fan
alt	Altitude
A_{rad}	Surface of the radiator
arctan	Arcustangens
a_{veh}	Acceleration in driving direction
bmep	Brake mean effective pressure, $\text{bmep} = P_{\text{eng,gross}} / (0.5 \cdot n_{\text{eng}} \cdot V_{\text{displ}})$ [all in SI-units]
bsfc	Brake specific fuel consumption, ratio of (consumed fuel mass) to (positive work output at clutch)
C_d	Air drag coefficient of straight air flow, without crosswind correction
$C_{d,\beta}$	Air drag coefficient, dependent on yaw angle of air flow

C_{eng}	Effective average heat capacity of coolant, engine oil and engine
CF	Consumption factor, ratio of (fuel consumption with saving measure) to (fuel consumption without saving measure)
cos	Cosinus
$C_{p,fr}$	Ram pressure coefficient at vehicle front, usually $c_{p,fr} > 0$
$C_{p,u}$	Ram pressure coefficient at vehicle undersurface, usually $c_{p,u} < 0$
CU	Capacity usage, ratio of (effective payload during all trips) to (theoretical max. payload during all trips), includes empty and loaded trips
d_{fan}	Diameter of fan cross sectional area
$E_{el,gain}$	Gain of electrical energy during regenerative braking
$E_{el,total}$	Electrical energy demand, total value
$E_{kin,air}$	Kinetic energy of air
el	Subscript, electrical, e. g. kWh _{el} - electrical energy
eng.	Engine
$E_{pot,air}$	Potential energy of air
ETF	Empty trip factor, ratio of (mileage without payload) to (total mileage)
$E_{v,air}$	Pressure energy of air, equals the mechanical work to move one volume unit
F0	Constant part of road load force, rolling resistance
F2	Part of second order of road load force, air drag
fact _{C_d,vel}	Correction due to cross wind, for the air drag coefficient of straight air flow (C_d), at one node of vehicle velocity
fact _{C_d,vel,60}	Correction due to cross wind, for the air drag coefficient of straight air flow (C_d), variable for vehicle velocity above 60 km/h, constant from 0 to 60 km/h
fact _{C_d,vel,full}	Correction due to cross wind, for the air drag coefficient of straight air flow (C_d), variable for full range of vehicle velocity
fact _{C_d,yaw}	Change of air drag coefficient with yaw angle
fact _{wear}	Factor for rolling resistance to depict half worn tires, here fact _{wear} = 0.88
F_{air}	Air drag force between vehicle body and surrounding air
$F_{air,avrg}$	Average air drag force at one velocity node for average crosswind, for wind angle ϕ_{wind} from 0 to 359°
$F_{air,wind}$	Force by wind, acting on vehicle body against driving direction
FC0	Mass flow, constant part of so called "FC-line"
FC _{meas}	Measured fuel consumption
FC _{meas,max}	Max. measured fuel consumption
FC _{sim}	Simulated fuel consumption
F_{grade}	Gradient force, component of vehicle weight force parallel to road surface
$F_{inert,dt}$	Equivalent inertia force at wheel hubs of rotating drivetrain parts from clutch to wheel hubs
$F_{inert,transl}$	Inertia force of translationally accelerated vehicle masses
$F_{inert,wh}$	Equivalent inertia force of all rotating accelerated wheels
$F_{inert,wh,non-dr}$	Equivalent inertia force of rotating accelerated non-driven wheels
$F_{road-load}$	Road load force, rolling resistance plus air drag
F_{roll}	Rolling resistance force of tires
F_{weight}	Weight force of laden vehicle
$F_{weight,vert}$	Weight force, component vertical to road surface
F_{wh}	Driving force: Tractive or brake force, parallel to longitudinal vehicle axis. Including the inertia forces of the rotating wheels.
$F_{z,lab}$	Vertical load on tire during official RRC-measurement in laboratory
g	Acceleration due to gravity (= 9.81 m/s ²)
h_i	Specific enthalpy, referred to amount or mass of substance
h_{rad}	Heat transfer coefficient of radiator, dependent on air flow velocity
h_{veh}	Height of vehicle

$i_{cl,fan}$	Ratio of (rotational speed of fan clutch) to (engine speed)
$i_{dt,k-wh}$	Ratio of (rotational speed of drivetrain component k) to (speed of driven hubs)
I_{el}	Electrical current
i_{fd}	Gear ratio of final drive, ratio of (speed of cardan shaft) to (speed of wheel shafts)
i_{gb}	Gear ratio of gear box, ratio of (speed of gearbox input shaft) to (speed of cardan shaft)
j	Subscript, index, placeholder for front (_{fr}) or undersurface (_u)
$J_{dt,k}$	Rotational inertia of drivetrain component "k" (shafts, clutches, gears)
J_{eng}	Rotational inertia of moving engine parts, referred to crankshaft
$J_{wh,dr}$	Rotational inertia of driven wheels
$J_{wh,i}$	Rotational inertia of wheels axle "i"
$J_{wh,non-dr}$	Rotational inertia of non-driven wheels
$k_{fan-off}$	Overall flow resistance coefficient of grille, radiator, idling fan, engine compartment; converted to fan cross sectional area, case fan-off
$k_{fan-off/on}$	Combined flow resistance coefficient of obstacles, for cases fan-off or fan-on, with and without idling fan as additional obstacle
k_{fan-on}	Combined flow resistance coefficient of grille, radiator and engine compartment, converted to fan cross sectional area, case fan-on
LF	Load factor, ratio of (effective payload during loaded trips) to (theoretical max. payload during loaded trips), excludes empty trips.
m_{air}	Air mass
$m_{air,tot}$	Total air mass, vessels brake front, brake rear, air suspension, miscellaneous
$m_{air,vessel}$	Air mass in one vessel
max	Subscript, maximum
m_{curb}	Curb mass of vehicle
$meas$	Subscript, related to measurement
$mech$	Subscript, mechanical, e. g. P_{mech} - mechanical power
$mf_{air} / mf_{air,meas,max}$	Ratio of (air mass flow through fan cross sectional area) to (max. air mass flow)
$mf_{air,norm,meas}$	Measured air mass flow through fan cross sectional area, normalised to maximum measured air mass flow
$mf_{air,norm,sim}$	Simulated air mass flow through fan cross sectional area, normalised to maximum measured air mass flow
$mf_{air,sim}$	Simulated air mass flow through fan cross sectional area
mf_{exh}	Exhaust mass flow
min	Subscript, minimum
m_{payl}	Mass of payload
$m_{rot,eq,dt}$	Equivalent mass of rotating drivetrain parts, clutch to wheel shafts
$m_{rot,eq,wh}$	Equivalent mass of all rotating wheels
m_{test}	Vehicle total test mass
m_{veh}	Sum of vehicle curb weight and payload
n	Rotational speed in rotations per minute
n_{alt}	Rotational alternator speed
n_{compr}	Rotational compressor speed
$n_{compr}(i)$	Rotational compressor speed at second "i" of delivery phase
n_{EM}	Rotational speed of electrical machine
$n_{EM,com}$	Rotational corner speed of electrical machine, $Tq_{EM,cont} \cdot (n_{EM,com} / 30 \cdot \pi) = P_{EM,mch,cont}$, for $[n_{EM,com}] = rpm$
n_{eng}	Rotational engine speed
$n_{eng,curr}$	Rotational engine speed, in current simulation time step
$n_{eng,idle}$	Rotational engine speed, at idle
$n_{eng,norm}$	Rotational engine speed, normal operation, no regenerative braking
$n_{eng,rated}$	Rotational engine speed at rated power

$n_{eng,regen}$	Rotational engine speed during regenerative braking
$n_{eng,rel}$	Relative rotational engine speed, $n_{eng,rel} = (n_{eng,curr} - n_{eng,idle}) / (n_{eng,rated} - n_{eng,idle})$
n_{fan}	Rotational fan speed
$n_{fan,cl}$	Rotational speed of fan clutch input shaft
$n_{fan,idle}$	Rotational speed of idling fan
n_{Oax}	Number of axles
nom	Subscript, nominal, absolute price at time of purchase
$n_{Owh,i}$	Number of wheels at axle "i", two or four
$overload_{1min,avrg}$	Subdivision of simulation results into intervals of one minute: Avrg. ratio (overload duration) to (interval duration); only for intervals, where overload occurs
$overload_{1min,max}$	Subdivision of results into intervals of one minute: Maximum ratio of (overload duration) to (interval duration); only for those intervals, where overload occurs
P	Power
p	Pressure
$P'_{fan,hub}$	Normalised mechanical power at fan hub, normalised to cubic rotational fan speed
$P_{A/C,chill}$	Mechanical power demand of the air conditioning chiller
$P_{A/C,chill,x,C-EU}$	Mechanical power demand of the chiller x kW_{th} with 2-point control only for the zone central Europe
$P_{A/C,el,2-point}$	Electrical power demand of a fully electrical A/C with 2-point controlled chiller. Power demand of motors for chiller and blower
$P_{A/C,el,blower}$	Electrical power demand of the A/C blower motors
$P_{A/C,el,cont}$	Electr. power demand of a fully electrical A/C with continuously controlled chiller
P_{air}	Power to overcome the air drag
$P_{alt,el}$	Electrical power output of alternator
$P_{alt,el,max}$	Maximum electrical power output of alternator
$P_{alt,mech}$	Mechanical alternator power input
$P_{alt,mech,norm}$	Mech. alternator power input during normal operation, w/o regenerative braking
$P_{alt,mech,regen}$	Reduced mechanical alternator power input during standing, driving & coasting due to regenerative braking
p_{amb}	Ambient pressure
P_{aux}	Power demand from engine auxiliary consumers
$P_{aux,avrg}$	Average mechanical power demand of engine auxiliary consumers
$P_{aux,i}$	Mechanical power demand, fictive auxiliaries for check of "FC-line", intermittent power, shifting from high power to low power and back
$P_{aux,norm,i}$	Mechanical power demand, fictive auxiliaries for check of "FC-line", current power normalised to average power
p_{br}	Air pressure in brake vessels
P_{br}	Simulated mechanical brake power at wheel shafts
$P_{chill,avrg}$	Average mechanical power, chiller of air conditioning
$P_{compr,off}$	Compressor power at idle
$P_{compr,off\&on}$	Compressor power for idle and delivery phases
$P_{compr,off\&on,norm}$	Compressor power for idle and delivery phases, normal operation, w/o regenerative braking
$P_{compr,off\&on,regen}$	Reduced compressor power during standing, driving & coasting due to regenerative braking
$P_{compr,on}$	Total compressor power at delivery
$P_{dt,loss}$	Power loss from drivetrain friction
P_{el}	Electrical power
$P_{el,avrg}$	Average electrical power demand of vehicle model
$P_{el,avrg,regen}$	Reduced electrical power demand during standing, driving & coasting due to regenerative braking
$P_{el,genset}$	Electrical power output of generating set, powered by a heat engine

$P_{EM,el}$	Electrical power of electrical machine, input (motor, > 0), output (generator, < 0)
$P_{EM,mech}$	Mechanical power, electrical machine, output (motor, > 0), input (generator, < 0)
$P_{eng,gross}$	Gross engine power
$P_{eng,gross,hybrid}$	Gross engine power hybrids, reduced by motor power from electr. machine
$P_{fan,avrg}$	Average mechanical fan power, at input shaft of fan clutch
$P_{fan,cl}$	Mechanical power at fan clutch input shaft
$P_{fan,hub}$	Mechanical power at fan hub
P_{grad}	Power to overcome (uphill) or brake (downhill) the gradient force
P_{ICE}	Mechanical power output from internal combustion engine
$P_{inert,dt}$	Mechanical power demand of rotating drivetrain parts, from clutch to wheel shafts
$P_{inert,eng}$	Power to overcome (engine speed increasing) or brake (engine speed decreasing) the inertias of moving engine parts
$P_{inert,veh}$	Power to overcome (acceleration) or brake (deceleration) the inertias of the masses of vehicle, payload and rotating drivetrain parts
P_{mech}	Mechanical power
P_{misc}	Air pressure in vessel for miscellaneous consumers
$P_{ORC,card}$	Mechanical output of ORC power machine, transmitted to cardan shaft, decreased by 10 % transmission losses
$P_{ORC,mech}$	Output of mechanical power at shaft of expander of ORC process.
$P_{ram,fr}$	Ram pressure by headwind, at vehicle front
$P_{ram,u}$	Ram pressure by headwind, at vehicle undersurface
P_{rat}	Rated engine power
P_{roll}	Power to overcome the rolling resistance
P_{stat}	Static pressure
$P_{stat,fr}$	Static pressure vehicle front, ambient pressure plus ram pressure headwind ($p_{ram,fr}$)
$P_{stat,u}$	Static pressure at vehicle undersurface, ambient pressure plus ram (under-) pressure by headwind ($p_{ram,u}$)
$P_{steer,idle}$	Average mechanical idle power steering pump
$P_{steer,steer}$	Average mechanical steering power
P_{susp}	Air pressure in vessel for air suspension
P_{vessel}	Air pressure in vessel
P_{wh}	Power at wheel hubs to drive or brake the vehicle
q	Subscript, counting index for time steps
r_{dyn}	Dynamic rolling radius of driven wheels
RPA	Relative positive acceleration, according (278 p. 34)
RRC	Average rolling resistance coefficient, weighted by share of axle load
$RRC_{cl,upper}$	Upper RRC from tire efficiency class, e. g. B: 4.9 N/kN, C: 5.9 N/kN ...
RRC_i	Rolling resistance coefficient of tires at axle "i"
$R_{s,air}$	Specific gas constant for dry air, 287.2 J/(kg·K)
s	Distance
sh_i	Share of axle load "i" at vehicle's total weight force
sim	Subscript, related to simulation
sin	Sinus
$S_{meas,max}$	Maximum measured distance of driving cycle
$stoich$	Subscript, stoichiometric
T	Temperature
t	Time
T_{air}	Air temperature
$T_{air,vs,avrg}$	Average air temperature in vessels
T_{amb}	Ambient temperature
$T_{br,fr,in}$	Air temperature in vessel front brake

$T_{br,fr,out}$	Material temperature of outer surface of vessel front brake
T_{cool}	Coolant temperature at engine outlet
$T_{cool,inner}$	Measured coolant temperature in inner engine circuit
$T_{cool,rad}$	Measured coolant temperature in outer radiator circuit
$T_{cool,sim}$	Simulated coolant temperature of effective thermal mass
t_{end}	End of driving cycle
$T_{exh,out}$	Exhaust temperature at outlet of aftertreatment
$T_{exh,out,stat}$	Exhaust temperature at outlet of aftertreatment, stationary case
$T_{exh,TC}$	Exhaust temperature downstream the turbocharger
$T_{exh,TC,stat}$	Exhaust temperature downstream the turbocharger, stationary case
t_h	Subscript, thermic, e. g. kWh_{th} - heat flow
$t_{interval}$	Time interval, fictive auxiliaries for check of "FC-line", time interval for shifting from high to low
T_q	Torque
T_{qEM}	Torque at shaft of electrical machine, output (motor, > 0), input (generator, < 0)
$T_{qEM,cont}$	Continuous torque of electrical machine, S1 operation, defined in (279 p. 13) as "Operation at a constant load maintained for sufficient time to allow the machine to reach thermal equilibrium."
$T_{qfan,cl}$	Torque at fan clutch input shaft
$T_{qfan,hub}$	Torque at fan hub
$T_{qgearbox-input}$	Torque at gearbox input shaft
$T_{qinert,wh}$	Inertia torque of accelerated rotating wheels
T_{qref}	Torque at reference input speed, hydraulic torque converter
T_{qwh}	Sum torque at hubs of driven wheels
$T_{qwh,act}$	Actuating torque at hubs of driven wheels
U_{el}	Electrical voltage
v	Velocity
$v_{air,fan}^*$	Air flow velocity in fan cross sectional area, normalised to rotational fan speed
v_{air}	Air flow velocity around moving vehicle, dependent on vehicle velocity, wind velocity and wind angle
V_{air}	Volume of air
$V_{air,amb,deliv(i)}$	Air volume delivered at second "i" of delivery phase, ambient density
$V_{air,consumpt}$	Volume of compressed air, consumed
$V_{air,deliv,fract}$	Air volume fraction, delivered in time step Δt
$V_{air,deliv,gain}$	Gain of delivered air during regenerative braking
$V_{air,deliv,tot}$	Total delivered air volume over driving cycle, equals total air consumption
$v_{air,fan}$	Air flow velocity in fan cross sectional area
$V_{air,tot,std}$	Total air content, unit of standard litres air
v_{avrg}	Average vehicle velocity, with stop phases
$V_{displacement}$	Displacement of reciprocating machine, internal combustion engine or piston compressor
$Vf_{cool,inner}^*$	Normalised measured coolant flow in inner engine circuit, normalised to max. coolant flow at rated engine speed
$Vf_{cool,rad}^*$	Normalised measured coolant flow in outer radiator circuit, normalised to max. coolant flow at rated engine speed
$v_{roll,avrg}$	Average vehicle velocity during rolling, w/o stop phases
v_{sim}	Simulated velocity
v_{targ}	Target velocity
v_{veh}	Vehicle velocity
V_{vessel}	Volume of air vessel
v_{wind}	Wind velocity in boundary layer, dependent on altitude above road surface

$V_{wind,eff}$	Effective wind velocity. Equals the air flow velocity, which causes the same air drag like the logarithmic wind profile from road surface to vehicle height.
$V_{wind,ref}$	Reference wind velocity at reference altitude, from wind atlas
$W_{alt,FC,norm}$	Accumulated work consumption of alternator during phases standing, driving and coasting, case normal operation
$W_{alt,FC,regen}$	Accumulated work consumption of alternator during phases standing, driving and coasting, case regenerative braking
$W_{aux,stop,shift}$	Work of engine auxiliaries, shifted from engine stop to driving, without steering pump idle losses
W_{compr}	Overall compressor work, idle and delivery phases
$W_{compr,deliv,spec}$	Additional specific compressor delivery work
$W_{compr,deliv,spec,avg}$	Average of additional specific delivery work, average over driving cycle
$W_{compr,FC,norm}$	Accumulated work consumption of compressor during phases standing, driving and coasting, case normal operation
$W_{compr,FC,regen}$	Accumulated work consumption of compressor during phases standing, driving and coasting, case regenerative braking
$W_{compr,off}$	Compressor work at idle
$W_{compr,tot,deliv}$	Total compressor work during air delivery, including all idle losses
$W_{compr,tot,spec}$	Specific total delivery work, $W_{compr,tot,spec} = P_{compr,on} / V_{f,air,deliv}$
$W_{eng,pos,cl}$	Positive mechanical engine work at clutch during driving cycle
$W_{ORC,mech}$	Mechanical work output from the expansion machine of an Organic Rankine Cycle process
$W_{tract,wh}$	Positive tractive mechanical work at hubs of driven wheels
W_{veh}	Width of vehicle
X_{fan}	Fan actuation grade
X_i	Mole fraction, equals volume fraction for ideal gases
Y_i	Gravimetric fraction, share at mass
z	Coordinate for altitude above ground, here the road surface
z_0	Aerodynamic roughness length, i.e. altitude above ground, where the wind velocity becomes zero
z_{ref}	Reference height, altitude above ground where the wind velocity is known

5.3 Units

For the SI base units ampere (A), kelvin (K), kilogram (kg), metre (m), mole (mol) and second (s) see (280 pp. 112-115). The US-American units are described in (281 pp. c8-c20).

#	Quantity, Number of
\$	Currency, United States of America, US-Dollar
%	Fraction, Percent, 10^{-2} of basis value
%/%	Ratio of (relative change of dependent parameter in %) to (relative change of basis parameter in %)
%-of-reading	Measurement accuracy, % of reading, uncertainty in $\pm\%$ of currently displayed value
€	Currency, European Union, Euro, since 2002-01
°	Angle, Degree
°C	Temperature differences, Degree Celsius, $1\text{ °C} = 1\text{ K}$
A	Electrical current, Ampère
bar	Pressure, Bar, $10^5\text{ kg m}^{-1}\text{ s}^{-2}$
bbl	(US) Volume, Barrel, $1.590\text{ }10^{-1}\text{ m}^3$
bhp	(US) Mechanical power, Brake horse power, $7.457\text{ }10^2\text{ W}$
bhp-h	(US) Energy, Brake horse power hour, $2.685\text{ }10^6\text{ J}$

Btu	(US) Energy, British thermal unit, $1.055 \cdot 10^3$ J
Btu/hr	(US) Heat flow, $2.931 \cdot 10^{-1}$ W _{th}
C	Normed charging power for batteries, normed to electrical power to charge the nominal battery capacity in 1 hour, e. g. 100 kW _{el} for a battery of 100 kWh _{el}
cal	(US) Energy, calorie, 4.184 J
cm	Distance, Centimetre, 10^{-2} m
cm ³	Volume, Cubic centimetre, 10^{-6} m ³
DGE	(US) Energy, Diesel gallon equivalent, $1.356 \cdot 10^8$ J
DM	Currency, Germany, Deutsche Mark, until 2001-12
dm	Distance, Decimetre, 10^{-1} m
EJ	Energy, Etajoule, 10^{18} J
ft	(US) Distance, Foot, $3.048 \cdot 10^{-1}$ m
g	Mass, Gram, 10^{-3} kg
g/L	Density, Gram per litre, 1 kg/m ³
gal	(US) Volume, US liquid gallon, $3.785 \cdot 10^{-3}$ m ³
gCO ₂ e	Mass of greenhouse gas with global warming potential equivalent to 10^{-3} kg CO ₂
GGE	(US) Energy, Gasoline gallon equivalent, $1.204 \cdot 10^8$ J
GL	Volume, Gigalitre, 10^6 m ³
Gt	Mass, Gigatonne, 10^{12} kg
h	Time, Hour, $3.6 \cdot 10^3$ s
Hz	Rotational speed, Hertz, s ⁻¹
in	(US) Distance, Inch, $2.54 \cdot 10^{-2}$ m
J	Energy, Joule, kg m ² s ⁻²
J/(kg·K)	Heat capacity, (Joule per kilogram) per Kelvin, m ² s ⁻² K ⁻¹
K	Absolute temperature, Kelvin, 273.16 K = 0 °C
kg	Mass, Kilogram
kg/(km/h) ²	Air drag, horizontal resistance in (kg-force) per (velocity to the power of two), $1.271 \cdot 10^2$ N/(m/s) ²
kg/h	Mass flow, Kilograms per hour, $2.778 \cdot 10^{-4}$ kg/s
kg/kg	Rolling resistance, ratio of (horizontal resistance in kg-force) to (vertical wheel load in kg-force)
kg/L	Density, Kilogram per Litre, 10^{-3} kg/m ³
kg/m ³	Density, Kilogram per cubic metre
kg·m ²	Rotational inertia
kg-force	Force, 1 kg · g, 9.81 N
km	Distance, Kilometre, 10^3 m
km/h	Velocity, Kilometre per hour, $2.778 \cdot 10^{-1}$ m/s
km ²	Area, Square-kilometre, 10^6 m ²
km ³ /year	Volume flow, Cubic-kilometres per year, $3.169 \cdot 10^1$ m ³ /s
kN	Force, Kilonewton, 10^3 N
ktoe	Energy, Kilo-tonne oil-equivalent, = $10^3 \cdot 10^3$ kg/t · 4.187 10^7 J/kg = $4.187 \cdot 10^{13}$ J
kW	Power, Kilowatt, 10^3 W
kW _{el}	Electrical power, Kilowatt electrical, 10^3 W _{el}
kWh	Energy, Kilowatthour, $3.6 \cdot 10^6$ J
kWh _{th} /kg	Gravimetric lower heating value, Kilowatthour per kilogram, $3.6 \cdot 10^6$ J/kg
kWh _{th} /L	Volumetric lower heating value, Kilowatthour per litre, $3.6 \cdot 10^9$ J/m ³
kW _{mech}	Mechanical power, Kilowatt mechanical, 10^3 W _{mech}
kW _{th}	Heat flow, 10^3 W _{th}
L	Volume, Litre, 10^{-3} m ³
L/min	Volume flow, Litres per minute, $1.667 \cdot 10^{-5}$ m ³ /s

L _{amb}	Volume, Litres of air at ambient density, 10 ⁻³ m ³
lb	(US) Mass, Pound, 4.536 10 ⁻¹ kg
lbf	(US) Force, Pound force, 4.450 N
lbf-ft	(US) Torque, Pound force feet, 1.356 Nm
lbf-in	(US) Torque, Pound force inch, 1.130 10 ⁻¹ Nm
m	Distance, Metre
m/s ²	Acceleration, deceleration, (Metres per second) per second
mi	(US) Distance, Mile, 1.609 10 ³ m
min	Time, Minute, 60 s
MJ	Energy, Megajoule, 10 ⁶ J
MJ _{th} /kg	Gravimetric lower heating value, Megajoule per kilogram, 10 ⁶ J/kg
mol	Amount of substance, Mole, 6.022 10 ²³ molecules
Mt	Mass, Megatonne, 10 ⁹ kg
N	Force, Newton, kg m s ⁻²
N/kN	Rolling resistance, ratio of (horizontal resistance force in N) to (vertical load in kN), 10 ⁻³ N/N
Nm	Torque, Newtonmeter, kg m ² s ⁻²
Pa	Pressure, Pascal, Newton per squaremetre, kg m ⁻¹ s ⁻²
pass.	Passenger in vehicle of urban public transport with standard mass of 68 kg
PJ	Energy, Petajoule, 10 ¹⁵ J
pkm	Haulage capacity, Passenger-kilometre, 6.8 10 ⁴ kg m
ppmv	Fraction, Parts per million volume, 10 ⁻⁶ of basis volume
psi	(US) Pressure, Pound force per square inch, 6.895 10 ³ Pa
rad	Angle, Radian, 360 / (2 π) ° = 57.30 °
rad/s	Rotational speed, Radians per second, 1/(2 π) Hz = 1.592 10 ⁻¹ Hz
rpm	Rotational speed, Rotations per minute, 1.667 10 ⁻² Hz
s	Time, Second
short-ton	(US) Mass, Short-ton, 9.072 10 ² kg
sl	Mass, Standard litre of dry air, 1.204 10 ⁻³ kg, at 1.013 bar and +20 °C
t	Mass, Metric tonne, 10 ³ kg
t·m	Lifting capacity of tail-lift. Horizontal distance of mass on tail-lift to rear loading sill. 1 t·m ≈ 9.81 10 ³ Nm
tkm	Haulage capacity, Tonne-kilometre, 10 ⁶ kg m
V	Electrical voltage, Volt, kg m ² s ⁻³ A ⁻¹
W	Power, Watt, kg m ² s ⁻³
Wh	Energy, Watthour, 3.6 10 ³ J
ZJ	Energy, Zetajoule, 10 ²¹ J

5.4 Driving cycles

5.4.1 VECTO target speed driving cycles¹⁰²

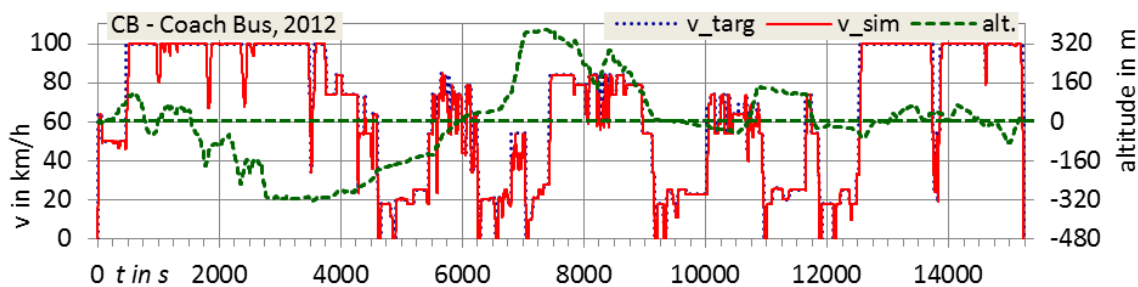


Figure 141. CB - Coach Bus cycle, 2012 (282 p. 1/58)

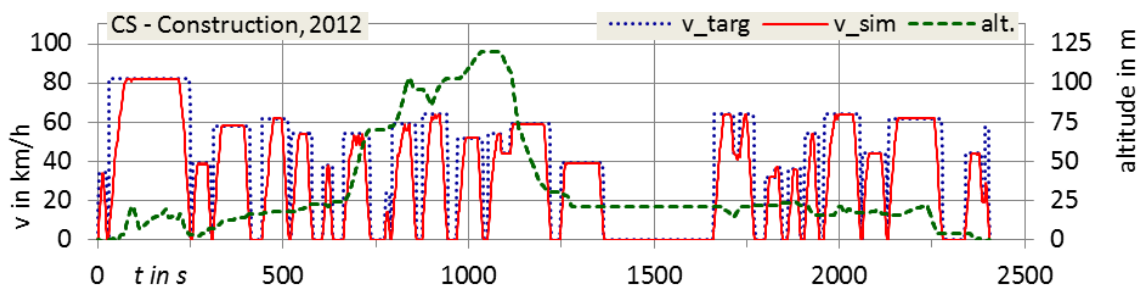


Figure 142. CS - Construction cycle, 2012 (282 p. 1/50)

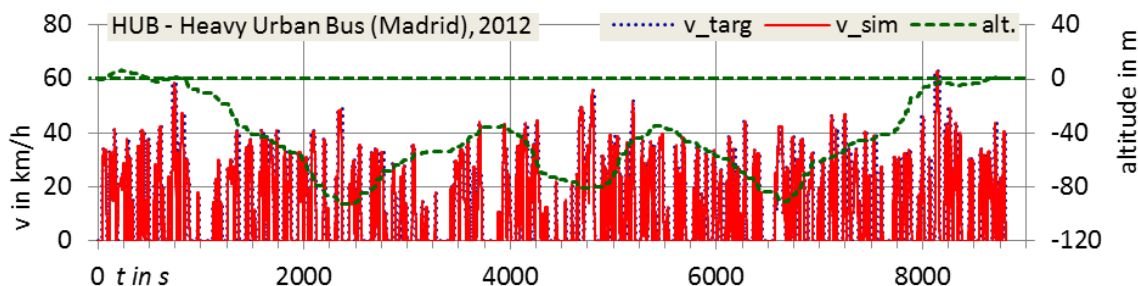


Figure 143. HUB - Heavy Urban Bus cycle, 2012 (282 p. 1/54)

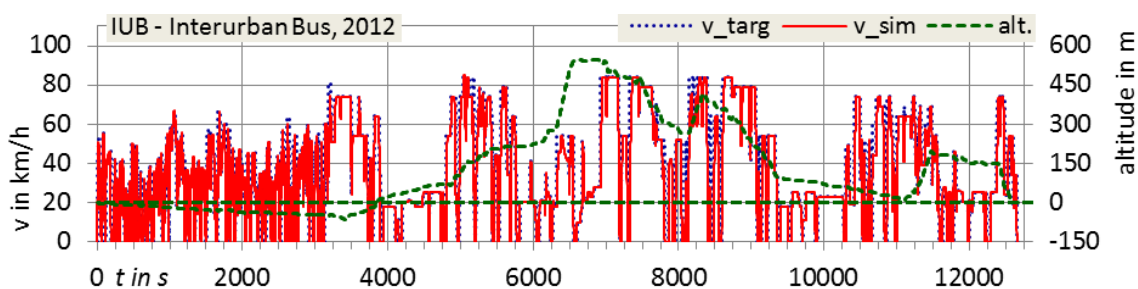


Figure 144. IUB - Interurban Bus cycle, 2012 (282 p. 1/57)

¹⁰² Status of cycles 2017-07.

Changes since first versions from 2011/2012: New Long Haul cycle 2015-04, new Suburban Bus cycle 2015-11, new Regional Delivery cycle 2016-12, new Municipal Utility cycle 2017-01, new Urban Delivery cycle 2017-06. Announcement by industry in 2017-04: Update planned in 2017 for construction cycle.

The up-to-date versions of the VECTO target speed cycles can be found in the folder ...\https://webgate.ec.europa.eu/CITnet/confluence/display/VECTO ; link as of 2017-07.

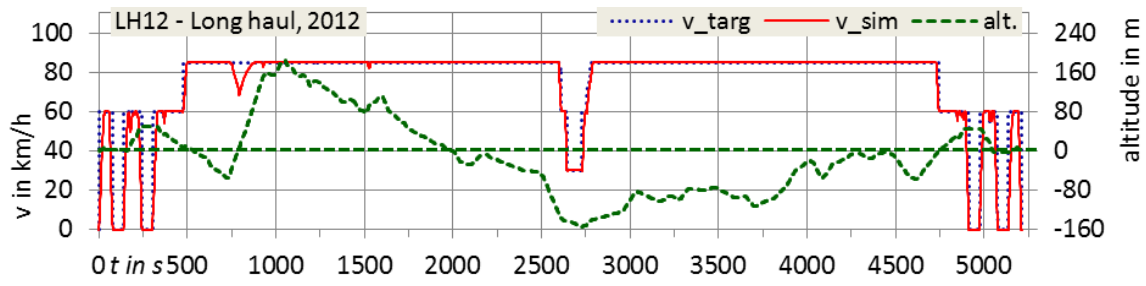


Figure 145. LH12 - Long Haul cycle, 2012 (282 p. 1/45)

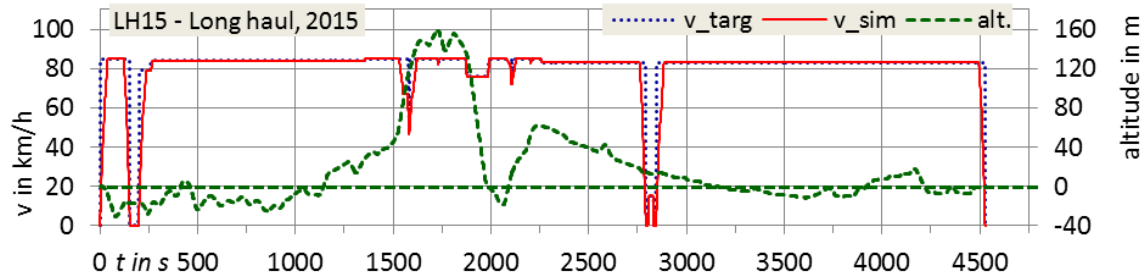


Figure 146. LH15 - Long Haul cycle, 2015 (149 p. 79)

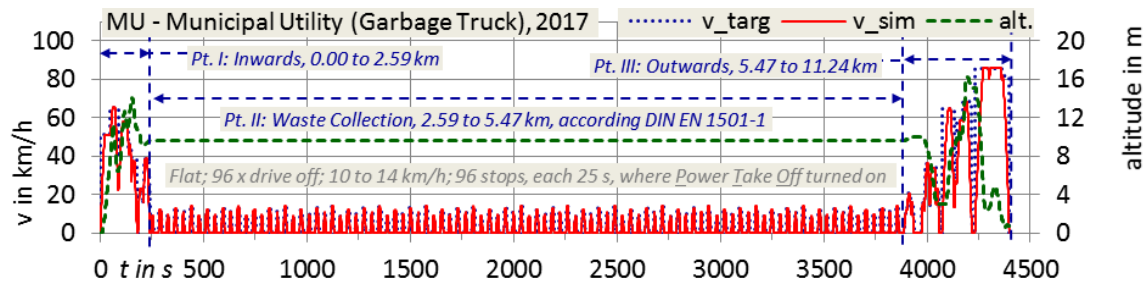


Figure 147. MU - Municipal Utility cycle (garbage truck), 2017, (283)

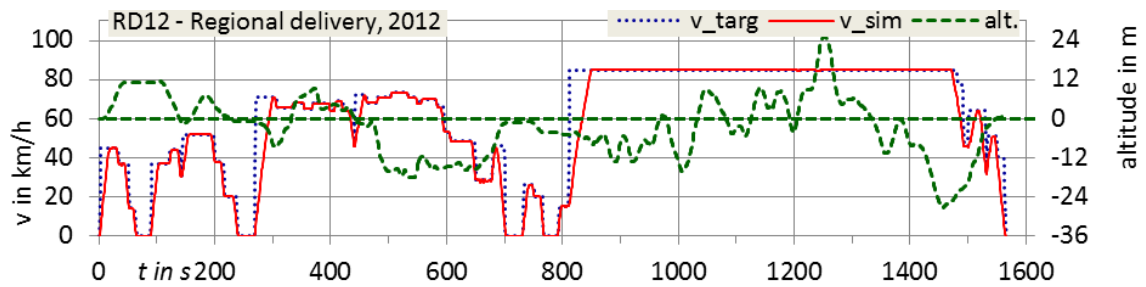


Figure 148. RD12, Regional Delivery cycle, 2012 (282 p. 1/36)

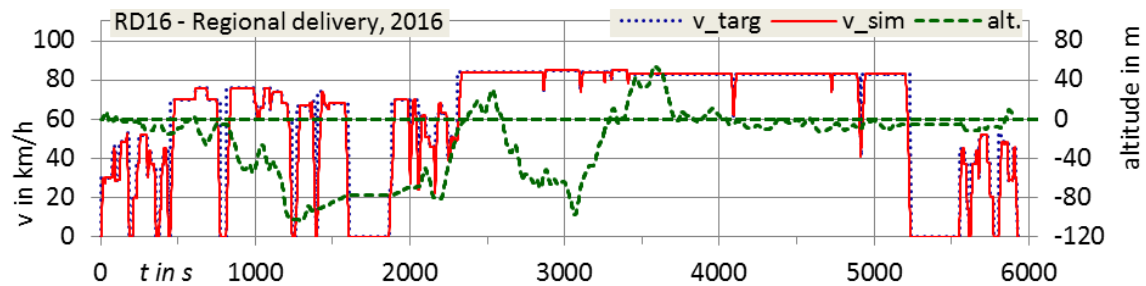


Figure 149. RD16 - Regional Delivery cycle, 2016 (284 p. 16)

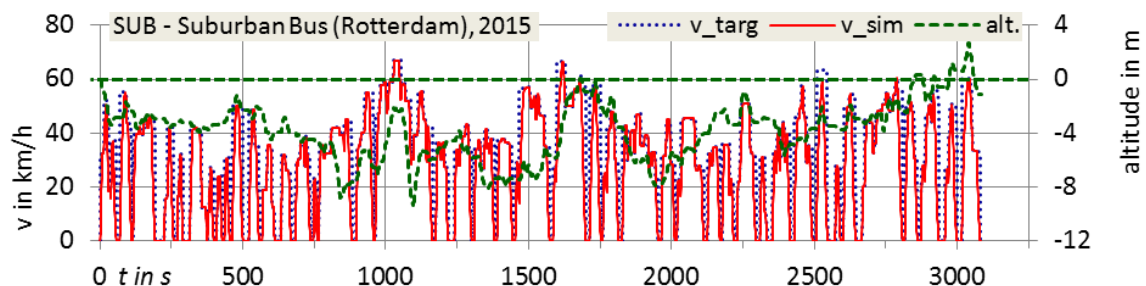


Figure 150. SUB - Suburban Bus cycle, 2015 (285 p. 93)

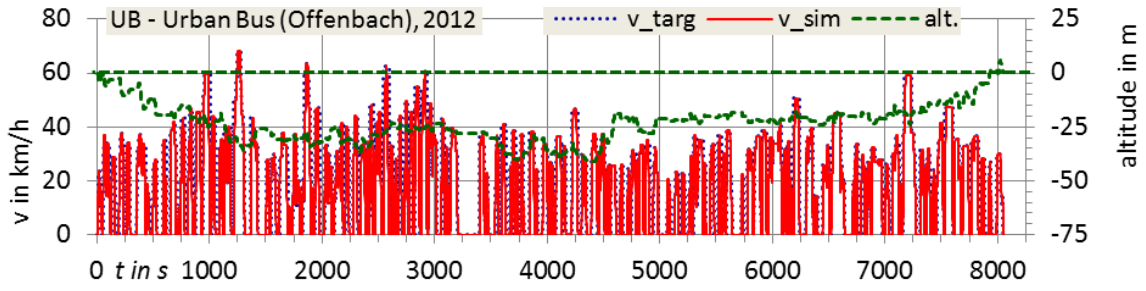


Figure 151. UB - Urban Bus cycle, 2012 (282 p. 1/55)

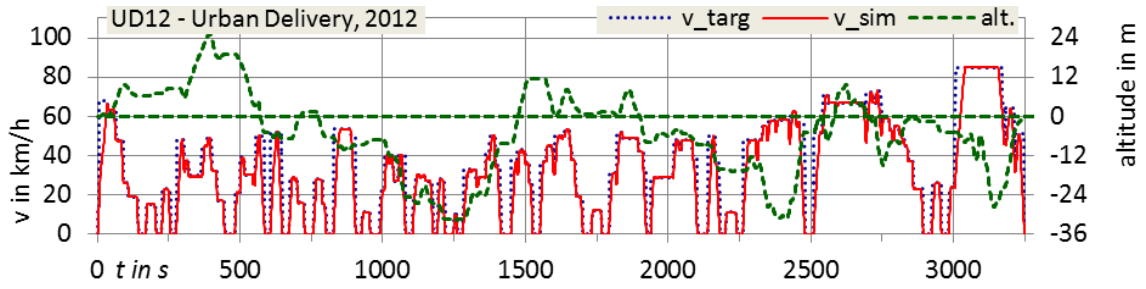


Figure 152. UD12 - Urban Delivery cycle, 2012 (282 p. 1/47)

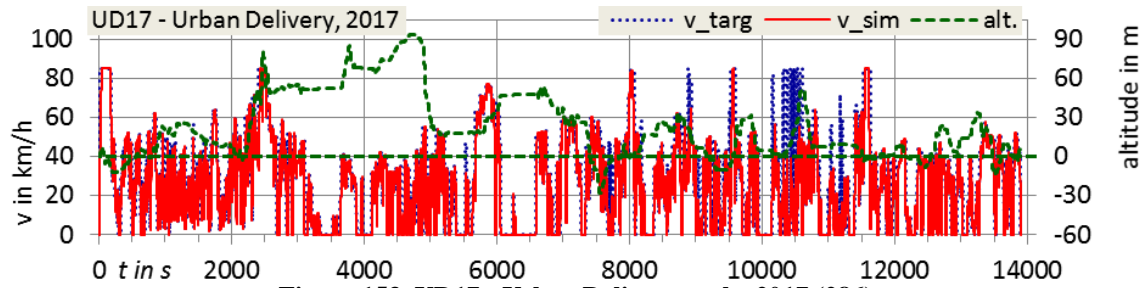


Figure 153. UD17 - Urban Delivery cycle, 2017 (286)

5.4.1.1 Variations of VECTO target speed driving cycles

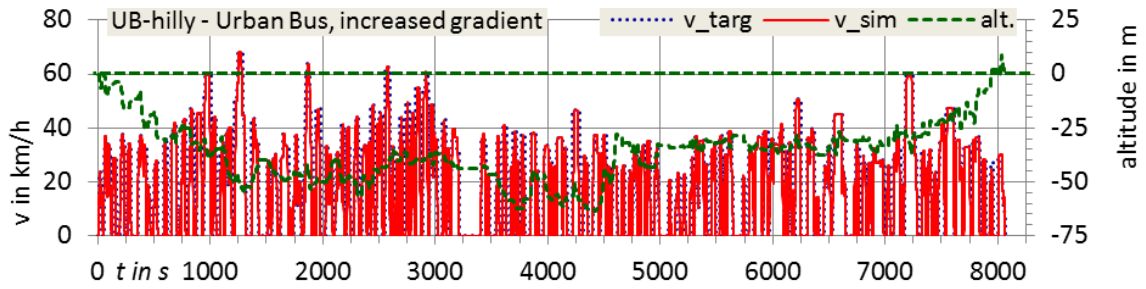


Figure 154. UB-hilly - Like Urban Bus cycle 2012, road gradient scaled with factor 1.554

- **UD12-flat:** Like Urban Delivery cycle 2012, see above, but without road gradient.

5.4.2 Further driving cycles

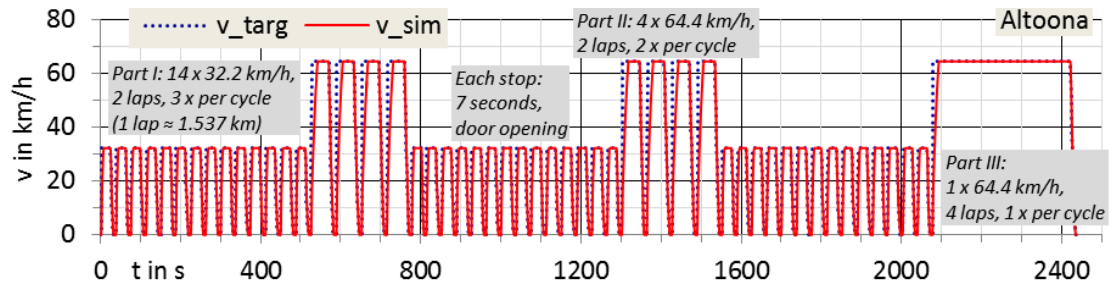


Figure 155. Altoona cycle (287 pp. 6-3 ff.), derivate from (288 p. 12). Weightings, I to III: 3/7, 2/7, 2/7

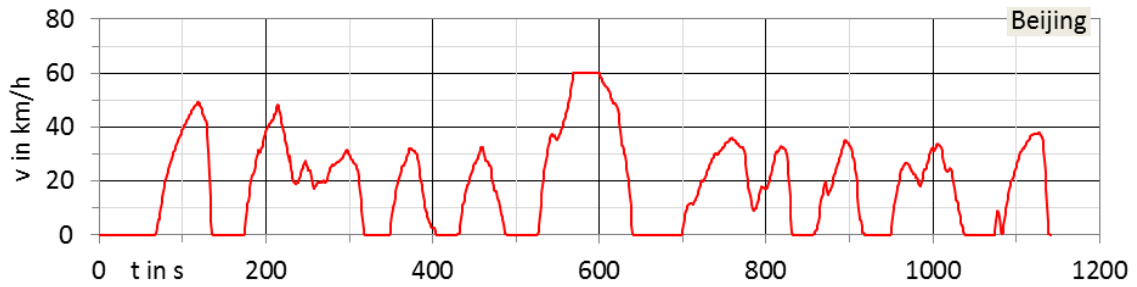


Figure 156. BJBC - Beijing Bus Cycle (289 pp. A-6)

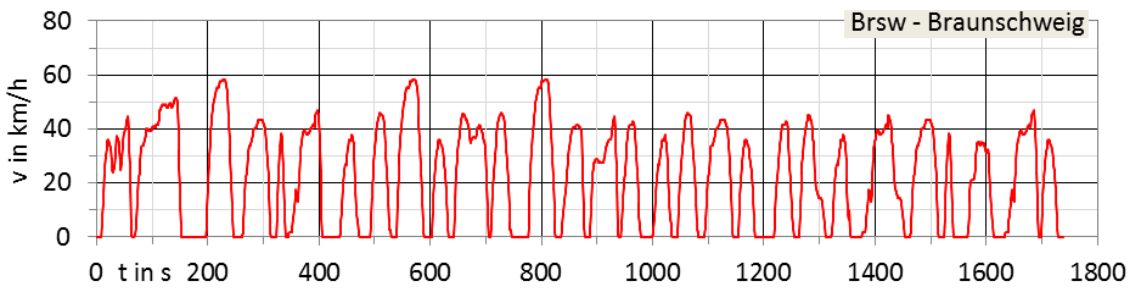


Figure 157. Brsw - Braunschweig bus cycle (290) (291)

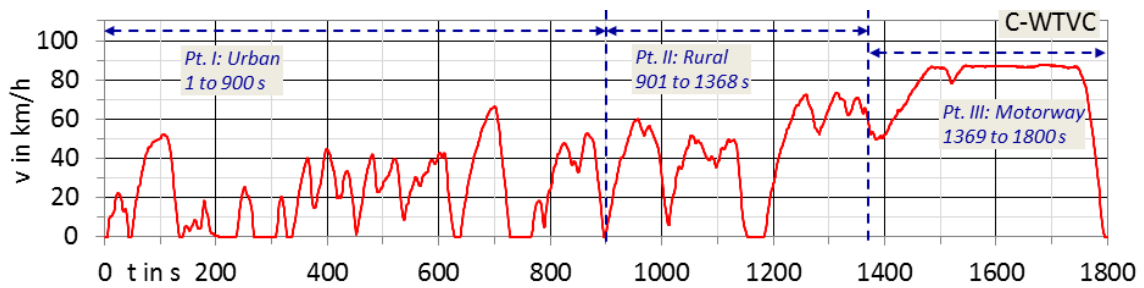


Figure 158. C-WTVC - Chinese World Transient Vehicle Cycle (292 p. 23 ff.)

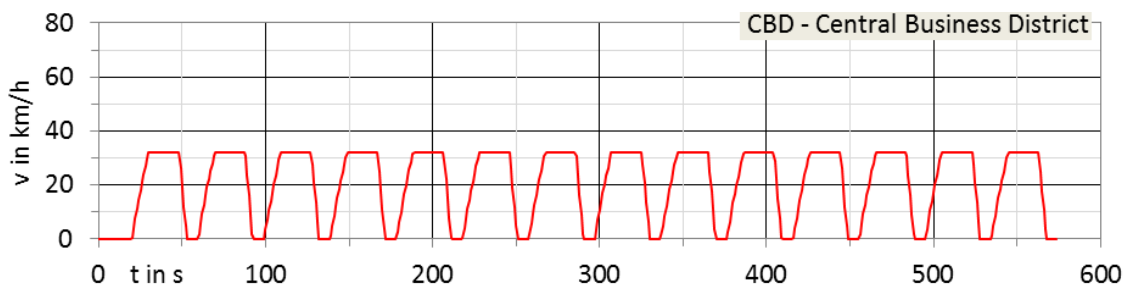


Figure 159. CBD (SAE) - Central Business District bus cycle (SAE) (288 p. 12)

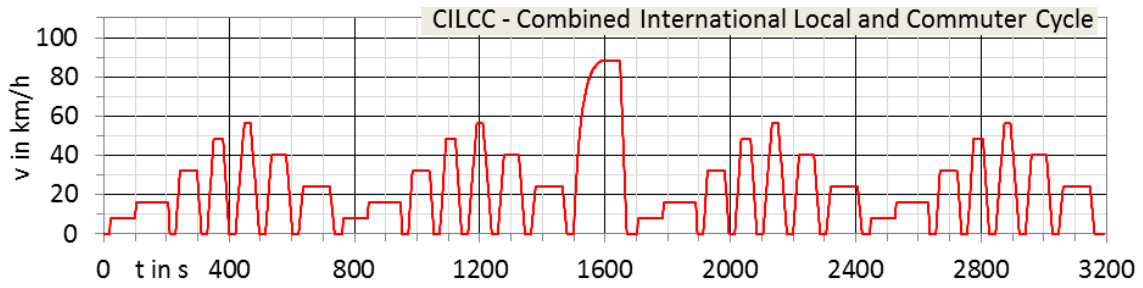


Figure 160. CILCC - Combined International Local and Commuter Cycle (293)

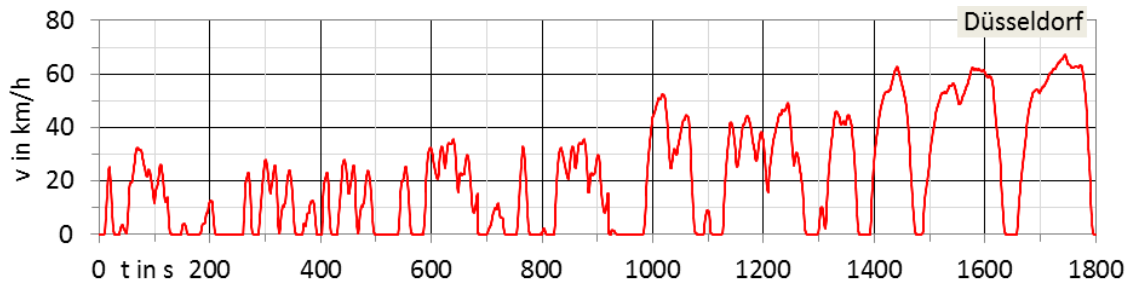


Figure 161. Düsseldorf bus cycle (294 p. 101 ff.)

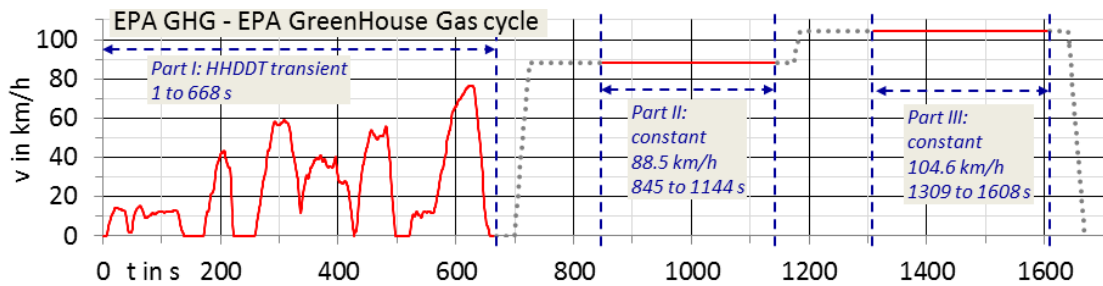


Figure 162. EPA GHG - EPA GreenHouse Gas cycle (170 pp. 149/150, 185).

Valid for GEM phase 1 until 2017, used in this work. Phase 2: Road gradient for constant parts (60 p. 74132).

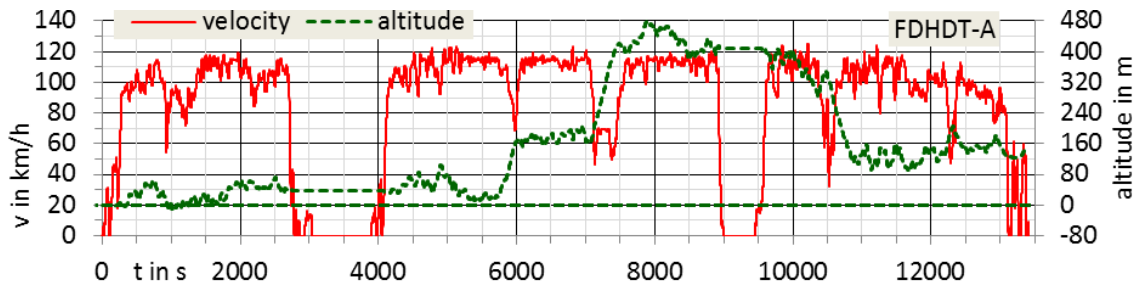


Figure 163. FDHDT-A - Freeway-Dominant Heavy Duty Truck cycle A (249 p. 101) (295 p. 165)

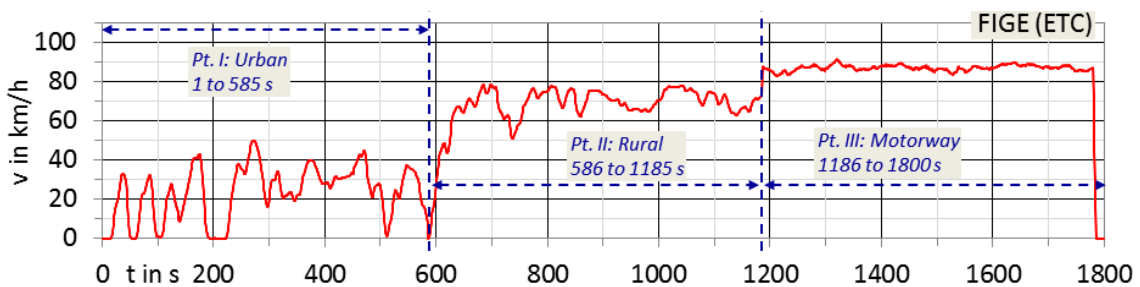


Figure 164. FIGE truck driving cycle (296 p. 68), basis for ETC

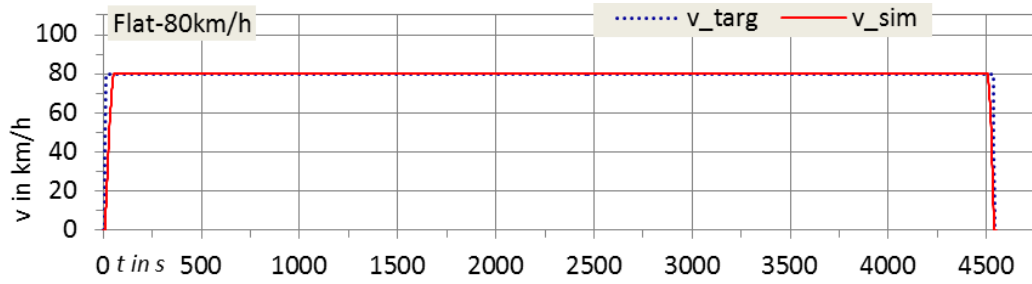


Figure 165. Flat-80km/h driving cycle: 100 km, flat.

Stand 10 s, acceleration until target speed 80 km/h, constant 80 km/h, braking, stand 10 s

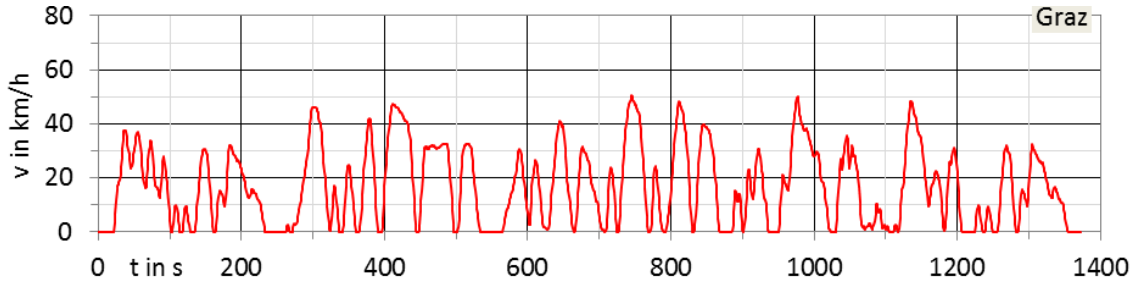


Figure 166. Graz bus cycle (297 p. 21/22) (298 p. 76 ff.)

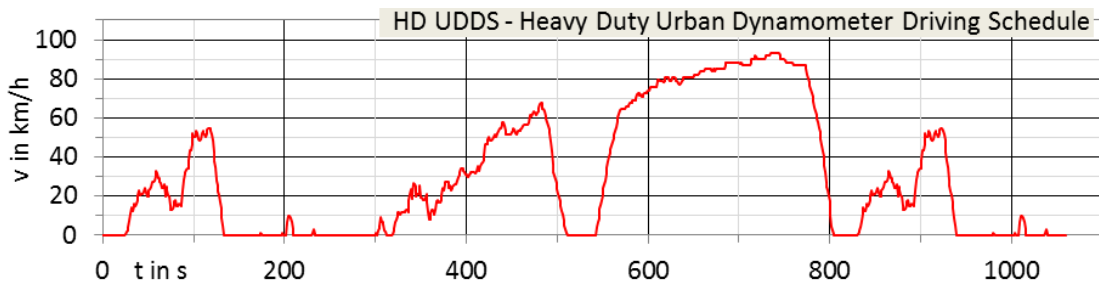


Figure 167. HD UDDS - Heavy Duty Urban Dynamometer Driving Schedule (299 p. 74 ff.) (300 p. 570 ff.)

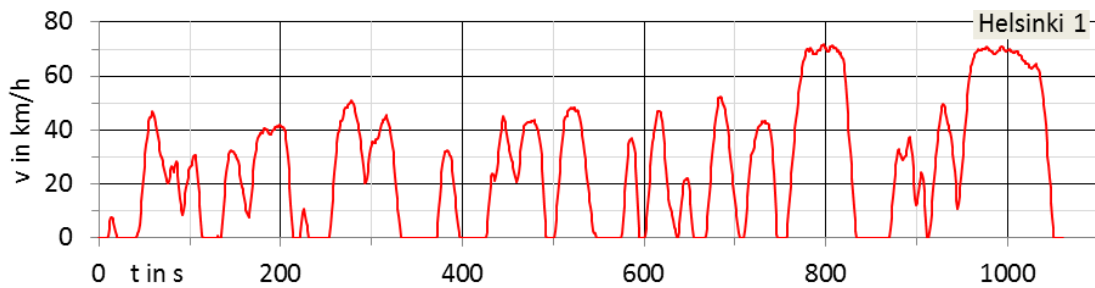


Figure 168. Helsinki 1 bus cycle (301 p. 8)

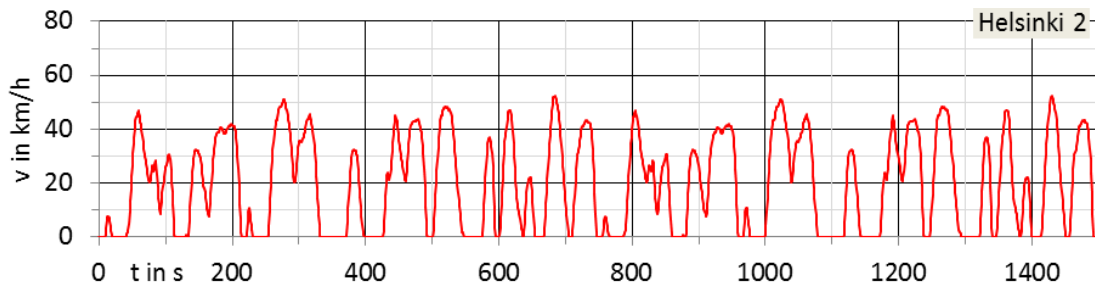


Figure 169. Helsinki 2 bus cycle (301 p. 9)

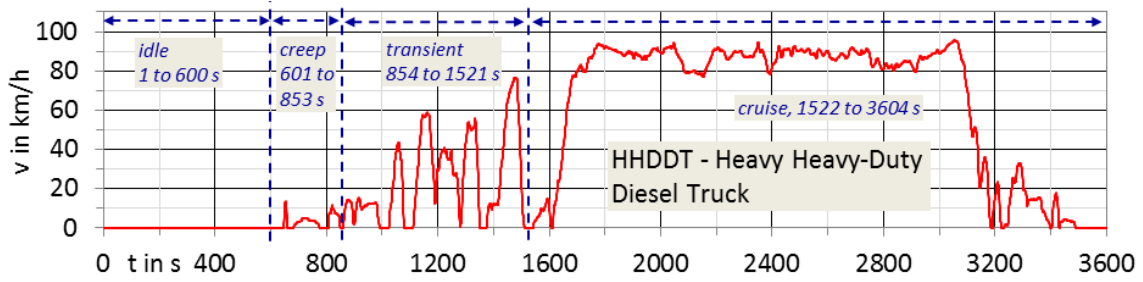


Figure 170. HHDDT - Heavy Heavy-Duty Diesel Truck cycle (302 p. 142)

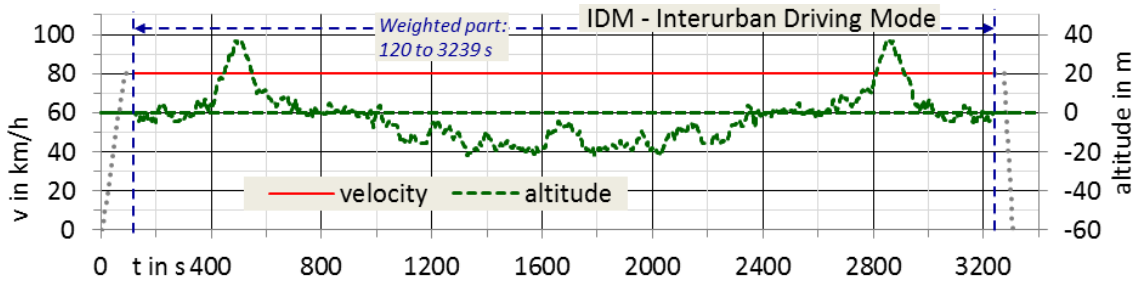


Figure 171. IDM - Interurban Driving Mode cycle (303)

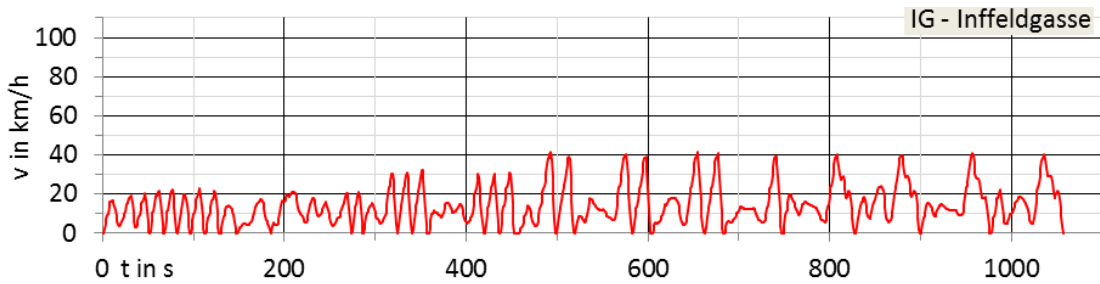


Figure 172. IG - Inffeldgasse cycle, measurement of air consumption of brakes, 2015-02-24

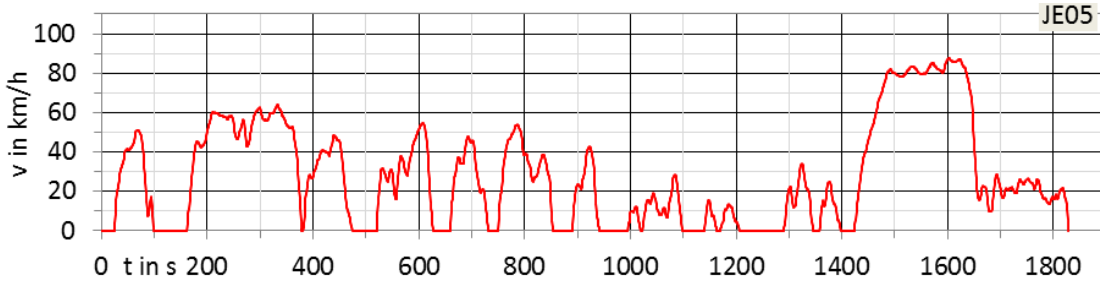


Figure 173. Japanese JE05 cycle (304)

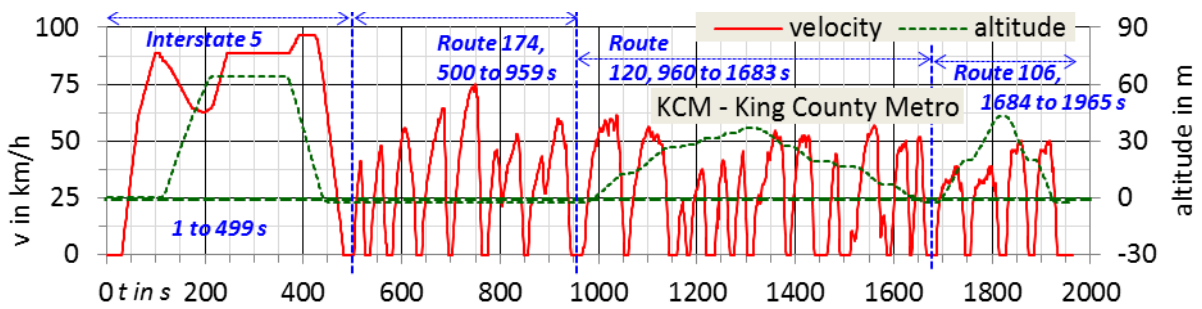


Figure 174. KCM - King County Metro bus cycle (305 p. 19)

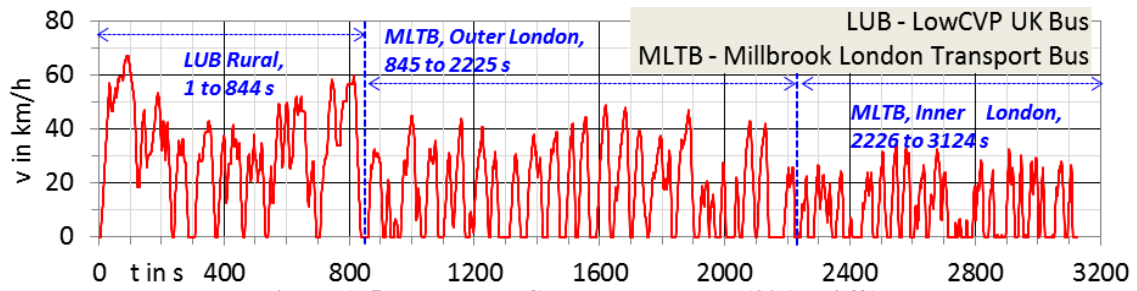


Figure 175. LUB - LowCVP UK Bus cycle (306 p. 4 ff.)
MLTB - Millbrooks London Transport Bus cycle (307)

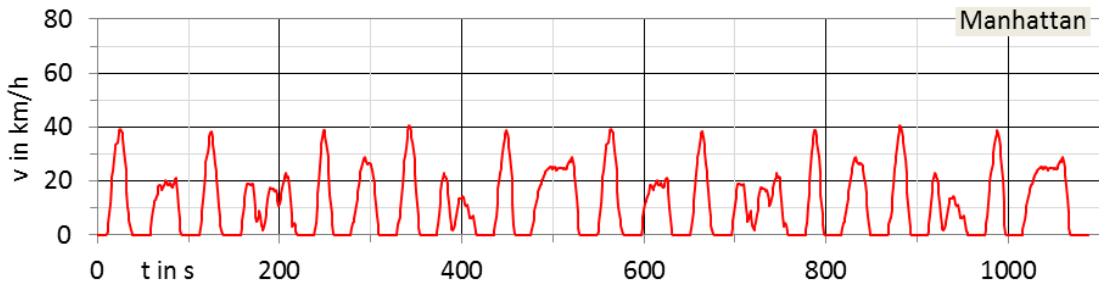


Figure 176. Manhattan bus cycle (308 p. 8/9)

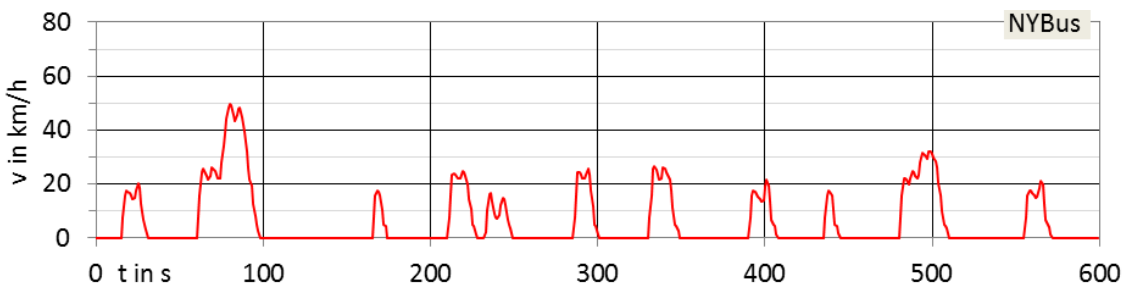


Figure 177. NYBus - New York Bus cycle (309 p. 4/5)

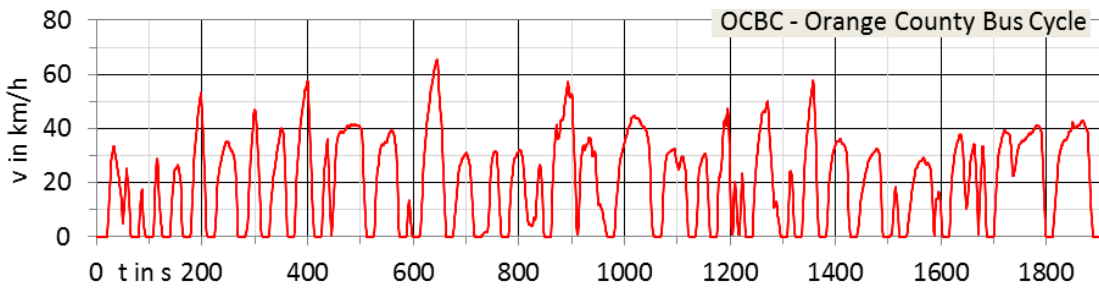


Figure 178. OCBC - Orange County Bus Cycle (310 pp. C-1 ff.)

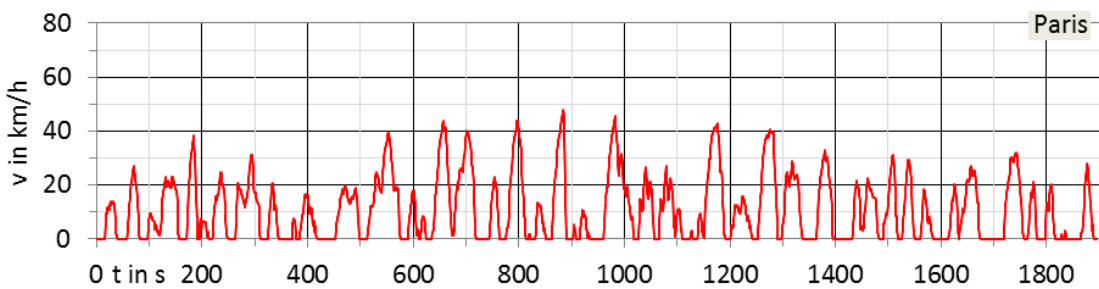


Figure 179. Paris bus cycle (311 p. 4)

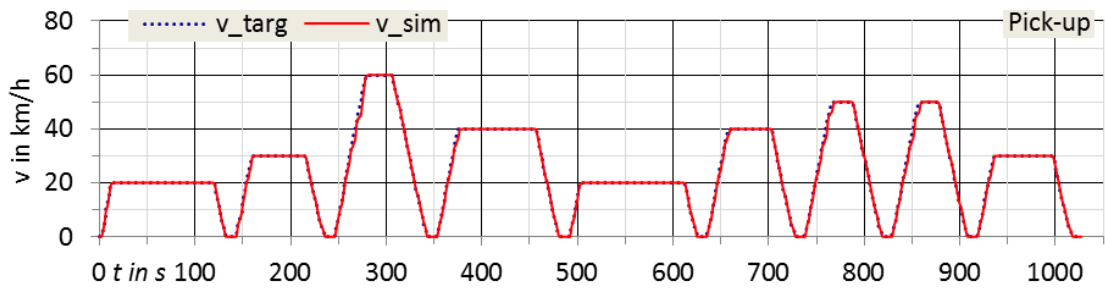


Figure 180. Pick-up - Pick up, delivery, utility and service operations driving cycle (312 p. 6)

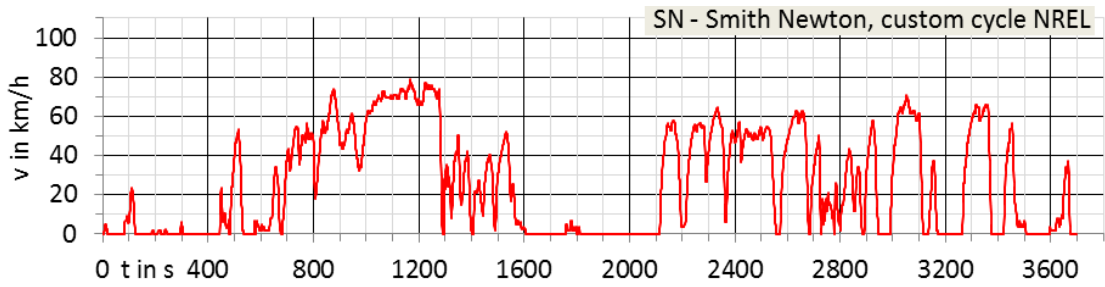


Figure 181. SN - Smith Newton truck cycle (269 p. 7)

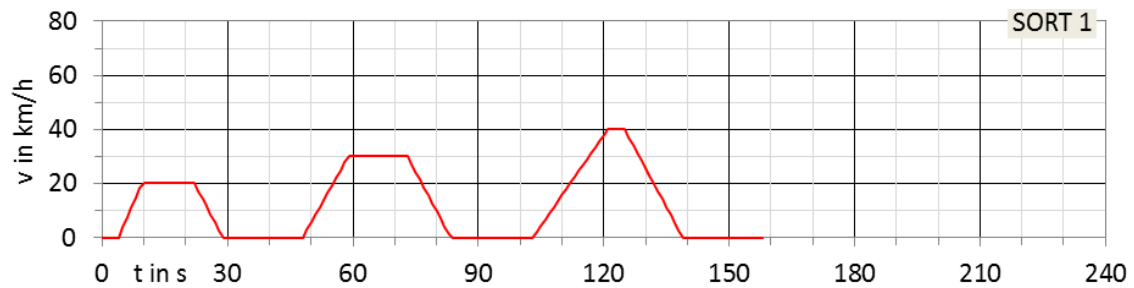


Figure 182. SORT 1 - Standardised OnRoad Test 1 bus cycle (313 p. 11 ff.)

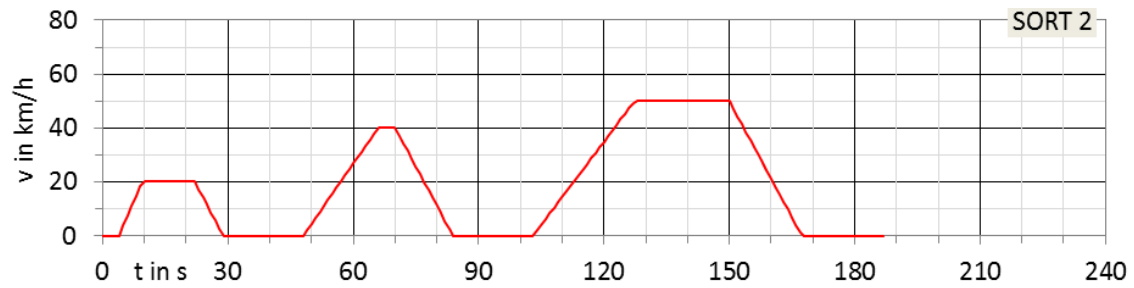


Figure 183. SORT 2 - Standardised OnRoad Test 2 bus cycle (313 p. 11 ff.)

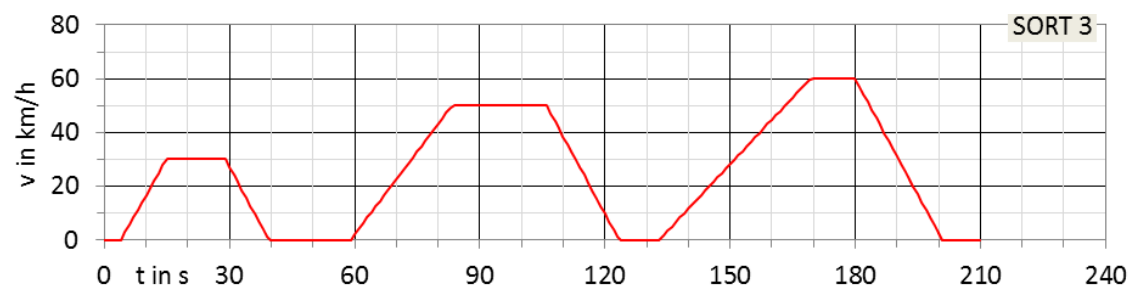


Figure 184. SORT 3 - Standardised OnRoad Test 3 bus cycle (313 p. 11 ff.)

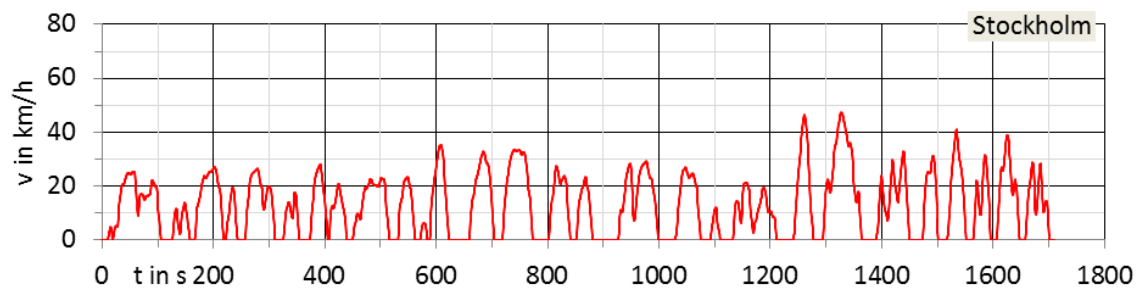


Figure 185. Stockholm bus cycle (314 p. 17)

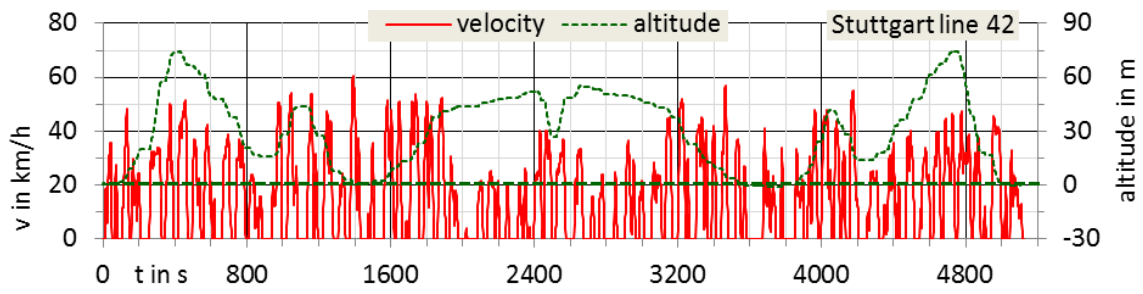


Figure 186. Stuttgart bus line 42, own GPS measurement 2016-03-24

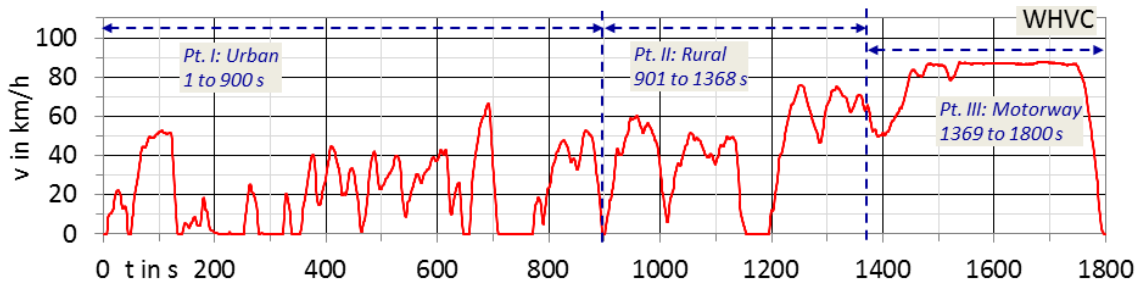


Figure 187. WHVC - World Harmonized Vehicle Cycle (315 p. 61 ff.) (316 p. 28 ff.), basis for WHTC

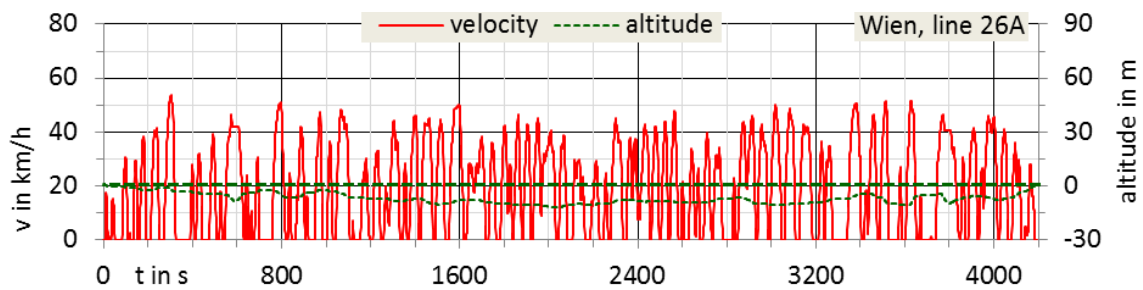


Figure 188. Wien bus line 26A, GPS measurement 2015-12-11

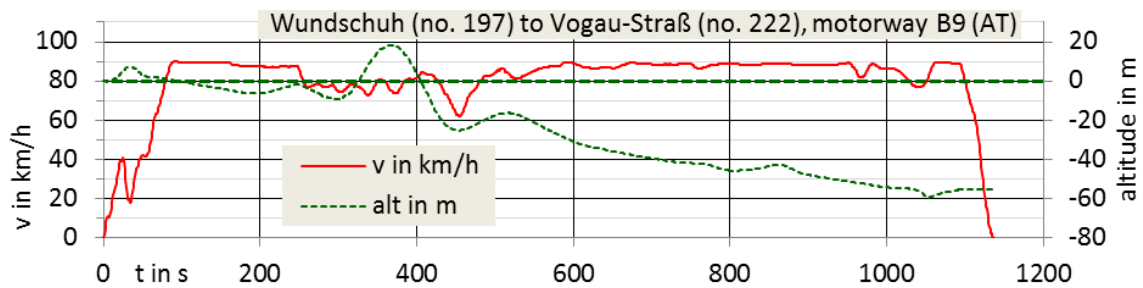


Figure 189. Wundschuh truck cycle, measurement of fuel consumption, 2010-10-15

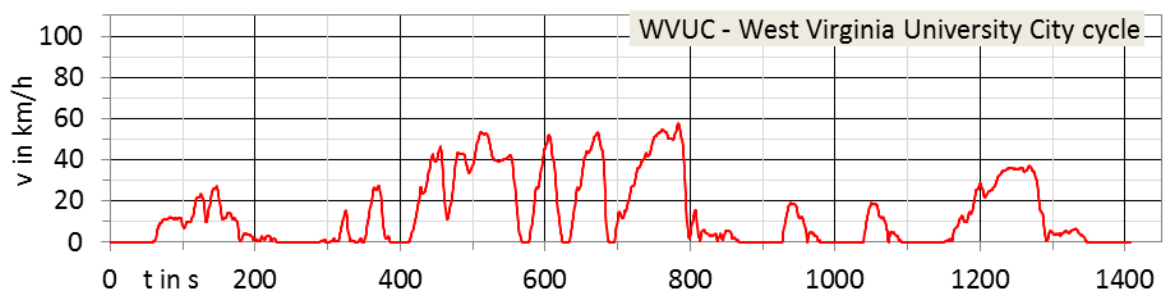


Figure 190. WVUC - West Virginia University City cycle (317)

5.4.3 Characteristic factors of driving cycles

Note: In case of target speed driving cycles the effective velocity course (simulated velocity (v_{sim}), red line in diagrams above) is individual for every single vehicle model, also the characteristic factors. It results from target speed (v_{targ} , blue line), change of altitude (alt., green line), demanded acceleration or deceleration and the available acceleration power. The factors were simulated with typical HDV models. \Rightarrow Models with a higher power-to-mass-ratio accelerate more quickly.

Table 28. Characteristic factors of driving cycles¹⁰³

	$t_{max};$ s	$s_{max};$ km	$v_{avg};$ km/h	$v_{roll,avg};$ km/h	stops/ km	Stand; % t_{max}	$ \Delta alt/\Delta s $ norm; %	RPA; m/s ²	$\tilde{a};$ m/s ²	TCF; -
VECTO target speed driving cycles										
CB, 2012	15'233	275.16	65.0	66.7	0.04	2.5	1.68	0.026	0.095	1.00
CS, 2012	2'406	21.21	31.7	42.7	1.0	25.7	1.95	0.123	0.182	1.03
HUB, 2012	8'808	30.47	12.5	21.8	5.0	42.8	1.38	0.229	0.259	1.04
IUB, 2012	12'667	123.58	35.1	40.2	0.7	12.7	1.80	0.116	0.177	1.02
LH12, 2012	5'212	108.18	74.7	78.3	0.05	4.5	1.43	0.013	0.078	1.00
LH15, 2015	4'529	100.17	79.6	80.7	0.03	1.4	0.94	0.012	0.053	1.00
MU, 2017	4'402	11.23	9.2	19.6	9.1	53.1	0.67	0.151	0.167	1.03
Pt. I, Inwards	243	2.58	38.2	39.0	0.8	2.1	1.27	0.151	0.217	1.00
Pt. II, Collection	3'636	2.88	2.8	7.5	33.4	62.0	0.00	0.174	0.173	1.04
Pt. III, Outwards	521	5.76	39.8	46.6	0.7	14.6	0.74	0.139	0.141	1.00
RD12, 2012	1'567	25.83	59.3	63.6	0.2	6.8	1.69	0.045	0.111	1.00
RD16, 2016	5'955	100.00	60.5	68.9	0.11	12.2	1.22	0.034	0.082	1.00
SUB, 2015	3'084	23.49	27.4	32.6	1.8	16.0	0.63	0.190	0.206	1.04
UB, 2012	8'054	39.54	17.7	26.3	3.0	32.9	1.45	0.178	0.214	1.04
UD12, 2012	3'250	27.81	30.8	37.8	0.9	18.6	1.71	0.107	0.152	1.03
UD17, 2017	13'903	100.00	25.9	33.4	1.0	22.6	1.53	0.167	0.197	1.03
Variations of VECTO target speed driving cycles										
UB-hilly	8'067	39.55	17.6	26.3	3.0	32.8	2.26	0.177	0.237	1.04
UD12-flat	3'253	27.81	30.8	37.8	0.9	18.5	0.00	0.102	0.100	1.03
Further driving cycles										
Altoona	2'438	21.51	31.8	35.8	2.4	11.3	0.00	0.145	0.145	1.03
Pt. I, CBD (<i>Altoona</i>) 3x	523	3.08	21.1	24.8	4.6	14.7	0.00	0.183	0.183	1.04
Pt. II, Arterial, 2x	251	3.08	44.1	48.3	1.3	8.8	0.00	0.208	0.208	1.03
Pt. III, Commuter, 1x	364	6.15	60.8	61.8	0.2	1.6	0.00	0.026	0.026	1.00
BJBC	1'142	5.75	18.1	25.8	1.4	29.8	0.00	0.128	0.124	1.04
Brsw	1'740	10.87	22.5	29.5	2.7	23.7	0.00	0.219	0.214	1.04

¹⁰³ $|\Delta alt/\Delta s|_{norm} = \sum_{q=1}^{q=q_{max}} |\Delta alt_q/\Delta s_q|/s_{max}$. Cumulated abs. value of change of altitude, normalised to s_{max}

$RPA = \sum_{q=1}^{q=q_{max}} [v_q \cdot \max(0; a_{veh,q}) \cdot \Delta t_q]/s_{max}$. Relative positive acceleration, (278 p. 34)

$\tilde{a} = \sum_{q=1}^{q=q_{max}-1} \max\{0; [0.5 \cdot (v_{q+1}^2 - v_q^2) + g \cdot (alt_{q+1} - alt_q)]\}/s_{max}$. Characteristic acceleration, (277 p. 4).

TCF: "Transient Correction Factor" to depict the behaviour of ICE. The integrated FC from the stationary engine performance map is multiplied with this factor, see also p. 36

	t_{\max} ; s	S_{\max} ; km	V_{avg} ; km/h	$V_{\text{roll,avg}}$; km/h	stops/ km	Stand; % t_{\max}	$ \Delta\text{alt}/\Delta s $ norm; %	RPA; m/s ²	\hat{a} ; m/s ²	TCF; -
C-WTVC	1'800	20.51	41.0	45.5	0.5	9.8	0.00	0.096	0.092	1.02
Pt. I, Urban	900	5.73	22.9	27.2	1.4	15.8	0.00	0.155	0.154	1.03
Pt. II, Rural	468	5.68	43.7	46.6	0.2	6.2	0.00	0.123	0.121	1.00
Pt. III, Motorway	432	9.10	75.8	76.7	0.11	1.2	0.00	0.042	0.034	1.00
CBD (SAE)	575	3.23	20.2	24.6	4.3	17.7	0.00	0.173	0.173	1.04
CILCC	3'192	19.80	22.3	26.6	1.3	16.0	0.00	0.085	0.085	1.03
Düsseldorf	1'800	10.74	21.5	27.7	2.1	22.4	0.00	0.154	0.152	1.04
EPA-GHG	1'268	20.67	58.7	64.1	0.2	8.4	0.00	0.034	0.033	1.00
Pt. I, Transient	668	4.57	24.6	29.4	0.9	16.0	0.00	0.153	0.150	1.04
Pt. II, 55 mi/h	300	7.37	88.5	88.5	0.00	0.0	0.00	0.000	0.000	1.00
Pt. III, 65 mi/h	300	8.72	104.6	104.6	0.00	0.0	0.00	0.000	0.000	1.00
FDHDT- A	13'409	316.22	84.9	95.8	0.04	11.4	1.52	0.054	0.076	1.00
FIGE	1'800	29.48	59.0	61.0	0.2	3.4	0.00	0.069	0.062	1.00
Pt. I, Urban	585	3.82	23.5	25.6	0.8	8.4	0.00	0.135	0.133	1.03
Pt. II, Rural	600	11.24	67.4	67.5	0.00	0.2	0.00	0.077	0.076	1.00
Pt. III, Motorway	615	14.43	84.5	86.5	0.07	2.3	0.00	0.039	0.026	1.00
Flat-80km/h	4'551	100.00	79.1	79.4	0.01	0.4	0.00	0.002	0.002	1.00
Graz	1'374	6.37	16.7	19.7	4.2	15.5	0.00	0.245	0.239	1.04
HD UDDS	1'061	8.93	30.3	44.5	1.5	32.0	0.00	0.137	0.124	1.03
Helsinki 1	1'062	7.52	25.5	33.5	2.1	23.9	0.00	0.223	0.216	1.04
Helsinki 2	1'503	8.16	19.5	26.7	3.2	26.9	0.00	0.255	0.249	1.04
HHDDT	3'604	41.90	41.9	57.1	0.3	26.7	0.00	0.054	0.053	1.00
Pt. I, Idle	600	0.00	0.0	0.0	0.00	100.0	0.00	0.000	0.000	1.00
Pt. II, Creep	253	0.20	2.8	4.7	15.0	39.9	0.00	0.065	0.064	1.04
Pt. III, Transient	668	4.57	24.6	29.4	0.9	16.0	0.00	0.153	0.150	1.03
Pt. IV, Cruise	2'083	37.12	64.2	69.3	0.13	7.4	0.00	0.042	0.041	1.00
IDM, weighted	3'120	69.33	80.0	80.0	0.00	0.0	1.36	0.000	0.064	1.00
Inffeldgasse	1'058	4.10	14.0	14.4	5.1	3.1	0.00	0.317	0.308	1.04
JE05	1'830	13.89	27.3	36.2	1.0	24.4	0.00	0.121	0.120	1.02
KCM	1'965	20.57	37.7	45.8	1.2	17.7	1.46	0.166	0.187	1.03
Pt. I, Interstate 5	499	9.35	67.5	74.7	0.11	9.6	1.40	0.055	0.102	1.00
Pt. II, Route 174	460	4.04	31.6	37.8	1.7	16.3	0.00	0.264	0.255	1.04
Pt. III, Route 120	724	5.31	26.4	33.5	2.3	21.3	1.49	0.263	0.243	1.04
Pt. IV, Route 106	282	1.87	23.9	31.7	2.1	24.8	4.84	0.233	0.308	1.04
LUB	3'124	16.37	18.9	24.5	3.5	23.0	0.00	0.218	0.211	1.04
Pt. I, LUB rural	843	7.40	31.6	34.1	0.9	7.4	0.00	0.190	0.184	1.00
Pt. II, MLTB, outer	1'381	6.47	16.9	22.6	3.7	25.4	0.00	0.229	0.221	1.04
Pt. III, MLTB, inner	900	2.50	10.0	15.1	10.4	33.8	0.00	0.276	0.264	1.04
Manhattan	1'089	3.32	11.0	16.7	6.0	34.3	0.00	0.282	0.270	1.04
NYBus	600	0.99	5.9	17.1	11.1	65.3	0.00	0.381	0.379	1.04
OCBC	1'909	10.52	19.8	24.7	2.9	19.6	0.00	0.218	0.215	1.02
Paris	1'896	5.71	10.8	15.7	7.4	30.7	0.00	0.253	0.238	1.04
Pick-up	1'028	6.90	24.2	26.6	1.3	9.1	0.00	0.081	0.081	1.03

	t_{\max} ; s	S_{\max} ; km	V_{avrg} ; km/h	$V_{\text{roll,avrg}}$; km/h	stops/ km	Stand; % t_{\max}	$ \Delta\text{alt}/\Delta s $ norm; %	RPA; m/s ²	\hat{a} ; m/s ²	TCF; -
Smith Newton	3'697	25.88	25.2	37.3	1.0	32.5	0.00	0.149	0.138	1.03
SORT 1	159	0.53	12.1	19.8	5.6	39.0	0.00	0.210	0.210	1.04
SORT 2	188	0.93	17.8	26.6	3.2	33.0	0.00	0.187	0.187	1.04
SORT 3	211	1.47	25.0	31.2	2.0	19.9	0.00	0.184	0.184	1.04
Stockholm	1'711	6.03	12.7	17.5	4.6	27.5	0.00	0.190	0.187	1.04
Stuttgart Line 42	5'126	21.30	15.0	23.9	3.6	37.5	2.68	0.254	0.292	1.04
WHVC	1'800	20.07	40.1	46.1	0.6	12.9	0.00	0.104	0.100	1.02
Pt. I, Urban	900	5.32	21.3	26.9	1.9	20.9	0.00	0.173	0.171	1.03
Pt. II, Rural	468	5.60	43.1	47.2	0.2	8.8	0.00	0.134	0.133	1.00
Pt. III, Motorway	432	9.15	76.3	77.0	0.11	0.9	0.00	0.046	0.038	1.00
Wien Line 26A	4'195	21.91	18.8	26.0	3.4	27.6	0.45	0.208	0.207	1.04
Wundschuh	1'139	25.27	79.9	80.0	0.04	0.2	0.66	0.037	0.043	1.00
WVUC	1'408	5.32	13.6	19.2	2.3	29.3	0.00	0.160	0.156	1.03

5.5 Fuel properties

Table 29. Generic fuel properties used for the analysis and for the well-to-wheel GHG factors

Fuel	p, bar	T, °C	ρ , kg/L	Lower heating value (LHV)	GHG per unit	GHG per LHV, kgCO _{2e} /kWh _{th}	Source
Biodiesel	1	+20	0.890	9.11 kWh _{th} /L	1.92 kgCO _{2e} /L	0.211	(208 p. 24)
Fossil diesel	1	+20	0.832	9.97 kWh _{th} /L	3.24 kgCO _{2e} /L	0.325	(208 p. 24)
LNG	6	-140	0.450	12.53 kWh _{th} /kg	3.36 kgCO _{2e} /kg	0.268	(318 p. 87)
CNG	200	+20	0.132	12.53 kWh _{th} /kg	3.07 kgCO _{2e} /kg	0.245	(208 p. 24)
Electricity	ENTSO-E-mix 2014, grid continental Europe: Portugal to Romania, Denmark to Greece, former grid UCTE. Radioactive waste of $7.11 \cdot 10^{-7}$ kg-radioact./kWh _{el}					0.340 kgCO _{2e} / kWh _{el}	(268 p. 37)

5.6 Detailed data of basis vehicle models and data sources

5.6.1 Basis vehicle models

Here more details and the data sources for the basis vehicle models are enlisted. The state of technology for MY 2014 and the single components were discussed with the HDV industry for a preceding project (5 pp. 55, 98, 211).

Table 30. Input data for basis vehicle models and sources

	Tractor-trailer 40 t	Delivery truck 12 t	City bus 18 t
RRC	<i>Chosen RRC classes: Tire availability 2014¹⁰⁴</i>		
	Front to rear: B - B - BBB	Front to rear: D - D	Front to rear: D - D
Axle load	0.20, 0.25, 3 x 0.183 (149 p. 108)	0.45, 0.55 (149 p. 108)	0.38, 0.62 (149 p. 112)
Curb weigh	Tractor: 7.2 t, Trailer: 6.2 t ¹⁰⁵	Chassis 4.5 t, rigid body 1.1 t, tail-lift 0.5 t ¹⁰⁶	11.0 t ¹⁰⁷
Pay-load	<i>For researched values for the avrg. payload of the analysed HDV classes see p. 187 Table 45</i>		
	14.5 t , incl. empty trips	1.8 t , incl. empty trips	16 passengers \approx 1.1 t
Air drag	$C_d = 0.51$, $A_{cr} = 10.0 \text{ m}^2$ Re-evaluation of air drag from constant speed measurement tractor-trailer. Corrected for 15 % decrease of RRC at low velocity, (100) (319) Standard crosswind correction (101 pp. 107-111) (103 p. 57)	$C_d = 0.57$, $A_{cr} = 9.1 \text{ m}^2$ Re-evaluation of air drag from constant speed measurement delivery truck. (50 p. 160 ff.), case "with windshield". Standard crosswind correction (101 pp. 107-111) (103 p. 57)	$C_d = 0.64$, $A_{cr} = 8.0 \text{ m}^2$ Default value C_d , city buses (101 p. 113) A_{cr} estimated from technical data of existing city buses ¹⁰⁸ Standard crosswind correction (101 pp. 107-111) (103 p. 57)
Rot. Inertia	<i>Default values for wheels, clutch plate, engine. (101 pp. 126-129)</i>		
	$J_{wheels} = 185 \text{ kg}\cdot\text{m}^2$	$J_{wheels} = 39 \text{ kg}\cdot\text{m}^2$	$J_{wheels} = 71 \text{ kg}\cdot\text{m}^2$
	$J_{clutch} = 1.3 \text{ kg}\cdot\text{m}^2$	$J_{clutch} = 1.3 \text{ kg}\cdot\text{m}^2$	$J_{clutch} = 1.3 \text{ kg}\cdot\text{m}^2$
r_{dyn}	<i>Default values. (149 p. 107)</i>		
	0.492 m	0.420 m	0.465 m
Transmission losses	<u>Final drive</u> Loss map, typical long-haul tractor axle, industry 2015-06 <u>Gearbox</u> Default loss maps, industry 2014 Input speed, input torque, torque loss referred to input torque	<u>Final drive</u> Calculated generic loss map, procedure similar to (103 p. 145) <u>Gearbox</u> Default loss maps from industry, state 2014. Input speed, input torque, torque loss ref. to input torque	<u>Final drive</u> $\eta_{mech,fd} = 0.953$, fix value <u>Gearbox</u> Specific loss maps, industry Input speed, input torque, torque loss ref. to input torque <u>Hydraulic torque converter</u> Specific data, industry Curves torque ratio and input torque over speed ratio

¹⁰⁴ Continental, Goodyear, Michelin, CP Reifen Trading GmbH, reifenleader.de

¹⁰⁵ e. g. Renault T 430 T4X2, Krone Profi Liner, Schmitz S.CS Universal

¹⁰⁶ MB Atego 1224, Volvo FL 42 R 812L, rigid body Saxas MKD61-M, tail-lift Bär BC 1500 S4

¹⁰⁷ Research technical data city buses 12 m, busmagazin.de , omnibusrevue.de

¹⁰⁸ Volvo 7700, MAN Lion's City EEV, MB Citaro EEV, MAN Lion's City Hybrid EEV, MB Citaro € 6

	Tractor-trailer 40 t	Delivery truck 12 t	City bus 18 t
Gear ratios	<u>Final Drive</u> $i_{fd} = 2.65$ datasheet € 6 tractor 320 kW <u>Gearbox</u> 12-speed AMT, 14.93 to 1.00 datasheet € 6 tractor 350 kW	<u>Final Drive</u> $i_{fd} = 4.63$ datasheet € 6 truck 154 kW <u>Gearbox</u> 6-speed AMT, 6.75 to 0.78 datasheet € 6 truck 175 kW	<u>Final Drive</u> $i_{fd} = 5.77$ <u>Gearbox</u> 4-speed AT power-split hydro-mechanical 1 st gear, mech. gears 1.36, 1.00, 0.74; specific data, industry
Shifting	Default shifting curves (149 pp. 149-152,159)		Fitted shifting curves to match avrg. engine speed of measured bus on Brsw. and Graz cycle.
Target accel.	Default curves for target acceleration and deceleration. (149 pp. 139-140)		Fitted curves to match measured acceleration and deceleration behaviour ¹⁰⁹ .
Idle retarder	Default curve. (103 p. 135) This work p. 23 Figure 23 right	<i>none</i>	Hydraulic torque converter with retarder mode
	<i>Avg. power auxiliaries (103 pp. 167-234), tech. level discussed with OEM (5 pp. 61-63, 211)</i>		
Fan	Viscous clutch $P_{mech} = 0.62$ kW (p. 167)	Viscous clutch $P_{mech} = 0.52$ kW (p. 167)	Direct hydraulic drive $P_{mech} = 1.8$ kW (p. 195)
Compressor	Large, <u>Energy Saving System</u> (reduced idle losses) $P_{mech} = 1.60$ kW (p. 188)	Small, <u>Energy Saving System</u> $P_{mech} = 0.80$ kW (p. 188)	Air demand ACEA (p. 211-218), own model, see p. 55 ff., data Voith LP 490, <u>Energy Saving System (ESS)</u> , $P_{mech,avrg} = 0.77$ kW
Steer. pump	Constant pump $P_{mech} = 0.72$ kW (p. 174)	Constant pump $P_{mech} = 0.31$ kW (p. 174)	Constant pump $P_{mech} = 1.05$ kW (p. 198-203)
A/C	Standard $P_{mech} = 0.35$ kW (p. 193)	Standard $P_{mech} = 0.15$ kW (p. 193)	2-point on/off control, 40 kW _{th} $P_{mech} = 1.70$ kW see also p. 29 section 2.2.3.1
Alternator	Compact type, map "Bosch" $P_{mech} = 1.46$ kW $\eta_{avrg} = 0.75$	Compact type, map "Bosch" $P_{mech} = 1.32$ kW $\eta_{avrg} = 0.74$	Compact type, map "Bosch" $P_{mech} = 2.03$ kW $\eta_{avrg} = 0.76$
Electr. power	$P_{el} = 1.10$ kW _{el} (p. 180)	$P_{el} = 0.98$ kW _{el} (p. 181)	$P_{el} = 1.55$ kW _{el} , 0.27 kW blowers A/C estimation: 0.98 kW deliv. truck + 0.3 kW bus equipment
FL	Full load curves for standard engines of each HDV class, from data sheets		
Engine map	Map € 5 12 L tractor engine, Lot 2 project, (50 p. 27), combined with readout deviation map tractor engine, € 6 to € 5, (320 p. 938). Downsizing factor 11/12 for torque and FC.	<u>7.7 L engine 6 cylinder:</u> 600 rpm: € 5 truck engine 6.4 L (50 p. 158) 1200 to 2500 rpm: € 6 truck engine 7.7 L (321) 700 to 1100 rpm: linear interpolation <u>5.1 L engine 4 cylinder:</u> Map 7.7 L engine, scaling factor 4/6 for torque and FC	

¹⁰⁹ (161 p. 35), Abbildung 28, Messung Straße, aggressive Fahrweise (# 22)

5.6.2 Aerodynamic measures

Table 31. Sources of input data, aerodynamic measures

<i>Aerodynamic measure</i>	<i>Change C_d</i>	<i>Source</i>	<i>Method of measurement</i>
Tractor-trailer			
Rear view cameras instead of mirrors	-3 %	(322 p. 16), Aero mirror, 0 °	Wind channel; 1:1, US conventional tractor-trailer
Side panels trailer	-8 %	(323); (105); p. 4 fig. 5b); COE + 14.6 m trailer; C _{d,0°} ≈ 0.43; p. 5 table 1, skirt clearance 533 mm, ΔC _d = 0.04 ≈ -9 %	Wind channel; model 1:2.5, EU COE tractor-trailer; model 1:10, US COE tractor-trailer
Underbody cover trailer, in addition to side panels	-2 %	Estimation manufacturer (Schmitz, Wildhagen M., meeting at UBA, Dessau-Roßlau 2014-11-03, (5 p. 211))	-
Boat tail 50 cm	-8 %	(323)	Wind channel; model 1:2.5, EU COE tractor-trailer
Boat tail 100 cm	-10 %	Estimation from measurements, that a longer boat tail causes a higher C _d reduction (324) p. 83 fig. 7.23 (325) p. 15 variants, p. 44 results, case 7 and 6	Road test, FC measurement, EU COE tractor-trailer Wind channel, model 1:25, US COE tractor-trailer
Additional mass aero package current: 200 kg		Estimation manufacturer (Schmitz)	-
Additional mass aero package future: 250 kg		Estimation manufacturer (Schmitz)	-
Delivery truck			
Aero package current	-10 %	Estimation from measurement (326)	Wind channel, 1:1, EU delivery truck 18 t
Aero package future	-13 %	Estimation, aero package current with rear view cameras	-
Additional mass aero packages: 130 kg		Estimation. 2/3 mass of aero package current tractor-trailer	

5.7 Technical data of vehicle variants and saving measures

In this section the technical data of the basis HDV models is summarised, and the changes of all variants towards the basis models are enlisted and described.

Table 32. Summarised technical data of basis vehicle models

TRACTOR-TRAILER (TT)	DELIVERY TRUCK (DT)	RIGID BUS 12 M (RB)
Powertrain diesel engine, basis vehicle models		
Tires B-B-BBB, RRC 4.5 N/kN $C_d \cdot A_{cr}$ 5.10 m ² Crosswind curve TT basis i_{FD} 2.65 Standard retarder 12-speed AMT, 14.93 to 1.00 Gearbox loss maps basis Alternator compact type, "Bosch" Compressor reduced idle losses, default mean power from industry, included in $P_{aux,mech}$ P_{aux} 3.29 kW _{mech} & 1.10 kW _{el} ¹¹⁰ Diesel engine 6 cyl. 11 L, 316 kW, map basis Accel. / decel. curves truck basis Tractor 7.2 t, 3-axle trailer 6.2 t GCWR 40 t, max. payload 26.6 t <i>With average payload 14.5 t:</i> 27.8 L/100km, 62.1 gCO ₂ e/tkm	Tires D-D, RRC 6.7 N/kN $C_d \cdot A_{cr}$ 5.19 m ² Crosswind curve DT basis i_{FD} 4.63 6-speed AMT, 6.70 to 0.73 Gearbox loss maps basis Alternator compact type, "Bosch" Compressor reduced idle losses, default mean power from industry, included in $P_{aux,mech}$ P_{aux} 1.78 kW _{mech} & 0.98 kW _{el} Diesel engine 4 cyl. 5.1 L, 154 kW, map basis Accel. / decel. curves truck basis Chassis 4.5 t, rigid body 1.1 t, tail-lift 0.5 t (capacity 1.5 t·m) GVWR 12 t, max. payload 5.9 t <i>With average payload 1.8 t:</i> 19.0 L/100km, 343.0 gCO ₂ e/tkm	Tires D-D, RRC 6.4 N/kN $C_d \cdot A_{cr}$ 5.12 m ² Crosswind curve RB basis i_{FD} 5.77 4-speed AT, hydraul. Tq-converter, mech. gears 1.36 to 0.74 Gearbox loss maps basis Alternator compact type, "Bosch" Compressor reduced idle losses, power curves "Voith", own model P_{aux} 4.55 kW _{mech} & 1.55 kW _{el} Diesel engine 6 cyl. 7.7 L, 220 kW, map basis Accel. / decel. curves bus basis Curb weight 11.0 t GVWR 18 t, max number of passengers: 80 ¹¹¹ <i>With average utilisation 16 pass.:</i> 41.0 L/100km, 83.2 gCO ₂ e/pkm

5.7.1 Single saving measures

Here the data of the analysed variants of the HDV models are enlisted. The incremental changes towards the basis modes are shown, hence only the components which were improved for a lower power consumption or for a higher efficiency.

Table 33. Technical data of basis vehicle models with single saving measures

TRACTOR-TRAILER (TT)	DELIVERY TRUCK (DT)	RIGID BUS 12 M (RB)
a) Tires lowest rolling resistance, current¹¹²		
Tires B-B-AAA, RRC 4.0 N/kN 27.0 L/100km, 60.4 gCO ₂ e/tkm	Tires C-D, RRC 6.3 N/kN 18.9 L/100km, 340.5 gCO ₂ e/tkm	Tires C-D, RRC 6.0 N/kN 40.8 L/100km, 82.7 gCO ₂ e/pkm
b) Tires lowest rolling resistance, future		
Tires A-A-AAA, RRC 3.6 N/kN 26.4 L/100km, 59.1 gCO ₂ e/tkm	Tires A-A, RRC 3.8 N/kN 17.9 L/100km, 322.6 gCO ₂ e/tkm	Tires A-A, RRC 3.6 N/kN 39.2 L/100km, 79.5 gCO ₂ e/pkm

¹¹⁰ Here P_{aux} in kW_{mech} is the constant mean value to be entered in VECTO. In addition the mech. power from the alternator, calculated from its performance map and the value for kW_{el}, plus in case of buses the power demand from the separate compressor model are considered in the simulations.

¹¹¹ The theoretical max. passenger capacity can be calculated by $(GVWR - m_{curb} - m_{driver}) / 0.068$ t, here ≈ 103 . Due to the limitation of 4 passengers/m² for stances the effective max. capacity is 80 passengers. This value decreases, if the theoretical max. capacity gets lower than 80 passengers by an increased curb weight of the bus.

¹¹² State 2015-10. Since 2016 tractor tires of RRC class A are available, see also the footnote on p. 99.

TRACTOR-TRAILER (TT)	DELIVERY TRUCK (DT)	RIGID BUS 12 M (RB)
c) Aero package current		
<u>Tractor-trailer:</u> Trailer with side panels and boat tail 0.5 m $C_d \cdot A_{cr}$ 4.28 m ² . Crosswind curve tractor-trailer panels Trailer 6.4 t (+0.2 t), max. payload 26.4 t (-0.2 t) 26.1 L/100km, 58.3 gCO ₂ e/tkm	<i>Rigid bus: Air drag not relevant.</i> <u>Delivery truck:</u> Cabin w. fairings to body, chassis w. underbody cover, body w. side panels, boat tail 0.5 m. $C_d \cdot A_{cr}$ 4.67 m ² . Crosswind curve deliv. truck panels. Chassis 4.55 t (+0.05 t), rigid body 1.18 t (+0.08 t), max. payload 5.77 t (-0.13 t) 18.7 L/100km, 337.9 gCO ₂ e/tkm	
d) Aero package future		
<u>Tractor-trailer:</u> Tractor w. rear view cameras, trailer w. underbody cover, side panels and boat tail 1.0 m. $C_d \cdot A_{cr}$ 3.93 m ² . Crosswind curve tractor-trailer panels Trailer 6.45 t (+0.25 t) max. payload 26.35 t (-0.25 t) 25.4 L/100km, 56.8 gCO ₂ e/tkm	<i>Rigid bus: Air drag not relevant.</i> <u>Delivery truck:</u> Cabin w. fairings to body, rear view cameras, chassis w. underbody cover, body w. side panels and boat tail 1.0 m $C_d \cdot A_{cr}$ 4.51 m ² . Crosswind curve deliv. truck panels. Chassis 4.55 t (+0.05 t), rigid body 1.18 t (+0.08 t), max. payload 5.77 t (-0.13 t) 18.6 L/100km, 335.7 gCO ₂ e/tkm	
e) Speed limit 80 km/h		
Max. velocity 80 km/h + 3.0 min/100km 26.8 L/100km, 60.0 gCO ₂ e/tkm	Max. velocity 80 km/h + 0.7 min/100km 18.9 L/100km, 340.4 gCO ₂ e/tkm	Max. target speed VECTO urban bus cycles: 68 km/h → Limit 80 km/h not relevant
f) Lightweight current		
3-axle trailer 5.5 t (-0.7 t) Max. payload 27.3 t (+0.7 t) 27.5 L/100km, 61.4 gCO ₂ e/tkm	Tail-lift 0.3 t (-0.2 t) (capacity 0.6 t-m, decrease by 0.9 t-m) Max. payload 6.1 t (+0.2 t) 18.8 L/100km, 339.3 gCO ₂ e/tkm	Curb weight 10.5 t (-0.5 t) 40.0 L/100km, 81.2 gCO ₂ e/pkm
g) Lightweight future		
Tractor 7.0 t (-0.2 t), 3-axle trailer 5.5 t (-0.7 t) Max. payload 27.5 t (+0.9 t) 27.4 L/100km, 61.3 gCO ₂ e/tkm	Chassis 4.3 t (-0.2 t), tail-lift 0.3 t (-0.2 t) Max. payload 6.3 t (+0.4 t) 18.5 L/100km, 334.1 gCO ₂ e/tkm	Curb weight 10.3 t (-0.7 t) 39.7 L/100km, 80.5 gCO ₂ e/pkm
h) 2-axle trailer		
<i>Delivery truck and rigid bus: No Trailer.</i> <u>Tractor-trailer:</u> 2-axle trailer 5.55 t (-0.65 t), axle distance ≥ 1.8 m, GCWR 38 t [Compare e. g. German StVZO §34 (6) 3. b)], max. payload 25.25 t (-1.35 t) 27.3 L/100km, 61.2 gCO ₂ e/tkm		
i) Retarder w. clutch		
Retarder w. clutch, no idle losses 27.4 L/100km, 61.32 gCO ₂ e/tkm	No retarder	Retarder integrated in hydraulic torque converter.
j) Reduced drivetrain friction		
Lump sum decrease of losses from gearbox and final drive by 25 %		
27.4 L/100km, 61.29 gCO ₂ e/tkm	18.8 L/100km, 338.8 gCO ₂ e/tkm	40.3 L/100km, 81.8 gCO ₂ e/pkm
k) Start-stop automatic		
Time share of stops ca. 1.5 % of cycle duration, not relevant for FC	Start-stop automatic 18.6 L/100km, 335.0 gCO ₂ e/tkm	Start-stop automatic 38.7 L/100km, 78.5 gCO ₂ e/pkm

TRACTOR-TRAILER (TT)	DELIVERY TRUCK (DT)	RIGID BUS 12 M (RB)
l) Efficient engine auxiliaries, current		
Variable steering pump, compressor w. clutch, LED lighting P _{aux} 2.31 kW _{mech} & 0.96 kW _{el} 27.5 L/100km, 61.5 gCO _{2e} /tkm	Variable steering pump, compressor w. clutch, LED lighting P _{aux} 1.55 kW _{mech} & 0.84 kW _{el} 18.8 L/100km, 338.8 gCO _{2e} /tkm	Compressor power curve "clutch". Variable hydraulic fan, variable steering pump, A/C compressor 3-point control (1, 0.5, 0), heat insulation glazing, insulation wall and doors, LED lighting P _{aux} 2.89 kW _{mech} & 1.41 kW _{el} 38.4 L/100km, 77.9 gCO _{2e} /pkm
m) Efficient engine auxiliaries, future		
Fan w. viscous clutch and decoupler, electrical steering pump, compressor w. clutch, LED lighting P _{aux} 1.52 kW _{mech} & 1.16 kW _{el} 27.4 L/100km, 61.2 gCO _{2e} /tkm	Compressor power curve "clutch", air demand and idle loss fitted to match industry value for P _{compr,avrg} . Fan w. viscous clutch and decoupler, electrical steering pump, LED lighting P _{aux} 0.47 kW _{mech} & 0.91 kW _{el} 18.6 L/100km, 334.8 gCO _{2e} /tkm	Compressor power curve "clutch". 2 nd alternator, electrical fan, electrical steering pump, A/C compressor continuous control, heat insulation glazing, insulation wall and doors P _{aux} 0.14 kW _{mech} & 2.13 kW _{el} 36.3 L/100km, 73.5 gCO _{2e} /pkm
n) Regenerative braking with engine future auxiliaries		
<i>The long haul cycle contains some long braking phases. It can be considered, that the standard energy storages, here battery and air vessels, cannot absorb the whole delivered current and air during braking. ⇒ No model for filling degree of 24 V batteries and air vessels, regen. braking not simulated</i>	Like m), "Efficient engine auxiliaries, future" Alternator and compressor at max. power during braking, filling of battery and air vessels. 18.3 L/100km, 330.4 gCO _{2e} /tkm	Like m), "Efficient engine auxiliaries, future" Alternator and compressor at max. power during braking, filling of battery and air vessels. 35.4 L/100km, 71.9 gCO _{2e} /pkm
o) Exhaust heat power generation		
Small steam power process (<u>O</u> rganic <u>R</u> ankine <u>C</u> ycle), max 20 kW _{mech} , powered by exhaust heat downstream aftertreatment. Expander coupled with chain drive to cardan shaft. Tractor 7.35 t (+0.15 t), max. payload 26.45 t (-0.15 t) 27.2 L/100km, 60.8 gCO _{2e} /tkm	<i>The instationary behaviour of the steam process during urban traffic cannot be calculated with the simple quasi-stationary model. Hence only the long haul cycle with slow changes of engine operation point and exhaust flow was simulated. In addition HDV in urban traffic have problems to reach sufficient exhaust temperatures for SCR catalysis and particle filter regeneration. It can be assumed, that the surplus heat downstream the aftertreatment is not enough to feed a steam power process.</i>	
p) Combustion engine higher efficiency		
Lump sum increase of average efficiency of ICE by + 0.01		
27.1 L/100km, 60.8 gCO _{2e} /tkm	18.6 L/100km, 334.5 gCO _{2e} /tkm	40.0 L/100km, 81.1 gCO _{2e} /pkm
q) EcoRoll and Look-Ahead-Coasting		
EcoRoll & Look-Ahead-Coasting -0.13 min/100km 27.3 L/100km, 61.0 gCO _{2e} /tkm	<i>EcoRoll and Look-Ahead-Coasting are only useful in constant driving phases on hilly roads, e. g. long haul or regional delivery traffic. These functions are not suited for urban traffic.</i>	
r) Limited braking deceleration		
<i>Limited braking deceleration does not match the use case long haulage.</i>	Basis acceleration curve truck, limited deceleration curve truck (min. -0.8 m/s ²), +1.9 min/100km 18.9 L/100km, 340.6 gCO _{2e} /tkm	Basis acceleration curve bus, limited deceleration curve bus (min. -0.8 m/s ²), +14.8 min/100km 40.1 L/100km, 81.4 gCO _{2e} /pkm

5.7.2 Alternative powertrain concepts

Here the technical data for the models with alternative powertrains are given. Like before, only the incremental changes towards the basis HDV models are enlisted, the rest of the virtual vehicles remained the same.

Table 34. Technical data of alternative powertrain concepts

TRACTOR-TRAILER (TT)	DELIVERY TRUCK (DT)	RIGID BUS 12 M (RB)
A) Gas engine		
i_{FD} 2.80 (higher rated speed than basis diesel engine) Stoichiometric gas engine, 6 cyl. 12.2 L, 316 kW @ 1900 rpm LNG @ 6 bar / -160 °C, tank 670 L, half-full (151 kg-gas) Range full tank, max. payload: 990 km Tractor 7.1 t (-0.1 t) Max. payload 26.7 t (+0.1 t) 25.9 kg/100km, 60.1 gCO _{2e} /tkm	i_{FD} 4.00 (lower rated speed than basis diesel engine) Stoichiometric gas engine, 4 cyl. 5.9 L, 154 kW @ 1900 rpm CNG @ 200 bar / +20 °C, tanks 500 L, half-full (33 kg-gas) Range full tank, max. payload: 310 km Chassis 4.7 t (+0.2 t) Max. payload 5.7 t (-0.2 t) 17.4 kg/100km, 296.2 gCO _{2e} /tkm	i_{FD} 5.00 (lower rated speed than basis diesel engine), $\eta_{mech,FD}$ 0.956 Stoichiometric gas engine, 6 cyl. 8.5 L, 220 kW @ 1900 rpm CNG @ 200 bar / +20 °C, tanks 1400 L, half-full (92 kg-gas) Range full tank, 80 pass.: 380 km Curb weight 11.6 t (+0.6 t) 39.3 kg/100km, 75.3 gCO _{2e} /pkm
B) Diesel-electrical parallel hybrid vehicles		
Additional powertr. components: Permanent magnet synchronous machine (PMSM) with clutch, ± 1200 Nm, ± 140 kW _{mech} , Tq _{EM,cont} 780 Nm, $n_{EM,com}$ 1470 rpm, (0.3 t, 3 kg·m ²) Li-Ion battery 12 kWh, SOC 40 to 60 %, 0.5 t (power cells) $\eta_{el,conv} = 0.95$, $\eta_{el,batt} = 0.95$ Start-stop automatic Tractor 8.0 t (+0.8 t), max. payload 25.8 t (-0.8 t) 27.2 L/100km, 60.9 gCO _{2e} /tkm	Additional powertr. components: PMSM w. clutch, ± 420 Nm, ± 45 kW _{mech} , Tq _{EM,cont} 270 Nm, $n_{EM,com}$ 920 rpm, (0.2 t, 1 kg·m ²) Li-Ion battery 2 kWh, SOC 40 to 60 %, 0.1 t (power cells) $\eta_{el,conv} = 0.95$, $\eta_{el,batt} = 0.95$ Start-stop automatic Chassis 4.8 t (+0.3 t), max. payload 5.6 t (-0.3 t) 17.4 L/100km, 313.6 gCO _{2e} /tkm	i_{FD} 4.78, $\eta_{mech,FD}$ 0.957 12-speed AMT ¹¹³ , 14.94 to 1.00, $\eta_{mech,gear,indir}$ 0.96, $\eta_{mech,gear,dir}$ 0.98 PMSM, +400/-800 Nm, +70 / -120 kW _{mech} , Tq _{EM,cont} 400 Nm, $n_{EM,com}$ 1670 rpm, (0.25 t, 2 kg·m ²) Li-Ion battery 5 kWh, SOC 40 to 60 %, 0.2 t (power cells) $\eta_{el,conv} = 0.95$, $\eta_{el,batt} = 0.95$ Start-stop automatic, electric auxiliaries "basis" (steering pump & compr. w/o idle), P _{aux} 6.41 kW _{el} Diesel engine 4 cyl. 5.1 L, 154 kW (0.55 t) Curb weight 11.7 t (+0.7 t) 30.7 L/100km, 62.3 gCO _{2e} /pkm
C) Diesel-electrical serial hybrid vehicles		
<i>Tractor-trailer and delivery truck: No serial hybrid.</i> Rigid bus 12 m: i_{FD} 5.77, $\eta_{mech,FD}$ 0.953 PMSM, ± 2000 Nm, +140/-240 kW _{mech} , Tq _{EM,cont} 1300 Nm, $n_{EM,com}$ 1470 rpm, (0.40 t, 5 kg·m ²). Supercapacitor 0.5 kWh, SOC 20 to 100 %, 200 kW _{el} (0.5 t). $\eta_{el,conv} = 0.95$, $\eta_{el,SCap} = 0.95$. Generator (PMSM) Tq _{EM,cont} 1000 Nm, $n_{EM,com}$ 1770 rpm, +170 kW _{el} @ 2200 rpm (0.35 t, 3 kg·m ²). Start-stop automatic Electrical auxiliaries "basis" (steering pump & compr. w/o idle). P _{aux} 6.41 kW _{el} Diesel engine 6 cyl. 6.4 L, 185 kW (0.62 t). Curb weight 12.3 t (+1.3 t). ICE on for SOC \leq 30 %. 33.0 L/100km, 67.0 gCO _{2e} /pkm		

¹¹³ Average payload 16 passengers: Driveaway in 5th gear (CAN Bus data from road measurement (244 pp. 17, 57)), effective gear ratios from 5.54 to 1.00. Full payload 80 passengers: Driveaway in 3rd gear (assumption, to reach acceptable acceleration performance), effective gear ratios from 9.04 to 1.00.

TRACTOR-TRAILER (TT)	DELIVERY TRUCK (DT)	RIGID BUS 12 M (RB)
D) Battery-electrical vehicle		
<i>Tractor-trailer: Not analysed.</i> Delivery truck: i_{FD} 3.70, 3-speed AT (w/o torque converter), 1.85, 1.36, 1.00, gear loss maps basis from AT of rigid bus PMSM, ± 1100 Nm, ± 160 kW _{mech} , Tq _{EM,cont} 720 Nm, n _{EM,com} 1470 rpm, (0.3 t, 3 kg·m ²), Li-Ion battery 150 kWh, SOC 20 to 100 %, 1.34 t (energy cells), $\eta_{el,conv} = 0.95$, $\eta_{el,batt} = 0.95$, max. range full payload.: 133 km Electrical. auxiliaries "basis" (no engine fan; steering pump & compressor w/o idle), cooling circuit for electrics (coolant pump, radiator, fan), basis lighting. P _{aux} 2.44 kW _{el} Chassis 5.3 t (+0.8 t). Max. payload 5.1 t (-0.8 t) Energy consumption from grid, $\eta_{charge} = 0.90$ 0.86 kWh _{el} /km, 162.5 gCO _{2e} /tkm		Rigid bus 12 m: i_{FD} 5.77, $\eta_{mech,FD}$ 0.953 PMSM, ± 2000 Nm, +140/-240 kW _{mech} , Tq _{EM,cont} 1300 Nm, n _{EM,com} 1470 rpm, (0.40 t, 5 kg·m ²), Li-Ion battery 300 kWh, SOC 20 to 100 %, 2.73 t (energy cells), $\eta_{el,conv} = 0.95$, $\eta_{el,batt} = 0.95$, max. range w. 80 pass.: 165 km (4 rounds UB cycle) Electrical. auxiliaries "basis" (no engine fan; steering pump & compressor w/o idle), cooling circuit for electrics (coolant pump, radiator, fan), basis lighting. P _{aux} 5.1 kW _{el} After 4 rounds (160 km, 8.8 h): Charging with 300 kW _{el} = 1 C for 40 min or with 26 kW _{el} = 0.087 C for 8 h Curb weight 13.3 t (+2.3 t). Max passengers: 69 (-11) Energy consumption from grid, $\eta_{charge} = 0.90$ 1.31 kWh _{el} /km, 27.8 gCO _{2e} /pkm
E) Battery-electrical vehicle with intermediate charging		
<i>Tractor-trailer and delivery truck: Not analysed.</i> Rigid bus 12 m: Like D), with: Li-Ion battery 80 kWh, SOC 20 to 100 %, 0.73 t (energy cells), max. range w. 80 pass.: 48 km. After 1 round on UB cycle (40 km, 2.2 h). Charging with 200 kW _{el} = 2.5 C for 14 min Curb weight 11.3 t (+0.3 t), max passengers: 80 (± 0) Energy consumption from grid, $\eta_{charge} = 0.90$ 1.20 kWh _{el} /km, 25.5 gCO _{2e} /pkm		

5.7.3 Bundles of current possible saving measures

In this section the changes of the models with the current possible technology bundles towards the basis vehicle models are given.

Table 35. Changes to basis vehicle models for bundles of saving measures "current"

TRACTOR-TRAILER (TT)	DELIVERY TRUCK (DT)	RIGID BUS 12 M (RB)
Measures which do not affect the powertrain structure		
Tires B-B-AA ¹¹⁴ , RRC 4.0 N/kN Aero package "current" (+0.2 t) Max. velocity 80 km/h, EcoRoll & Coasting (+2.6 min/100km) Lightweight 2-axle trailer, 5.25 t (-0.95 t), GCWR 38 t Retarder w. clutch, no idle losses Auxiliaries "current" P _{aux} 2.31 kW _{mech} & 0.96 kW _{el}	Tires C-D, RRC 6.3 N/kN Aero package "current" (+0.13 t) Max. velocity 80 km/h & limited braking decel. (+2.2 min/100km) Start-stop automatic Auxiliaries "current" P _{aux} 1.55 kW _{mech} & 0.84 kW _{el} Rigid body 1.18 t (+0.08 t), tail-lift 0.3 t (-0.2 t)	Tires C-D, RRC 6.0 N/kN Start-stop automatic Auxiliaries "current" P _{aux} 2.89 kW _{mech} & 1.41 kW _{el} Limited braking deceleration (+14.8 min/100km)
Diesel engine, bundle "current"		
Max. payload 25.55 t (-1.05 t) 22.7 L/100km, 50.7 gCO _{2e} /tkm	Chassis 4.55 t (+0.05 t), max. payload 5.97 t (+0.07 t) 17.4 L/100km, 313.0 gCO _{2e} /tkm	Curb weight 10.5 t (-0.5 t) 34.2 L/100km, 69.4 gCO _{2e} /pkm

¹¹⁴ State 2015-10. Since 2016 tractor tires of RRC class A are available, see also the footnote on p. 99.

TRACTOR-TRAILER (TT)	DELIVERY TRUCK (DT)	RIGID BUS 12 M (RB)
A) Gas engine, bundle "current"		
Gas engine & LNG tank. Range w. full tank & payload: 1'190 km Tractor 7.1 t, max. payload 25.65 t (-0.95 t) 21.4 kg/100km, 49.7 gCO _{2e} /tkm	Gas engine & CNG tanks. Range w. full tank & payload: 330 km Chassis 4.55 t (+0.05 t), max. payload 5.97 t (+0.07 t) 15.7 kg/100km, 268.5 gCO _{2e} /tkm	Gas engine & CNG tanks. Range w. full tank & 80 pass.: 450 km Curb weight 11.1 t (+0.1 t) 33.2 kg/100km, 63.6 gCO _{2e} /pkm
B) Diesel-electrical parallel hybrid vehicles, bundle "current"		
Additional hybrid components Tractor 8.0 t (+0.8 t), max. payload 24.75 t (-1.85 t) 22.1 L/100km, 49.5 gCO _{2e} /tkm	Additional hybrid components Chassis 4.85 t (+0.35 t), max. payload 5.67 t (-0.23 t) 16.0 L/100km, 288.7 gCO _{2e} /tkm	Powertrain parallel hybrid Electrical auxiliaries "current" (steering pump w/o idle) P _{aux} 4.71 kW _{el} Curb weight 11.2 t (+0.2 t) 27.5 L/100km, 55.8 gCO _{2e} /pkm
C) Diesel-electrical serial hybrid vehicles, bundle "current"		
<i>Tractor-trailer and delivery truck: No serial hybrid.</i>		
<u>Rigid bus 12 m:</u> Powertrain serial hybrid. Electrical auxiliaries "current" (steering pump w/o idle), P _{aux} 4.71 kW _{el} . Curb weight 11.8 t (+0.8 t). 28.8 L/100km, 58.4 gCO _{2e} /pkm		
D) Battery-electrical vehicle, bundle "current"		
<i>Tractor-trailer: Not analysed.</i> <u>Delivery truck:</u> Powertrain battery electrical., battery 140 kWh, 1.27 t. Range w. full payload.: 141 km Electrical auxiliaries "current" (no engine fan; steering pump w/o idle), cooling circuit for electrics (coolant pump, radiator, fan), LED lighting, 2.3 kW _{el} Chassis 5.28 t (+0.78 t), max. payload 5.24 t (-0.66 t) Energy consumption from grid, η _{charge} = 0.90 0.79 kWh _{el} /km, 149.7 gCO _{2e} /tkm	<u>Rigid bus 12 m:</u> Tires C-D, RRC 6.0 N/kN Powertrain battery electrical., battery 280 kWh, 2.55 t. Range w. 80 pass.: 172 km (4 rounds) Electrical auxiliaries "current" (no engine fan; steering pump w/o idle), cooling circuit for electrics (coolant pump, radiator, fan), LED lighting, 3.87 kW _{el} Curb weight 12.6 t (+1.6 t) Max passengers: 79 (-1) Energy consumption from grid, η _{charge} = 0.90 1.21 kWh _{el} /km, 25.6 gCO _{2e} /pkm	
E) Battery-electrical vehicle with intermediate charging, bundle "current"		
<i>Tractor-trailer and delivery truck: Not analysed.</i>		
<u>Rigid bus 12 m:</u> Like D) "current", with: Li-Ion battery 70 kWh (0.64 t), max. range w. 80 pass.: 45 km. Curb weight 10.7 t (-0.3 t), max passengers: 80 (+/- 0). Energy consumption from grid, η _{charge} = 0.90 1.13 kWh _{el} /km, 24.1 gCO _{2e} /pkm		

5.7.4 Bundles of future possible saving measures

Here the data for the models with the future possible technology bundles are shown. Only the incremental changes towards the basis HDV models are enlisted.

Table 36. Changes to basis vehicle models for bundles of saving measures "future"

TRACTOR-TRAILER (TT)	DELIVERY TRUCK (DT)	RIGID BUS 12 M (RB)
Measures which do not affect the powertrain structure		
Tires A-A-AA ¹¹⁵ , RRC 3.6 N/kN Aero package "future" Max. velocity 80 km/h, EcoRoll & Coasting (+2.6 min/100km) Lightweight tractor, lightweight 2-axle trailer 5.30 t (-0.9 t), GCWR 38 t Reduced gearbox losses Retarder w. clutch, no idle losses Auxiliaries "future" P_{aux} 1.52 kW _{mech} & 1.16 kW _{el} Exhaust heat power generation Diesel engine η_{avrg} +0.01	Tires A-A, RRC 3.8 N/kN Aero package "future" Max. velocity 80 km/h & limited braking decel. (+2.2 min/100km) Reduced gearbox losses Start-stop automatic Auxiliaries "future" with regenerative braking P_{aux} 0.47 kW _{mech} & 0.91 kW _{el} Diesel engine η_{avrg} +0.01 Rigid body 1.18 t (+0.08 t), tail-lift 0.3 t (-0.2 t)	Tires A-A, RRC 3.6 N/kN Reduced gearbox losses Start-stop automatic Auxiliaries "future" with regenerative braking P_{aux} 0.14 kW _{mech} & 2.13 kW _{el} Diesel engine η_{avrg} +0.01 Limited braking deceleration (+14.8 min/100km)
Diesel engine, bundle "future"		
Tractor 7.15 t (-0.05 t), max. payload 25.55 t (-1.05 t) 20.1 L/100km, 45.0 gCO _{2e} /tkm	Chassis 4.35 t (-0.15 t), max. payload 6.17 t (+0.27 t) 15.0 L/100km, 270.7 gCO _{2e} /tkm	Curb weight 10.3 t (-0.7 t) 28.2 L/100km, 57.1 gCO _{2e} /pkm
A) Gas engine, bundle "future"		
Gas engine η_{avrg} + 0.01, LNG tank, max. range : 1'310 km Tractor 7.05 t (-0.15 t), max. payload 25.65 t (-0.95 t) 19.0 kg/100km, 44.1 gCO _{2e} /tkm	Gas engine η_{avrg} + 0.01, CNG tanks, max. range : 380 km Chassis 4.55 t (+0.05 t), max. payload 5.97 t (+0.07 t) 13.7 kg/100km, 233.6 gCO _{2e} /tkm	Gas engine η_{avrg} + 0.01, CNG tanks, max. range : 540 km Curb weight 10.9 t (-0.1 t) 27.4 kg/100km, 52.6 gCO _{2e} /pkm
B) Diesel-electrical parallel hybrid vehicles, bundle "future"		
Additional hybrid components Tractor 8.0 t (+0.8 t), max. payload 24.75 t (-1.85 t) 19.5 L/100km, 43.7 gCO _{2e} /tkm	Additional hybrid components Chassis 4.65 t (+0.15 t), max. payload 5.87 t (-0.03 t) 13.9 L/100km, 249.9 gCO _{2e} /tkm	Powertrain parallel hybrid Electrical auxiliaries "future", P_{aux} 2.93 kW _{el} Curb weight 11.0 t (\pm 0 t) 20.5 L/100km, 41.6 gCO _{2e} /pkm
C) Diesel-electrical serial hybrid vehicles, bundle "future"		
<i>Tractor-trailer and delivery truck: No serial hybrid.</i>		
Rigid bus 12 m: Powertrain serial hybrid. Reduced gearbox losses. Electrical auxiliaries "future", P_{aux} 2.93 kW _{el} , curb weight 11.6 t (+0.6 t). 22.1 L/100km, 44.8 gCO _{2e} /pkm		

¹¹⁵ State 2015-10. Since 2016 tractor tires of RRC class A are available, see also the footnote on p. 99.

TRACTOR-TRAILER (TT)	DELIVERY TRUCK (DT)	RIGID BUS 12 M (RB)
D) Battery-electrical vehicle, bundle "future"		
<i>Tractor-trailer: Not analysed.</i> <u>Delivery truck:</u> Drivetrain battery electrical. Reduced gearbox losses. Battery 120 kWh, 1.09 t. Range full payload.: 139 km Electrical. auxiliaries "future" (no engine fan), cooling circuit for electrics (coolant pump, radiator, fan), P_{aux} 2.30 kW _{el} Chassis 4.9 t (+0.4 t), max. payload 5.62 t (-0.28 t) Energy consumption from grid, $\eta_{charge} = 0.90$ <i>0.68 kWh_{el}/km, 128.1 gCO_{2e}/tkm</i>	<u>Rigid bus 12 m:</u> Powertrain battery electrical. Reduced gearbox losses. Battery 220 kWh, 2 t. Range w. 80 pass.: 169 km (4 rounds) Electrical. auxiliaries "future" (no engine fan), cooling circuit for electrics (coolant pump, radiator, fan), P_{aux} 2.93 kW _{el} Curb weight 11.9 t (+0.9 t) Max passengers: 80 (+/-0) Energy consumption from grid, $\eta_{charge} = 0.90$ <i>0.95 kWh_{el}/km, 20.1 gCO_{2e}/pkm</i>	
E) Battery-electrical vehicle with intermediate charging, bundle "future"		
<i>Tractor-trailer and delivery truck: Not analysed. Rigid bus 12 m: Like D) "future", with: Li-Ion battery 60 kWh (0.55 t). Range w. 80 pass.: 47 km. Curb weight 10.6 t (-0.4 t). Energy consumption from grid, $\eta_{charge} = 0.90$ <i>0.91 kWh_{el}/km, 19.2 gCO_{2e}/pkm</i></i>		

5.7.5 Vehicle models to simulate own measurements

Below the data for the HDV models is given, which were used to simulate own measured cycles.

Table 37. Technical data of vehicle models of measurements at the emissions department of IVT

LONG HAUL TRACTOR € 5	DELIVERY TRUCK € 5	RIGID BUS € 5
<i>Vehicle model used for:</i> • FC motorway "Wundschuh". Compare p. 84 Table 14 Tires RRC B, 4.5 N/kN $C_d \cdot A_{cr}$ 5.1 m ² Crosswind curve tractor-trailer basis i_{FD} 3.07; drive tires 385/55R22.5, total J_{wh} 189 kg·m ² , r_{dyn} 0.522 m 12-speed AMT, 14.93 to 1.00 Gearbox loss maps basis Standard retarder HDV alternator compact type P_{aux} 3.29 kW _{mech} & 1.10 kW _{el} Diesel ICE 350 kW, map 12 L € 5 Tractor 8.5 t, 3-axle trailer total 19.4 t, m_{test} 27.9 t (50 pp. 154 ff., Actros € 5)	<i>Vehicle model used for:</i> • Simulation chassis dyno tests IVT, cycles RD12 & UD12-flat, rigid body 7.2 m 17 pallets, m_{test} 9.3 t, RRC 7.8 N/kN, $C_d \cdot A_{cr}$ 4.83 m ² , no crosswind, P_{aux} intermitt. from measurement, avrg. 4.4 kW (1.9 to 8.0) for RD12, 3.5 kW (1.9 to 9.5) for UD12 • Simulation road tests, m_{test} 12.00 t for cycle "Inffeldgasse", RRC 7.2 N/kN, $C_d \cdot A_{cr}$ 5.19 m ² , side-wind curve deliv. truck basis, P_{aux} intermittent for cycle IG 3.8 kW (2.1 to 9.3). Compare p. 29 Figure 30, p. 61 Figure 61, p. 85 Table 15 i_{FD} 4.30, drive tires 265/70R22.5, total J_{wh} 39 kg·m ² , r_{dyn} 0.421 m 6-speed AMT, 6.70 to 0.73 Gearbox loss maps basis Diesel ICE 175 kW, map 6.4 L € 5 (50 p. 160 ff.)	<i>Vehicle model used for:</i> • FC "Braunschweig", "Graz", dyno, m_{test} 15.06 t, RRC 6.5 N/kN, $C_d \cdot A_{cr}$ 5.17 m ² , no side-wind Compare p. 86 Table 16 i_{FD} 5.47, drive tires 275/70R22.5, total J_{wh} 97 kg·m ² , r_{dyn} 0.465 m 4-speed AT, power split 1 st gear with hydraul. Tq-converter, mech. gears 1.36 to 0.74 Gearbox loss maps basis HDV alternator compact type Compressor ESS (energy saving system, reduced idle losses, own model, separate input data) P_{aux} 2.1 kW _{mech} & 1.28 kW _{el} Diesel ICE 235 kW, map 11 L € 5 Curb weight 12.44 t (Dyno IVT, 2016-01)

For the vehicle model "Delivery truck € 5" the driving resistances needed to be adopted for the simulation of the chassis dyno tests, to meet the overall positive tractive work at the axles of the driven wheels ($W_{\text{tract,wh}}$). This value was calculated from the measurands velocity and tractive force at the dynamometer¹¹⁶, in the contact points with the driven wheels of the truck. Hence from the equilibrium of forces the positive tractive power and subsequently the work at the axles of the vehicle were determined. It was found, that with the original dyno settings the work would be 2 to 6 % below the measured value. These influences contributed amongst others to the uncertainty of measurement:

- Slip and power losses between the driven wheels and the rollers of the dynamometer.
- Deviations between assumed and effective losses of the idling drivetrain from gearbox output to wheels during the calibration via the loss run procedure.
- Temperature of the tires
- Uncertainty of measurement of the dynamometer itself.

The reason of the deviation from the calculated to the measured tractive work could not be determined afterwards. To approximate the tractive work, the rolling resistance coefficient (RRC) of the model was increased, because it is independent on the velocity and contributes only during driving. The correlation between rolling resistance and the deviations of simulated tractive work and FC from the measured values are shown in Figure 191.

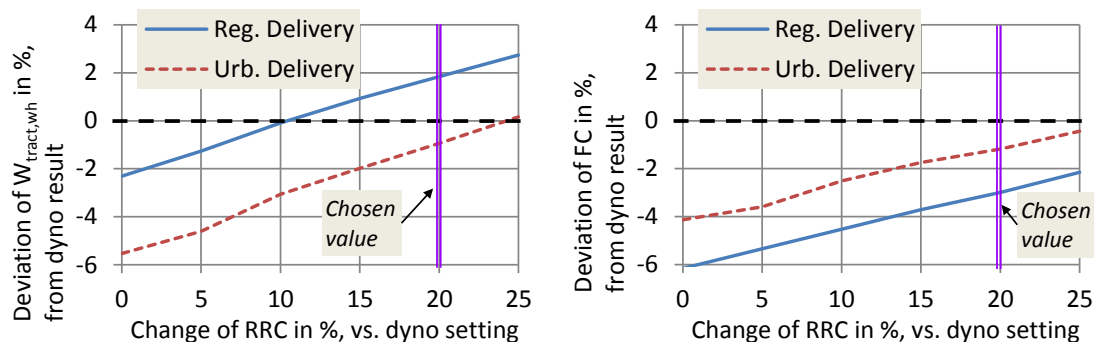


Figure 191. Change of simulated RRC, deviation of tract. work $W_{\text{tract,wh}}$ & FC from the measurands.

The simulated RRC of the delivery truck EURO V was increased by 20 % to better meet $W_{\text{tract,wh}}$ and FC, compare p. 85 Table 15.

In case of the model "Rigid bus € 5" the tractive work was met for the Graz and Braunschweig cycle with a deviation of -1.4 and +0.1 % with the original dyno settings, see also p. 86 Table 16. That is acceptable and in the uncertainty of the whole measurement chain.

¹¹⁶ The dynamometer calculates the tractive force at the contact point between wheels and roller via the measured force at the engine brake plus taking into account the acceleration forces of the rollers and the losses between tires and rollers. The necessary parameters are determined by a so-called "loss-run" procedure.

5.7.6 Additional vehicle models for check of plausibility

In this section the VECTO input for the models is shown, which were applied for the simulation on cycles, where published results for fuel- or energy consumption were available.

Table 38. Technical data of additional vehicle models, similar to measured vehicles

AB: ARTICULATED BUS	AB PHEV: DIESEL-ELECTRICAL PARALLEL HYBRID ARTIC. BUS	DTS: BATTERY-ELECTRICAL DELIVERY TRUCK "SMITH"
<p><u>Used for:</u> FC; cycles HUB, UB, SUB Compare p. 94 section 2.6.3.4 Tires D-D-D, RRC 6.2 N/kN $C_d \cdot A_{cr}$ 5.12 m² Crossw. basis i_{FD} 6.21, $\eta_{mech,FD}$ 0.952, tires 275/70R22.5, $J_{wh,tot}$ 119 kg·m², r_{dyn} 0.465 m 4-speed AT, power split 1st gear with hydraul. Tq-converter, gears 1.36 to 0.74 Gearbox loss maps basis HDV alternator compact type Compressor ESS (energy saving system, reduced idle losses, own model) $\dot{Q}_{A/C,cool,max} = 60 \text{ kW}_{th}$ P_{aux} 5.6 kW_{mech} & 1.81 kW_{el} Diesel ICE 260 kW, map 7.7 L € 6 Curb weight 16.5 t, avrg. usage 26/130 pass. = 20 %, ≈ 1.8 t payload (327)</p>	<p><u>Used for:</u> FC; cycles HUB, UB, SUB Compare p. 115 section 3.1.11.4. Tires D-D-D, RRC 6.2 N/kN $C_d \cdot A_{cr}$ 5.12 m², Crosswind basis i_{FD} 4.78, $\eta_{mech,FD}$ 0.957, tires 275/70R22.5, $J_{wh,tot}$ 119 kg·m², r_{dyn} 0.465 m 12-speed AMT¹¹⁷, 14.94 to 1.00, $\eta_{mech,gear,indir}$ 0.96, $\eta_{mech,gear,dir}$ 0.98 EM, +400/-1200 Nm, +70/-150 kW_{mech}, Tq_{EM,cont} 400 Nm, n_{EM,com} 1670 rpm, (J_{EM} 3 kg·m²) Li-Ion battery 9.8 kWh, SOC 40 to 60 %, power cells $\eta_{el,conv} = 0.95$, $\eta_{el,batt} = 0.95$ Electrical. auxiliaries "artic. bus basis" (steering pump & compr. w/o idle) $\dot{Q}_{A/C,cool,max} = 60 \text{ kW}_{th}$, P_{aux} 7.90 kW_{el} Diesel ICE 177 kW, map 5.1 L € 6 Curb weight 16.4 t, average capacity usage 26/130 passengers = 20 %, ≈ 1.8 t payload (258 p. 12 ff.) (328)</p>	<p><u>Used for:</u> EC_{batt,drv}; cycle SN Compare p. 123 Table 24 Tires RRC 9 N/kN, (270 p. 3) (271 pp. C-22) $C_d \cdot A_{cr}$ 4.68 m², Crosswind curve "DTS" i_{FD} 3.42, $\eta_{FD,mech}$ 0.96, drive tires 245/70R19.5, total J_{wh} 36 kg·m², r_{dyn} 0.403 m 1-speed reduction gear, ratio 4.0, $\eta_{gb,mech}$, 0.97 P_{aux} 2.44 kW_{el} EM ±600 Nm, ±120 kW_{mech}, Tq_{EM,cont} 300 Nm, n_{EM,com} 1900 rpm, (0.2 t, 1.5 kg·m²) Battery Li-Ion 120 kWh GVWR 11.8 t, curb weight chassis 4.52 t, body + tail-lift 1.6 t, payload 1.80 t, m_{test} 7.92 t (163) (329)</p>
DTT: DELIVERY TRACTOR-TRAILER	DTT PHEV: DIESEL-ELECTRICAL PARALLEL HYBRID DELIV. TRACTOR-TRAILER	
<p><u>Used for:</u> FC; cycles WVUC, CILCC, HHDDT, dyno, no crosswind, m_{test} 15.4 t, RRC 8.4 N/kN • FC; cycle UD12-flat, road, m_{test} 19.5 t, custom crosswind curve, RRC 8.4 N/kN Compare p. 111 section 3.1.11.2. $C_d \cdot A_{cr}$ 7.84 m²; i_{FD} 3.58, drive tires 275/80R22.5, total J_{wh} 169 kg·m², r_{dyn} 0.491 m 6-speed AMT, 6.70 to 0.73; $\eta_{mech,FD}$ 0.96, $\eta_{mech,gear,indir}$ 0.96, $\eta_{mech,gear,dir}$ 0.98 HDV alternator compact; P_{aux} 2.54 kW_{mech} & 1.1 kW_{el} Diesel ICE 210 kW, map 7.7 L € 6 Tractor 5.06 t, 2-axle trailer 5 t, payload 5.34 t (dyno), 9.43 t (cycle UD12-flat) (252) (253 pp. 3/4, 30-32, 37/38)</p>	<p><u>Used for:</u> FC; cycles WVUC, CILCC, HHDDT, dyno, m_{test} 15.6 t, RRC 9.4 N/kN • FC; cycle UD12-flat, road, m_{test} 19.7 t, custom crosswind curve, RRC 8.4 N/kN Compare p. 111 section 3.1.11.2. $C_d \cdot A_{cr}$ 7.84 m²; i_{FD} 5.38, drive tires 275/80R22.5, total J_{wh} 169 kg·m², r_{dyn} 0.491 m 6-speed AMT, 6.70 to 0.73, $\eta_{mech,FD}$ 0.96, $\eta_{mech,gear,indir}$ 0.96, $\eta_{mech,gear,dir}$ 0.98 PMSM w. clutch, ±420 Nm, ±45 kW_{mech}, Tq_{EM,cont} 270 Nm, n_{EM,com} 920 rpm, (0.2 t, 1 kg·m²) Li-Ion battery 2 kWh, SOC 40 to 60 %, 0.1 t $\eta_{el,conv} = 0.95$, $\eta_{el,batt} = 0.95$, Start-stop automatic HDV alternator compact, P_{aux} 2.54 kW_{mech} & 1.1 kW_{el} Diesel ICE 210 kW, map 6.4 L € 6 Tractor 5.27 t, 2-axle trailer 5 t, payload 5.34 t (dyno), 9.43 t (cycle UD12-flat) (252) (253 pp. 3/4, 30-32, 37/38)</p>	

¹¹⁷ Average payload 26 passengers: Driveaway in 5th gear, compare footnote to AMT of rigid bus PHEV on p. 172, effective gear ratios from 5.54 to 1.00. Full payload 130 passengers: Driveaway in 3rd gear, effective gear ratios from 9.04 to 1.00.

5.7.7 Driving performance of models with alternative powertrains

Each model of the basis technology level with gas engine or (hybrid) electrical powertrain was simulated with max. payload for full load acceleration and on a demanding hilly and/or transient driving cycle. For the acceleration test the distinction was made for charged and discharged battery in case of parallel hybrid electrical HDV ("ch." & "disch."). The driving performance in terms of acceleration and average rolling velocity ($v_{roll,avrg}$) was compared to the basis vehicle models with a conventional diesel powertrain, see Figure 192 to Figure 195.

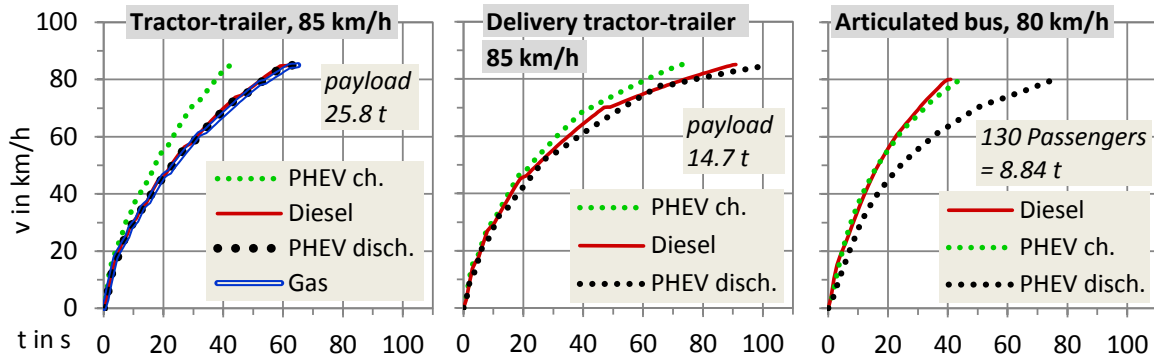


Figure 192. Full load acceleration on flat: Models tractor-trailers, deliv. tractor-trailers, articulated buses.

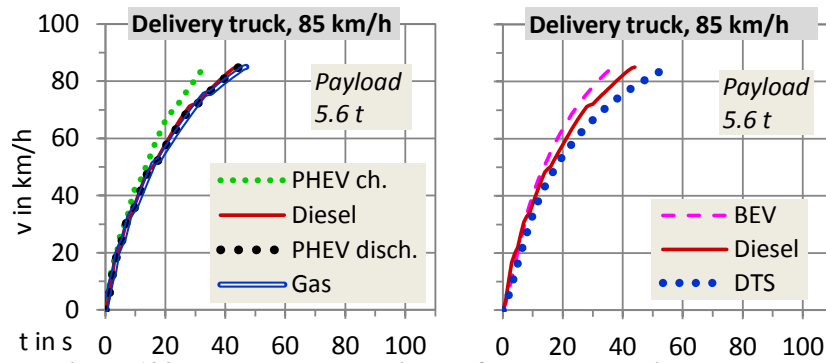


Figure 193. Full load acceleration on flat: Models delivery trucks.

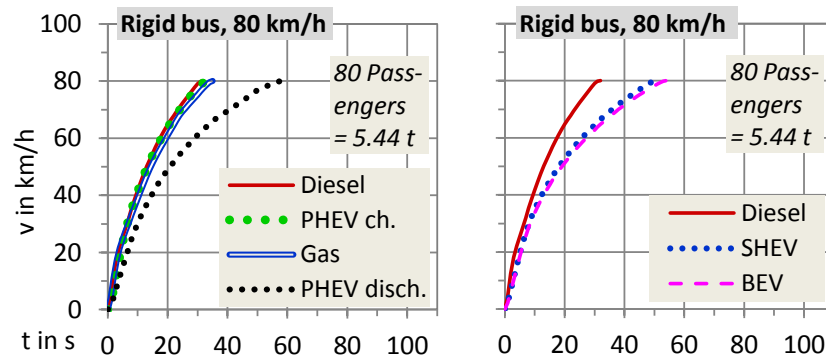


Figure 194. Full load acceleration on flat: Models rigid buses.

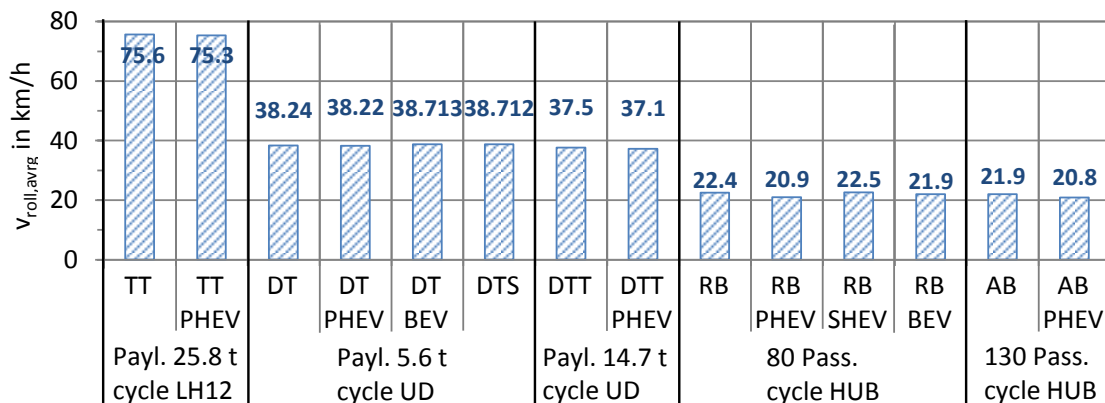


Figure 195. Avrg. rolling velocity, models full payload. Standard curves for acceleration & deceleration.

where: AB - Articulated bus, BEV - Battery-electrical vehicle, DT - Delivery truck, DTS - Battery-electrical delivery truck "Smith", DTT - Delivery tractor-trailer, HUB - Heavy Urban Bus cycle, LH12 - Long Haul cycle 2012, PHEV - Parallel hybrid electrical vehicle, RB - Rigid bus, SHEV - Serial hybrid electrical vehicle, TT - Tractor-trailer, UD12 - Urban Delivery cycle 2012

For the full load acceleration there are some differences in the driving performance, but more important is the average rolling velocity on demanding driving cycles, simulated with the standard curves for desired acceleration and deceleration. The max. deviation towards the conventional vehicle model is ca. -7 % in average rolling velocity for the parallel hybrid rigid bus, 20.9 vs. 22.4 km/h. I. e. the hybrid model could not follow the conventional model during all acceleration phases. The total cycle duration, incl. stand phases, increased by 1.6 % from 147.4 min to 149.8 min.

5.8 Engine performance data

Here the basis engine maps for this thesis are shown and compared with published values for the FC of diesel- and gas engines. Maps from real engines were available for

12 L, € 5, 350 kW, 12 L, € 6, 350 kW, 7.7 L, € 6, 220 kW, 6.4 L, € 5, 228 kW,
see also p. 167 Table 30 "Engine map". The other maps were calculated by scaling or extrapolation.

For the gas engine the map of a medium HDV engine was available and also scaled.

5.8.1 Performance maps, diesel and gas engines, basis electrical machine

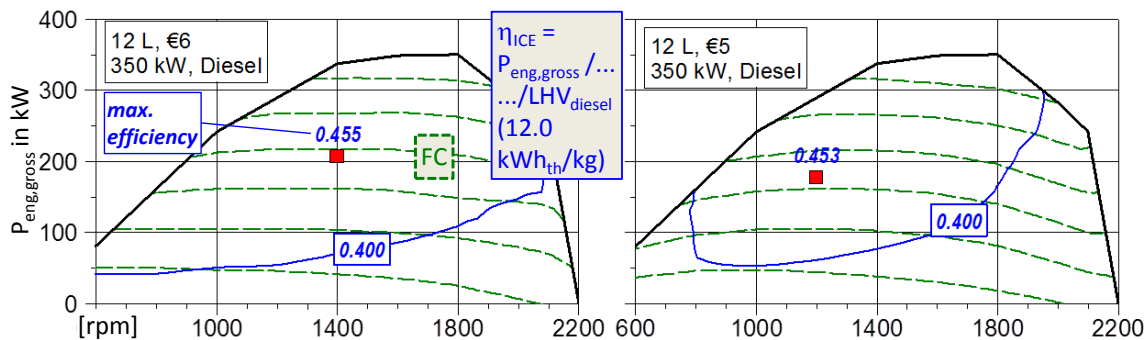


Figure 196. Performance maps, 6-cyl. diesel engines 12 L, € 5 and € 6

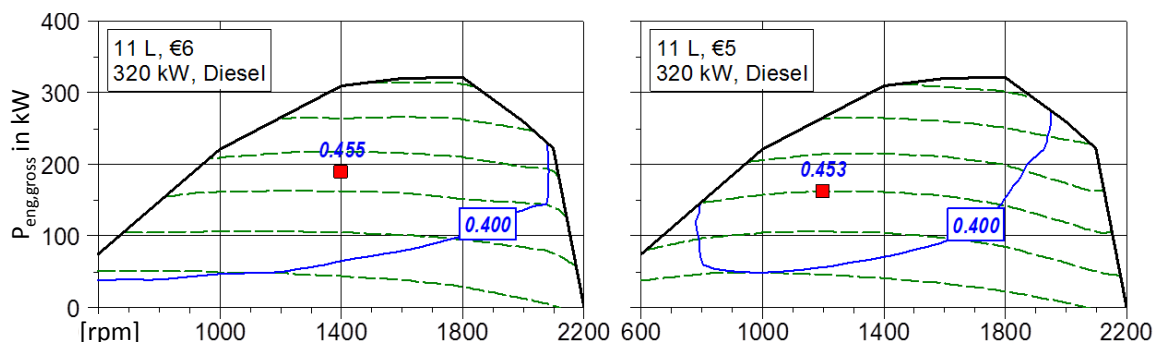


Figure 197. Performance maps, 6-cyl. diesel engines 11 L, € 5 and € 6

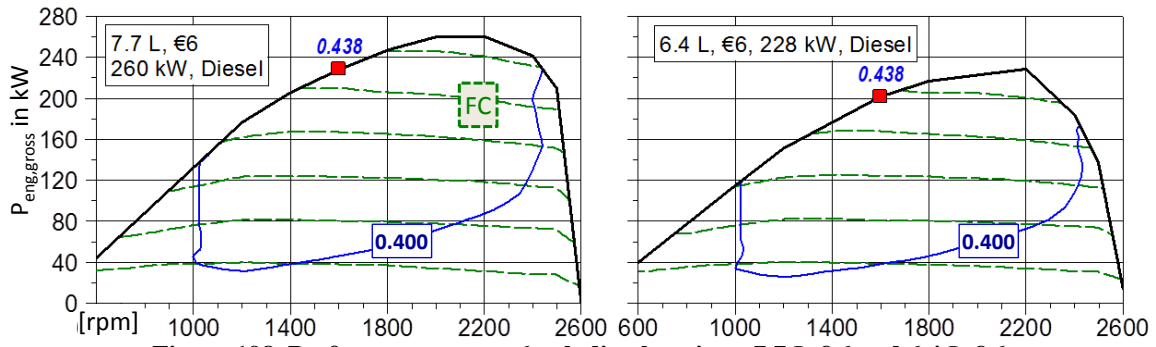


Figure 198. Performance maps, 6-cyl. diesel engines, 7.7 L € 6 and 6.4 L € 6

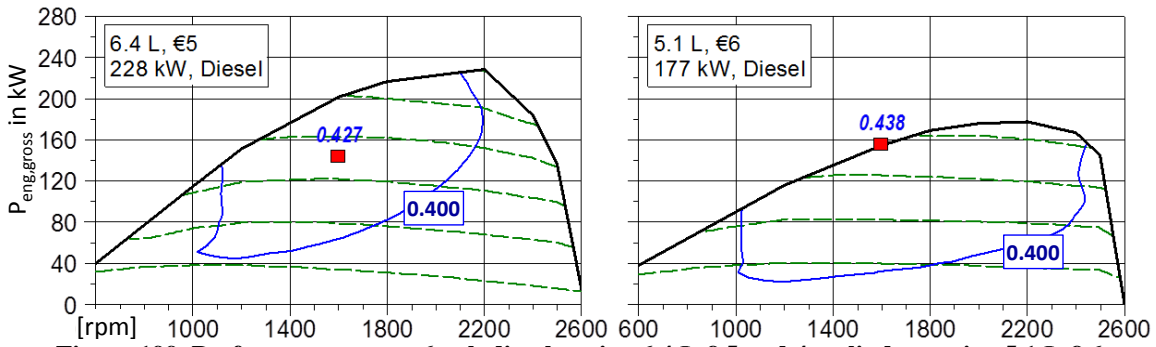


Figure 199. Performance maps, 6-cyl. diesel engine 6.4 L € 5 and 4- cylinder engine 5.1 L € 6

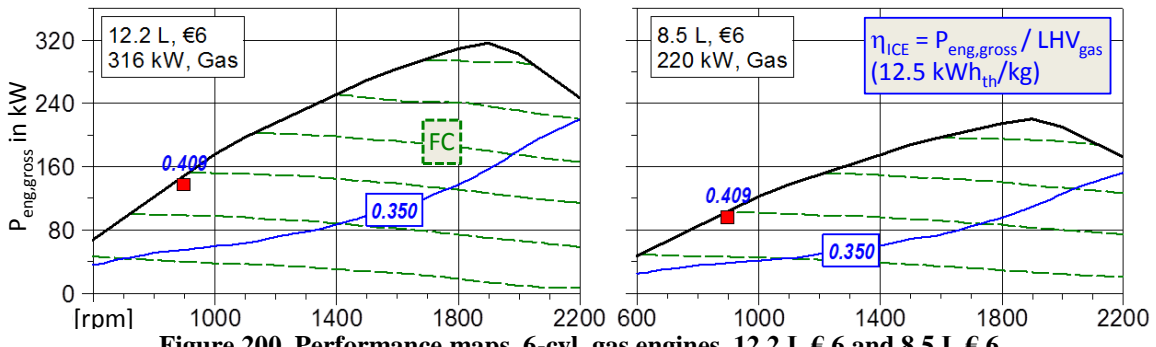


Figure 200. Performance maps, 6-cyl. gas engines, 12.2 L € 6 and 8.5 L € 6

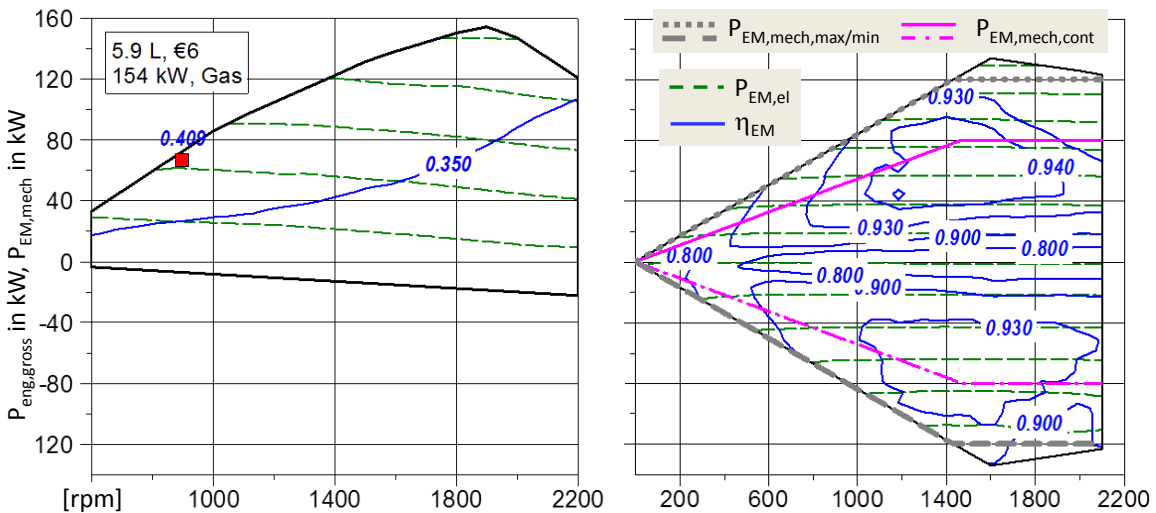
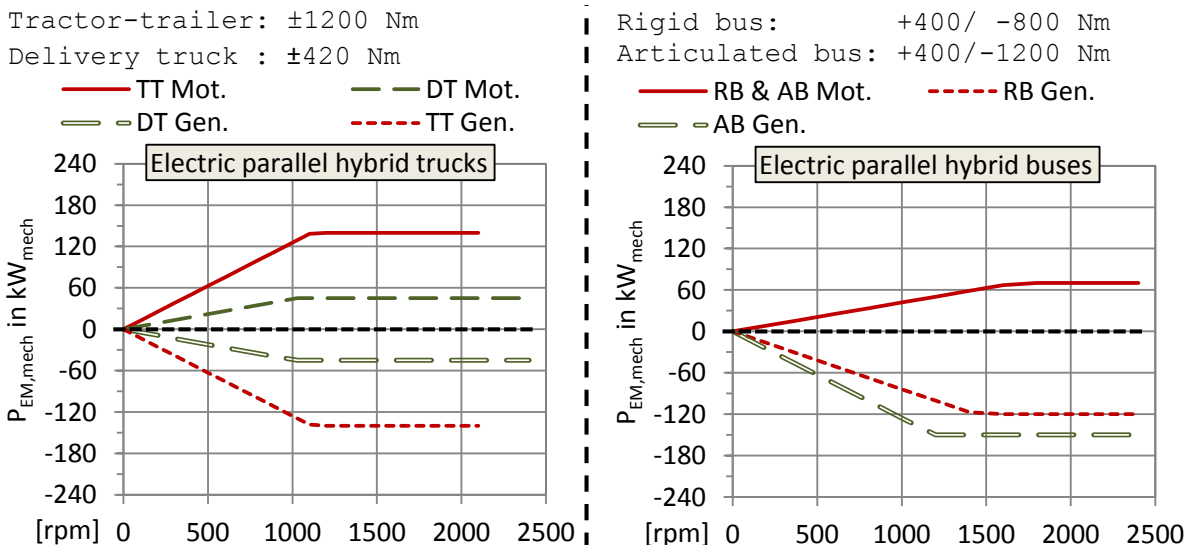
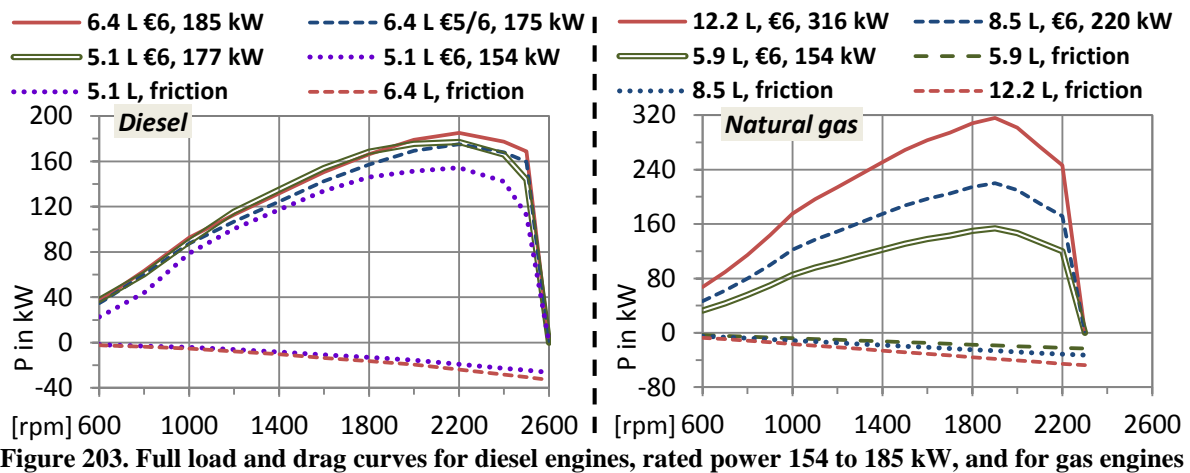
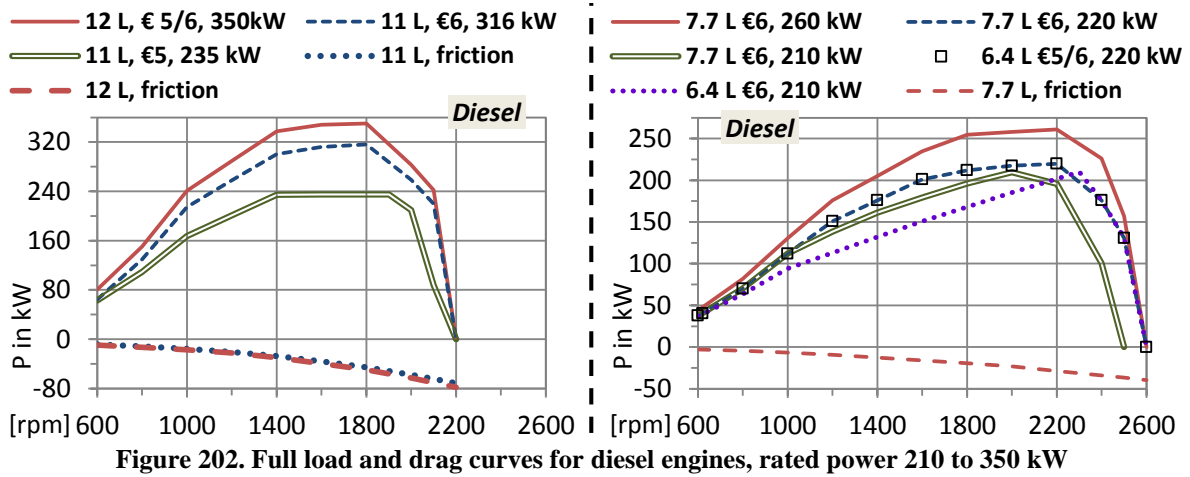
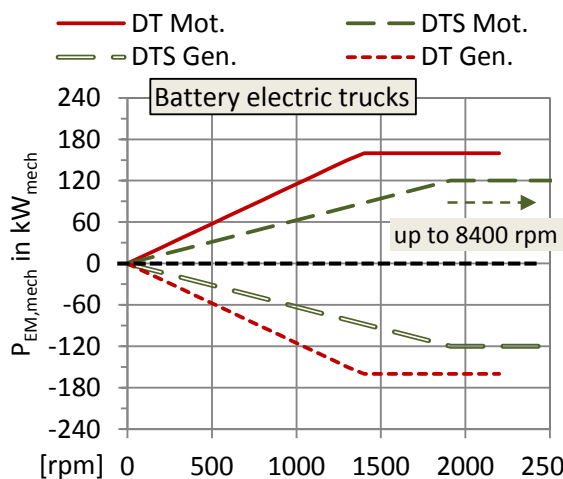


Figure 201. Performance maps, 4-cyl. gas engine 5.9 L € 6 and electrical machine (PMSM)¹¹⁸

¹¹⁸ Nominal voltage 630 V, max. current 200 A, corner speed 1470 rpm, $T_{q, cont} \pm 520$ Nm, $P_{cont} \pm 80$ kW, $T_{q, max} \pm 800$ Nm, $P_{max} \pm 120$ kW, inertia $2 \text{ kg}\cdot\text{m}^2$. Other efficiency maps of PMSM for comparison can be found e. g. in (595 p. 103) (596 p. 12) (597 p. 77) (598 p. 570) (599 p. 2765) (600 p. 99) (601 p. 5272) (602 p. 14003) (603 p. 583). The available machine with the shown map had typical efficiency values of PMSM.



Delivery truck BEV: ± 1100 Nm
 Delivery truck "Smith": ± 600 Nm



Rigid bus SHEV & BEV: ± 2000 Nm
 EM for Genset SHEV: 1x -1000 Nm

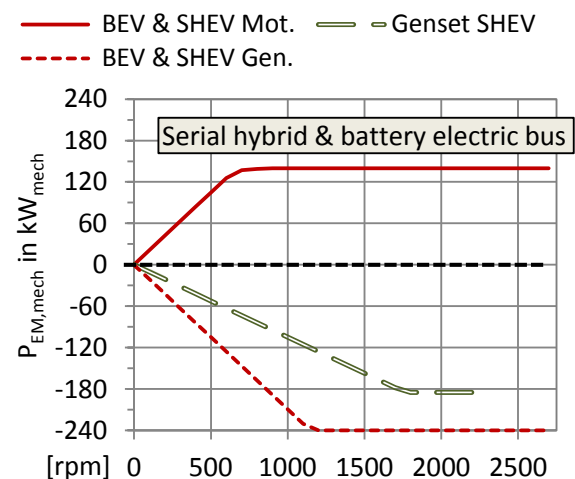


Figure 205. Full load curves for motor- and generator operation of the electrical machines for electrical vehicles. The basis performance map, see Figure 201, is scaled to the generator torque.

5.8.2 Internal combustion engines, check of performance maps

In this chapter the FC from several engine performance maps of this thesis is compared with published numbers for the average FC from engine tests for the specific FC.

In case of simulated transient engine cycles like ETC, FTP or WHTC the power was calculated *without* the rotational inertias of engine and dynamometer, like foreseen for VECTO (55) Annex V, Appendix 8, § 5.3. For these cycles the integrated FC as outcome of the interpolation in the performance maps was multiplied with the overall "WHTC-factor", which was assumed to be 1.03 in this thesis to depict the increase of FC for transient operation. This factor is a practical experience from the own work, when comparing the interpolated FC from stationary engine maps with real measured WHTC results. For known engines it ranges from ca. 1.02 to ca. 1.04.

Table 39. Diesel engines; FC in WHTC engine cycle (130 pp. 29 ff., 87 ff.); maps of this work; measurement of EU engines

Engine type	MY	V _{displ} in L	T _{qmax} , bmep in bar	P _{rated} in kW	P _{rated} , n in rpm	P _{rated} , bmep in bar	WHTC hot, FC, g/kWh	Source
<i>Interpolated from the fuel maps used in this work</i>								
6 cyl., map 12 L € 5, FL 350 kW	-	12.00	24.1	350	1800	20.2	207	-
6 cyl., map 12 L € 6, FL 350 kW	-	12.00	24.1	350	1800	20.2	204	
6 cyl., map 7.7 L € 6, FL 260 kW	-	7.70	22.8	260	2200	18.5	209	
6 cyl., map 6.4 L € 5, FL 220 kW	-	6.40	23.6	220	2200	18.7	217	
6 cyl., map 6.4 L € 6, FL 220 kW	-	6.40	23.6	220	2200	18.7	208	
<i>Measured values from various sources (* = Nonroad engine)</i>								
MAN D2676, € 6	2015	12.40	23.3	353	1800	19.0	212	(235 p. 11)
Deutz TCD* 7.8 € 5	2015	7.80	22.6	250	2200	17.5	213	(330 p. 62)
Daimler OM 926, € 5	2012	7.20	22.7	240	2200	18.2	-	(331 p. 11)
Daimler OM 936, € 6	2012	7.70	22.8	260	2200	18.4	-2 % to OM 926	

Table 40. Diesel engines; FC in ESC/SET and FTP engine cycles; maps of this work; measurement of US engines¹¹⁹, emission standard EPA-2010

Engine type (EPA: no. of engine family)	MY	V _{displ} in L	T _{qmax} , bmep in bar	P _{rated} in kW	P _{rated} , n in rpm	P _{rated} , bmep in bar	SET, CO ₂ in g/bhp.h	FTP hot, CO ₂ in g/bhp.h	SET/ ESC	FTP hot
									FC, g/kWh	
<i>Interpolated from engine maps used in this work, engine maps 6 to 9 L</i>										
6 cyl., map 7.7 L € 6, FL 260 kW	-	7.70	22.8	261	2200	18.5	-	-	197	211
6 cyl., map 6.4 L € 6, FL 220 kW		6.40	23.6	220	2200	18.7			197	212
6 cyl., map 6.4 L € 5, FL 220 kW		6.40	23.6	220	2200	18.7			206	225
<i>Measured from several sources, engine maps 6 to 9 L</i>										
Cummins ISB 6.7 ECEXH0408BAP	'14	6.69	20.4	268	2600	18.5	494.2	563.4	207	236
Navistar S350 ENVXH05700SA	'14	9.35	21.0	261	2000	16.7	503.0	541.9	211	227
Navistar A350 ENVXH05700GA	'14	9.35	21.0	261	2000	16.7	541.8	586.5	227	247
<i>Interpolated from engine maps used in this work, engine maps 11 to 13 L</i>										
6 cyl., map 12 L € 6, FL 350 kW	-	12.00	24.1	350	1800	20.2	-	-	196	213
6 cyl., map 12 L € 5, FL 350 kW		12.00	24.1	350	1800	20.2			192	206
<i>Measured from several sources, engine maps 11 to 13 L</i>										
Paccar MX-13 FPCRH12.9M01	'15	12.90	24.4	373	1700	20.4	466.4	501.5	196	210
Navistar A475 FNVXH07570SB	'15	12.41	23.4	354	1700	20.2	-	529.4	-	222
Navistar A475 ENVXH07570SB	'14	12.41	23.4	354	1700	20.2	-	529.5	-	222
Detroit DD13 FDDXH12.8FED	'15	12.80	22.0	350	1800	18.3	454.4	525.2	195	223
Volvo MP7 FVPTH10.8G01	'15	10.80	25.2	295	1500	21.8	468	541.9	196	227

¹¹⁹ Test engine data and specific CO₂ from (604) (605).

Carbon mass fraction US diesel ca. 0.872 [#2 diesel: 0.869 (606 p. 706), reference diesel fuel: 0.874 (60 p. 74025)], carbon mass fraction CO₂ ca. 0.2727, ⇒ CO₂ factor US diesel is 3.20 kgCO₂/kg.

LHV_{diesel,US} is 11.97 kWh_{th}/kg (60 p. 74025).

Supplemental emission test (SET), equals European Steady state Cycle (ESC), from (157 pp. 10, 55 ff.) (300 p. 320 ff.) (607 p. 586 ff.). FC calculated with original weighting factors from SET/ESC. In 2016-10 USEPA introduced new weighting factors for CO₂, reflecting the trend towards engine downspeeding (60 p. 73550/73551). Federal Test Procedure's transient HD diesel engine cycle (FTP) from (606 p. 676) (607 pp. 585 ff., 880 ff.)

Table 41. Diesel engines. Comparison of minimum brake specific fuel consumption (bsfc)¹²⁰

Min bsfc in g/kWh	Description of engine	Source
<i>Engine maps used in this work</i>		
184	6 cyl., map 12 L € 6, FL 350 kW (also scaled to engine 11 L)	-
185	6 cyl., map 12 L € 5, FL 350 kW	
191	6 cyl., map 7.7 L € 6, FL 260 kW (also scaled to engines 6.4 L and 5.1 L)	
196	6 cyl., map 6.4 L € 5, FL 220 kW	
<u>Published data, measurement or default, if so from engine performance map</u>		
ca. 171	Default map GEM tool, MY 2027, 6 cyl. 15 L, 339 kW @ 1800 rpm	(332 pp. 2-136)
ca. 182	Default map GEM tool, MY 2018, 6 cyl. 15 L, 339 kW @ 1800 rpm	(332 pp. 2-85)
ca. 182	Detroit Diesel, DD15, MY 2013, 6 cyl. 14.8 L, 377 kW @ 1800 rpm	(333 p. 14)
186	Cummins, ISX 475, MY 2010, 6 cyl. 15 L, 391 kW @ 1800 rpm	(249 p. 101) (250 p. 770)
189	Detroit Diesel, DD60, early 1990ies, 6 cyl 11.1 L, 239 kW @ 1800 rpm	(334 p. 159)
ca. 190	Make, model and MY unknown, 312 kW @ 1800 rpm	(335 p. 656)
ca. 190	MAN, D0826 LOH 17, MY 1995 to 2001, 6 cyl. 6.9 L, 158 kW @ 2400 rpm	(336 p. 2870)
ca. 190	Make unknown, MY 2001 to 2004, 6 cyl. ca. 11 L, ca. 295 kW @ 1900 rpm	(337 p. 400)
191	MAN, model and MY unknown, 6 cyl. 12 L, 300 kW @ 1800 rpm	(171 p. 14)
191	Caterpillar, MY unknown, 6 cyl. 10 L, 261 kW @ 1800 rpm	(338 p. 1709)
194	Cummins, N14-460E, early 1990ies, 6 cyl. 14 L, 343 kW @ 1800 rpm	(334 p. 144)
201	Make unknown, MY 2009, 4 cyl. 3 L, 110 kW @ 2800 rpm	(339 p. 385)
202	Cummins, ISB 385, MY 2012, 6 cyl. 6.7 L, 287 kW @ 2750 rpm	(340)
210	Mack, Maxidyne ENDT 676, mid 1970ies, 6 cyl. 11 L, 213 kW @ 1800 rpm	(341 p. 41)
240	First commercial diesel engines, 1910s, stationary machines	(203 p. 1) (342 p. 15)

Table 42. Stoichiometric gas engines; FC in engine cycles ETC (157) and WHTC, map of this work; measurement¹²¹

Engine type	MY	V _{displ} in L	T _{qmax} , bmep in bar	P _{rated} in kW	P _{rated} , n in rpm	P _{rated} , bmep in bar	ETC hot, FC in g/kWh	WHTC hot, FC in g/kWh	Source
<i>Interpolated from engine maps used in this work</i>									
6 cyl., map 8.5 L € 6, FL 220 kW	-	8.5	17.6	220	1900	16.3	226	234	-
<u>Measured from various sources</u>									
Iveco Cursor 8 € 6	2013	7.8	20.9	243	2000	18.7	-	233	(343 p. 6)
Make unknown, € 6	-	7.8	20.9	243	2000	18.7	234	221	(344 p. 352)

¹²⁰ $\eta [-] = 1 / (\text{bsfc} [\text{g/kWh}] \cdot \text{LHV} [\text{kWh}_{\text{th}}/\text{kg}] \cdot 0.001)$, bsfc calculated from η with $\text{LHV}_{\text{Diesel}} = 11.95 \text{ kWh}_{\text{th}}/\text{kg}$. When looking at the rather slow decrease of *minimum bsfc* during the decades, it shall be regarded that for a low FC on a driving cycle the *overall average bsfc* of the engine needs to be low. Most times it is not operated in the single point of lowest bsfc. In addition the manufacturers needed to implement costly exhaust aftertreatment systems between 1990 to 2010 to meet the decreasing limits for pollutant emissions, what claimed resources.

¹²¹ Transient correction for simulated FC on ETC and WHTC: 1.03, see also the explanation on p. 183. Measured FC calculated from CO₂ emissions with TTW CO₂-factor 2.68 kgCO₂/kgCNG (208 p. 24).

Table 43. Stoichiometric gas engines. Comparison of minimum brake specific fuel consumption (bsfc)¹²²

Min bsfc in g/kWh	Description of engine	Source
<i>Engine map used in this work</i>		
195	6 cyl., map 8.5 L € 6, FL 220 kW (also scaled to gas engines 12.2 and 5.9 L)	-
<u>Published data, measurement, if so from engine performance map</u>		
193	MBtech, CoNAG 4C, MY 2013, 4 cyl 6 L, 220 kW @ 1800 rpm	(345 p. 7)
199	Make and MY unknown, 200 kW @ 2000 rpm	(346 p. 876)
200	Daimler, M936G € 6, MY 2014, 6 cyl. 7.7 L, 222 kW @ 2200 rpm	(347 p. 8)
ca. 200	Optimised test engine (Opel), MY 2003, 3 cyl. 1.0 L, 66 kW @ 5200 rpm	(348 p. 91)
205	Daimler, M936G € 6, MY 2015, 6 cyl. 7.7 L, 222 kW @ 2200 rpm	(349 p. 238)
205	Iveco, Cursor 8, MY 2004, 6 cyl. 7.8 L, 200 kW @ 2000 rpm	(350 p. 55)
ca. 207	Make unknown, MY 2001 to 2004, 6 cyl. ca. 9 L, ca. 230 kW @ 1900 rpm	(337 p. 401)

5.9 Transmission performance data

Here an overview of published values for measured, guidance and default values for the mechanical efficiency of transmissions, hence shift gearboxes and final drives, is given, see Table 44.

Table 44. Published efficiency values for transmissions, shift gearboxes and final drives.

$\eta_{tm,mesh}$ - mesh efficiency, only friction between gears;

$\eta_{tm,ova}$ - overall efficiency of transmission, ratio of (work-out) to (work-in)

Efficiencies in -	Description	Source
<u>Measurement</u>		
0.749; 0.854; 0.957; 0.967	Input power 10.5 kW @ 5000 rpm; 2.1 kW @ 1000 rpm; 104.7 kW @ 5000 rpm; 20.9 kW @ 1000 rpm $\eta_{tm,ova}$, planetary gearbox, passenger car	(351 p. 24)
0.900; 0.975	Input power 1.07 kW @ 600 rpm; 28.3 kW @ 3000 rpm $\eta_{tm,mesh}$, hypoid gear pair, ratio not given, oil temperature 90 °C	(352 p. 61)
0.779; 0.942	Input power 5 kW @ 1000 rpm; 17 kW @ 1000 rpm $\eta_{tm,ova}$, final drive, ratio 3.55, oil temp. 113 °C, pickup truck	(353 pp. 3-13)
0.891; 0.943	Used final drives; new final drives Average $\eta_{tm,ova}$, each two drives over two driving cycles, ratio 2.64, light truck GVWR 3.5 t	(354 p. 672)
<u>Guidance and default values</u>		
0.900 to 0.930; 0.990 to 0.998	Bevel gear pairs; spur gear pairs Guidance values, $\eta_{tm,mesh}$	(355 p. 67)
0.950 to 0.990; 0.990 to 0.998	Bevel gear pairs; spur gear pairs Guidance values, $\eta_{tm,mesh}$	(356 p. 75)
0.940 to 0.960; 0.980 to 0.985	Hypoid gear pairs in final drives; spur gear pairs in gearboxes Guidance values, max. $\eta_{tm,ova}$, automotive components, rated power	(357 p. 222)
0.960 to 0.980; 0.990 to 0.995	Hypoid gear pairs in final drives; spur gear pairs in gearboxes Guidance values, max. $\eta_{tm,mesh}$, automotive components, rated power	(357 p. 222)
0.920 to 0.970; 0.900 to 0.970; 0.900 to 0.950	Spur gearbox flood lubrication passenger car; spur gearbox flood lubrication, HDV; planetary gearbox Guidance values, $\eta_{tm,ova}$	(355 p. 67)

¹²² If so bsfc calculated from η with $LHV_{gas} = 12.53 \text{ kWh}_{th}/\text{kg}$

0.930 to 0.980; 0.900 to 0.980; 0.900 to 0.970	Spur gearbox flood lubrication passenger car; spur gearbox flood lubrication, HDV; planetary gearbox with bridgeable torque converter Guidance values, $\eta_{tm,ova}$	(356 p. 75)
0.950	Spur gearbox, medium commercial vehicle Guidance value, $\eta_{tm,ova}$	(358)
0.950; 0.950; 0.980	Final drive; stepped-up gears; direct gears (1:1) Default values, $\eta_{tm,ova}$, Japanese simulation tool for CO ₂ -label HDV	(56 p. 19)
0.955; 0.960; 0.980	Final drive; stepped-up gears; direct gears (1:1) Default values, $\eta_{tm,ova}$, US simulation tool for CO ₂ -label HDV	(359 p. 15)
0.980; 0.950; 0.970	Final drive; stepped-up gears; direct gears (1:1) Default values, $\eta_{tm,ova}$, S-Korean simulation tool for CO ₂ -label HDV	(360 p. 3)

5.10 Average payload of analysed vehicle classes

CU Capacity usage, ratio of (effective payload during *all* trips, $m_{\text{payload,avrg,all}}$) to (theoretical max. payload during *all* trips, $m_{\text{payload,max,all}}$), includes empty and loaded trips.

ETF Empty trip factor, ratio of (mileage without payload) to (total mileage).

LF Load factor, ratio of (effective payload during *loaded* trips, $m_{\text{payload,avrg,loaded}}$) to (theoretical max. payload during *loaded* trips, $m_{\text{payload,max,loaded}}$), excludes empty trips.

$$m_{\text{payload,avrg,all}} = m_{\text{payload,max,all}} \cdot \text{CU} = m_{\text{payload,max,all}} \cdot \text{LF} / (1 + \text{ETF}), \text{ (361 p. 25)}$$

Assumptions for max. payload:

Tractor-trailer (TT), GCWR 40 t: 26 t (3 p. 19) (362 p. 53).

Delivery truck (DT), GVWR 12 t: 6 t (362 p. 53).

Rigid city bus (RB), GVWR 18 t: 80 Passengers. Case: 4 passengers per m² on standing areas (363) (364) (365) (366), 68 kg/pass. (367)

Table 45. Average payload of HDV classes, empty trips included or excluded

Payl. [t]	Tractor-trailer (TT), GCWR 40 t, mainly long haulage	Source
12.5	Incl. empty trips, TT (Ensemble articul�), diverse goods (Marchandises diverses), long haul, GCWR 40 t, statistics FR 2010	(368)
12.9	Default value for VECTO, regional delivery cycle, 2016	(149 p. 186)
13.0	Incl. empty trips, LF 0.60, ETF 0.20, default data EcoTransIT, 2016	(361 p. 27/28)
13.0	Incl. empty trips, CU 0.50, default value NTMCalc Basic, 2016	(369)
13.5	Incl. empty trips, CU 0.52 (AT, CH, DE, FR, NO, SE), TT 34 to 40 t, HBEFA 2014	(370)
14.0	Incl. empty trips, calculated via weighted avrg. GVW, long haul TT in whole EU-28, mass classes 10 to 45 t, GVW calculated from accelerations after gear change, data collection by Scania 2012-01 to 2014-04	(371 p. 17)
14.6	Incl. empty trips, calculated via weighted avrg. GVW, long haul TT 5-axles, mass classes 10 to 45 t, GVW measured by 10 weigh-in-motion systems on NL motorways, 384'500 vehicles, 4 weeks, 2012-06 to 2012-08	(372 pp. 16, 22)
14.6	Incl. empty trips, avrg. payload "hire or reward", trip length \geq 2000 km, based on Eurostat 2010	(373 p. 49)
14.6	Excl. empty trips, LF 0.56, 9 fleets TT on motorways (primary distribution level), food supply chain, survey UK 2002	(374 p. 226) (375 p. 13)
14.8	Excl. empty trips, LF 0.57, representative payload distribution, around 2000, based on research of NEA Transportonderzoek, Rijswijk, nea.nl	(376 p. 15)
15.5	Incl. empty trips, LF 0.66, ETF 0.11, HDV statistics DE 2014, TT 30 to 40 t	(377 p. 8) (378 p. 14)
15.6	Incl. empty trips, CU 0.60, based on survey DE early 1990ies (379)	(380 p. 28)

19.3	Default value for VECTO, long haul cycles, 2016	(149 p. 186)
19.8	Incl. empty trips, LF 0.86, ETF 0.13, trucks 34 to 44 t, 6180 trucks on Inntal motorway near Kundl, 2008	(381)
Payl. [t] Delivery truck (DT), GVWR 12 t, mainly urban delivery traffic Source		
1.9	Excl. empty trips, LF 0.32, 14 fleets DT on city streets (tertiary distribution level), food supply chain, survey UK 2002	(374 p. 226) (375 p. 13)
2.1	Incl. empty trips, LF 0.49, ETF 0.42, HDV statistics DE 2014 truck-class payload 4 to 10 t	(377 p. 8) (378 p. 14)
2.1	Incl. empty trips, CU 0.30 to 0.40, based on survey DE early 1990ies (379)	(380 p. 28)
2.9	Incl. empty trips, CU 0.49, DT 12 to 14 t, HBEFA 2014	(370)
3.0	Default value for VECTO, trucks class 1 to 3 (4x2, 7.5 to 16 t), 2016	(149 p. 187)
3.7	Incl. empty trips, LF 0.73, ETF 0.20, trucks 7.5 to 12 t, 276 trucks, 2008	(381)
Pass. [#] Rigid bus 12 m, GVWR 18 t, mainly urban bus traffic Source		
15	CU 0.19, public transportation association VDV, statistics DE 2014	(382 p. 38)
17	CU 0.21, research of avrg. payload HDV in EU, ARTEMIS project, 1999	(383 p. 17)
18	CU 0.22, public transportation association VDV, email, DE 2014	(366)
47	Avrg. payload 3.2 t, SORT test conditions, early 2000s	(313 p. 25)
48	CU 0.60, urban bus, HBEFA 2014	(370)
83	CU 1.04, default value for VECTO, city buses, 2016	(149 p. 195)

5.11 Cooling capacity of air conditioners of city buses

Table 46. Maximum cooling capacity of air conditioners of city buses

Make	Model	MY	A/C Cabin, $\dot{Q}_{A/C,cool,max}$ in kW _{th}	A/C Driver, $\dot{Q}_{A/C,cool,max}$ in kW _{th}	Full electr. A/C	Source
Rigid buses 12 m						
Diverse		2008	20 to 30	?	–	(384 p. 3)
Diverse		2012	23 to 45	?	–	(385 p. 2)
MAN	Lion's City, EEV	2008	29.0	3.2	–	(386 p. 36)
MAN	Lion's City H, EEV, <i>hybrid</i>	2012	18.0	?	x	(267 p. 74)
MAN	Lion's City, € 6	2013	32.0	5.0	–	(387 p. 58)
MAN	Lion's City, € 6	2016	32.0	5.0	–	(388 p. 52)
MB	Citaro, € 5/EEV	2011	32.0	8.0	–	(389 p. 84) (266 p. 48)
MB	Citaro, € 6	2014	32.0	8.0	–	(273 p. 52) (390)
MB	Citaro Ü, € 6	2016	32.0	7.0	–	(391)
Otokar	Kent C, € 6	2015	39.0	3.5	–	(392 p. 14)
VDL	Citea SLF, € EEV	2011	26.0	8.0	–	(265 p. 50)
Volvo	7700LH, <i>hybrid</i>	2010	7.2	3.5	x	(393 p. 33) (394 p. 2)
Volvo	7900LH, <i>hybrid</i>	2015	28.0	?	x	(395 p. 15)

Articulated buses 18 m						
Diverse		2012	42 to 45	?	–	(385 p. 2)
MB	Citaro G, € 6	2016	36.0	8.0	–	(390)
Solaris	Urbino 18, € 6	2016	24.0	4.3	–	(396 p. 58)
Volvo	7900LAH, <i>hybrid</i>	2015	38.0	?	x	(328 p. 2)

5.12 Organic Rankine Cycle performance data

Here is the researched performance data enlisted, which was used to create the characteristic line of the ORC efficiency, see p. 70 Figure 68.

Publication 1: (397 p. 14); HDV diesel engine, ca. 320 kW; waste heat from EGR line and exhaust as heat sources; turbine as expansion machine of ORC process; toluene as working fluid; simulation with validated model.

Publication 2: (398 p. 403), based on (399); 6 cyl. diesel engine, 12 L, 300 kW, € 6; waste heat from exhaust as heat source; piston machine as expander of ORC process; ethanol as working fluid; measurement.

Table 47. Performance data of Organic Rankine Cycle systems

Publi- cation	Point ESC	n_{eng} in rpm	$P_{eng,gross}$ in kW _{mech}	$T_{exh,out}$ in °C	$\dot{H}_{exh,out}$ in kW _{th}	$P_{ORC,mech} /$ $P_{eng,gross}$ in -	$P_{ORC,mech}$ in kW _{mech}	$\eta_{ORC,mech}$ in -
1	B25	1516	80.2	264	71.9	0.032	2.6	0.036
	B50		160.4	367	131.2	0.049	7.9	0.060
	B75		240.6	431	190.8	0.062	14.9	0.078
2	A25	1190	65.5	255	45.3	0.026	1.7	0.038
	A50		131.0	370	94.2	0.035	4.6	0.049
	A75		196.5	435	149.3	0.038	7.5	0.050
	B25	1516	80.2	264	71.9	0.033	2.6	0.037
	B50		160.4	367	131.2	0.036	5.8	0.044
	B75		240.6	431	190.8	0.042	10.1	0.053
	C25	1842	82.3	279	82.4	0.033	2.7	0.033
	C50		164.6	358	136.7	0.033	5.4	0.040
C70	247.0		437	198.0	0.040	9.9	0.050	

where: $\eta_{ORC,mech}$ Efficiency of ORC, ratio of mech. power at shaft of expander to exhaust loss
 $\dot{H}_{exh,out}$ Exhaust loss, calculated from exhaust mass flow and difference of specific enthalpy between exhaust temperature at aftertreatment outlet and ambient temperature.
 n_{eng} Engine speed
 $P_{eng,gross}$ Gross engine power
 $P_{ORC,mech}$ Mechanical power at shaft of expander of Organic Rankine Cycle
Point ESC Operation point of engine according (157 pp. 10, 55 ff.), see p. 70 Figure 67.
 $T_{exh,out}$ Exhaust temperature at ORC inlet, here assumed to equal the temperature at turbocharger outlet.

5.13 Current consumption standards for heavy-duty vehicles

In this section the details on the consumption standards are enlisted, which are already mandatory in Canada, China, Japan and the USA. The results for the basis HDV models from this thesis are shown on p. 93 in section 2.6.3.3.

Canadian procedure : (58 p. 450 ff.). Aligned to the US-procedure, e. g. the same CO₂ limits are applied, compare (58 pp. 482-484) and (170 pp. 133-134).

Chinese procedure : (57) (292), (400)

Japanese procedure : (56), (401 pp. 22-24), (402)

US procedure : (60) (170 pp. 133-189), (332 pp. 3/1-4/46) (403 pp. 125-127)

Table 48. Driving cycles for certification

Country	Driving cycle	Part I	Part II	Part III
China	C-WTVC	Urban	Rural	Motorway
Japan	JE05, IDM	JE05	IDM	-
USA & CA	EPA GHG	HHDDT transient	55 mi/h (88.5 km/h)	65 mi/h (104.6 km/h)

Table 49. Tractor-trailer, allocation and weighting factors for cycle parts

Country	Allocation for weighting of cycle parts	Weighting factors for cycle parts		
		Part I	Part II	Part III
China	Tractor-trailer, GCWR > 27 t	0.00	0.10	0.90
Japan	Tractor-trailer, GCWR > 20 t	0.90	0.10	-
USA & CA	Tractor, sleeper cab	0.05	0.09	0.86

Table 50. Delivery truck, allocation and weighting factors for cycle parts

Country	Allocation for weighting of cycle parts	Weighting factors for cycle parts		
		Part I	Part II	Part III
China	Truck, 5.5 t < GVWR ≤ 12.5 t	0.10	0.60	0.30
Japan	Truck, GVWR ≤ 20 t	0.90	0.10	-
USA & CA	Vocational vehicle	0.42	0.21	0.37

Table 51. Rigid bus, allocation and weighting factors for cycle parts

Country	Allocation for weighting of cycle parts	Weighting factors for cycle parts		
		Part I	Part II	Part III
China	City bus, GVWR > 3.5 t	1.00	0.00	0.00
Japan	Route bus, all GVWR	1.00	0.00	0.00
USA & CA	<i>Buses not covered in phase 1 until 2017</i>			

Table 52. Tractor-trailer, allocation, payload and fuel consumption limit

Country	Allocation for FC limit	Payload [t]	FC limit [L/100km]
China	Tractor-trailer, 35 t < GCWR ≤ 40 t	26.6 max. payload	40.0
Japan	Tractor, TT2, GCWR > 20 t, model data see Table 55	20.06	49.8
USA & CA	Tractor, class 8, high roof sleeper cab, MY 2016, GVWR > 33'000 lb (14.97 t)	19 short-tons (17.24 t)	7.3 gal/ (1'000 short-ton · mi) ⇒ 32.6 L/100km

Table 53. Delivery truck, allocation, payload and fuel consumption limit

Country	Allocation for FC limit	Payload [t]	FC limit [L/100km]
China	Truck, 10.5 t < GVWR ≤ 12.5 t	5.9 max. payload	25.0
Japan	Truck, T7, 10 t < GVWR ≤ 12 t, model data see Table 55	3.80	16.7
USA & CA	Vocational vehicle, class 7, MY 2016 26'000 lb < GVWR ≤ 33'000 lb (11.79 to 14.97 t)	5.6 short-tons (5.08 t)	23.0 gal/ (1'000 short-ton · mi) ⇒ 30.3 L/100km

Table 54. Rigid bus, allocation, payload and fuel consumption limit

Country	Allocation for FC limit	Payload [t]	FC limit [L/100km]
China	City bus, 16.5 t < GVWR ≤ 18.0 t	7.0 max. payload	37.5
Japan	Route bus, BR5, GVWR > 14 t, model data see Table 55	2.17	23.6
USA & CA	<i>Buses not covered in phase 1 until 2017</i>		

Table 55. Table values for Japanese HDV models¹²³

HDV model	Curb weight in kg	Pay-load in kg	Vehicle width in m	Vehicle height in m	RRC in N/kN	C _d · A _{cr} in m ²	Inertia wheels in kg·m ²
Tractor-trailer	19'028	20'055	2.49	2.89	5.6	4.427	322.4
Delivery truck	4'048	3'797	2.35	2.541	7.4	3.643	50.2
Rigid bus	9'790	2'173	2.49	2.962	6.6	3.089	148.2

¹²³ RRC = "μ_r" = 0.00513 + 17.6 / (m_{curb} + m_{payl}), [kg/kg];

(C_d · A_{cr} · ρ_{air}/2)_{truck} = (μ_a A)_{truck} = 0.00299 · w_{veh} · h_{veh} - 0.000832, [kg/(km/h)²]; (μ_a A)_{bus} = 0.68 · (μ_a A)_{truck};
J_{wheels} = 0.07 · m_{curb} · r_{dyn}², [kg·m²], η_{mech,gear,indir} 0.95, η_{mech,gear,dir} 0.98, η_{mech,FD} 0.95; no retarder; no auxiliaries

5.14 Published values for fuel consumption

In the following tables a selection of numbers for fuel- and energy consumption from publicly available sources is given. The focus was set on HDV from the last ten years on the markets Europe and North America, where the technical level is similar.

Diesel fuel: LHV 43.0 MJ/kg = 9.94 kWh_{th}/L, Natural gas: 45.1 MJ/kg = 12.53 kWh_{th}/kg

5.14.1 Tractors 4x2

5.14.1.1 Conventional tractors, diesel-fuelled

From technical magazines and multiple internet resources FC values for vehicles with known and unknown payload were collected, see Table 56.

Table 56. Consumption values for tractor trailers (TT), diesel-fuelled, mainly motorway operation

* marked FC values with known payload are compared directly to the simulation results, see p. 90 Figure 90

L/ 100km	Description	Source
	TT - Tractor-trailer	
Road measurement		
25.4	Route "Wundschuh" MB, Actros 3 1848 LS, MY 2010; curb weight 8.5 t; engine MB OM 501, 6 cyl. 11.9 L € 5, 2300 Nm @ 1400 rpm, 350 kW @ 1800 rpm; 12-speed AMT MB G281, 14.93 to 1.00; i _{FD} 3.07; tires 315/80R22.5, r _{dyn} 0.522 m, 3-axle trailer curtainsider 19.4 t, overall test mass 27.9 t	own measurement 2010-10-10 (50 p. 154 ff.)
Measurements by technical magazines		
18.0 *	Route "Verkehrsrundschau empty", average FC TT, € 3, € 5, € 6 (17.9 to 18.2 L/100km), test mass close 15 t, <i>payload 0 t</i>	Verkehrsrundschau ¹²⁴
26.7 *	Route "Verkehrsrundschau full", average FC TT, € 3, € 5, € 6 (26.5 to 27.0 L/100km), test mass close 40 t, <i>payload ca. 25 t</i>	
28.1 *	Route "KFZ-Anzeiger motorway", average FC four TT € 6 MY 2014 to 2015, test mass close 40 t, <i>payload ca. 25 t</i>	KFZ-Anzeiger ¹²⁵
32.0 (25.2) *	Route "güterverkehr motorway", average FC nine TT € 6 MY 2012 to 2014, test mass ca. 39 t (26 t), <i>payload ca. 25 t (12.4 t)</i>	güterverkehr ¹²⁶
32.6 (25.5) *	Route "DVZ motorway", average FC nine TT € 6 MY 2012 to 2014, test mass ca. 39 t (26 t), <i>payload ca. 25 t (12.4 t)</i>	Deutsche Verkehrs-Zeitung ¹²⁷
34.3 *	Route "lastauto omnibus", avrg. FC seven TT € 6 MY 2013 to 2015, test mass close 40 t, <i>payload ca. 25 t</i>	lastauto omnibus ¹²⁸

¹²⁴ Verkehrsrundschau; multiple TT class 301 to 338 kW; easy / moderate altitude profile; sections without payload: Unterschleißheim - Allershausen - Pfaffenhofen - München, trip 65 km, 69 % motorway, 31 % state road; sections with full payload: Allershausen - Regensburg - Nürnberg - Langenbruck - Dasing - Unterschleißheim, trip 358 km; 86 % motorway, 14 % state road; (46 p. 31) (171 p. 10) (608 p. 78)

¹²⁵ KFZ-Anzeiger; motorway, FC 26.1 to 29.7 L/100km, P_{rated,avrg} 311 kW (302 to 324 kW); Köln-Heumar to Oberhonnefeld, moderate motorway, roundtrip 120 km; (609) (610) (611) (612) (613)

¹²⁶ güterverkehr; motorway, FC 30.7 to 34.1 L/100km (24.4 to 26.5 L/100km), P_{rated,avrg} 324 kW (301 to 338 kW); 154 km, 40 % flat, 39 % medium, 21 % hilly; (614) (615) (616) (617) (618) (619) (620) (621) (622)

¹²⁷ DVZ, FC 31.4 to 34.0 L/100km (23.5 to 26.8 L/100km), P_{rated,avrg} 322 kW (301 to 338 kW); mixed motorway flat to hilly, 521 km, incl. A7 "Kasseler Berge" with road gradient up to 7 %; (623) (624) (625)

¹²⁸ lastauto omnibus; FC 32.0 to 35.9 L/100km, P_{rated,avrg} 317 kW (301 to 331 kW); Konken to Schloßheck, hilly motorway, roundtrip 270 km; (238) (239) (626) (627) (628) (629) (630) (631)

Fleet operation, mainly long haul		
<i>If EURO-stage not published: Estimation by date. Name (headquarter) of transport company given</i>		
23.5 *	Avrg. FC TT, MB Actros 1842 € 6, 310 kW, GIRR (Graben), 2014-10, avrg. GVW 20.8 t, <i>avrg. payload assumed 6.8 t</i>	(404)
23.9 *	FC TT Renault Premium € 5, Bartkowiak (Hildesheim), 2012-03-23, Hildesheim - Goslar - Hamburg - Hildesheim, roundtrip 468 km, flat motorway, <i>avrg. payload 12 t (1/2 trip w. 24 t, Goslar to Hamburg)</i>	(405)
24.6	Avrg. FC TT, MB Actros 1842 € 6, (22.7 to 26.5 L/100km), Andres (Hanau), 2014-07; Meiberg (Soest), 2015-01; Kreykenbohm (Holzminden), 2015-05; Hövener (Rheine), 2015-11; Achtermann (Hörstel), 2015-11	(404)
25.0 *	Avrg. FC MB Axor 1843 € 5, tank semitrailer (24.2 to 26.9 L/100km), Talke (Hürth), 2013-08 to 2013-10, Hürth to Loos, 61 roundtrips 652 km, avrg. GVW 25.9 t (<i>1/2 trip with 27.2 t payload</i>), tires RRC classes B-C-BBB	(406) (407)
25.0	Avrg. FC TT fleet € 5, Papstar (Kall), 2012, tempo limit 85 km/h	(408 p. XCI)
27.4	Avrg. FC whole TT fleet € 4, Grampian (Aberdeen), 2008	(409)
28.3	Avrg. FC whole TT fleet € 5, linehaul, TNT Express (Hoofddorp), 2015, majority of vehicles assumed € 5, FC calculated from 917 gCO ₂ e/km	(410 p. 25)
29.0 *	Avrg. FC TT fleet € 3, tank semitrailers, mineral oil trade association MWV (Berlin), 2006, <i>avrg. payload assumed 13.3 t (1/2 max. payload)</i> , calculated from weighted average density of transported gasoline and diesel fuel	(411 p. 6)
29.0	Avrg. FC TT € 4, Rigterink (Nordhorn), Hermsdorf to Ohrdruf, roundtrips 210 km, 2008-07 to 2009-05,	(412 p. 12)
29.1	Avrg. FC 13 TT € 6, Bartkowiak (Hildesheim), 2014 to 2015 ¹²⁹	(413)
29.7	Avrg. FC three TT € 6, DB Schenker (Frankfurt), Große-Vehne (Rhede), Elflein (Bamberg), 5 days in 2015, motorway ¹³⁰	(272)
29.9	Avrg. FC long haul trucks ("Fjärr"), DB Schenker (Göteborg), SE 2014	(414 p. 36)
30.0	19 roundtrips 1'190 km, Wundschuh to Göppingen via Schober Pass Volvo, FH12, MY 2013, eng. Volvo D13K460 € 6, 6 cyl. 12.8 L, 2300 Nm @ 1400 rpm, 338 kW @ 1800 rpm, 12-speed AMT, 14.94 to 1.00 Semitrailer with curtainsider body, payload 1.4 to 13.0 t	(415 pp. 14-16)
30.4 *	Avrg. FC TT € 4 (26 to 33 L/100km), reg. delivery traffic Aix-en-Provence, 2010 to 2011, $v_{roll,avrg}$ 70 km/h, <i>avrg. payload ca. 8 t</i> , vehicles assumed € 4	(416 p. 18)
30.5	Avrg. FC whole TT fleet € 5, Hebtling (Schweighouse), 2014	(417)
31.1	Avrg. FC seven TT € 6, avrg. 333 kW (323 to 345 kW), Fehrenkötter (Ladbergen), 2014-02 to 2016-07, per TT avrg. 133'420 km p. a., avrg. m_{curb} tractor & trailer 18.79 t (18.46 to 19.04 t)	(418 p. 25)
31.2	Avrg. FC two TT € 5, Fritz (Heilbronn), 2015	(419 p. 11)
32.0 *	Avrg. FC MB Actros 1845 € 5, Schröder (Ebernhahn), 2015, GVW always 40 t, <i>avrg. payload assumed 26 t</i>	(420)
33.8	Avrg. FC six TT € 5, Fehrenkötter (Ladbergen), 2007 to 2011, per TT avrg. 138'600 km/a, transport of agricultural machines	(421)
34.0	Avrg. FC whole TT fleet (33 to 35 L/100km), DB Schenker (Frankfurt a. M.), Germany 2010, vehicles assumed € 4	(422)
35.0 *	Avrg. FC TT, Renault Premium 460 € 5, 338 kW, 8 roundtrips 228 km Thüringen, 68 % motorway, 32 % state road, v_{avrg} 70.1 km/h, <i>payload 24 t</i>	(423 p. 46/47)

¹²⁹ Fuelling protocols 2014-07-29 to 2015-06-23; 7 tractors MB, 6 Renault; avrg. FC 29.1 L/100km (27.6 to 30.6 L/100km), avrg. mileage 104'170 km (85'780 to 119'430 km), avrg. fuelling date 2014-12-24 (2014-07-05 to 2015-06-19); tractor IDs 148, 1846, 1847, 1848, 1849, 1900, 2700, 6010, 6011, 6012, 6013, 6014, 6016

¹³⁰ Motorways in Germany; roundtrips, daily mileage 860, 840 and 570 km; FC 27.7, 30.6 and 31.5 L/100km

Table values and statistics, long haul		
26.3	Table values, TT € 6, 34 to 40 t GCWR, motorway flat, 14.5 t payload ¹³¹	(45 p. 153)
30.1	Table values FR, TT GCWR 42 t, highway cycle, 14.5 t payload	(424 p. 23)
30.7	Table values, TT € 6, 34 to 40 t GCWR, motorway hilly, 14.5 t payload. Also used as default by German hauliers association DSLV	(45 p. 158) (362 pp. 45, 53)
32.6	Statistics FR, avrg. FC all TT (tracteur & semi-remorque), 2014	(49 p. 28)
32.8	Table values DE, truck with trailer € 5, 34 to 40 t GCWR, motorway, 14.4 t payload (60 %), ProBas data	(425)
35.2	Table values, TT € 6, 34 to 40 t GCWR, motorw. mountains, 14.5 t payload	(45 p. 163)
35.7	Statistics DE, avrg. FC all TT (Sattelzugm.), 2008 6'426 10 ⁶ L-Diesel / (18 10 ⁹ km)	(426 p. 40)

5.14.1.2 Payload-specific GHG emission factors, tractor-trailers, diesel-fuelled

For the vehicles where the payload was known, the payload-specific GHG emissions in gCO₂e/tkm were calculated, see Table 57. In addition other published data was added.

Table 57. Payload-specific GHG emissions, tractor-trailers, diesel-fuelled, 3'240 gCO₂e/L-Diesel

* marked GHG values with known payload are compared directly to the simulation results, see p. 90 Figure 91.

gCO ₂ e/tkm	Description	Source
Measurements by technical magazines, vehicles € 5 and € 6		
35 *	Verkehrsrundschau, TT € 3, € 5, € 6, <i>payload ca. 25 t</i>	Compare p. 192 ff. Table 56
36 *	KFZ-Anzeiger, TT € 6, <i>payload ca. 25 t</i>	
41 (66) *	güterverkehr, TT € 6, <i>payload ca. 25 t (12.4 t)</i>	
42 (67) *	Deutsche Verkehrs-Zeitung, TT € 6, <i>payload ca. 25 t (12.4 t)</i>	
44 *	lastauto omnibus, <i>payload ca. 25 t</i>	
Fleet operation, mainly long haul		
40 *	TT € 5, Schröder (Ebernhahn), <i>payload ca. 26.0 t</i>	Table 56
47 *	Measurement Thüringen, Renault Premium 460 € 5, <i>payload ca. 24.0 t</i>	
60 *	TT € 5, Talke (Hürth), <i>avrg. payload 13.6 t</i>	
65 *	TT € 5, Bartkowiak (Hildesheim), <i>avrg. payload 12.0 t</i>	
71 *	TT € 3, MWV (Berlin), <i>avrg. payload assumed 13.3 t</i>	
72	TT € 5 & € 6, road transport 2015, DSV (Hedehusene)	(427 p. 28)
79	TT € 5, road transport 2013, XPO (Lyon)	(428)
112 *	TT € 6, Girr (Graben), <i>avrg. payload ca. 6.8 t</i>	Table 56
123 *	TT € 4, Aix-en-Provence, $v_{roll,avrg}$ 70 km/h, <i>avrg. payload ca. 8 t</i>	
Table values and GHG calculators, long haul		
59	Table values, TT € 6, 34 to 40 t GCWR, motorway flat, 14.5 t payload	(45 p. 153)
69	Table values, TT € 6, 34 to 40 t GCWR, motorway hilly, 14.5 t payload. Also used as default by German hauliers association DSLV	(45 p. 158) (362 pp. 45, 53)
72	Table values, German hauliers association DSLV	(362 p. 13)
74	Table values, truck with trailer € 5, 34 to 40 t GCWR, 14.4 t payl., ProBas	(425)
75	GHG calculator for transport, EcoTransIT, according EN 16258 (208), 100 t goods from Graz to Lisboa, truck € 6, 21 t-CO ₂ e / (100 t · 2'787 km)	(429)
79	Table values, TT € 6, 34 to 40 t GCWR, motorw. mountains, 14.5 t payl.	(45 p. 163)
96	Table values FR, TT (Ensemble articulé), diverse goods (Marchandises diverses), long haul, GCWR 40 t	(368)

¹³¹ HBEFA data, linear interpolation with payload, $[21.8 + (29.9 - 21.8) \cdot 14.5 \text{ t} / 26 \text{ t} = 26.3]$ L/100km

5.14.1.3 Conventional tractors, CNG-fuelled

For gas-fuelled tractors only data from one direct comparison of a CNG-vehicle and a conventional diesel-vehicle was found, compare Table 58.

Table 58. Comparison measurement of diesel- and CNG-fuelled tractors

Value	Description	Source
	Iveco, Stralis tractor, Diesel- vs. CNG-engine, 12-speed AMT ZF AS 1930, 15.68 to 1.00, i_{FD} 3.70, tires 315/70R22.5; 3-axle trailers, total mass each trailer 19.1 t. Test route 158 km with 47 km/h	(430 p. 18)
3.50 kWh _{th} /km	Engine Iveco Cursor 8 Diesel, 6 cyl. 7.8 L € 5/EEV, 1500 Nm @ 1700 rpm, 243 kW @ 2400 rpm; curb weight tractor 6.4 t, test mass tractor-trailer 25.5 t FC 35.2 L/100km	
4.47 kWh _{th} /km +28 %	Engine Iveco Cursor 8 CNG, 6 cyl. 7.8 L € 5/EEV, 1300 Nm @ 1700 rpm, 243 kW @ 2000 rpm; curb weight tractor 6.9 t, test mass tractor-trailer 26.0 t FC 35.7 kg/100km	

5.14.2 Delivery trucks 4x2

5.14.2.1 Conventional delivery trucks, diesel-fuelled

For the absolute FC of conventional delivery trucks of GVWR 12 t in general less data was available, the found numbers are shown in Table 59.

Table 59. Consumption values for delivery trucks (DT), diesel-fuelled, urban traffic

L/100km	Description	Source
Chassis dynamometer		
20.3, 20.9	VECTO cycles RD12, UD12-flat MB, Atego 1224 L, MY 2011; curb weight w. body 6.9 t; engine MB OM 906, 6 cyl. 6.4 L € 5, 850 Nm @ 1600 rpm, 175 kW @ 2200 rpm; 6-speed AMT, 6.70 to 0.73; i_{FD} 4.30; tires 265/70R19.5, r_{dyn} 0.421 m <u>Chassis dyno</u> : total vehicle mass 9.3 t; $F_0 = 598$ N, $F_2 = 2.87$ N/(m/s) ²	own measurement 2015-02-20
Road measurement		
25.2	Urban traffic MB, Atego 1222, MY 2012; GVWR 12 t, curb weight w. body 6.48 t; engine MB OM 924 LA, 4 cyl. 4.8 L € 5/EEV, 810 Nm @ 1600 rpm, 160 kW @ 2200 rpm; 6-speed MT, 6.70 to 0.73; tires 265/70R19.5; test mass 11.76 t	(431 p. 26)
20.5	Urban traffic, 30 km Iveco, Eurocargo 120E25, MY 2008; GVWR 12 t, curb weight w. body 6.40 t; engine Iveco, 6 cyl. 5.9 L € 5, 850 Nm @ 2280 rpm, 185 kW @ 2700 rpm; 6-speed AMT, 6.58 to 0.78; i_{FD} 4.11; tires 245/70R19.5, test mass 11.87 t	(432)
Fleet operation, urban delivery		
21.5	Urban delivery traffic region Stockholm, 2013 & 2014 Conventional diesel truck GVWR 12 t, € 5, test mass unknown	(433 p. 18)
16.1, 17.2, 21.8	Field test, each truck ca. 3'000 km, 4 weeks, London (47.8 km/h, 0.8 stops/km), Eindhoven (33.2 km/h, 0.8 stops/km), Hull (19.3 km/h, 1.3 stops/km) <i>Average FC three delivery trucks</i> : DAF, LF 45.160; GVWR 12 t; engine Paccar FR 118, 4 cyl. 4.5 L € 5/EEV, 600 Nm @ 1800 rpm, 118 kW @ 1900 rpm; 5-speed AMT; i_{FD} 3.73; tires 225/75R17.5 Test mass unknown.	(434) (435 p. 36/37)

Table values		
17.9	Truck € 6, 7.5 to 12 t GVWR, intra-urban flat, 1.8 t payload	(436 p. 150)
17.9	Truck GVWR 7.5 to 12 t, avrg. road gradient, intra-urban, 1.8 t payload, German hauliers association DSLV	(362 pp. 45, 53)
18.4	Truck € 6, 7.5 to 12 t GVWR, intra-urban hilly, 1.8 t payl.	(436 p. 155)
18.8	Truck € 6, 7.5 to 12 t GVWR, intra-urban mountains, 1.8 t pl.	(436 p. 160)
19.6	Truck € 5, 7.5 to 12 t GVWR, 2 t payload (40 %), intra-urban, ProBas	(437)

5.14.2.2 Hybrid diesel-electrical delivery trucks

For the comparison of conventional and hybrid delivery trucks more FC values are published, see the list in Table 60.

Table 60. Comparison measurements of conventional and hybrid electrical delivery trucks

Change FC	Description	Source
Chassis dynamometer		
	Conv.: Freightliner, M2 106, MY 2012; GVWR 11.8 t; engine Cummins ISB 220, 6 cyl. 6.7 L, 705 Nm @ 1600 rpm, 160 kW @ 2600 rpm; test mass 14.3 t	<i>Delivery trucks, pair 1</i> (254 p. 28 ff.)
	HEV: Freightliner, M2 106 Hybrid, MY 2010; GVWR 15.8 t; engine Cummins ISB 325, 6 cyl. 6.7 L, 1020 Nm @ 1800 rpm, 235 kW @ 2600 rpm; parallel hybrid system Eaton, motor-generator ±250 (420) Nm, ±26 (44) kW, battery Li-Ion 1.8 kWh; 6-speed AMT Eaton, test mass: 14.8 t	
-21 % FC	Cycle WVUC, FC _{HEV} 33.1 L/100km, FC _{conv} 41.8 L/100km	
-10 % FC	Cycle HD UDDS, FC _{HEV} 27.3 L/100km, FC _{conv} 30.4 L/100km	
+6 % FC	Cycle EPA-GHG, FC _{HEV} 26.7 L/100km, FC _{conv} 25.2 L/100km	
	Conv.: Freightliner, M2 106, tractor 4x2, MY 2009; GVWR 15.8 t; curb weight 5.1 t; engine Cummins ISC 285, 6 cyl. 8.3 L, 1085 Nm @ 1300 rpm, 213 kW @ 2000 rpm; 7-speed MT Eaton; i _{FD} 3.58; tires 275/80R22.5, r _{dyn} 0.491 m <u>Chassis dyno:</u> test mass 15.4 t; RRC 8.4 N/kN; C _d ·A _{cr} 7.84 m ²	<i>Delivery tractor-trailer, chassis dyno</i> (253 p. 12) (252)
	HEV: Kenworth, T370 Hybrid, tractor 4x2, MY 2010; GVWR 15.8 t, curb weight 5.3 t; engine Paccar PX 6 280, 6 cyl. 6.7 L, 896 Nm @ 1600 rpm, 209 kW @ 2000 rpm; parallel hybrid system Eaton, <i>see above</i> ; i _{FD} 5.38; tires 275/80R22.5, r _{dyn} 0.491 m <u>Chassis dyno:</u> test mass 15.6 t; RRC 9.4 N/kN; C _d ·A _{cr} 7.84 m ²	
-23 % FC	Cycle WVUC, FC _{HEV} 40.7 L/100km, FC _{conv} 53.1 L/100km	
-18 % FC	Cycle CILCC, FC _{HEV} 31.2 L/100km, FC _{conv} 38.1 L/100km	
±0 % FC	Cycle HHDDT, FC _{HEV} 38.2 L/100km, FC _{conv} 38.2 L/100km	
Test track, Pick-up cycle		
	Conv.: Navistar Int., Dura Star, truck 4x2 class 7, MY 2010; curb weight 7.9 t; engine Navistar MaxxForce7, V8 6.4 L EPA '10, 900 Nm @ 1600 rpm, 224 kW @ 2600 rpm; 6-speed MT Eaton; i _{FD} 4.30; tires 11R22.5; test mass 12.5 t	<i>Delivery trucks, pair 2</i> (255 p. 9)
	HEV: <i>Two trucks of same type;</i> Kenworth, T370 Hybrid, truck 4x2 class 7, MY 2009; curb weight 7.55 t (7.34 & 7.76 t); engine Paccar PX-6, 6 cyl. 6.7 L EPA '07, 760 Nm @ 1600 rpm, 179 kW @ 2600 rpm; parallel hybrid system Eaton, <i>see above</i> ; i _{FD} 5.57; tires 11R22.5; test mass 12.2 t (11.90 & 12.48 t)	
-20 % FC	FC _{HEV} 23.4 L/100km (22.0 to 24.9 L/100km), FC _{conv} 29.2 L/100km	

Road measurement		
-24 % FC	Urban traffic, hybrid vs. conventional truck MB, Atego 1222 Hybrid, MY 2012; GVWR 12 t, curb weight w. body 6.79 t; engine MB OM 924 LA, 4 cyl. 4.8 L € 5/EEV, 810 Nm @ 1600 rpm, 160 kW @ 2200 rpm; parallel hybrid system Eaton, <i>see above</i> ; 6-speed AMT, 6.70 to 0.73; tires 265/70R19.5; test mass 11.84 t FC _{HEV} 19.2 L/100km, FC _{conv} 25.2 L/100km	(431 p. 26)
-10 % FC	Urban traffic, hybrid vs. conventional truck Iveco, Eurocargo Hybrid 75E16, MY 2012; GVWR 7.5 t, curb weight w. body 5.69 t; engine Iveco Tector 4, 4 cyl. 3.9 L € 5/EEV; 535 Nm @ 1250 rpm, 118 kW @ 2700 rpm; parallel hybrid system Eaton, <i>see above</i> ; 6-speed AMT Eaton; i _{FD} 3.91; tires 205/75R17.5; test mass 7.5 t	(438 p. 37) (439 p. 16)
-10 % FC	Urban delivery traffic, hybrid vs. conventional trucks Iveco, Eurocargo 75E160 Hybrid; MB, Atego 1222 Hybrid, <i>see above</i> DAF, LF 45.160 Hybrid, MY 2012; GVWR 12 t, curb weight 3.76 t; engine Paccar FR 118, 4 cyl. 4.5 L € 5/EEV, 600 Nm @ 1800 rpm, 118 kW @ 1900 rpm; parallel hybrid system Eaton, <i>see above</i> ; 6-speed AMT Eaton, 7.05 to 0.78; i _{FD} 4.10; tires 245/70R17.5 MAN, TGL 12.220 Hybrid, GVWR 12 t, engine MAN D834, 4 cyl. 4.6 L € 5/EEV, 850 Nm, 162 kW; parallel hybrid system, motor-generator peak ±60 kW, battery Li-Ion 2.0 kWh; 6-speed AMT Volvo, FE 300 Hybrid [Renault, Premium Distribution Hybrys], chassis 6x2 GVWR 26 t; engine D7F300 [DX7i], 6 cyl. 7.2 L € 5, 1160 Nm [1153 Nm], 223 kW [231 kW]; parallel hybrid system Volvo, motor-generator ±70 (120) kW, battery Li-Ion 1.2 kWh; 12-speed AMT Volvo I-Shift [Optidriver+]	(440 p. 36)
Fleet operation, urban delivery		
-11 % FC	Urban delivery traffic region Stockholm, 2013 & 2014, 7 hybrid trucks € 5 vs. conventional diesel trucks € 5 Volvo, FE 300 Hybrid, <i>see above</i> FC _{HEV} 27.5 L/100km, FC _{conv} 31.0 L/100km	(433 p. 17)
-9 % FC	Urban delivery traffic region Stockholm, 2013 & 2014, 7 hybrid trucks € 5 vs. conventional diesel trucks € 5 DAF, LF45-160 Hybrid, <i>see above</i> FC _{HEV} 19.6 L/100km, FC _{conv} 21.5 L/100km	(433 p. 15)
+0.5 % FC	Urban delivery traffic region Stockholm, 2013 & 2014, 2 hybrid trucks € 5 vs. conventional diesel trucks € 5 MB, Atego 1222 Hybrid, <i>see above</i> FC _{HEV} 21.6 L/100km, FC _{conv} 21.5 L/100km	(433 p. 18)
14.9, 14.9, 17.2 -8, -13, -21 % FC	Field test urban delivery, each truck ca. 3'000 km, 4 weeks London (46.1 km/h, 0.8 stops/km), Eindhoven (32.1 km/h, 0.8 stops/km), Hull (20.9 km/h, 1.3 stops/km) Average FC three parallel hybrid electric delivery trucks: DAF, LF 45.160 Hybrid, <i>see above</i> ; i _{FD} 3.73; tires 225/75R17.5	(434) (435 p. 36/37)

-12 % FC	Urban delivery traffic Miami (flat), 2010-05 to 2011-05, 70 km per day, 1.0 stops/km, v_{avg} 36.5 km/h, $k_{i,avg}$ 0.468 1/km (0.23 to 0.64 1/km) Kenworth, T370 Hybrid vs. Freightliner, M2 1206, <i>see above</i> average test masses with trailer ca. 19.6 t FC _{conv} 41 L/100km (38.9 to 46.7 L/100km) FC _{HEV} 37 L/100km (34.4 to 38.5 L/100km)	<i>Delivery tractor-trailer, urban delivery traffic</i> (252) (253 p. vii ff.)
-10 % FC	Urban delivery traffic London, 2008-11 to 2010-04 Mitsubishi, Canter Eco Hybrid, MY 2008; GVWR 7.5 t; engine Mitsubishi 4M42 T2, 4 cyl. 3 L € 4, 362 Nm @ 1700 rpm, 107 kW @ 3200 rpm; parallel hybrid system Mitsubishi, motor-generator ±15 (35) kW, battery Li-Ion 1.9 kWh, 5-speed AMT Inomat-II, <i>no start-stop</i> FC _{HEV} 17.0 L/100km, FC _{conv} 18.8 L/100km	(441 p. 32)

5.14.2.3 Battery-electrical delivery trucks

In case of battery-electrical delivery trucks the data basis from publications was small. Only one fleet test was found, see Table 61.

Table 61. Energy consumption of battery electrical delivery trucks

EC in kWh/km	Description	Source
0.786	Urban delivery traffic, 40 US cities, 2013-01 to 2014-09 → Basis for cycle Smith Newton Electrical (SN) Avg EC _{batt,drive} 200 delivery trucks: " <i>Driving DC Electrical Energy Consumption</i> ", <i>energy demand during driving (consumpt. - regen.), w/o stops</i> Smith, Newton gen. 2, chassis 4x2; GVWR 11.8 t, curb weight 4.4 to 4.6 t; motor-generator peak ±600 Nm, ±120 kW; battery Li-Ion 80 or 120 kWh; 1-speed reduction gear; tires 245/70R19.5, r_{dyn} 0.402 m	(163) (269 p. 7)
0.9 to 1.2	Urban delivery traffic, payload unknown MAN, TGL Elektro, battery mass 1.5 t	(442 p. 31)

5.14.3 City buses 12 m 4x2

5.14.3.1 Conventional city buses 12 m, diesel-fuelled

For the basis diesel-fuelled 12 m city bus much FC values were published. Some are from the comparison vehicles from fleet tests of hybrid buses. The relative saving potential is given later on p. 204 ff. in sections 5.14.3.3 and 5.14.3.4, where also the hybrids are described.

Table 62. FC of conventional diesel city buses 12 m, 4x2 GVWR 18 t

L/100km	Description	Source
Chassis dynamometer		
42.8, 48.0	Cycles Braunschweig, Graz Van Hool, A330-2; MY 2009; curb weight 12.44 t; engine MAN D2066 LOH26, 6 cyl. 10.5 L € 5, 1600 Nm @ 1400 rpm, 235 kW @ 1900 rpm; 4-speed AT Voith 854.5, 8.00 ¹³² to 0.74, i_{FD} 5.74; tires 275/70R22.5, r_{dyn} 0.465 m Chassis dyno: Test mass 15.06 t; $F_0 = 960$ N, $F_2 = 3.07$ N/(m/s) ²	own measurement 2016-01-28
44.4	Cycle Braunschweig Avrg. FC of 23 buses € 5/EEV, half payload, test mass around 15 t	(443 p. 54) (444 p. 9)
44.7, 49.3, 38.6, 50.8	Cycles Braunschweig, Helsinki 1, Helsinki 2, Stockholm Avrg. FC of 3 buses; MY 2007, 2011, 2011; € 5/EEV, 1/2 payl., test mass 15.5 t	(314 p. 19 ff.)
42, 32, 30, 96, 55, 28	Cycles Braunschweig, HD UDDS, JE05, NYBus, Paris, WHVC Bus; engine 6 cyl. 7.2 L € 5/EEV; test mass 15.1 t	(256 pp. 107, 176)
Test track, SORT cycles, payload 3.2 t, procedure according (313)		
38.0	SORT 2 Autosan, Sancity 12LF, MY 2015; curb weight 10.8 t; engine Cummins ISB, 6 cyl. 6.7 L € 6, 204 kW; 4-speed AT Voith, 8.00 to 0.74; test mass 14.0 t	(392 p. 17)
33.6, 38.9	SORT 2. Two buses € 6	(445 p. 5)
47.9, 38.8	SORT 1, 2. Bus € 5	(446 p. 81)
47.3, 38.7, 35.4	Cycles SORT 1, 2, 3; <i>chassis dyno</i> Bus € 5/EEV	(260 p. 30)
45.2	SORT 2. Bus € 5/EEV, 7-speed AT ZF 6 HP	(447 p. 12)
51.1, 40.1, 36.0	SORT 1, 2, 3. Bus € 5/EEV	(448 p. 5)
54.7, 43.3, 38.0	SORT 1, 2, 3 Solaris, Urbino 12, MY 2009; engine DAF € 5, 231 kW	(449 p. 206)

¹³² In this overview the variable ratio of the (power split) first gear with the active hydraulic torque converter is set to 8.00 for all AT models.

Test track, Altoona cycle, w/o air conditioning		
48.9 Pt. I to III: 59.8, 52.6, 28.7	Cycle Altoona. Bus 12.2 m 4x2 New Flyer, XD40, MY 2012; GVWR 19.3 t, curb weight 12.6 t; engine Cummins ISL 280, 6 cyl. 8.8 L, 1220 Nm @ 1300 rpm, 209 kW @ 2000 rpm; 7-speed AT Allison, 8.00 to 0.64; i_{FD} 4.63; tires 305/70R22.5, test mass 15.1 t	(263 p. 41)
76.8 Pt. I to III: 90.3, 79.6, 53.8	Cycle Altoona. Bus 12.8 m 4x2 New Flyer, D40LF, MY 2006; GVWR 19.3 t, curb weight 13.3 t; engine Cummins ISM 280, 6 cyl. 10.8 L, 1560 Nm @ 1200 rpm, 209 kW @ 2100 rpm; 7-speed AT ZF, 8.00 to 0.59; i_{FD} 5.40; tires 305/70R22.5, test mass 14.5 t	(450 p. 34)
53.2 Pt. I to III: 67.3, 53.4, 31.8	Cycle Altoona. Bus 12.2 m 4x2 Gillig, Low Floor, MY 2004; GVWR 18.0 t, curb weight 12.4 t; engine Cummins ISM 280, 6 cyl. 10.8 L, 1560 Nm @ 1200 rpm, 209 kW @ 2100 rpm; 4-speed AT Voith DIWA; i_{FD} 5.38; tires 12R22.5, test mass 14.8 t	(451 p. 93)
Road measurement, w/o air conditioning		
56.3	Stuttgart line 42, Schlossplatz to Erwin-Schoettle-Platz, roundtrip 21 km MAN, Lion's City Evolution, MY 2016; curb weight 11.93 t; engine MAN D2066 LUH, 6 cyl. 10.52 L € 6, 1600 Nm @ 1400 rpm, 235 kW @ 1900 rpm; 7-speed AT ZF, 8.00 to 0.62; i_{FD} 5.13; tires 275/70R22.5, test mass 15.94 t	(388 p. 52)
45.4	Novi Sad 2014-11, urban bus line, roundtrip 10.9 km, v_{avg} 17.7 km/h, $v_{roll,avg}$ 23.6 km/h, stand ratio 25 %, 3.4 total-stops/km Iveco, Crossway LE; engine Iveco Cursor 8, 6 cyl. 7.9 L € 5, 243 kW; 4-speed AT Voith D864.5, 8.00 to 0.74; payload around 1.5 t \approx 24 pass. FC calculated via carbon-balance from mobile measured CO ₂ emissions	(452 p. 98)
53.1	Stuttgart line 42, Schlossplatz to Erwin-Schoettle-Platz, roundtrip 21 km MAN, Lion's City, MY 2013; curb weight 12.07 t; engine MAN D2066 LUH, 6 cyl. 10.52 L € 6, 1600 Nm @ 1400 rpm, 235 kW @ 1900 rpm; 7-speed AT ZF Ecolife, 8.00 to 0.62; i_{FD} 5.13; tires 275/70R22.5, test mass 15.79 t	(387 p. 58)
29.1	Beijing, cycle BJBC. Avg. FC of four buses € 5, payload 1 t, w/o A/C FC calculated via carbon-balance from mobile measured CO ₂ emissions, normalised to BJBC driving cycle (27.5, 27.8, 29.1 and 31.9 L/100km)	(289 p. 1653)
58.2	Stuttgart line 42, Schlossplatz to Erwin-Schoettle-Platz, roundtrip 21 km MB, Citaro, MY 2011; curb weight 11.34 t; engine MB OM 906 LA, 6 cyl. 7.2 L € 5/EEV, 1120 Nm @ 1600 rpm, 210 kW @ 220 rpm; 4-speed AT Voith Diwa 854.5, 8.00 to 0.74; i_{FD} 5.77; tires 275/70R22.5, test mass 16.10 t	(266 p. 48)
51.2	Berlin, urban bus traffic, roundtrip 47 km, v_{avg} 17.6 km/h, 1.9 bus-stops/km, 3.3 total-stops/km VDL, Citea SLF-120; MY 2010; curb weight 11.16 t; engine DAF PR228, 6 cyl. 9.2 L € 5/EEV, 1275 Nm @ 1700 rpm, 228 kW @ 2200 rpm; 4-speed AT Voith 864.5, 8.00 to 0.74; i_{FD} 6.1; tires 275/70R22.5, test mass 15.94 t	(453)
62.4	Stuttgart line 42, Schlossplatz to Erwin-Schoettle-Platz VDL, Citea SLF-120, <i>see above</i> , i_{FD} 5.13, test mass 16.40 t	(265 p. 50)
Fleet tests and line operation		
42.8	Heidenheim (2014-04 to 2014-07). Line 1, Iglauer Str. to Wehrenfeld, roundtrip 17.0 km, v_{avg} ca. 21 km/h, peak time 2.5 bus-stops/km. Avg. FC one bus € 5	(262 p. 66)
42.5, 42.9, 40.8, 36.9	Ingolstadt (2014-03 to 2014-08), Hamburg 1 (2013-09 to 2014-06), Hamburg 2 (2014-03 to 2014-08), Hannover (2014-04 to 2014-08). (Sub-) urban bus lines, v_{avg} 17 to 22 km/h, flat terrain. Avg. FC of buses € 5	(454 p. 20) (455)
35.6	Wolfsburg, 2014-08. (Sub-) urban bus lines, flat terrain. Avg. FC one bus € 6	(454 p. 20)
41.1	Aarau (2013). Urban bus traffic, $v_{avg} \approx$ 17 km/h, ca. 3 total-stops/km MAN, Lion's City, curb weight ca. 12 t; engine MAN D 2066 LUH 41, 6 cyl. 10.5 L € 5/EEV, 1250 Nm @ 1400 rpm, 206 kW @ 1900 rpm; 4-speed AT Voith DIWA, 8.00 to 0.74; i_{FD} 5.74	(456 p. 9)

36.9	Helsinki (summer 2012). Line 42, Kamppi(M) to Kannelmäen asema, roundtrip 29 km, v_{avg} ca. 28 km/h, peak time 1.7 bus-stops/km. Avg. FC three buses, Scania, € 5/EEV	(457 p. 25)
36.6	Tampere (2013-03 to 2013-10, w/o 2013-07). <u>Line 21</u> , Turtola to Länsitori, roundtrip 44 km, v_{avg} ca. 26 km/h, peak time 2.4 bus-stops/km. <u>Line 25</u> , Janka to Tahmela, roundtrip 20 km, v_{avg} ca. 19 km/h, peak time 3 bus-stops/km Avg. FC one bus 13 m, Volvo, € 5/EEV, MY 2011	(457 p. 26)
55.7	Ames, IA (2011-07 to 2012-08) 12 (sub-)urban bus lines Avg. FC 7 buses 12.2 m 4x2: Gillig, Low Floor, MY 2008 to 2010; curb weight 11.35 t; engine Cummins ISL 280, 6 cyl. 8.8 L, 1220 Nm @ 1300 rpm, 209 kW @ 2000 rpm; 4-speed AT Voith DIWA 864.5, 8.00 to 0.74	(458 p. 20)
41.2	Cagliari. Urban bus lines. MB, Citaro € 5, 7-speed AT ZF EcoLife, 8.00 to 0.62	(447 p. 12)
46.7	Darmstadt, München, Ruhr region. (Sub-) urban bus lines, 2010 & 2011 Avg. FC four buses € 5	(459 p. 59)
47, 40, 35	(Heavy) urban, suburban, interurban bus lines. Buses € 5, guiding values MAN	(460 p. 152)
60, 45, 38	German cities, urban bus traffic. Heavy urban (12 km/h), urban (18 km/h), suburban (27 km/h) bus lines Avg. FC buses € 5/EEV, payload 1.5 t \approx 22 pass.	(461 p. 74)
45.5	Leipzig line 89 (2009-09-25 to 2009-10-03), Hauptbahnhof to Connewitz Kreuz, roundtrip 17.6 km, v_{avg} ca. 18 km/h, peak time 1.8 bus-stops/km Average FC two buses (45.4 and 45.6 L/100km) Solaris Urbino 12, MY 2009; GVWR 18 t, curb weight ca. 12 t; engine Paccar PR 183, 6 cyl. 9.2 L € 5/EEV, 1050 Nm @ 1700 rpm, 183 kW @ 2000 rpm; Transmission 1: 7-speed AT ZF, 8.00 to 0.62; Transmission 2: 4-speed AT Voith DIWA, 8.00 to 0.74	(168 p. 18)
67.8	Washington, DC (2006-09 to 2007-05). Suburban bus lines, v_{avg} ca. 28 km/h Avg. FC 10 buses 12.8 m 4x2 New Flyer, D40LF, MY 2006; GVWR ca. 19.3 t, curb weight ca. 13.3 t; engine Cummins ISM 280, 6 cyl. 10.8 L, 1560 Nm @ 1200 rpm, 209 kW @ 2100 rpm; AT Allison B-400R	(450 p. 6 ff.) (462 pp. B-15 ff.)
103.3 & 99.0	New York, bus depots West Farms & Mother Clara Hale (2004-06 to 2005-05). Heavy urban traffic, $v_{avg} \approx 10.3$ km/h Avg FC, 9 & 9 buses 12.2 m 4x2: Orion, V, MY 1994 and 1999; GVWR 18.2 t, curb weight 12.9 t; engine DDC S50, 4 cyl. 8.5 L, 1200 Nm @ 2300 rpm, 205 kW @ 2100 rpm; AT Allison B-400R	(463 p. 25)
Table values		
30.3, 44.1, 56.4	Intra-urban bus traffic, free flow, dense, stop+go Table values DE, bus GVWR 15 to 18 t, based on HBEFA	(464 p. 23)
37.4	Table values DE, bus GVWR 15 to 18 t, € 5, 18 passengers (30 %), intra-urban bus traffic, ProBas data	(465)
Double decker bus 10.5 m, line operation		
47.5	London line 159 (2011-02-06 to 2011-03-05), Streatham Station to Marble Arch, roundtrip 26 km, v_{avg} ca. 14 km/h, peak time 4.9 bus-stops/km Avg. FC two buses (47.6 and 47.3 L/100km): ADL, Enviro 400, MY 2010; engine Cummins ISB, 6 cyl. 6.7 L € 4, 950 Nm @ 1600 rpm, 186 kW @ 2300 rpm Wright, Gemini 2, chassis Volvo B9TL, MY 2010; curb weight 12.1 t; engine Cummins ISB, 6 cyl. 6.7 L € 5, 950 Nm @ 1600 rpm, 186 kW @ 2300 rpm (assumptions, power stage of Cummins engine unknown)	(466 p. 26)

Table 63. FC of optimised conventional diesel city buses 12 m, 4x2 GVWR 18 t

L/100km	Description	Source
Road measurement		
49.0	Stuttgart line 42, Schlossplatz to Erwin-Schoettle-Platz, roundtrip 21 km MB, Citaro, MY 2013; curb weight 11.42 t; engine MB OM 936, 6 cyl. 7.7 L € 6, 1200 Nm @ 1600 rpm, 220 kW @ 2200 rpm; 7-speed AT ZF Ecolife, 8.00 to 0.62; i_{FD} 5.77; tires 275/70R22.5, test mass 15.68 t. <i>Regenerative braking with three alternators, each ca. 3.6 kWh_{el}, energy storage SCap 0.024 kWh_{el}</i>	(273 p. 52)
38.4	Wiesbaden (2012-10-22 to 2012-10-26), line 17, Graf-von-Galen-Str. to Wolfsfeld, roundtrip 18.6 km, v_{avg} 16.6 km/h, 1.35 bus-stops/km, $ \Delta alt/\Delta s _{norm}$ 2.3 %, 1'360 km in 5 days MB, Citaro, <i>see above</i> , curb weight 10.5 t, test mass 13.7 t	(183) (274)

5.14.3.2 Conventional city buses 12 m, CNG-fuelled

Also for gas-fuelled rigid buses sufficient published data for comparison purposes is available, see the list in the following Table 64. The relative change of fuel energy per km in comparison to the diesel buses from p. 199 ff. Table 62 is also given. The corresponding diesel vehicles can be identified by the driving cycle and/or by the source number, if not written.

Table 64. FC of natural gas-fuelled city buses 12 m, CNG pressure tanks, 4x2 GVWR 18 t and change of energy consumption (EC in terms of LHV) vs. corresponding diesel buses from Table 62

kg/100km, change EC	Description	Source
Chassis dynamometer		
43.4, 52.4	Cycles LUB, MLTB Scania/ADL, Enviro 300, MY 2015; curb weight 11.77 t; engine Scania OC09 101 280, 5 cyl. 9 L € 6, 1350 Nm @ 1400 rpm, 206 kW @ 1900 rpm; 7-speed AT ZF 6AP1200B, 8.00 to 0.62; tires 275/70R22.5, test mass 13.3 t	(467)
56.7	Cycle MLTB MAN, Lion's City CNG, MY 2015; curb weight 11.1 t; engine MAN E2876 LUH, 6 cyl. 12.8 L € 6, 200 kW; 4-speed AT Voith DIWA.5, 8.00 to 0.74; test mass 14.4 t	(468)
47.1 +33 % EC	Cycle Braunschweig Avrg. FC of 8 buses € 5/EEV, half payload, test mass around 15 t ⇒ CNG 5.89 kWh _{th} /km vs. Diesel 4.42 kWh _{th} /km → +33 %	(443 p. 54) (444 p. 9)
47.8, 51.8, 37.4, 52.0 +29 to +35 % EC	Cycles Braunschweig, Helsinki 1, Helsinki 2, Stockholm Avrg. FC of 2 buses; MY 2005, 2009; stoichiometric gas engines € 5/EEV; half payload, test mass 15.8 t ⇒ CNG 6.00, 6.50, 4.69 and 6.53 kWh _{th} /km vs. Diesel 4.44, 4.89, 3.83 and 5.06 kWh _{th} /km → +35, 33, 22 and 29 %	(314 p. 19 ff.)
Test track, Altoona cycle, w/o air conditioning		
37.2 +38 % ¹³³ Pt. I to III: 42.1, 42.7, 24.3 +28, +48, +54 %	Cycle Altoona. Bus 12.5 m 4x2: New Flyer, C40LF, MY 2012; GVWR 19.3 t, curb weight 14.2 t; engine Cummins ISL G280, 6 cyl. 8.8 L, 1220 Nm @ 1300 rpm, 209 kW @ 2000 rpm; 7-speed AT Allison B400R, 8.00 to 0.65; i_{FD} 5.44; tires 305/70R22.5; test mass 16.7 t ⇒ CNG 5.99 (6.77, 6.88, 3.91) kWh _{th} /km vs. Diesel 4.33 (5.29, 4.66, 2.54) kWh _{th} /km → +38 (+28, +48, +54) %. vs. New Flyer, XD40, MY 2012	(469 p. 42)

¹³³ ABRTC utilised fuels with these lower heating values: CNG 16.10 kWh_{th}/kg, Diesel 10.64 kWh_{th}/L

Road measurement, w/o air conditioning		
49.2 +26 % EC	Stuttgart, line 42, Schlossplatz to Erwin-Schoettle-Platz, roundtrip 21 km MB, Citaro NGT, MY 2016; curb weight 11.72 t; engine MB M 936 G, 6 cyl. 7.7 L € 6, 1200 Nm @ 1200 rpm, 222 kW @ 2000 rpm; 7-speed AT ZF, 8.00 to 0.62; i_{FD} 5.82; tires 275/70R22.5, test mass 15.60 t. <i>Regenerative braking with three alternators, each ca. 3.6 kW_{el}, energy storage SCap 0.024 kWh_{el}</i> ⇒ CNG 6.16 kWh _{th} /km vs. Diesel 4.88 kWh _{th} /km → +26 %, vs. <i>Citaro € 6</i>	(470 p. 100)
44.8	Ljubljana (2012-04 to 2012-05), line 2, Nove Jarse to Zelena Jama, roundtrip 25 km, v_{avg} ca. 21 km/h, Δt ca. 70 min, 2.2 bus-stops/km Bus 12 m, MY 2011; curb weight 12.59 t, engine Otto cycle, 6 cyl. 7.8 L € 5, 213 kW; <i>FC calculated from mobile measured CO₂ and CO₂ factor of CNG, average payload during road measurement.</i>	(471 p. 438)
42.6 +18 % EC	Novi Sad 2014-11, urban bus line Solaris, Urbino 12 CNG, engine Iveco Cursor 8 CNG, 6 cyl. 7.9 L € 5/EEV, 200 kW; 4-speed AT Voith 854.5, 8.00 to 0.74; payload around 1.5 t ≈ 24 pass. ⇒ CNG 5.33 kWh _{th} /km vs. Diesel 4.50 kWh _{th} /km → +18 %	(452 p. 98)
29.8 +29 % EC	Beijing, cycle BJBC. Avg. FC of 2 buses € 5, payload 1 t, w/o A/C ⇒ CNG 3.72 kWh _{th} /km vs. Diesel 2.89 kWh _{th} /km → +29 %	(289 p. 1653)
Fleet tests and line operation		
39.6	Pomona, CA (2014-10 to 2015-07). (Sub-) urban bus lines, v_{avg} 28 km/h Avg. FC 8 buses 12.8 m 4x2. NABI, 42-BRT; MY 2014; GVWR 19.3 t, curb weight 15.4 t; engine Cummins ISL G, 6 cyl. 8.8 L, 1220 Nm @ 1500 rpm, 209 kW @ 2200 rpm; 7-speed AT Allison, 8.00 to 0.65; tires 305/70R22.5	(472 p. 20)
34.0	Kragujevac. (Sub-) urban bus lines, each bus ca. 280 km/d Average FC of 2 types of CNG buses, 33 to 35 kg/100km: MAZ-BIK, 203CNG-S, MY 2009; curb weight 12.1 t; engine Cummins Westport C Gas Plus 280, 6 cyl. 8.3 L € 4, 1150 Nm @ 1400 rpm, 209 kW @ 2400 rpm; 7-speed Allison T-325R, 8.00 to 0.65; i_{FD} 6.20; tires 275/70R22.5 MAZ-BIK, 203 CNG-S; curb weight 11.36 t; engine Cummins ISL G, 6 cyl. 8.8 L € 6, 990 Nm @ 1300 rpm, 192 kW @ 2000 rpm; 7-speed AT Allison T280, 8.00 to 0.65; tires 275/70 R 22.5	(473) (474 pp. 61, 69) (475)
40.7	Beograd (2009-05-26 to 2009-06-17). (Heavy) urban bus lines 55, 58, 74, 94 MAZ-BIK, 203CNG-S, MY 2009, <i>see above</i>	(474 p. 70)
106.0 +29 % EC	New York, bus depot West Farms (2004-10 to 2005-09) Heavy urban traffic, v_{avg} ≈ 10.4 km/h Avg. FC 10 buses 12.2 m 4x2: Orion, VII CNG, MY 2002; GVWR 19.3 t, curb weight 14.3 t; engine DDC S50 G, 4 cyl. 8.5 L, 1220 Nm @ 1200 rpm, 205 kW @ 2100 rpm; AT Allison B-400R ⇒ CNG 13.3 kWh _{th} /km vs. Diesel 10.3 kWh _{th} /km → +29 %	(463 p. 23)

5.14.3.3 Diesel-electrical parallel hybrid city buses 12 m

The found FC values for parallel hybrid city buses 12 m are shown in Table 65. The enlisted vehicles were equipped with a powertrain of specifications similar to the simulated one.

In the table also the change in FC vs. the conventional diesel buses from p. 199 ff. Table 62 is given. The corresponding diesel vehicles can be identified by the driving cycle and/or by the source number.

Table 65. FC of parallel hybrid city buses 12 m, 4x2 GVWR 18 t, powertrain similar to model

L/100km change FC	Description	Source
Chassis dynamometer		
32, 27, 22, 59, 35, 24	Cycles Braunschweig, HD UDDS, JE05, NYBus, Paris, WHVC Parallel hybrid bus; engine 4.8 L € 5/EEV, battery energy storage; total vehicle mass 15.1 t. <i>Change FC: -24, -27, -39, -36, -16, -14 %</i>	(256 pp. 107, 179)
Test track, SORT cycles, payload 3.2 t, procedure according (313)		
-30 % FC	SORT 1 Volvo, 7700LH, MY 2009 pre-series; curb weight 12.2 t; engine Volvo D5F215, 4 cyl. 4.8 L € 5, 800 Nm @ 1700 rpm, 161 kW @ 2200 rpm; parallel hybrid system Volvo, motor-generator ±400 (800) Nm, ±70 (120) kW, battery Li-Ion 4.8 kWh; 12-speed AMT Volvo AT2412D, 14.94 to 1.00; i_{FD} 4.72; tires 275/70T22.5; test mass 15.4 t	(476 p. 426)
Fleet tests and line operation		
28.8	Aarau (2015). Urban bus traffic, $v_{avg} \approx 17$ km/h, ca. 3 stops/km Volvo, 7900LH, € 5, MY 2013; curb weight 11.7 t; <i>powertrain like model 7700LH, see above</i>	(259 p. 14) (456 p. 12)
-25 % FC	Dortmund, Hamburg, Hannover, 2013-01 to 2014-09, urban bus, $v_{avg} \approx 20$ km/h 41 parallel hybrid buses € 5 vs. conventional buses € 5	(477 pp. 10-24)
30.5, 33.0 -23, 24 %	Hamburg 1 (2013-09 to 2014-06), Hamburg 2 (2014-03 to 2014-08) (Sub-) urban bus lines, flat terrain. Avg. FC Volvo, 7900LH, € 5, <i>see above</i>	(454 p. 20)
-20 % FC	Hamburg. (Sub-) urban bus lines, flat terrain Change FC, 21 hybr. buses vs. conv. buses. Volvo, 7700LH, <i>see above</i>	(478 p. 8) (479 p. 52)
29.3 -30 % FC	Aarau (2013). Urban bus traffic, $v_{avg} \approx 17$ km/h, ca. 3 total-stops/km Volvo, 7900LH, € 5, <i>see above</i>	(456 p. 9)
29.2 -21 % FC	Helsinki (summer 2012). Line 42, Kamppi(M) to Kannelmäen asema Avg. FC two buses: Volvo, 7700LH € 5/EEV, <i>see above</i>	(457 p. 24)
32.6	Luzern (2011-02 to 2012-01). Six urban bus lines (v_{avg} ca. 20 km/h) Avg. FC six hybrid buses: Volvo, 7700LH € 5/EEV, <i>see above</i>	(480 p. 10/11)
36.5	Graz (2011-08 to 2011-09). Line 39, Wirtschaftskammer to Urnenfriedhof, roundtrip 11 km, v_{avg} ca. 13 km/h, 3.5 bus-stops/km, 4.5 total-stops/km Avg. FC one hybrid bus: Volvo 7700LH € 5/EEV, MY 2010, <i>see above</i>	(481 p. 8)
32.3 -29 % FC	Leipzig line 89, Hauptbahnhof to Connewitz Kreuz Volvo 7700LH € 5/EEV, MY 2009 pre-series, <i>see above</i>	(168 p. 18)
Double decker bus 10.5 m, line operation		
35.4 -25 % FC	London line 159 (2011-02-06 to 2011-03-05) Volvo, B5L; MY 2010; double decker, <i>powertrain like model 7700LH, see above</i>	(466 p. 26)

In Table 66 found FC values for hybrid buses with parallel or power split powertrains are given, where the design differs from the simulated parallel hybrid bus.

Table 66. FC of parallel hybrid city buses 12 m, 4x2 GVWR 18 t, powertrain different from model

L/100km change FC	Description	Source
Test track, SORT cycles, payload 3.2 t, procedure according (313)		
36.5, 33.7, 30.8 -33, -22, -19 %	SORT 1, 2, 3 Solaris, Urbino H12, MY 2009; curb weight ca. 11.2 t; engine Cummins ISB 6.7 EV 225 B, 6 cyl. 6.7 L € 5, 850 Nm, 165 kW; parallel hybrid system Eaton, motor-generator ±250 (420) Nm, ±26 (44) kW, battery Li-Ion 3.6 kWh; 6-speed AMT Eaton EH8E306, 7.05 to 0.78, test mass ca. 14.4 t	(449 p. 206)
Test track, Altoona cycle, w/o air conditioning		
56.6 -26 % FC Pt. I to III: 65.6, 61.0, 38,6	Cycle Altoona. Bus 12.2 m 4x2. <i>FC change vs. New Flyer, D40LF, MY 2006</i> New Flyer, DE40LF, MY 2005; GVWR 18.4 t, curb weight 13.6 t; engine Cummins ISL 280H, 6 cyl. 8.8 L, 1220 Nm @ 1300 rpm, 209 kW @ 2200 rpm; parallel/power-split hybrid system Allison EP40, automated CVT, three planetary gear sets with two integrated motor-generators each ±38 (75) kW, battery NiMH; tires 205/70R22.5; test mass 16.2 t. <i>FC change: -27, -23, -28 %</i>	(482 p. 18)
41.3 -22 % FC Pt. I to III: 44.8, 48.5, 28.9	Cycle Altoona. Bus 12.2 m 4x2. <i>FC change vs. Gillig, Low Floor, MY 2004</i> Gillig, Low Floor Hybrid, MY 2004; GVWR 18.0 t, curb weight 12.8 t; engine Cummins ISB 260 H, 6 cyl. 6.7 L, 895 Nm @ 1600 rpm, 194 kW @ 2500 rpm; parallel/power-split hybrid system Allison EP40, <i>see above</i> ; i_{FD} 5.38; tires 12R22.5, test mass 15.5 t. <i>FC change: -33 %, -9 %, -9 %</i>	(483 p. 98)
Fleet tests and line operation		
ca. 30.0	Hannover. (Sub-) urban bus lines, v_{avg} around 22 km/h, flat terrain Avg. FC 9 hybr. buses: Solaris, Urbino H12 € 5, <i>see above</i> , MY 2013	(484) (477 p. 21)
33.7 -18 % FC	Aarau (2013). Urban bus traffic, $v_{avg} \approx 17$ km/h, ca. 3 stops/km Solaris, Urbino H12 € 5/EEV, <i>see above</i>	(456 p. 9)
32.3 -12 % FC	Tampere (2013-03 to 2013-10, w/o 2013-07) Line 21, Turtola to Länsitori, Line 25, Janka to Tahmela Avg. FC two buses 13 m: Solaris, Urbino H12 € 5/EEV, <i>see above</i> , MY 2012	(457 p. 26)
49.8 -11 % FC	Ames, IA (2011-07 to 2012-08). Operation on 12 (sub-) urban bus lines Avg. FC ten buses 12.2 m: Gillig, Low Floor Hybrid; MY 2010; curb weight 13.39 t; engine Cummins ISL 280, 6 cyl. 8.8 L, 1220 Nm @ 1300 rpm, 209 kW @ 2000 rpm; parallel hybrid system Voith, motor-generator peak ±150 kW, supercaps 0.5 kWh; 4-speed AT Voith DIWA 864.5, 8.00 to 0.74	(458 p. 20)
56.9 -16 % FC	Washington, DC (2006-09 to 2007-05). Suburb. bus lines, v_{avg} ca. 28 km/h Avg. FC 10 hybrid buses 12.2 m 4x2. New Flyer, DE40LF, MY 2006; GVWR ca. 18.4 t, curb weight ca. 13.6 t; engine Cummins ISL 280H, 6 cyl. 8.8 L, 1220 Nm @ 1300 rpm, 209 kW @ 2200 rpm; parallel/power-split hybrid system Allison EP40, <i>see above</i>	(462 pp. B-15 ff.) (482 p. 6)

5.14.3.4 Diesel-electrical serial hybrid city buses 12 m

The found FC values for serial hybrid buses 12 m are shown in Table 65, for buses with a powertrain characteristic similar to the model. Also the change in FC vs. the diesel buses from p. 199 ff. Table 62 is given. The diesel vehicles can be identified by the driving cycle and/or by the source number.

Table 67. FC of serial hybrid city buses 12 m, 4x2 GVWR 18 t, powertrain similar to model

L/100km	Description	Source
SORT cycles, test track, payload 3.2 t, procedure according (313)		
34.7, 30.4 -28, -23 % FC	SORT 1, 2 Hess, Hybrid, MY 2012; curb weight 13.6 t; engine € 5, 1000 Nm @ 1600 rpm, 170 kW @ 1800 rpm; serial hybrid system Voith, generator 1000 Nm, 165 kW, supercap 0.63 kWh, motor-generator, peak ±1600 Nm, ±280 kW; overall ratio, gearbox and final drive, 9.82; test mass 16.8 t	(446 pp. 7-15, 82) (262 p. 66)
35.7, 29.5, 28.3	SORT 1, 2, 3; chassis dyno MAN, Lion's City Hybrid, MY 2012; curb weight 12.76 t; engine MAN D 0836 LOH, 6 cyl. 6.9 L € 5/EEV, 1000 Nm @ 1750 rpm, 184 kW @ 2300 rpm; serial hybrid system Siemens ELFA, generator 1FV5168-8WS24, 700 (950) Nm, 180 (250) kW, supercap 0.4 kWh, 2 x motor-generator 1PV5138-4WS24, ±220 (530) Nm, ±85 (150) kW, summation gearbox Flender 152, ratio 4.05, i_{FD} 5.77, tires 275/70R22.5; test mass 15.96 t	(260 p. 30) (267 p. 74) (485) (486)
35.9, 29.1	SORT 1, 2. MAN, Lion's City Hybrid, <i>see above</i>	(261 p. 13)
Test track, Altoona cycle, w/o air conditioning		
40.3 -18 % FC Pt. I to III: 43.2, 46.1, 30.2	Cycle Altoona. Bus 12.2 m 4x2. FC change vs. New Flyer, XD40, MY 2012: New Flyer, XDE40, MY 2010; GVWR 19.3 t, curb weight 12.7 t; engine Cummins ISB 6.7, 6 cyl. 6.7 L €, 895 Nm @ 1600 rpm, 209 kW @ 2600 rpm; serial hybrid system BAE HybriDrive, generator 830 Nm, 200 kW, battery, motor-generator ±2400 (5100) Nm, ±160 (200) kW; i_{FD} 4.11; tires 305/70R22.5; test mass 15.4 t. Change FC: -28, -12, +5 %	(264 p. 40)
Road measurement, w/o air conditioning		
47.2 -22 % FC	Stuttgart line 42, Schlossplatz to Erwin-Schoettle-Platz, roundtrip 21 km MAN Lion's City Hybrid, <i>see above</i> , test mass 17.08 t, FC change vs. conventional buses € 5/EEV	(267 p. 74)
Fleet tests and line operation		
31.9 -25 % FC	Heidenheim (2014-04 to 2014-07). Line 1 Hess, Hybrid, <i>see above</i>	(262 p. 66)
-15 % FC	Baden (2012 to 2015) . Mixed urban bus lines MAN, Lion's City Hybrid, MY 2012, € 5/EEV, <i>see above</i> FC change vs. conv. bus MAN Lion's City, MY 2009, € 5/EEV, <i>see above</i>	(487 p. 13)
-18 % FC	Anklam, Dresden, Grevesmühlen, Hagen, Heidenheim, Ingolstadt, Leipzig, München, Wolfsburg, 2013-01 to 2014-09. Urban bus, v_{avg} around 19 km/h 20 serial hybrid buses € 5 vs. conventional buses € 5	(477 pp. 10-24)
30.5 -28 % FC	Ingolstadt (2014-03 to 2014-08). (Sub-) urban bus lines, flat terrain MAN Lion's City Hybrid, <i>see above</i> , vs. conv. bus € 5/EEV	(455)
29.1	Wolfsburg, 2014-08. (Sub-) urban lines. MAN, Lion's City Hybrid, <i>see above</i>	(454)
33.3 -19 % FC	Aarau (2013). Urban bus, $v_{avg} \approx 17$ km/h, ca. 3 stops/km MAN, Lion's City Hybrid, <i>see above</i>	(456 p. 9)
73.8 -25 % FC	New York, bus dep. Mother Clara Hale, 2004-10 to 2005-09. Heavy urban traffic, $v_{avg} \approx 10.2$ km/h 10 buses 12.2 m 4x2: Orion, VII Hybrid, MY 2002; GVWR 19.31 t, curb weight 14.45 t; engine Cummins ISB, 6 cyl. 6.7 L, 895 Nm @ 1600 rpm, 201 kW @ 2500 rpm; serial hybrid system BAE HybriDrive, generator -120 kW, battery lead-acid, motor-generator peak ±3660 Nm, ±186 (239) kW	(463 p. 22)

In Table 68 the researched FC values for serial hybrid buses is shown, where the vehicle or the design of the powertrain differ from the simulation.

Table 68. FC of serial hybrid city buses 12 m, 4x2 GVWR 18 t, powertrain different from model

L/100km	Description	Source
Chassis dynamometer		
26.2 <u>double-decker</u> <u>10.4 m</u>	Cycle MLTB Wright, New Routemaster, MY 2012; curb weight ca. 12.0 t; engine Cummins ISBe 185, 4 cyl. 4.5 L € 5, 700 Nm @ 1200 rpm, 138 kW @ 2500 rpm; serial hybrid system Siemens ELFA 2, generator 1FV5168-8WS24, -700 (950) Nm, ±180 (250) kW, battery Li-Ion, motor-generator 1DB2016-WS54, ±1500 (2500) Nm, ±160 kW @ 1500 rpm, tires 275/70R22.5	(485) (486) (488 p. 4) (489)
30, 35, 27, 60, 34, 29	Cycles Braunschweig, HD UDDS, JE05, NYBus, Paris, WHVC Serial hybrid bus; engine 5.9 L € 5/EEV, battery energy storage; total vehicle mass 15.2 t. <i>Change FC: -29, -10, -38, -38, -9, -4 %</i>	(256 pp. 107, 179)
28.2 <u>double-decker</u> <u>10.4 m</u>	Cycle MLTB Wright, Gemini 2 H, MY 2009; curb weight ca. 11.7 t; engine Ford Puma T, 4 cyl. 2.4 L € 4, 305 Nm @ 3000 rpm, 108 kW @ 3900 rpm; serial hybrid system Siemens ELFA, generator 1FV5139-6WS28, -320 (450) Nm, -110 (150) kW, battery Li-Ion, 2 x motor-generator 1PV5138-4WS24, ±220 (530) Nm, ±85 (150) kW, summation gearbox Flender 152, ratio 4.05, tires 275/70R22.5	(490) (485) (486)
Fleet tests and line operation		
32.3 -32 % FC <u>double-decker</u> <u>10.4 m</u>	London line 159 (2011-02-06 to 2011-03-05) ADL, Enviro 400H, MY 2010; curb weight ca 11.5 t; engine Cummins ISBe 185, 4 cyl. 4.5 L € 4, 700 Nm @ 1200 rpm, 138 kW @ 2500 rpm; serial hybrid system BAE HybriDrive, generator -120 (195) kW, battery Li-Ion, motor-generator ±2400 (5100) Nm, ±160 (200) kW; tires 275/70R22.5	(466 p. 26)
27.7 -41 % FC	<u>Double decker 10.4 m</u> . London line 159 (2011-02-06 to 2011-03-05) Wright, Gemini 2 H, MY 2010, <i>see above</i>	(466 p. 26)

5.14.3.5 Battery-electrical city buses 12 m

For battery-electrical city buses some published values for the energy consumption, mostly from the battery, were found to judge the simulation results. In Table 69 the EC values from vehicles are given, where the powertrain characteristic was similar to the simulated BEV bus.

Table 69. Energy consumption of battery-electrical city buses 12 m, 4x2 GVWR 18 t, similar to model

EC _{batt} in kWh _{el} /km	Description	Source
Chassis dynamometer		
0.84, 0.96, 1.45, 0.98	Cycles Braunschweig, MLTB, NYBus, Paris Kabus Oy, eBUS Test Mule, prototype 2012; curb weight 8.4 t; battery Li-Fe-Po 56 kWh; motor-generator, ±1000 (3000) Nm, ±262 kW; test mass 12.4 t	(491 p. 7)
Test track, Altoona cycle, w/o air conditioning		
1.08 Pt. I to III: 1.05, 1.35, 0.85	Cycle Altoona. <i>Avg EC two buses, avg. test mass 15.25 t</i> Proterra, Catalyst BE40; MY 2014; GVWR 18.0 t, curb weight 12.4 t; battery Li-Ti; motor-generator UQM PowerPhase HD 220, ±700 Nm, ±120 (220) kW; 2-speed AMT Eaton EEV-7202, 3.53 to 1.00; i _{FD} 7.38; tires 305/70E22.5; test mass 15.3 t. ⇒ <i>EC 1.04 (0.97, 1.31, 0.88) kWh_{el}/km</i> Proterra, BE35, MY 2013; GVWR 16.2 t, curb weight 12.8 t; battery Li-Ti; motor-generator UQM PowerPhase HD 220, ±700 Nm, ±120 (220) kW; 3-speed AMT BorgWarner eGearDrive 34-01, 3.13 to 1.00, i _{FD} 9.82; tires 305/70R22.5, test mass 15.2 t. ⇒ <i>EC 1.12 (1.14, 1.39, 0.83) kWh_{el}/km</i>	(492 p. 134) (493 p. 39)

Fleet tests and line operation		
1.34 Bus 10.7 m	Pomona, CA (2014-04 to 2015-07) Line 291, La Verne to Pomona, roundtrip 26 km, v_{avg} 13.5 km/h, $v_{roll,avg}$ 28.4 km/h, stand ratio 52 %, 2.3 total-stops/km, $k_{i,avg}$ 1.06 1/km Avg. EC 12 buses, intermediate charging: Proterra, BE35, <i>see above</i> , curb weight 12.6 t; Li-Ti battery 88 kWh; motor-generator peak power 220 kW	(472 p. 20)

In Table 70 EC values from BEV buses are shown, where the powertrain differs from the model. For the SORT cycles some were nevertheless used for comparison purposes. The max. mechanical power at the EM on the SORT 1, 2, 3 cycles from the BEV bus model with a test mass of 14.6 t is ± 120 , ± 150 and ± 166 kW_{mech}. Hence a comparison is still possible with a small curtailment.

Table 70. Energy consumption of battery-electrical city buses 12 m, 4x2 GVWR 18 t, different from model

EC _{batt} in kWh/km	Description	Source
Test track, SORT cycles, used for comparison, payload 3.2 t, procedure according (313)		
1.06	SORT 2. Bus, curb weight ca. 11.2 t; central motor-generator, test mass 14.4 t	(494 p. 7)
1.10	SORT Euracom, Eurabus gen. 2, MY 2013; curb weight ca. 12 t; battery Li-Fe-Po 214 kWh; motor-generator 2200 Nm, 130 kW; test mass ca. 15.2 t	(495 p. 450)
1.15, 1.14, 1.15	SORT 1, 2, 3. Ebusco, YTP-1, MY 2012; curb weight 11.8 t; battery Li-Fe-Po 242 kWh; motor-gen. peak ± 2500 Nm, ± 120 (150) kW; test mass 14.41 t (payload 2.61 t)	(496 p. 11) (497 p. 3) (498 p. 13)
Test track, SORT cycles, further values, payload 3.2 t, procedure according (313)		
1.2, approx. value	SORT 1, 2, 3 Euracom, Eurabus gen. 1, MY 2012; curb weight ca. 12.5 t; test mass ca. 15.7 t	(499 p. 20)
1.05 Bus 10.5 m	SORT 2 SOR, EBN 10.5, MY 2012; GVWR 16.5 t, curb weight 10.1 t; battery Li-Ion 170 kWh (1.98 t); motor-generator ± 120 kW, i_{FD} 6.14; tires 285/70R19.5; test mass 12.8 t (payload 2.7 t)	(500 p. 25)
Test track, Altoona cycle, w/o air conditioning		
1.19 Pt. I to III: 1.16, 1.50, 0.91	Cycle Altoona. Avg EC two buses, avg. test mass 17.25 t New Flyer, XE 40; MY 2014; GVWR 20.1 t, curb weight 14.9 t; battery Li-Ion 7 kWh (intermediate charging); motor-generator Siemens ELFA 2 1DB2016, ± 1500 (2500) Nm, ± 160 kW @ 1500 rpm; i_{FD} 5.67; tires 305/70R22.5; test mass 17.6 t. $\Rightarrow EC$ 1.14 (1.09, 1.42, 0.93) kWh _e /km BYD, K9, MY 2014; GVWR 17.8 t, curb weight 14.5 t; Li-Fe-Po battery 324 kWh; 2 x motor-generator, hub drives, ± 350 Nm, ± 75 (90) kW, hub reduction gears, ratio 14.50; tires 275/70R22.5; test mass 16.9 t $\Rightarrow EC$ 1.23 (1.24, 1.58, 0.89) kWh _e /km	(501 p. 116) (502 p. 141)
Road measurement, w/o air conditioning		
1.62	(Heavy) urban traffic Macao, v_{avg} 15.0 km/h. Avg. EC two buses. Ankai, HFF6128G03EV, MY 2014; curb weight 13.8 t; battery Li-Fe-Po 170 kWh; motor-generator ± 100 kW; test mass 15.7 t. $\Rightarrow EC$ 1.84 kWh _e /km BYD, K9, <i>see above</i> , curb weight 13.8 t; test mass 15.5 t. $\Rightarrow EC$ 1.40 kWh _e /km	(503 p. 608)

Fleet tests and line operation		
1.31	Mannheim (2015-07 to 2015-10). Line 63, Hauptbahnhof to Pfalzplatz, roundtrip 9 km, v_{avg} km/h, peak time 2.6 bus-stops/km Avrg. EC two buses, intermediate charging Hess, Swiss Primove, MY 2014; curb weight 12 t; battery Li-Ion 60 kWh; 2 x motor-generator Bombardier Primove 140-2, hub drives, ± 60 (140) kW; rear axle ZF AVE 130, hub reduction gears, ratio 22.66; tires 275/70R22.5	(504 p. 10)
1.30	Dresden (2015-06 to 2015-09). Line 79, Mickten to Übigau, roundtrip 5.2 km, v_{avg} ca. 19.5 km/h, peak time 2.5 bus-stops/km Solaris, Urbino 12 electrical, MY 2015; battery Li-Fe-Po 200 kWh; 2 x motor-generator, hub drives, ± 60 kW; rear axle ZF AVE 130, hub reduction gears, ratio 22.66; tires 275/70R22.5	(505 p. 12)
0.93	Breda, Espoo and Maastricht, urban bus lines, v_{avg} 16.8 km/h (17.5, 18.0 and 14.9 km/h) Avrg. EC: Ebusco, YTP1, <i>see above</i> : 0.87, 0.98, 0.93 kWh/km	(497 p. 4 ff.)
1.27	Barcelona, Beograd, Copenhagen, London, Milano. 2013-11 to 2014-04 Avrg. EC: BYD, K9, <i>see above</i> : 1.44, 1.30, 1.40, 1.07 and 1.16 kWh/km	(506 p. 90)
1.14	Urban bus lines, 2.5 total-stops/km SOR, EBN 10.5 (10.5 m), <i>see above</i> , guidance value from manufacturer	(507 p. 76)

5.14.4 City buses 18 m 6x2

5.14.4.1 Conventional city buses 18 m, diesel-fuelled

Published FC values were also researched for 18 m articulated city buses to assess the simulation model, see the selection in Table 71.

Table 71. FC of conventional diesel city buses 18 m, articulated, 6x2 GVWR 28 t

L/100km	Description	Source
Chassis dynamometer		
161.4, 109.6, 107.6, 81.2	Cycles Manhattan, OCBC, CBD, KCM Bus 18.5 m 6x2: New Flyer, D60 LF, MY 2004; GVWR 30.32 t; curb weight 19.75 t; engine Caterpillar C9, 6 cyl. 8.8 L, 1560 Nm @ 1400 rpm, 246 kW @ 2100 rpm; AT Allison B-500; i_{FD} ca. 4.50, tires 305/70R22.5, test mass 22.3 t	(305 p. 10)
Test track, SORT cycles, payload 5.0 t, procedure according (313)		
56 to 58, 49 to 51, 46 to 48	SORT 1, 2, 3, measurement 2016 <i>Range of FC</i> , articulated bus, MY 2015; engine ϵ 6, 260 to 280 kW, test mass 21 to 23 t.	Bus manufacturer, 2016
59.6, 50.9, 47.8	SORT 1, 2, 3 Iveco, Urbanway 18, MY 2015; engine Cursor 9, 6 cyl. 8.7 L ϵ 6, 1650 Nm @ 1200 rpm, 265 kW @ 2200 rpm; 7-spd. AT ZF, 8.00 to 0.62	(508 p. 17)
48.3	SORT 2. Bus ϵ 6	(257 p. 9)
57.2	Cycle SORT 1 Solaris, Urbino 18, MY 2013; engine DAF PR 228, 6 cyl. 9.2 L ϵ 5, 1280 Nm @ 1100 rpm, 231 kW @ 1900 rpm; 7-speed AT ZF 6 AP	(509 p. 62)
52.3	Cycle SORT 2. Avrg. FC three buses ϵ 6 (50.2, 50.9, 55.7 L/100km)	(445 p. 5)
75.1, 58.7, 53.8	Cycles SORT 1, 2, 3; chassis dyno. Bus ϵ 5	(260 p. 30)
79.6, 61.2, 57.3	Cycles SORT 1, 2, 3. Bus ϵ 5	(510 p. 7)
74.7/72.8, 62.4/59.6, 56.0/53.1	Cycles SORT 1, 2, 3, shifting modes normal/Topodyn Bus ϵ 5	(511 p. 10)

Test track, Altoona cycle, w/o air conditioning		
73.7 Pt. I to III: 91.0, 77.2, 44.1	Cycle Altoona Bus 18.6 m 6x2: New Flyer, D60LF, MY 2002; GVWR 30.2 t, curb weight 18.4 t; engine Cummins ISL 330, 6 cyl. 8.8 L, 1490 Nm @ 1300 rpm, 246 kW @ 2200 rpm; AT Allison B 500R; i_{FD} 4.80; tires 305/70R22.5, test mass 22.2 t	(512 p. 32)
Road measurement, w/o air conditioning		
68.2	Stuttgart line 42, Schlossplatz to Erwin-Schoettle-Platz, roundtrip 21 km Solaris, Urbino 18, MY 2016; GVWR 28 t, curb weight 16.31 t; engine DAF MX 11 271 H1, 6 cyl. 10.8 L ϵ 6, 1600 Nm @ 1650 rpm, 271 kW @ 1650 rpm; 7-speed AT ZF Ecolife 6 AP 2000, 8.00 to 0.62; i_{FD} 5.77; tires 275/70R22.5, test mass 24.03 t. <i>Regenerative braking with three alternators, each ca. 3.6 kW_{el}, energy storage SCap 0.026 kWh_{el}</i>	(396 p. 58)
50.1, 57.0	Wien Line 26A, Kagran to Groß-Enzersdorf, roundtrip 22 km Payload 0.4 t and 5.4 t: MB, Citaro G; curb weight 16.86 t; engine MB OM 470, 6 cyl. 10.7 L ϵ 6, 1900 Nm @ 1000 rpm, 290 kW @ 1800 rpm; gearbox not known, test mass 17.26 and 22.26 t. <i>Regenerative braking with three alternators, each ca. 3.6 kW_{el}, energy storage SCap 0.024 kWh_{el}</i> <i>FC calculated from mobile measured CO₂ emissions with carbon-balance ($m_{C,out} \approx m_{C,in}$), checked by fuelling protocol</i>	measurement 2015-12 TU Graz IVT Dept. Emis- sions
51.0	Bad Neuenahr to Bonn ZOB, (sub-) urban test route, roundtrip 100 km, v_{avg} 23 km/h, 1.4 total-stops/km MB, Citaro G, <i>see above</i> , MY 2014; curb weight 17.06 t; 7-speed AT ZF 6 AP 2000, 8.00 to 0.62; i_{FD} 5.82; tires 275/70R22.5, test mass 24.15 t	(513)
68.5	Stuttgart line 42, Schlossplatz to Erwin-Schoettle-Platz, roundtrip 21 km MB, Citaro G, <i>see above</i> , MY 2014; curb weight 17.06 t; 7-speed AT ZF 6 AP 2000, 8.00 to 0.62; i_{FD} 5.82; tires 275/70R22.5, test mass 24.15 t	(514 p. 46)
38.9	Cycle Düsseldorf MB, Citaro G, engine MB OM 457 hLA 934, 6 cyl. 12 L ϵ 3, 1250 Nm @ 1100 rpm, 220 kW @ 2000 rpm; 4-speed AT Voith DIWA, 8.00 to 0.73; i_{FD} 5.77; tires 275/70R22.5, test mass 21.42 t $W_{eng,pos,cl} = 1.48$ kWh/km, $\eta_{rel,avg} = 0.282$ <i>Engine cycle work at clutch calculated from denormed cycle and full load curve (294 pp. 35, 101 ff.), FC calculated from CO₂ in g/kWh (294 p. 65).</i>	(294 pp. 12, 28, 38, 64/65)
Fleet tests and line operation		
57.0	Aarau (2015). Urban bus, $v_{avg} \approx 17$ km/h, ca. 3 stops/km Scania/Hess N 310 UA, ϵ 5	(259 p. 15) (456 p. 12)
52.1, 57.7, 55.9, 52.0	Beograd (2014-03-01 to 2014-04-15). (Heavy) Urban lines 17, 23, 65, 88 Solaris, Urbino 18, MY 2013, <i>see above</i>	(509 p. 62)
52.0	Luzern (2013-07 to 2014-07). (Sub-) urban bus lines no. 12, 18, 19, 20, 22, 23,24; v_{avg} around 21 km/h Bus ϵ 6, comparison vehicle for test of hybrid bus.	(258 p. 16/17)
55.3	Hannover (2014-04 to 2014-08). (Sub-) urban bus, v_{avg} ca. 22 km/h, flat MAN, A23, MY 2008 to 2011; curb weight 16.5 t; engine MAN D2066, 6 cyl. 10.5 L ϵ 5/EEV, 1600 Nm @ 1400 rpm, 235 kW @ 1900 rpm; 4-speed AT Voith DIWA	(454 p. 20) (477 p. 21)
60.0	Lausanne (2014-05). Heavy urban bus, v_{avg} ca. 14 km/h, 3 total-stops/km MAN, Lion's City GL (18.8 m), MY 2014; curb weight 17.4 t; engine MAN D2066, 6 cyl. 10.5 L ϵ 6, 1800 Nm @ 1400 rpm, 265 kW @ 1800 rpm; 4-speed AT Voith DIWA	(515 p. 7)
56.0	Bremen, Dresden, Hamburg, Leipzig, München, Ruhr region, Stuttgart, 2010 & 2011. (Sub-) urban bus lines Avg. FC 20 buses ϵ 5	(459 p. 59)

59.0	Stuttgart. Urban bus lines, v_{avg} ca. 18 km/h, ca. 3 total-stops/km MB, Citaro G; engine MB OM 457hLA, 6 cyl. 12.0 L € 5/EEV, 1600 Nm @ 1100 rpm, 260 kW @ 2000 rpm; 7-speed AT ZF EcoLife, 8.00 to 0.62	(516 p. 28) (517 p. 37)
63.2	Hannover (12 months). Line 121, Altenbekener Damm to Haltenhoffstr., roundtrip 24 km, v_{avg} 18.5 km/h, peak time 2.3 bus-stops/km MAN, A23, <i>see above</i>	(518 p. 12/14) (519 p. 25)
67, 50	(Heavy) urban, suburban bus lines Buses € 5, guiding values from manufacturer MAN	(460 p. 152)
57.1	Dresden line 62 (former line 82, 2007-07 to 2008-03), Johannstadt to Dölzschen, roundtrip 21.2 km, v_{avg} 17 km/h, peak time 3.5 bus-stops/km Avg FC one bus 18 m 6x2: Solaris, Urbino 18, MY 2006; GVWR 28 t, curb weight 17.6 t; engine PR 265, 6 cyl. 9.2 L € 5, 1450 Nm @ 1700 rpm, 265 kW @ 2100 rpm; 7-speed AT ZF; i_{FD} 6.2; tires 275/70R22.5	(520 pp. 9-11)
94.2	Seattle, Ryerson base (2005-04 to 2006-03). (Sub-) urban, 20.0 km/h, hilly Avg. FC ten buses: New Flyer, D60 LF, <i>see above</i>	(305 p. 15) (521 p. 22)
Table values		
39.4, 56.0, 62.6	Intra-urban bus traffic, free flow, dense, stop+go Table values DE, bus GVWR > 18 t, based on HBEFA	(464 p. 23)
48.3	Table values DE, bus GVWR 18 to 30 t, € 5, 27 passengers (30 %), intra-urban bus traffic, ProBas data	(522)

5.14.4.2 Diesel-electrical parallel hybrid city buses 18 m

The researched FC values for parallel hybrid city buses 18 m is shown in Table 65. The vehicles were equipped with a powertrain of specifications close to the simulated one.

In the table also the change of FC vs. the diesel buses from p. 209 ff. Table 71 is given. The diesel buses can be identified by the driving cycle and/or by the source number.

Table 72. FC of parallel hybrid city buses 18 m, 6x2 GVWR 28 t, powertrain similar to model

L/100km	Description	Source
Test track, SORT cycles, payload 5.0 t, procedure according (313)		
38.4 -20.5 % FC	SORT 2 Volvo, 7900 LAH, MY 2015; GVWR 29.0 t, curb weight 16.4 t; engine Volvo D5K240, 4 cyl. 5.1 L € 6, 920 Nm @ 1600 rpm, 177 kW @ 2200 rpm; parallel hybrid system Volvo, motor-generator ±400 (1200) Nm, ±70 (150) kW, battery Li-Ion 9.6 kWh; 12-speed AMT, 14.94 to 1.00; i_{FD} 4.72; tires 275/70R22.5, test mass 21.4 t	(257 p. 9)
Fleet tests and line operation		
39.4	Aarau (2015-05 to 2016-04) Mixed urban bus traffic, $v_{avg} \approx 17$ km/h, ca. 3 total-stops/km Volvo 7900 LAH, MY 2015, € 6, <i>see above</i>	(259 p. 15) (456 p. 12)
40.0 -23 % FC	Luzern (2013-07 to 2014-07). (Sub-) urban bus lines no. 12, 18, 19, 20, 22, 23,24; v_{avg} around 21 km/h Avg. FC hybrid bus: Volvo, 7900 LAH, <i>see above</i> , prototype 2013	(258 p. 16/17)

The found FC values for hybrid buses 18 m with parallel or power split powertrains, where the design differs from the model, is given in Table 73.

Table 73. FC of parallel hybrid city buses 18 m, 6x2 GVWR 28 t, powertrain different from model

L/100km	Description	Source
Chassis dynamometer		
92.0, 72.7, 72.5, 62.3 -43,-34, -33, -23.3 % FC	Cycles Manhattan, OCBC, CBD, KCM New Flyer, DE60 LF (18.5 m), 6x2 articulated bus, MY 2004; GVWR 30.32 t; curb weight 20.25 t; engine Caterpillar C9, 6 cyl. 8.8 L, 1560 Nm @ 1400 rpm, 246 kW @ 2100 rpm; parallel/power-split hybrid system Allison EP50, automated CVT, three planetary gear sets with two integrated motor-generators, each ± 38 (75) kW, battery NiMH ca. 10 kWh; i_{FD} ca. 5.40, tires 305/70R22.5, test mass 22.93 t	(305 p. 10)
Test track, SORT cycles, payload 5.0 t, procedure according (313)		
71.3, 56.6, 49.5	Cycles SORT 1, 2, 3. Avrg FC two buses (Dresden, Leipzig) Solaris, Urbino H18, MY 2006; curb weight ca. 18.6 t; engine Cummins ISL 330H, 6 cyl. 8.8 L ϵ 5, 1490 Nm @ 1300 rpm, 243 kW @ 2100 rpm; parallel/power-split hybrid system Allison EP50, <i>see above</i> , tires 275/70R22.5, test mass ca. 23.6 t	(510 p. 7) (511 p. 10) (523)
Test track, Altoona cycle, w/o air conditioning		
53.1 -28 % FC Pt. I to III: 63.0, 55.8, 35.4 (-31, -28, -20 %)	Cycle Altoona. Bus 18.3 m 6x2. <i>FC change vs. New Flyer, D60LF:</i> New Flyer, DE60LF, MY 2003; GVWR 28.8 t, curb weight 19.3 t; engine Cummins ISL 330H, 6 cyl. 8.8 L, 1490 Nm @ 1300 rpm, 246 kW @ 2200 rpm; parallel/power-split hybrid system Allison EP50, <i>see above</i> ; i_{FD} ca. 5.00; tires 305/70R22.5; test mass 22.6 t	(524 p. 109)
Fleet tests and line operation		
50.8	Aarau (2015). Urban bus traffic, $v_{avrg} \approx 17$ km/h, ca. 3 stops/km Solaris, Urbino H18, MY 2014, ϵ 6, <i>see above</i>	(259 p. 15) (456 p. 12)
-13 % FC (range -3 to -25 %)	Bochum, Hannover, Leipzig, München, 2013-01 to 2014-09 Urban bus lines, v_{avrg} around 18 km/h 2 parallel hybrid and 9 parallel/power-split hybrid buses ϵ 5	(477 pp. 10 - 24)
43.1 -23 % FC	Hannover (2014-04 to 2014-08). (Sub-) urban bus, v_{avrg} ca. 22 km/h, flat Avrg. FC 4 hybrid buses: Solaris, Urbino H18, <i>see above</i>	(454 p. 20) (477 p. 21)
48.6 -23 % FC	Hannover (12 months). Line 121, Altenbekener Damm to Haltenhoffstr. Avrg. FC hybrid bus: Solaris, Urbino H18, MY 2008, curb weight ca. 16.8 t, engine Cummins ISBe 250, 6 cyl. 6.7 L ϵ 5, 950 Nm @ 1700 rpm, 186 kW @ 2300 rpm; parallel/power-split hybrid system Allison EP50, <i>see above</i>	(518 p. 12/14) (519 p. 25)
49.3 -14 % FC	Dresden line 62, Johannstadt to Dölzchen Average FC one hybrid bus 18 m 6x2: Solaris, Urbino H18, MY 2006; GVWR 28 t, curb weight 17.2 t; engine Cummins ISL 330H, 6 cyl. 8.8 L ϵ 4, 1490 Nm @ 1300 rpm, 246 kW @ 2100 rpm; parallel/power-split hybrid system Allison EP50, <i>see above</i> ; i_{FD} 6.2; tires 275/70R22.5	(520 pp. 9-11)
74.3 -21 % FC	Seattle, bus depot Atlantic Base (2005-04 to 2006-03) (Sub-) urban bus lines, v_{avrg} 18.7 km/h, hilly terrain Avrg. FC ten hybrid buses: New Flyer, DE60 LF, <i>see above</i>	(305 p. 15) (521 p. 22)

5.15 Fan power demand

In Figure 206 to Figure 208 some simulation results for the fan operation are shown. The model is described on p. 37 ff. chapter 2.3.1. The main result from measurement and simulation is, that the fan is only engaged during longer phases of high engine load, i. e. for uphill driving or full load acceleration.

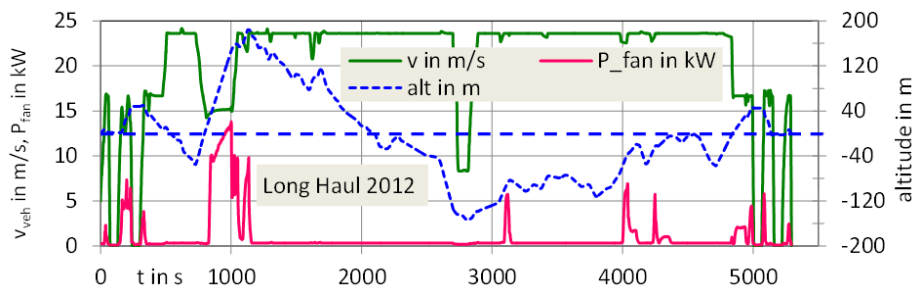


Figure 206. Tractor-trailer 330 kW, payload 19.3 t, Long Haul cycle 2012, measurement by MAHLE

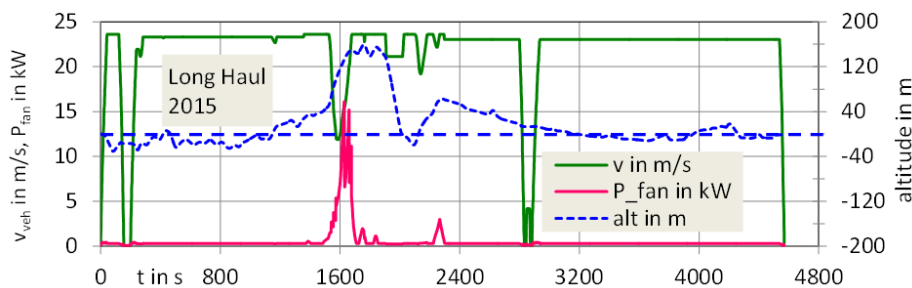


Figure 207. Tractor-trailer 330 kW, payload 19.3 t, Long Haul cycle 2015, own simulation

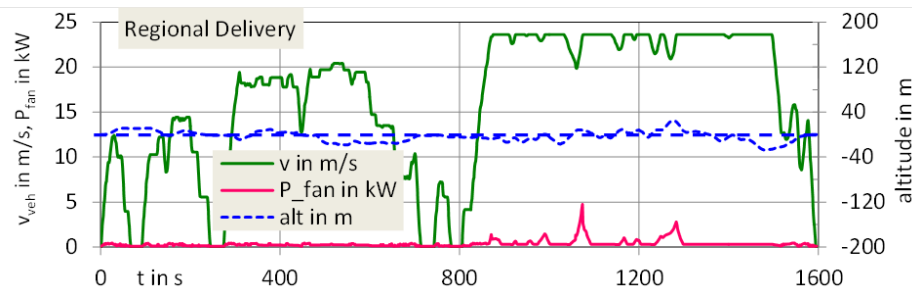


Figure 208. Tractor-trailer 330 kW, payload 19.3 t, Regional Delivery cycle 2012, own simulation

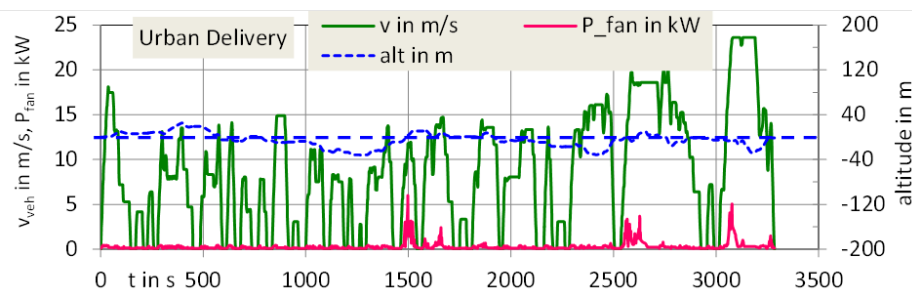


Figure 209. Tractor-trailer 330 kW, payload 19.3 t, Urban Delivery cycle 2012, own simulation

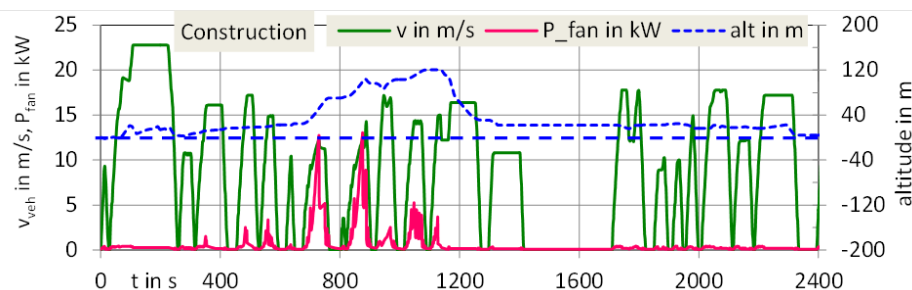


Figure 210. Tractor-trailer 330 kW, payload 19.3 t, Construction cycle, own simulation

5.16 Miscellaneous

The calculation flow of the model for the compressor power, which is the starting point for the analysis on p. 55 ff. in section 2.3.2.2, is shown in Figure 211.

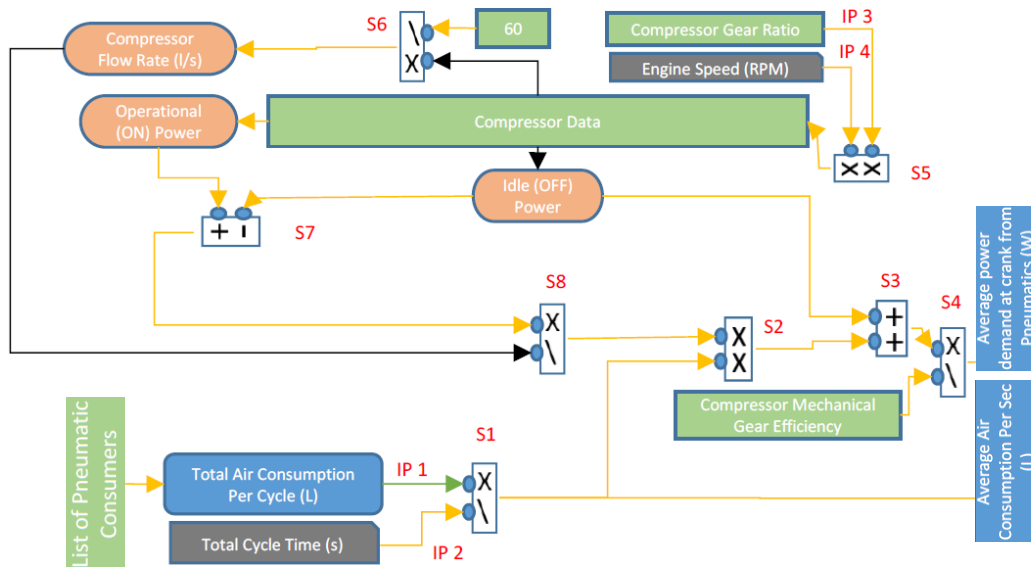


Figure 211. Simulation approach for compressor from Ricardo (115 p. 79)

5.16.1 Utilised simulation programs

An overview of the applied simulation programs is given in Table 74.

Table 74. Simulation programs.

Program name	version no.	Release data	Used for
VECTO	3.2.0/925	2017-07-14	Comparison of basis HDV models in VECTO v2 and v3
VECTO	2.2	2015-09-10	Main simulation program
VECTO	1.4 RC 7	2013-11-29	Electrical vehicles and serial hybrid bus
PHEM	11.4	2014-04-01	Tractor-trailer, simulation of exhaust gas: mass flow
PHEM	7.2	2013-07-09	Parallel hybrid bus

6 References

6.1 Institutions and abbreviations

ABRTC	Altoona Bus Research and Testing Center, Altoona PA
ACEA	Association des Constructeurs Européens d'Automobiles, Bruxelles
ADEME	Agence de l'environnement et de la maîtrise de l'énergie, Angers
ADVISOR	ADvanced VehIcle SimulatOR, adv-vehicle-sim.sourceforge.net , c/o NREL, Golden CO
AET	Association for European Transport, Henley-in-Arden
AG-IAB	Arbeitsgruppe Innovative Antriebe Bus, c/o thinkstep, Leinfelden-Echterdingen
AN	Assemblée nationale, Paris
ANL	Argonne National Laboratory, Argonne IL
Ann.	Annex
AOCS	American Oil Chemists' Society, Urbana IL
AREMA	American Railway Engineering and Maintenance of Way Association, Lanham MD
Art. on hp.	Article on homepage
ASSTRA	Associazione Trasporti, Roma
ATZ	Automobiltechnische Zeitschrift, c/o Springer Verlag, Berlin
AVL	Anstalt für Verbrennungskraftmaschinen List, Graz
BAG	Bundesamt für Güterverkehr, Köln
BASt	Bundesanstalt für Straßenwesen, Bergisch Gladbach
BBR	Bundesamt für Bauwesen und Raumordnung, Bonn
BGL	Bundesverband Güterkraftverkehr Logistik und Entsorgung, Frankfurt a. M.
BIFA	British International Freight Association, Feltham
BIPM	Bureau international des poids et mesures, Sèvres
BLS	Bureau of Labor Statistics, Washington DC
BMBF	Bundesministerium für Bildung und Forschung, Berlin
BMUB	Bundesumwelt- und -bauministerium, Berlin
BMVI	Bundesministerium für Verkehr und digitale Infrastruktur, Berlin
BMVJ	Bundesministerium der Justiz und für Verbraucherschutz, Berlin
BP	British Petroleum, London
Bull.	Bulletin
BVL	Bundesvereinigung Logistik, Bremen
C3S	Copernicus Climate Change Service, c/o ECMWF, Reading
CARB	California Air Resources Board, Sacramento CA
CDIAC	Carbon Dioxide Information Analysis Center, c/o ORNL, Knoxville TN
CEN	Comitee Europeen de Normalisation, Bruxelles
CF-AIPCR	Comité français de l'association mondiale de la Route, Marne-la-Vallée
CFR	Code of Federal Regulations,
CIESIN	Center for International Earth Science Information Network, c/o Uni Columbia, New York NY
CIT	California Institute of Technology, Pasadena CA
CLECAT	Comité de Liaison Européen des Commissionnaires et Auxiliaires de Transport du Marché Commun, Bruxelles
CNR	Comité National Routier, Paris
Conf.	Conference, meeting
CORDIS	Community Research and Development Information Service, c/o Europ. Commiss., Luxembourg

CSR	Corporate Social Responsibility
CTA	Center for Transportation Analysis, c/o ORNL, Knoxville TN
DBFZ	Deutsches Biomasseforschungszentrum, Leipzig
DBU	Deutsche Bundesstiftung Umwelt, Osnabrück
DG	Directorate General, c/o Europ. Commiss., Bruxelles
DGMK	Deutsche Gesellschaft für Mineralölwissenschaft und Kohlechemie, Hamburg
DIN	Deutsches Institut für Normung, Berlin
Diss.	Dissertation
Doc.	Document
doi	Digital object identifier
DSLVB	Deutscher Speditions- und Logistikverband, Berlin
DVZ	Deutsche Verkehrs-Zeitung, c/o Deutscher Verkehrs-Verlag, Hamburg
DWD	Deutscher Wetterdienst, Offenbach
ECCJ	Energy Conservation Center Japan, Tokyo
ECMWF	European Centre for Medium-Range Weather Forecasts, Reading
EDGAR	Emissions Database for Global Atmospheric Research, c/o JRC, Ispra
EERE	Office of Energy Efficiency and Renewable Energy, c/o USDOE, Washington DC
ETH	Eidgenössische Technische Hochschule, Zürich
EU-28	European Union, 28 member states, 2013-07 to 2019 (Brexit?)
FAT	Forschungsvereinigung Automobiltechnik, c/o VDA, Berlin
FFG	Forschungsförderungsgesellschaft, Wien
FIGE	Forschungsinstitut Geräusche und Erschütterungen, Herzogenrath
FISITA	Fédération Internationale des Sociétés d'Ingénieurs des Techniques de l'Automobile, Stansted
FKFS	Forschungsinstitut für Kraftfahrwesen und Fahrzeugmotoren, Stuttgart
GRPE	Working Party on Pollution and Energy, c/o UNECE, Genf
GSFC	Goddard Space Flight Center, c/o NASA, Greenbelt MD
HBEFA	HandBook Emission Factors, c/o INFRAS, Bern
IAA	Internationale Automobil-Ausstellung, Frankfurt a. M. (LDV) & Hannover (HDV)
ICCT	The International Council on Clean Transportation, Washington DC
IEC	International Electrotechnical Commission, Genf
IEEE	Institute of Electrical and Electronics Engineers, Piscataway NJ
IES	Industrial Electronics Society, c/o IEEE, Piscataway NJ
IET	Institute for Energy and Transport, c/o JRC, Ispra
IFA	Institut für Fahrzeugantriebe und Automobiltechnik, c/o TU, Wien
IFSTTAR	Institut français des sciences et technologies des transports, de l'aménagement et des réseaux, Marne-la-Vallée
IGF	Industrielle Gemeinschaftsforschung, c/o BMWI, Berlin
IMEchE	Institution of Mechanical Engineers, London
INRETS	Institut national de recherche sur les transports et leur sécurité, Bron
IPCC	Intergovernmental Panel on Climate Change, c/o WMO, Genf
IVE	Ingenieurgesellschaft für Verkehrs- und Eisenbahnwesen, Hannover
IVI	Fraunhofer-Institut für Verkehrs- und Infrastruktursysteme, Dresden
IVT	Institut für Verbrennungskraftmaschinen und Thermodynamik, c/o TU, Graz
J.	Journal
JPL	Jet Propulsion Laboratory, c/o CIT, Pasadena CA
JRC	Joint Research Center, c/o Europ. Commiss., Ispra
JSAE	Society of Automotive Engineers of Japan, Tokyo
KNEG	Klimatneutrala godstransporter, c/o Chalmers TH, Göteborg
KTBB	Kommission Technik und Betrieb Bus, c/o VöV, Bern

KTH	Kungliga Tekniska högskolan, Stockholm
LANUV	Landesamt für Natur, Umwelt und Verbraucherschutz, Recklinghausen
Lect.	Lecture
LowCVP	Low Carbon Vehicle Partnership, London
MEEM	Ministère de l'Environnement, de l'Énergie et de la Mer, Paris
MetOffice	Meteorological Office, Exeter
MLIT	Ministry of Land, Infrastructure, Transport and Tourism, Tokyo
MOE	Ministry of Environment, Tokyo
MTZ	Motortechnische Zeitschrift, c/o Springer Verlag, Berlin
MVIBW	Ministerium für Verkehr und Infrastruktur Baden-Württemberg, Stuttgart
MVW	MineralölWirtschaftsVerband, Berlin
NASA	National Aeronautics and Space Administration, Washington DC
NCGIA	National Center for Geographic Information and Analysis, c/o Uni California, St. Barbara CA
NEMA	National Electrical Manufacturers Association, Arlington VA
NHTSA	National Highway Traffic Safety Administration, Washington DC
NIST	National Institute of Standards and Technology, Gaithersburg MD
NOAA	National Oceanic and Atmospheric Administration, Silver Spring MD
NREL	National Renewable Energy Laboratory, Golden CO
NTM	Network for Transport Measures, Stockholm
NTRC	National Transport Research Center, c/o ORNL, Knoxville TN
OCLC	Online Computer Library Center, Dublin
OPEC	Organization of the Petroleum Exporting Countries, Wien
ORNL	Oak Ridge National Laboratory, Knoxville TN
PR	Press release
ProBas	Prozessorientierte Basisdaten für Umweltmanagement-Instrumente, c/o UBA, Dessau-Roßlau
Proc.	Proceedings
PSPC	Public Services and Procurement Canada, Gatineau
Rep.	Report
RNL	Risø National Laboratory, Roskilde
RWTH	Rheinisch-Westfälische Technische Hochschule, Aachen
SAE	Society of Automotive Engineers, Warrendale PA
saena	Sächsische Energieagentur, Dresden
SAG	Scientific Advisory Group, c/o ACEA, Bruxelles
SIA	Société des Ingénieurs de l'Automobile, Suresnes
SMUL	Sächsisches Staatsministerium für Umwelt und Landwirtschaft, Dresden
SPC	Standards Press of China, Beijing
Std.	Standard
STIB	Société des Transports Intercommunaux de Bruxelles
STU	Sustainable Transport Unit, c/o JRC, Ispra
TAP	Transport and Air Pollution Conference
TCMV	Technical Committee Motor Vehicles, c/o Europ. Commiss., DG Growth, Bruxelles
TCRP	Transit Cooperative Research Program, Washington DC
TfL	Transport for London
TH	Technische Hochschule
TMA	Truck Manufacturers Association, Chicago IL
TML	Transport & Mobility Leuven
TNO	Nederlandse Organisatie voor toegepast-natuurwetenschappelijk onderzoek, Den Haag
TRB	Transportation Research Board, Washington DC
TU	Technische Universität

TY	Teknillinen Yliopisto
UITP	Union internationale des transports publics, Bruxelles
UNECE	UN, Economic Commission for Europe, Genf
UNFCCC	UN Framework Convention on Climate Change, Bonn
USDOE	United States Department of Energy, Washington DC
USEPA	United States Environmental Protection Agency, Washington DC
USGPO	United States Government Publishing Office, Washington DC
üstra	Überlandwerke und Straßenbahnen Hannover
VDA	Verband der Automobilindustrie, Berlin
VDI	Verein Deutscher Ingenieure, Düsseldorf
VDL	van der Leegte Bus & Coach, Eindhoven
VDV	Verband Deutscher Verkehrsunternehmen, Köln
VEIC	Vermont Energy Investment Corporation, Burlington VT
VKM	Verbrennungskraftmaschine
VöV	Verband öffentlicher Verkehr, Bern
VR	Verkehrsrundschau, c/o Springer Verlag, München
VSVI	Vereinigung der Straßenbau- und Verkehrsingenieure, Hamburg
VTT	Valtion Teknillinen Tutkimuskeskus, Espoo
WABCO	Westinghouse Air Brake Company, c/o Wabtec, Wilmerding PA
WAC	World Automotive Congress, c/o FISITA, Stansted
WEVA	World Electric Vehicle Association, Washington DC
WEVJ	World Electric Vehicle Journal, c/o WEVA, Washington DC
WG	Workgroup
WSP	William Sale Partnership, Stockholm-Globen
WVU	West Virginia University, Morgantown WV
ZAMG	Zentralanstalt für Meteorologie und Geodynamik, Wien

6.2 References

1. **EuCom-M.** 2016. *EU transp. in figures*. [Rep.]. Bruxelles : Europ. Commiss., DG Mobility, 09 2016. Vol. 20, p. 156. ISSN 2363-2739, ISBN 9789279515279.
2. **BMVI.** 2016/2017. *Verkehr in Zahlen*. [Rep.]. Hamburg : DVV, 11 2016. Vol. 45, p. 372. ISSN 1863-527X, ISBN 9783871545917.
3. **BGL.** 2014/2015. *Verkehrswirtschaftliche Zahlen*. [Rep.]. Frankfurt a. M. : BGL, 01 2016. Vol. 55, p. 96. ISSN 0083-5021.
4. **EuCom-E.** 2016. *EU Energy in figures*. [Rep.]. Bruxelles : Europ. Commiss., DG Energy, 09 2016. Vol. 5, p. 264. ISSN 1977-4559, ISBN 9789279582479.
5. **Dünnebeil, F.** Zukünftige Maßnahmen zur Kraftstoffeinsparung und Treibhausgasminde rung bei schweren Nutzfahrzeugen. *Texte*. [Rep.]. Dessau-Roßlau : UBA, 04 2015. Vol. 32/2015, p. 154 + app. 58. ISSN 1862-4804, rep. no. UBA-FB 002058.
6. **BP.** 2016. *65 BP Statistical Review of World Energy*. [Rep.]. London : BP, 06 2016. p. 44. bp.com/statisticalreview.
7. **Dickinson, R.** Future global warming from atmospheric trace gases. *Nature*. 09 01 1986, Vol. 319, pp. 109-115. ISSN 0028-0836, doi 10.1038/319109a0.
8. **Oreskes, N.** The Scientific Consensus on Climate Change. *Science*. 03 12 2004, Vol. 306, 5702, p. 1686. ISSN 1095-9203, doi 10.1126/science.1103618.
9. **Anderegg, W.** Expert credibility in climate change. *Proc. NAS*. 06 07 2010, Vol. 107, 27, pp. 12107–12109. ISSN 1091-6490, doi 10.1073/pnas.1003187107.
10. **Cook, J.** The Scientific Guide to Global Warming Skepticism. [Rep.]. Warner, AU : Cook J., Climate Communicat. Fellow, Glob. Change Inst., Uni Queensland, Brisbane, AU, 12 2010. p. 16. skepticalscience.com, Guide_to_Skepticism.pdf.
11. **ZAMG.** Informationsportal Klimawandel. [Art. on hp.]. Wien : ZAMG, Abt. f. Klimaforschung, 2012. zamg.ac.at.
12. **Cook, J.** Quantifying the consensus on anthropogenic global warming (...). *Environm. Rsrch. Letters*. 15 05 2013, Vol. 8, 2, pp. 1-7. ISSN 1748-9326, doi 10.1088/1748-9326/8/2/024024.
13. **NASA.** Scientific consensus: Earth's climate is warming. [Art. on hp.]. Pasadena, CA : CIT, NASA, SPL, Earth Science Communications Team, 2013. climate.nasa.gov/scientific-consensus.
14. **Barnosky, A.** Introducing the Scientific Consensus on Maintaining Humanity's Life Support Systems in the 21st Century. *Anthropoc. Rev.* 04 2014, Vol. 1, 1, pp. 78-109. ISSN 2053-0196, doi 10.1177/2053019613516290.
15. **IPCC.** Climate Change 2014: Synthesis Report. [Rep.]. Genf : IPCC, 03 2015. p. 151. ISBN 9789291691432.
16. **Météo-France.** 2014. *Rapport Climat*. [Rep.]. Saint-Mandé : Météo-France, 23 04 2015. Vol. 3, p. 30. ISSN 2269-9007, Rep. no. DOC00030431.
17. **Powell, J.** Climate Scientists Virtually Unanimous: Anthropogenic Global Warming Is True. *Bull. Science, Tech. & Society*. 28 03 2016, Vol. 35, 5-6, pp. 121-124. ISSN 0270-4676, doi 10.1177/0270467616634958.
18. **WMO.** 2015. *Statem. status glob. climate*. [Rep.]. Genf : WMO, 04 2016. Vol. 23, p. 26. WMO-no. 1167, OCLC no. 33200899.
19. **MetOffice.** Climate Guide. [Art. on hp.]. Exeter : Meteorological Office, 12 09 2016. metoffice.gov.uk.
20. **WMO.** 2015. *GHG Bull.* [Rep.]. Genf : WMO, 24 10 2016. Vol. 12, p. 8. ISSN 2078-0796.
21. **DWD.** 2016. *Nationaler Klimareport*. [Rep.]. Offenbach : DWD, 09 11 2016. Vol. 1, 2. ISSN 2509-3622.
22. **C3S.** Earth on the edge: Record breaking 2016 was close to 1.5°C warming. [PR]. Reading : ECMWF, C3S, 05 01 2017. climate.copernicus.eu.
23. **WMO.** WMO confirms 2016 as hottest year on record, about 1.1°C above pre-industrial era. [PR]. Genf : WMO, 18 01 2017. PR no. 1/2017, public.wmo.int.
24. **IPCC.** Climate Change 2013: The Physical Science Basis. [Rep.]. Cambridge, UK : Cambridge University Press, 04 2014. p. 1535. ISBN 9781107661820.
25. **Harries, J.** Increases in greenhouse forcing inferred from the outgoing longwave radiation spectra of the Earth in 1970 and 1997. *Nature*. 15 03 2001, Vol. 410, pp. 355-357. ISSN 0028-0836, doi 10.1038/35066553.
26. **Chen, C.** Spectral signatures of climate change in the Earth's infrared spectrum between 1970 and 2006. *EUMETSAT publ.* 26 09 2007, Vol. 50, p. 5. ISSN 1011-3932, ISBN 929110079X, eumetsat.int, pdf_conf_p50_s9_01_harries_v.pdf.
27. **Booth, B.** Climate feedbacks. [Art. on hp.]. Exeter : Meteorological Office, 16 06 2016. metoffice.gov.uk.
28. **Dessler, A.** Water-vapor climate feedback inferred from climate fluctuations, 2003–2008. *Geophys. Rsrch. Lett.* 23 10 2008, Vol. 35, 20, p. 4. ISSN 1944-8007, doi 10.1029/2008GL035333.
29. **Clausius, R.** Ueber die bewegende Kraft der Wärme (...), part 2 of 2. [ed.] J. Poggendorf. *Annalen Physik Chemie*. 1850, Vol. 155, pp. 500-524. ISSN 0003-3804, doi 10.1002/andp.18501550403.

30. **Baehr, D.** *Thermodynamik*. 15. Wiesbaden : Springer Vieweg, 2012. p. 667. ISBN 9783642241604.
31. **Boden, T.** Global, Regional, and National Fossil-Fuel CO2 Emissions. [Rep.]. Knoxville, TN : ORNL, CDIAC, 10 06 2015. doi 10.3334/CDIAC/00001_V2015.
32. **GCP.** Global Carbon Budget 2015. [ed.] C. Le Quéré. [Pres. slides]. Norwich : Uni East Anglia, 07 12 2015. p. 68. globalcarbonproject.org, GCP_budget_2015_v1.pdf.
33. **EDGAR.** Global GHG time series. [Data table]. Ispra : Europ. Commiss., JRC, IET, EDGAR, 26 09 2014. edgar.jrc.ec.europa.eu, EDGARv42FT2012_GHG.xls.
34. **Blunden, J.** State of the Climate in 2014. *Bull. AMS*. [Rep.]. Boston, MA : AMS, 07 2015. Vol. 96, 7, p. 267. ISSN 0003-0007, doi 10.1175/2015BAMSSStateoftheClimate.1.
35. **Murphy, D.** An observationally based energy balance for the Earth since 1950. *J. Geophys. Resch.* D: Atmospheres, 09 09 2009, Vol. 114, 17, p. 14. ISSN 2169-8996, doi 10.1029/2009JD012105.
36. **Helm, V.** Elevation and elevation change of Greenland and Antarctica derived from CryoSat-2. *The Cryosphere*. 20 08 2014, Vol. 8, 2, pp. 1539-1559. ISSN 1994-0416, doi 10.5194/tc-8-1539-2014.
37. **Buth, M.** Vulnerabilität Deutschlands gegenüber dem Klimawandel. *Climate Change*. [Rep.]. Dessau-Roßlau : UBA, 11 2015. Vol. 24/2015, p. 688 + app. 182. ISSN 1862-4359, rep. no. UBA-FB 002226.
38. **Tobler, W.** The Global Demography Project. [Rep.]. Santa Barbara, CA : NCGIA, 1995. p. 69. Rep. no. TR-95-6, ncgia.ucsb.edu/pubs/gdp/pop.html.
39. **CIESIN.** Population Density Grid, 2015: Global. [Map]. New York, NY : Uni Columbia, CIESIN, 06 2016. p. 1. doi 10.7927/H4NP22DQ.
40. **Lloyd, W.** *Two lectures on the checks to population*. Oxford, UK : Uni Oxford, 1833. p. 75. Vol. 1, hdl.handle.net/2027/uc1.a0006830269.
41. **Hardin, G.** The Tragedy of the Commons. *Science*. 13 12 1968, Vol. 162, 3859, pp. 1243-1248. ISSN 1095-9203, doi 10.1126/science.162.3859.1243.
42. **UNFCCC.** Adoption of the Paris Agreement. [Treaty]. Paris : UNFCCC, 12 12 2015. p. 32. Doc. no. FCCC/CP/2015/L.9/Rev.1, unfccc.int, 109r01.pdf.
43. **Kossov, A.** State and Trends of Carbon Pricing 2015. [Rep.]. Washington, DC : The World Bank, 20 09 2015. p. 85. ISBN 9781464807251, hdl.handle.net/10986/22630.
44. **EEX.** Emission Spot Primary Market Auction Rep. 2015. [Data Table]. Leipzig : EEX, 01 01 2016. eex.com, emission_spot_primary_market_auction_report_2015.xls.
45. **Kranke, A.** *CO2-Berechnung in der Logistik*. München : Vogel, 2011. p. 336. ISBN 9783574260957.
46. **Burgdorf, J.** FC of trucks and transporters. *VR*. 07 03 2014, Vol. 69, 10, pp. 29-31. ISSN 0341-2148.
47. **Zeitzen, F.** Fuel consumption of tractor-trailers on motorways. *lastauto omnibus*. 03 2014, Vol. 88, 4, pp. 10-12. ISSN 1613-1606. Overview of measurements 1966 to 2014.
48. **CNR.** 2007. *Enquête longue distance*. [Rep.]. Paris : CNR, 01 06 2008. p. 31. cnr.fr, <E CNR LD 2007.pdf>.
49. —. 2015. *Enquête longue distance*. [Rep.]. Paris : CNR, 07 04 2016. p. 33. cnr.fr, <CNR - Enquête longue distance - 2015.pdf>.
50. **Hausberger, S.** Reduction and Testing of Greenhouse Gas Emissions from Heavy Duty Vehicles. [Rep.]. Graz : TU, IVT, 09 01 2012. p. 193 + app. 18. ec.europa.eu, hdv_2011_01_09_en.pdf.
51. **Aarnink, S.** Market Barriers to Increased Efficiency in the European On-road Freight Sector. [Rep.]. Delft : CE Delft, 10 2012. p. 101. Rep. no.: 12.4780.66, cedelft.eu/publications.
52. **Fontaras, G.** Development of a CO2 certification and monitoring methodology for HDV. [Rep.]. Ispra : Europ. Commiss., JRC, IET, STU, 2014. ISBN 9789279351464, doi 10.2790/12582.
53. **Luz, R.** Development and validation of a methodology for monitoring and certification of greenhouse gas emissions from heavy duty vehicles through vehicle simulation. [Rep.]. Graz : TU, IVT, 26 05 2014. p. 170. Rep. No. I 07/14/Rex EM-I 2012/08 699, ec.europa.eu, final_report_co2_hdv_en.pdf.
54. —. Simulationsbasierte Methode zur Zertifizierung der CO2 Emissionen von schweren Nutzfahrzeugen. [Diss.]. Graz : TU, IVT, 02 2015. p. 107.
55. **EuCom-G.** Commission Regulation (EU) .../... of XXX (...) as regards the determination of the CO2 emissions and fuel consumption of heavy-duty vehicles (...). *Comitology register, Dossier*. [Draft rule]. Bruxelles : Europ. Commiss., DG Growth, TCMV, 11 05 2017. pp. 21, + 11 annexes p. 283. 67th meeting, dossier no. CMTD(2017)0478, doc. no. D051106/2, <https://circabc.europa.eu/w/browse/c99d7c7e-cb99-421a-bb74-f75447b287ec>, ec.europa.eu/transparency/regcomitology/index.cfm.
56. **ECCJ.** Final Report by Heavy Vehicle Fuel Efficiency Standard Evaluation Group. [Rep.]. Tokyo : ECCJ, 11 2005. p. 51. eccj.or.jp, heavy_vehicles_nov2005.pdf.
57. **Zheng, T.** Development of Fuel Consumption Test Method Standards for HD CV in China. *SAE Tech. Papers*. 14 09 2011, Vol. 65, 2011-01-2292, p. 9. ISSN 0148-7191, doi 10.4271/2011-01-2292.
58. **CG.** HDV and Engine Greenhouse Gas Emission Regulations. II, Official Regulations *Canada Gazette*. [Rule]. Ottawa : PSPC, 13 03 2013. Vol. 147, 6, pp. 450-572. ISSN 1494-6122, gazette.gc.ca, g2-14706.pdf.

59. **Hao, H.** An overview of energy efficiency standards in China's transport sector. *Renew. Sustain. Energy Rev.* 23 08 2016, Vol. 67, pp. 246-256. ISSN 1364-0321, doi 10.1016/j.rser.2016.08.044.
60. **FR.** Greenhouse Gas Emissions and Fuel Efficiency Standards for Medium- and Heavy-Duty Engines and Vehicles - Phase 2. *Fed. Register.* [Rule]. Washington, DC : USGPO, 25 10 2016. Vol. 81, 206, pp. 73478-74274. ISSN 0097-6326, gpo.gov, 2016-21203.pdf.
61. **Park, J.** Development of Driving Cycle for CO2 Emission Test of HDV. *SAE Tech. Papers.* 14 10 2013, Vol. 67, 2013-01-2520, p. 8. ISSN 0148-7191, doi 10.4271/2013-01-2520.
62. **Sharpe, B.** Testing methods for heavy-duty vehicle fuel efficiency. [Paper]. San Francisco, CA : ICCT, 20 04 2015. p. 20. Paper no. 2015-3, theicct.org.
63. **Lukey, I.** Calculating Car Performance with a Digital Computer. [5th year thesis]. Flint, MI : GM Institute (today: Kettering University), 1957.
64. **Louden, R.** Computer simulation of automotive fuel economy and acceleration. *SAE Tech. Papers.* 1960, Vol. 14, 600132. ISSN 0148-7191, doi 10.4271/600132.
65. **Arno, R.** Digital computer utilization in the design of the experimental truck, 2-1/2-ton XM521 at Detroit Arsenal. *SAE Tech. Papers.* 1961, Vol. 15, 610408. ISSN 0148-7191, doi 10.4271/610408.
66. **Noon, W.** Computer Simulated Vehicle Performance. *SAE Tech. Papers.* 1962, Vol. 16, 620573, pp. 22-28. ISSN 0148-7191, doi 10.4271/620573.
67. **Campbell, R.** Energy Recovery Incentive for Regenerative Braking. *SAE Tech. Papers.* 1962, Vol. 16, 620143. ISSN 0148-7191, doi 10.4271/620143.
68. **Guzella, L.** *Vehicle Propulsion Systems. Introduction to Modeling and Optimization.* 3. Berlin : Springer, 2012. p. 409. ISBN 9783642359125.
69. **Milliken, W.** General Introduction to a Programme of Dynamic Research. *Gen. Meeting of the Automob. Divis.* [Conf.]. London : IMechE, 13 11 1956. Vol. 10, 1, pp. 287-309. ISSN 0367-8822, doi 10.1243/PIME_AUTO_1956_000_031_02.
70. **Whitcomb, D.** Design Implications of a General Theory of Automobile Stability and Control. *Gen. Meeting of the Automob. Divis.* [Conf.]. London : IMechE, 03 11 1956. Vol. 10, 1, pp. 367-391. ISSN 0367-8822, doi 10.1243/PIME_AUTO_1956_000_035_02.
71. **JSAE.** Stability/Controllability/Maneuverability of Automobiles (3). *J. JSAE.* 1953, Vol. 7, 5, pp. 104-106. JSAE paper no. 535044, bookpark.ne.jp/jsae.
72. —. Stability/Controllability/Maneuverability of Automobiles (4). *J. JSAE.* 1953, Vol. 7, 6, pp. 136-140. JSAE paper no. 535054, bookpark.ne.jp/jsae.
73. **Iguchi, M.** A study on characteristics of Driver Control Action with a model automobile. *JSAE Transact.* 1960, Vol. 7, 1, pp. 1-7. JSAE paper no. 606001, bookpark.ne.jp/jsae.
74. **Sheridan, T.** Vehicle Handling: Mathematical Characteristics of the Driver. *SAE Tech. Papers.* 1963, Vol. 17, 630068. ISSN 0148-7191, doi 10.4271/630068.
75. **McKenzie, R.** Computerized Evaluation of Driver-Vehicle-Terrain Systems. *SAE Tech. Papers.* 1967, Vol. 21, 670168, pp. 945-956. ISSN 0148-7191, doi 10.4271/670168.
76. **Pew, R.** Human Information-Processing Concepts for System Engineers. [book auth.] R. Machol (ed.). *System Engineering Handbook.* New York, NY : McGraw-Hill, 1965, 31, pp. 31-3 - 31-19. ISBN 9780070393714.
77. **Hartwich, E.** Simulation der Längsdynamik eines Straßenfahrzeugs. *ATZ.* 1972, Vol. 74, 8, pp. 315-323. ISSN 0001-2785.
78. **Schramm, D.** *Modellbildung und Simulation der Dynamik von Kraftfahrzeugen.* Wiesbaden : Springer-Vieweg, 2013. p. 412. ISBN 9783642338878.
79. **Blundell, M.** *The Multibody Systems Approach to Vehicle Dynamics.* Oxford, UK : BH, 2014. p. 741. ISBN 9780080994253.
80. **Mastinu, G.** *Road and Off-Road Vehicle System Dynamics Handbook.* Boca Raton, FL : CRC, 2014. p. 1662. ISBN 9780849333224.
81. **Wood, N.** *Rail-Roads.* 1. London : Knight & Lacey, 1825. p. 314. hdl.handle.net/2027/nyp.33433004638577.
82. **Parent, M.** Sur La Plus Grande Perfection Possible Des Machines. [ed.] Acad. Royale Des Sciences. *Histoire.* [Conf.]. Paris : G. Martin, 1745. Vol. MDCCIV, pp. 116-123 (Histoire), 323-337 (Mémoires). Lect. of 1704-11-19, hdl.handle.net/2027/ucm.5327383770.
83. **Borda, Le Chev. M. de.** Expériences sur la Resistance des Fluides. [ed.] Acad. Royale Des Sciences. *Histoire.* [Conf.]. Paris : Imprimerie Royal, 1766. Vol. MDCCLXIII, pp. 118-126 (Histoire), 358-376 (Mémoires). Lect. of 1763-12-20, hdl.handle.net/2027/ucm.5327384079.
84. **Sigloch, H.** *Technische Fluidmechanik.* Berlin : Springer, 2008. p. 583. ISBN 9783540446330.
85. **Pambour, F.-M. Guyonneau de.** *Locomotive Engines.* 2. London : Weale, 1840. p. 583. hdl.handle.net/2027/uc1.\$b25879.
86. **McNab, W.** On the economics of railway location. [Proc.]. Chicago, IL : AREMA, 1907. Vol. 8, pp. 143-254. hdl.handle.net/2027/mdp.39015068170284.

87. **UNECE**. Regulation No. 117 - Rev.3 - Tyre rolling resistance, rolling noise and wet grip. [Std.]. Genf : UNECE, WP.29, 02 2014. p. 97. Std. no. E/ECE/324/Rev.2/Add.116/Rev.3.
88. **OJ**. Regulation (EC) No 1222/2009. L (Legislation) *Official J. EU*. [Rule]. Luxembourg : Publ. Office EU, 22 12 2009. Vol. 52, 342, pp. 46-28. ISSN 1725-2555, CELEX no. 32009R1221.
89. **Ullrich, S.** Der Einfluss der Textur auf Reifen-Fahrbahngeräusch und Rollwiderstand. S, Straßenbau *Ber. BASt*. [Rep.]. Bremen : Schünemann, 01 1996. Vol. 4, 11, p. 92. ISSN 0943-9323, ISBN 9783894299279, bast.opus.hbz-nrw.de/volltexte/2015/929.
90. **Sander, K.** Vergleichsmessungen des Rollwiderstandes auf der Straße und im Prüfstand. *Ber. BASt. F, Fahrzeugtechnik*, 06 1996, Vol. 4, 20, p. 58. ISSN 0943-9307, ISBN 9783894297183, bast.opus.hbz-nrw.de/volltexte/2015/885.
91. **Glaeser, K.** Der Rollwiderstand von Reifen auf Fahrbahnen. *Fortschr.-Ber. VDI. 12, Verkehrstechnik*, 26 09 2005, Vol. 603, pp. 116-046. ISSN 0178-9449, ISBN 3183603128.
92. **Bode, O.** Untersuchung des Rollwiderstands von Nutzfahrzeugreifen auf echten Fahrbahnen. *FAT-Schriftenreihe*. [Rep.]. Berlin : FAT, 13 06 2013. Vol. 255, p. 72. ISSN 2192-7863.
93. **Michelin**. *Rollwiderstand und Kraftstoffersparnis*. Karlsruhe : Michelin, 2005. p. 120. ISBN 9782067116580.
94. **Kleffmann, J.** Bus Tire Rolling Resistance. [Pres. slides]. Hannover : Continental, 08 07 2009. p. 24.
95. **Bode, M.** Der Reifenrollwiderstand von Nutzfahrzeugen - Wie korrelieren die Werte bei unterschiedlichen Messverfahren? *VDI-Ber.* 26 10 2011, Vol. 2137, pp. 231-246. ISSN 0083-5560, ISBN 9783180921372.
96. **Pflug, H.** Einflüsse auf den Rollwiderstand von Lkw-Reifen auf realen Fahrbahnen. *Nutzfahrzeug Workshop*. [Conf.]. Graz : TU, Inst. f. Fahrzeugtechn., 12 05 2016. Vol. 7, p. 19.
97. **Bode, O.** Untersuchung des Rollwiderstands von Nutzfahrzeugreifen auf realer Fahrbahn. *FAT-Schriftenreihe*. [Rep.]. Berlin : FAT, 18 05 2016. Vol. 285, p. 36. ISSN 2192-7863.
98. **Buchholz, T.** Europäischer Transportpreis für Nachhaltigkeit: Die Preisträger 2016. *Transport*. [Art. on hp.]. München : Huss, 26 11 2015. Vol. 25, 23/24. ISSN 0946-7416, transport-online.de.
99. **Michelin**. Michelin X Line Energy gewinnen den "Europäischen Transportpreis für Nachhaltigkeit". [Art. on hp.]. Karlsruhe : Michelin Reifenwerke, 30 11 2015. lkw.michelin.de.
100. **Fontaras, G.** (...) Methodology for Measuring of Aerodynamic Resistances of HDV (...). *SAE Int. J. Commer. Veh.* 01 04 2014, Vol. 7, 1, pp. 102-110. ISSN 1946-3928, doi 10.4271/2014-01-0595.
101. **ACEA**. CO2 declaration procedure HDV. 3 [Rep.]. Bruxelles : ACEA, WG CO2HDV, 17 04 2014. p. 224.
102. **Rentema, D.** Aerodynamic optimization aspects of the DAF XF Euro 6 truck. *VDI-Ber.* 05 06 2013, Vol. 2186, pp. 13-24. ISSN 0083-5560, ISBN 9783180921860.
103. **ACEA**. CO2 declaration procedure HDV, Annex. 4 [Rep.]. Bruxelles : ACEA, WG CO2HDV, 21 04 2015. p. 269.
104. **Assen, R.** Base Drag Reduction of Articulated Trucks by Means of Boat-Tailing. [Master's thesis]. Delft : TU, Fac. Luchtvaart- en Ruimtevaarttech., 2007. lr.tudelft.nl.
105. **Cooper, K.** Wind Tunnel and Track Tests of Class 8 Tractors Pulling Single and Tandem Trailers Fitted with Side Skirts and Boat-tails. *SAE Int. J. Commer. Veh.* 2012, Vol. 5, 1, pp. 1-17. ISSN 1946-3928, doi 10.4271/2012-01-0104.
106. **Veldhuizen, R.** Results windtunnel measurement tractor-trailer with side-panels and boat-tail, model 1:16. [Email]. Rotterdam : WABCO - Optiflow, 03 07 2015. wabco-optiflow.com.
107. **WMO**. Guide to Meteorological Instruments and Methods of Observation. 7 [Std.]. Genf : WMO, 2012. p. 702 + app. 2. WMO-no. 8, ISBN 9789263100085.
108. **Troen, I.** *European Wind Atlas*. 1. Roskilde : RNL, 1989. p. 631 + app. 24. ISBN 9788755014824, orbit.dtu.dk, European_Wind_Atlas.pdf.
109. **DWD**. Windgeschwindigkeit in der BRD. *Windkarten*. [Map]. Offenbach a. M. : DWD, 2009. p. 1. Deutschland (200 m Raster), mittl. Windgeschw., 10m über Grund, dwd.de, windkarten.html.
110. —. Klimakarte der Windgeschwindigkeit für den Zeitraum 1995 bis 2008. *Windfelder für Deutschland (CLM4TRY)*. [Art. on hp.]. Offenbach a. M. : DWD, 2016. Avrg. wind velocity DE, 10 m above ground, dwd.de.
111. **BBR**. Handbuch Testreferenzjahre von Deutschland (...). [Rep.]. Bonn : BBR, 09 2014. p. 74. bbsr-energieeinsparung.de, TRY_Handbuch.pdf.
112. **VDI**. Hydrodynamische Leistungsübertragung. *VDI-Handbuch Getriebetechnik*. II, Gleichförmig übersetzte Getriebe, 04 1994, p. 44. Std. no. 2153, doc. no. 62-585.22(083.132).
113. **Voith**. *Hydrodynamik in der Antriebstechnik*. Mainz : VFV, 1987. p. 352. ISBN 9783783002270.
114. **Ayoubi, M.** Fahrzeugphysik. [book auth.] S. Pischinger. *Vieweg Handbuch Kraftfahrzeugtechnik*. 8. Wiesbaden : Springer Vieweg, 2016, 3, pp. 57-130. ISBN 9783658095277.
115. **Norris, J.** Quantifying energy consumption of HDV auxiliary components (...). 3 [Rep.]. Didcot : Ricardo Energy & Environment, 07 10 2015. p. 149 + app. 23. Ref. no. ED59309.
116. **Willans, P.** Steam Engine Trials. *Proc. ICE*. 11 04 1893, Vol. 114, 4, pp. 2-54. Paper no. 2622, ISSN 1753-7843, doi 10.1680/imotp.1893.20134.

117. **Pachernegg, S.** A Closer Look at the Willans-Line. *SAE Tech. Papers.* 1969, Vol. 23, 690182, pp. 1-10. ISSN 0148-7191, doi 10.4271/690182.
118. **Rizzoni, G.** Unified Modeling of Hybrid Electric Vehicle Drivetrains. *IEEE/ASME Transact. Mechatron.* 09 1999, Vol. 4, 3, pp. 246-257. ISSN 1083-4435, doi 10.1109/3516.789683.
119. **Nam, E.** Fuel Consumption Modeling of Conventional and Advanced Technology Vehicles in the Physical Emission Rate Estimator. [Rep.]. Washington, DC : USEPA, 02 2005. p. 122. Rep. no. EPA420-P-05-001, epa.gov, 420p05001.pdf.
120. **Ligterink, N.** Correction algorithms for WLTP chassis dynamometer and coast-down testing. [Rep.]. Delft : TNO, 05 08 2014. p. 70 + app. 43. Project no. 060.03678, www2.unece.org/wiki/display/trans/WLTP+8th+session.
121. **Norris, J.** Technical support to the correlation of CO2 emissions measured under NEDC and WLTP. [Rep.]. Didcot : Ricardo-AEA, 16 02 2015. p. 95. Ref. no. ED59049, SR#2 to Framework Contract CLIMA.C.2/FRA/2012/006.
122. **Zyl, S. van.** Using a simplified Willans line approach as a means to evaluate the savings potential of CO2 reduction measures in heavy-duty transport. *TAP.* [Conf.]. Lyon : IFSTTAR, Lab. transp. et environ., 24 05 2016. Vol. 21, pp. 784-797. ISBN 9782857827160, ifsttar.fr.
123. **VDV.** Klimatisierung von Linienbussen der Zulassungsklassen I und II (...). *VDV-Schriften.* [Std.]. Köln : Beka, 06 2015. Vol. 236, 2, p. 19.
124. **Kuitunen, S.** Determination of Carbon Dioxide Emissions of HVAC Systems for Buses. [Rep.]. Dresden : IVI, 25 04 2013. p. 111. webgate.ec.europa.eu/CITnet/jira/browse/VECTO.
125. —. HVACCO2SIM - ein Tool zur simulativen Ermittlung des CO2-Emissionsanteils von Klimatisierungssystemen in Bussen. *Wärmemgmt d. Kfz.* [Conf.]. Renningen : expert, 06 2014. Vol. 9, pp. 272-284. ISBN 9783816932758, publica.fraunhofer.de/documents/N-294171.html.
126. **CEN.** Calculation of room temperatures and of load and energy for buildings with room conditioning systems. *Ventilation for buildings.* [Draft std.]. Bruxelles : CEN, 07 2006. p. 155. Std. no. prEN 15243, cres.gr/greenbuilding/PDF/prend/set3.
127. **DIN.** Energy efficiency of buildings. [Std.]. Berlin : DIN, 02 2007. Std. no. DIN V 18599-1 to DIN V 18599-10, tc76.org, files 18599-1.pdf to 18599-10.pdf.
128. **Daimler.** Diesel and gas engine systems for EURO VI on-highway applications. [Prod. info]. Stuttgart : Daimler, 31 07 2013. p. 20. powertrain.mercedes-benz.com.
129. **Pischinger, R.** *Thermodynamik der Verbrennungskraftmaschine.* 3. Wien : Springer, 2009. p. 475. ISBN 9783211992760.
130. **UNECE.** Test procedure for compression-ignition (C.I.) engines (...). [Std.]. Genf : UNECE, 25 01 2007. p. 86 + ann. 40. Global technical regulation (GTR) No. 4, doc. no. ECE/TRANS/180/Add.4, unece.org, ECE-TRANS-180a4e.pdf.
131. **Eichlseder, W.** Designing Vehicle Cooling Systems Using Simulation Calculations. *ATZ.* 1997, Vol. 99, 10, pp. 638-647. ISSN 0001-2785.
132. **Yoo, I.** An Engine Coolant Temperature Model and Application for Cooling System Diagnosis. *SAE Tech. Papers.* 06 03 2000, Vol. 54, 2000-01-0939, p. 11. ISSN 0148-7191, doi 10.4271/2000-01-0939.
133. **Won, J.** Thermal Flow Analysis of Vehicle Engine Cooling System. *WAC.* [Conf.]. Seoul : FISITA, 12 06 2000. p. 6. 210.101.116.115/fisita/pdf/H202.pdf.
134. **Gumpoldsberger, T.** Simulating the thermal management of commercial vehicles. *Autotechnology.* 2003, Vol. 3, 1, pp. 84-87. ISSN 1616-8216, doi 10.1007/BF03246761.
135. **Dupree, R.** Cooling fan and system performance and efficiency improvements. [Rep.]. Peoria, IL : Caterpillar, 31 07 2005. p. 107. DOE contract no.: FC26-02AL68081, doi 10.2172/1028966.
136. **Mao, S.** Off-highway heavy-duty truck under-hood thermal analysis. *Appl. Thermal Engrg.* 13 05 2010, Vol. 30, 13, pp. 1726-1733. ISSN 1359-4311, doi 10.1016/j.applthermaleng.2010.04.002.
137. **Yao, Y.** Experiment and Simulation Research of Engine Cooling Fan in Dump Truck. *EMEIT.* [Conf.]. Harbin : IEEE, 12 08 2011. Vol. 9, pp. 742-745. ISBN 9781612840871, doi 10.1109/EMEIT.2011.6023202.
138. **Nessim, W.** A Simulation Study of an Advanced Thermal Management System for Heavy Duty Diesel Engines. *AISR.* [Conf.]. Amsterdam : Atlantis, 11 2012. Vol. 27, pp. 287-290. ISSN 1951-6851, ISBN 9789078677598, doi 10.2991/mems.2012.176.
139. **Minovski, B.** Study of software system integration for transient simulation of future cooling system for heavy truck applications. [Master thesis]. Göteborg : Chalmers TH, Fordonstekn. och autonoma syst., 2013. p. 54. studentarbeten.chalmers.se/publication/185292.
140. **Magna.** KULI Software. [Prod. info]. Sankt Valentin : Magna Powertrain, 16 06 2016. p. 6. kuli-software.com/Flyer.5336.0.html.
141. **Banzhaf, M.** Verbrauchsreduzierung bei Nutzfahrzeugen durch Visco-Lüfter und -Wasserpumpen. [Pres. slides]. Stuttgart : Behr, 12 05 2010. p. 14. yumpu.com/en/document/view/9451007.

142. **Kies, A.** Options to consider future advanced fuel saving technologies in the CO2 test procedure for HDV. [Rep.]. Graz : TU, IVT, 19 12 2013. p. 108. Rep. no. FVT -104/13/ Rex Em 06/13-6790, theicct.org.
143. **Voisins, J.** *Traité d'hydraulique, à l'usage des ingénieurs*. 1. Paris : Levrault, 1834. p. 564. hdl.handle.net/2027/nyp.33433066366661.
144. **Bernoulli, D.** *Hydrodynamica*. [ed.] Imp. acad. of Sciences St. Petersburg. Strasbourg : Dulsecker, 1738. p. 304. doi 10.3931/e-rara-3911 , engl. transl. by I. Bruce, 17centurymaths.com.
145. **Wagner, W.** *Strömung und Druckverlust*. 7. Würzburg : Vogel, 2012. p. 318. ISBN 9783834332738.
146. —. *Lufttechnische Anlagen*. Würzburg : Vogel, 2007. p. 226. ISBN 9783834330956.
147. **Clapeyron, E.** Mémoire sur la Puissance Motrice de la Chaleur. *J. École polytechn.* 1834, Vol. 14, 23, pp. 153-190. ISSN 0368-2013, ISBN 9782876472839, hdl.handle.net/2027/mdp.39015013153542.
148. **Knorr.** High Performance Compressors. [Prod. info]. München : Knorr-Bremse, 11 03 2009. p. 4. Doc. no. P-3505_EN_005, knorr-bremsecvs.com.
149. **ACEA.** CO2 declaration procedure HDV. 4 [Rep.]. Bruxelles : ACEA, WG CO2HDV, 21 04 2015. p. 238.
150. **Voith.** Air compressors. [Prod. info]. Zschopau : Voith, 10 2012. voith.com, air-compressors-9812.html.
151. **Ennemoser, A.** Optimized Strategic Auxiliary Operation in Commercial Vehicles. *MTZ worldw.* 10 02 2012, Vol. 73, 3, pp. 28-32. ISSN 2192-9114, doi 10.1365/s38313-012-0151-4.
152. **Hydac.** Bladder Accumulators Standard. [Prod. info]. Sulzbach : HYDAC, 09 2014. pp. 29-35. Doc. no. E 3.201.27/09.14, hydac.com.
153. **Marx, M.** Feedback on Electrical System - VECTO2.0.4 - AUX.Alpha.3. [Pres. slides]. Bruxelles : ACEA, WG CO2HDV, Task Force 5, 30 11 2015. p. 6. acea.be.
154. **Espinosa, N.** Waste heat recovery, Refrigerant Rankine system. *Trucks/Off-Road Powertrain*. [Conf.]. Lyon : SIA, 21 11 2012.
155. **Zeitzen, F.** MAN TGA tractor with Knorr Pneumatic Booster System, MB Actros tractor with Voith WHR System. *lastauto omnibus*. 12 2011, Vol. 86, 1/2, pp. 32-35. ISSN 1613-1606.
156. **NIST.** Thermophysical Properties of Fluid Systems. *Chemistry WebBook*. [Database]. Gaithersburg, MD : NIST, 2016. webbook.nist.gov.
157. **OJ.** Directive 2005/55/EC. L (Legislation) *Official J. EU*. [Rule]. Luxembourg : Publ. Office EU, 20 10 2005. Vol. 48, 275, pp. 1-163. ISSN 1725-2555, CELEX no. 32005L0055.
158. **Hausberger, S.** Emission Factors from the Model PHEM for the HBEFA Version 3. [Rep.]. Graz : TU, IVT, 07 12 2009. p. 76. Rep. no. I-20/2009 Haus-Em 33/08/679.
159. **Rexeis, M.** Ascertainment of Real World Emissions of HDV. [Diss.]. Graz : TU, IVT, 10 2009. p. 237.
160. **Kies, A.** Eco Drive for Hybrid Electric Vehicles, Zwischenbericht 2. [Interim Rep.]. Graz : TU, IVT, 27 07 2012. p. 15. FFG, project no. 829966.
161. —. EHEV - Eco Drive for Hybrid Electric Vehicles. [Rep.]. Graz : TU, IVT, 22 11 2013. p. 80. FFG, project no. 829966, klimafonds.gv.at, EHEVAntonius-KiesEndberichtNE-2020-4AS829966.pdf.
162. **VEIC.** An Assessment of Level 1 and Level 2 Electric Vehicle Charging Efficiency. [Rep.]. Burlington, VT : VEIC, 20 03 2013. p. 16. veic.org, 20130320-EVT-NRA-Final-Rep..pdf.
163. **Ragatz, A.** Smith Newton Vehicle Performance Evaluation. [Rep.]. Golden, CO : NREL, 10 2014. p. 4. Rep. no. NREL/BR-5400-64238, osti.gov/scitech/biblio/1215262.
164. **IEC.** Electrical insulation – Thermal evaluation and designation. 4 [Std.]. Genf : IEC, 07 11 2007. Std. no. 60085, ISBN 2831893879.
165. —. Permanent magnet synchronous electrical machines connected to an electronic converter. 1 *Electric traction - Rotating electrical machines for rail and road vehicles*. [Std.]. Genf : IEC, 11 12 2012. 4. Std. no. 60349-4, ISBN 9782832205471.
166. **Andersson, R.** Design and evaluation of electrical machine for parallel hybrid drive for heavy vehicles. *ICEM*. [Conf.]. Marseille : IEEE, 02 09 2012. Vol. 20, pp. 2622-2628. ISBN 9781467301428, doi 10.1109/ICEIMach.2012.6350255.
167. **Breemersch, T.** GHG reduction measures for the Road Freight Transport sector. [Rep.]. Leuven : TML, 2014. p. 39. tmlleuven.be/project/hgvc02.
168. **Breitkopf, M.** Leipzig testet Hybridbus. *Der Nahverkehr*. 02 2010, Vol. 28, 3, pp. 17-20. ISSN 0722-8287.
169. **Tschakert, W.** IBC 2014: MAN Lion's City, MB Citaro, Scania Citywide, Solaris Urbino, VDL Citea. *Bus-Fahrt*. 04 2014, Vol. 62, 5, pp. 10-21. ISSN 0341-5244.
170. **CFR.** Title 40, Protection of Environment, Part 1000 to End. *CFR*. [Rule]. Washington, DC : USGPO, 01 07 2015. p. 1237. ISSN 1946-4975, gpo.gov/fdsys/pkg/CFR-2015-title40-vol33.
171. **Süßmann, A.** Technische Möglichkeiten für die Reduktion der CO2-Emissionen von Nfz. *Ber. BAST. F, Fahrzeugtechnik*, 30 07 2015, Vol. 23, 103, p. 64. ISSN 0943-9307, ISBN 9783956061592, bast.opus.hbz-nrw.de/volltexte/2015/1412.
172. **Sherwood, A.** A study of the wind resistance of tractors and truck-trailers. [Rep.]. College Park, MD : Uni Maryland, Wind Tunnel Operations Dept., 24 09 1954. p. 46. worldcat.org/oclc/489236172.

173. **Cooper, K.** CV Aerodynamic Drag Reduction. [book auth.] E. McCallen. *The Aerodynamics of Heavy Vehicles*. Berlin : Springer, 2004, pp. 9-28. ISBN 9783642535864.
174. **Willms, O.** MB Atego Aero. *lastauto omnibus*. 10 2014, Vol. 91, 11, p. 18. ISSN 1613-1606.
175. **OJ.** Commission Regulation (EU) No 1230/2012. L (Legislation) *Official J. EU*. [Rule]. Luxembourg : Publ. Office EU, 21 12 2012. Vol. 55, 353, pp. 31-79. ISSN 1977-0677, CELEX no. 32012R1230.
176. **EuCom.** Impact Assessment. [Rep.]. Bruxelles : Europ. Commiss., 15 04 2013. p. 72. CELEX no. 52013SC0108.
177. **OJ.** Directive (EU) 2015/719. L (Legislation) *Official J. EU*. [Rule]. Luxembourg : Publ. Office EU, 06 05 2015. Vol. 58, 115, pp. 1-10. ISSN 1977-0677, CELEX no. 32015L0719.
178. **UNECE.** Proposal for a draft Supplement to the 04 series of amendments to Regulation No. 46. [Draft std.]. Genf : UNECE, WP.29, GRSG, CMS, 29 09 2015. p. 102. Doc. no. GRSG-108-46-Rev.2.
179. **Daimler.** Mercedes-Benz Aerodynamics Truck und Trailer. [PR]. Stuttgart : Daimler, 18 09 2012. media.daimler.com/dcmmedia/0-921-657321-49-1533366-1-0-1-0-0-1-12639-614240-0-1-0-0-0-0-0.html.
180. **Colombano, M.** An optimized transport concept for tractor-semitrailer combination. *ATZ worldw.* 01 2008, Vol. 110, 2, pp. 32-36. ISSN 2192-9076, doi 10.1007/BF03224985.
181. **Wildhage, H.** Slow Steaming lohnt sich auch beim LKW. *DVZ*. 17 05 2013, Vol. 67, 40, pp. 20-21. ISSN 0342-166X.
182. **Zeitzen, F.** Iveco Stralis AS440S45. *lastauto omnibus*. 09 2010, Vol. 87, 10, pp. 11-14. ISSN 1613-1606.
183. **Zeilinger, M.** Record Run Buses 2012. [Pres. slides]. Wiesbaden : Daimler, Buses, 29 10 2012. p. 27. daimler.com, 2246408_Record_Run_Buses_2012_Martin_Zeilinger_.pdf.
184. **VDL.** Citea, Tech. spec. Euro 6. [Prod. info]. Valkenswaard : VDL, 2013. vdlbuscoach.com/Producten/Openbaar-vervoer/Citea/Technische-specificatie.aspx.
185. **Wildhagen, M.** Möglichkeiten der Verbrauchsoptimierung durch Aerodynamik und weitere Maßnahmen am Trailer. *VDI-Ber.* 20 05 2011, Vol. 2128, pp. 89-104. ISSN 0083-5560, ISBN 9783180921280.
186. **Kraneburg, P.** Die Entwicklung eines Leichtlaufgetriebeöls. *ATZ*. 12 2005, Vol. 108, 1, pp. 34-37. ISSN 0001-2785, doi 10.1007/BF03221760.
187. **Hargreaves, D.** Assessing the energy efficiency of gear oils via the FZG test machine. *Tribology Int.* 18 01 2009, Vol. 42, pp. 918-925. ISSN 0301-679X, doi 10.1016/j.triboint.2008.12.016.
188. **Winkelmann, L.** The Capacity of Superfinished Vehicle Components to Increase Fuel Economy. *Gear Tech.* 02 2009, Vol. 26, 1/2, pp. 50-60. ISSN 0743-6858.
189. **Killian, M.** Efficiency Improvement through Reduction in Friction and Wear in Powertrain Systems. [Rep.]. Milwaukee, WI : Eaton, 30 09 2009. p. 134. Contr. no. FC26-04NT42263, doi 10.2172/989104.
190. **Green, D.** The Effect of Engine, Axle and Transmission Lubricant, and Operating Conditions on Heavy Duty Diesel Fuel Economy. Part 1: Measurements. *SAE Int. J. Fuels Lubr.* 30 08 2011, Vol. 5, 1, pp. 480-487. ISSN 1946-3952, doi 10.4271/2011-01-2129.
191. **Doyer, A.** How Bearing Design Improves Gearbox Performance. *Gear Tech.* 09 2012, Vol. 29, 9, pp. 52-57. ISSN 0743-6858.
192. **Joachim, F.** How to Minimize Power Losses in Transmissions, Axles and Steering Systems. *Gear Tech.* 09 2012, Vol. 29, 9, pp. 58-66. ISSN 0743-6858.
193. **Fernandes, C.** Gearbox power loss. Part I: Losses in rolling bearings. *Tribology Int.* 03 12 2014, Vol. 88, pp. 298-308. ISSN 0301-679X, doi 10.1016/j.triboint.2014.11.017.
194. —. Gearbox power loss. Part II: Friction losses in gears. *Tribology Int.* 18 12 2014, Vol. 88, pp. 309-316. ISSN 0301-679X, doi 10.1016/j.triboint.2014.12.004.
195. —. Gearbox power loss. Part III: Application to a parallel axis and a planetary gearbox. *Tribology Int.* 27 03 2015, Vol. 88, pp. 317-326. ISSN 0301-679X, doi 10.1016/j.triboint.2015.03.029.
196. **Macian, V.** Potential of low viscosity oils to reduce CO2 emissions and fuel consumption of urban buses fleets. *Transp. Rsrch. D, Transp. and Environm.*, 29 06 2015, Vol. 39, pp. 76-88. ISSN 1361-9209, doi 10.1016/j.trd.2015.06.006.
197. **Sgroi, M.** Engine bench and road testing of an engine oil containing MoS2 particles as nano-additive for friction reduction. *Tribology Int.* 20 10 2016, Vol. 105, pp. 317-325. ISSN 0301-679X, doi 10.1016/j.triboint.2016.10.013.
198. **Wildhage, H.** Scania R 520. *Kfz-Anzeiger*. 04 2015, Vol. 68, 7, pp. 11-14. ISSN 0341-9681.
199. **Steininger, U.** Im Praxistest - Mehrverbrauch durch Retarder? *VDI-Ber.* 27 05 2009, Vol. 2068, pp. 83-95. ISSN 0083-5560, ISBN 9783180920689.
200. **Dold, R.** Abgasenergieerückgewinnung für schwere Fernverkehrsnutzfahrzeuge. *VDI-Ber.* 05 06 2013, Vol. 2186, pp. 43-52. ISSN 0083-5560, ISBN 9783180921860.
201. **Glensvig, M.** Testing of a Long Haul Demonstrator Vehicle with a Waste Heat Recovery System on Public Road. *SAE Tech. Papers*. 27 09 2016, Vol. 70, 2016-01-8057, p. 9. ISSN 0148-7191, doi 10.4271/2016-01-8057.

202. **Lutz, R.** Use of Exhaust Gas Energy in Heavy Trucks Using the Rankine Process. *MTZ worldw.* 06 09 2012, Vol. 73, 10, pp. 32-36. ISSN 2192-9114, doi 10.1007/s38313-012-0224-4.
203. **Diesel, R.** *The present status of the Diesel engine in Europe.* Saint Louis, MO : Busch-Sulzer, 1912. p. 48. hdl.handle.net/2027/chi.087192032.
204. —. *Die Entstehung des Dieselmotors.* 1. Berlin : Springer, 1913. ISBN 9783642649400, doi 10.3931/e-rara-11467.
205. **Knothe, G.** Historical perspectives on vegetable oil-based diesel fuels. *inform.* 2001, Vol. 12, 11, pp. 1103-1107. ISSN 0897-8026.
206. **Knothe, G. (ed.).** *The Biodiesel Handbook.* 1. Champaign, IL : AOCS, 2005. p. 296. ISBN 9781893997790.
207. **O.J.** Directive 98/70/EC. L, Legislation *Official J. EC.* [Rule]. Luxembourg : Publ. Office EU, 28 12 1998. Vol. 41, 350, pp. 58-67. ISSN 0378-6988, CELEX no. 01998L0070-20151005, update 2015-09-15 by Directive (EU) 2015/1513.
208. **CEN.** Methodology for calculation and declaration of energy consumption and GHG emissions of transport services (freight and passengers). [Std.]. Bruxelles : CEN, 21 11 2012. p. 66. Std. no. EN 16258.
209. **Pflaum, H.** Potential of Hydrogenated Vegetable Oil (HVO) in a Modern Diesel Engine. *SAE Tech. Papers.* 28 09 2010, Vol. 64, 2010-32-0081, p. 11. ISSN 0148-7191, doi 10.4271/2010-32-0081.
210. **Pandey, A.** *Biofuels.* 1. Oxford, UK : Academic Press, 2011. p. 630. ISBN 9780123850997.
211. **Eichseder, H.** *Wasserstoff In Der Fahrzeugtechnik.* 3. Wiesbaden : Springer-Vieweg, 2012. p. 320. ISBN 9783834817549.
212. **Geringer, B.** Alternative Antriebe. [Lect. notes]. Wien : TU, IFA, 06 2012. Lect. no. 315.725.
213. **Dedl, P.** Screening von potenziellen sauerstoffhaltigen erneuerbaren Dieselkomponenten für kraftstoffbasierende Emissionsreduktion. *VDI-Ber.* 06 11 2012, Vol. 2183, pp. 159-172. ISSN 0083-5560, ISBN 9783180921839.
214. **Kaltschmitt, M. (ed.).** *Renewable Energy Systems.* 1. New York, NY : Springer, 2012. p. 1896. ISBN 9781461458197.
215. **Kegl, B.** *Green Diesel Engines.* 1. London : Springer, 2013. p. 264. ISBN 9781447153245.
216. **Evans, P.** The System Performance Benefits of Lubrication Flow Control. *SAE Tech. Papers.* 26 10 2004, Vol. 58, 2004-01-2687, p. 9. ISSN 0148-7191, doi 10.4271/2004-01-2687.
217. **Reichert, J.** Reduced friction in engine sealing system for truck engines. *MTZ worldw.* 03 2010, Vol. 71, 4, pp. 30-35. ISSN 2192-9114, doi 10.1007/BF03227989.
218. **Wickerath, B.** Fully variable mechanical coolant pump for commercial vehicles. *MTZ worldw.* 23 12 2010, Vol. 72, 1, pp. 28-32. ISSN 2192-9114, doi 10.1365/s38313-011-0006-4.
219. **Voigt, D.** Variable Flow Spur Gear Oil Pump for utility vehicle engines. *MTZ.* 11 03 2011, Vol. 72, 4, pp. 24-29. ISSN 0024-8525, doi 10.1365/s38313-011-0037-x.
220. **Taylor, I.** Impact of Lubricants on Engine Friction and Durability. *Tribology Days.* [Conf.]. Trollhättan : TU Lulea, Machine Elements, 08 11 2011. p. 36. itu.se, IanTaylor.pdf.
221. **Schultheiß, G.** Visco Coolant Pump Demand-based Flow Rate Control. *MTZ worldw.* 10 02 2012, Vol. 73, 3, pp. 34-39. ISSN 2192-9114, doi 10.1365/s38313-012-0152-3.
222. **Carden, P.** The Effect of Low Viscosity Oil on the Wear, Friction and Fuel Consumption of a HD Truck Engine. *SAE Int. J. Fuels Lubr.* 08 04 2013, Vol. 6, 2, pp. 311-319. ISSN 1946-3952, doi 10.4271/2013-01-0331.
223. **Shin, Y.** Use of electromagnetic clutch water pumps in vehicle engine cooling systems to reduce fuel consumption. *Energy.* 21 06 2013, Vol. 57, pp. 624-631. ISSN 0360-5442, doi 10.1016/j.energy.2013.04.073.
224. **Gerhardt, J.** Beitrag des Einspritzsystems zur Absenkung der CO₂-Emission. *Der Arbeitsprozess des Verbrennungsmotors.* [Proc.]. Graz : TU, IVT, 24 09 2013. Vol. 14, 1, pp. 53-67. ISBN 9783851252958.
225. **Stanton, D.** Highly Efficient and Clean Engines to Meet Future CV GHG Regulations. *SAE Int. J. Engines.* 24 09 2013, Vol. 6, 3, pp. 1395-1480. ISSN 1946-3936, doi 10.4271/2013-01-2421.
226. **Mo, H.** The effect of cylinder deactivation on the performance of a diesel engine. *Proc. IMechE. D, J. Automob. Engrg.,* 24 10 2013, Vol. 228, 2, pp. 199-205. ISSN 0954-4070, doi 10.1177/0954407013503627.
227. **Zammit, J.** The influence of cylinder deactivation on the emissions and fuel economy of a four-cylinder direct-injection diesel engine. *Proc. IMechE. D, J. Automob. Engrg.,* 28 10 2013, Vol. 228, 2, pp. 206-217. ISSN 0954-4070, doi 10.1177/0954407013506182.
228. **Franke, M.** Development Trends for Commercial and Industrial Engines. *SAE Int. J. Engines.* 30 09 2014, Vol. 7, 4, pp. 1629-1636. ISSN 1946-3936, doi 10.4271/2014-01-2325.
229. **Thiruvengadam, A.** Heavy-Duty Vehicle Diesel Engine Efficiency Evaluation and Energy Audit. [Rep.]. Morgantown, WV : WVU, Mech. and Aerosp. Engrg., 10 2014. p. 62. theicct.org, HDV_engine-efficiency-eval_WVU-rpt_oct2014.pdf.
230. **Dam, W. van.** Taking HD Diesel Engine Oil Performance to the Next Level, Part 1: Optimizing for Improved Fuel Economy. *SAE Tech. Papers.* 13 10 2014, Vol. 68, 2014-01-2792, p. 8. ISSN 0148-7191, doi 10.4271/2014-01-2792.

231. **Cipollone, R.** Sliding vane rotary pump in engine cooling system for automotive sector. *Appl. Therm. Engrg.* 08 11 2014, Vol. 76, pp. 157-166. ISSN 1359-4311, doi 10.1016/j.applthermaleng.2014.11.001.
232. **Granottier, N.** Engine Thermal Management on Volvo Heavy Duty Engines. *MTZ worldw.* 01 01 2015, Vol. 76, 2, pp. 4-9. ISSN 2192-9114, doi10.1007/s38313-014-1013-z.
233. **Macian, V.** Low viscosity engine oils: Study of wear effects and oil key parameters in a heavy duty engine fleet test. *Tribology Int.* 28 08 2015, Vol. 94, pp. 240-248. ISSN 0301-679X, doi 10.1016/j.triboint.2015.08.028.
234. **Ratzberger, R.** Evaluation of Valve Train Variability in Diesel Engines. *SAE Int. J. Engines.* 06 09 2015, Vol. 8, 5, pp. 2379-2393. ISSN 1946-3936, doi 10.4271/2015-24-2532.
235. **Theißl, H.** Miller Valve Timing for Future Commercial Diesel Engines. *MTZ worlww.* 03 10 2015, Vol. 76, 11, pp. 4-11. ISSN 2192-9114, doi 10.1007/s38313-015-0053-3.
236. **Kraxner, T.** Cylinder deactivation for Heavy Duty Diesel Engines. *Powertrain.* [Conf.]. Rouen : SIA, 01 06 2016. p. 9. sia.fr.
237. **Mollenhauer, K.** *Handbuch Dieselmotoren.* 3. Berlin : Springer, 2007. p. 702. ISBN 9783540721642.
238. **Zeitzen, F.** Iveco Stralis AS440S42. *lastauto omnibus.* 12 2014, Vol. 91, 1, pp. 10-14. ISSN 1613-1606.
239. —. Scania R450 LA Topline. *lastauto omnibus.* 06 2015, Vol. 92, 7, pp. 20-25. ISSN 1613-1606.
240. **Bennühr, S.** European Truck Challenge 2014. *DVZ.* 18 12 2014, Vol. 68, 101, pp. 2-11. ISSN 0342-166X, european-truck-challenge.com, ETC-DVZ-2014.pdf.
241. **Kern, M.** Tractors with EcoRoll: MB Actros 1845, Scania G 450, Volvo FH 460. *lastauto omnibus.* 07 2013, Vol. 90, 8, pp. 14-19. ISSN 1613-1606.
242. **Lattemann, F.** The Predictive Cruise Control - A System to Reduce Fuel Consumption of HD Trucks. *SAE Tech. Papers.* 26 10 2004, Vol. 58, 2004-01-2616, p. 8. ISSN 0148-7191, doi 10.4271/2004-01-2616.
243. **Kies, A.** Influence of the driving style on fuel consumption and battery wear of a parallel hybrid city bus. *Automot. Engine Tech.* [Conf.]. Stuttgart : FKFS, 27 02 2013. Vol. 13, pp. 127-142.
244. —. EHEV - Eco Drive for Hybrid Electric Vehicles. *Science Brunch Energieeffz. Fahrzeugtech.* [Conf.]. Wien : Klima- und Energiefonds, 09 04 2015. p. 11. klimafonds.gv.at.
245. **Oulette, P.** Which technology for Natural Gas HD engines? *Trucks/Off-Road Powertrain.* [Conf.]. Lyon : SIA, 21 11 2012. p. 23. sia.fr.
246. **Dunn, M.** High efficiency and low emission natural gas engines for heavy duty vehicles. [book auth.] IMechE. *Internal Combustion Engines.* Philadelphia, PA : Woodhead, 2013, pp. 123-136. ISBN 9781782421832, doi 10.1533/9781782421849.4.123.
247. **Figer, G.** Commercial Vehicle Natural Gas Engines with Diesel Efficiency. *MTZ worldw.* 09 09 2014, Vol. 75, 10, pp. 10-15. ISSN 2192-9114, doi 10.1007/s38313-014-0229-2.
248. **Gao, Z.** Comparative Study of Hybrid Powertrains on Fuel Saving, Emissions, and Component Energy Loss in HD Trucks. *SAE Int. J. Commer. Veh.* 30 09 2014, Vol. 7, 2, pp. 414-431. ISSN 1946-3928, doi 10.4271/2014-01-2326.
249. —. Exploring Fuel-Saving Potential of Long-Haul Truck Hybrid. *TRR.* 2015, Vol. 2502, pp. 99-107. ISSN 0361-1981, doi 10.3141/2502-12, FDHDT-A via email, 2016-10-31, Gao Z., Knoxville TN, ORNL, NTRC.
250. —. The evaluation of developing vehicle technologies on the fuel economy of long-haul trucks. *Energy Cnv. and Mgmt.* 23 10 2015, Vol. 106, pp. 766-781. ISSN 0196-8904, doi 10.1016/j.enconman.2015.10.006.
251. —. Pers. communication. [Email]. Knoxville, TN : ORNL, NTRC, 2016. Emails 2016-11-03, 2016-11-10.
252. **NREL.** Project Startup: Evaluating Coca-Cola's Class 8 Hybrid-Electric Delivery Trucks. [Rep.]. Golden, CO : NREL, 01 03 2011. p. 2. Rep. no. NREL/FS-5400-49621, doi 10.2172/1009686.
253. **Walkowicz, K.** Coca-Cola Refreshments Class 8 Diesel Electric Hybrid Tractor Evaluation. [Rep.]. Golden, CO : NREL, 01 08 2012. p. 38. doi 10.2172/1052910.
254. **Thornton, M.** Data Collection, Testing, and Analysis of Hybrid Electric Trucks and Buses (...). [Rep.]. Golden, CO : NREL, 12 06 2015. p. 72. Rep. no. NREL/TP-5400-62009, doi 10.2172/1215000.
255. **Proust, A.** Evaluation of Class 7 Diesel-Electric Hybrid Trucks. *SAE Tech. Papers.* 24 09 2012, Vol. 67, 2012-01-1987, p. 13. ISSN 0148-7191, doi 10.4271/2012-01-1987.
256. **Nylund, N.** Fuel and Technology Alternatives for Buses. *VTT Tech.* [Rep.]. Espoo : VTT, 08 2012. 46, p. 294 + app. 94. ISSN 2242-122X, ISBN 9789513878696, urn.fi/URN:ISBN:978-951-38-7869-6.
257. **Anderegg, M.** 21 umweltfreundliche Hybrid-Gelenkbusse für BERNMOBIL. [Pres. slides]. Bern : Bernmobil, 10 09 2015. p. 9. bernmobil.ch, 2015-09-10-Präsentation_MO_V4.pdf.
258. **Zumsteg, C.** Erfahrungen Volvo Diesel-Hybridbusse. *Fachtagung KTBB.* [Conf.]. Granges-Paccot : VöV, 21 05 2014. p. 21. voev.ch.
259. **Grünenfelder, M.** Hybridbusse im Linienbetrieb. *Fachtagung KTBB.* [Conf.]. Granges-Paccot : VöV, 24 05 2016. p. 18. voev.ch.
260. **Bourbon, G.** Hybridbusse für einen umweltfreundlichen ÖPNV. [Rep.]. Berlin : BMUB, 05 2012. p. 130. erneuerbar-mobil.de, abschlussbericht-begleitprogramm-public.pdf.

261. **WSP**. Energieeffektivisering av bussar och busstrafik. [Rep.]. Stockholm-Globen : WSP, 24 05 2012. p. 78. snt.se/portfolio/WSP_Rapporter_fran_WSP.
262. **Elbert, P.** Systematic Optimisation of a Serial Hybrid Electric Bus. *MTZ worldw.* 15 04 2016, Vol. 77, 5, pp. 62-67. ISSN 2192-9114, doi 10.1007/s38313-016-0031-4.
263. **ABRTC**. New Flyer, XD40. [Rep.]. Duncansville, PA : ABRTC, 11 2012. p. 61. Rep. no. PTI-BT-R1211, altoonabustest.psu.edu/buses/416.
264. —. New Flyer, XDE40. [Rep.]. Duncansville, PA : ABRTC, 12 2011. p. 56. Rep. no. PTI-BT-R1015, altoonabustest.psu.edu/buses/388.
265. **Unruh, R.** VDL Citea SLF-120. *lastauto omnibus.* 03 2011, Vol. 88, pp. 48-52. ISSN 1613-1606.
266. —. MB Citaro Euro 5. *lastauto omnibus.* 09 2011, Vol. 85, pp. 47-50. ISSN 1613-1606.
267. —. MAN Lion's City Hybrid Euro 5. *lastauto omnibus.* 09 2012, Vol. 89, 10, pp. 72-76. ISSN 1613-1606.
268. **E-CONTROL**. Stromkennzeichnungsbericht 2015. [Rep.]. Wien : Energie-Control Austria, 01 2016. p. 190. e-control.at/EC_Stromkennzb15_NEU.pdf.
269. **Prohaska, R.** Statistical Characterization of Medium-Duty Electric Vehicle Drive Cycles. [Paper]. Golden, CO : NREL, 05 2015. p. 10. Rep. no. NREL/CP-5400-63607, osti.gov/scitech/biblio/1215109, SN via email, 2016-03-10, Prohaska R., NREL, Transp. and Hydrogen Syst.,.
270. **Steele, L.** Vocational Vehicle Tire Rolling Resistance Test Data Evaluation. [Memo]. Ann Arbor, MI : USEPA, 11 05 2015. p. 6. regulations.gov/#!documentDetail;D=EPA-HQ-OAR-2014-0827-0116.
271. **Reinhart, T.** Commercial Medium- and Heavy-Duty Truck Fuel Efficiency Technology Study. [Rep.]. Washington, DC : NHTSA, 02 2016. p. 122 + app. 131. Rep. no. DOT HS 812 194, nhtsa.gov.
272. **Jordan, M.** Mercedes-Benz reduziert CO2-Ausstoß beim „Efficiency Run 2015“ um bis zu 14 Prozent. [Art. on hp.]. Höttingen : MBpassion, 19 10 2015. blog.mercedes-benz-passion.com.
273. **Unruh, R.** MB Citaro Euro 6. *lastauto omnibus.* 07 2013, Vol. 90, 8, pp. 51-54. ISSN 1613-1606.
274. **Daimler**. Record Run Buses. [Art. on hp.]. Milton Keynes : Daimler, Mercedes-Benz UK Ltd., 2013. mercedes-benz.co.uk/record_run.html.
275. **Breemersch, T.** GHG reduction measures for the Road Freight Transport sector up to 2020. [Rep.]. Leuven : TML, 29 07 2015. p. 43. tmlleuven.be/project/followuphdvco2/home.htm.
276. **Zacharof, N.** Report on VECTO technology simulation capabilities and future outlook. [Rep.]. Luxembourg : Publ. Office EU, 12 2016. p. 46. ISBN 9789279641589, doi 10.2790/10868.
277. **O'Keefe, M.** Duty Cycle Charact. and Eval. Towards Heavy Hybrid Vehicle Applicat. *SAE Tech. Papers.* 16 04 2007, Vol. 61, 2007-01-0302, p. 13. ISSN 0148-7191, doi 10.4271/2007-01-0302.
278. **Weijer, C. J. T. van de.** Heavy-duty emission factors. [Diss.]. Graz : TU, Fakultät für Maschinenbau, 10 1997. p. 155. permalink.obvsg.at/AC02228456.
279. **IEC**. Rating and performance. 12 *Rotating electrical machines*. [Std.]. Genf : IEC, 03 02 2010. 1. Std. no. 60034-1, ISBN 2831810741.
280. **BIPM**. Le Système international d'unités (SI). 8 [Std.]. Paris : BIPM, 05 2006. p. 180. ISBN 9282222136, bipm.org/si_brochure_8.pdf.
281. **NIST**. Specifications, Tolerances, and Other Technical Requirements for Weighing and Measuring Devices. [Std.]. Gaithersburg, MD : NIST, 11 2015. Vol. 44, p. 516. doi 10.6028.NIST.HB.44.
282. **ACEA**. CO2 declaration procedure HDV. 2 [Rep.]. Bruxelles : ACEA, WG CO2HDV, 12 2012. p. 65+145.
283. —. Integration of DIN Cycle in ACEA Refuse Cycle. [Pres. slides]. Stuttgart : ACEA, WG CO2HDV, Task Force 1, 31 01 2017. p. 9. Cycle from folder VECTO v3.2.0/925, ...\\Mission Profiles\MunicipalUtility.vdri.
284. **Bierbooms, R.** 1. Comparison missions, 2. Optimization Regional, 3. Urban cycle. [Pres. slides]. Eindhoven : Sioux LIME B.V., 01 06 2016. p. 22. limebv.nl, document not public; RD16 via email, 2017-01-16, Trentzsch A., Stuttgart, Daimler, Powertrain Homologation.
285. **ACEA**. CO2 declaration procedure HDV. 5 [Rep.]. Bruxelles : ACEA, WG CO2HDV, 21 04 2016. p. 292.
286. **Herpen, R. van.** New 100 km urban cycle. [Email]. Eindhoven : Sioux LIME B.V., 22 06 2017. limebv.nl, email to ACEA, WG CO2HDV, Task Force 1.
287. **ABRTC**. Fuel Economy Test. [Std.]. Duncansville, PA : ABRTC, 04 2006. p. 25. altoonabustest.psu.edu/bus-tests.htm, 6-1.fueconomy.pdf.
288. **SAE**. Fuel Economy Measurement Test (Engineering Type) for Trucks and Buses. [Std.]. Warrendale, PA : SAE, 01 07 1982. p. 13. Std. no. J1376, cycle from ADVISOR, standards.sae.org/j1376_198207.
289. **Zhang, S.** Real-world fuel consumption and CO2 emissions of urban public buses in Beijing. *Appl. Energy.* 11 10 2013, Vol. 113, pp. 1645–1655. ISSN 0306-2619, doi 10.1016/j.apenergy.2013.09.017, BJBC via email, 2016-02-22, Zhang S., Ann Arbor MI, Uni Michigan, Dept. Mech. Engrg.,.
290. **Dreyer, W.** Stochastischer Fahrzyklus für Stadt-Linienomnibusse. *Berichte*. [Rep.]. Braunschweig : TU, SFB 97 Fahrzeuge und Antriebe, 02 1975. Vol. 34. dieselnet.com, braunschweig.txt.
291. **Braun, H.** Ein Standard Fahrzyklus für Stadt-Linienomnibusse. *ATZ.* 12 1978, Vol. 81, 1, pp. 29-32. ISSN 0001-2785.

292. **SPC**. FC test methods for med. and HD CV (中重型商用车辆燃料消耗量测量方法). [Std.]. Beijing : SPC, 01 01 2012. p. 35. Std. no. GB/T 27840-2011; spc.net.cn; camra.org.cn, GB-T 2027840-2011.pdf; zbs.miit.gov.cn, n13242371.doc.
293. **Zou, Z.** A New Composite Drive Cycle for Heavy-Duty Hybrid Electric Class 4-6 Vehicles. *SAE Tech. Papers*. 08 03 2004, Vol. 58, 2004-01-1052. ISSN 0148-7191, doi 10.4271/2004-01-1052, CILCC via email, 2016-02-27, Besch M., Morgantown WV, WVU, Dept. for Mech. and Aersp. Engrg..
294. **Kleinebrahm, M.** Emissionsverhalten von Linienbussen - Teil 1. *LANUV-Fachberichte*. [Rep.]. Recklinghausen : LANUV, 05 2009. Vol. 14, p. 119. lanuv.nrw.de, 30014.pdf.
295. **Daw, C.** Simulated Fuel Economy and Emissions Performance during City and Interstate Driving for a Heavy-Duty Hybrid Truck. *SAE Int. J. Commer. Veh.* 08 04 2013, Vol. 6, 1, pp. 161-182. ISSN 1946-3928, doi 10.4271/2013-01-1033.
296. **Steven, H.** Influence of the Transient Operating Mode of Commercial Vehicles and its Consideration in Emission Measurement According to ECE R 49. [Rep.]. Herzogenrath : FIGE, 01 1994. p. 93. Rep. no. 104 05 316, dieselnet.com, etc_fige.txt.
297. **Hausberger, S.** Saubere Stadtbusstechnologien. *ICUT*. [Rep.]. Graz : TU, IVT, 12 02 2010. p. 56. eltis.org, icut_broschuere_aktuell1_11.pdf, Graz cycle from own resource.
298. **Scheer, H.** Applikation eines SCR-Nachrüstsystems in einen Stadtbus. [Dipl. thesis]. Graz : TU, IVT, 22 03 2010. p. 97.
299. **France, C.** Recommended Practice for Determining Exhaust Emissions from Heavy-Duty Vehicles Under Transient Conditions. [Rep.]. Washington, DC : USEPA, 02 1979. p. 77. Rep. no. SDSB 79-08, nepis.epa.gov/Adobe/PDF/9100RVLQ.PDF, epa.gov, huddscol.txt.
300. **CFR**. Title 40, Protection of Environment, Part 86 (86.600-1 - End). *CFR*. [Rule]. Washington, DC : USGPO, 01 07 2001. p. 679. ISSN 1946-4975, gpo.gov/fdsys/pkg/CFR-2001-title40-vol16.
301. **Kaijalainen, O.** Osahanke 5: Linja-auton energiankulutuksen mallinnus. *Raskaan kaluston energiankäytön tehostaminen*. [Rep.]. Espoo : Teknillinen Korkeakoulu, Autotekniikan laboratorio, 02 11 2004. p. 27. Helsinki + Stockholm cycles via email, 2016-02-29, Kytö M., Espoo, VTT, Engines and emissions.
302. **Gautam, M.** Qualification of the Heavy HD Diesel Truck Schedule and Development of Test Procedures. [Rep.]. Morgantown, WV : WVU, Mech. and Aersp. Engrg., 03 2002. p. 145. Project No. E-55-2, crcao.org. Pt. I, creep: dieselnet.com, hhdtdt_creep.txt; pt. II, transient: CFR title 40, subchapter U, part 1037, appendix I; pt. III, cruise: ADVISOR.
303. **MLIT**. 80km/h Constant Speed Mode with Road Gradient (縦断勾配付き80キロメートル毎時定速モード). [Velocity pattern]. Tokyo : MLIT, 28 06 2007. p. 23. mlit.go.jp, 05santeikokuji.pdf.
304. **MOE**. Traveling mode file (走行モードファイル). [Velocity pattern]. Tokyo : MOE, 21 05 2003. p. 51. env.go.jp, c_d_moe_ed12.pdf.
305. **Hayes, R.** King County Metro Transit: Allison Hybrid Electric Transit Bus Laboratory Testing. [Rep.]. Golden, CO : NREL, 01 09 2006. p. 23. Rep. no. NREL/TP-540-39996, doi 10.2172/893005, KCM via email, 2016-03-22, Walkowicz K., NREL, Transp. and Hydrogen Syst..
306. **Eastlake, A.** Defining and supporting the 2015 Low Emission Bus (LEB) scheme. [Rep.]. London : LowCVP, 28 04 2015. p. 20. Rep. no. BWG-P-15-09, lowcvp.org.uk, leb_apr_bwg_presentation.ppt, LUB via email, 2016-04-08, Hayes D., LowCVP.
307. **LowCVP**. MLTB test cycle. [Velocity Pattern]. London : LowCVP, 07 05 2003. lowcvp.org.uk, mltb-test-cycle.xls, lowcvp.org.uk/initiatives/lceb/lceb-testing.htm.
308. **MJB**. Hybrid-Electric Drive Heavy-Duty Vehicle Testing Project. [Rep.]. Manchester, NH : M.J. Bradley & Associates, 15 02 2000. p. 74. Agreem. No.: NAVC1098-PG009837, walshcarlines.com/pdf/Navc9837.pdf, Manhattan from ADVISOR.
309. **Kitchen, M.** Development of Conversion Factors for Heavy-Duty Bus Engines g/bhp-hr to g/mile. [Rep.]. Washington, DC : USEPA, 27 07 1992. p. 23. Rep. no.: EPA-AA-EVRB-92-01. NYBus from ADVISOR, nepis.epa.gov/Exe/ZyPURL.cgi?Dockey=9100UO2L.txt.
310. **CARB**. Proposed Modifications to the Public Transit Bus Fleet Rule (...). [Std.]. Sacramento, CA : CARB, 06 09 2002. p. 63 + app. 76. arb.ca.gov/regact/bus02/bus02.htm.
311. **Coroller, P.** Comparative Study on Exhaust Emissions from Diesel- and CNG-Powered Urban Buses. *DEER*. [Conf.]. Newport, RI : EERE, 08 2003. Vol. 9, p. 12. osti.gov/scitech/biblio/829628, Paris cycle from own resource.
312. **Surcel, M.** Development of a Fuel Consumption Test Procedure for Representative Urban Duty Cycles. *SAE Tech. Papers*. 13 09 2011, Vol. 65, 2011-01-2291, p. 14. ISSN 0148-7191, doi 10.4271/2011-01-2291.
313. **UITP**. Project 'SORT'. Standardised On-Road Test Cycles. [Std.]. Bruxelles : UITP, 07 2014. p. 38.
314. **Kytö, M.** WP 6.5 Bus Emission Measurements on Chassis Dynamometer. [Rep.]. Espoo : VTT, 12 09 2012. p. 29. balticbiogasbus.eu; Helsinki, Stockholm via email, 2016-02-29, Kytö M., VTT, Engines and emissions.
315. **TNO**. Development of a World-wide Heavy-Duty Engine Test Cycle. [Rep.]. Delft : TNO, 09 05 2000.

316. **OJ.** Commission Regulation (EU) 2016/1718. L (Legislation) *Official J. EU*. [Rule]. Luxembourg : Publ. Office EU, 27 09 2016. Vol. 59, 259, pp. 1-41. ISSN 1977-0677, CELEX no. 32009R1221.
317. **Clark, N.** West Virginia City Driving Schedule. *ADVISOR*. [Data table]. Morgantown, WV : WVU, Mech. and Aerosp. Engrg., 1998. Cycle from ADVISOR.
318. **Edwards, R.** Well-To-Tank Version 4.a. [Rep.]. Luxembourg : Publ. Office EU, 04 2014. p. 146. ISBN 9789279338885, doi 10.2790/95629.
319. **Kies, A.** Constant Speed Evaluation Tool V1.0. [Rep.]. Graz : TU, IVT, 06 12 2012. p. 43. Rep.-no. I 22/12/Rex EM I 10/12/679.
320. **Krüger, W.** 10.7-L Daimler HD Truck Engine for Euro VI and Tier 4. *MTZ worldw.* 2012, Vol. 73, 12, pp. 932-939. ISSN 2192-9114, doi 10.1007/s38313-012-0246-y.
321. **Daimler.** Kraftstoffverbrauch OM 936, EURO VI. [Data sheet]. Stuttgart : Daimler, Dept. TG/LPS, 19 12 2013. Doc. no. 100 93 616, map via email, 2014-02-04, Daimler, Stuttgart, cs.aut at cac.mercedes-benz.com.
322. **TMA.** Test (...) of Practical Devices/Systems to Reduce Aerodyn. Drag of Tractor/Semitr. Combi. Unit Trucks. [Rep.]. Washington, DC : TMA, 30 04 2007. p. 77. doi 10.2172/926158.
323. **Daimler.** Der Mercedes-Benz Aerodynamics Trailer. [Art. on hp.]. Stuttgart : Daimler, 09 2012. daimler.com/dccom/0-5-1608998-49-1609004-1-0-0-1609343-0-0-135-7165-0-0-0-0-0-0.html.
324. **Raemdonck, G. van.** Design of Low Drag Bluff Road Vehicles. [Diss.]. Delft : TU, Dept. of Flight Perform. and Propuls., 11 05 2012. p. 247. ISBN 9789461912572, resolver.tudelft.nl/uuid:7f7d98b2-aac4-433b-92b9-a990975c0b23.
325. **Muirhead, V.** An Investigation of Drag Reduction for Tractor Trailer Vehicles with Air Deflector and Boattail. [Rep.]. Washington, DC : NASA, 1981. p. 59. Rep. no. CR-163104, ntrs.nasa.gov.
326. **Daimler.** Der Mercedes-Benz Aerodynamics Truck. [Art. on hp.]. Stuttgart : Daimler, 09 2012. daimler.com/dccom/0-5-1608998-49-1609007-1-0-0-1609343-0-0-135-7165-0-0-0-0-0-0.html.
327. —. Die Citaro Stadtbusse. [Prod. info]. Stuttgart : Daimler, 11 09 2015. p. 24. mercedes-benz.de, TechInfo_Citaro_Stadt_de.pdf.
328. **Volvo.** Volvo 7900 Hybrid-Gelenkbus. [Prod. info]. Göteborg : Volvo Bussar, 2015. p. 3. volvobuses.com, bernmobil.ch, <Technische Daten Volvo 7900 LAH Hybrid-Gelenkbus DE.pdf>.
329. **Smith.** The Newton. [Prod. info]. Kansas City, MO : Smith Electric Vehicles, 2011. p. 2. smithelectric.com, SmithNewtonUS_SpecSheet_2011.pdf.
330. **Laible, T.** Light-off/out Support at Catalyst of Diesel Engine. *MTZ worldw.* 03 10 2015, Vol. 76, 11, pp. 58-64. ISSN 2192-9114, doi 10.1007/s38313-015-0058-y.
331. **Herrmann, H.** Mercedes-Benz Medium-Duty Commercial Engines. *MTZ worldw.* 06 09 2012, Vol. 73, 10, pp. 4-11. ISSN 2192-9114, doi 10.1007/s38313-012-0220-8.
332. **USEPA.** Regulatory Impact Analysis. [Rep.]. Washington, DC : USEPA, 16 08 2016. p. 1115. Doc. no. EPA-420-R-16-900, epa.gov, 420r16900.pdf.
333. **Gruden, I.** New 14.8-l HD Truck Engine from Daimler for NAFTA. *MTZ worldw.* 31 10 2013, Vol. 74, 12, pp. 12-18. ISSN 2192-9114, doi 10.1007/s38313-013-0121-5.
334. **Fitch, J.** *Motor Truck Engineering Handbook*. 4. Warrendale, PA : SAE, 1994. p. 444. ISBN 9781560913788.
335. **Schütz, T. (ed.).** *Hucho - Aerodynamik Des Automobils*. 6. Wiesbaden : Springer Vieweg, 2013. p. 1150. ISBN 9783834819192.
336. **Banjac, T.** Energy conversion efficiency of hybrid electric heavy-duty vehicles (...). *Energy Cnv. and Mgmt.* 29 07 2009, Vol. 50, pp. 2865-2878. ISSN 0196-8904, doi 10.1016/j.enconman.2009.06.034.
337. **Bach, C.** Diesel-und Erdgasmotoren für schwere Nutzfahrzeuge. *MTZ*. 04 2005, Vol. 66, 5, pp. 394-402. ISSN 0024-8525, doi 10.1007/BF03226743.
338. **Ramdam, M.** Optimal design of a power-split hybrid hydraulic bus. *J. Automob. Engrg.* 2016, Vol. 230, 12, pp. 1699-1718. ISSN 0954-4070, doi 10.1177/0954407015621817.
339. **Mizushima, N.** A Study on High-Accuracy Test Method for Fuel Consumption of HD Diesel Vehicles (...). *SAE Int. J. Fuels Lubr.* 05 04 2016, Vol. 9, 2, pp. 383-391. ISSN 1946-3952, doi 10.4271/2016-01-0908.
340. **MacIsaac, J.** Submission to Docket No. NHTSA-2014-0132; Southwest Research Institute (SwRI) engine maps or delta maps (...). [Memo & data table]. Washington, DC : NHTSA, 25 09 2015. nhtsa.gov, SwRI-Engine-Maps-NPRM-Docket-Memo.pdf, Cummins-ISB_PU385-Fuel-Maps.xlsx.
341. **Urlaub, A.** Wege zur besseren Energieausnutzung im Fahrzeugmotor. *Fortschr.-Ber. VDI-Z.* 12, Verkehrstechnik, 03 1979, Vol. 34, pp. 33-42. ISSN 0506-3167.
342. **Busch-Sulzer.** *The Diesel engine*. Saint Louis, MO : Busch-Sulzer, 1913. p. 112. hdl.handle.net/2027/nyp.33433090905831.
343. **Flach, M.** Euro VI alternatively fuelled truck supply session. *Low Carbon Trucks Trial workshop*. [Conf.]. Gaydon : Centre of Excell. for Low Carbon and Fuel Cell Tech., 30 01 2014. p. 11. cenex.co.uk/knowledge.

344. **Grigoratos, T.** (...) emissions from a prototype heavy-duty compressed natural gas engine under transient and real life conditions. *Energy*. 25 03 2016, Vol. 103, pp. 340-355. ISSN 0360-5442, doi 10.1016/j.energy.2016.02.157.
345. **lastauto omnibus.** Gas engine CoNAG 4C. *lastauto omnibus*. 08 2013, Vol. 90, 10, p. 7. ISSN 1613-1606.
346. **Soriano, F.** (...) powertrains for refuse-collecting vehicles based on real routes - Part I (...). *J. Automot. Tech.* 30 06 2016, Vol. 17, 5, pp. 873–882. ISSN 1229-9138, doi 10.1007/s12239-016-0085-y.
347. **Hoffmann, K.** The New Mercedes-Benz Medium Duty Commercial Natural Gas Engine. *MTZ worldw.* 09 2014, Vol. 75, 11, pp. 4-10. ISSN 2192-9114, doi 10.1007/s38313-014-0251-4.
348. **Berner, H.** Ein CO₂-minimales Antriebskonzept auf Basis des Kraftstoffes Erdgas. [book auth.] O. Dingel. *Gasfahrzeuge*. Renningen : expert, 2004, pp. 74-97. ISBN 9783816924395.
349. **Dold, R.** LNG - Future Fuel for Trucks? *VDI-Ber.* 10 06 2015, Vol. 2247, pp. 235-243. ISSN 0083-5560, ISBN 9783180922478.
350. **Pidello, F.** CNG Application to Commercial Vehicles. [book auth.] O. Dingel. *Gasfahrzeuge*. Renningen : expert, 2004, pp. 51-57. ISBN 9783816924395.
351. **Fischer, R.** *Das Getriebebuch*. 1. Berlin : Springer, 2012. p. 342. ISBN 9783709108765.
352. **Niemann, G.** *Maschinenelemente III*. 2. Berlin : Springer, 1983. p. 294. ISBN 9783540103172.
353. **Gangopadhyay, A.** Rear Axle Lubrication. [book auth.] G. Totten (ed.). *Handbook of Lubrication and Tribology*. Boca Raton, FL : CRC, 2006, Vol. I, pp. 3.1-3.21. ISBN 9780849320958, doi 10.1201/9781420003840.ch3.
354. **Dykas, B.** HMMWV Axle Testing Methodology to Determine Efficiency Improvements with Superfinished Hypoids. *SAE Int. J. Passeng. Cars. Mech. Syst.*, 08 04 2013, Vol. 6, 2, pp. 665-673. ISSN 1946-3995, doi 10.4271/2013-01-0605.
355. **Naunheimer, H.** *Fahrzeuggetriebe*. 2. Berlin : Springer, 2007. p. 710. ISBN 9783540306252.
356. **Kirchner, E.** *Leistungsübertragung In Fahrzeuggetrieben*. 1. Berlin : Springer, 2007. p. 699. ISBN 9783540352884.
357. **Niemann, G.** *Maschinenelemente II*. 2. Berlin : Springer, 1983. p. 376. ISBN 9783540111498.
358. **Kozuch, M.** Personal communication. IAA. Hannover : VDA, 26 09 2014. Eaton Corp. site Tczew, Polska.
359. **USEPA.** Greenhouse Gas Emissions Model (GEM) User Manual. [Rep.]. Washington, DC : USEPA, 06 2015. p. 48. Rep. no. EPA-420-B-15-076, nepis.epa.gov/Exe/ZyPURL.cgi?Dockey=P100MKXF.txt.
360. **Lee, H.** (...) Vehicle System Model for the First Medium- and HD CV FE Standards in Korea. *SAE Tech. Papers*. 29 09 2015, Vol. 69, 2015-01-2774, p. 19. ISSN 0148-7191, doi 10.4271/2015-01-2774.
361. **IVE.** Ecological Transport Information Tool for Worldwide Transports. [Rep.]. Hannover : IVE, 04 12 2014. ecotransit.org, EcoTransIT_World_Methodology_Rep._2014-12-04.pdf.
362. **DSLVL.** Berechnung von Treibhausgasemissionen in Spedition und Logistik gemäß DIN EN 16258. [Rep.]. Bonn : DSLVL, 03 2013. p. 67. dslv.org/dslv/web.nsf/id/li_fdih9a3thv.html.
363. **VDV.** Richtlinie zur Bestimmung des Fassungsvermögens von Fahrzeugen des Personenverkehrs für statistische Zwecke. [Std.]. Köln : VDV, 1990. p. 3. no. from calculation example.
364. **NWM.** Häufig gestellte Fragen zum Einsatz von „Schulbussen“. [Info]. Eschwege : Nahverkehr Werra-Meißner, 2009. p. 6. nwm-esw.de, <Haeufig gestellte Fragen zum Einsatz von Schulbussen.pdf>.
365. **NVB.** Erläuterungen zum Ziel „ausreichende Kapazitäten (...)“. [Info]. Heidelberg : Nahverkehrsberat. Südw., 14 06 2011. p. 2. kn-kreistag.de/buergerinfo/getfile.php?id=9161&type=do.
366. **Pütz, R.** Mittlere Passagierzahl Solobus. [Email]. Köln : VDV, 18 06 2014.
367. **BMJV.** Zulässige Zahl von Sitzplätzen und Stehplätzen in Kraftomnibussen. *German StVZO, Anlage XIII (§ 34a Absatz 3)*. [Rule]. Berlin : BMJV, 2012. gesetz-im-internet.de.
368. **ADEME.** Scope 3 : émissions indirectes - autres, Transport de marchandises, Routier. *Bilans GES*. [Art. on hp.]. Angers : ADEME, 2015. bilans-ges.ademe.fr.
369. **NTM.** Vehicle type characteristics and default load factors. [Art. on hp.]. Stockholm : NTM, 2016. transportmeasures.org.
370. **HBEFA.** Handbook emission factors for road transport (HBEFA). [Rep.]. Bern : INFRAS, 17 07 2014.
371. **Znidaric, A.** Heavy-Duty Vehicle Weight Restrictions in the EU. *SAG Meeting*. [Rep.]. Bruxelles : ACEA, 02 2015. Vol. 23, p. 27. acea.be, SAG_23_Heavy-Duty_Vehicle_Weight_Restrictions_in_the_EU.pdf.
372. **Kuiper, E.** Voertuigcategorieën en gewichten van voertuigcombinaties op de Nederlandse snelweg (...). [Rep.]. Delft : TNO, Sustain. Transp. Logistics, 05 12 2013. p. 26. Rep. no. TNO 2013 R12138, resolver.tudelft.nl/uuid:f2203fc7-099e-4f67-889c-18bd6afb90af.
373. **Hill, N.** Reduction and Testing of Greenhouse Gas (GHG) Emissions from Heavy Duty Vehicles - Lot 1: Strategy. [Rep.]. Didcot : Ricardo-AEA, 2011. p. 290. Rep. no. ED46904, ec.europa.eu, ec_hdv_ghg_strategy_en.pdf.

374. **McKinnon, A.** Use of a synchronised vehicle audit to determine opportunities for improving transport efficiency in a supply chain. *Int. J. Logistics*. 01 09 2004, Vol. 7, 3, pp. 219-238. ISSN 1367-5567, doi 10.1080/13675560412331298473.
375. —. European Freight Transport Statistics. *SAG Meeting*. [Rep.]. Bruxelles : ACEA, 08 09 2010. Vol. 15, p. 23. acea.be, [SAG_15_European_Freight_Transport_Statistics.pdf](http://acea.be/SAG_15_European_Freight_Transport_Statistics.pdf).
376. **Lumsden, K.** Truck Masses and dimensions. *SAG meeting*. [Rep.]. Bruxelles : ACEA, 02 2005. Vol. 8. acea.be, [SAG_8_Trucks_Masses_Dimensions.pdf](http://acea.be/SAG_8_Trucks_Masses_Dimensions.pdf).
377. **KBA.** Verkehr deutscher Lastkraftfahrzeuge (VD). [Statistics]. Flensburg : Kraftfahrt-Bundesamt, 09 2015. p. 45. kba.de, [vd5_201412_pdf.pdf](http://kba.de/vd5_201412_pdf.pdf).
378. **BAG.** Marktbeobachtung Güterverkehr. [Rep.]. Köln : BAG, 05 2015. p. 49. bag.bund.de, [Jahresbericht_2014.pdf](http://bag.bund.de/Jahresbericht_2014.pdf).
379. **Steigerwald, G.** Systemvergleich für unterschiedliche verkehrliche Prozessabläufe und Transportketten (...). [book auth.] Dt. Bundestag. *Studienprogramm*. 4, Verkehr. Bonn : Economica, 1994, Vol. 2, C, pp. 1-259. ISBN 9783870810146.
380. **Wenzel, B.** Der Einfluß internationaler Arbeitsteilung auf den Energiebedarf und die CO2-Emissionen bei der Herstellung ausgewählter Konsumgüter. *Fortschr.-Ber. VDI*. 16, Technik und Wirtschaft, 1999, Vol. 103, p. 135. ISSN 0178-9597, ISBN 9783183103164, ifne.de, [diss_kea_konsumgueter.pdf](http://ifne.de/diss_kea_konsumgueter.pdf).
381. **HERRY.** Lkw und Pkw Erhebung Tirol. [Art. on hp.]. Wien : HERRY Consult, 2009. Table with data on truck payload usage, traffic census, data not public, herry.at.
382. **VDV.** Statistik 2014. [Rep.]. Köln : VDV, 10 2015. p. 99. vdv.de/statistik-2014.pdf.
383. **Adra, N.** Analysis of the load factor and the empty running rate for road transport. [Rep.]. Bron : INRETS, 11 2004. p. 63. Rep. no. INRETS-LTE 0419, hal.archives-ouvertes.fr/hal-00546125.
384. **Sonnekalb, M.** CO2 basierte Air-Condition und Heizung für Stadtbusse. [Rep.]. Osnabrück : DBU, 12 2008. p. 50. Ref. no. 23864, dbu.de, [DBU-Abschlussbericht-AZ-23864.pdf](http://dbu.de/DBU-Abschlussbericht-AZ-23864.pdf).
385. **Spheros.** REVO EvoBus / City bus. [Prod. info]. Gilching : Spheros, 23 10 2012. p. 13. Doc. no. 11117292A, spheros.eu, [ET_REVO_EvoBus_Stadtbuss_DE_EN_1211.pdf](http://spheros.eu/ET_REVO_EvoBus_Stadtbuss_DE_EN_1211.pdf).
386. **Unruh, R.** MAN Lion's City Euro 5. *lastauto omnibus*. 07 2008, Vol. 85, 8, pp. 32-38. ISSN 1613-1606.
387. —. MAN Lion's City Euro 6. *lastauto omnibus*. 11 2013, Vol. 90, 12, pp. 57-60. ISSN 1613-1606.
388. **Wagner, T.** MAN Lion's City Evo. *lastauto omnibus*. 06 2016, Vol. 93, 7, pp. 50-54. ISSN 1613-1606.
389. **Görgler, J.** MB Citaro Euro 5. *V+T*. 02 2011, Vol. 64, 3, pp. 79-84. ISSN 0340-4536.
390. **Daimler.** Der neue Citaro mit EU-Abgasnorm Euro VI. [Prod. info]. Stuttgart : Daimler, 07 2016. [mercedes-benz.de, technical_data_e6.0003.html](http://mercedes-benz.de/technical_data_e6.0003.html).
391. —. Der Citaro Ü. [Prod. info]. Stuttgart : Daimler, 07 2016. [mercedes-benz.de, technical_dat.html](http://mercedes-benz.de/technical_dat.html).
392. **Bünnagel, C.** Autosan Sancity 12LF. *Busmagazin*. 01 2015, Vol. 24, 2, pp. 16-18. ISSN 0942-346X.
393. **Spheros.** Citysphere S. [Prod. info]. Gilching : Spheros, 08 2012. p. 80. Doc. no. 11117332A, spheros.eu, [BA_Citysphere_S_DE_EN_SV_2015_02_11117332A.pdf](http://spheros.eu/BA_Citysphere_S_DE_EN_SV_2015_02_11117332A.pdf).
394. **Eberspächer.** AC 403 E & AC 420. [Prod. info]. Esslingen a. N. : Eberspächer, 27 01 2015. p. 2. eberspaecher-na.com, [EB_AC403_420_Spec_WEB_READY_01_27_15.pdf](http://eberspaecher-na.com/EB_AC403_420_Spec_WEB_READY_01_27_15.pdf).
395. **Volvo.** Hybridbus Volvo 7900 H. [Prod. info]. Göteborg : Volvo Bussar, 07 10 2015. p. 16. volvobuses.de, [Volvo-7900-Hybrid-Brochure-2016-DE.pdf](http://volvobuses.de/Volvo-7900-Hybrid-Brochure-2016-DE.pdf).
396. **Wagner, T.** Solaris Urbino 18. *lastauto omnibus*. 07 2016, Vol. 90, 8, pp. 56-60. ISSN 1613-1606.
397. **Seher, D.** Waste Heat Recovery for Commercial Vehicles with a Rankine Process. *Aachen Colloquium*. [Conf.]. Aachen : RWTH, Inst. f. Kfz, VKM, 10 2012. Vol. 21, p. 15.
398. **Edwards, S.** Waste Heat Recovery. *SAE Int. J. Commer. Veh.* 16 04 2014, Vol. 5, 1, pp. 395-406. ISSN 1946-3928, doi 10.4271/2012-01-1205.
399. **Schmiederer, K.** The Potential Fuel Consumption of a Truck Engine plus Rankine Cycle System. *Fortschr.-Ber. VDI*. 12, Verkehrstechnik, 26 04 2012, Vol. 749, 1, pp. 351-376. ISSN 0178-9449, ISBN 9783183749126.
400. **SPC.** FC limits for HD CV (重型商用车燃料消耗量限值). [Std.]. Beijing : SPC, 01 07 2014. p. 4. Std. no. GB 30510-2014; spc.net.cn; vecc-mep.org.cn, [GB_2030510-2014.pdf](http://vecc-mep.org.cn/GB_2030510-2014.pdf); miit.gov.cn, [n14830171.pdf](http://miit.gov.cn/n14830171.pdf).
401. **MLIT.** Test procedure for FC rate and exhaust emissions of HD HEV using hardware-in-the-loop simulator system. [Std.]. Tokyo : MLIT, 16 03 2007. p. 122. Kokujikan No. 281.
402. **Ueda, J.** Overview of HDV fuel economy improvement policy in Japan. *Measurement and Monitoring CO2 emission from HDVs*. [Conf.]. Ispra : Europ. Commiss., JRC, IET, STU, 29 05 2013. p. 23. iet.jrc.ec.europa.eu, [ueda.130530-31_japan_presentation.pdf](http://uet.jrc.ec.europa.eu/ueda.130530-31_japan_presentation.pdf).
403. **CFR.** Title 49, Transportation, Parts 400 to 571. *CFR*. [Rule]. Washington, DC : USGPO, 01 07 2015. p. 1134. ISSN 1946-4975, gpo.gov/fdsys/pkg/CFR-2015-title49-vol6.
404. **Daimler.** Fuel Duel. Fleet test of MB Actros 1842 Euro 6 at hauliers. [Art. on hp.]. Stuttgart : Daimler, 11 2015. fuelduel.de/de_DE.

405. **Jentzsch, G.** Spedition Bartkowiak GmbH spart auf Vergleichsfahrt rund zehn Prozent Kraftstoff. [PR]. Brühl : Renault Trucks, 30 04 2012. p. 3.
406. **Vaßen, A.** Langzeitfahrversuch als Beweis für hohe Effizienzpotenziale. *Flexibilisierung komplexer Netzwerke*. [Conf.]. Frankfurt a. M. : BVL, 04 02 2014. p. 23. bvl.de, FAL14_Praesentation_Vassen_Axel.pdf.
407. **Granzow, A.** Unterwegs auf Spritsparsohlen. *DVZ*. [Art. on hp.]. Hamburg : DVV, 11 11 2013. ISSN 0342-166X, dvz.de.
408. **Kersten, W.** Durchsetzung ökologischer Standards in Stückgutkooperationen (ÖkoStar). A. Schlussbericht [Rep.]. Hamburg : TU, Inst. f. Logistik, 31 10 2015. p. 179 + app. 109. IGF project no. 17936 N, bvl.de, OekoStar_Abschlussbericht_Final_17936.pdf.
409. **Conti.** Continental tyres marked by longer life. [PR]. Hannover : Continental, 15 01 2009. conti-online.com, pm_grampian_en.html.
410. **TNT.** Annual Report 2015. [Rep.]. Hoofddorp : TNT Express, 16 02 2016. p. 176. tnt.com, tnt-express-annual-report-2015.pdf.
411. **DGMK.** Gefahrgut-Risikobetrachtung bei Tankfahrzeugen mit höheren Nutzlasten in der Tankstellenversorgung. *Information*. 06 09 2006, Vol. 07/06, p. 7. dgmk.de, Info_0706_659.pdf.
412. **Hils, P.** 40t-EuroCombi. [Pres. slides]. Erfurt : FH Erfurt, Fachgebiet Straßenverkehrstechnik, 03 09 2010. p. 22. blogs.taz.de, 40t-EuroCombi_Sept_2010_Presse.pdf.
413. **Bartkowiak.** Verbräuche. [Art. on hp.]. Hildesheim : Sped. Bartkowiak, 23 06 2015. spedition-bartkowiak.de/24.html.
414. **DBS.** Verksamhetsåret 2014. *Hållbarhetsredovisning*. [Rep.]. Göteborg : DB Schenker, 06 2015. Vol. 3, p. 48. dbschenker.se, hallbarhetsredovisningen_2014.pdf.
415. **Prenner, M.** Potential of variable roof shape to reduce the fuel consumption of semitrailers. *Nutzfahrzeug Workshop*. [Conf.]. Graz : TU, Inst. f. Fahrzeugtechn., 13 05 2016. p. 19.
416. **Chaari, H.** Fuel Consumption Assessment in Delivery Tours (...). *AET Papers*. 2012, Vol. 40, p. 21. ISSN 2313-1853, abstracts.aetransport.org/paper/index/id/3886.
417. **Hebting, J.** Praktische Erfahrungen bei der Reduzierung von Verbrauch und Emissionen. *IAA-Symposium „Reduzierung der CO₂-Emissionen im Straßengüterverkehr“*. [Conf.]. Hannover : VDA, 26 09 2014.
418. **Braun, M.** Operational cost and fuel consumption, seven tractors Euro 6. *lastauto omnibus*. 11 2016, Vol. 93, 12, pp. 24-30. ISSN 1613-1606.
419. **Fritz.** Umweltbericht 2015. [Rep.]. Heilbronn : Fritz Sped., 29 04 2016. p. 24. fritz-gruppe.de, Umweltbericht_2015.pdf.
420. **Bennühr, S.** Tires low rolling resistance at Sped. Gebr. Schröder. *DVZ*. 23 09 2014, Vol. 116, 79, p. 6. ISSN 0342-166X.
421. **Rosenberger, T.** Operational cost and fuel consumption, six tractors Euro 5. *lastauto omnibus*. 11 2011, Vol. 85, 12, pp. 18-23. ISSN 1613-1606.
422. **Kranke, A.** Ist der Schienengütertransport wirklich umweltfreundlicher? *VR*. [Art. on hp.]. München : Springer, 22 07 2010. ISSN 0341-2148, verkehrsrundschau.de.
423. **Kienzler, H.** Studie über wirtschaftliche und ökologische Vorteile von nutzlastoptimierten Fahrzeugen im LKW-Verkehr. [Rep.]. Gundelfingen : K+P Transport Consultants, 19 03 2012. p. 57. berger-ecotrail.com, hwh_K_P_Transport_Consultants_2012.pdf.
424. **Jacob, B.** Massification et Enjeux Energetiques. *Cycle poids lourds 2016-2019*. [Conf.]. Champs-sur-Marne : CF-AIPCR, 31 03 2016. p. 26. cf-aipcr.org, 775-S2-1_jacob.pdf.
425. **UBA.** Lastzug 34-40 t, Euro-5, Autobahn, Auslastungsgrad 60 %. *ProBas*. [Database]. Dessau-Roßlau : UBA, 2010. probas.umweltbundesamt.de.
426. **Mayer, H.** (...) Weiterentwicklung der Berechnungen zum Energieverbrauch und zu den CO₂ -Emissionen des Straßenverkehrs (...). *Umweltökonomische Gesamtrechnungen*. [Rep.]. Wiesbaden : Statistisches Bundesamt, 25 03 2011. p. 86. Article no. 5850009119004, destatis.de.
427. **DSV.** CSR Report. [Rep.]. Hedehusene : DSV, 04 02 2016. p. 32. documents.dsv.com/dsv/816.
428. **XPO.** CSR-Commitments. [Art. on hp.]. Lyon : XPO, 2014. europe.xpo.com/CSR-Commitments.
429. **IVE.** EcoTransIT World. [Art. on hp.]. Hannover : IVE, 12 11 2015. ecotransit.org.
430. **Schwarz, A.** Comparison Iveco Stralis 330, diesel and gas engine Cursor 8. *KFZ-Anzeiger*. 07 2012, Vol. 65, 13, pp. 16-19. ISSN 0341-9681.
431. **Willms, O.** MB Atego 1222 Hybrid. *lastauto omnibus*. 03 2013, Vol. 90, 4, pp. 24-26. ISSN 1613-1606.
432. **Tschakert, W.** Iveco Eurocargo 120E25. *KFZ-Anzeiger*. 01 2009, Vol. 62, 1, pp. 11-12. ISSN 0341-9681.
433. **Stockholm.** Evaluation Report for CleanTruck. [Rep.]. Stockholm : Stockholms stad, Miljöförvaltningen, 31 03 2015. p. 31. Rep. no. LIFE08 ENV/S/000269, stockholm.se/cleantruck.
434. **Jong, B. de.** Hybrid Truck Fieldtest. *HCV Final workshop*. [Conf.]. Göteborg : Volvo, 28 05 2014. p. 15. Europ. Commiss, CORDIS, 7th Framework Progr., project "Hybrid Commercial Vehicle", grant no. 234019, hcv-project.eu, DAF_Hybrid_truck_field_test.pdf.

435. **Erkfeldt, S.** Hybrid Commercial Vehicle. [Rep.]. Göteborg : Volvo, 07 09 2015. p. 51. Europ. Commiss., CORDIS, 7th Framework Progr., project "Hybrid Commercial Vehicle", grant no. 234019, hcv-project.eu, HCV-Final_report_publishable_Rev1-PUBLIC.pdf.
436. **Kranke, A.** (...) CO₂-Fußabdruck. *VR*. 03 01 2011, Vol. 65, 51/52, pp. 36-38. ISSN 0341-2148.
437. **UBA.** Lkw 7,5-12 t, Euro-5, Innerorts, Auslastungsgrad 40 %. *ProBas*. [Database]. Dessau-Roßlau : UBA, 2010. probas.umweltbundesamt.de.
438. **Tschakert, W.** Iveco Eurocargo 75E16 H. *KFZ-Anz.* 05 2012, Vol. 65, 9, pp. 35-37. ISSN 0341-9681.
439. **Willms, O.** Iveco Eurocargo Hyb. 75E16. *lastauto omnibus omnib.* 06 2012, Vol. 89, 7, pp. 14-16. ISSN 1613-1606.
440. —. DAF LF45-160 Hybrid, Iveco Eurocargo 75E160 Hybrid, MAN TGL 12.220 Hybrid, MB Atego 1222 Bluetec Hybrid, Renault Premium Distribution Hybrys, Volvo Trucks FE 300 Hybrid. *lastauto omnibus.* 03 2012, Vol. 89, 4, pp. 30-36. ISSN 1613-1606.
441. **Rosenberger, T.** Mitsubishi Fuso Canter Eco Hybrid. *lastauto omnibus.* 04 2010, Vol. 87, 6/7, pp. 32-33. ISSN 1613-1606.
442. **Hipp, E.** Postfossile Gütermobilität. *Postfossile Mobilität*. [Conf.]. Tutzing : Evangel. Akadem., 15 05 2011. p. 31. web.ev-akademie-tutzing.de/cms/get_it.php?ID=1525.
443. **Olofsson, M.** Enhanced emission performance and fuel efficiency for HD methane engines. [Rep.]. Haninge : AVL, 10 05 2014. p. 91. Rep. no. OMT 1032, iea-amf.org, AMF_Annex_39-2.pdf.
444. **Erkkilä, K.** Ten years of VTT's bus performance evaluation. *Kehittyvä bussitekniikka ja vaihtoehtoiset energiamuodot*. [Conf.]. Helsinki : VTT, 06 02 2012. p. 27. transeco.fi.
445. **Zürcher, R.** SORT-Zyklen in Ausschreibungen. *Fachtagung KTBB*. [Conf.]. Granges-Paccot : VöV, 22 05 2014. p. 9. voev.ch.
446. **Elbert, P.** Noncausal and causal optimization strategies for hybrid electric vehicles. [Diss.]. Zürich : ETH, Inst. f. Dyn. Systems and Control, 2014. p. 108. Diss. no. 21522, doi 10.3929/ethz-a-010060690.
447. **Gasparini, P.** CTM e l'efficientamento energetico. *Il Risparmio energetico nelle aziende di TPL*. [Conf.]. Roma : ASSTRA, 13 10 2011. p. 21. www.asstra.it/eventi/download_allegato/374.html.
448. **Wagenknecht, T.** Fuel consumption. *La strada dell'economia per il nuovo bus*. [Conf.]. Friedrichshafen : ASSTRA, 09 09 2010. p. 13. www.asstra.it/eventi/download_allegato/546.html.
449. **Uhlenhut, A.** Solaris Urbino 12 Hybrid. *V+T*. 05 2010, Vol. 63, 6, pp. 203-208. ISSN 0340-4536.
450. **ABRTC.** New Flyer, D40LF. [Rep.]. Duncansville, PA : ABRTC, 05 2006. p. 47. Rep. no. PTI-BT-R0607, altoonabustest.psu.edu/buses/116.
451. —. Gillig, Low Floor. [Rep.]. Duncansville, PA : ABRTC, 12 2004. p. 105. Rep. no. PTI-BT-R0410, altoonabustest.psu.edu/buses/86.
452. **Zivanovic, Z.** Natural Gas Buses in Serbia Public Transport. *FME Transact.* 2015, Vol. 43, 2, pp. 89-98. ISSN 1451-2092, doi 10.5937/fmet1502089Z.
453. **OR.** VDL Citea SLF 120-310. *Omnibusrevue.* 03 2011, Vol. 62, 4, pp. 3-8. ISSN 1436-9974.
454. **Faltenbacher, M.** Prüfprogramm Diesel-Hybridbusse. *Abschlusskonferenz zur Hybridbusförderung*. [Conf.]. Berlin : BMUB, 06 10 2014. p. 41. erneuerbar-mobil.de.
455. **Frank, R.** MAN-Hybridbusse - Innovation und Nachhaltigkeit im Stadtverkehr Ingolstadt. *Hybridbusse für den Stadtverkehr Ingolstadt*. [Conf.]. Berlin : BMUB, 10 2014. p. 19. erneuerbar-mobil.de.
456. **Grünenfelder, M.** Hybridbusse im Regelbetrieb. *Fachtagung KTBB*. [Conf.]. Granges-Paccot : VöV, 21 05 2014. p. 24. voev.ch.
457. **Liimatainen, H.** Hybridibussit - kokemuksia käyttöönnotosta, liikennöinnistä ja energiankulutuksesta. [Rep.]. Tampere : Tampereen TY, Liikenteen tutkimuskeskus Verne, 03 2014. p. 41. ISBN 9789521532504, tut.fi/verne/tutkimusraportti-hybridibussit.
458. **Hallmark, S.** Evaluation of In-Use Fuel Economy and On-Board Emissions for Hybrid and Regular CyRide Transit Buses. [Rep.]. Ames, IA : Iowa State Uni, Center for Transp. Rsrch and Educat., 10 2012. p. 37. publications.iowa.gov/id/eprint/14772.
459. **Faltenbacher, M.** Plattform Innovative Antriebe Bus. [Rep.]. Leinfelden-Echterdingen : PE International (today: thinkstep), 10 2011. p. 28. Rep. no.: FKZ 03KP5001, ssb-ag.de, iab_abschlussbericht.pdf.
460. **Buschbacher, H.** RegInnoMobil. [Rep.]. Wien : Buschbacher, H., 11 2010. p. 174. buschbacher.at/EndberichtPunktbahn.pdf.
461. **Pütz, R.** Strategische Optimierung von Linienbusflotten. [Diss.]. Düsseldorf : Alba, 03 2010. p. 195. ISBN 9783870946852.
462. **Clark, N.** Assessment of Hybrid-Electric Transit Bus Technology. *TCRP*. [Rep.]. Washington, DC : TRB, 2009. p. 78 + app. 148. ISSN 1073-4872, ISBN 9780309118033, rep. no. R-132.
463. **Barnitt, R.** New York City Transit (NYCT) Hybrid (125 Order) and CNG Transit Buses. [Rep.]. Golden, CO : NREL, 01 11 2006. p. 49. Rep. no. NREL/TP-540-40125, doi 10.2172/894985.

464. **BMVI**. Berechnung des Energieverbrauchs und der Treibhausgasemissionen des ÖPNV. [Rep.]. Berlin : BMVI, 06 2014. p. 60. bmvi.de.
465. **UBA**. Linienbus, 15-18 t, Euro-5, Innerorts, Auslastungsgrad 30 %. *ProBas*. [Database]. Dessau-Roßlau : UBA, 2010. probas.umweltbundesamt.de.
466. **Misanovic, S.** Exploitation and Environmentally Aspects of Hybrid Buses in European Cities. *MVM*. 2014, Vol. 40, 1, pp. 19-31. ISSN 1450-5304, mvm.fink.rs.
467. **LowCVP**. Scania KUB / ADL 300: Biomethane. [Certificate]. London : LowCVP, 18 01 2016. Test no. ML02015298, ML02015299, ML02015300, lowcvp.org.uk/initiatives/leb.htm.
468. —. MAN Euro 6 Biomethane. [Certificate]. London : LowCVP, 09 2015. Test no. ML02014567, ML02014568, ML02014574, lowcvp.org.uk/initiatives/leb.htm.
469. **ABRTC**. New Flyer, C40LF. [Rep.]. Duncansville, PA : ABRTC, 06 2012. p. 63. Rep. no. PTI-BT-R1205, altoonabustest.psu.edu/buses/414.
470. **Wagner, T.** MB Citaro NGT. *lastauto omnibus*. 09 2016, Vol. 93, 10, pp. 98-102. ISSN 1613-1606.
471. **Gerbec, M.** Cost benefit analysis of three different urban bus drive systems using real driving data. *Transp. Rsrch. D, Transp. and Environm.*, 06 11 2015, Vol. 41, pp. 433-444. ISSN 1361-9209, doi 10.1016/j.trd.2015.10.015.
472. **Eudy, L.** Foothill Transit Battery Electric Bus Demonstration Results. [Rep.]. Golden, CO : NREL, 01 2016. p. 49. Rep. no. NREL/TP-5400-65274, doi 10.2172/1237304.
473. **Milojevic, S.** CNG Buses for Clean and Economical City Transport. [Email]. Kragujevac : Uni Kragujevac, Faculty of Engrg., 28 03 2016. Info to paper, mfkgrs.
474. —. CNG Buses for Clean and Economical City Transport. *MVM*. 04 2011, Vol. 37, 4, pp. 57-71. ISSN 1450-5304, mvm.fink.rs.
475. **Vulovic**. MAZ-BIK 203CNG, EURO VI. [Datasheet]. Kragujevac : Vulovic Transp., 2010. vulovictransport.com, MAZ-BIK203CNG-.pdf.
476. **Görgler, J.** Busworld 2009. *V+T*. 11 2009, Vol. 62, 12, pp. 423-426. ISSN 0340-4536.
477. **AG-IAB**. Hybrid- und Elektrobus-Projekte in Deutschland. [Rep.]. Berlin : BMVI, AG-IAB, 01 2015. p. 50. starterset-elektromobilitaet.de, Statusbericht_Elektromobilitaet_2014_Hybrid-_und_Elektro.pdf.
478. **May, J.** Über 50 neue Hybridbusse für die Hansestadt. *SaHyb - Saubere parallele Dieselybridbusse in Hamburg*. [Conf.]. Berlin : BMUB, 10 2014. p. 10. erneuerbar-mobil.de.
479. —. Erprobung paralleler Dieselybridbusse. *VSVI Info*. 2012, pp. 47-54. vsvi-hamburg.de, vsvi_2012.pdf.
480. **Zumsteg, C.** Erfahrungen mit 12m- Volvo Hybridbus. *Fachtagung KTBB*. [Conf.]. Granges-Paccot : VöV, 27 04 2012. p. 19. voev.ch.
481. **Kies, A.** Eco Drive for Hybrid Electric Vehicles, Zwischenbericht 1. [Interim Rep.]. Graz : TU, IVT, 24 02 2012. p. 18. FFG, project no. 829966.
482. **ABRTC**. New Flyer, DE40LF. [Rep.]. Duncansville, PA : ABRTC, 08 2005. p. 48. Rep. no. PTI-BT-R0511-P, altoonabustest.psu.edu/buses/102.
483. —. Gillig, Low Floor Hybrid. [Rep.]. Duncansville, PA : ABRTC, 10 2004. p. 110. Rep. no. PTI-BT-R0405, altoonabustest.psu.edu/buses/81.
484. **üstra**. Die Hybridbusse. [Art. on hp.]. Hannover : üstra, 04 2016. uestra.de/unternehmen/betriebstechnik/stadtbus/hybridbusse.
485. **Siemens**. ELFA Components. [Prod. info]. München : Siemens, 25 03 2011. p. 18. siemens.com, elfa-components-data-sheets.pdf.
486. **Claudino, A.** ELFA Hybrid. [Prod. info]. Sao Paulo : Siemens, 07 2009. p. 33. emtu.sp.gov.br, p21siemens.pdf.
487. **Grütter, F.** Serieller Hybrid von MAN bei den RVBW. *Fachtagung KTBB*. [Conf.]. Granges-Paccot : VöV, 24 05 2016. p. 15. voev.ch.
488. **Robb, A.** The New Bus for London. London : TfL, 22 09 2014. p. 5. clean-fleets.eu, New_Bus_for_London_Case_Study_for_Clean_Fleets_-_final.pdf.
489. **Prior, M.** New Bus for London driven. *Autocar*. 16 12 2011, Vol. 117. ISSN 1355-8293, autocar.co.uk/car-news/new-cars/new-bus-london-driven.
490. **B&C**. 10mpg from Wrightbus hybrid. *B&C*. 03 04 2009. ISSN 1472-1759, busandcoach.com/news/articles/archive/10mpg-from-wrightbus-hybrid.
491. **Erkkilä, K.** eBUS - Electric bus test platform in Finland. *EVS*. [Conf.]. Barcelona : WEVA, 17 11 2013. Vol. 27, p. 10. transsmart.fi/julkaisut/edistykselliset_ajoneuvot.
492. **ABRTC**. Proterra, BE40. [Rep.]. Duncansville, PA : ABRTC, 05 2015. p. 150. Rep. no. LTI-BT-R1406, altoonabustest.psu.edu/buses/454.
493. —. Proterra, BE35. [Rep.]. Duncansville, PA : ABRTC, 05 2013. p. 45. Rep. no. PTI-BT-R1305-P, altoonabustest.psu.edu/buses/425.

494. **Klett, S.** Hocheffizienter getriebeloser Direktantrieb für Elektrobusse. *Innovation Elektrobus*. [Conf.]. Dresden : saena, 10 12 2015. p. 11. saena.de/aktuelles/veranstaltung.html?eid=255.
495. **Görgler, J.** Busworld. *V+T*. 11 2013, pp. 443-452. ISSN 0340-4536.
496. **Goethem, S. van.** Performance of Battery Electric Buses in Practice. [Rep.]. Delft : TNO, 05 02 2013. p. 18 + app. 7. Rep. no. TNO-060-DTM-2013-00409, publications.tno.nl.
497. **Bijvelds, P.** Ebusco YTP1. *Elektrobusse*. [Conf.]. Berlin : VDV, 17 02 2014. p. 12. vdv-akademie.de.
498. **Hanke, D.** New developments in the field of electro buses. *Omnibus Spiegel*. 10 2012, Vol. 34, 9, pp. 8-17. ISSN 0724-7664, ebusco.eu, Omnibus-Magazine-small.pdf.
499. **Seitz, C.** Elektrobus aus China. *Fachtagung KTBB*. [Conf.]. Granges-Paccot : VöV, 21 05 2014. p. 31. voev.ch.
500. **Vytous, Z.** E-Busse im Betrieb. *Neue Horizonte im Stadtverkehr*. [Conf.]. Leipzig : trolley:motion, 23 10 2012. p. 33. trolleymotion.ch.
501. **ABRTC.** New Flyer, XE40. [Rep.]. Duncansville, PA : ABRTC, 07 2015. p. 128. Rep. no. LTI-BT-R1405, altoonabustest.psu.edu/buses/458.
502. —. BYD, K9. [Rep.]. Duncansville, PA : ABRTC, 06 2014. p. 156. Rep. no. LTI-BT-R1307, altoonabustest.psu.edu/buses/441.
503. **Zhou, B.** Real-world performance of battery electric buses. *Energy*. 01 02 2016, Vol. 96, pp. 603-613. ISSN 0360-5442, doi 10.1016/j.energy.2015.12.041.
504. **Menges, S.** rnv Primove - Induktiv geladene Elektrobusse im Echtbetrieb. *Innovation Elektrobus*. [Conf.]. Dresden : saena, 10 12 2015. p. 12. saena.de/aktuelles/veranstaltung.html?eid=255.
505. **Roch, R.** Die Elektromobilitätsprojekte der DVB AG gehen weiter. *Innovation Elektrobus*. [Conf.]. Dresden : saena, 10 12 2015. p. 15. saena.de/aktuelles/veranstaltung.html?eid=255.
506. **Zivanovic, Z.** Fully Electric Buses are Promising Technology in the Future. *MVM*. 2014, Vol. 40, 2, pp. 65-99. ISSN 1450-5304, mvm.fink.rs.
507. **Unruh, R.** SOR EBN 10.5. 02 2013, Vol. 90, 2, pp. 76-77. ISSN 1613-1606.
508. **Bulut, A.** Iveco Urbanway articulated bus. *Busmagazin*. 10 2015, Vol. 24, 11, pp. 16-17. ISSN 0942-346X.
509. **Misanovic, S.** Measurement the Fuel Consumption of Buses for Public Transport by the Methodology "SORT". *MVM*. 05 2015, Vol. 41, 2, pp. 55-63. ISSN 1450-5304, mvm.fink.rs.
510. **Juhrs, R.** Die Hybridbusse der Leipziger Verkehrsbetriebe GmbH. *Innovation Elektrobus*. [Conf.]. Dresden : saena, 10 10 2011. p. 23. saena.de/aktuelles/veranstaltung.html?eid=56.
511. **Klingner, M.** Neue Antriebskonzept om öffentlichen Verkehr. *grünes forum pillnitz*. [Conf.]. Pillnitz : SMUL, 13 10 2009. p. 21.
512. **ABRTC.** New Flyer, D60LF. [Rep.]. Duncansville, PA : ABRTC, 08 2002. p. 42. Rep. no. PTI-BT-R0220-P, altoonabustest.psu.edu/buses/42.
513. **Görgler, J.** MB Citaro G Euro 6. *Busmagazin*. 09 2014, Vol. 23, 10, pp. 6-10. ISSN 0942-346X.
514. **Wagner, T.** MB Citaro G. *lastauto omnibus*. 07 2014, Vol. 91, 8, pp. 44-48. ISSN 1613-1606.
515. **Seydoux, P.** Retour expériences Euro 6. *Fachtagung KTBB*. [Conf.]. Granges-Paccot : VöV, 21 05 2014. p. 13. voev.ch.
516. **Wiedemann, M.** Stimmen zuversichtlich: Erfahrungen mit Hybridbussen im Linienbetrieb. *Der Nahverkehr*. 08 2011, Vol. 29, 9, pp. 26-28. ISSN 0722-8287.
517. **Bargende, M.** Moderne Dieselmotorentechnik im Zusammenspiel mit alternativen Antrieben. *ÖPNV Innovationskongress*. [Conf.]. Freiburg i. Br. : MVIBW, 10 03 2015. Vol. 7, p. 60. innovationskongress-bw.de.
518. **Ernsting, J.** Hybridbusse bei der üstra. 1. *Workshop "Hybridbusse"*. [Conf.]. Berlin : BMUB, 10 05 2011. p. 26. erneuerbar-mobil.de.
519. **Uhlenhut, A.** Hannover: Auf ganzer Linie Hybridbusse. *Stadtverkehr*. 10 2011, Vol. 56, 11, pp. 24-25. ISSN 0038-9013.
520. **Lange, J.** Ab wann rechnet sich ein Hybridfahrzeug im Linienbetrieb? *Der Nahverkehr*. 05 2008, Vol. 26, 6, pp. 8-14. ISSN 0722-8287.
521. **Chandler, K.** King County Metro Transit Hybrid Articulated Buses: Final Evaluation Results. [Rep.]. Golden, CO : NREL, 01 12 2006. p. 48. Rep. no. NREL/TP-540-40585, doi 10.2172/896328.
522. **UBA.** Linienbus 18-30 t, Euro-5, Innerorts, Auslastungsgrad 30 %. *ProBas*. [Database]. Dessau-Roßlau : UBA, 2010. probas.umweltbundesamt.de.
523. **Tschakert, W.** Solaris Urbino 18 Hybrid. *Bus-Fahrt*. 12 2006, Vol. 55, pp. 12-15. ISSN 0341-5244.
524. **ABRTC.** New Flyer, DE60LF. [Rep.]. Duncansville, PA : ABRTC, 10 2003. p. 121. Rep. no. PTI-BT-R0305, altoonabustest.psu.edu/buses/54.
525. **Sandkühler, G.** Entwicklung eines Hybridantriebes für Abfallsammelfahrzeuge. *Baumaschinentechnik*. [Conf.]. Dresden : TU, Inst. f. Verarbeitungsmasch. u. Mob. Arbeitsmasch., 15 05 2009. pp. 237-245. baumaschine.de, a237_246.pdf.

526. **Katsis, P.** CO2 emissions of heavy duty vehicles, EU-28, 2012. [Email]. Thessaloniki : EMISIA, 08 12 2015. emisia.com, data from emissions calculator COPERT.
527. **Charette, M.** The Volume of Earth's Ocean. *Oceanography*. 2010, Vol. 23, 2, pp. 112-114. ISSN 1042-8275, doi 10.5670/oceanog.2010.51.
528. **Létréguilly, A.** The Greenland ice sheet (...). *Palaeogeogr., Palaeoclimatol., Palaeoecol.* 1991, Vol. 90, 4, pp. 385-394. ISSN 0031-0182, doi 10.1016/S0031-0182(12)80037-X.
529. **Fretwell, P.** Bedmap2: improved ice bed, surface and thickness datasets for Antarctica. *The Cryosphere*. 28 02 2013, Vol. 7, 1, pp. 375-393. ISSN 1994-0416, doi 10.5194/tc-7-375-2013.
530. **Olivier, J.** Global CO2 emissions from fossil fuel use and cement production 1970-2014. [Data table]. Ispra : Europ. Commiss., JRC, IET, EDGAR, 25 11 2015. edgar.jrc.ec.europa.eu, CO2_1970-2014_dataset_of_CO2_report_2015.xls.
531. **IPCC.** Climate Change 2014: Mitigation. [Rep.]. Cambridge, UK : Cambridge University Press, 03 2015. p. 1465. ISBN 9781107654815.
532. **EuCom-M.** 2015. *EU transp. in figures*. [Rep.]. Bruxelles : Europ. Commiss., DG Mobility, 09 2015. Vol. 19, p. 146. ISSN 1831-998X, ISBN 9789279439155.
533. **Tol, R.** The Social Cost of Carbon: Trends, Outliers and Catastrophes. *Economics*. 12 08 2008, Vol. 2, 25, pp. 1-22. ISSN 1864-6042, doi 10.5018/economics-ejournal.ja.2008-25.
534. **Nordhaus, W.** Estimates of the Social Cost of Carbon: Background and Results from the RICE-2011 Model. *NBER Working Papers*. 10 2011, Vol. 39, 17540, p. 48. ISSN 1058-8450, doi 10.3386/w17540.
535. **Greenstone, M.** Developing a Social Cost of Carbon for US Regulatory Analysis. *Rev. Environm. Econ. Policy*. 2013, Vol. 7, 1, pp. 23-46. ISSN 1750-6824, doi 10.1093/reep/res015.
536. **Nordhaus, W.** Estimates of the Social Cost of Carbon: Concepts and Results from the DICE-2013R Model (...). *J. AERE*. 2014, Vol. 1, 1/2, pp. 273-312. ISSN 2333-5963, doi 10.1086/676035.
537. **Waldhoff, S.** The Marginal Damage Costs of Different Greenhouse Gases: An Application of FUND. *Economics*. 01 10 2014, Vol. 8, 31, pp. 1-33. ISSN 1864-6042, doi 10.5018/economics-ejournal.ja.2014-31.
538. **BLS.** CPI Detailed Report, Nov. 2015. [Rep.]. Washington, DC : BLS, 12 2015. p. 115. bls.gov/cpi.
539. **Icha, P.** Entwicklung der spezifischen Kohlendioxid-Emissionen des deutschen Strommix (...). *Climate Change*. [Rep.]. Dessau-Roßlau : UBA, 06 2015. Vol. 09/2015, p. 21. ISSN 1862-4359.
540. **Verschuur, M.** Der Kohlenbergbau in der Energiewirtschaft der BRD im Jahre 2014. [Rep.]. Herne : Statistik der Kohlenwirtschaft, 11 2015. p. 82. kohlenstatistik.de, rag_kohlenwirt_silberbuch_web.pdf.
541. **BGL.** Kostenentwicklung im Güterkraftverkehr. [Art. on hp.]. Frankfurt a. M. : BGL, 2014. bgl-ev.de.
542. **AN.** Projet de loi de finances pour 2014. *Doc. d'information*. [Rule]. Paris : AN, 19 12 2013. Vol. 21. Texte adopté n° 267, ISSN 1240-831X, ISBN 9782111327658.
543. **MEEM.** La fiscalité des produits pétroliers (...). *La fiscalité dans les dernières lois de finances*. [Rule]. Paris : MEEM, 13 01 2016. Taxes on diesel fuel (gazole), 2002 to 2016, developpement-durable.gouv.fr.
544. **Hütte.** *Des Ingenieurs Taschenbuch*. 1. Berlin : Ernst & Korn, 1857. Vol. 1, ISBN 9783981190304.
545. **Newton, I.** *Philosophiae Naturalis Principia Mathematica*. London : Royal Society, 1687. p. 510. doi 10.3931/e-rara-440.
546. **Lüdde, H.** Klassische Mechanik. [Lecture notes]. Frankfurt a. M. : Goethe Uni, Inst. f. Theor. Physik, 2012. p. 128. th.physik.uni-frankfurt.de/~luedde.
547. **Gasch, R.** *Windkraftanlagen*. 4. Wiesbaden : Teubner, 2005. ISBN 9783519363347.
548. **Mansour, M.** Development of novel control strategy for multiple circuit, roof top bus air conditioning (...). *Energy Cnv. and Mgmt*. 21 02 2008, Vol. 49, 6, pp. 1455-1468. ISSN 0196-8904, doi 10.1016/j.enconman.2007.12.032.
549. **Boltz, N.** *Klimasysteme im Bus*. 1. München : SV Onpact, 2011. p. 72. ISBN 9783862360239.
550. **Kossel, R.** Hybride Simulation thermischer Systeme am Beispiel eines Reisebusses. [Diss.]. Braunschweig : TU, Institut für Thermodynamik, 02 2012. p. 112. katalog.ub.tu-braunschweig.de/vufind/Record/689041969.
551. **Reitz, T.** Ideen für eine wirtschaftliche und effiziente Klimatechnik von Morgen. [Conf.]. Leipzig : trolley:motion, 23 10 2012. p. 18. trolley:motion.ch.
552. **Hegar, M.** Bus HVAC energy consumption test method based on HVAC unit behavior. *Refrigeration*. 12 11 2012, Vol. 36, 4, pp. 1254-1262. ISSN 0140-7007, doi 10.1016/j.ijrefrig.2012.10.023.
553. **Kaiser, C.** Konzepte für die Reduzierung des Kraftstoffverbrauchs von Omnibusklimaanlagen. *VDI-Ber.* 05 06 2013, Vol. 2186, pp. 269-282. ISSN 0083-5560, ISBN 9783180921860.
554. **Großmann, H.** *Pkw-Klimatisierung*. 2. Berlin : Springer, 2013. p. 309. ISBN 9783642398407.
555. **Imam, R.** Design of Air Conditioning System in Automobile. *Innovative Rsrch. in Science, Engrg. Tech.* 12 2013, Vol. 2, 12, pp. 7460-7464. ISSN 2319-8753.
556. **Sukri, M.** Achieving a better energy-efficient automotive air-conditioning system. *Energy Efficiency*. 26 08 2015, Vol. 8, 6, pp. 1201-1229. ISSN 1570-646X, doi 10.1007/s12053-015-9389-4.
557. **Bitzer.** Reciprocating compressors, KP-570-3. [Prod. info]. Sindelfingen : Bitzer, 08 2010. p. 8. bitzer.de.

558. **Bock**. Bock Compressors for Mobile Applications. [Prod. info]. Frickenhausen : GEA - Bock, 08 2014. p. 92. Doc. no. 09689-08.2014-Gb, gea.com, 09689_Vehicle Compressors_tcm24-19452.pdf.
559. **March, M.** Simulation einer PKW-Klimaanlage. [Bachelor Thesis]. Graz : TU, IVT, 16 10 2014. p. 71.
560. **Linden, D. ed.** *Handbook Of Batteries*. 3. New York, NY : McGraw Hill, 2002. p. 1468. ISBN 9780071359788.
561. **Schröder**. *Leistungselektronische Schaltungen*. 2. Berlin : Springer, 2008. p. 1304. ISBN 9783540693000.
562. **Sauer, D.** Lithium-Ionen Batterien. [book auth.] O. Sirch. *Elektrik/Elektronik in Hybrid- und Elektrofahrzeugen*. Renningen : expert, 2009, pp. 1-8. ISBN 9783816928171.
563. **Graf, I.** Semiconductors in Hybrid Drives Applications. [book auth.] O. Sirch. *Elektrik/Elektronik In Hybrid- Und Elektrofahrzeugen*. Renningen : expert, 2009, pp. 51-62. ISBN 9783816928171.
564. **Lunz, B.** Potenziale von Energiespeichern zur Elektrifizierung des Nahverkehrs. *Der Nahverkehr*. 06 2009, Vol. 27, 7/8, pp. 23-27. ISSN 0722-8287.
565. **Riegel, B.** Energiespeicher: Schlüsseltechnik für die Elektromobilität. *Der Nahverkehr*. 06 2009, Vol. 27, 7/8, pp. 28-30. ISSN 0722-8287.
566. **Broussely, M.** Battery Requirements for HEVs, PHEVs, and EVs: An Overview. [book auth.] G. Pistoia. *Electric And Hybrid Vehicles*. Amsterdam : Elsevier, 2010, 13, pp. 305-346. ISBN 9780444535658.
567. **März, M.** Leistungselektronik für e-Fahrzeuge. *DRIVE-E-Akademie*. [Conf.]. Erlangen : BMBF, 12 03 2010. p. 36. drive-e.org, 15_Fr_Maerz_Leistungselektronik.pdf.
568. **Burke, A.** Testing of electrochemical capacitors. *Electrochim. Acta*. 29 04 2010, Vol. 55, 25, pp. 7538–7548. ISSN 0013-4686, doi 10.1016/j.electacta.2010.04.074.
569. —. The power capability of ultracaps and Li batteries for EV & HEV applications. *J. Power Sources*. 31 07 2010, Vol. 196, 1, pp. 514–522. ISSN 0378-7753, doi 10.1016/j.jpowsour.2010.06.092.
570. **Rashid, M.** *Power Electronics Handbook*. 3. Burlington, MA : Butterworth-Heinemann, 2011. p. 1389. ISBN 9780123820365.
571. **Gerssen-Gondelach, S.** Performance of batteries for electric vehicles on short and longer term. *J. Power Sources*. 10 04 2012, Vol. 212, pp. 111-129. ISSN 0378-7753, doi 10.1016/j.jpowsour.2012.03.085.
572. **Korthauer, R. ed.** *Handbuch Lithium-Ionen-Batterien*. 1. Wiesbaden : Springer-Vieweg, 2013. p. 436. ISBN 9783642306525.
573. **Zach, F.** *Leistungselektronik*. 5. Wiesbaden : Springer-Vieweg, 2015. p. 2784 + app. 94. Vol. 2, ISBN 9783658048983.
574. **Tschöke, H. (ed.)**. *Die Elektrifizierung des Antriebsstrangs*. 1. Wiesbaden : Springer-Vieweg, 2015. p. 207. ISBN 9783658046439.
575. **Malottki, S. von.** Elektrischer Traktionsmotor Am Stromzwischenkreis-Wechselrichter. [Diss.]. Aachen : RWTH, Fak. f. Elektrotechn. u. Informationstechn. p. 152. ISBN 9783844038392.
576. **Specovius, J.** *Grundkurs Leistungselektronik*. 7. Wiesbaden : Springer-Vieweg, 2015. p. 402. ISBN 9783658033088.
577. **Sahin, F.** Design and development of a high-speed axial-flux permanent-magnet machine. [Diss.]. Eindhoven : TU, Electr. Engrg., 03 2001. p. 229. ISBN 9038613801, doi 10.6100/IR544267.
578. **Chin, Y.** A PMSM for an EV. *TRITA-ETS*. [Licentiate thesis]. Stockholm : KTH, Elektro- och systemteknik, 05 07 2004. Vol. 4, p. 77. ISSN 1650-674, ISBN 9172838035, urn.kb.se/resolve?urn=urn:nbn:se:kth:diva-1763.
579. **Hey, J.** Transient thermal modelling of an Axial Flux Permanent Magnet (AFPM) machine (...). *VTMS*. [Conf.]. Warwickshire : IMechE, 19 05 2011. Vol. 10, pp. 411-421. doi 10.1533/9780857095053.6.411.
580. **Huang, Z.** Thermal Design of EM. [Licentiate Thesis]. Lund : Uni Lund, Industriell Elektroteknik, 10 2013. p. 129. ISBN 9789188934628, lup.lub.lu.se/search/record/42e8e271-f2f4-42e5-9130-d010c94de6d8.
581. **Boglietti, A. (...)** Thermal Analysis of Electrical Machines. *IEEE Transact. Industr. Electron.*, 27 02 2009, Vol. 56, 3, pp. 871-882. ISSN 0278-0046, doi 10.1109/TIE.2008.2011622.
582. **Kolondzovski, Z.** Thermal and mechanical analyses of high-speed permanent-magnet electrical machines. *TKK dissertations*. [Diss.]. Aalto : Yliopisto, Sähkötekniikan laitos, 08 2010. Vol. 233, p. 93. ISSN 1795-2239, ISBN 9789526032795, urn.fi/URN:ISBN:978-952-60-3280-1.
583. **Nategh, S.** Thermal Analysis and Management of High-Performance Electrical Machines. *TRITA-EE*. [Diss.]. Stockholm : KTH, Elektro- och systemteknik, 28 05 2013. Vol. 22, p. 83. ISSN 1653-5146, ISBN 9789175017334, urn.kb.se/resolve?urn=urn:nbn:se:kth:diva-122695.
584. **La Rocca, A.** Thermal analysis of a high speed electrical machine. [Diss.]. Nottingham : Uni Nottingham, 11 2015. p. 135 + app. 44. eprints.nottingham.ac.uk/id/eprint/33156.
585. **Demetriades, G.** A Real-Time Thermal Model of a Permanent-Magnet Synchronous Motor. *Power Electron*. 18 08 2009, Vol. 25, 2, pp. 463-474. ISSN 0885-8993, doi 10.1109/TPEL.2009.2027905.
586. **Yanhua, S.** Thermal Behavior of PM in-Wheel Motor used in Off-Road Motor Driven Truck. *Proc. Engrg*. 2011, Vol. 23, pp. 222-228. ISSN 1877-7058, doi 10.1016/j.proeng.2011.11.2493.

587. **Marquez-Fernandez, F.** Dynamic evaluation of the overloading potential of a convection cooled permanent magnet synchronous motor. *IEMDC*. [Conf.]. Niagara Falls, CA : IEEE, 15 05 2011. pp. 13-18. ISBN 9781457700606, doi 10.1109/IEMDC.2011.5994812.
588. **Martinovic, M.** Influence of winding design on thermal dynamics of permanent magnet traction motor. *SPEEDAM*. [Conf.]. Ischia : IEEE, 18 06 2014. Vol. 22, pp. 397-402. ISBN 9781479947492, doi 10.1109/SPEEDAM.2014.6872026.
589. **Huger, D.** An advanced lifetime prediction method for permanent magnet synchronous machines. *ICEM*. [Conf.]. Berlin : IEEE, 02 09 2014. 21, pp. 696-691. ISBN 9781479943890, doi 10.1109/ICELMACH.2014.6960255.
590. **Pohlandt, C.** Thermal models of electric machines with dynamic workloads. *Landtechnik*. [Article]. Düsseldorf : VDI, 15 07 2015. Vol. 70, 4, pp. 97–112. ISSN 0023-8082, doi 10.15150/lt.2015.2664.
591. **Götz, H.** Die Aerodynamik des Nutzfahrzeuges. *Fortschr.-Ber. VDI-Z. 12, Verkehrstechnik*, 03 1978, Vol. 31, pp. 187-197. ISSN 0506-3167.
592. **Hau, E.** Über den Luftwiderstand von Fernlastzügen. *Fortschr.-Ber. VDI-Z. 12, Verkehrstechnik*, 03 1978, Vol. 31, pp. 199-210. ISSN 0506-3167.
593. **Hucho, W. (ed.)**. *Aerodynamik Des Automobils*. 1. Würzburg : Vogel, 1981. p. 440. ISBN 9783802306426.
594. **Naumann, K.** Monitoring Biokraftstoffsektor. 3 [Rep.]. Leipzig : DBFZ, 07 09 2016. p. 132. Rep. no. 11, ufop.de, DBFZ_Report_11_3.pdf.
595. **Kraßer, B.** Optimierte Auslegung einer Modularen Dauermagnetmaschine für ein Autarkes Hybridfahrzeug. [Diss.]. München : TU, Elektr. Masch. und Geräte, 08 02 2000. p. 113. nbn-resolving.de/urn/resolver.pl?urn:nbn:de:bvb:91-diss2000092315246.
596. **Immonen, P.** Hybrid Drive System For Mobile Work Machine. [Pres. slides]. Lappeenranta : TY, Sähkötekn., 13 11 2009. p. 18. prizz.fi, linkki2ID431.pdf.
597. **Lee, S.** Development and Analysis of Interior Permanent Magnet Synchronous Motor with Field Excitation Structure. [Diss.]. Knoxville, TN : Uni Tennessee, 12 2009. p. 190. trace.tennessee.edu/utk_graddiss/613.
598. **Dereyne, S.** Variable Speed Drive Evaluation Using Iso Efficiency Maps. *EEMODS*. [Conf.]. Alexandria, VA : NEMA, 12 09 2011. pp. 566-278. ISBN 9789279282218, doi 10.2790/76744.
599. **Demmelmayr, F.** Advantages of PM-machines (...). *IECON*. [Conf.]. Melbourne : IEEE, IES, 07 11 2011. Vol. 37, pp. 2762-2768. ISSN 1553-572X, ISBN 9781612849720, doi 10.1109/IECON.2011.6119749.
600. **Immonen, P.** Energy Efficiency of a Diesel-Electric Mobile Working Machine. *Acta Univ. Lappeenranta*. [Diss.]. Lappeenranta : TY, Sähkötekn., 06 06 2013. Vol. 518, p. 133. ISSN 1456-4491, ISBN 9789522654144, urn.fi/URN:ISBN:978-952-265-415-1.
601. **Sato, D.** Evaluation Method of Energy Consumption for Permanent Magnet Synchronous Motor Drive System. *IECON*. [Conf.]. Yokohama : IEEE, IES, 09 11 2015. Vol. 41, pp. 5267-5272. ISSN 1553-572X, ISBN 9781479917624, doi 10.1109/IECON.2015.7392929.
602. **Gu, W.** Design and Optimization of Permanent Magnet Brushless Machines for Electric Vehicle Applications. *energies*. 10 12 2015, Vol. 8, 12, pp. 13996-14008. ISSN 1996-1073, doi 10.3390/en81212410.
603. **Guan, Y.** Comparison between induction machine and interior permanent magnet machine for electric vehicle application. *COMPEL*. [Article]. Bingley : Emerald, 07 03 2016. Vol. 35, 2, pp. 572-585. ISSN 0332-1649, doi 10.1108/COMPEL-02-2015-0110.
604. **USEPA**. On-highway Heavy-duty Diesel and Gasoline Certification Data for 2014. *Engine Certification Data*. [Data table]. Washington, DC : USEPA, 03 2015. Vol. 19. epa.gov, on-hwy-2014e.xls.
605. —. On-highway Heavy-duty Diesel and Gasoline Certification Data for 2015. *Engine Certification Data*. [Data table]. Washington, DC : USEPA, 05 2016. epa.gov, on-hwy-2015.xls.
606. **CFR**. Title 40, Protection of Environment, Part 1000 to End. *CFR*. [Rule]. Washington, DC : USGPO, 01 07 2010. p. 965. ISSN 1946-4975, gpo.gov/fdsys/pkg/CFR-2010-title40-vol32.
607. —. Title 40, Protection of Environment, Parts 85 to 86. *CFR*. [Rule]. Washington, DC : USGPO, 01 07 2015. p. 962. ISSN 1946-4975, gpo.gov/fdsys/pkg/CFR-2015-title40-vol19.
608. **Grünig, G.** MB Actros 1851 Euro 6 and presentation of new test route. *VR*. 03 08 2012, Vol. 67, 31-32, pp. 76-80. ISSN 0341-2148.
609. **Schwarz, A.** Scania G 410 Streamline. *KFZ-Anzeiger*. 02 2014, Vol. 67, 3, pp. 16-21. ISSN 0341-9681.
610. —. Iveco Stralis Hi-Way 420. *KFZ-Anzeiger*. 04 2015, Vol. 68, 7, pp. 17-21. ISSN 0341-9681.
611. —. MB Actros 1842. *KFZ-Anzeiger*. 08 2015, Vol. 68, 16, pp. 10-15. ISSN 0341-9681.
612. —. DAF CF 440. *KFZ-Anzeiger*. 09 2015, Vol. 68, 18, pp. 11-14. ISSN 0341-9681.
613. —. Volvo FL 240 and presentation new test route. *KFZ-Anzeiger*. 06 2007, Vol. 60, 12, pp. 8-11. ISSN 0341-9681.
614. **Wildhage, H.** Scania G 440. *güterverkehr*. 04 2012, Vol. 61, 5, pp. 8-13. ISSN 0017-5137.
615. —. MB Actros 1845. *güterverkehr*. 09 2012, Vol. 61, 10, pp. 8-12. ISSN 0017-5137.
616. —. MB Actros 1843. *güterverkehr*. 07 2013, Vol. 62, 8/9, pp. 8-11. ISSN 0017-5137.

617. — Iveco Stralis 460. *güterverkehr*. 10 2013, Vol. 62, 11/12, pp. 8-10. ISSN 0017-5137.
618. — Volvo FH 460. *güterverkehr*. 12 2013, Vol. 63, 1/2, pp. 10-12. ISSN 0017-5137.
619. — Scania G 410. *güterverkehr*. 02 2014, Vol. 63, 3, pp. 11-13. ISSN 0017-5137.
620. — DAF XF 460. *güterverkehr*. 06 2014, Vol. 63, 6, pp. 8-10. ISSN 0017-5137.
621. — Renault T 430. *güterverkehr*. 07 2014, Vol. 63, 8/9, pp. 8-10. ISSN 0017-5137.
622. — DAF XF 440. *güterverkehr*. 09 2014, Vol. 63, 10/11, pp. 8-10. ISSN 0017-5137.
623. — MB Actros 1845. *DVZ*. 19 04 2013, Vol. 67, 32, pp. 14-15. ISSN 0342-166X.
624. — Scania G 450. *DVZ*. [Art. on hp.]. Hamburg : DVV, 08 05 2014. ISSN 0342-166X , dvz.de.
625. — Scania G410, Volvo FH 460, DAF XF 440, MAN TGX 18.440, Renault T 430, MB Actros 1843, Iveco Stralis 460. *DVZ*. 23 09 2014, Vol. 68, 79, pp. 7-9. ISSN 0342-166X.
626. **Zeitzen, F.** MB Actros 1843 LS. *lastauto omnibus*. 07 2013, Vol. 90, 8, pp. 24-28. ISSN 1613-1606.
627. — MAN TGX 18.440 XLX. *lastauto omnibus*. 08 2013, Vol. 90, 9, pp. 14-17. ISSN 1613-1606.
628. — Scania G410 LA. *lastauto omnibus*. 01 2014, Vol. 91, 2, pp. 12-16. ISSN 1613-1606.
629. — DAF XF 440. *lastauto omnibus*. 08 2014, Vol. 91, 9, pp. 9-13. ISSN 1613-1606.
630. — Scania G410 Highline. *lastauto omnibus*. 11 2014, Vol. 91, 12, pp. 12-17. ISSN 1613-1606.
631. — Description of new test route. *lastauto omnibus*. 03 2010, Vol. 87, 4, pp. 16-17. ISSN 1613-1606.